NBS SPECIAL PUBLICATION 484

U.S. DEPARTMENT OF COMMERCE / National Bureau of Standards

Flow Measurement in Open Channels and Closed Conduits

Volume 2

NATIONAL BUREAU OF STANDARDS

The National Bureau of Standards[1] was established by an act of Congress March 3, 1901. The Bureau's overall goal is to strengthen and advance the Nation's science and technology and facilitate their effective application for public benefit. To this end, the Bureau conducts research and provides: (1) a basis for the Nation's physical measurement system, (2) scientific and technological services for industry and government, (3) a technical basis for equity in trade, and (4) technical services to promote public safety. The Bureau consists of the Institute for Basic Standards, the Institute for Materials Research, the Institute for Applied Technology, the Institute for Computer Sciences and Technology, the Office for Information Programs, and the Office of Experimental Technology Incentives Program.

THE INSTITUTE FOR BASIC STANDARDS provides the central basis within the United States of a complete and consistent system of physical measurement; coordinates that system with measurement systems of other nations; and furnishes essential services leading to accurate and uniform physical measurements throughout the Nation's scientific community, industry, and commerce. The Institute consists of the Office of Measurement Services, and the following center and divisions:

Applied Mathematics — Electricity — Mechanics — Heat — Optical Physics — Center for Radiation Research — Laboratory Astrophysics[2] — Cryogenics[2] — Electromagnetics[2] — Time and Frequency[2].

THE INSTITUTE FOR MATERIALS RESEARCH conducts materials research leading to improved methods of measurement, standards, and data on the properties of well-characterized materials needed by industry, commerce, educational institutions, and Government; provides advisory and research services to other Government agencies; and develops, produces, and distributes standard reference materials. The Institute consists of the Office of Standard Reference Materials, the Office of Air and Water Measurement, and the following divisions:

Analytical Chemistry — Polymers — Metallurgy — Inorganic Materials — Reactor Radiation — Physical Chemistry.

THE INSTITUTE FOR APPLIED TECHNOLOGY provides technical services developing and promoting the use of available technology; cooperates with public and private organizations in developing technological standards, codes, and test methods; and provides technical advice services, and information to Government agencies and the public. The Institute consists of the following divisions and centers:

Standards Application and Analysis — Electronic Technology — Center for Consumer Product Technology: Product Systems Analysis; Product Engineering — Center for Building Technology: Structures, Materials, and Safety; Building Environment; Technical Evaluation and Application — Center for Fire Research: Fire Science; Fire Safety Engineering.

THE INSTITUTE FOR COMPUTER SCIENCES AND TECHNOLOGY conducts research and provides technical services designed to aid Government agencies in improving cost effectiveness in the conduct of their programs through the selection, acquisition, and effective utilization of automatic data processing equipment; and serves as the principal focus wthin the executive branch for the development of Federal standards for automatic data processing equipment, techniques, and computer languages. The Institute consist of the following divisions:

Computer Services — Systems and Software — Computer Systems Engineering — Information Technology.

THE OFFICE OF EXPERIMENTAL TECHNOLOGY INCENTIVES PROGRAM seeks to affect public policy and process to facilitate technological change in the private sector by examining and experimenting with Government policies and practices in order to identify and remove Government-related barriers and to correct inherent market imperfections that impede the innovation process.

THE OFFICE FOR INFORMATION PROGRAMS promotes optimum dissemination and accessibility of scientific information generated within NBS; promotes the development of the National Standard Reference Data System and a system of information analysis centers dealing with the broader aspects of the National Measurement System; provides appropriate services to ensure that the NBS staff has optimum accessibility to the scientific information of the world. The Office consists of the following organizational units:

Office of Standard Reference Data — Office of Information Activities — Office of Technical Publications — Library — Office of International Standards — Office of International Relations.

---

[1] Headquarters and Laboratories at Gaithersburg, Maryland, unless otherwise noted; mailing address Washington, D.C. 20234.

[2] Located at Boulder, Colorado 80302.

Flow Measurement in Open Channels and Closed Conduits

Volume 2

Proceedings of the Symposium on Flow Measurement in Open Channels and Closed Conduits held at the National Bureau of Standards in Gaithersburg, Maryland on February 23-25, 1977

Lafayette K. Irwin, Editor

Mechanics Division
Institute for Basic Standards
National Bureau of Standards
Washington, D.C. 20234

U.S. DEPARTMENT OF COMMERCE, Juanita M. Kreps, Secretary

Dr. Sidney Harman, Under Secretary
Jordan J. Baruch, Assistant Secretary for Science and Technology

U.S. NATIONAL BUREAU OF STANDARDS, Ernest Ambler, Acting Director

Issued October 1977

Library of Congress Cataloging in Publication Data

Symposium on Flow Measurement in Open Channels and Closed Conduits, National Bureau of Standards, 1977.
Flow measurement in open channels and closed conduits.
(National Bureau of Standards special publication ; 484)
Includes index.
Supt. of Docs. no.: C13.10:484
1. Flow meters—Congresses. I. Irwin, Lafayette K. II. Title. III. Series: United States. National Bureau of Standards. Special publication ; 484.
QC100.U57 no. 484 [TC177] 602'.1s [6a0.1'064] 77-14243

National Bureau of Standards Special Publication 484/2
Nat. Bur. Stand. (U.S.), Spec. Publ. 484/2, 490 pages (Oct. 1977)
CODEN: XNBSAV

U.S. GOVERNMENT PRINTING OFFICE
WASHINGTON: 1977

For sale by the Superintendent of Documents, U.S. Government Printing Office
Washington, D.C. 20402 - Price $12.25 per 2 part set ; sold in sets only

Stock No. 003–003–01845–7

PREFACE

These Proceedings include most of the papers presented at the three-day symposium on fluid flow measurements held at the National Bureau of Standards, Gaithersburg, Maryland, on February 23, 24, and 25, 1977. The papers dealt with flow in open channels and closed conduits and a special related session on international standards.

The impetus to hold the symposium came from several sources. These included (1) continuing requests for the information presented at the 1974 Flow Measurement Conference held to establish connections between flow measurement and national needs (conference presentations not published), (2) increasing use of measurement technology by regulators to monitor or enforce the effects of their rule making, and (3) rising awareness of the importance of international standards to this nation, particularly, for quantifying energy-related fluids. The purpose of the symposium was to bring together a significant group of the producers and users of flow measurement technology, to provide a forum for presenting and discussing both the new and the proven ideas for making useful flow measurements, and to assemble and disseminate the resulting information.

Initially, the theme was to emphasize identification and assessment of sources of errors, formulation of error analysis techniques and recommendations for resolving the uncertainties for flow measurement. The strong interests of investigators in presenting related research, of instrument developers in describing the performance of flow measurement devices and systems, and of users in discussing applications resulted in a broader spectrum and larger number of papers than was envisioned. An optimum ordering of papers in the resulting two volumes has not evolved.

Lafayette K. Irwin, Editor

Conversions for Customary to International System (SI) Units*

Reflecting the transitional stage of the measurement units in this technological area, both U. S. customary and SI units of measurement are used in different papers of these Proceedings. The U.S.A. is a member of the General Conference on Weights and Measures which gave official status to the SI metric units in 1960. Conversion factors for selected units in these Proceedings are:

Quantity	Conversion customary to SI	Factor, approximate
Length	inch (in) to meter (m)	0.0254†
	foot (ft) to meter (m)	0.3048†
Area	$inch^2$ (in^2) to $meter^2$ (m^2)	0.0006452
	$foot^2$ (ft^2) to $meter^2$ (m^2)	0.09290
Volume	$inch^3$ (in^3) to $meter^3$ (m^3)	0.00001639
	$foot^3$ (ft^3) to $meter^3$ (m^3)	0.02832
	gallon†† (gal) to $meter^3$ (m^3)	0.003785
Mass	pound, avoirdupois (lb) to kilogram (kg)	0.4536
Force	pound (lbf) to newton (N)	4.448
	kilogram (kgf) to newton (N)	9.807
Pressure, or Stress	pound/$inch^2$ (psi) to newton/$meter^2$ (N/m^2)	6895
	inch of mercury, 60 °F (inHg) to newton/$meter^2$ (N/m^2)	3377
	inch of water, 60 °F (inH_2O) to newton/$meter^2$ (N/m^2)	248.8
	millimeter of mercury, 0 °C (mmHg) to newton/$meter^2$ (N/m^2)	133.3
Velocity	inch/second (in/s) to meter/second (m/s)	0.0254†
	foot/second (ft/s) to meter/second (m/s)	0.3048†
Acceleration	foot/$second^2$ (ft/s^2) to meter/$second^2$ (m/s^2)	0.3048†
	free fall, standard (g) to meter/$second^2$ (m/s^2)	9.807
Density	pound/$foot^3$ (lb/ft^3) to kilogram/$meter^3$ (kg/m^3)	16.02
	pound/gallon†† (lb/gal) to kilogram/$meter^3$ (kg/m^3)	119.8
Flow	$foot^3$/second (ft^3/s) to $meter^3$/second (m^3/s)	0.02832
	$foot^3$/minute (ft^3/min) to $meter^3$/second (m^3/s)	0.0004719
	gallon††/minute (gal/min) to $meter^3$/second (m^3/s)	0.00006309
	pound/second (lb/s) to kilogram/second (kg/s)	0.4536
Temperature	degree Fahrenheit to degree Celsius	$t_{°C}=(t_{°F}-32)1.$

* See NBS SP330, 1977 ed., The International System of Units (SI) and ASTM E380-76, Metric Practice Guide for more complete information.

† Exact

†† U. S. liquid

TABLE OF CONTENTS - Volume 1

PREFACE iii

Conversions for Customary to International (SI) Units iv

ABSTRACT ix

Measuring the Repeatability of Flowmeters 1
A. T. J. Hayward

The Navy Liquid Flow Correlation Program 25
J. H. Tabler and C. G. Kullman

A Laboratory Study of Turbine Meter Uncertainty 33
G. Mattingly, P. Pontius, H. Allion, and E. Moore

Evolution of a Modern Petroleum Measurement Manual 55
L. M. Davis

Building Blocks Towards Flowmeter Reliability 61
Dezsoe Halmi

Open Channel Flow Monitoring or Metering, That is the Question ... 83
Kenneth W. Martig, Jr.

Instrument Errors in Open Channel Flow Measurement Systems 91
D. M. Grant

Marine Dynamics and Its Effects on Current Measuring Transducers . 109
Thomas Mero, Gerald Appell, and Raul S. McQuivey

Some Error Sources in Price and Pygmy Current Meter Traverses 123
G. Kulin

Flow Measurements in the Canals of Power Plant Closed Loop Cooling Systems 145
Joseph F. O'Brien, James Skridulis, John Annett, G. Wayne Singley and Harold L. Koenig

Errors in Flow Measurement and Their Importance in Infiltration/ Inflow Analysis 173
D. L. Guthrie, D. R. Washington and C. Vincenty

Rating Broad-Crested V-Notch Weirs with Narrow, Sloping Approach Channels and Sediment Deposits 187
James F. Ruff, Keith Saxton and Clement Dang

Compensating for Construction Errors in Critical-Flow Flumes and Broad-Crested Weirs 201
John A. Replogle

Table of Contents - Volume 1 (Continued)

Numerical Modeling of Two-Dimensional Flumes 219
Ronald W. Davis

The Design of Open Channel Acoustic Flowmeters for Specified Accuracy: Sources of Error and Calibration Test Results 243
Francis C. Lowell, Jr.

Application Considerations & Performance Capability of the Time Differential Clamp-On Ultrasonic Flowmeter 267
J. Baumoel

Theoretical and Experimental Assessment of Uncertainties in Non-Intrusive, Ultrasonic Flow Measurement 277
Ronald F. Bruner

A New Ultrasonic Flowmeter for the Natural Gas Industry 293
N. E. Pedersen, J. E. Bradshaw, L. C. Lynnworth and P. F. Morel

A New Non-Intrusive Flowmeter 319
R. S. Flemons

Reconstructing Three-Dimensional Fluid Velocity Vector and Temperature Fields from Acoustic Transmission Measurements 335
S. A. Johnson, J. F. Greenleaf, M. Tanaka, and G. Flandro

Validation of Use of Dye-Dilution Method for Flow Measurement in Large Open and Closed Channel Flows 361
W. H. Morgan, D. Kempf, R. E. Phillips

Dilution Method of Discharge Measurement in Pipes 395
E. R. Holley

Application of a Fluorescence Technique to Dye-Concentration Measurements in a Turbulent Jet 423
Hsien-Ta Liu, Jung-Tai Lin, Donald P. Delisi and Frank A. Robben

The Application of Monte Carlo and Bayesian Probability Techniques to Flow Prediction and Determination 447
Frank J. Berté

Author Index 470-A

TABLE OF CONTENTS - Volume 2

Laser Doppler Anemometry for Flow Measurement 471
William W. Durgin and Lawrence C. Neale

On Improving the Pitot-Tube Determination of Flows in Large Pipes. 479
J. M. Robertson and M. E. Clark

Numerical Modeling and Turbulent Flow Through Thin Orifice Plates. 491
R. W. Davis and G. E. Mattingly

Table of Contents - Volume 2 (Continued)

Studies of Pulsating Incompressible Flow Through Orifice Meters .. 523
R. A. Bajura and M. T. Pellegrin

A Vortex Flowmeter - Calibration Results and Application Experiences 549
R. W. Miller, J. P. DeCarlo, and J. T. Cullen

Temperature Field Measurements in Turbulent Thermals 571
Mohamed Gad-el-Hak

Flow Measurement Up-Date 597
Robert B. Suhoke

Near Wall Velocity Measurements for Wall Shear Inference in Turbulent Flows 621
F. J. Pierce and D. S. Gold

On Reduction of Errors Arising in Hot-Wire Anemometry of Thin Turbulent Shear Layers 649
J. Gaviglio and J. P. Dussauge

Probe and Method for Simultaneous Measurements of 'True' Instantaneous Temperature and Three Velocity Components in Turbulent Flow 659
Gracio Fabris

Measurement of Boundary Layer Transition Using Acoustic Techniques 687
Donald C. Sachs, Thomas F. V. Meagher, and Vernon D. Peckham

Measurement of Recirculating Flow Behind a Cylinder with Spray Cooling 705
R. S. Rudland

A New Type of Velocity Probe 719
W. B. Brower, Jr. and Alan Servoz

The Influence of Turbulence on Static and Total Pressure Probes .. 737
V. E. Scottron

Determination and Elimination of Errors in Velocity Readings at Ventilation Tubing Inlets 755
Robert A. Haney

Indirect Two-Phase Flow Measurement: Analysis and Reduction of Methods Errors 765
N. N. Kondic

Measurements of Density and Density Gradient With an Oscillating Conductivity Probe 783
Donald P. Delisi and Robert H. Kirchhoff

New Techniques for Automotive Fuel Flow Measurements 803
Milton Baker

A New Digital Technique for Temperature and Viscosity Compensation of Turbine and Positive-Displacement Flow Transducers 821
Roger Jennings

Viscosity Effects on the Turbine Flowmeter 847
John M. Ball

Turbine Meters for the Measurement of Gaseous Hydrocarbons 871
Paul J. LaNasa

On a New Method of Gas Flow Measurement Using Cryogenic Techniques 881
D. B. Mann and J. A. Brennan

An Anatomy of the International Standards Producing System - Flow Measurement 895
L. K. Irwin

OIML and EEC, Their Impact on the International Standards Producing System 921
D. E. Edgerly

The Interface Between Industrial, National and International Standards 929
Wallace N. Seward

The Adequacy of the Data Bases Available for Promulgating International Standards 935
H. H. Dijstelbergen

Equitable Implementation of National and International Allocation Programs - Summary of Remarks 945
James A. West

Of Form and Substance for Effective Standards 947
E. A. Spencer

Comments On: Role of International Standards in Measuring and Allocating Hydrocarbons - A Program for Solution of our Present Problems 957
F. H. Abernathy

Author Index 960

ABSTRACT

The wide range and complexity of problems and potential solutions that must be considered for useful flow measurements are emphasized by the papers contained in these proceedings. Fifty-three presentations cover: characteristics of new and improved instruments; applications of traditional and new measuring devices in field environments; procedures for identifying and analyzing errors or uncertainties in data under specific conditions; uses of physical and numerical models; politico-economic changes that affect international standards for flow measurement; and philosophical bases for making measurements. The fluids of most interest are water and waste water, petroleum and related refined products, air, natural gas and stack gas.

Experimental and analytical investigations on instrument performance and interpretation of results include innovative applications of traditional and new flow measurement techniques to fluid flows in open channels and closed conduits. The traditional devices or techniques include weirs, flumes, current meters, orifice plates, turbines, hot-wires, pitot-static tubes, velocity traverses, dye-dilution, and others. More recent instrumentation developments and procedures such as laser doppler anemometry, acoustic and thermal imaging, acoustic pulse velocity and doppler anemometry, numerical modeling, vortex shedding and digital computation are covered for particular measurement purposes.

The most significant trend reflected in these presentations is the general awareness that uncertainties in measured quantities at the lowest point in the measurement chain, i.e., in the field or plant, are more important than accuracy statements derived from controlled laboratory studies. Other trends in evidence are the rising importance of turbine meters for use as transfer standards and in-line measurements of liquids and gases in filled pipes and the increasing number of applications for acoustics and laser technology for flow measurements in both open channels and closed conduits.

Key Words: Acoustic flow meters; closed conduit flows; current meters; dye-dilution methods; errors in flow measurement; flow measurement; fluid flow modeling; fluid velocity; flumes; gas flow standard; hot-wire anemometry; international flow standards; laser anemometry; open channel flows; orifice meters; pitot-static meters; turbine meters; weirs.

DISCLAIMER:

Certain trade names and company products are identified in order to adequately specify the experimental procedure. In no case does such identification imply recommendation or endorsement by the National Bureau of Standards, nor does it imply that the products are necessarily the best available for the purpose.

National Bureau of Standards Special Publication 484, Proceedings of the Symposium on Flow in Open Channels and Closed Conduits held at NBS, Gaithersburg, MD, February 23-25, 1977. (Issued October 1977)

LASER DOPPLER ANEMOMETRY FOR FLOW MEASUREMENT

William W. Durgin

Alden Research Laboratories
Worcester Polytechnic Institute
Holden, Massachusetts

Lawrence C. Neale

Charles T. Main, Inc.
Boston, Massachusetts

Laser doppler anemometers are non-invasive, linear, and inherently precise. Calibration, in the usual sense, is not necessary; length and frequency measurements suffice to establish velocity at a spatial point. Measurements were made at points in the cross-sections of two square ducts containing water flow. The points were selected in conformance with a numerical integration scheme to be used for volumetric flow rate determination from the velocity measurements. The experiments were performed in a primary calibration facility at flows up to 1.25 m^3/sec using ducts with sides 46 and 92 cm. The anemometer, operating in forward scatter differential mode with a 15 mw He Ne laser, was positioned with a special traversing frame. Windows in the ducts allowed transmission of the beams into the flow and reception of scattered light. Two grid patterns, 4 x 11 and 11 x 11, were used so that 44 and 121 velocities were measured for each test. A total of eight tests were conducted covering a Reynolds number range from 1.1 to 3.9 x 10^6. After accounting for errors due to the discreet integration scheme of 0.61% and 0.13% for the 4 x 11 and 11 x 11 schemes, respectively, comparison with the calibration facility indicated extreme errors of +0.81/-0.16 and +0.84/-0.61. The major limitation of the set-up used was the time required to move the anemometer and obtain a new velocity value. It was pointed out that either better mechanical positioning or optical scanning could be employed to reduce the time required for a flow determination.

1. Introduction

As part of a test program to evaluate the performance of a four path acoustic flow meter, it was necessary to establish the velocity distribution at the metering section. The measurements were made using a laser doppler anemometer and a pattern which allowed numerical integration for volumetric flow rate. The experiments were set up in a primary flow calibration facility using gravimetric determination of water flow rate. Square ducts were used with windows provided for the anemometer. A traversing mechanism was used to position the anemometer measuring volume at spatial locations where velocity measurements were made. The facilities, procedures, and results of the entire program are reported in [1, 2]*, while this paper discusses only those aspects pertaining to determination of flow rate from laser doppler measurements.

2. Test Facility

Square ducts (46 and 92 cm) were installed in the large primary calibration facility at the Alden Research Laboratories, Figure 1. This facility consisted of a sump with a capacity of 760 m^3 of water, which was maintained at temperatures from 30C to 40C, a pumping capacity of 1.27 m^3/s at a head of 37 m, a straight pipe run of 25 m, and a weigh tank with capacity of 45,000 kg. A diverter was provided to allow static weighing for all tests and a timing activator for mid-stroke operation. At the maximum flow rate, the filling time for a weigh tank run was approximately 30 seconds.

The weighing system was a Toledo beam scale arranged with a direct reading dial and nine individual drop weights. Timing was accomplished by a photoelectric system mounted on the diverter which activated a 100 KH_z counter synchronized with a precision time base. Dead weight calibration of the scale and load cell was carried out on a routine basis every 6 months, while the time base was checked on a continuing basis each week. The culmative error associated with this facility was known to be approximately 0.1% so that it formed a good primary standard for the LDA flow measurements.

3. Laser Doppler Anemometer

A laser doppler anemometer (LDA) operating in the forward scatter differential mode was used. The light beam from a 15 mw He Ne laser was split into two beams which passed into the test section through a plane window, Figure 2. The beams were brought to a focus at the crossing point where the velocity measurement was made. A photomultiplier on the opposite side of the duct detected light scattered from particles in the measuring volume modulated at the doppler frequency. Figure 3 shows the 46 cm test section, traversing frame, laser, and transmission optics. The receiving optics were also mounted on the frame, but out of view. Figure 4 shows the measuring volume just inside the window on the 92 cm duct.

*Figures in brackets indicate the literature references at the end of this paper.

The instantaneous particle velocity, u, was given by the equation

$$u = \frac{\lambda f_D}{2 \sin \theta/2}$$

where λ was the wavelength of the laser radiation, f_D was the doppler frequency, and θ was the beam angle. The radiation wavelength was known accurately, and the beam angle was determined by projecting the two beams onto a distant screen and using careful geometrical measurements. The accuracy of a velocity measurement thus hinged on measurement of the doppler frequency. This measurement was made with a frequency tracker which utilized a voltage controlled oscillator and an error detector to track the doppler signal. Either the control voltage or the VCO output could be monitored as an indication of velocity. The measurements of mean velocity reported here were made using a digital voltmeter with variable time constants, although it was later found that a frequency meter monitoring the VCO gave better results. In either case, the system was conveniently and accurately calibrated using a crystal frequency source.

Thus, all quantities associated with a velocity measurement were accurately and easily traceable. Furthermore, the velocity and signal output were linearly related, which simplified subsequent processing. An error analysis indicated that the accuracy of the velocity measurements was approximately ±0.18%.

4. Integration for Flowrate

The traversing mechanism provided for the LDA facilitated positioning the measuring volume at specific locations in the cross-section. The positions were chosen as 4 x 11 and 11 x 11 matrices such that the flow rate could be obtained from the mean velocities using Gaussian quadrature [3].

The volumetric flowrate was determined as

$$Q = 4A \sum_{i}^{11} \sum_{j}^{4,11} \mu_i \mu_j u_{ij}$$

where

A = duct area

x_i, x_j = fractional location of point from centerline

μ_i, μ_j = weights

u_{ij} = measured velocity at i, j

The Gaussian weights and fractional locations are given in Table I.

TABLE I

	11 POINTS		4 POINTS	
i, j	x_i	μ_i	x_j	μ_j
1	0.978	0.056	0.861	0.348
2	0.887	0.126	0.340	0.652
3	0.730	0.186	0.340	0.652
4	0.519	0.233	0.861	0.348
5	0.269	0.263		
6	0.000	0.273		
7	0.269	0.263		
8	0.519	0.233		
9	0.730	0.186		
10	0.887	0.126		
11	0.978	0.056		

To the extent that velocity profiles could be represented by Legendre polynominals, the integration would be exact. For more realistic profiles, the accuracy was checked by integrating over a theoretical velocity distribution derived from a law of the wall. An exact integration was made and compared to the 4 x 11 and 11 x 11 schemes corresponding to the measurements. Based on this calculation, the 4 x 11 and 11 x 11 schemes should have overestimated the flow rate by 0.61% and 0.13%, respectively.

5. Results

Mean and rms velocity measurements were made at each of the 165 grid points. Each measurement required approximately two minutes to insure proper time averaging. A flow rate determination was made after each 11 measurements and slight temporal variations accounted for in subsequent data reduction. Three useful runs were made using the smaller duct, while five were made for the larger. The results are summarized in Table II.

TABLE II

Size cm	Test No.	Test Date	Flow m^3/s	% 11 x 11	% 4 x 11	$\mathbb{R} \times 10^{-6}$
46 x 46	4	1/29/75	1.2013	+0.37	+0.70	3.5
46 x 46	5	2/05/75	1.2098	-0.01	+0.45	3.9
46 x 46	6	2/07/75	0.5955	+0.30	+0.73	1.9
92 x 92	7	5/06/75	1.2470	-0.24	+0.83	1.8
92 x 92	8	5/12/75	0.6370	-0.12	+0.68	1.0
92 x 92	9	5/19/75	1.2418	+0.97	+1.42	2.0
92 x 92	10	5/20/75	0.6222	+0.65	+1.16	1.1
92 x 92	11	6/17/75	1.2498	-0.48	+0.59	1.8

Keeping in mind that errors of 0.61% and 0.13% should be expected for the 4 x 11 and 11 x 11 schemes, respectively, because of the integration method, it can be seen that flow rate determinations using the LDA are quite good. In fact, after accounting for the integration error, the maximum percentage flow rate error for the 4 x 11 scheme was +0.81/-0.16 while the 11 x 11 scheme was +0.84/-0.61. Similarly, the mean errors were +0.21% and -0.35%, respectively.

6. Conclusions

The precision of the system, including the LDA and the integration, was good. The system required no calibration other than a tape measure to determine beam angle and a frequency standard to calibrate the tracker. The possibility of using standards other than volume or mass in connection with flow metering is thus open. The major limitation is seen to be the length of time required to make a flow rate determination. It is speculated, however, that suitable hardware could be arranged to provide fast scanning of the flow cross-section.

7. Acknowledgements

Much of the work described herein was originally supported by the Oceanic Division of Westinghouse Electric Corporation in connection with the development of their LEFM flow meter. Matching funds from an internal development fund enabled acquisition of the laser Doppler system.

8. References

[1] Tassinari, P.J., "Fluid Flow Characteristics in Square Ducts at High Reynolds Numbers," M.S. Thesis, Worcester Polytechnic Institute, (May 1975).

[2] Tassinari, P.J. and W.W. Durgin, "Flow Measurement in Rectangular Ducts," Report 87-75/M91F, Alden Research Laboratories, Worcester Polytechnic Institute, (November 1975).

[3] Benedict, R.P. and J. Wyler, "Determining Flow Rate from Velocity Measurements," Instruments and Control Systems, pp. 47-50, February 1974.

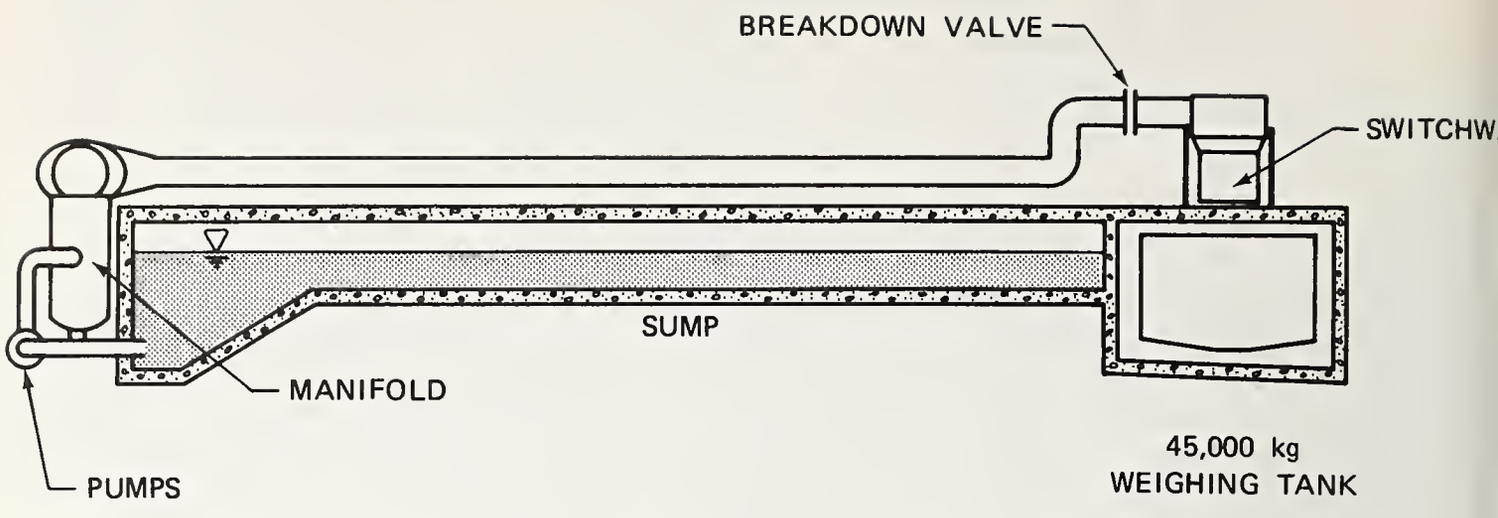

FIGURE 1 TEST FACILITY

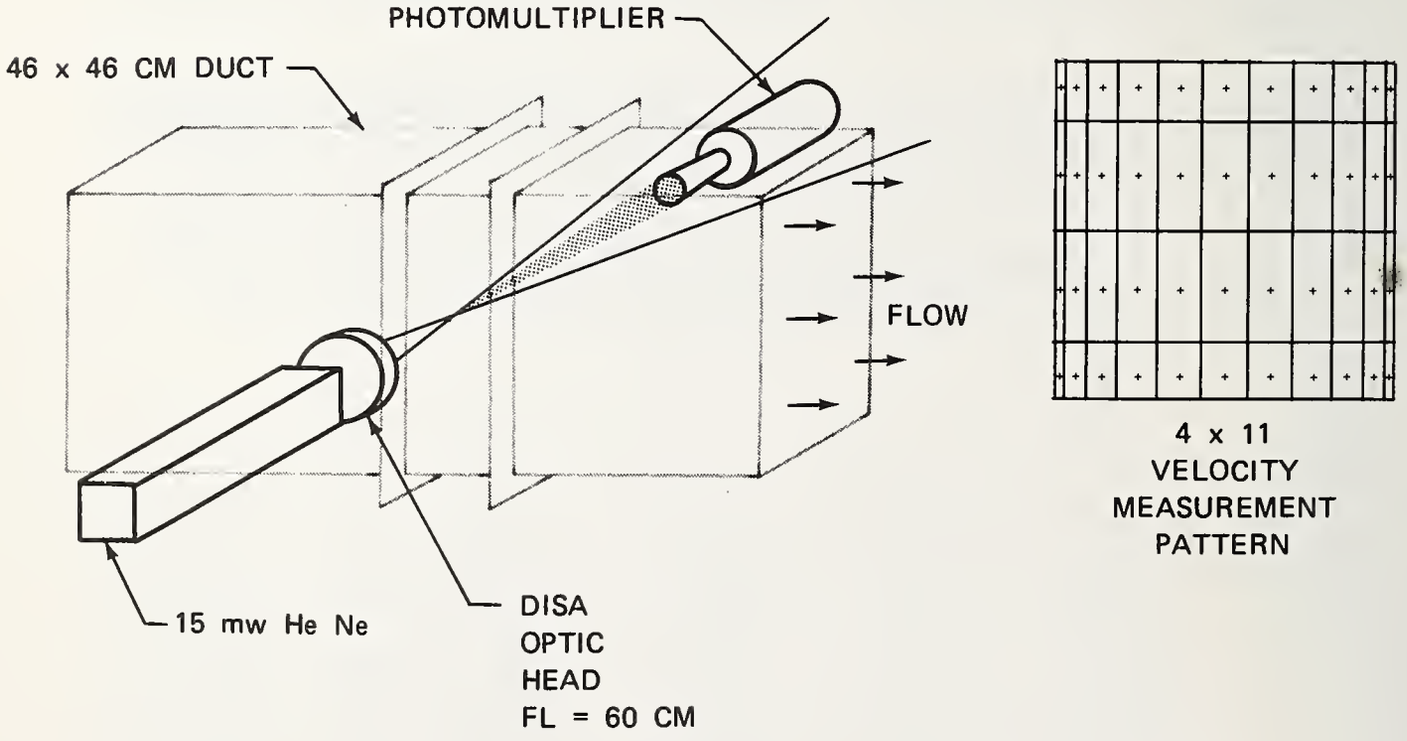

FIGURE 2 TEST SECTION

FIGURE 3 46 cm DUCT, LDA, AND TRAVERSING FRAME

FIGURE 4 BEAM CROSSING IN 92 cm DUCT

National Bureau of Standards Special Publication 484, Proceedings of the Symposium on Flow in Open Channels and Closed Conduits held at NBS, Gaithersburg, MD, February 23-25, 1977. (Issued October 1977)

ON IMPROVING THE PITOT-TUBE DETERMINATION OF FLOWS IN LARGE PIPES

J. M. Robertson and M. E. Clark
Department of Theoretical and Applied Mechanics
University of Illinois at Urbana-Champaign
Urbana, Illinois 61801

Reliable and accurate flow measurements in large pipes are becoming increasingly important in assessing the performance of power plant equipment in these days of energy crises. Since the Pitot-static tubes that are used for the determination of flows in large (diameters from 4 to 8 ft) pipes are being calibrated in a smaller (24-in.) pipe, various uncertainties arise in the use of the Pitot and in the interpretation of its coefficient. These uncertainties include the correction for the area blockage by the Pitot tube, the effect of tip proximity to the wall on velocity indications, and the effect of asymmetric velocity profiles on the accuracy of the flow rate prediction. Additionally, the problems associated with fluctuating manometer readings and vibration of the Pitot tube can be significant. Studies and considerations of these uncertainties are reported. Specifically, the blockage correction has been studied via traverses with several Pitot tubes in the 24-in. pipeline and with a reduced-size model in 8- and 24-in. pipelines. Test results indicate that this type of correction is necessary to achieve true flow rate predictions but that it needs a better definition and is not unique. Velocity gradients and proximity to the far wall also significantly affect velocity indications. Conventional integration techniques applied to asymmetric velocity profiles, obtained from laboratory measurements following a pipe bend, are shown to yield inaccurate flow rate predictions. A study of Pitot tube vibration effects suggests that the resultant over-indicated velocities should be discarded from the average and more appropriate values, estimated from the trend of the profile, should be substituted for them.

Key Words: Pipe flow; Pitot tubes; flow metering; velocity indication; flow in large pipes.

1. Introduction

The flow rate in large pipelines can be found using several methods (integral flow meters, dilution methods, velocity probes, etc). Because of the small initial cost and the relative ease in conducting the test in the field, the current conventional method of choice involves the integration of velocity profiles obtained by traversing a Pitot-static head mounted at the end of a cylindrical rod cantilevered into the pipe. Usually a pair of orthogonal traverses are used with velocities taken at the centroids of ten or more annular areas of equal increments of the cross section. The geometries of the commercial Pitot-static heads deviate considerably from that of the optimum Pitot design which gives a direct indication of velocity. This difference is commonly accounted for by attaching a coefficient to each Pitot tube with this coefficient taken as a unique constant. Calibration is thus required and is

usually accomplished in a pipe appreciably smaller than the pipeline in the field. Specifically, the authors have been calibrating standard Pitot tubes in a 24-in. pipe for use in pipelines with diameters of 4 to 8 ft. This paper addresses questions which arise on using the coefficient obtained in the smaller pipe to evaluate the flow rate in the large pipelines.

Uncertainties. Various uncertainties arise in the use of the Pitot tube. The cantilevered device introduces a variable blockage (reduction in flow area) as it is extended into the pipe. How should a correction for this blockage be introduced when one is using the calibration determined in a small pipe to obtain flow rates in large pipes? When the Pitot head is near a wall, the flow patterns and, hence, the velocity indications are modified. Since these modifications depend upon tip size, how do they affect the establishing of calibration coefficients for pipes of various sizes? Evaluation of average pipe velocity from two orthogonal traverses can involve serious errors when the velocity profiles are appreciably distorted by upstream fittings. Periodic flow separation from the rod can cause the cantilevered Pitot tube to vibrate, or "sing". Unsteady separation of the flow about the Pitot head or turbulence can cause appreciable fluctuations in the manometer readings. Thus, it is difficult to interpret the indicated velocities. Results of studies of these factors are presented in what follows. The objective of these continuing studies is to improve the Pitot head, our methods of using it, and our methods of interpreting its indications so that more reliable flow-rate measurements can be achieved in large pipelines.

Background. Since its invention by Henri de Pitot in 1732, the Pitot or Pitot-static tube has been extensively studied, modified, and used. The 1955 review of this device by Folsom [1][1] indicates the status of our knowledge of it. Folsom and others note that the real reason why the Pitot-tube fails as an absolute velocity-indicating device lies in the measurement of the static or reference pressure. The impact pressure or total head is usually obtained with sufficient accuracy. A number of designs for Pitot heads are indicated in Fig. 1. Two long heads with coefficients near unity are (a) the Prandtl tube and (b) the NPL-type tube; this latter tube seems to be much like that developed by Gregory in 1903. These elongated tubes, however, tend to be unsuitable for introduction into pipelines through moderate-sized valves or corporation cocks. Various compact heads, which can be inserted through openings about the size of their support rods, are illustrated by Fig. 1c, d and e. The typical one of Fig. 1c was used for traversing flow in 4-in. pipes at the University of Illinois [2] and in 10-in. pipes at the Pennsylvania State University [3]. The Pitot-static head commonly used for large pipeline flow measurements (see Fig. 1e) is compact enough to be moved through openings less than one-inch in diameter. Information on the design of this specific head, which has a coefficient of about 0.8, is not available in the literature. The reference pressure taps of this head are half way around a circular cylinder in a region particularly susceptible to flow separation and to oscillations due to variations in the flow direction. In another type of standardized Pitot head - the Pitometer of Cole [4] - the Darcy scheme of getting the reference pressure from an opening at the rear was adopted and, according to Cole, this led to much more consistent calibrations.

---

[1]Figures in brackets indicate the literature references at the end of this paper.

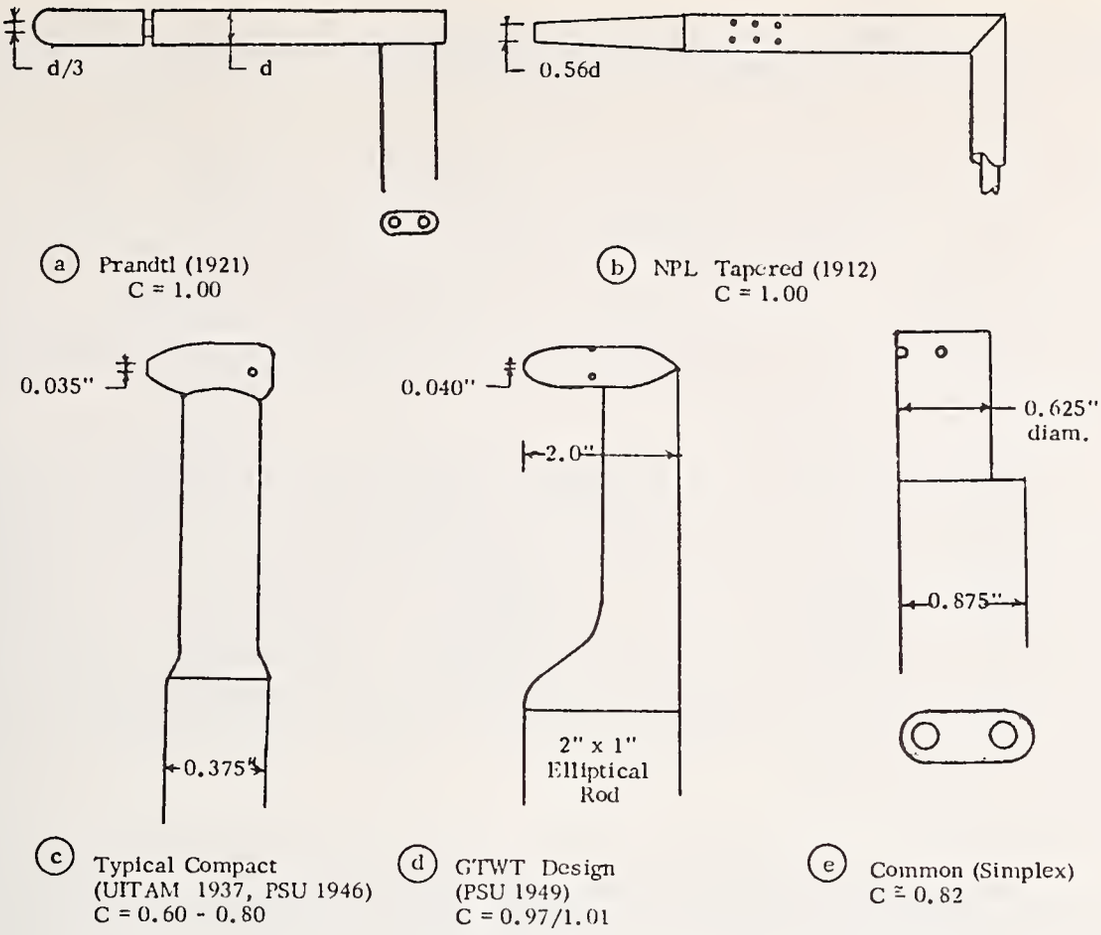

Fig. 1. Various Long and Compact Pitot-Static Heads

The design of a larger head (see Fig. 1d) capable of being moved through a 2-in. opening, has been reported [5]. This head was mounted on a one- by two-in. elliptical cantilever rod. It was designed for use in large circular conduits (up to 12-ft diameter) and for large velocities (80 fps in 4-ft pipe). In towing-tank calibration, it had a coefficient of 1.010, four percent above the design value -- presumably due to errors in placing the static holes in the head. Such a tube would be difficult to fabricate in a size that would move through a one-inch hole. The cantilevered Pitot cylinder of Winternitz [4] on the other hand is quite simple in geometry but exhibits a considerable wall-interference effect.

An alternative design to the cantilever arrangement is the transverse Pitot tube, which may consist simply of a cylinder completely spanning the pipe along a diameter [5,6] with static reference pressures obtained from wall-piezometer taps. A more sophisticated device of this type with integral reference pressure taps has been developed by Numachi, et al [7]. Unfortunately, it is not always convenient or easy to drill the holes and to mount such transverse tubes and wall piezometers are affected by wall roughness.

2. Errors and Corrections

Blockage Correction. Since the Pitot head and support rod assembly reduces the pipe flow area and thereby increases the velocity, some correction for blockage

is necessary. This effect is localized near the rod, so that for Pitot tubes with long heads (Fig. 1a or 1b), it should be negligible; Hubbard [10] has noted that a long head could produce a significant blockage only if it was large relative to the pipe. Cole [2] gave lengthy consideration to the blockage effect for the cantilevered Pitometer and detailed various experiments which yielded a correction factor of between one and one and a half times the projected area of the Pitometer (extended to the pipe center). Additional work by Cole and Cole [11] in pipes of various sizes indicated a correction of about 1.2 times the projected area of the Pitometer. The blockage correction certainly depends upon the geometry of the Pitot head and, hence, studies are reported here of the design shown in Fig. 1e which is often used for flow measurements in large pipelines.

The Pitot tube of Fig. 1e (Simplex design) has a cylindrical head, one inch long and 0.625 in. in diameter, mounted at the end of a oval rod having a thickness normal to the flow of 0.34 in. When introduced into a 24-in. pipe to indicate the centerline velocity, the flow area is reduced by one percent. In a 4-ft pipe, the reduction is 0.48 percent and, in a 6-ft pipe, 0.31 percent. This rod is also used in long lengths but then it is stiffened against vibration by encasing it in a 1.5-in. steel cylinder. When stiffened to within 11 in. of the pressure taps, the blockage in the 2-ft pipe is then 1.3 percent and, in the 4- and 6-ft pipes, is 1.4 and 1.0 percent, respectively.

The blockage acts to increase the average velocity indicated by the Pitot tube. If C is defined as the true Pitot coefficient obtained by calibration with a blockage correction based on the projected area of the tube extended to give the centerline velocity, the flow rate can be calculated by the following relation.

$$(1) \qquad Q = (A - A_{bl})\ C\ \bar{V}_p = A\,(1 - B)\ C\ \bar{V}_p$$

where A is the actual cross-sectional area of the pipe, $A_{bl} = B\,A$ is the projected Pitot tube area when extended to give the centerline velocity, B is the fractional blockage (A_{bl}/A), and $\bar{V}_p$ is the average uncorrected velocity indicated by the Pitot traverse. The nominal coefficient for the tube is defined, ignoring the blockage, as follows

$$(2) \qquad C_{nom} = \frac{Q}{A\,\bar{V}_p} = C\,(1 - B)$$

For a Pitot of true coefficient C = 0.820, the nominal coefficient in pipes of 2- to 8-ft diameter would be as listed in Table I. The variation in C_{nom} is appreciable. If blocking were the only factor, calculation of a true C from C_{nom} would be relatively simple; unfortunately, other factors varying with pipe size also enter.

Experiments with the Simplex Pitot in a 24-in. pipe and a model (0.59 times as large) of it in 24- and 8-inch pipes have been made to further evaluate the problem. The coefficient values found from these tests (via Eq. 1) are presented in Table II together with the associated pipe and skewness factors. Some of the results were found from single traverses (not one or more pairs at 90 degrees, as for the others). Included are results for the reinforced Pitot rod with different lengths (Y) of non-reinforced end. The trends of these results are qualitatively as indicated by Eq. 2 and Table I, but there is much scatter. As an example, the coefficient for the model varies from 0.81 in the 8-in. pipe to 0.83 in the 24-in. pipe. Other factors must affect the coefficient, as will be noted in later sections.

If blockage were the only factor affecting the coefficient, then the C values should be the same no matter what Pitot or pipe size was involved.

Table I. Variation in Nominal Coefficient with Pipe Size for C = 0.820

Pipe Diameter	C_{nom}	
	Std. Simplex	Reinf. Simplex Y = 11 in.
2 ft	0.812	0.810
4 ft	0.816	0.809
6 ft	0.817	0.812
8 ft	0.818	0.813

Table II. Pitot Coefficients and Flow Factors Found for Two Sizes of the Simplex Pitot Tube in Two Pipes

Pipe	Pitot	$B = \frac{A_{bl}}{A}$	Coefficients		Flow Factors	
			C_{nom}	C	P	S
24 in.	Reinf. Simplex Pitot A					
	Y = 11 in.	0.013	0.812	0.823	0.866	1.082
	Y = 5 in*	0.028	0.794	0.817	0.864	1.116
	Pitot B					
	Y = 5 in.	0.028	0.808	0.831	0.873	1.160
24 in.	Simplex**	0.0097	0.796 to 0.824	0.804 to 0.832	0.85 to 0.87	1.08 to 1.14
24 in.	Model Simplex	0.0055	0.826	0.831	0.843	1.076
8 in.	Model Simplex	0.018	0.795	0.810	0.847	1.141

*Single Traverse
**Six Pitots/23 Traverses

In addition to the Pitot coefficient, certain other ratios or factors characterizing the flow also indicate effects of blockage. These are the pipe factor and the skewness of the velocity profiles. The ratio of average to centerline velocity -- dubbed the pipe factor P by Cole [2] -- is a useful indicator of the nature of the flow,

as well as a direct factor for flow metering. At a sufficient distance downstream of flow disturbances, this factor is a unique function of Reynolds number and the relative roughness of the pipe [10, 11]. However, for a Pitot of finite size, blockage effects result in an over-indication of the velocities. In Table II, there is a definite tendency for these data for the 24-in. pipe to increase with B. The model Pitot traverses in the 8-in. pipe gave a value somewhat above the value of 0.83 which was established earlier [11] in the same pipe using a Pitot with negligible blockage.

Since the blockage is larger when the Pitot is extended to indicate far-wall velocities than for near-wall velocities, the ratio of velocities equidistant from but on opposite sides of the centerline depends on blockage when the pipe flow is symmetrical. The skewness factor S of Table II is thus taken as the ratio of the two velocities found at wall distances of 0.09D. These factors are seen to increase with B, but not in a simple linear fashion. Calculations of S, based on blockage alone, yield values of 1.05 and 1.015 for values of B equal to 0.028 and 0.0097, respectively. As can be seen from the table, the experimentally-determined values are considerably larger but the trends are as predicted.

Wall-Proximity and Velocity-Gradient Effects. The specialized flow field about the end of a Pitot tube is affected by wall-proximity and by transverse velocity gradients. These two effects will be considered separately, although in practice they occur simultaneously since steep velocity gradients appear near walls.

The extensive study of Pitot tube errors by Hubbard [10] did not consider the effect of wall proximity on the the flow and on corresponding velocity indications but, on a reciprocity basis, his studies of the rod effects on wall piezometer taps would infer an effect of the wall on the tip pressure field leading to near-wall errors in the reference static pressure. Winternitz [4] in his study of a round tip on the end of a cylindrical cantilever tube found a significant wall-interference effect; errors in static pressure, up to the order of ten percent, occurred near walls and were of different signs for the near and far walls. Since the wall-proximity effect must depend greatly on the Pitot head design, the common Pitot tube (Fig. 1e) has been investigated for its wall effect. Changes in the velocity indicated by this tube in uniform flow (except for a boundary layer about 0.06-in. thick) near a flat plate in an air stream are summarized in Fig. 2. From this figure, the Pitot is seen to significantly over-indicate velocities when the tip is within a few inches of the far wall. In fact, for a flow-rate evaluation (using a 14-point concentric-area integration) the two velocity indications nearest the wall would be 1.0 and 0.5 percent too high. Studies have yet to be made of near-wall effects; there the wall opening through which the tube enters the pipeline will also disturb the flow field.

An error -- tantemount to a shift in the effective location of the measuring tip -- appears in the indicated velocity of Pitots, even the elongated forward-pointing types, when measurements are made in transverse velocity gradients. This effect was first studied by Young and Maas [14] and later by Livesey [15], Davies [16] and Dhawan and Vasudeva [17]. No studies of the common pipeline Pitot seem to have been made and the authors' experiments in shear flows away from walls are still in the planning stage. Further studies of this effect and that of wall interference seem necessary.

Pulsation and Support-Rod Vibration Effects. Turbulent flow is inherently unsteady so that a manometer connected to a Pitot in a pipeline will show pulsations. Additionally, pulsation can result from unsteady flow about the Pitot head due to vortex-street occurrences. Both Cole [4] and Hubbard [10] have considered this problem

of properly interpreting the manometer indication in the presence of pulsations. Cole's suggestion that the readings be taken over a full cycle of variation is fine except that the variations are generally random and one is not able to define the cycle. The authors have observed less manometer pulsation with one Pitot design that with another, but ferretting out the explanation for this and optimizing it is difficult.

Rod vibration effects are more easily recognized. Cole [4], Cole and Cole [11] and Bean [18] have all noted effects of vibration. These effects are small when the amplitude of vibration is small but the overindication becomes large with increase in amplitude. Winternitz [19] has studied this problem extensively and explains it on the basis of the streaming flow near the reference static-pressure taps as induced by the lateral vibration of the Pitot rod assembly. The vibration is due to fluid-dynamic forces generated by the oscillating vortex street behind the cantilevered rod. When the frequency of these oscillations matches the natural frequency of the Pitot tube system (including the support mechanism), resonance occurs. Except to make the rod and its support as stiff as possible not a lot can be done to prevent these vibrations. Common fluid-dynamic fixes, in the form of strakes or trailing plates, are not feasible since they must be applied to the outside surface of the rod and this would lead to difficulties with packing seals. For the common pipeline Pitot tube (Fig. 1e), the authors have noted "singing" (forced vibration evidenced by an audible hum) in their 24-in. pipeline at velocities between 5.6 and 7.2 fps when the tube was extended 1.71 ft from the near wall and at velocities between 7.4 and 10.0 fps when extended 1.27 ft. These speeds must certainly depend upon the rigidity of the Pitot in its support. The resultant increase of indicated velocity is generally only a few percent but this debilitates the validity of a flow-rate evaluation. As an operational procedure, the authors suggest that elevated readings, caused by vibration effects, be reduced in calculating an average velocity. Generally, one can smooth the velocity profile, taking the trend of the curve below the values indicated by the vibrating

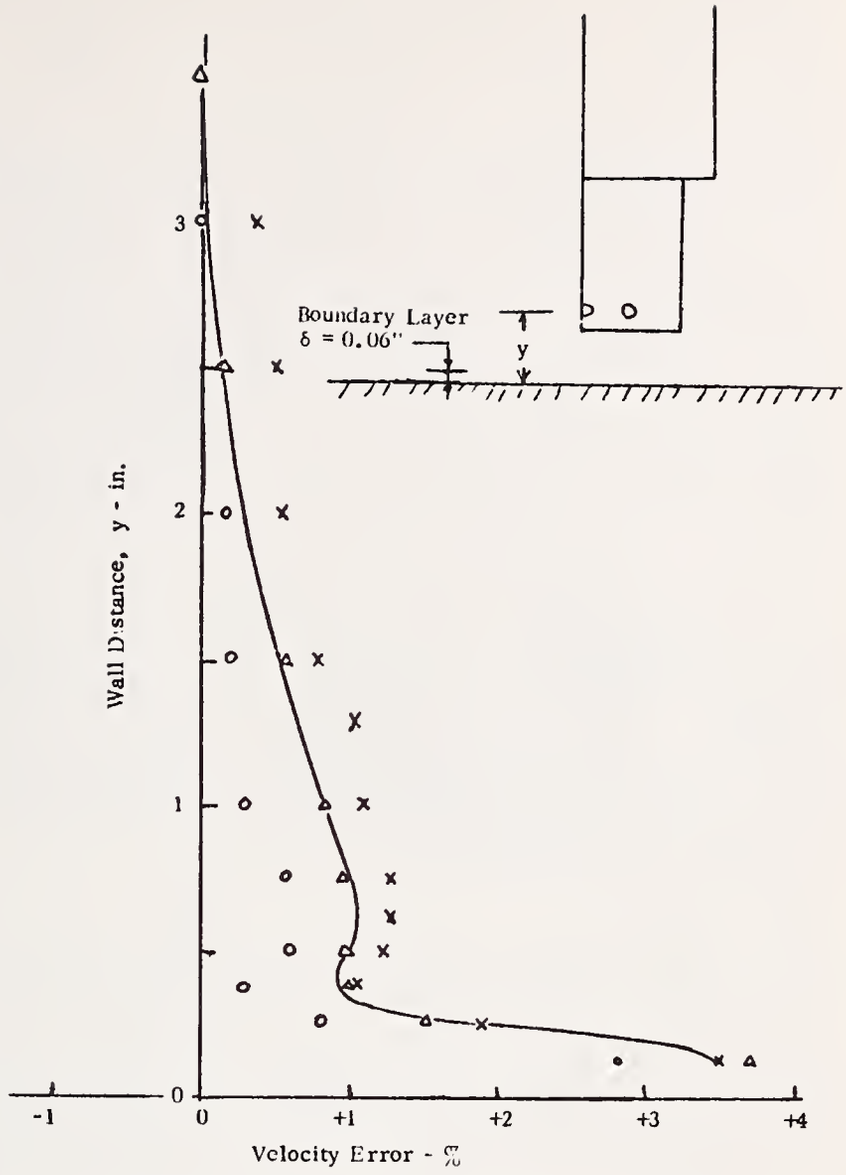

Fig. 2. Wall Proximity Effects on Simplex Pitot in Uniform Air Flow of 86 fps

tube. To quantify the correction requires correlation of the error with the amplitude of vibration; this has not been done. An alternative approach is to have two Pitot tubes or support geometries of significantly different natural frequency (stiffness) so that the vibration region of one may be avoided with the other.

Flow Rate Evaluation in Disturbed Flow. It is sometimes necessary to make flow measurements in the field at sites where the flow profiles have not been fully developed. The field engineer then asks, "How accurately can I determine the flow rate by the probe method?" In an attempt to provide a partial answer to such a question in a laboratory context where the actual flow rate was determinable, horizontal and vertical traverses were taken in the 24-in. pipeline two diameters downstream of a short-radius bend. The flow upstream of this bend was disturbed from the fully-developed profile by other bends. Vertical (in plane of bend) and horizontal 14-point traverses were taken with the common Pitot; the resultant velocity profiles are shown in Fig. 3. Both profiles are obviously skewed. The tube coefficient C, determined in the same pipe with fully-developed flow according to standardized procedures with the appropriate blockage correction, was 0.823 for the average of a horizontal and a vertical traverse. The 14-point averages of the Pitot tube indications downstream from the elbow were 8.08 and 8.77 fps for horizontal and vertical traverses, respectively; corresponding average velocities (obtained through multiplication by C) were 6.65 and 7.22 fps. Using the same amount of blockage as used in the calibration calculations, the indicated flow rates were 20.74 and 22.51 cfs. The corresponding values of the flow rate, determined volumetrically, were 20.20 and 20.49 cfs; thus giving percentage errors in the flow rate of 2.7 and 11.4, respectively.

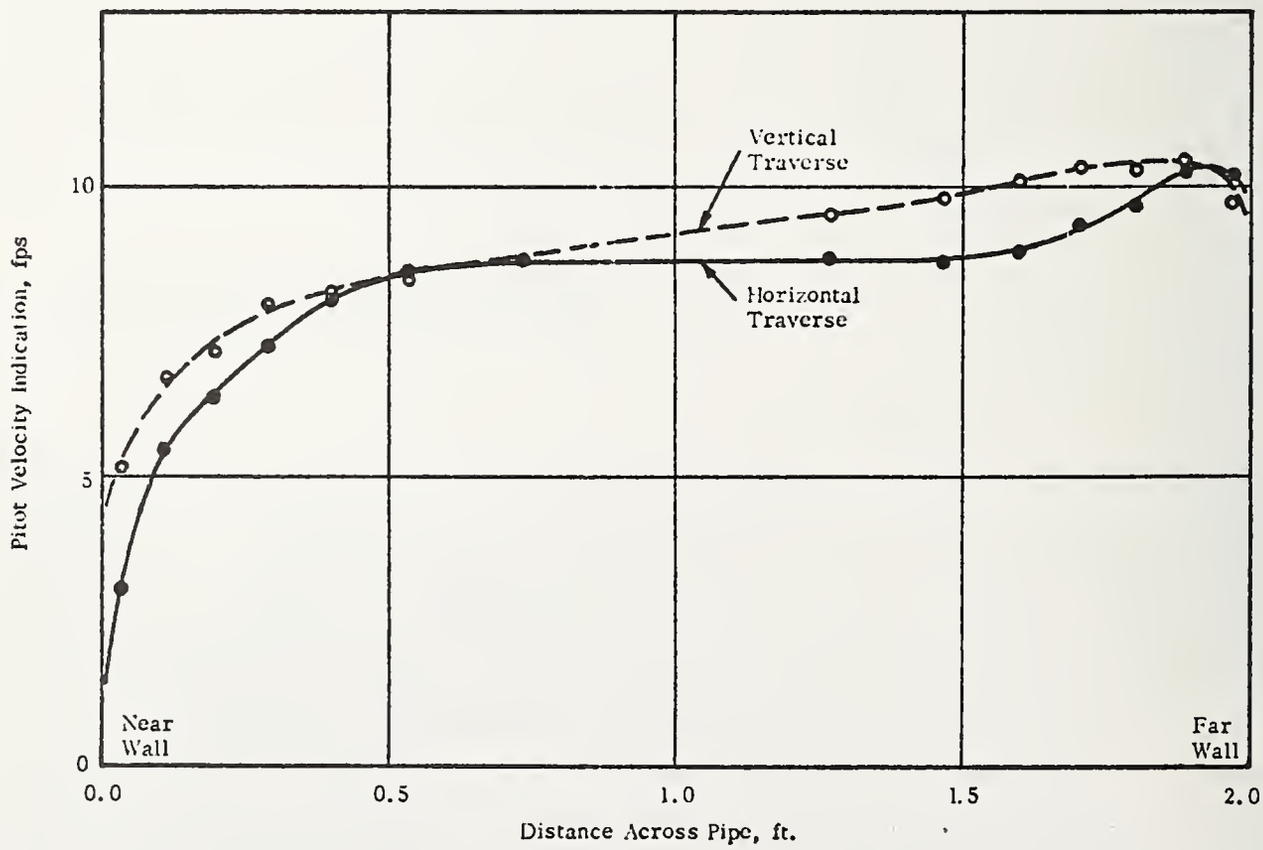

Fig. 3. Pitot Traverses Taken Downstream of a Pipe Bend At a Flow Rate of 20 cfs.

From these results, it can be seen that some individual velocity traverses taken in disturbed flow will give fair approximations to the true flow rate (e.g., the horizontal traverse of Fig. 3 predicts a flow rate to within three percent of the actual one). However, other traverses can give a poor prediction of flow rate. In the single case investigated, both traverses over-predicted the flow rates. Hence, other traverse directions should exist which would have under-predicted the flow rate by comparable amounts. Only if the total cross-sectional area had been sufficiently probed to give a true average value of the velocity would the indicated flow rate agree with the actual value. One would presume that two more orthogonal traverses midway between the horizontal and vertical traverses already taken would have been sufficient to formulate a proper average. Without going through the additional work required to secure such data, however, the foregoing statement remains a presumption. Under field conditions there would be no way to determine the validity of such a four-traverse result. Therefore, at a site where skewed profiles are found, a sufficient number of traverses must be taken so as to obtain a trustworthy average velocity. Otherwise, errors in flow rate of as much as 10 to 20 percent can be expected.

Other Considerations. Certain significant features of the Pitot tube problem are not addressed here. Thus Cole's [4] studies indicated a small, but finite, velocity effect -- as a decrease in coefficient from 0.89 to 0.86 as the pipe velocity increased from 2 to 10 fps. The common Pitot (Fig. 1e) is usually taken to have a coefficient invariant with velocity; the authors' limited studies tend to support this view. Another feature of flow evaluations from velocity traverses involves the number of annular-area increments used for averaging the velocity profile. Often five areas -- giving a ten-point average -- are used. Folsom [1] presents calculations based on the one-seventh-power velocity profile of turbulent flows indicating overcalculation of the average velocity by 0.91 percent for a six-point traverse, by 0.53 percent for a ten-point one and by 0.25 percent for 20 points. The authors have compared 10-point and 14-point averages from an actual traverse in a 24-in. pipe and have found a 0.1 percent decrease (suggesting a larger Pitot coefficient) in the indicated average velocity with the larger number of points. The choice of an optimum number of points involves such considerations modified by concern for wall-proximity effects.

3. Summary

Obviously, this study of the Pitot tube commonly used in field measurements of large pipeline flows is far from complete. Even though firm conclusions from this study would be premature at this time, some of the uncertainties have been clarified.

Blockage and wall-proximity effects on the Pitot tube significantly affect flow rate evaluation in pipes of different size (larger) than those used for the calibration of the tube. Further study is needed to quantify the needed corrections. Pitot vibration effects on indicated flows can be reduced with care in taking and interpreting traverses. Flow rate evaluations at sites of disturbed flow require more than the usual two orthogonal traverses, otherwise significant errors may be encountered.

The results of numerous calibrations of the commonly-used Pitot in the 2-ft pipe are indicated as well as those of a 0.59 model in the 2-ft and in an 8-in.

pipe. These calibrations do not yield the unique coefficient one would expect -- the variation certainly stems from the effects discussed but also presumably from small dimensional differences between the measuring heads due, in part at least, to rough handling in the field. The coefficient has a value of 0.82 + 0.01. The studies of this Pitot in uniform flow (see Fig. 2 at large values of $\bar{y}$) yield a coefficient of 0.81. The difference between this value and 0.82 is presumably due to the characteristics of the pipe flow, i.e., blockage, wall-proximity, turbulence, etc.

Improvement of this type of measurement is not easy since the effects involved amount to only a few percent and are due to factors not always clearly understood. Improvement in the design of the Pitot measuring head is not imminent. Changes in the geometry or in placement of the pressure ports affect the overall performance only slightly and sometimes unpredictably.

References

[1]. Folsom, R. G., "Review of the Pitot Tube", Trans. A.S.M.E., 78, 1447-1460, (1956).

[2]. Robertson, J. M., "A Study of the Flow of Water Around Bends in Pipes", B.S. Thesis in Civil Engineering, Univ. of Illinois, (1938).

[3]. Turchetti, A. J., and Robertson, J. M., "Design of Vaned-Turns for a Large Water Tunnel", A.S.M.E. paper 48-SA-15, (1948).

[4]. Cole, E. S., "Pitot Tube Practice", Trans. A.S.M.E., 57, 281-294, (1935).

[5]. Shuster, F. E., "Design of Pitot-Static Tube for a Large Water Tunnel", M.S. Thesis in Civil Engineering, Penn. State Univ., (1949).

[6]. Winternitz, F. A. L., "Cantilevered Pitot Cylinder", The Engineer, May 27, 739-732, (1955).

[7]. Christensen, J. E., and French, O. C., "Characteristics of Transverse Pitot Tubes", Agricultural Engineering., 18, 21-24, (1937).

[8]. Robertson, J. M., and Shuster, F. E., "Coefficient of a Pitot-Tube Flow Detector", Instruments and Control Systems, 34, 645-647, (1961).

[9]. Numachi, F., Murai, H., and Abe, S., "Streamlined Pitot-Tube Bar for Measuring Water Flow in Large Pipe", Trans. A.S.M.E., 78, 1079-1089, (1956).

[10]. Hubbard, C. W., "Investigation of Errors of Pitot Tubes", Trans. A.S.M.E., 61, 477-506, (1939).

[11]. Cole, E. S., and Cole, E. Shaw, "Pitot Tubes in Large Pipes", Trans. A.S.M.E., 61, 465-475, (1939).

[12]. Folsom, R. G., and Iverson, H. W., "Pipe Factors for Quantity Rate Flow Measurements with Pitot Tubes", A.S.M.E. paper 48-A35, (1948); abstract in Mech. Engineering, 20, 1019-1020, (1948).

[13]. Robertson, J. M., Martin, J. D., and Burkhart,T."Turbulent Flow in Rough Pipes", I&EC Fundamentals, 7, 253-265, (1968).

[14]. Young, A. D., and Maas, J. N., "The Behavior of a Pitot Tube in a Transverse Total Pressure Gradient", British Aero. Res. Council, R&M No. 1770, (1937).

[15]. Livesey, J. L., "The Behavior of Transverse Cylindrical and Forward Facing Total Pressure Probes in Transverse Total Pressure Gradients", Jour. Aero. Sci., 23, 949-955, (1956).

[16]. Davies, P.O.A.L., "The Behavior of a Pitot Tube in Transverse Shear", Jour. Fluid Mchs., 3, 441-7, (1957).

[17]. Dhawan, S., and Vasudeva, B. R., "The Pitot Tube Displacement Effect in Boundary Layer Flows", Jour. Aero. Soc. of India, 11, 1-18, (1959).

[18]. Bean, H. S., discussion of reference 9, 473.

[19]. Winternitz, F. A. L., "Effects of Vibration on Pitot Probe Readings", The Engineer, 201, 273-75, 282-290, (March 30 and April 6, 1956).

National Bureau of Standards Special Publication 484, Proceedings of the Symposium on Flow in Open Channels and Closed Conduits held at NBS, Gaithersburg, MD, February 23-25, 1977. (Issued October 1977)

NUMERICAL MODELING OF TURBULENT FLOW THROUGH THIN ORIFICE PLATES

R. W. Davis and G. E. Mattingly

Mechanics Division, IBS
National Bureau of Standards
Department of Commerce
Washington, D.C. 20234

A study is presented which uses the two-equation turbulence model developed at Imperial College, London to model high Reynolds number flow through orifice plates. This turbulence model employs the eddy viscosity concept for the Reynolds stresses. Two transport equations are solved for turbulence variables and are combined to form a spatially dependent eddy viscosity. This eddy viscosity is used in the numerical solution of the time-averaged momentum equations. The resulting solution is in terms of velocities, pressure, and turbulence intensity. The flow fields modeled are axisymmetric; the orifice plates are infinitely thin with beta ratios from 0.4 to 0.7. Reynolds numbers are in the approximate range 10^4 - 10^6. The incoming velocity profile at one pipe diameter upstream of the orifice plate is varied to assess its effect on meter performance. The results of the calculations give such orifice flow features as discharge coefficients for various tap locations, vena contracta, points of minimum pressure, and reattachment locations, and overall pressure loss through the meter. The numerical results are compared with available experimental data, and the agreement between computed and experimental discharge coefficients is within 4 percent. It is concluded that this type of computer simulation can be extremely useful in conjunction with experiments in future investigations of the performance of numerous types of differential pressure meters.

Key Words: Closed conduit meter; differential pressure; flow measurement; mathematical modeling; meter performance; orifice meter; turbulence flow.

1. Introduction

There are two objectives in the present study. The first is to test the feasibility of using turbulence modeling to study the flow through orifice meters. The second is to establish a unified, comprehensive picture of orifice flow that will produce more reliable metering with this widely used device.

Reliable and accurate flow meter performance becomes increasingly important when, in our present world with its ever expanding population, we envision equitable exchange, transmission and consumption of our finite resources. An example of the economic impact that optimizing flow meter performance can have can be taken from the natural gas industry. Miller and Kneisel [1][1] have shown that there is a significant bias in the measured values of flow coefficients for recently manufactured orifice meters as compared with the published (and widely used) values. Conservatively, the reported bias was more than 0.3 percent. Using this value, it was estimated [2] that in 1974 the daily average error value associated with the uncertainty of orifice metering natural gas amounted to $87,500 per day. Because orifice meters are relatively inexpensive and hence widely used in industry the impact of the effects of optimized orifice meter performance becomes more apparent.

In an earlier effort [3] we computed laminar orifice flow for a variety of meter configurations. The present results for the turbulent case include flow fields for the axisymmetric, incompressible flow through four (4) different meters. In addition, the variations produced by a range of velocity profiles and Reynolds numbers are described.

Critical to any effort directed toward optimizing orifice meter performance is a thorough understanding of the flow field through the meter and its interaction with the readout instrumentation. Furthermore, it is essential to quantify the effects of well-known sources of variation such as upstream meter tube length, centeredness of the orifice hole in the pipe, orifice lip shape and sharpness, orifice plate smoothness, orifice hole roundness, etc. To date, users are guided by recommended procedure and practice that have evolved over many years [4,5,6]. Orifice discharge coefficients have been tabulated for many meter and pressure tap configurations. Values presented are the results of averaging the massive amounts of data taken in experimental studies over the past 80 years. In these studies, experimental control was not uniformly proper and, as a result, variability is large and individual effects such as those mentioned above cannot be determined. It is therefore apparent that a new approach to orifice metering has to be initiated and carried out according to proper measurement theory [7]. To do this, a dual effort is envisioned. One effort will consist of conducting properly controlled experiments; the other will be producing, via computer methods, the flow fields through meters. In this manner, widely ranging parameters and meter variations can be introduced and

[1]Bracketed numbers refer to references listed at the end of this paper.

evaluated using computer methods and, for selected cases, validation experiments would demonstrate credibility. The results of this dual approach should produce reliable flow measurements using orifice meters.

Orifice meter performance is based upon an obstruction to the fluid flow in a pipe which is designed to produce a flow rate dependent change in the fluid pressure across it. The general form of this obstruction is a thin round plate with a hole in its center. The pressure difference across this plate is monitored by means of a variety of schemes each with its own advantages and disadvantages. The fluid pressures are measured via pressure "taps" along the pipe wall. Figure 1 presents a sketch of the flow through an orifice meter equipped with a particular arrangement of taps. The salient features of the flow field are the pressure distribution along the wall, the characteristics of the recirculating eddy downstream of the orifice plate, and the nature of the jet flow through the orifice hole. Determining how these characteristics change with the various factors affecting them is the central objective of these efforts to reduce the variability attributed to the orifice meter. Also significant in the operation of the orifice meter are the positions along the pipe wall of the taps which measure the static pressure difference across the orifice plate.

The four schemes most widely used in orifice installations are corner, flange, so called "D-D/2," and vena contracta taps. Corner taps (prevalent in Europe) are located in the corners produced by the pipe wall and the up and downstream surfaces of the orficie plate. Flange taps are placed one inch (2.54 cm) up and downstream of each surface of the orifice plate. They have the advantage of being conveniently installed via a radial hole drilled through flange discs that sandwich the orifice plate in the pipe. Since for most large pipe sizes, flange taps are located small fractions of a pipe diameter from the orifice plate, the pressure difference they sense approximates that given by corner taps. The major disadvantage with flange taps is that their location does not scale with diameter according to the principles of geometric similitude. Taps located one diameter up and one half diameter downstream from the upstream surface of the orifice plate are referred to as D-D/2 taps. The advantage of these taps is that they are displaced from the orifice plate and give a smaller but "smoother" pressure difference, i.e., less affected by pressure fluctuations than those obtained via the corner or flange taps. Vena contracta taps are located one diameter upstream of the upstream surface of the orifice and a variable distance downstream from this surface. This variable distance is intended to align the downstream tap with the minimum pressure which, at one time, was assumed to occur at the vena contracta. Previous results [3,8] indicate that the minimum wall pressure and the vena contracta occur at different locations. In spite of this misalignment, the advantage of these taps is that they render a smaller, but supposedly even "smoother" pressure difference than that of the D-D/2 taps.

To properly assess orifice meter variability, consideration is given: (a) to the primary device - the orifice meter and its associated flow field and (b) to the secondary device - the readout system which

senses the pressure difference. Orifice metering practice will benefit considerably when the combined variability of these two components of the total variation is properly characterized.

The present study is to assess the variability of the primary device, i.e., the orifice meter and its flow field. The particular turbulence model that is used to simulate this flow field is the kε-model developed at Imperial College, London [9]. This turbulence model is economical, in wide use, and has given reasonable results in situations similar to orifice flow [10,11,12].

2. Basic Equations

The momentum and continuity equations for turbulent incompressible stationary flow are

$$\rho(\underset{\sim}{q} \cdot \nabla)\underset{\sim}{q} = -\nabla P - \nabla x[\mu_{eff}(\nabla x\underset{\sim}{q})] \tag{1}$$

$$\nabla \cdot \underset{\sim}{q} = 0 \tag{2}$$

in which q = (U, V), where U and V are the mean velocity components in the radial and axial directions in an axisymmetric cylindrical reference frame; P is the mean pressure; ρ is the constant density; and μ_{eff} is the sum of the laminar and turbulent viscosities. The turbulent viscosity, μ_t, is assumed to be a function of the turbulent kinetic energy, k, and the dissipation rate, ε, of k; i.e.,

$$\mu_t = C_\mu \rho\, k^2/\varepsilon \tag{3}$$

where $C_\mu = 0.09$. The values of k and ε to be inserted in (3) are determined from the following transport equations written in axisymmetric cylindrical coordinates (r,z):

$$\rho\left(V\frac{\partial k}{\partial z} + U\frac{\partial k}{\partial r}\right) = \frac{\partial}{\partial z}\left(\frac{\mu_{eff}}{\sigma k}\frac{\partial k}{\partial z}\right) + \frac{1}{r}\frac{\partial}{\partial r}\left(\frac{r\mu_{eff}}{\sigma k}\frac{\partial k}{\partial r}\right) + \mu_t G - C_D\rho\varepsilon \tag{4}$$

$$\rho\left(V\frac{\partial \varepsilon}{\partial z} + U\frac{\partial \varepsilon}{\partial r}\right) = \frac{\partial}{\partial z}\left(\frac{\mu_{eff}}{\sigma_\varepsilon}\frac{\partial \varepsilon}{\partial z}\right) + \frac{1}{r}\frac{\partial}{\partial r}\left(\frac{r\mu_{eff}}{\sigma_\varepsilon}\frac{\partial \varepsilon}{\partial r}\right) +$$

$$C_1\varepsilon\frac{\mu_t}{k}G - C_2\rho\frac{\varepsilon^2}{k} \tag{5}$$

where $\sigma_k = 1.0$, $\sigma_\varepsilon = 1.3$, $C_D = 1.0$, $C_1 = 1.44$, $C_2 = 1.92$, and

$$G \equiv 2\left[\left(\frac{\partial V}{\partial z}\right)^2 + \left(\frac{\partial U}{\partial r}\right)^2 + \left(\frac{U}{r}\right)^2\right] + \left[\frac{\partial V}{\partial r} + \frac{\partial U}{\partial z}\right]^2 .$$

The justification for the values of the empirical constants is given in [9].

3. Numerical Scheme

The SIMPLE finite difference scheme has been developed and incorporated into the TEACH-T, Fortran computer code at the Department of Mechanical Engineering, Imperial College of Science and Technology, London, England. Since a complete description of TEACH-T is available [13,14] and, also, of SIMPLE [15,16], only a brief review of the computer code will be given here.

The system of equations (1) to (5) is finite differenced and solved iteratively by underrelaxation. The convective terms in these equations are differenced using a hybrid scheme [17] comprised of central and conservative upwind differencing. At each iterative step, the finite difference analogs of equation (1) are solved implicitly using a line-by-line procedure involving a tridiagonal matrix solver. The velocity field resulting from this solution of the momentum equations for a given iteration will probably not satisfy the continuity equation (2). Using this known (but probably incorrect) velocity field, equation (2) can be transformed into an equation for the pressure correction required to make the velocity field solenoidal. This pressure correction is calculated in the same implicit manner and is used to determine the final velocity field for a given iteration. These velocities are then used in the solution (by the usual implicit scheme) of equations (4) and (5) for k and ε. Finally, equation (3) for μ_t is updated and the next iteration begins. The iterations proceed until the sum of the absolute values of the residual mass and momentum sources is less than some predetermined small value. This summation is performed separately for the mass flow and each component of momentum, with the resulting sums to each be less than some small percentage, δ, of the mass flow and largest component of momentum, respectively, at the inlet to the computational test section.

4. Numerical Modeling of Orifice Flow

The computational test section containing the orifice plate is shown in Figure 2. The mesh selected had 13 computational cells in the radial direction and up to 68 cell axially. Variable mesh spacing was used, with the radial cell dimension, Δr, only a function of r and the axial cell dimension, Δz, only a function of z. The variation in Δr was from $0.05R_o$ to $0.10R_o$, while that for Δz was from $0.05R_o$ to $0.50R_o$, where R_o is pipe radius. Cells were concentrated axially in the area of the orifice plate and radially near the plate lip and pipe wall. Normal velocities were specified along cell boundaries, and pressure, turbulent kinetic energy, and dissipation rate were specified at cell centers. An orifice plate of zero thickness was created by setting axial velocities to zero along a strip of cell boundaries whose length

varied with β ratio. The inlet velocity profile was specified at a distance of about $2R_o$ upstream of the orifice plate, while the outlet profile was determined by setting axial gradients to zero. Inlet distributions of turbulent kinetic energy and dissipation rate were specified via a pipe flow computation. This computation produced results which satisfactorily agreed with available experimental data. For the orifice flow computations, boundary conditions along the pipe wall were based on the logarithmic law (i.e., the wall-function method [9]), and the radial velocity and the radial derivative of the streamwise velocity were set to zero along the axis. The value of the convergence criterion, δ, that was chosen was five percent. Computation times on the NBS UNIVAC 1108 ranged up to 17 minutes, but were generally less than 10 minutes per case.

5. Results and Discussion

The flow patterns through four orifice meters for values of β, the ratio of orifice hole to pipe diameter, in the range from 0.4 to 0.7 are shown in Figure 3. The Reynolds number of 2×10^5 is based upon pipe radius and average velocity. The inlet conditions (V,k,ε) at a distance of about $2R_o$ upstream of the orifice plate are based on the results of $200R_o$-long straight, smooth pipe calculations using the same computer program at the same Reynolds number. The exit conditions from these pipe calculations were in good agreement with available experimental data and were thus used to simulate fully-developed flow entering an orifice meter. In what follows, all velocities are nondimensionalized by average inlet velocity, V_0, pressure by V_0^2, and all lengths by R_o thus producing $R = r/R_o$ and $Z = z/R_o$. To exhibit the flow patterns through the orifice plate, the computational test section is only shown axially for six radii; the actual computed test section extends for 14 to 17 radii depending on β ratio. In these plots are shown segmented streamlines produced by the short line segments drawn from a point at the center of each computational cell tangent to the local velocity vector. The length of each segment is constant. Several radial rows of cells located at axial locations adjacent to the plate are omitted for clarity. With these exceptions, Figure 3 exhibits the general distribution of cells in the portion of the flow field shown.

Shown via the segmented streamlines in Figure 3 is the way the pipe flow is turned through the orifice hole and forms the jet flow downstream of the plate. The shape of the eddy downstream of the plate is also evident with its radial and axial dimensions perceived via the streamline that could be drawn from the orifice lip to the reattachment point on the pipe wall. The dynamics of the flow within this eddy can also be seen.

The streamwise distributions of the mean static pressure along the pipe wall and the centerline are shown in Figure 4 along with the centerline velocity. Evident here are the locations of the points of maximum centerline velocity, minimum centerline and wall static pressures, and the differences between centerline and wall pressures. From such distributions, one is able, with any particular choice of pressure taps, to

determine the corresponding discharge coefficient, C_d given by

$$C_d = \sqrt{\frac{1-\beta^4}{2\beta^4 \Delta p}}$$

where Δp is the upstream - downstream pressure difference taken at the respective tap locations. Discharge coefficients will be presented below for particular tap configurations and compared with published values.

Radial distributions of the streamwise component of velocity, plotted at six axial locations, are shown in Figure 5. The inlet profile plotted is the specified power law profile whose 1/9th exponent was determined via the pipe flow computation noted previously. Profiles adjacent to the orifice plate are shown and exhibit the flow into and out of the hole in the plate. The profile downstream of the plate shows that the velocity distribution in the jet flow is not uniform. In fact for the smaller β's, the maximum velocity in the profile is located, not on the pipe centerline, but off of it, in the flow adjacent to the orifice lip where the axial pressure gradients are large - an effect that has been observed experimentally [18]. Velocity profiles are also plotted at the maximum centerline velocity location, near the reattachment point, and at the outlet of the computational test section. This outlet profile is noted to have developed into one closely resembling that at the inlet.

The axial location of the vena contracta, the point of maximum orifice jet convergence, is found from radially integrating velocity profiles downstream of the orifice plate. This location is where the orifice jet radius is minimized. This minimum jet radius is then taken as the vena contracta radius, $R_{v.c.}$, and the axial location is considered specified to within the local axial grid spacings and the tolerances applied to the calculated results.

Figure 6 presents plots of the streamwise distribution of the shear stress at the pipe wall. The plots show the axial extent of the recirculating eddy downstream of the orifice plate by virtue of the sign change at the reattachment point.

The turbulent intensity, I, which is proportional to the square root of the turbulent kinetic energy normalized by the square root of the mean kinetic energy, is plotted against streamwise coordinate in Figure 7. Shown here are the distributions along the wall and the pipe centerline. The peaks in the wall intensity distributions are of interest in that at these locations turbulent effects can be considered locally significant relative to the mean flow dynamics. These peaks occur adjacent to the orifice plate and in the region near the point of reattachment. In fact, the turbulent intensity values near the point of reattachment attain values which exceed scale limits and are, therefore, omitted from these graphs.

That peaks in the turbulent intensity at the wall occur adjacent to the orifice plate are interesting in that it is in these regions where it is common practice to measure the pressure for the determination of flow rate. It has been well established that pressure pulsations can significantly limit the accuracy and precision of "head-type" meters by the way they influence the pressure measuring instrumentation [19,20,21]. For example, the error attributed to pulsations is related to the ratio of the streamwise component of the turbulent velocity to the average streamwise velocity. This error, which is termed the square root error, is such that the measured flow rate is greater than the actual. The value of the error depends upon the nature of the pulsation. For a single frequency of pulsation, the time averaged square root of the pressure difference which is read is, where overbars are to indicate time averages,:

$$\overline{\sqrt{\Delta p}}\Big|_r = \sqrt{\overline{\Delta p}_a}\ \left[1 - \left(\frac{\Delta p_a}{4\overline{\Delta p}_o}\right)^2\right]$$

and where Δp_r, Δp_a, and Δp_o denote, respectively, the recorded, the oscillation amplitude, and the true mean differential pressures. This relationship applies for small ratios of Δp_a to Δp_o. It is apparent that to reduce this square root error, that a small amplitude of pressure pulsation is preferable, i.e., the taps should not be placed in regions where there are large pressure fluctuations.

Since pressure pulsation intensity is related to the square of the intensity of the streamwise component of the pulsating velocity, the present computer solutions can, in principle, be used as a guide. It is conceivable that an optimal tap location might be found where both the mean pressure difference across the orifice plate is maximized and the detrimental pulsation effects are minimized. Judging from Figure 7 one would want to place taps away from regions where the intensity distribution along the pipe wall is peaked. Figure 7 also illustrates that the centerline values of turbulent intensity exhibit an increase downstream of the reattachment point. This increase is also seen in the experimental results of Turner and Lightning [22].

The effects of upstream velocity profile were demonstrated for the $\beta = 0.7$ orifice in Figures 8-12. In these, we have placed at the inlet section three different velocity profiles to span a wide range possible for axisymmetric flows. The average flow rate and Reynolds number are the same for all three profiles. In Figure 8 are shown the segmented streamline patterns for a portion of the flow field computed. In 8 (a) is an admittedly unrealistic parabolic profile, in 8 (b) the realistic 1/9th power law profile, and in 8 (c) an admittedly unrealistic uniform profile. The figure shows that the streamwise length of the large recirculating eddy downstream of the orifice plate is increased as the velocity profile approaches the uniform one.

It is also noted that, for the parabolic case, a small reversed flow occurs in the corner produced by the upstream surface of the orifice plate and the adjacent pipe wall. This reversed flow is undoubtedly due to the presence of an eddy trapped in this corner and having sufficient momentum to produce the small but visible reversed flow. Actually, several radial rows of cells were not plotted for reasons of graphical clarity at axial locations adjacent to the orifice plate. These omitted cells confirm the presence of this eddy upstream of the plate. Figures 8(b) and 8(c) indicate that no such eddy is evident in the same corner; the omitted cells in this region show no effects of reversed flow. Figures 8(b) and 8(c) are noted to be quite similar. While this observation appears to indicate that these two profile variations do not change the fluid flow pattern, it shall be found in what follows that the detailed features of the two flows are different. More important are the differences found in the discharge coefficients for the two flows.

Figure 9 presents streamwise distributions in the $\beta = 0.7$ meter of centerline and wall static pressures and centerline velocity. It is seen here that while the maximum values for centerline velocity are essentially the same, the pressure distributions show significant differences. The largest difference is noted between the parabolic and uniform profiles. Comparing the wall pressure distributions for the 1/9th and the uniform profile, differences are found both upstream and downstream of the plate. The increased inertial effects of the uniform flow elevate the pressure levels upstream of the plate relative to those of the 1/9th profile. Downstream, the uniform flow calculation exhibits reduced pressure levels. The head loss for the meter with the parabolic flow is the smallest of the three while those of the 1/9th and uniform profiles are essentially the same.

Streamwise velocity distributions for the $\beta = 0.7$ meter with the three different inlet velocity profiles are shown in Figure 10. Here the different inlet profiles, with constant average velocities, are clearly shown. The velocity profiles adjacent to the orifice plate indicate the variation in velocity across the orifice jet, the edge of which is located at $R = 0.7$. It is apparent that the orifice jet velocity varies markedly in the parabolic case while in the other cases the velocity is quite uniform over about 80 percent of the jet radius with significant variation occurring over the remaining 20 percent. Further downstream, the differences between the three cases are reduced further due to turbulent diffusion. At the outlet, the three profiles are practically the same.

The fluid shearing stress, τ_w at the pipe wall is shown in Figure 11 for the three profiles. Here, the parabolic flow produces a significantly different distribution from the other two. The 1/9th and uniform distributions exhibit slight differences in the region upstream of the plate and otherwise are very similar. The orifice jet reattachment to the pipe wall located via the zero stress point downstream of the plate lies closest to the orifice plate for the parabolic profile. The

reattachment point for the uniform flow lies slightly downstream of that for the 1/9th profile.

In Figure 12 are shown streamwise distributions for turbulent intensity. Again, the parabolic distribution stands out as the most different of the three with increased levels of turbulent intensity along the pipe wall upstream of the plate. In this region just upstream of the orifice plate, a large peak in the intensity distribution is observed. This is probably the result of the reduced velocity and reversed flow resulting from the presence of an eddy in this corner. Intensity distributions along the pipe centerline are quite similar for all three inlet profiles.

In Table 1 are presented comparisons of the computed discharge coefficient for two tap configurations i.e., corner and D-D/2 with corresponding values taken from an ISO Draft International Standard (ISO/DIS 5167) [6]. Table 1 shows that for constant diametral Reynolds number, $Re_D = 4 \times 10^5$, the computed discharge coefficients for corner and D-D/2 taps behave quite differently. For corner taps, the discharge coefficients decrease monotonically with increasing β and constant inlet velocity profile. The corresponding ISO values are noted not to follow this trend. For each β, the deviations occurring between the sets of values is nominally 2 percent or less. The effects of inlet velocity profile on the $\beta = 0.7$ meter are considered especially significant since the maximum variation is 23 percent for corner taps. The D-D/2 tap configuration produces computed coefficients which, with increasing β, first decrease and then increase with constant inlet profile. It is noted that this trend is not duplicated in the ISO results. However, the differences here are small and may be insignificant. The effects of profile variations on discharge coefficients can be estimated from the computed values given. For D-D/2 taps, the maximum variation attributed to the profiles examined in the $\beta = 0.7$ meter is 27 percent. For both tap configurations, the discharge coefficients are found to decrease as the velocity profile approaches uniform flow. At $\beta = 0.5$, it is noted that for both corner and D-D/2 taps, the reduced Reynolds number results indicate that the discharge coefficients increase slightly. In Table 2, discharge coefficients obtained via computation are compared with tabulated results for flange and D-D/2 taps taken from the ASME Fluid Meters [4]. The computed results for flange taps were produced by assuming a pipe diameter of 2 in. ($\sim$ 5 cm). The flange taps comparison duplicates that noted from Table 1 for the case of corner taps, i.e., the monotonically increasing trend in ASME values follows that for the computed results only for $0.5 \leq \beta \leq 0.7$. However, the difference between the computed flange tap coefficients for $\beta = 0.4$ and 0.5 is too small to be significant. As seen in Table 1, variations in inlet profile for $\beta = 0.7$ produce significant variations in flange tap coefficients. Trends similar to those noted in Table 1 are seen in the ASME values for D/D/2 coefficients.

In view of the changes produced here by the different velocity profiles, it seems pertinent to note that the oft repeated and conventional process of calibrating orifice meters can lead to systematic errors.

When a meter is removed from its "native" pipeline and sent to a "foreign" one for calibration, the differences in the inlet velocity profile conditions are not considered. If, for example, other sources of meter variation such as upstream piping roughness, roundness, or vibration can be neglected and inlet velocity characteristics are the major source of differences, the present results indicate that such differences can be important. In this regard, one can envision that a more precise calibration for an orifice meter could, in principle, be achieved by computer. These calibrations by computer might be done by precisely determining the inlet velocity profile and meter geometries, and then having the calibration done via computer without removing the meter from its "native" pipeline.

The present results permit tabulation of the salient features of turbulent orifice flow and their respective locations in the flow field. These individual features are shown in Table 3. Here, for constant $Re_D = 4 \times 10^5$ and the 1/9th profile, the location of the vena contracta as determined by mass flow integrations across the jet appears to lie furthest downstream for the $\beta = 0.5$ meter. The radius of the orifice jet at the vena contracta increases with β and is, typically, 90 percent of the orifice radius. The maximum centerline velocity decreases with increasing β ratio from a value of about 10 at $\beta = 0.3$ to a minimum of about 3 at $\beta = 0.7$. The location of this maximum centerline velocity occurs at $X = 0.75$ independent of β and lies downstream of the vena contracta. This is due to the distribution of velocity in the orifice jet. Along the pipe centerline, the static pressure decreases markedly from that at the orifice plate for the lower β ratios. The minimum centerline static pressure location is nominally one pipe radius downstream of the plate. Since liquid cavitation effects would begin wherever the local pressure reached vapor pressure levels, the location of the minimum static pressure is one place where one could expect incipient cavitation. Another place would be wherever mean pressure levels were low and the turbulent component of the pressure was sufficiently large to produce instantaneous values at the vapor pressure level. In this event one would expect sporadic cavitation to occur. Given the distributions of pressure in these meters, the prospects for sporadic cavitation could exist in or adjacent to the large recirculating eddy downstream of the orifice plate. The reattachment location, X_R, gives the streamwise length of the large recirculating eddy downstream of the orifice plate. This eddy length decreases with increasing β ratio. The location of the minimum static pressure along the pipe wall, X_{pmw} is also found to decrease with increasing β. It is also noted that the minimum static pressure along the pipe wall occurs at or upstream of the minimum pressure on the centerline.

To assess the accuracy of the computed results, it is necessary to compare them with experimental values. The experimental results available [4] for the overall pressure loss across thin-plate orifices are shown in Figure 13. The agreement is considered good. At $\beta = 0.7$, the three values shown for the present study represent the effects of the different inlet velocity profiles. The parabolic value lies below the line, the 1/9th profile point lies just above the line, and the

uniform profile point gives the maximum loss.

An interesting comparison of the present computed values to graphical results given in [4] is shown in Figure 14. Here, spatial ranges for the position of minimum static pressure along the pipe wall are presented as they depend upon β ratio. These were obtained by averaging data from "numerous experiments by different investigators over a wide range of pipe sizes of 2 in or larger." The resulting range of minimum pressure positions for any β ratio is interpreted to be due to the wide range of Reynolds numbers and other pertinent parameters the graph is undoubtedly intended to encompass, since no ranges are specified. As stated further in [4], it is "the general assumption that this plane of minimum pressure coincides with that of the vena contracta." The present results for the minimum pressure along the pipe wall are observed to fall considerable short of the ranges presented for the experimental data. In addition, the computed results for vena contracta positions are graphed. For the range of β ratios presented and, as shown in Table 3, the vena contracta lies downstream of the minimum wall pressure for the higher values of β, but it lies upstream for the lower values. Thus, the graphed results for the presently computed values indicate the degree to which the conventional assumption regarding the coincidence of minimum pressure and vena contracta points is valid. Concurrently, it is concluded that presently unexplained discrepancies exist between the experimental data and the computed positions for these points. It is expected that further experimental investigation of these features will properly resolve these issues.

Conclusions

It has been demonstrated that the k,ε - turbulence model can provide a reasonably accurate description of the important features of turbulent, incompressible flow through an axisymmetric, thin-plate orifice meter. The effects of β ratio variation are described through the range typically used in metering practice. A wide range of inlet velocity profiles is used to determine this effect on a $\beta = 0.7$ meter, and a limited range of Reynolds number is examined for a $\beta = 0.5$ meter.

The present results include radial and axial distributions of the fluid velocities and pressure anywhere in the flow field. Consequently, comparisons can be made with a wide variety of measurable quantities. Such comparisons are made for quantities such as discharge coefficients, pressure distributions, and the locations of salient features in the flow field. The comparison of the computed discharge coefficients with published values is considered reasonable. Generally, the trends found in discharge coefficients parallel those published. Qualitatively, good agreement is also found between computed and published axial pressure distributions through these meters. However, quantitative discrepancies are noted between computed and published values for the locations of salient features of the flow such as minimum pressure points and the vena contracta. The present computations have extended the range of earlier efforts which have demonstrated that the vena contracta and the points of minimum pressure along the pipe wall are not aligned. It is

shown here that for certain β ratios, $\beta > 0.6$, the vena contracta lies downstream of the point of minimum wall pressure while for $\beta < 0.6$ the vena contracta lies upstream of this point.

The present results show that numerical turbulence models are capable of describing the complete orifice flow field and corresponding meter performance. As such, computational methods have to be considered a feasible and fertile complement to similarly directed theoretical and experimental analyses. Furthermore, these methods are not intended to be limited solely to orifice-type head meters. It seems only logical to include other head meters such as nozzles and venturies, as well as other types of meters operating in a wide variety of turbulent flow conditions.

It is also concluded that, while there does exist a considerable volume of experimental data pertaining to orifice meter characteristics, further efforts are now required to firmly establish realistic tolerances on much of the so-called "well-established" results such as discharge coefficients and the locations of salient flow features. It is toward this end that the full complement of numerical methods in conjunction with the most recent developments in experimental measurement techniques should be directed.

Acknowledgements

The authors gratefully acknowledge contributions of a wide variety from several persons at the National Bureau of Standards. The efforts of Ms. E. F. Moore, in maintaining the organization of and running the computer programs and plotting routines, enabled this phase of the present study to proceed with high efficiency. In addition, her efforts in reducing the computed results to proper form for tabulation and comparisons of the results are greatly appreciated. We are indebted for several helpful discussions with Mr. L. K. Irwin and Mr. K. R. Benson. The secretarial assistance provided by P. Beall, P. Gurewitz, and J. Preet is also greatly appreciated.

References

[1] Miller, R. W. and Kneisel, O. A., Comparison Between Orifice and Flow Nozzle Laboratory and Published Coefficients, *ASME Journal of Fluids Engineering*, Vol. 96, p. 139-149, June 1974.

[2] API/Committee on Gas Measurement internal document, November 1975.

[3] Mattingly, G. E. and Davis, R. W., Numerical Solutions for Laminar Orifice Flow (submitted, June 1976 for publication in the *ASME Journal of Fluids Engr.*)

[4] Bean, H. S., ed, *Fluid Meters - Their Theory and Applications*, 6th ed, ASME, New York, 1971.

[5] American Gas Association - *Report No. 3. Orifice Metering of Natural Gas*, Arlington, Va, 1972.

[6] Measurement of Fluid Flow by Means of Orifice Plates, Nozzles, and Venturi Tubes Inserted in Circular Cross-sectional Conduits Running Full, *ISO Draft International Standard 5167*, April 1976.

[7] Pontius, P. E., Notes on the Fundamentals of Measurement and Measurement as a Production Process, *NBSIR 74-545*, 1974.

[8] Wilson, M. P. and Teyssandier, R. G., The Paradox of the Vena Contracta, *Trans ASME*, Sept. 1975, pp 366-370.

[9] Launder, B. E. and Spalding D. B., The Numerical Computation of Turbulent Flows, *Computer Methods in Applied Mechanics and Engineering*, Vol. 3, pp 269-289, 1974.

[10] *Proceedings of Symposium on Turbulent Shear Flows*, University Park, Penn, April 18-20, 1977.

[11] Kubo, I. and Gouldin, F. C., Numerical Calculations of Turbulent Swirling Flow, *ASME Journal of Fluids Engineering*, Vol. 97, p. 310, Sept. 1975.

[12] Moon, L. F., and Rudinger, G., Velocity Distribution in an Abruptly Expanding Circular Duct, *ASME Journal of Fluids Engineering*, Vol. 98, p. 226, March, 1977.

[13] Salimonu, Dauda O., Mathematical and Programming Details of the TEACH T and L Recirculating Flow Code, *Argonne National Laboratory Technical Memorandum ANL-CT-76-22*, October 1975.

[14] Gosman, A. D., Khalil, E. E., and Whitelaw, J. H., The Calculation of Two-Dimensional Turbulent Recirculating Flows, *Proceedings of Symposium on Turbulent Shear Flows*, University Park, Penn, p. 13,35, April 18-20, 1977.

[15] Caretto, L. S., Gosman, A. D., Patankar, S. V., and Spalding, D. B., Two Calculation Procedures for Steady, Three-Dimensional Flows with Recirculation, *Proceedings of the Third International Conference on Numerical Methods in Fluid Mechanics*, ed. by Henri Cabannes and Roger Temam, Vol. II, Springer-Verlag, New York, p. 60, (1973).

[16] Patankar, S. V., Numerical Prediction of Three-Dimensional Flows, *Studies in Convection*, Vol. 1, ed. by B. E. Launder, Academic Press, New York, p. 1, (1975).

[17] Spalding, D. B., A Novel Finite Difference Formulation for Differential Expressions Involving Both First and Second Derivatives, *International Journal for Numerical Methods in Engineering*, Vol. 4, pp 551-559, (1972).

[18] Pearson, J., An Experimental Investigation of Turbulent Flow Through Orifice, Masters item submitted to the Dept. of Mech. Engr. and Appl. Mech., University of Rhode Island, 1975.

[19] Sparks, C. W., A Study of Pulsation Effects on Orifice Metering of Compressible Flow, *ASME Flow Measurement Symposium*, Pittsburgh, Pa., pp 124-138 (1966).

[20] Miller, R. W., Precise Measurements of Differential Pressure When Calibrating a Head Class Flow Meter, *Trans ASME*, Dec. 1970, pp 742-757.

[21] Watanabe, N. and Komiya, K., Pulsating Gas Flow Measurement by Orifice Meter, *Bulletin of the National Research Laboratory of Metrology Series No. 26*, April 1972, pp 22-27.

[22] Turner, J. T. and Lightning, G., Measurement of Mean Flow and Turbulent Structure in an Axisymmetric Pipe Flow with High Initial Shear, *Proceedings of Symposium on Turbulent Shear Flows*, University Park, Pa., p. 8.29, April 1977.

Table 1. Comparisons of discharge coefficients with ISO [6] values

β	Re_D	Inlet* Profile	C_{corner}		$C_{D-D/2}$	
			Computed	ISO (DIS)	Computed	ISO (DIS)
0.4	$4 \cdot 10^5$	1/9	.616	.602	.615	.600
0.5	$4 \cdot 10^4$	1/7	.609	.609	.610	.609
0.5	$4 \cdot 10^5$	1/9	.607	.604	.609	.605
0.6	$4 \cdot 10^5$	1/9	.602	.606	.616	.609
0.7	$4 \cdot 10^5$	P	.706	-	.788	-
0.7	$4 \cdot 10^5$	1/9	.591	.604	.637	.612
0.7	$4 \cdot 10^5$	U	.573	-	.622	-

*The inlet profile is that imposed at the entrance of the computed test section: "1/9" indicates a power law profile with this exponent, "P" denotes a parabolic and "U" denotes a uniform profile.

Table 2. Comparison of discharge coefficients for flange and D-D/2 taps [4]

β	Re_D	Inlet* Profile	C_{flange}**		$C_{D-D/2}$**	
			Computed	ASME	Computed	ASME
0.4	$4 \cdot 10^5$	1/9	0.613	0.603	0.615	0.599
0.4	$4 \cdot 10^4$	1/7	0.610	0.618	0.610	0.615
0.5	$4 \cdot 10^5$	1/9	0.608	0.607	0.609	0.604
0.6	$4 \cdot 10^5$	1/9	0.616	0.611	0.616	0.610
0.7	$4 \cdot 10^5$	P	0.783	-	0.788	-
0.7	$4 \cdot 10^5$	1/9	0.636	0.610	0.637	0.615
0.7	$4 \cdot 10^5$	U	0.621	-	0.622	-

*The inlet profile is that imposed at the entrance of the computed test section. "1/9" indicates a power law profile with this exponent, "P" denotes a parabolic, and "U" denotes a uniform profile.

**To determine these coefficients, a 2 inch pipe size (~ 5 cm) is assumed.

Table 3. Salient features and their locations* in turbulent orifice flow

β	Re_D	Inlet(1) Profile	(2) $X_{v.c.}$	(3) $R_{v.c.}$	(4) V_{max}	(5) $X_{v.m.}$	(6) P_{plt}	(7) P_{min}	(8) X_{pm}	(9) X_R	(10) X_{pmw}
0.4	4.10^5	1/9	0.46	0.37	9.93	0.75	-19.7	-49.7	1.05	4.75	1.05
0.5	4.10^4	1/7	0.46	0.45	6.35	0.75	-8.12	-19.7	0.85	3.90	0.65
0.5	4.10^5	1/9	0.55	0.44	6.37	0.75	-8.08	-19.8	1.05	4.12	0.65
0.6	4.10^5	1/9	0.46	0.53	4.29	0.75	-3.71	-8.59	0.85	3.21	0.45
0.7	4.10^5	P	0.26	0.65	2.97	0.55	-1.39	-2.59	0.65	1.61	0.30
0.7	4.10^5	1/9	0.38	0.63	2.97	0.75	-1.79	-3.79	0.85	2.23	0.30
0.7	4.10^5	U	0.38	0.63	2.99	0.75	-1.79	-3.96	0.85	2.32	0.30

* All radial distances are given in pipe radii from the center of the pipe. Axial distances are given in pipe radii from the orifice plate; upstream distances are negative; downstream are positive.

(1) The inlet profile in that imposed at the entrance of the computed test section: "1/9" indicates a power law profile with this exponent, "P" denotes a parabolic profile, and "U" denotes a uniform profile.

(2) $X_{v.c.}$ is the location of the vena contracta.

(3) $R_{v.c.}$ is the radius of the orifice jet at the vena contracta.

(4) V_{max} is the maximum centerline velocity.

(5) X_{vm} is the location of the maximum centerline velocity.

(6) P_{plt} is the centerline static pressure at the location of the orifice plate.

(7) P_{min} is the centerline static pressure at the minimum pressure location.

(8) X_{pm} is the location of the minimum centerline static pressure.

(9) X_R is the location of the orifice jet reattachment to the pipe wall.

(10) X_{pmw} is the location of the minimum static pressure along the pipe wall.

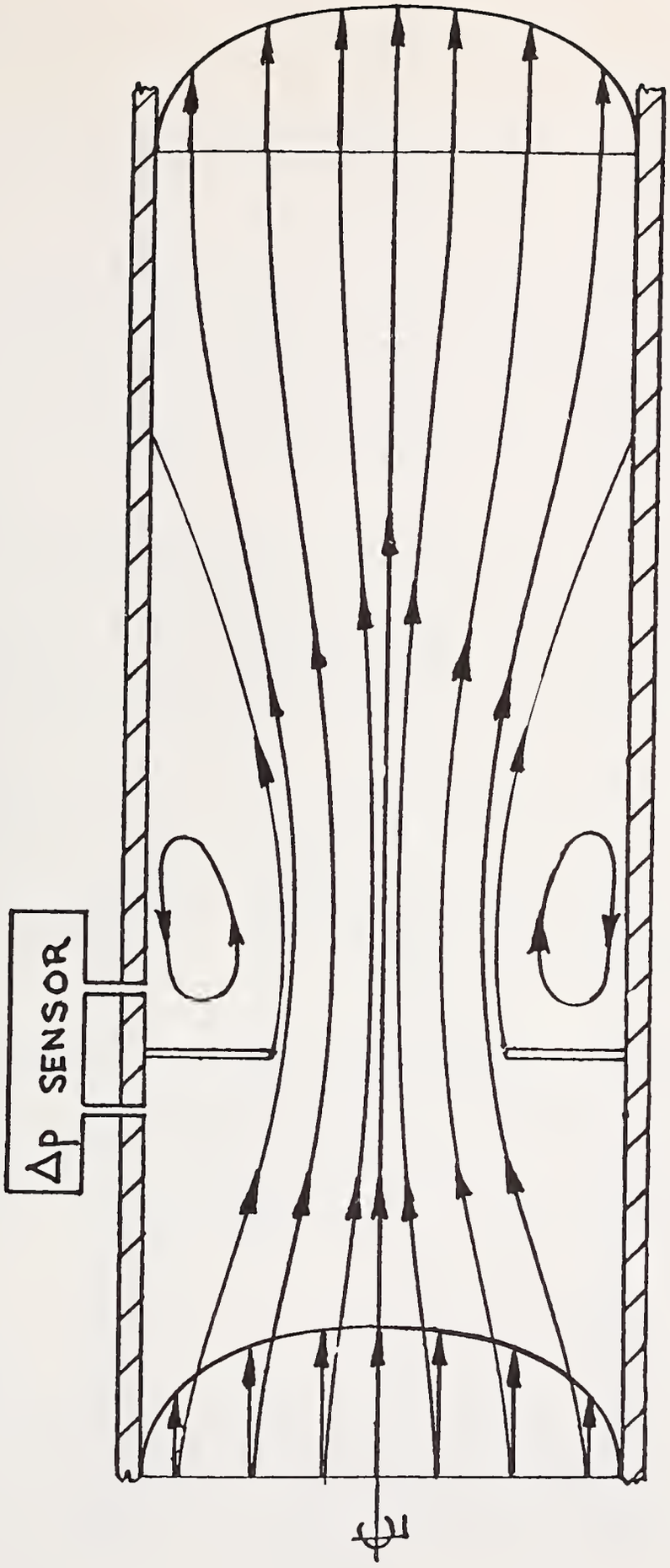

Fig 1. Sketch of orifice flow.

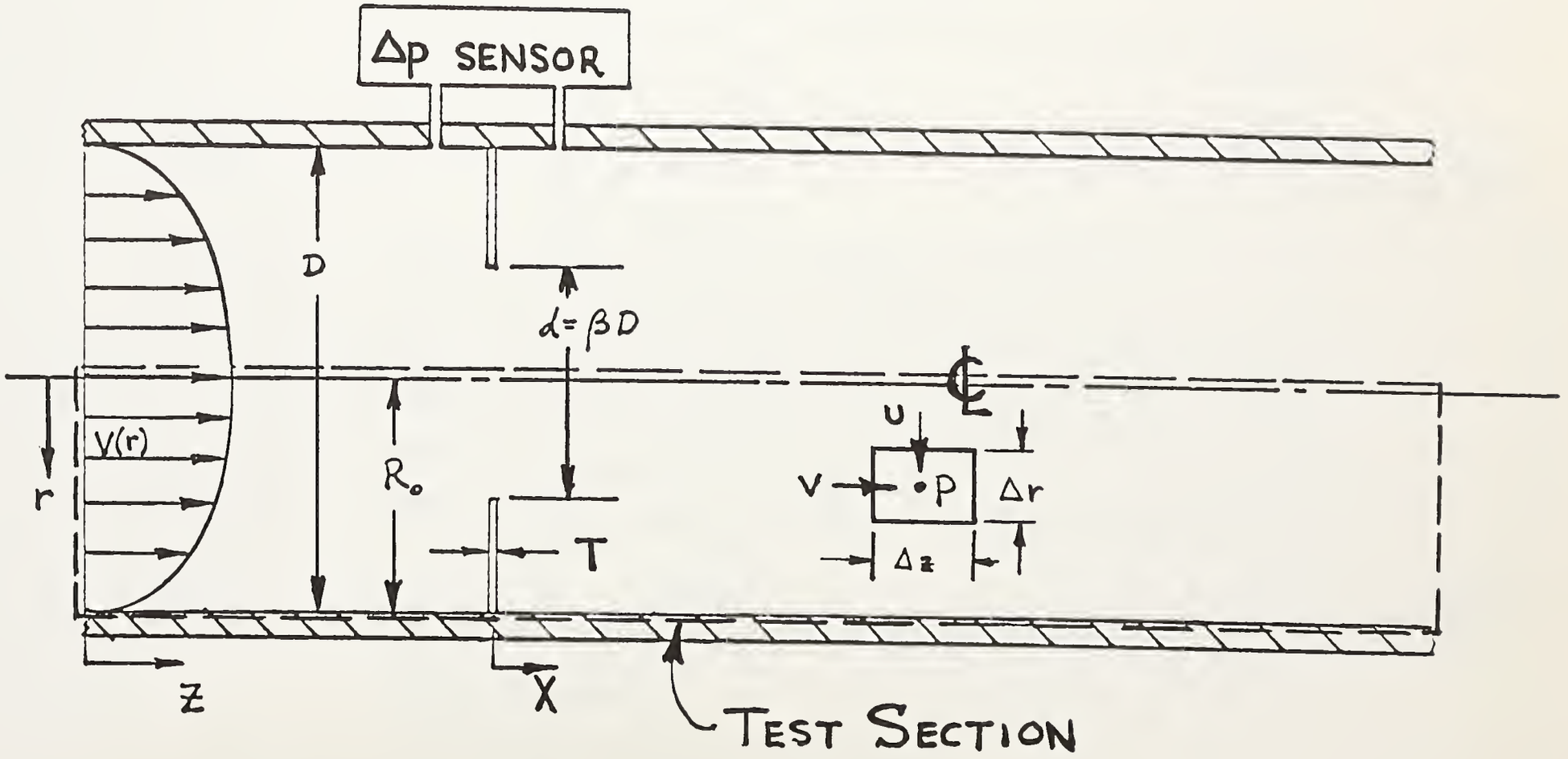

Fig 2. The computational test section.

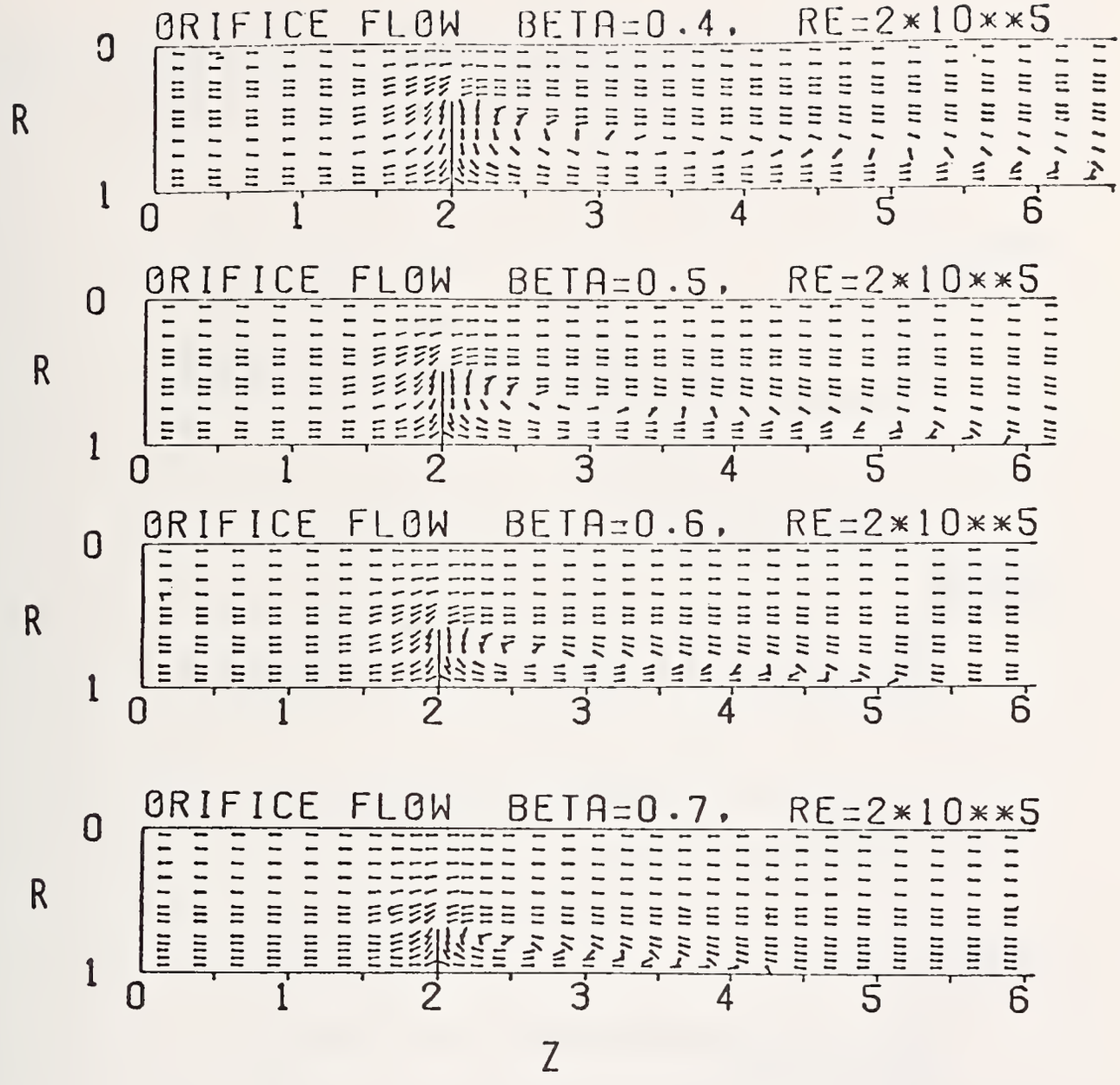

Fig 3. β effects on orifice flows.

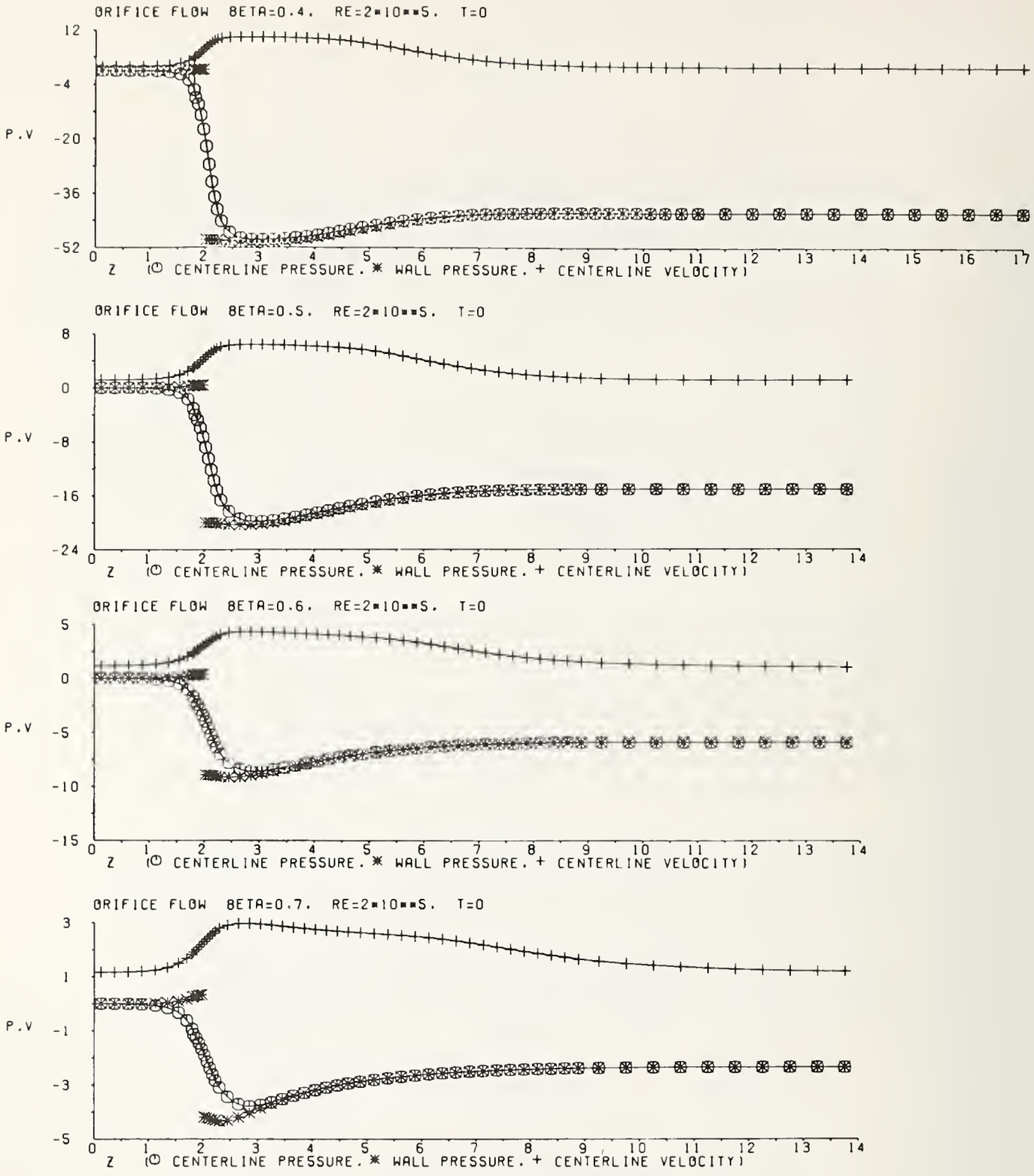

Fig 4. β effects on the centerline and wall static pressures and centerline velocity distributions.

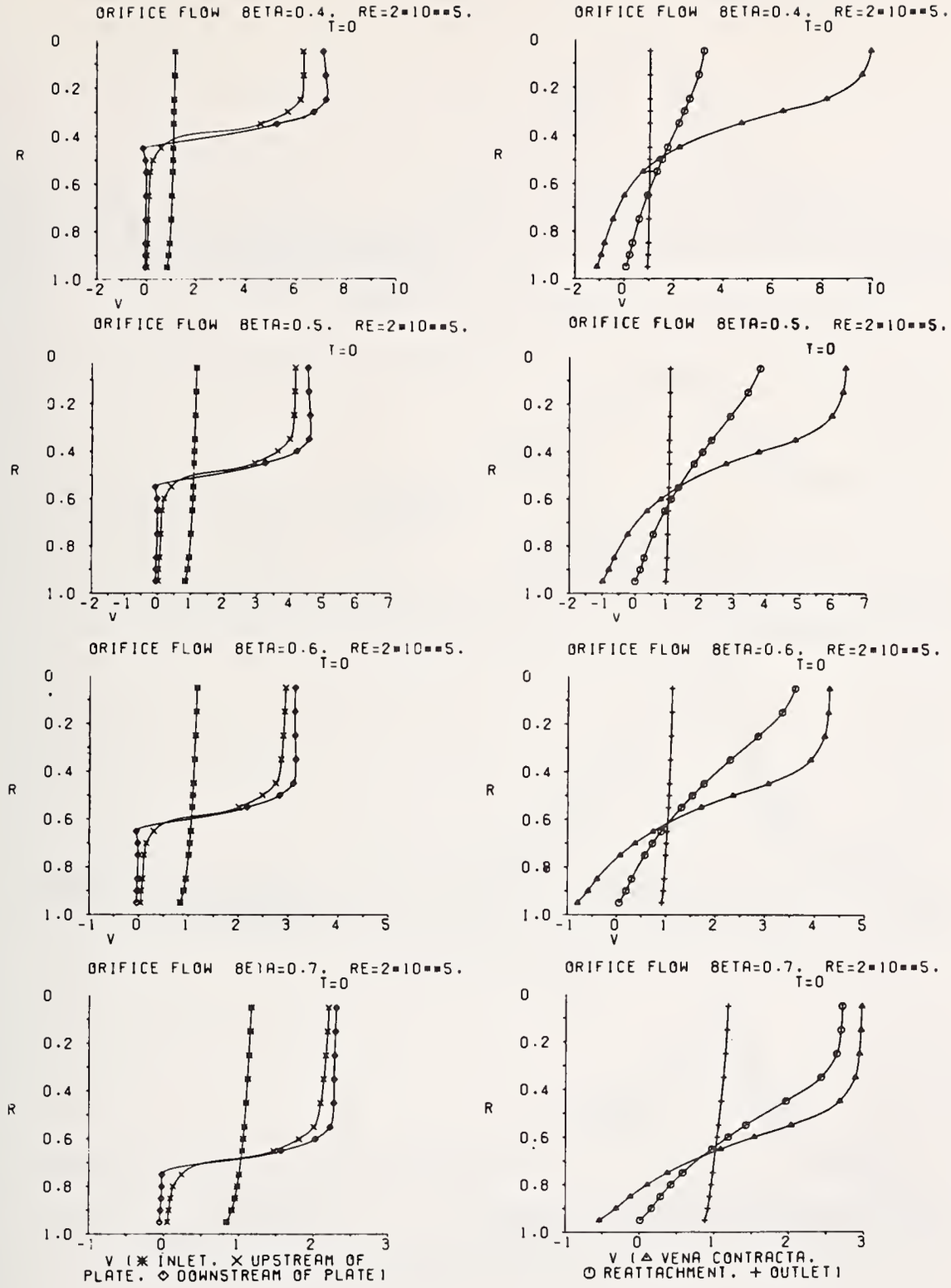

Fig 5. β effects on radial profiles of the streamwise velocity component.

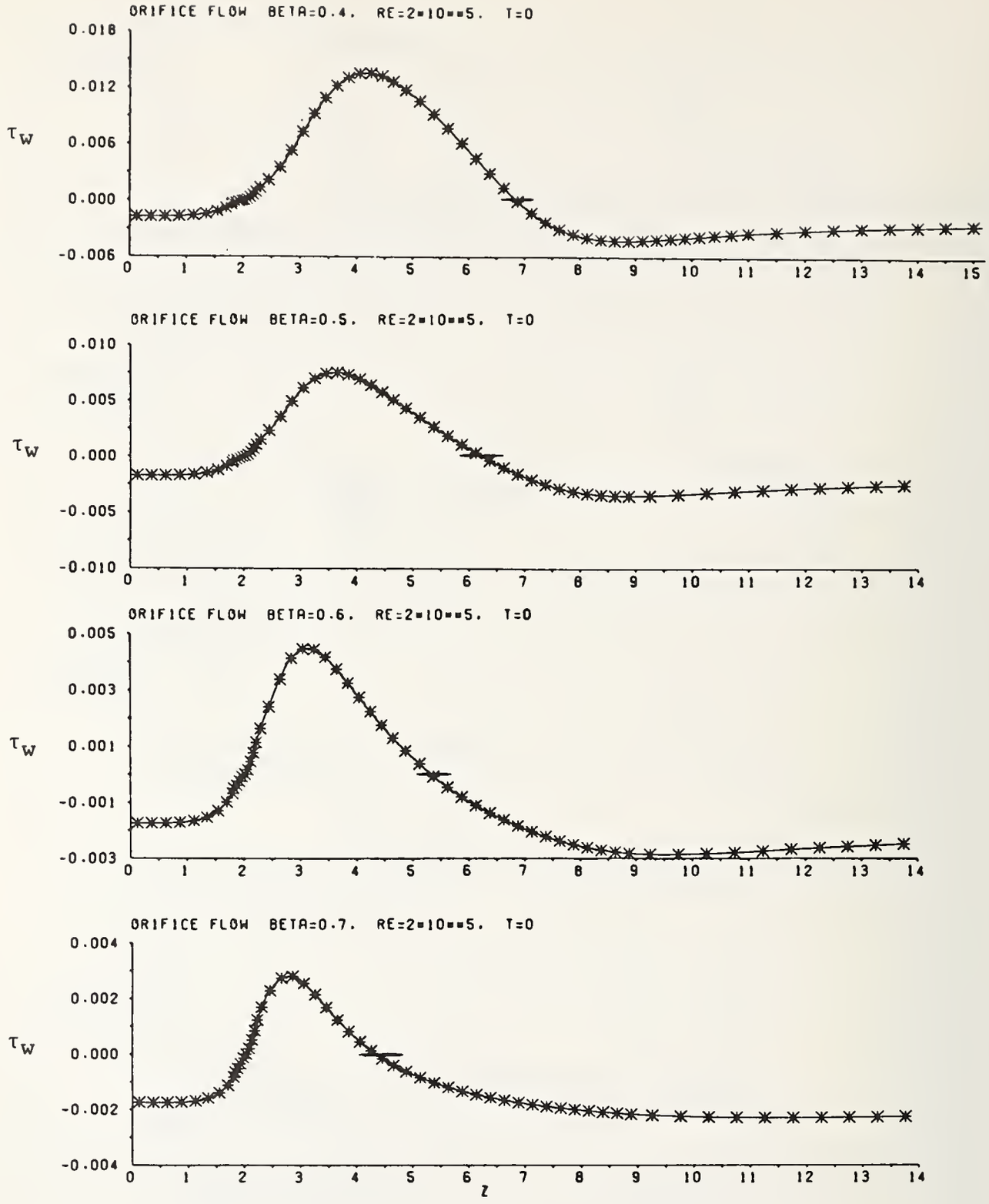

Fig 6. β effects on the wall shearing stress distribution.

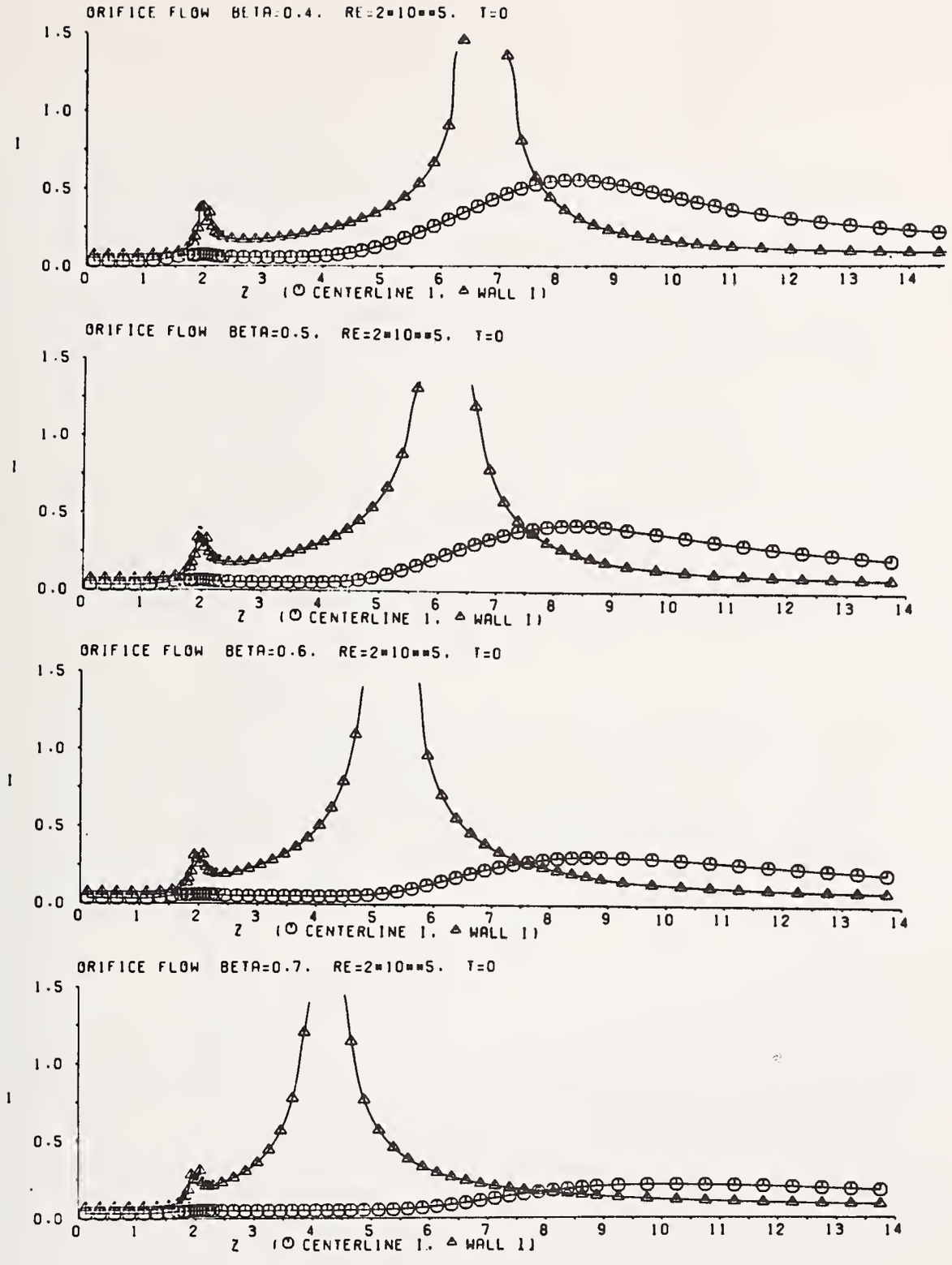

Fig 7. β effects on the centerline and wall turbulent intensity distributions.

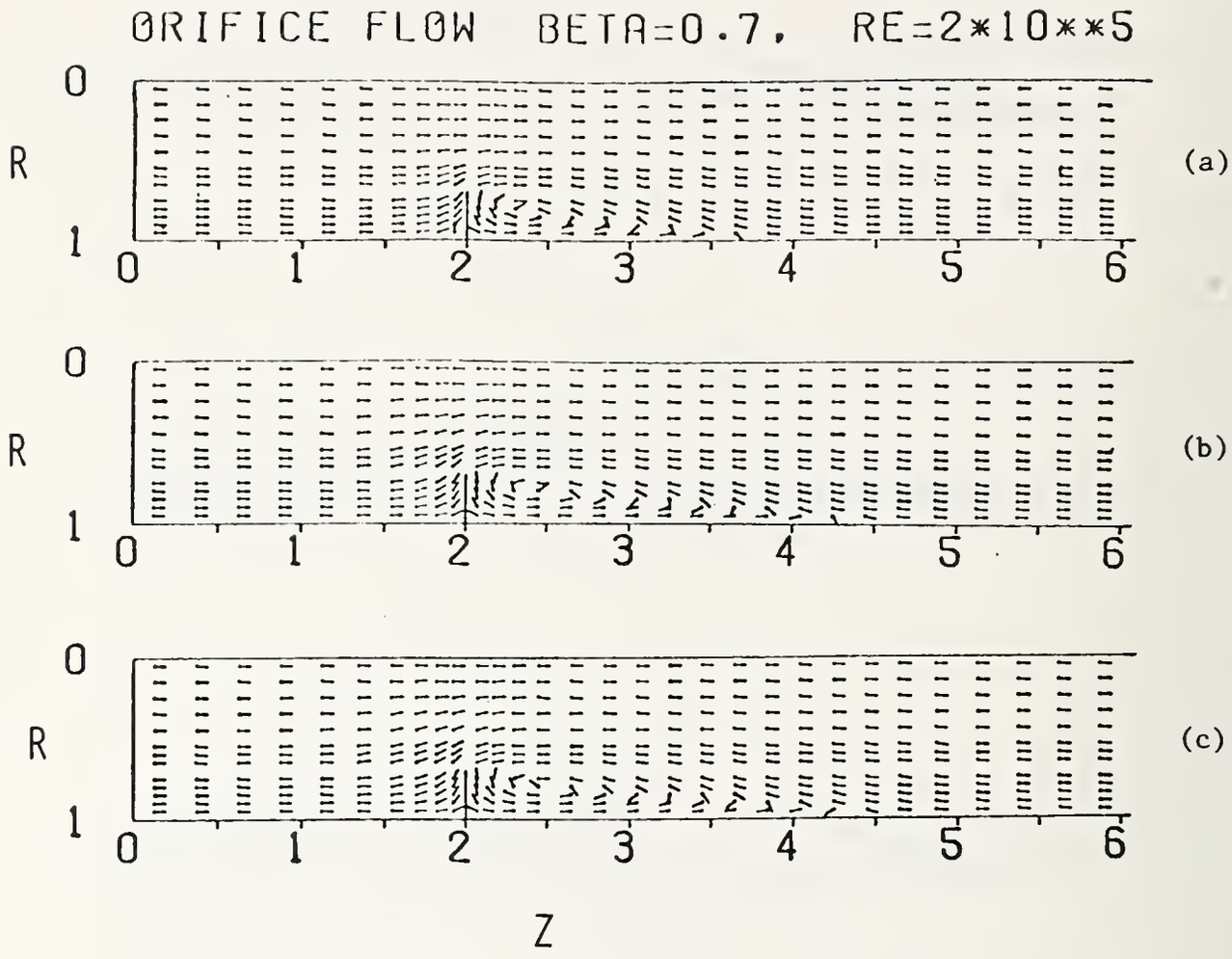

Fig. 8. Inlet velocity profiles effects on a $\beta = 0.7$ orifice meter. The profiles are: (a) parabolic, (b) "1/9"th power law, and (c) uniform.

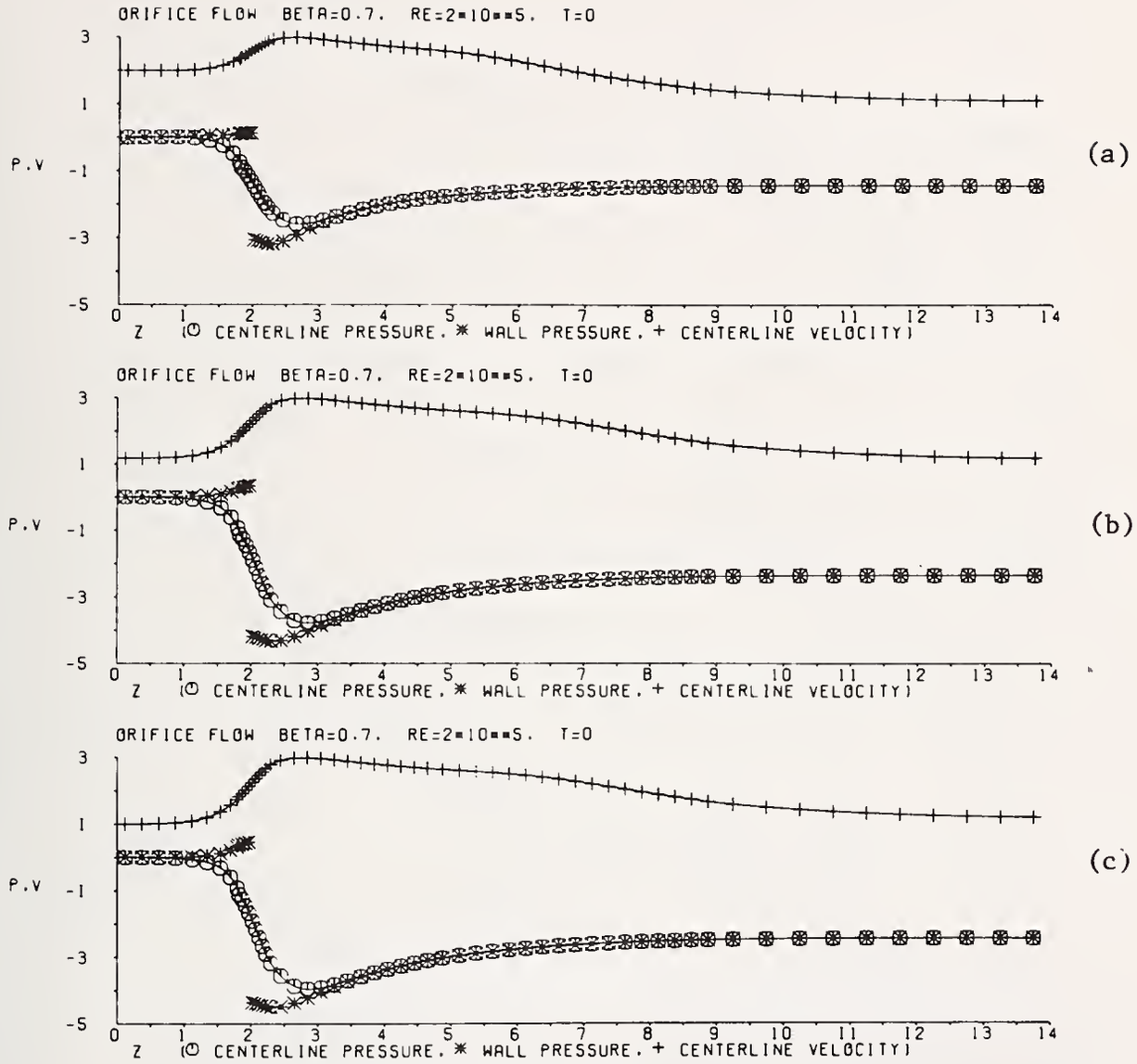

Fig. 9. Inlet velocity profile effects on the centerline and wall static pressures and the centerline velocity distribution for a $\beta = 0.7$ orifice meter. The profiles are: (a) parabolic, (b) "1/9"th power law, and (c) uniform.

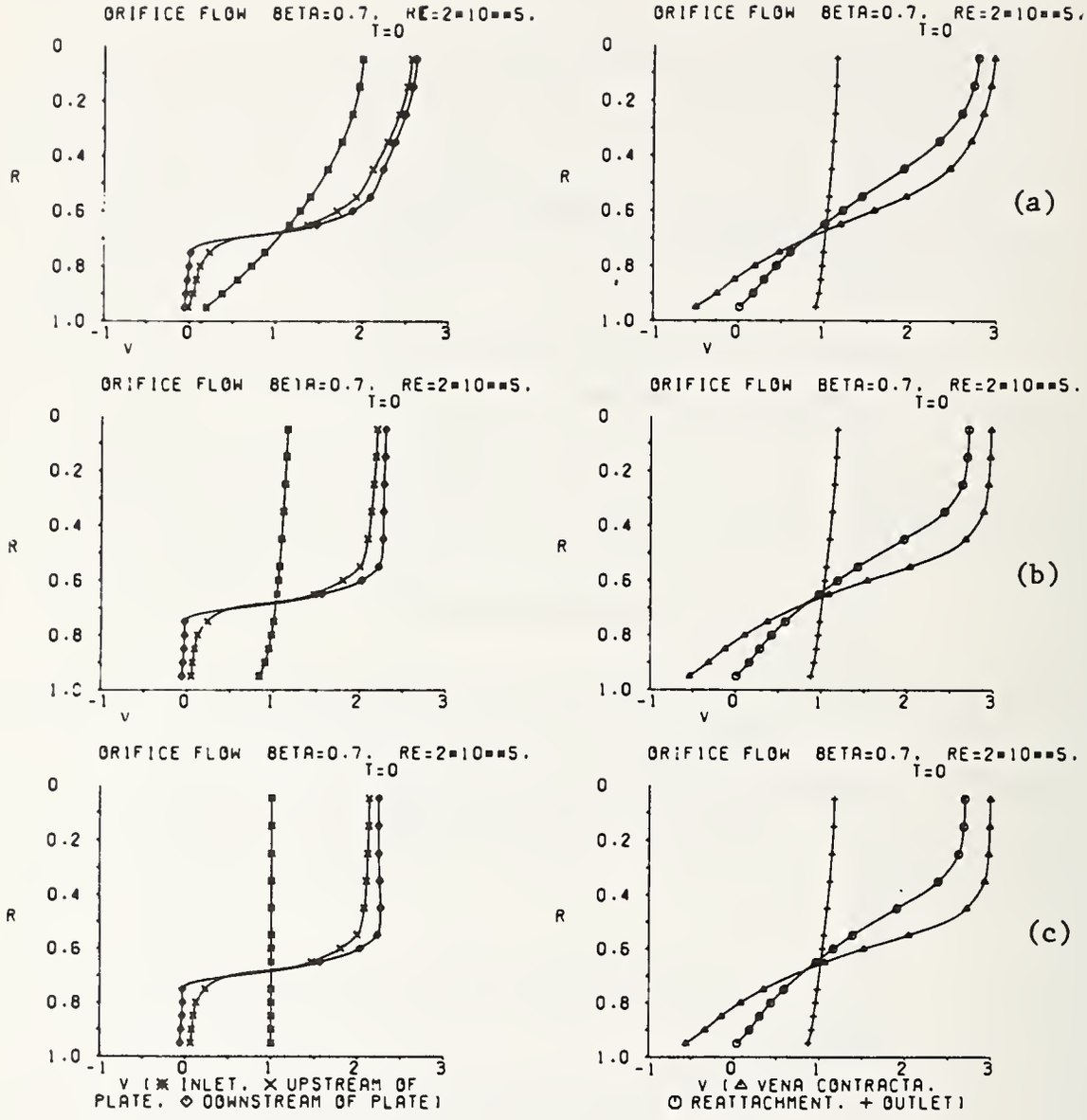

Fig. 10. Inlet velocity profile effects on radial profiles of the streamwise velocity component in a $\beta = 0.7$ orifice meter. The profiles are: (a) parabolic, (b) "1/9"th power law, and (c) uniform.

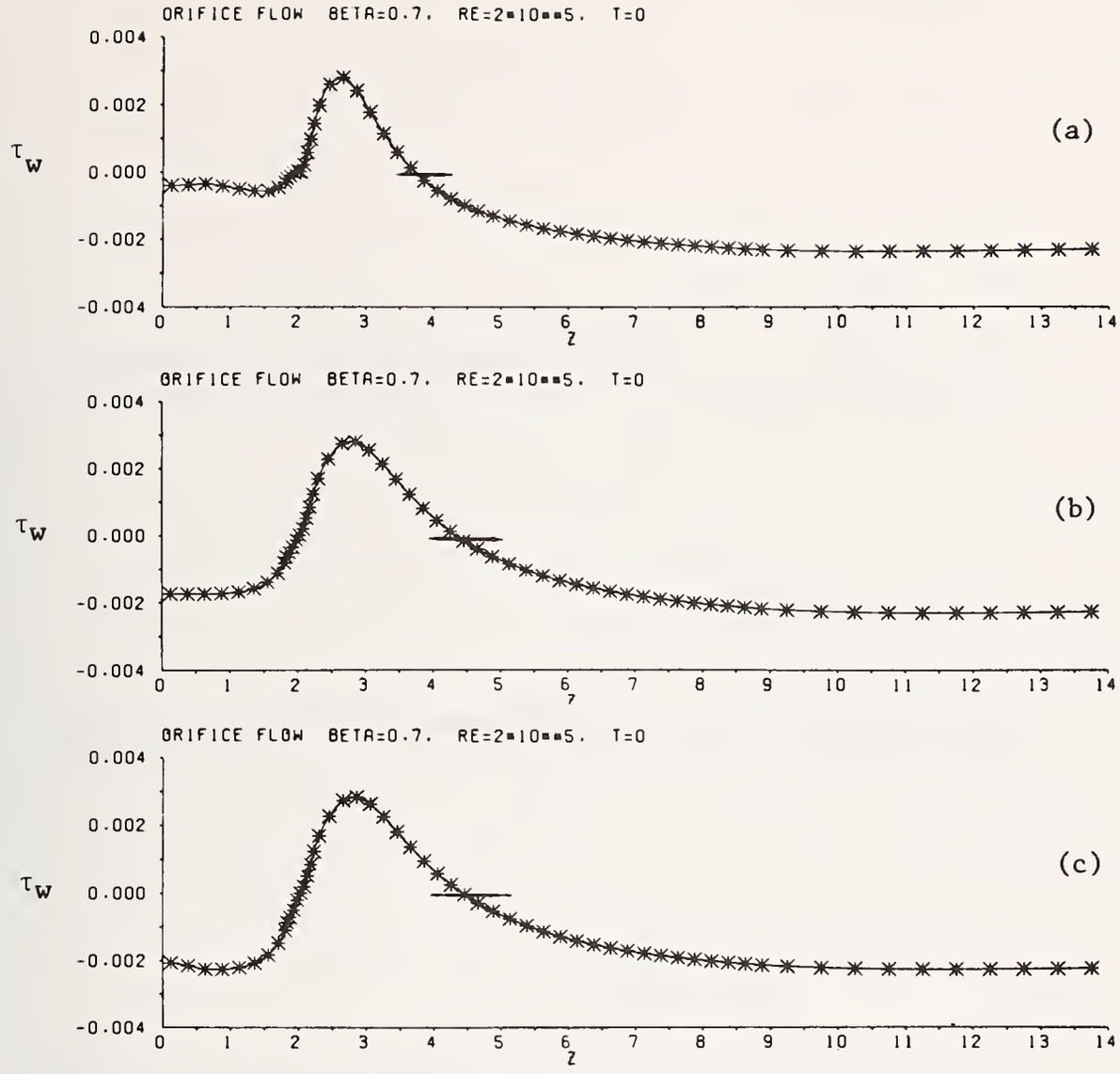

Fig. 11. Inlet velocity profile effects on the wall shearing stress distribution in a $\beta = 0.7$ orifice meter. The profiles are: (a) parabolic, (b) "1/9"th power law, and (c) uniform.

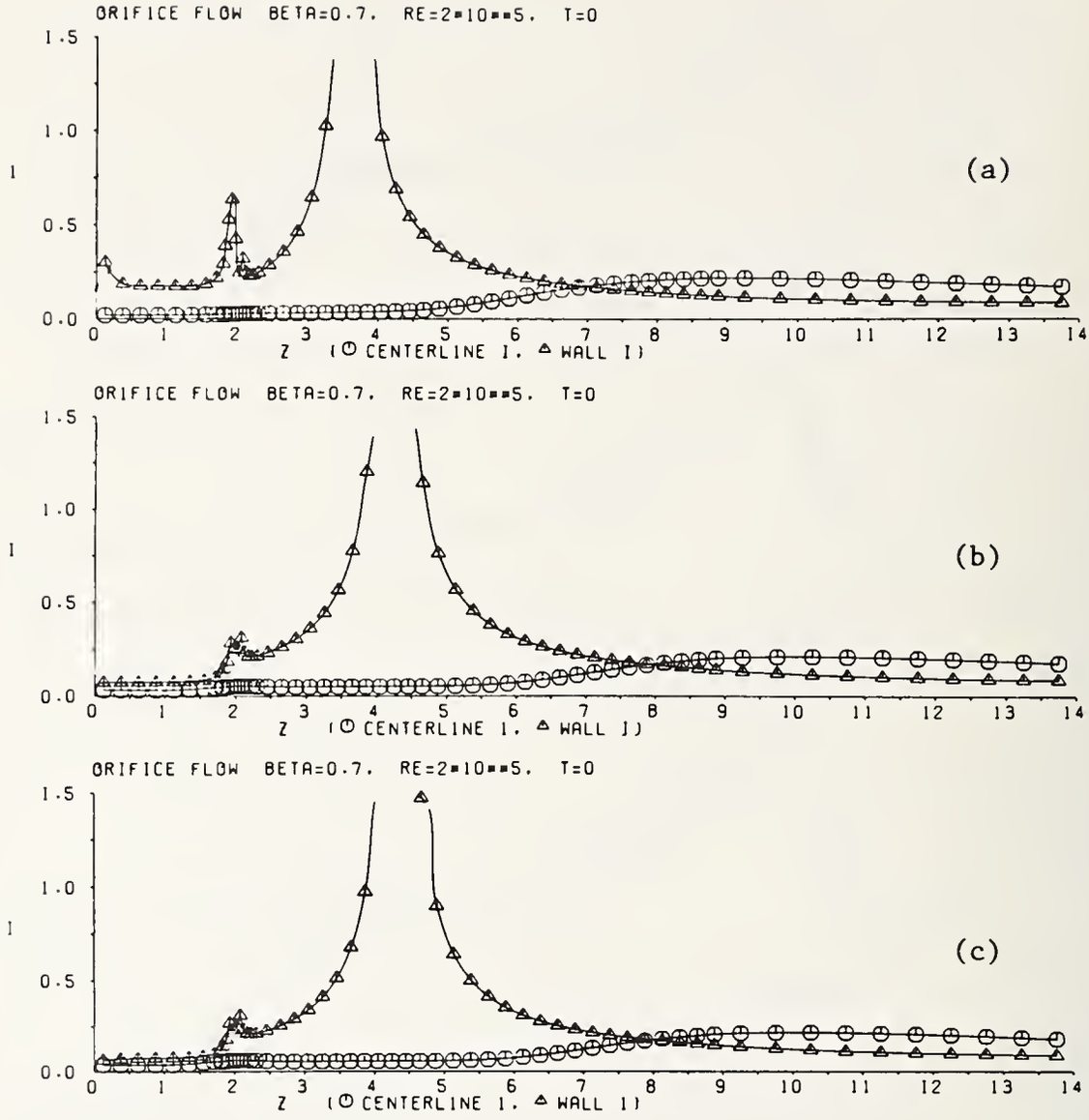

Fig. 12. Inlet velocity profile effects on the centerline and wall turbulent intensity distributions in a $\beta = 0.7$ orifice meter. The profiles are: (a) parabolic, (b) "1/9"th power law, and (c) uniform.

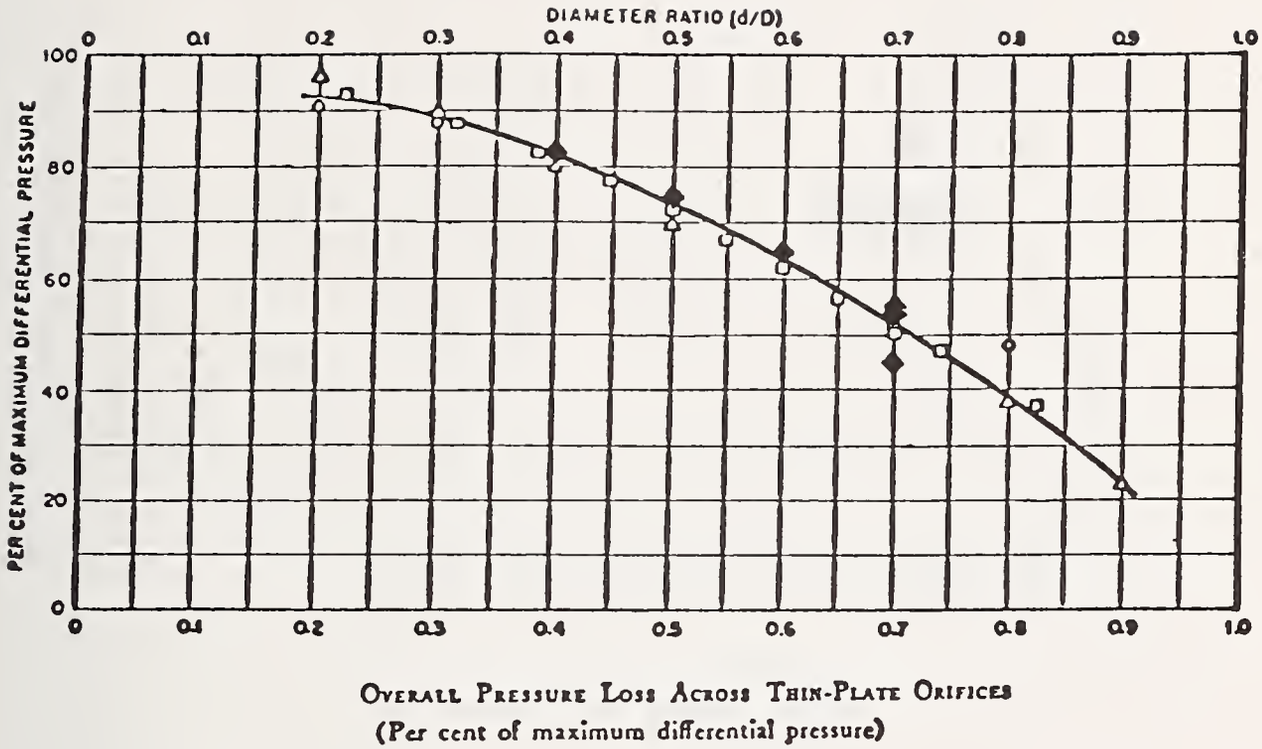

Fig. 13. Comparison of computed and experimental results for the overall pressure loss across thin plate orifices. Symbols Δ, 0, and □ denote previous results [3]; ◆ denote present results.

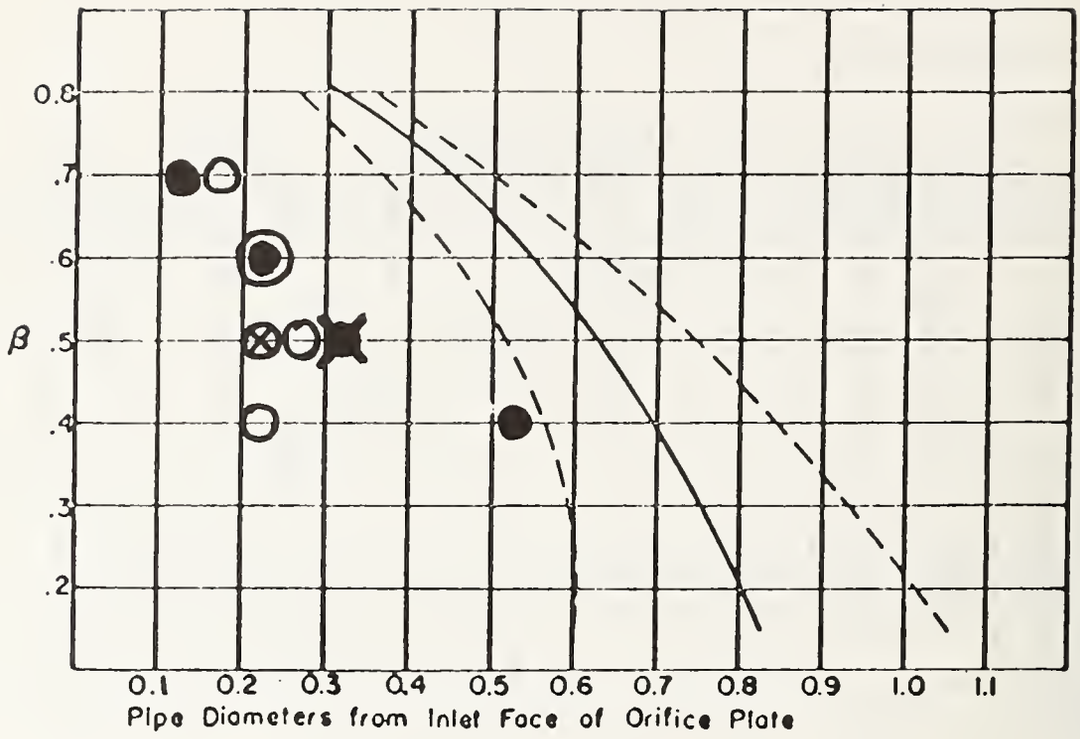

Fig. 14. Comparison of computed and experimental results for the locations of minimum wall pressure and vena contracta in thin plate orifice flows.

National Bureau of Standards Special Publication 484, Proceedings of the Symposium on Flow in Open Channels and Closed Conduits held at NBS, Gaithersburg, MD, February 23-25, 1977. (Issued October 1977)

STUDIES OF PULSATING INCOMPRESSIBLE FLOW THROUGH ORIFICE METERS

R. A. Bajura and M. T. Pellegrin

Department of Mechanical Engineering and Mechanics
West Virginia University
Morgantown, West Virginia 26506

The differential pressure-flow relationship for standard ASME concentric sharp-edged orifice meters subjected to pulsating incompressible flow was investigated experimentally and analytically. Tests were conducted with water at pipe Reynolds numbers between 8,000 and 24,000. Strouhal numbers of pulsation were varied between 0 and 1.8. The source of pulsation was located 15 diameters downstream of the orifice and provided flow pulsation amplitudes of up to 30% of the mean flow with differential pressure pulsation amplitudes of up to 250% of the mean differential pressure across the orifice. Three orifices with beta ratios of 0.35, 0.50 and 0.70 were used in the tests. A vortex shed from the edge of the orifice during pulsatile flow distorts the downstream flow channel as the vortex is convected away from the orifice. A marked distortion of the orifice flow channel occurs for pulsation conditions where the wavelength of the pulsation is approximately equal to the bore diameter of the orifice. The effect of the inertia of the fluid mass between pressure taps was determined over a range of pulsation Strouhal numbers. The effective discharge coefficient of the orifice decreases during pulsatile flow conditions. An analytical model which included the effects of fluid inertia and the increased friction losses which occur during pulsatile flow was developed and compared with the experimental data.

Key Words: Pulsating flow measurements; orifice meters; flow metering error; pulsations; flow oscillations; jet flow; vortex; differential pressure; turbulence.

1. Introduction

Orifices are the most common differential producers used in industrial flow metering because of their ease of installation, low cost, accuracy, and the interchangeability of orifice plates without the need for recalibration. The total flow metering system is comprised of three parts. The first part, or primary element, consists of the orifice plate and the remainder of the metering run. The second part, or secondary system, consists of the impulse piping, the differential pressure sensor, and the associated read-out devices and/or recording elements. An illustration of these two hardware components is given by Figure 1. The third part of the metering system is conceptual in nature and involves the formulation and interpretation of system equations which relate the output from the hardware elements to the flow rate for a given set of conditions.

The dimensionless equation for the one dimensional unsteady flow of an incompressible fluid through an orifice can be represented by a relationship between the flow rate*, q(t), and the differential pressure, $\Delta h(t)$, which has the form:

$$\frac{dq(t)}{dt} + CQ\, q^2(t) = CP\, \Delta h(t) - CLOSS \quad \ldots\ldots\ldots\ldots\ldots\ldots (1)$$

The term CQ is a coefficient for the convective acceleration of the fluid, CP is a coefficient related to the differential pressure, and CLOSS represents the effects of friction losses. Equation (1) is obtained by integrating the momentum equation between the upstream and downstream pressure taps using suitable assumptions for the shape of the flow channel. One of the most common assumptions is to require the shape of the flow channel to remain constant during pulsation. Under this condition, no mass or momentum storage occurs in the flow channel due to changes in the size of the control volume. A change in the size of the control volume can be interpreted as a capacitance effect which leads to a compressibility condition that alters the propagation of flow signals through the downstream jet region [1].** For steady flow, the dimensionless metering equation can be reduced to a more elementary relationship, namely:

$$q = CD\ \mathrm{sqrt}\ (\Delta h) \quad \ldots\ldots\ldots\ldots\ldots\ldots\ldots\ldots\ldots\ldots\ldots\ldots (2)$$

Orifice meters can be calibrated to an accuracy of $\pm$ 0.5% under steady flow conditions. For unsteady flow, a calibration relationship such as equation (2) will lead to inaccurate predictions of the flow rate. Flow metering errors arise due to a number of reasons, such as neglecting the effects of fluid inertia in the measurement volume and in the transmission lines leading to the pressure transducer, and the introduction of acoustical effects due to the impedance of the orifice. Under the analytical model known as square root theory [2,3], it is assumed that the inertial effects may be neglected and the flow rate may be accurately predicted if the square root of the differential pressure is obtained from the secondary system before time-averaging the output signal. This quasi-steady flow approximation is useful when the characteristic frequency of the unsteadiness is low and the differential pressure across the orifice is always positive. When the characteristic frequency of the unsteadiness is large, changes in the assumed flow channel for the orifice will occur, the inertial and friction loss terms become important, the flow coefficients CP and CQ may vary during the cycle of the oscillation, and the differential pressure across the orifice may become negative. These conditions lead to a strong non-linearity in the metering relationship which prohibits obtaining an accurate flow rate estimate from a simple time-averaging of an output differential pressure signal.

An indication of the degree of unsteadiness in the flow is given by the Strouhal number, which is defined as:

$$S = fd/U_j \quad \ldots\ldots\ldots\ldots\ldots\ldots\ldots\ldots\ldots\ldots\ldots\ldots\ldots\ldots (3)$$

---

*Terms are defined in the Nomenclature Section at the end of the paper.

**Numbers in brackets denote references in the Bibliography Section.

where f is the pulsation characteristic frequency, d is the orifice bore diameter, and U_j is the maximum jet velocity downstream of the orifice. The boundary between steady, quasi-steady, and unsteady flow is a function of the Strouhal number.

The objectives of the present research program are to determine the characteristics of an orifice flow meter under pulsatile flow conditions. Specific areas of investigation were defined in three broad categories: 1) the pressure and velocity fields near the orifice, 2) the response of typical secondary systems under pulsatile flow conditions, and 3) the development of an analytical model to accurately predict the flow rate under pulsatile flow conditions. The present paper discusses results obtained from studies of the pressure and velocity fields near the orifice plate. A discussion of a one-dimensional, fixed flow channel analytical model for the orifice is also presented.

2. Review of Literature

Flow metering with concentric orifices has long been a standard practice to obtain flow rate measurements in pipelines. Accurate values of the orifice calibration coefficients have been obtained from statistical studies of the data of various experimenters and experimental facilities under steady flow conditions [4,5,6]. The dependence of the discharge coefficient on the Reynolds number and the pressure tap location has been described by Halmi [7] and is documented in detail in flow metering reference books [8]. Minor corrections due to changes in the edge sharpness [9,10] and in the approaching velocity profile [11,12], have also been identified in order to account for scatter in discharge coefficient data. These analytical studies [11,12,13] which incorporate the approaching velocity profile into the orifice flow model predict discharge coefficients which are in close agreement with experimental data. In summary, the main direction of the steady flow work has been to modify the one-dimensional orifice hydraulic equation to account for the effects of Reynolds number, pipe diameter and orifice diameter ratio, and the pressure tap location.

However, steady flow conditions often do not prevail in industrial piping systems. Examples of severe pulsating flow and pressure conditions have been given in several review papers [14,15,16]. Flow metering errors have been observed under these conditions and were assumed to be dependent on an unsteadiness parameter which took various forms such as the Hodgson and Strouhal numbers [17,18] and an intensity parameter as proposed by Head [19]. Some investigators [3,20,21] have suggested that the Strouhal number is not a criterion for pulsating flow measurement.

Earlier attempts to explain the discrepancy between the actual mean flow and the predicted flow based on the hydraulic equation focused on the interpretation of the output of the secondary system when the readings oscillated at large amplitudes due to the unsteadiness of the flow [17,22, 23]. Severe throttling of the impulse lines was often used to obtain steady readings under the assumption that the output device would produce the "true" differential pressure reading if the secondary system response

were linear. Later, "square root theory" was proposed as a possible solution to the problem of obtaining accurate flow measurements under pulsating flow conditions [23,24]. Using this method, the output of the secondary system is processed to obtain the square root of the differential pressure before time-averaging the output signal. The basis of this method is the square root relationship between the differential pressure and the flow rate if the steady flow hydraulic equation is used as the correlation between these two variables. The square root method proved satisfactory in most cases, but always produced a positive error in the measurement (i.e., the indicated flow rate was always greater than the actual flow rate). This method is unsatisfactory if the differential pressure becomes negative during a portion of the cycle of oscillation.

Much discussion has appeared in the literature concerning the causes of the metering error and the difficulties of obtaining flow measurements under conditions of pulsation [25,26,27,28,29,30,31]. Randall [32] examined the operation of the orifice meter under unsteady conditions and noted in summary that the error in measurement was attributable to the following factors:

1. The inertia of the fluid mass between pressure taps introduces an additional factor into the metering equation which is not taken into account in steady flow calibrations.

2. The flow rate is related to the square root of the differential pressure if a quasi-steady flow relationship is assumed for the pulsating flow condition.

3. The inertia of the fluid in the impulse piping and the output transducer introduces additional factors into the response of the secondary system which contribute to errors in flow measurement.

4. Acoustic waves which arrive out-of-phase at the measuring taps due to the impedance of the orifice can impose negative differential pressures across the orifice which are much larger than the average differential pressure due to flow.

These observations suggest that a combination of factors such as orifice beta ratio, the pulsation Strouhal number and amplitude ratio, the pressure tap location, and the response characteristics of the secondary system must all be considered in evaluating the error under pulsatile conditions. Various investigators have measured the flow metering error under a wide range of pulsation conditions. A summary of their results is presented in Pellegrin [33].

While some insight into the characteristics of the error behavior may be gained by calibration experiments, a physical understanding of the orifice flow metering relationship cannot be developed without a careful study of the dynamic flow field near the orifice plate. Experimental data for the orifice flow field in steady flow have been obtained by Teyssandier [34] and others; however, detailed flow field data under pulsation are scarce.

Some of the characteristics of the downstream orifice jet flow can be deduced from the behavior of free jets and shear layers. A large scale organized vortex structure has been found in the transition region of free jets between the nozzle and the fully developed zone [35,36,37]. The natural excitation frequencies for this vortex structure lie in the Strouhal number range of 0.3 to 0.6. The presence of bounding walls in the orifice jet zone and the stagnation region at the upstream face of the orifice introduce complicating factors which differentiate the orifice jet flow from the free jet flow case. Some observations of the vortex structure for two dimensional slit orifices have been reported by Rockwell [38] and Farr [39]. The authors present in this paper the results of a detailed study of the flow and pressure fields near the orifice under conditions of pulsation.

3. Experimental Facility

The metering run was constructed from 10.2 cm diameter clear acrylic pipe in a manner consistent with ASME specifications. Orifice plates of 0.95 cm thickness were threaded so that they could be installed in the metering run without the need for flanges which would impair flow visualization studies near the orifice. The three test orifices had beta ratios of 0.35, 0.50, and 0.70, respectively. Pressure tap arrangements corresponded to the Flange, D-D/2, and Vena Contracta locations for each orifice. Velocity measurements were obtained from hot film and hot wire probes and flow visualization techniques, including high speed movies. Pressure measurements were made at the pipe wall using crystal pressure sensors. The average differential pressure across the orifice was obtained from manometers and capacitance-type pressure transducers. Signal averaging techniques were used to obtain ensemble-averaged waveforms of the pulsating differential pressure and velocity as a function of the phase angle of the pulsation.

Most of the testing program was conducted with water except for a few initial experiments with air. A schematic illustration of the orifice and the water test facility is given by Figures 1 and 2, respectively. The flow through the system was regulated by two upstream constant head reservoirs in order to attain a steady supply flow independent of any pressure or flow disturbances from the pump. The water was recirculated through the system to maintain constant temperature operation for the hot film probes. Pulsations were induced from the downstream end of the metering run by a rotating valve arrangement driven by a variable speed DC motor. The valve rotation frequency range was 0-17 Hz. Velocity and flow rate variations could be adjusted to rms levels of from 5% to 30% of the temporal mean values of these parameters. Corresponding rms pressure oscillations approached 250% of the mean differential pressure across the orifice. Typical Reynolds numbers for the experiments were in the range of 8,000 to 24,000 (based on the metering run diameter of 10.2 cm and the volumetric average velocity of the flow approaching the orifice).

4. Velocity Measurements Near the Orifice

A. Steady Flow. The flow approaching the orifice was determined to be without swirl and corresponded to a fully developed power law profile with an exponent of (1/6.6). The location of the maximum velocity in the downstream orifice jet coincided with the predicted vena contracta region for the 0.70 and 0.50 beta ratio orifices. The maximum velocity location for the 0.35 beta ratio orifice was found to occur slightly upstream of the predicted vena contracta region. Frequency spectra taken for the lower flow rates near the edge of the shear zone in the contracting jet region downstream from the orifice indicated that a laminar-turbulent transition process was intermixed with lower frequency turbulent fluctuations convected from upstream. At higher flow rates, the upstream turbulence dominated the frequency spectra in this region and no regular velocity fluctuations were observed.

B. Pulsatile Flow. The amplitude and waveform characteristics of the pulsation were functions of the frequency of oscillation, the pulsator valve design, and the overall resistance, capacitance and inductance of the metering run. An example of the change in waveform with frequency for low and high Reynolds number flows is given by Figure 3. In general, higher oscillation frequencies produced lower amplitudes of flow fluctuation through the orifice.

The metering run was modeled using a lumped parameter description of the resistive, inductive and capacitative elements of the system. Several analytical functions describing the pulsator valve opening and closing time history were studied using a computer analysis. Results from the computer analysis were in qualitative agreement with the experimentally-observed differential pressure and centerline velocity measurements. The computer analysis also verified the experimentally-observed sensitivity of the system characteristics to different valve designs (area-of-opening vs. angular position). The natural frequency of the metering run was in the neighborhood of 4 Hz as determined from experiments and the lumped parameter computer analysis. The system natural frequency was dominated by the characteristics of the entire metering run and appeared to be only slightly dependent on the beta ratio of the orifice being tested.

Figure 4 illustrates mean velocity profiles in pulsating flow at 4 positions along the metering run for the 0.50 beta ratio orifice. For cases where the steady flow mean velocity profile differs from the pulsatile flow case, the steady flow mean velocity profiles are shown by the dotted lines. The example of Figure 4 is typical of the velocity profile characteristics for all three beta ratio orifices. Upstream of the orifice, the mean velocity profiles were similar to the steady flow cases. In the downstream region, time averaged velocity profiles were generally broader than the corresponding profiles for steady flow conditions. The location of the maximum velocity region also moved further upstream toward the orifice under pulsating flow conditions.

The rms amplitude of the pulsation component, u'_{rms}, appeared to be constant over the core regions of the flow both upstream and downstream of the orifice. Figure 4 illustrates the profiles for the fluctuating velocity component in the lower portion of the figure. The fluctuating velocity (rms magnitude) consists of both turbulence and the periodic change in velocity due to the pulsation. The amplitude of the fluctuating velocity is larger in the downstream shear layer than in the core region at that location, partially due to the greater turbulence activity and partially due to the characteristic response of the shear layer to the pulsation. The larger amplitude of the fluctuating component of streamwise velocity was especially noted for Strouhal numbers between 0.4 and 0.8 where large variations in the orifice flow channel boundaries occurred. The broadening of the mean velocity profile in pulsatile flow is due to increased friction losses and also indicates that pressure recovery downstream from the orifice may occur sooner than for the steady flow condition.

Figure 5 gives an illustration of a conceptual model of the downstream flow channel for cases where the Strouhal number is such that the wavelength of the pulsation corresponds with the dimensions of the orifice. The model assumes that the shape of the flow channel (i.e., the flow channel radius at any point along the centerline) varies with time. On the average, however, the time mean flow channel does not correspond to a contracting jet cylinder but retains this wavelike structure as shown by Figure 5. The cause of the waviness in the flow channel is attributed to a well-defined vortex which is shed from the lip of the orifice during each pulsation cycle.

Due to the growth of the shear layer downstream, it is not possible to define a zone in which all the fluid is moving at the centerline velocity. The velocity profiles at each station were analyzed to determine the point for which the jet momentum flux was 25% of the momentum flux at the centerline. In steady flow, this location corresponds to the point where the velocity is one half of the centerline velocity. The time averaged flow channel was defined as the locus of points where the jet momentum flux was 25% of the centerline momentum flux. An analysis of the experimental data showed that this flow channel encompassed approximately 95% of the total momentum flux of the jet velocity profile. Experimentally-determined shapes for the orifice flow channel boundary are shown on Figure 6. A wavelike structure is seen in the locus of points defining the flow channel. However, the shape of the flow channel changes with the Strouhal number and the amplitude of the flow oscillation. This characteristic behavior was noted for all three orifice beta ratios.

The size and location of the starting vortex in relation to the shear layer of the downstream jet flow is a function of the orifice beta ratio, the Strouhal number, and the amplitude of the pulsation. The convection velocity, U_c, of the vortex varied almost linearly between 0.4 U_j for Strouhal numbers of 0.4 to approximately 0.8 U_j for Strouhal numbers of 1.5. The optimum vortex formation was observed for Strouhal numbers between 0.4 and 0.8 where the wavelength of the pulsation was of the order of the bore diameter of the orifice. Visual studies confirmed that the smaller vortices occurred for the higher Strouhal number cases. This effect is partially due

to the fact that the amplitude of the oscillation decreased with increasing frequency due to the response characteristics of the metering run. The smaller vortices tended to remain in the high velocity portion of the shear layer and were therefore convected downstream at speeds closer to the core region velocity. The larger vortices spread over more of the shear layer and were convected downstream at a lower average speed. For a given amplitude of pulsation, oscillations with Strouhal numbers in the range of 0.4 to 0.8 produced large wavelike spatial variations in the time-averaged cross-sectional area of the flow channel downstream from the orifice. Regions where the flow channel cross-sectional area were increased were coincident with regions where the rms velocity fluctuations were decreased. The opposite effect was observed in regions where the cross-sectional area was decreased. These observations were confined to regions between the orifice plate and the furthest vena contracta tap location downstream.

Figure 7 shows the velocity profile (ensemble average) at different times in the cycle of oscillation at three downstream locations. The time-mean velocity profile for pulsation is shown by the dotted line. These profiles were obtained by signal averaging techniques, using the upstream pressure signal as a trigger for the averaging process to ensure that the zero phase angle for each profile coincided to the same reference time in the cycle of oscillation. The effects of turbulence are averaged out of the profiles in Figure 7. These data clearly show that the maximum swing in the value of the velocity occurs in the shear layer region. The data also show phase differences between stations which are due to the time lag caused by the convective characteristics of the orifice vortex. These results show that the pressure and the flow rate do not coincide due to the effects of both inertia and the convective lag, or capacitance effect, caused by the orifice vortex. This latter effect has not been considered in any analytical model for the orifice as a flow meter.

5. Pressure Measurements Near the Orifice

Static pressure measurements were obtained across the jet profile at a location 5.1 cm downstream from the leading edge of the orifice. The average static pressure at any radial location was found to be equal to the pressure observed at the wall tap. The largest rms pressure fluctuation was observed in the shear layer for the steady flow case. In pulsatile flow, the system pressure level oscillation is so much larger than the shear layer turbulent pressure fluctuations that the local static pressure fluctuation is practically constant over the cross-section. These results support the assumption that the pressure pulse is propagated along the test section as a one-dimensional wave. Since the waveform of the pressure signal was similar at both the upstream and downstream pressure taps, it was concluded that the orifice was not acting as an acoustic impedence for the test conditions studied.

Analytical models for the orifice under pulsatile flow conditions show that the inertial coefficient for the time dependent term should increase as the spatial separation between pressure taps in increased. The major

contribution to the inertial coefficient is the length of the high kinetic energy region in the downstream orifice jet zone. The downstream jet zone may be hypothesized to be a cylinder in which the fluid behaves in a slug-like manner. This idealized flow channel is shown on Figure 5. Experiments with the 0.7 beta ratio orifice were in agreement with this concept. The rms differential pressure was observed to increase as the distance between the upstream and downstream pressure taps was increased. Velocity measurements showed that the fluid moved through the 0.7 beta ratio orifice in a slug-like manner. The increase in the magnitude of the fluctuating differential pressure, $\Delta p'_{rms}$, with tap separation is shown on Figure 8a.

For the 0.5 beta ratio orifice, the rms differential pressure increased only slightly with increases in the tap separation distance. For the 0.35 beta ratio orifice, the rms differential pressure decreased slightly as the tap separation distance was increased. This behavior is illustrated by Figures 8b and 8c, respectively.

The observations for the 0.35 beta ratio orifice are consistent with the velocity profile experiments which show an increased turbulent dissipation. The slug-like motion of the fluid through the orifice under pulsatile flow conditions is not as well-defined for the lower beta ratio orifices in comparison with the high beta ratio orifice. Decreases in the level of the flow oscillation in the test section were accompanied by corresponding decreases in the rms level of the differential pressure fluctuation.

6. Calibration Experiments

All three orifices were calibrated for both steady and pulsating flow by collecting approximately 135 kg of water in a weigh tank. The tests were repeatable to 0.3% differences for the same flow conditions. The orifice calibration constants were in agreement with ASME standards ($\pm$ 0.5% accuracy) for the 0.35 and the 0.50 beta ratio orifices in steady flow [8]. However, the 0.70 beta ratio orifice differed from the ASME standards for flows in the Reynolds number range of 20,000 to 30,000 (based on the bore of the orifice). The calibration constant was approximately 15% higher than the recommended values in reference [8]. However, the behavior of the 0.70 beta ratio data is in agreement with the data of Stearns, et al, [40]. Steady state values of the flow coefficients obtained by calibration were used in all cases for comparison with pulsatile flow results.

Each orifice was tested for metering error for various combinations of Strouhal number and amplitude of oscillation. Data taken for the D-D/2 pressure tap combination are presented in Figure 9. In all cases, the orifice passed less flow under pulsatile flow conditions than would be predicted using the steady flow hydraulic equation, steady flow coefficients, and the average value of the differential pressure across the orifice. The amplitude parameter shown on Figure 9 is the oscillation in flow rate and not the oscillation in the differential pressure across the orifice. Square root theory was not used in calculating the flow rate since the differential pressure across the orifice became negative for some portions of the cycle of oscillation. The dashed lines on Figure 9 illustrate

three regions delineating flow pulsation amplitudes between 5 and 10%, 10 and 20%, and 20 to 30%, respectively. The data appear to be consistent in that the magnitude of the error increases with increases in both the amplitude of the oscillation and the Strouhal number. One data point, for the 0.70 beta ratio orifice at high pulsation amplitudes, however, indicates a significantly lower error than would be expected based upon the general trends of the data. Two comments are in order here. First, the error which would be obtained using the flange tap arrangement is approximately 16% and is much greater than the 1% error predicted for the D-D/2 taps. Second, the Strouhal number of the oscillation for this case is in the range where the flow channel was markedly deformed by the orifice vortex. This deformation was also verified by visual observations with dye streaks. Additional experiments are required to formulate the overall relationship between the measurement error and the independent parameters (Strouhal number, tap separation, flow pulsation amplitude, orifice beta ratio, and Reynolds number).

7. Analytical Model

An analytical model was developed for the unsteady flow of an incompressible fluid through a sharp-edged orifice under the assumption that the flow channel for the orifice did not vary with time. The orifice flow channel is idealized as shown by the cylindrical volumes on Figure 5. Inputs from the experimental velocity profiles were used in formulating estimates for the radius of the cylinders in the upstream and downstream regions. The length of the control volume extends from the upstream to the downstream pressure taps. Values for the friction loss coefficient, CLOSS, were developed from the experimental data and some preliminary computations with the analytical model. An indication of the variation in the friction loss coefficient is given by Figure 10.

One complete period of pulsation for the experimentally observed differential pressure signal was obtained by time averaging techniques and recorded on strip charts. This differential pressure trace was nondimensionalized and digitized to provide discrete values of the differential pressure for 50 times in the cycle of pulsation. Numerical computations were performed with this input signal to obtain a solution for the dimensionless velocity waveform through the orifice. These numerical predictions were compared with experimentally-determined velocity waveforms.

Two cases of analysis are shown in Figures 11 and 12, respectively. Figure 11 illustrates the comparison between the model and the theory for a Strouhal number of approximately 0.14. The dashed line represents the solution obtained from another analytical model patterned after square root theory. Note that the square root theory solution is similar to the differential pressure signal, as should be expected. The analytical model developed by the authors provides a better fit to the data than does the square root theory model. Figure 12 illustrates the case of a Strouhal number near 0.34. The agreement between the present analytical model and the experimental data is still good while the square root theory solution is clearly inadequate. These examples show that the inertia effects must be taken into account in formulating a hydraulic equation for the orifice

which is applicable to pulsating flow. In those instances where the flow channel was markedly deformed by the orifice vortex, the agreement between the model and the experimental results was not as well-matched as the results illustrated by Figures 11 and 12. The amplitude of the waveform predicted by the model was larger than the amplitude of the experimentally-determined waveform, although predictions of phase angle were accurate. In these instances, the fixed area flow channel assumption is questionable.

Simple arguments based upon the analytical model can be used to show the dependence of the flow metering error upon the amplitude of oscillation parameter and the Strouhal number. The analytical model can also be used to show that the effective discharge coefficient for the orifice under pulsating flow must be less than the steady flow discharge coefficient for the same average differential pressure. This result is in agreement with the experimental data for the flow metering error shown on Figure 9. The data of Figures 11 and 12 also illustrate the relationship between the differential pressure and the flow rate variable as a function of the Strouhal number. Referring to equation (1), when the Strouhal number is small, the inertia term may be eliminated and the pressure is related to the square of the flow. For this case the extrema in the pressure and flow curves should occur at approximately the same time in the cycle of oscillation. This condition is illustrated by the experimental data of Figure 11. When the Strouhal number becomes large, the inertia term becomes dominant and the convective acceleration term may be neglected. For this case, the pressure variable and the time derivative of the flow variable should have maxima and minima at corresponding times in the cycle of oscillation. The higher Strouhal number case is illustrated on Figure 12, where the maximum flow occurs at the location where the pressure is changing rapidly, and vice versa.

8. Conclusions

When the wavelength of the pulsation is of the order of the bore diameter of the orifice, the vortex shed from the edge of the orifice distorts the downstream flow channel sufficiently to introduce significant errors in the one-dimensional flow metering equation. The orifice passes less flow during pulsatile flow conditions than for steady flow at the same average differential pressure. Reversal of flow through the orifice was not observed even when the differential pressure became negative. A variable area flow channel analytical model is needed to predict the flow field adequately when the Strouhal number is in the range of 0.4-0.8. The present results suggest that the accurate prediction of the flow rate under unsteady conditions may require information concerning the amplitude of the flow fluctuation in addition to the more readily observed fluctuations in the differential pressure.

Acknowledgments

This research program is sponsored by the National Science Foundation, Fluid Mechanics Program, under Grant ENG-10399-A01 and is being conducted

as a cooperative effort with the Babcock & Wilcox Company, the DeLaval Turbine Division, and West Virginia University. Project reports issued by the investigators under this program of research are listed as references [41,42,43].

Nomenclature

CD	Discharge coefficient
CLOSS	Friction coefficient
CP	Differential pressure coefficient
CQ	Convective acceleration coefficient
d	Orifice bore diameter
D	Pipe diameter (10.4 cm)
f	Frequency, hz
Δh	Dimensionless differential pressure
ℓ	Length of orifice jet zone between orifice and downstream pressure tap.
p	Pressure
$\Delta\bar{p}$	Average differential pressure
Δp_{rms}	Root mean square value of fluctuating differential pressure
q	Dimensionless volume flow rate
R	Pipe radius (5.2 cm)
R_D	Reynolds number based on pipe diameter and bulk velocity in pipe.
R_d	Reynolds number based on orifice bore diameter and velocity through orifice
S	Strouhal number, fd/U_j
t	Dimensionless time
$\bar{u}$	Average velocity
U_c	Vortex convection velocity
U_j	Maximum velocity on centerline in downstream jet region
u'_{rms}	Room mean square of fluctuating velocity component
U_{ℓ}	Velocity on centerline
x	Axial location
y	Radial position measured from centerline
β	Orifice beta ratio
λ	Wavelength of pulsation
θ	Phase angle of pulsation

Bibliography

1. A. H. Shapiro, "Fluid Mechanics in Bioengineering," Invited Lecture presented to the Fluids Engineering Division Luncheon, ASME Winter Annual Meeting, New York, December 8, 1976.

2. D. S. Moseley, "Measurement Error in the Orifice Meter on Pulsating Water Flow," Flow Measurement Symposium, ASME, p. 103, September 26-28,

3. H. J. Sauer, R. D. Smith, and L. V. Field, "Metering Pulsating Flow in Orifice Installations," Instrumentation Technology, pp. 41-44, March, 1969.

4. R. W. Miller, "Precise Measurement of Differential Pressure When Calibrating a Head Class Flow Meter," ASME J. of Basic Engineering, p. 743, December, 1970.

5. R. B. Dowdell and V. L. Chen, "A Statistical Approach to the Prediction of Discharge Coefficients of Concentric Orifice Plates," ASME J. of Basic Engineering, v. 92, pp. 752-765, 1970.

6. R. W. Miller and O. Kneisel, "A Comparison Between Orifice and Flow Nozzle Laboratory Data and Published Coefficients," ASME Paper 73-WA/FM-5, 1973.

7. D. Halmi, "Practical Guide to the Evaluation of the Metering Performance of Differential Producers," ASME Journal of Fluids Engineering, pp. 127-141, March, 1973.

8. Report of ASME Research Committee on Fluid Meters, "Fluid Meters, Their Theory and Application," Sixth Edition, H. S. Bean, ed., ASME, 1971.

9. K. A. Crockett and E. L. Upp, "The Measurement and Effects of Edge Sharpness on the Flow Coefficients of Standard Orifices," ASME Paper 72-WA/FM-4, 1972.

10. R. P. Benedict, J. S. Wyler and G. B. Brandt, "The Effect of Edge Sharpness on the Discharge Coefficient of an Orifice," ASME Paper 74-WA/FM-4, 1974.

11. H. S. Ghazi, "On Nonuniform Flow Characteristics at the Vena Contracta," ASME Journal of Basic Engineering, pp. 883-888, December, 1970.

12. R. G. Teyssandier, "Flow Coefficient Variation for Concentric Orifices from an Analysis of Turbulent Velocity Profiles," ASME Paper 75-WA/FE-19, 1975.

13. R. B. Dowdell and M. P. Wilson, Jr., "Status of the Analysis of Flow Through Concentric Square Edged Orifices," ASME Paper 75-WA/FM-4, 1975.

14. H. Diederichs and W. D. Pomeroy, "The Occurrence and Elimination of Surge or Oscillating Pressures in Discharge Lines from Reciprocating Pumps," Transactions of ASME, Paper PET-51-2, pp. 9-49, 1929.

15. E. G. Chilton and L. R. Handley, "Pulsations in Gas Compressor Systems," Transactions of ASME, p. 931, 1952.

16. J. L. Dussourd, "An Investigation of Pulsations in the Boiler Feed System of a Central Power Station," ASME J. of Basic Engineering, p. 607, December, 1968.

17. A. K. Oppenheim and E. G. Chilton, "Pulsating-Flow Measurement--A Literature Survey," Transactions of ASME, p. 231, 1955.

18. F.V.A. Engel, "Fluid Dynamic Problems Awaiting Solution," Measurement and Control, v. 4, pp. T-6--T-14, 1971.

19. V. P. Head, "A Practical Pulsation Threshold for Flowmeters," Transactions of ASME, v. 78, pp. 1471-1479, 1956.

20. J. M. Zarek, "Metering Pulsating Flow-Coefficients for Sharp-Edged Orifices," Engineering, v. 179, pp. 17-19, 1955.

21. B. J. Jeffery, "Pulsating Flow Through an Orifice," Ph.D. Dissertation, University of London, 1965.

22. T. J. Williams, "Pulsation Damping in Pressure Gauge Connections," The Engineer, pp. 378-379, March, 1959.

23. S.W.E. Earles, B. J. Jeffery, T. S. Williams, and J. M. Zarek, "Pulsating Flow Measurement Using an Orifice-Manometer System," The Engineer, v. 224, pp. 822-825, 1967.

24. C. R. Sparks, "A Study of Pulsation Effects on Orifice Metering of Compressible Flow," Flow Measurement Symposium, ASME, p. 124, 1966.

25. E. J. Lindahl, "Pulsation and Its Effect on Flow Meters," Transactions of ASME, v. 68, pp. 883-894, 1946.

26. A. R. Deschere, "Basic Difficulties in Pulsating-Flow Metering," Transactions of ASME, v. 74, pp. 919-923, 1952.

27. N. A. Hall, "Orifice and Flow Coefficients in Pulsating Flow," Transactions of ASME, v. 74, pp. 925-929, 1952.

28. S.W.E. Earles and J. M. Zarek, "Use of Sharp-Edged Orifices for Metering Pulsating Flow," Proc. Instn. Mech. Engrs., v. 177, pp. 997-1024, 1963.

29. G. A. Karim and M. Rashidi, "The Measurement of a Pulsating Air Flow Using a Sharp-Edged Orifice Meter," ASME Paper 72-WA/FE-36, 1972.

30. B. W. Imrie and R. A. Evans, "An Investigation of Resonance Conditions for Pulsating Flow of Air Through an Orifice in a Pipe," Measurement and Control, v. 6, pp. 41-46, 1973.

31. R. C. Mottram, "The Measurement of Pulsating Flow Using Orifice Plate Meters," Flow - Its Measurement and Control in Science and Industry, v. 1, R. B. Dowdell, ed., Instrument Society of America, pp. 197-208, 1974.

32. L. N. Randall, "Some Experimental Results in Precise Measurement of Unsteady Fluid Flow Using a Unique Flow Sensor," Flow Measurement Symposium, ASME, 1966.

33. M. T. Pellegrin, "Pulsating Flow of an Incompressible Fluid Through a Sharp-Edged Orifice Meter," Ph.D. Dissertation, West Virginia University, 1976.

34. R. G. Teyssandier and M. P. Wilson, Jr., "The Paradox of the Vena Contracta," ASME Paper 73-WA/FM-9, 1973.

35. S. C. Crow and F. H. Champagne, "Orderly Structure in Jet Turbulence," Journal of Fluid Mechanics, v. 48, pp. 547-592, 1971.

36. J. C. Lau and M. J. Fisher, "The Vortex Structure of 'Turbulent' Jets, Part I," Journal of Fluid Mechanics, v. 67, pp. 299-337, 1975.

37. G. S. Beavers and T. A. Wilson, "Vortex Growth in Jets," Journal of Fluid Mechanics, v. 44, pp. 97-112, 1970.

38. D. O. Rockwell, "Vortex Stretching Due to Shear Layer Instability," ASME Paper 76-WA/FLCS-11, 1976.

39. L. R. Farr, "Pulsating Flow Through a Slit Orifice," MSME Thesis, West Virginia University, 1976.

40. R. F. Stearns, R. M. Jackson, R. R. Johnson, and C. A. Larson, "Flow Measurement with Orifice Meters," Van Nostrand Company, New York, 1951.

41. R. A. Bajura, M. T. Pellegrin and L. R. Farr, "Pulsatile Flow Through an Orifice," Available from NTIS, Springfield, Virginia, accession number PB 255179, 85 pages, January, 1976.

42. M. T. Pellegrin and R. A. Bajura, "Pulsating Flow of an Incompressible Fluid Through a Sharp-Edged Orifice Meter," Available from NTIS, Springfield, Virginia, accession number PB 261182, 355 pages, July, 1976.

43. L. R. Farr and R. A. Bajura, "Pulsating Flow Through a Slit Orifice," Available from NTIS, Springfield, Virginia, accession number PB 261147, 129 pages, July, 1976.

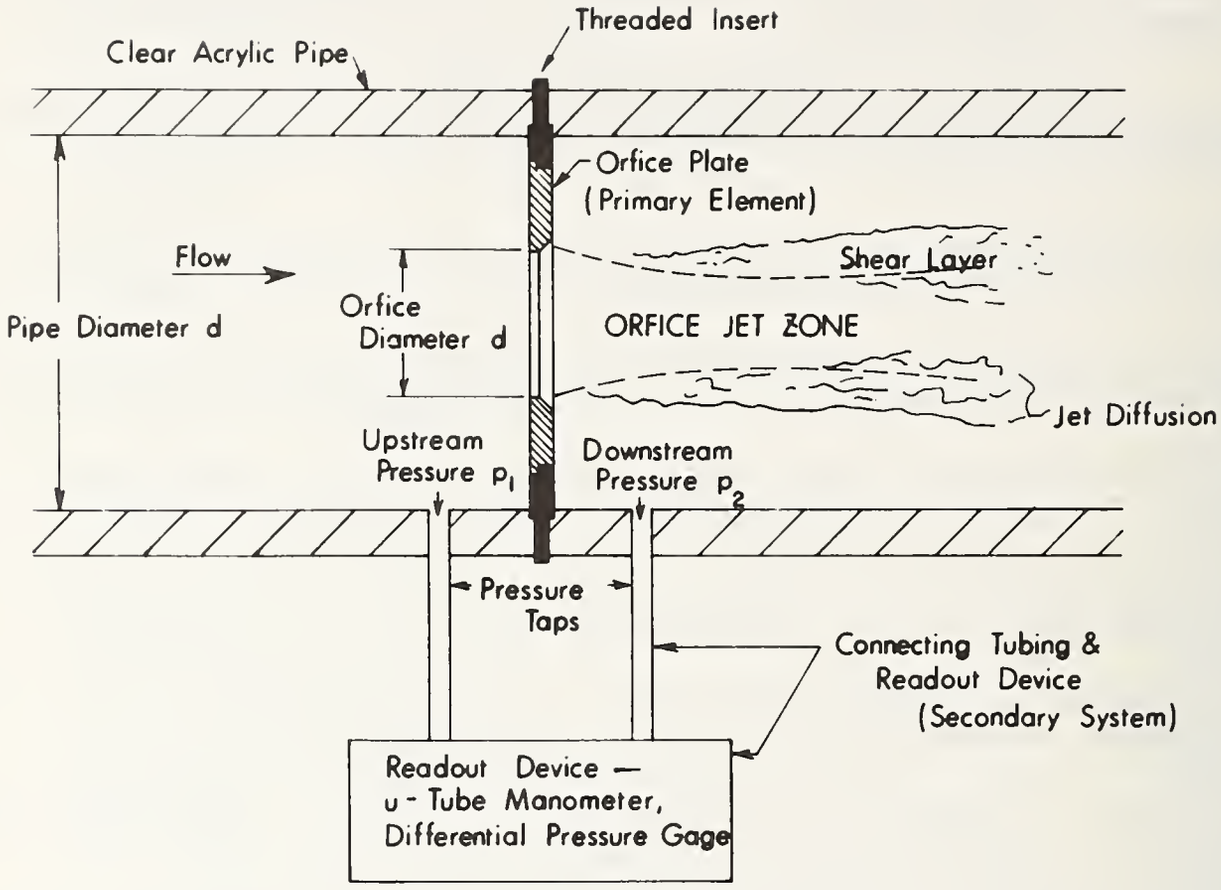

Figure 1. Description of Orifice Meter and Flow Field.

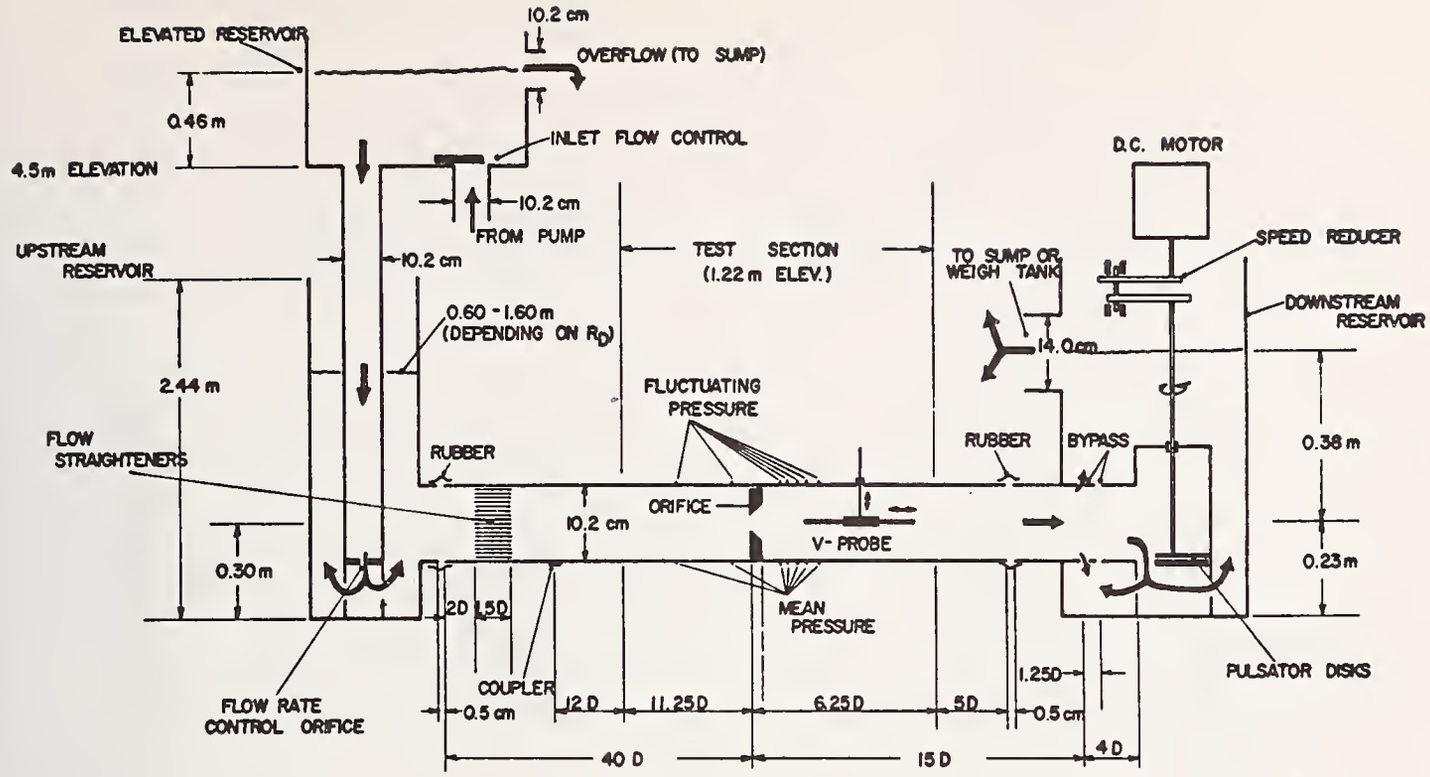

Figure 2. Elevation Schematic of Water Test Facility.

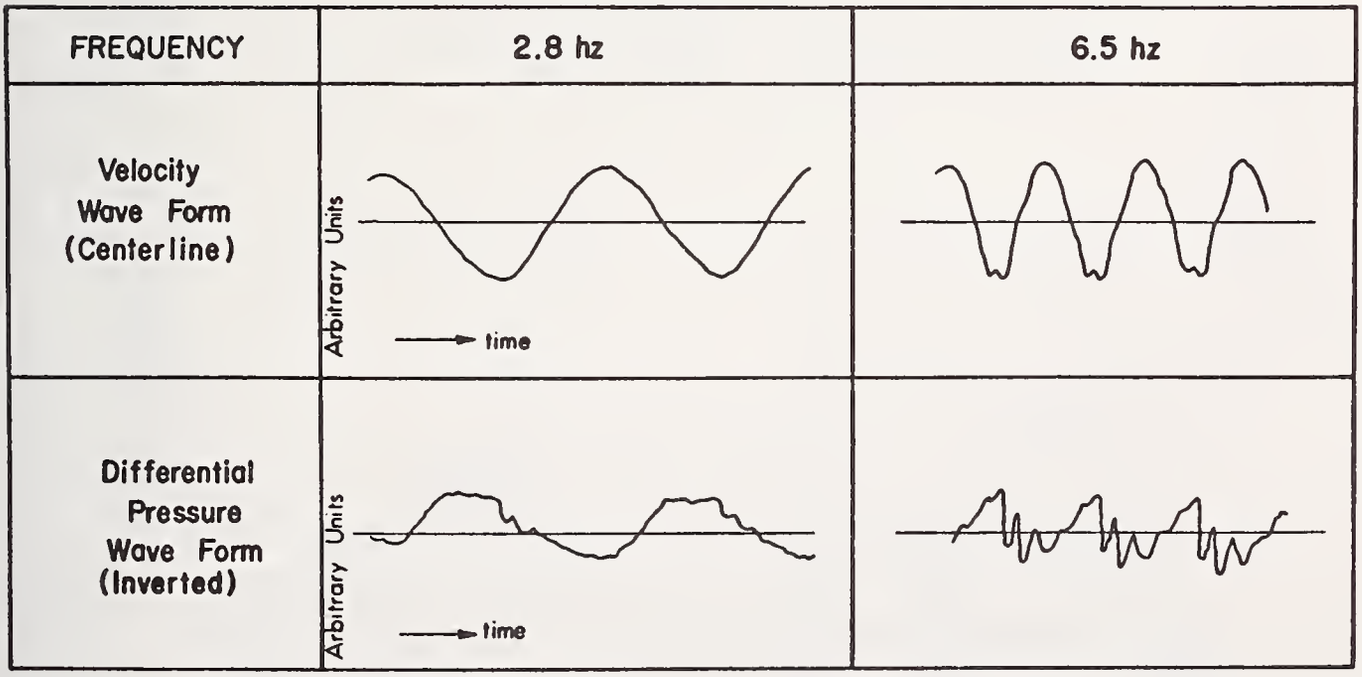

Figure 3. Characteristics of the Velocity and Differential Pressure Waveforms for Two Pulsation Frequencies.

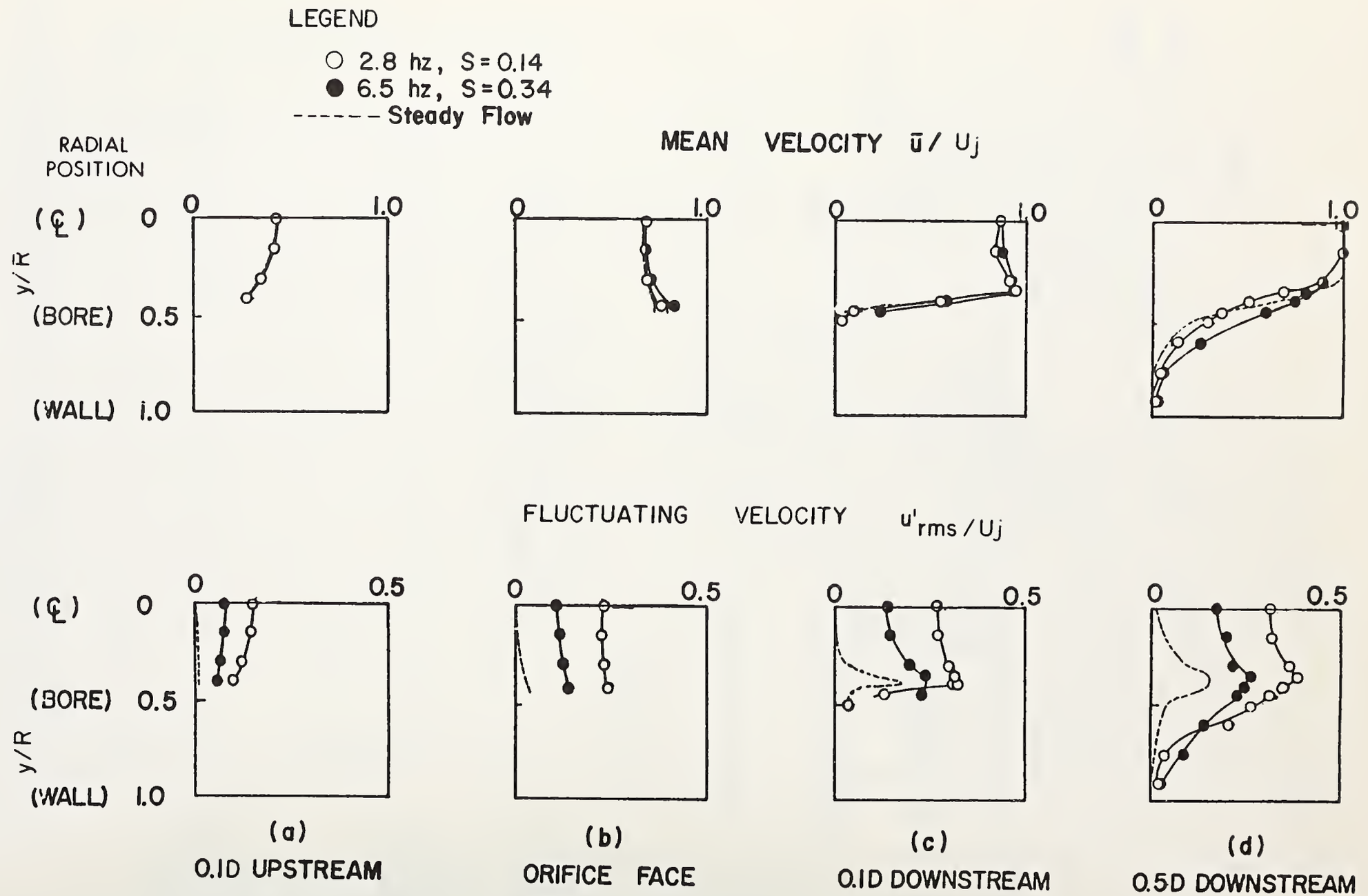

Figure 4. Dimensionless Mean and RMS Axial Velocity Profiles in Pulsating Flow for a 0.50 Beta Ratio Orifice at R_D = 17,000

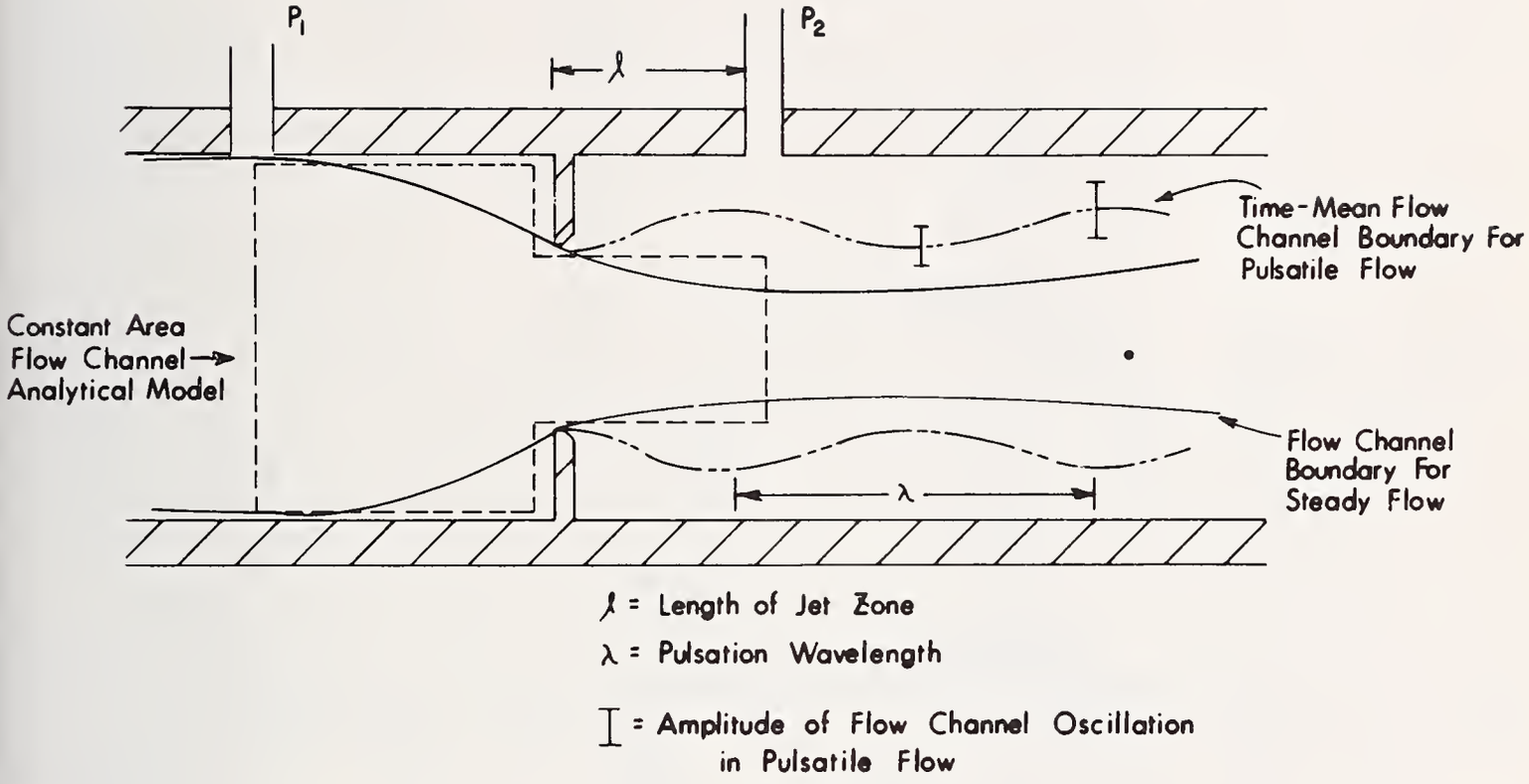

Figure 5. Conceptual Models of Flow Channel for an Orifice.

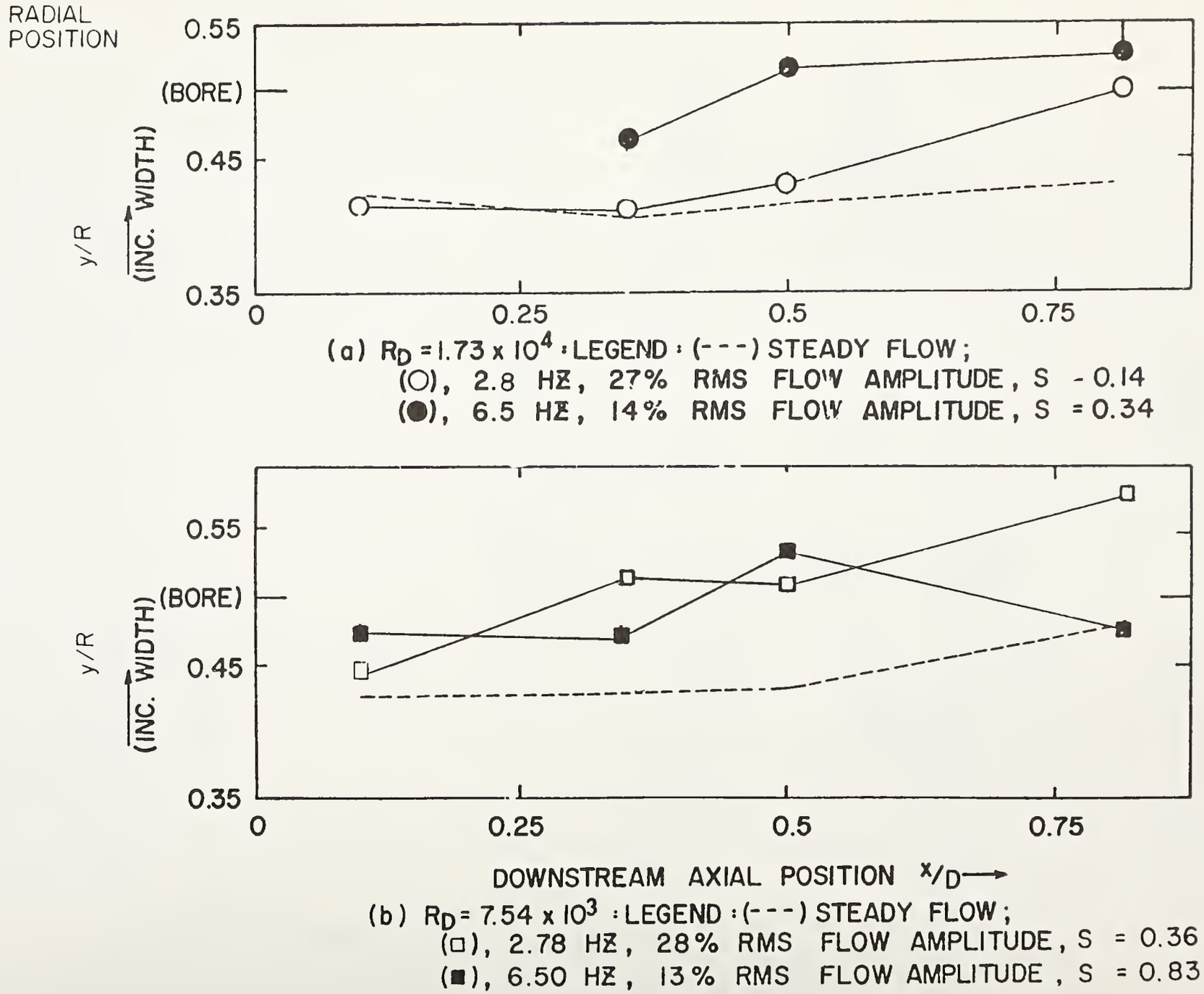

Figure 6. Mean Flow Channel Boundary for 0.50 Beta Ratio Orifice.

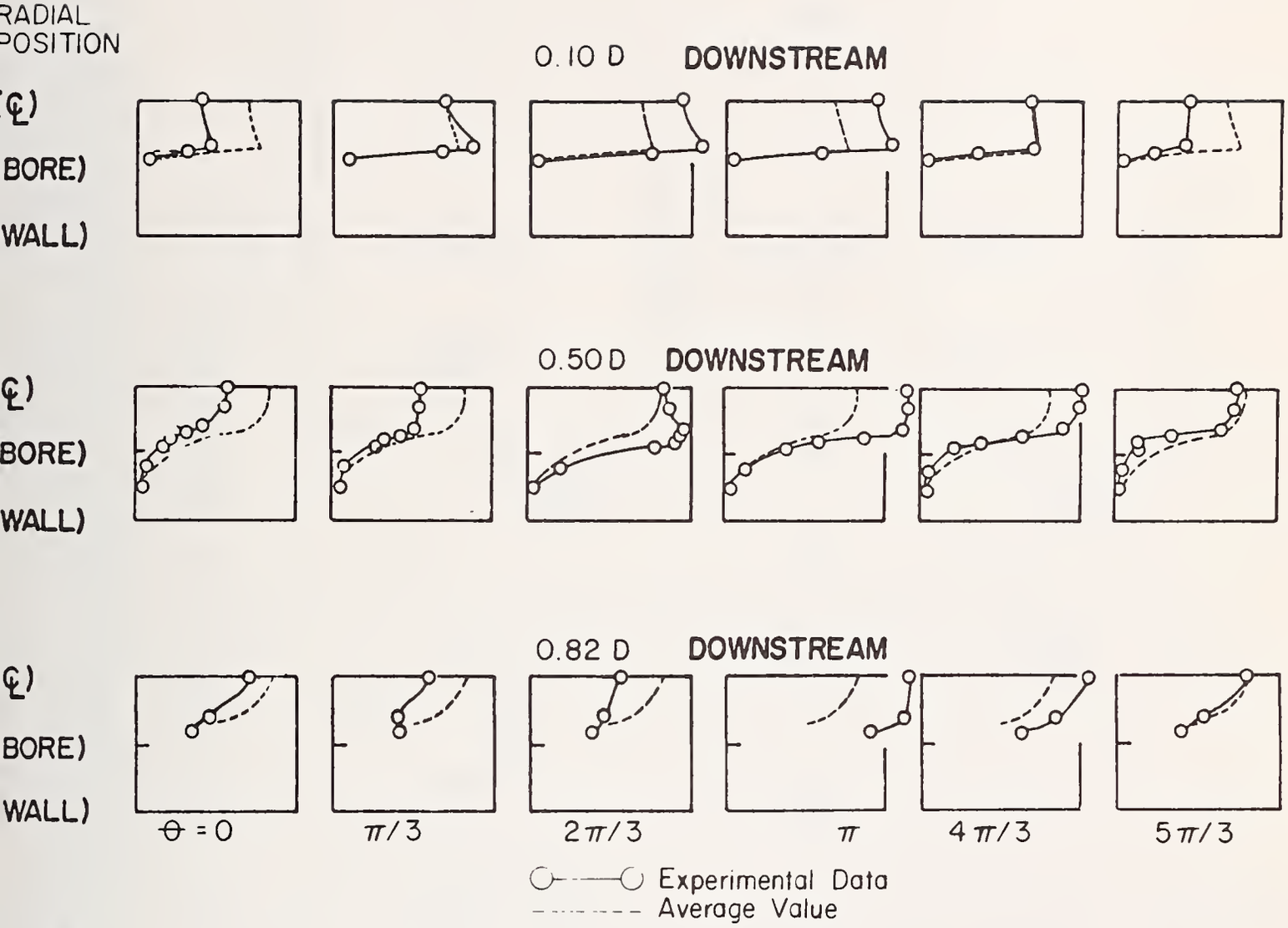

Figure 7. Ensemble-Averaged Axial Velocity Profiles for Six Equally Spaced Intervals in the Cycle of Pulsation for a 0.50 Beta Ratio Orifice at R_D = 17,000, 2.8 hz, 27% RMS Flow Pulsation Amplitude, S = 0.14.

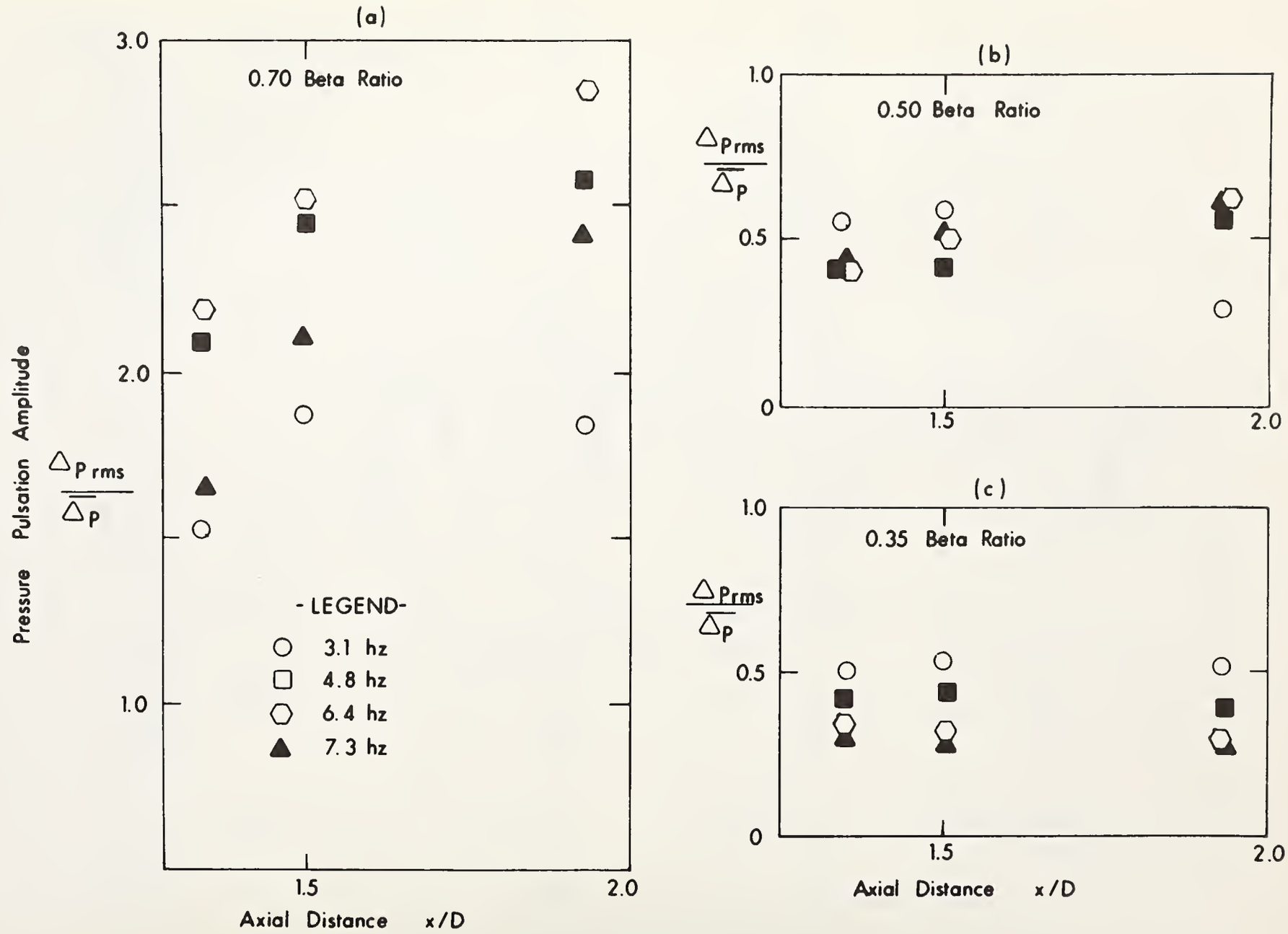

Figure 8. RMS Fluctuation in the Differential Pressure Across the Orifice as a Function of the Separation Distance Between Pressure Taps for the Tap Combinations: D-Flange, D-D/2, and Vena Contracta (0.35 Beta Ratio).

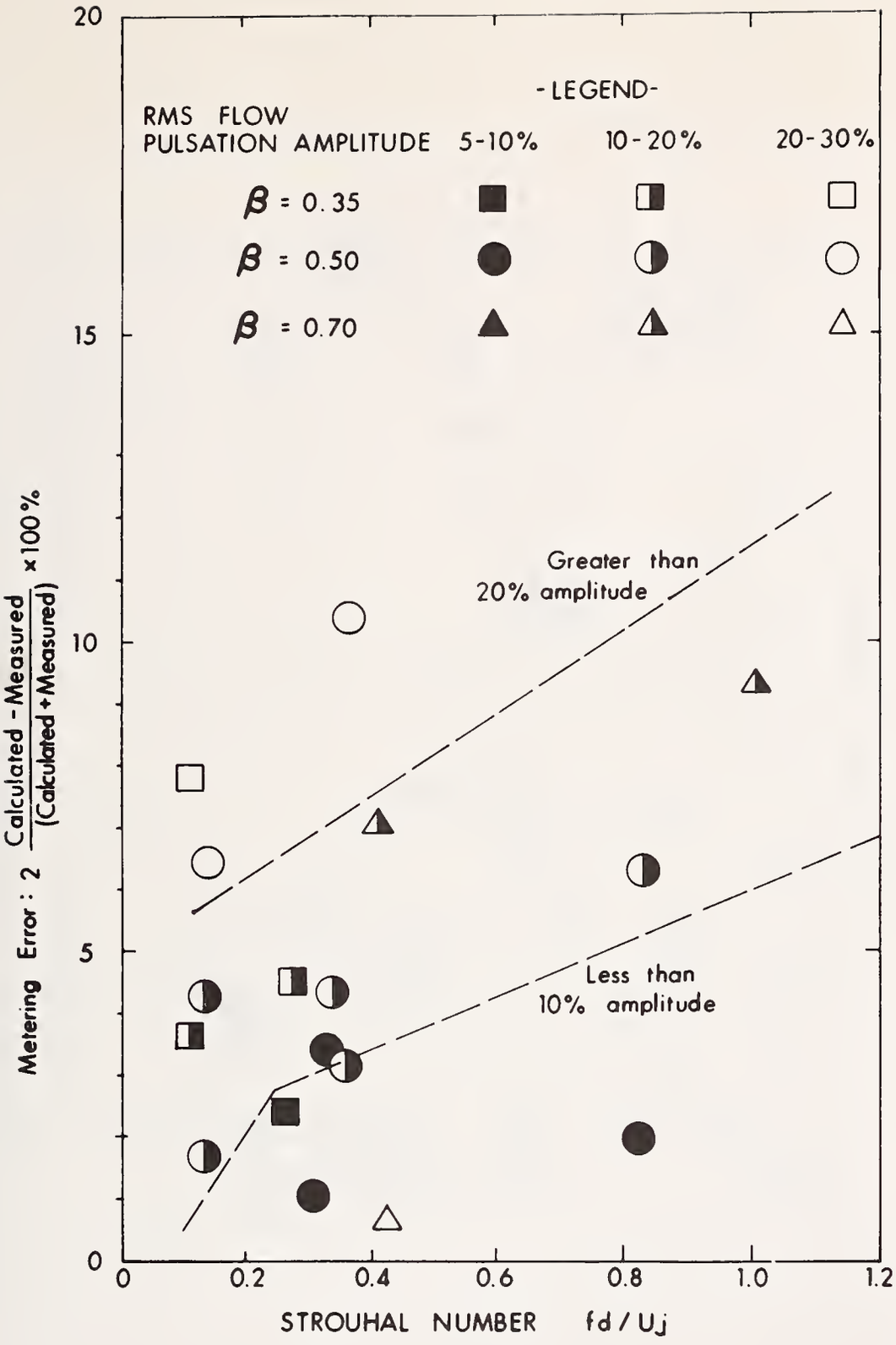

Figure 9. Metering Error as a Function of Strouhal Number and Amplitude of Pulsation in Flow for D-D/2 Pressure Taps.

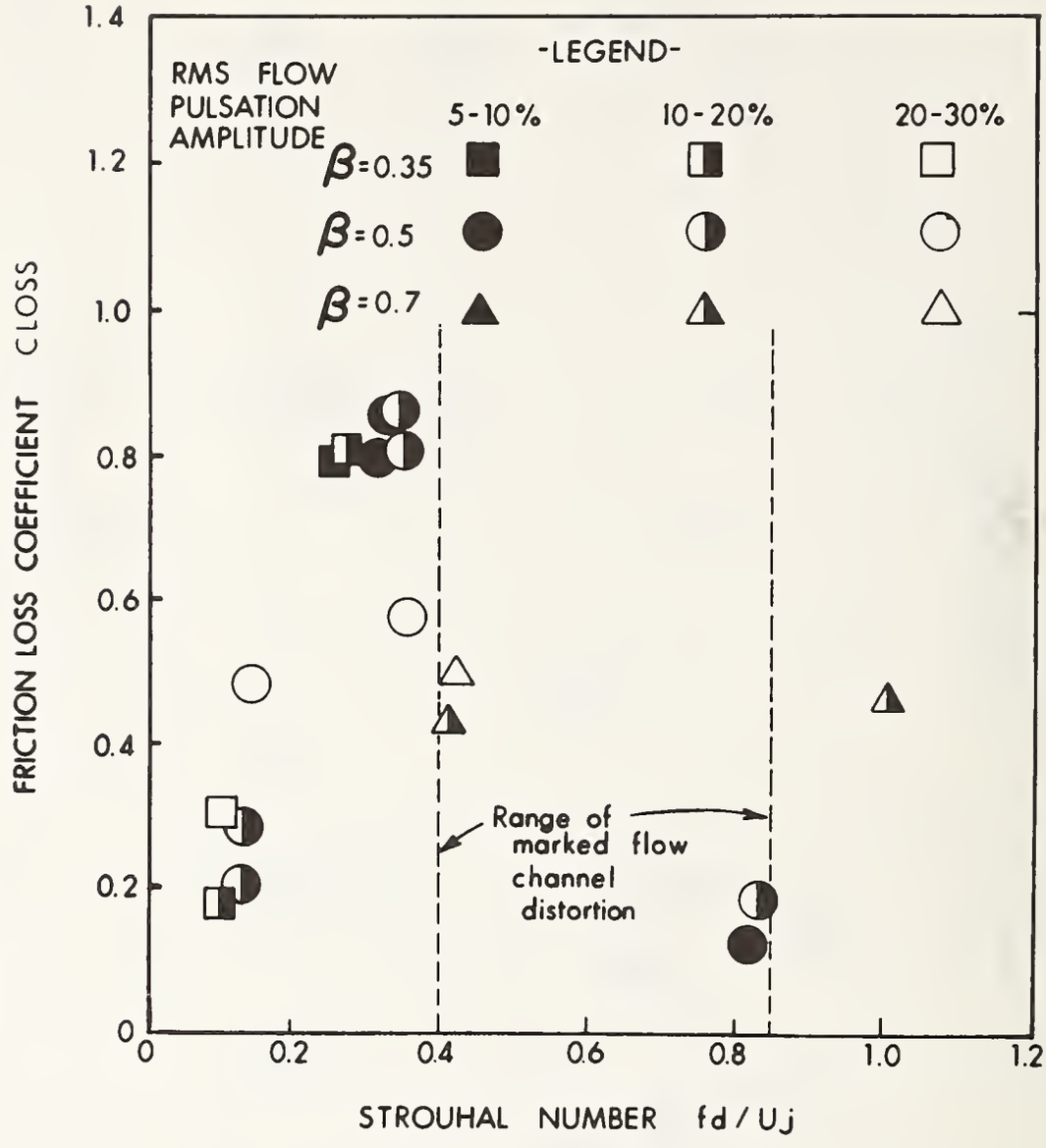

Figure 10. Dependence of Friction Loss Coefficient on Strouhal Number and Pulsation Amplitude.

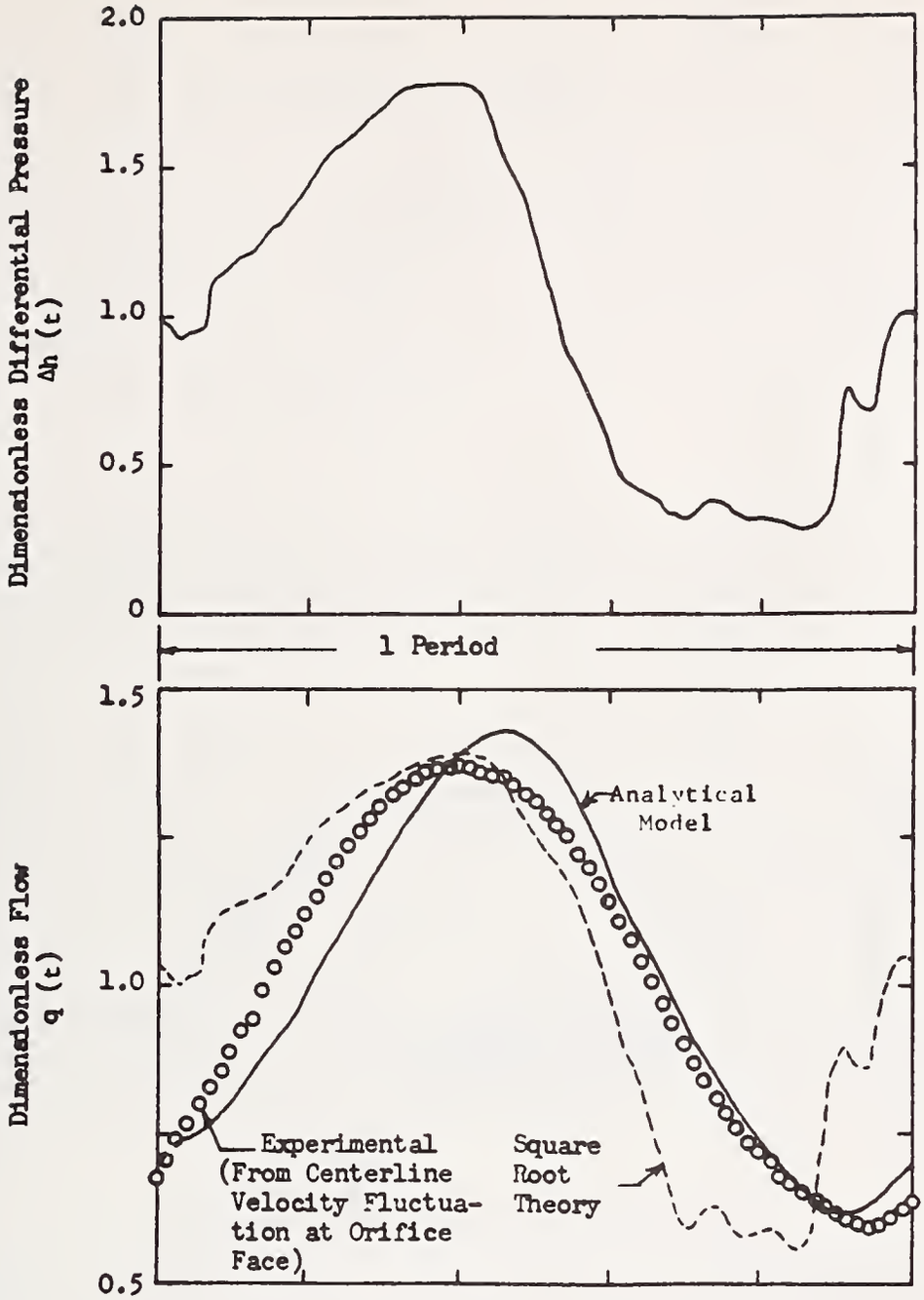

Figure 11. Comparison of Analytical Models with Experimental Velocity Waveform for a Strouhal Number of 0.14. Beta Ratio = 0.5, 27% Flow Pulsation Amplitude.

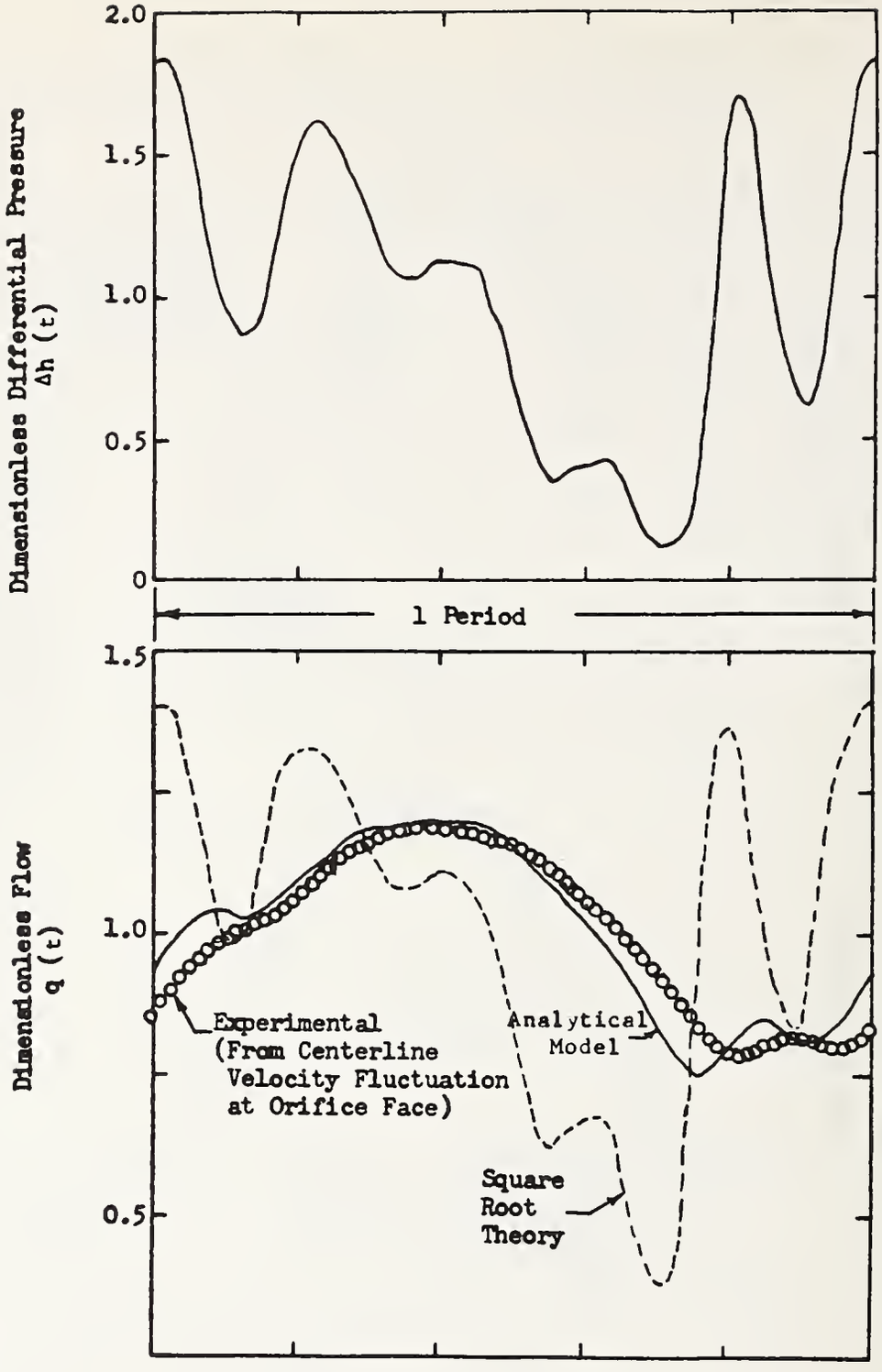

Figure 12. Comparison of Analytical Models with Experimental Velocity Waveforms for a Strouhal Number of 0.34. Beta Ratio = 0.5, 14% Flow Pulsation Amplitude.

National Bureau of Standards Special Publication 484, Proceedings of the Symposium on Flow in Open Channels and Closed Conduits held at NBS, Gaithersburg, MD, February 23-25, 1977. (Issued October 1977)

A VORTEX FLOWMETER - CALIBRATION RESULTS AND APPLICATION EXPERIENCES

R. W. Miller, J. P. DeCarlo, and J. T. Cullen

The Foxboro Company
Foxboro, Massachusetts 02035 U.S.A.

Key Words: Vortex shedding; linearity; shedding frequency; vortex flowmeter; vortex generating element.

1. Introduction

Over the past few years the vortex flowmeter has come into prominence because of its potentially high degree of accuracy and low cost. Although several meter manufacturers offer this type flowmeter, little calibration data has been published to support specifications that are claimed.

The purpose of this paper is to present a substantial body of calibration data on a particular vortex flowmeter design. Over 1300 data points on 167 meters in 2" (50 mm), 3" (75 mm), and 4" (100 mm) line sizes were obtained in a high quality hydraulic test laboratory. These data are statistically analyzed to arrive at specifications for this particular type of vortex flowmeter. These results are not necessarily representative of the performance of any other vortex flowmeter design.

This paper will not deal with the theoretical aspect of vortex shedding, of which little is known, but will describe the broad fundamentals of vortex shedding. Details of the experimental and fluid mechanic studies necessary to design a practical industrial type flowmeter are left to the reader's imagination.

2. General Description of Flowmeter

Generally, vortex flowmeters are made up of three parts: a vortex generating element fully spanning a pipe, a sensor to convert the vortex shedding energy into an electrical pulse signal, and a transmitter for signal amplification and conditioning. The significant differences between vortex flowmeter designs are the shape of the element, the complexity of the sensor, and the location of the electronic transmitter. These three factors affect performance, as well as cost.

Vortex flowmeters measure flow rate by detecting pressure or velocity changes in the flow field resulting from the periodic generation and shedding of vortices. Vortices are rotational flow zones that form and shed alternately, as shown in Figure 1, at a frequency proportional to the fluid velocity [1].[1] Associated with these vortices is a sinusoidal differential pressure, which is created aft of the generating body. By sensing the sinusoidal differential pressure, the frequency of vortex shedding and hence the fluid velocity is determined. For a given line size, a vortex

[1]Numbers in brackets refer to references given at the end of this paper.

flowmeter may then be considered a volumetric type flowmeter suitable for both a flow rate measurement (gal/min;m^3/s) and totalizing (gals;m^3).

The presence of the vortex generating element causes the separation of fluid particles that form a shear layer, where a high velocity gradient exists. The fluid within the shear layer is inherently unstable and breaks down after some length of travel into well-formed vortices. At the outer extremities of the vortices, called the edge of the wake, there exists a zone of random fluid turbulence. The edge of the wake represents the extrapolated path of the shear layer if the layer could remain stable without vortex formation.

The shear layer is a complex fluid mechanic phenomenon having a zero velocity at the lower part of the layer and a large velocity gradient through to the upper part of the layer. Some of the fluid necessary to feed the vortex is drawn from the lower part of the layer, and it is this fluid feed that is believed to lead to instability in the layer and to initiate the vortex shedding.

A region extending upstream from the point where the shear layer breaks down is normally referred to as "outside" the wake. The region inside the lower part of the layer to the point of shear layer breakdown is commonly referred to as "inside" the wake.

Within the shear layer and at its upper extremity random turbulence exists. When the layer begins to break down, pressure and velocity changes exist that are at the vortex shedding frequency, close to the shedding frequency, or completely random in nature.

Consequently, detecting the vortex shedding frequency outside the wake, particularly after the layer breakdown point, is difficult and requires sophisticated filtering and sensitive detector schemes. Care also must be taken to ensure that the detector configuration does not alter the basic flow field.

3. The Foxboro Vortex Flowmeter [2]

The vortex generator shape was designed for detecting vortex shedding inside the wake where the dominant vortex frequency exists. When viewed from the inlet end, the vortex generator appears as a simple rectangular plate with a width (h) to meter bore (D) ratio of approximately 0.27, Figure 1. In terms of blockage, the net flow area approximates a 0.8 beta ratio orifice plate. When viewed in cross section, the vortex generator appears as a flat plate with a centered tail, Figure 2. Vortex shedding generates an alternating differential pressure across the differential pressure sensor located within the tail.

This vortex flowmeter uses a particular shape of vortex generating element. Its shape evolved in conjunction with the type sensor employed. The sensor, a rugged piezoelectric differential pressure detector, is completely sealed from the process fluid and located in a "quiet" fluid zone on the vortex generating body. In addition, the location of the sensor is protected from the impacting of any solid particles carried by the flow stream. In the development phase, the type of sensor and sensor location played just as important a role in determining the vortex generator shape as did the performance potential of the shape itself.

A thorough research and development program was initiated to study the effects of vortex generator body shapes on the performance of a vortex flowmeter. Hundreds of tests and thousands of hours of data analysis finally resulted in a vortex element shape that is essentially a flat plate. However, a tail type section mounted downstream of the flat plate proved to be a significant factor in the control of stable vortex shedding. Specifically, the geometry of the end of the tail section proved to be a critical vortex-stabilizing control parameter. In addition, the tail section served as an excellent location for a sensor. The flow zone inside the wake surrounding the tail is low in noise, consequently the signal-to-noise ratio is high. Because the tail is behind the flat plate, the plate also acts as a shield to prevent damage to the sensor.

The flowmeter's primary device, Figure 3, consists of a wafer-style housing, a removable vortex element with integrally mounted differential pressure sensor, and associated mounting hardware.

The integral secondary device consists of a two-compartment electrical housing; the amplifier compartment contains the electronics; the junction box compartment contains the wiring terminals and optional flow rate indicator. The amplifier options are: (1) amplified and conditioned voltage pulse output, or (2) a 4-20 mA analog output.

4. Flowmeter Performance

Vortex flowmeter performance is similar to that of a turbine meter. The frequency of shedding is linear with pipeline velocity, and hence to the volumetric flow rate for a given bore. In the case of a turbine flowmeter, the rotational speed of the blades is proportional to pipeline velocity. By counting the blades passing a fixed point, the flow rate is determined. Because of the similarity in both readout and the relationship to volumetric flow rate, the accepted terminology and performance standards for turbine meters [3] were selected to present the data. The ISO Standard [4] is used to establish accuracy specifications.

The relationship between input (volumetric flow rate) and output (pulse rate) defines the flow "coefficient". This relationship, expressed as the ratio of pulse rate to volumetric flow rate, is called the K-factor. The units are pulses/unit volume (pulses/gallon, pulses/cubic metre, etc.).

A plot of the K-factor against the pipe Reynolds number (R_D) establishes a signature curve. Because the K-factor remains essentially constant for pipe Reynolds numbers greater than 10,000, a mean K-factor is used to characterize the flow performance over a designated flow rate range. A linearity band, expressed as a percentage, defines the performance over the designated linearity range. This band is calculated from the maximum and minimum K-factor determined by a flow calibration.

The mean K-factor is:

$$\text{Mean K-factor} = \frac{K_{max} + K_{min}}{2}$$

where K_{max} is the maximum K-factor and K_{min} is the minimum K-factor over the flow rate range, the values of each being determined by a flow calibration.

Two design flow rate ranges were of interest; first, a 1-10 ft./sec. (0.3 - 3 m/s) range, the normal operating range for most pipeline installations, and second, a 1-20 ft./sec. (0.3 - 6 m/s) range encountered in wide turn-down control, batching or totalizing. As is the case in turbine meters, the linearity and "designated" linear range are specified in terms of a water calibration factor. Adjustments to flow rate range limits, due to viscosity effects (Reynolds number) or the minimum velocity the detector would operate, is checked by a simple calculation procedure. Flow tests using oil at varying viscosities confirmed the Reynolds number signature curve, while the differential pressure created by the shedding was experimentally determined as a constant times the product of the fluid density and the square of the pipeline velocity. These factors allow a water test to fully define the operating characteristics and the operating flow rate limits.

In Table 1, the parameters for defining the low velocity limit of the flowmeter as a function of viscosity are presented.

5. Flow Laboratory

Ninety 2-inch (50 mm), fifty-one 3-inch (75 mm), and twenty-six 4-inch (100 mm) flowmeters were calibrated to determine the mean K-factor and linearity.

Calibration work was performed at the Engineering-Development Flow Laboratory of The Foxboro Company, in Foxboro, Massachusetts. The meter run and piping arrangement are illustrated in Figure 4.

Water is brought from a weir type head tank, located 55 feet above the test facility, and similar to that described by Spencer and Hayward [5], into a 6-inch horizontal header located in the main facility. This header branches into a permanently installed 4-inch (100 mm) test meter run. Flow straighteners are located upstream of the meter test section. These flow straightener are of the multiple-multiholed type [6]. They consist of three multiholed 1/4-inch (6.3 mm) thick circular plates mounted in series with approximately 2 inches (50 mm) between plates. Downstream of the meter run are 29 pipe diameters of straight horizontal pipe. A vertical length of pipe with a throttling valve leads to the flow nozzle diffuser and diverter system. The diverter and nozzle diffuser are similar in construction to those described by Shafer and Ruegg [7]. The flow is directed into the 10,000 lbs. (4536 kg) calibrated weigh receiver or returned to the reservoir by the diverter system. The mass rate of flow is calculated as the collected mass, corrected for buoyancy and scale calibration, divided by the measured test time interval.

Eight calibration points were obtained on each flowmeter over a velocity range of approximately 1-20 ft./sec./ (0.3 - 6 m/s). The meter's output pulses were gated and counted when the diverter directed the flow into the calibrated weigh receiver. The count was stopped when the flow was redirected into the reservoir.

The actual K-factor, at each flow rate point, is calculated as the recorded pulses divided by the volume of water collected. Volume is derived from the mass of collected water and the water density values given in ASME Steam Tables [8] of water density as a function of temperature. It is estimated that the random systematic error, in the determination of volumetric flow rate, is ±0.1 percent and that the random uncertainties including counters, timers, and scales are ±0.15 percent computed for a 95 percent confidence level.

6. Data Analysis

A typical 2-inch (50 mm) flowmeter calibration plot is shown in Figure 5. Similar plots were made for the 167 flowmeters tested to date. Plots were generated on a high speed plotter after the laboratory data had been computer-calculated to determine the actual K-factor at each flow rate point. The plus symbols are actual test points plotted on the ordinate as a percentage deviation from the mean K-factor established over the range of velocities shown on the abscissa. The upper and lower dashed lines run through the minimum and maximum K-factors and represent the upper and lower linearity limit over the entire test range. The average of these points is the mean K-factor, and the percent deviation is the linearity over the designated flow rate range.

The calculated mean K-factor and linearity over three designated linear ranges are indicated on each plot. Reading from left to right, the first is for the complete range tested, the second a nominal 1-10 ft./sec. range (0.3 - 3 m/s), and the third a 1-20 ft./sec. (0.3 - 6 m/s). For this particular flowmeter, the linearity (±.28 percent) and mean K-factor (24.187) are independent of the linear range selected. The linearity is expressed as a percent of flow rate reading.

This was generally true of the 2-inch (50 mm) and 3-inch (75 mm) flowmeters, because the minimum and maximum K-factors occurred within the 1-10 ft./sec. (0.3 - 3 m/s) range. This is not true, however, for the 4-inch (100 mm) flowmeter where the minimum K-factor, because of a higher Reynolds number, occurred at approximately 20 ft./sec. (6 m/s).

In Figure 6 are shown all the data points (435) taken on fifty-one 3-inch (75 mm) flowmeters. These points are plotted as the percent difference of each point from the average of the mean K-factors for all fifty-one flowmeters over the entire flow rate range. The upper and lower dashed lines are the uncertainty limit of the data (statistically referred to as upper and lower range) calculated for a 95 percent confidence level (±2 sigma). The 95 percent confidence level uncertainty limit was selected because it is the international standard proposed for specifying flowmeter uncertainties [4].

The standard deviation estimate was calculated in accordance with ISO/DIS 5168 [4]. The range of values within which the mean K-factor and linearity are expected to lie, at a 95 percent confidence level, is calculated as:

Range of Mean K-factors

$$R_{\bar{K}} = \bar{K} \pm t\, S_K \tag{1}$$

where: $\bar{K}$ = Average Mean K-factor

t = Student "t" value at a 95 percent confidence level. [4]

and $$S_K = \left[\frac{\sum_{i=1}^{i=n} (K - \bar{K})^2}{n - 1}\right]^{\frac{1}{2}} \tag{2}$$

with: K = Mean K-factor for each flowmeter.

$\bar{K}$ = Average of Mean K-factors for (n) flowmeters.

n = Number of flowmeters.

Range of Linearity

$$R_{\bar{L}} = \bar{L} \pm t\, S_L$$

where: $\bar{L}$ = Average Linearity of n flowmeters.

S_L = Standard deviation estimation calculated from Eq. 2.

Sigma was adjusted using the student's "t" method for the estimation of sigma for a 51 sample size. These statistical calculations are covered in detail in reference [4].

The ±0.71 percent two sigma value, computed for the 3-inch (75 mm) flowmeters, includes not only linearity but the inherent systematic differences between flowmeters when tests are conducted on multiple flowmeters.

In the case of vortex flowmeters, as with turbine flowmeters, the performance specifications are given as a mean K-factor, established by flow calibration and a linearity specification over a specified linear flow rate range. This linearity value may be based on the actual calibrated curve or more generally as an upper limit value below which all the data is expected to fall for a 95 percent confidence level.

If twice the standard deviation, corrected by the use of student "t" for sample size, is computed, and the value of each flowmeter mean K-factor is used to eliminate systematic differences between flowmeters, the data point plot of Figure 7 is obtained.

The heavy lines represent the averaged linearity over the entire flow rate range, and the dashed lines represent the lower and upper linearity uncertainty limits. Within these two dashed lines, the linearity of 95 percent of all flowmeters tested, or the linearity of any future flowmeters, are estimated to fall.

Similar plots and statistical computations made for each line size and for two designated linear range (1-10 ft./sec. and 1-20 ft./sec.; .3 - 3 m/s and .3 - 6 m/s) are not presented here because of repetition and lack of space. Table 2 lists the mean K-factors and linearities for the 167 flowmeters.

Of the 167 flowmeters tested, two early production 2-inch (50 mm) and one 3-inch (75 mm) flowmeters were outliers as indicated by the Thomson's Tau (τ) technique [4] or Dixon's illegitimate error test [4]. These flowmeters, marked by an asterisk in Table 2, were considered outliers and excluded in the final computation of the mean and standard deviations of both the mean K-factor and linearity values. It should be noted, however, that their inclusion only affects the results by $\leq \pm 0.05$ percent.

Table 3 summarizes the test results. The average mean K-factor ($\overline{K}$) and range of values within which the mean K-factors are expected to lie for a 95 percent confidence level are presented for the two designated linear ranges (1-10 and 1-20 ft./sec. or 0.3 - 3 and 0.3 - 6 m/s).

For example, the 2" (50 mm) flowmeters have a mean K-factor of 24.129, and the values range ±0.77 percent about this mean. Ninety-five percent of these meters, or future meters, would be expected to have a mean K-factor ranging between 23.943 and 24.315 if water tested over a 1-10 ft./sec. (0.3 - 3 m/s) range. This uncertainty in the mean K-factor is academic, since each flowmeter was calibrated, and the mean K-factor established, within the flow laboratory accuracy limits previously stated. However, if, in the future, uncalibrated flowmeters are used, these values would be the assigned mean K-factor "tolerance"; analogous to the tolerance assigned to orifice, venturi, or flow nozzles.

It should be noted, however, that only one 2" (50 mm) meter was outside this estimated range. Therefore, it is felt that the range limits presented are conservative.

The lower half of Table 3 presents the mean linearity ($\overline{L}$) and the random uncertainty (tS_L) over the two designated flow rate ranges. For example, the 3" (75 mm) flowmeters had a mean linearity of ±0.43 percent with a random uncertainty (tS_L) of ±0.21 percent when tested over a nominal 1-10 ft./sec. (0.3 - 3 m/s) flow rate range. Ninety-five percent of all 3-inch (75 mm) flowmeters tested are estimated to have a linearity ranging between ±0.22 and ±0.64 percent. For a nominal 1-20 ft./sec. (0.3 - 6 m/s) flow rate range these values are ±0.25 to ±0.63 percent.

7. Flowmeter Accuracy Specifications

The accuracy of a measurement may be characterized by giving the random uncertainty to be expected and the systematic uncertainty bounds [4, 9, 10]. For this particular test work, the laboratory and the mean linearity would constitute the systematic errors, assuming these errors are randomized. The random uncertain portion is the computed uncertainty (tS_L) with respect to the average linearity, with the assumption that the ±0.15 percent laboratory random uncertainty is included in the estimated linearity uncertainty (tS_L)

The overall uncertainty over a given flow rate range can be computed as:

$$\text{Overall uncertainty} = \sqrt{e_S^2 + \bar{L}^{-2} + (e_R)_{95}^2}$$

with a random uncertainty of

$$(e_R)_{95} = \frac{(tS_L)}{\sqrt{n}}$$

where n = number of flowmeters tested in a given line size.

For example: the 3" (75 mm) flowmeter has an overall estimated uncertainty over a 1-20 ft./sec. (0.3 - 6 m/s) flow rate range of

$$\text{Overall uncertainty} = \sqrt{0.1^2 + .44^2 + .19^2} = \pm 0.49\%$$

NOTE: To be conservative the random uncertainty (tS_L) of 0.19 percent was not reduced by $\sqrt{n}$ in the above computation.

The random uncertainty would be:

$$(e_R)_{95} = .19/\sqrt{51} = \pm 0.03\%$$

Although recommended by ISO/DIS 5168, it is confusing to some readers to give both components in an accuracy statement. The authors prefer to algebraically add the overall uncertainty and the random uncertainty computed above to arrive at a conservative estimate of the maximum errors to be expected, and to call this accuracy.

In Table 4, the accuracy specifications for the three line size flowmeters calibrated are presented to the nearest tenth of a percent.

8. Application Experiences

Since the release of the Foxboro Vortex Flowmeter, applications for the device have been found in the five basic areas of batching, control, totalizing, recording, and blending. Some examples of field trial applications are shown in Table 5.

Meters that were on field trial and used with such fluids as ammonia, ammonia sulphate, and hydrocarbons, were recalibrated at the Foxboro RD&E Laboratories after several hundred hours of field operation. The results of a comparison of the before and after field-test calibrations indicated no change in linearity and a mean meter factor (K-factor) within ±0.1 percent of the factor stamped on the meter data label. Two calibration data sets, one taken before and one taken after field use, are shown in Figure 8. Note, the agreement between the two calibration data sets is within the estimated random uncertainty for the data.

9. Conclusions

In order to achieve confidence in the specifications for a flowmeter, the number of units tested should represent a valid statistical sample. Using a statistical approach in the analysis of data correlates numerous data points and portrays the results in terms familiar to the user. It is expected that others will consider using statistical procedures as outlined in ISO Standards so that flowmeters may be compared on some common basis.

Based on the data obtained from the 167 flowmeters tested under reference laboratory conditions, these vortex shedding type flowmeters consistently provide an accuracy of ±0.5 percent over a 10 to 1 flow rate range. This accuracy is in percent of actual flow rate reading.

Application experience shows that no performance degradation occurred after considerable in-line use.

10. References

1. Lamb, Sir Horace, "Hydrodynamics", Dover Publication, Sixth Edition.

2. The Foxboro Company, PUB 416, "E83 Series Vortex Flowmeter".

3. International Standard ISO/2715, "Liquid Hydrocarbons - Volumetric Measurement of Turbine Meter Systems".

4. International Standard ISO/DIS 5168, "Measurement of Fluid Flow - Estimation of Uncertainty of a Flow Rate Measurement".

5. Spencer, E. A., and Hayward, A. T. J., "The Accurate Calibration of Flowmeters with Water", Trans. of the Society of Instrument Technology, Volume 9.

6. Sprenkle, R. W., and Courtright, N. S., "Straightening Vanes for Flow Measurement", ASME Paper No. 57-A-76.

7. Shafer, M. R., and Ruegg, F. W., "Liquid Flowmeter Calibration Techniques", ASME Paper No. 52-A-70.

8. Meyer, C. A., et. al., "Thermodynamic and Transport Properties of Steam", A.S.M.E., 1967.

9. Filban, T. J. Jr., Shafer, M. R. Jr., "Flow Measurement Standardization", ISA Transactions 1964, New York.

10. "Proceedings of the 1962 Standards Laboratory Conference", NBS Miscellaneous Publication 248, Issued August 16, 1963.

TABLE 1. PARAMETERS FOR LOW VELOCITY LIMIT

Meter Size	Viscosity Centistokes	Minimum Flow Rate Ft./Sec.
2" (50 mm)	$\nu_{cs} \leq 1.6$	$1/\sqrt{G_L}$
	$\nu_{cs} > 1.6$	$.62\ \nu_{cs}$ if $1/\sqrt{G_L}$
3" (75 mm)	$\nu_{cs} \leq 2.2$	$1/\sqrt{G_L}$
	$\nu_{cs} > 2.2$	$0.45\ \nu_{cs}$ if $1/\sqrt{G_L}$
4" (100 mm)	$\nu_{cs} \leq 3.0$	$1/\sqrt{G_L}$
	$\nu_{cs} > 3.0$	$0.34\ \nu_{cs}$ if $1/\sqrt{G_L}$

where G_L = Specific Gravity at line conditions.

TABLE 2. COMPLETE DATA SET FOR ALL FLOWMETERS CALIBRATED

2" (50 MM)

	LINEAR RANGE					LINEAR RANGE					LINEAR RANGE			
	1-10 FT/SEC (.3 - 3 M/SEC)		1-20 FT/SEC (.3 - 6.1 M/S)			1-10 FT/SEC (.3 - 3 M/SEC)		1-20 FT/SEC (.3 - 6.1 M/S)			1-10 FT/SEC (.3 - 3 M/SEC)		1-20 FT/SEC (.3 - 6.1 M/S)	
NO.	MEAN K-FACTOR	LINEARITY	MEAN K-FACTOR	LINEARITY	NO.	MEAN K-FACTOR	LINEARITY	MEAN K-FACTOR	LINEARITY	NO.	MEAN K-FACTOR	LINEARITY	MEAN K-FACTOR	LINEARITY
1	23.807	±.38	23.807	± .38	31	24.117	±.18	24.048	±.47	61	24.040	±.30	24.024	±.37
2	24.293	±.47	24.293	± .47	32	24.108	±.16	24.060	±.36	62	24.094	±.24	24.034	±.49
3*	24.190	±.76	24.119	±1.05	33	24.205	±.29	24.205	±.29	63	24.179	±.29	24.179	±.29
4	24.239	±.12	24.239	± .12	34	23.949	±.13	23.873	±.44	64	24.208	±.17	24.164	±.35
5	24.373	±.65	24.373	± .65	35	24.034	±.14	23.961	±.44	65	24.249	±.37	24.249	±.37
6	24.129	±.40	24.129	± .40	36	24.030	±.11	23.982	±.31	66	24.120	±.12	24.091	±.24
7	24.223	±.50	24.223	± .50	37	24.195	±.35	24.195	±.35	67	24.193	±.36	24.193	±.36
8	24.182	±.34	24.182	± .34	38	24.284	±.28	24.276	±.32	68	24.050	±.32	24.050	±.32
9	24.117	±.13	24.086	± .26	39	24.033	±.49	24.033	±.49	69	24.126	±.11	24.062	±.38
10	24.120	±.19	24.080	± .36	40	24.270	±.52	24.270	±.52	70	24.132	±.14	24.131	±.14
11	24.059	±.21	24.036	± .30	41	24.020	±.20	24.074	±.78	71	24.128	±.57	24.125	±.58
12	23.974	±.16	23.935	± .32	42	24.066	±.30	24.066	±.30	72	24.287	±.61	24.287	±.61
13*	23.997	±.89	23.954	±1.07	43	24.054	±.37	23.965	±.74	73	24.039	±.35	24.015	±.44
14	24.076	±.21	24.008	± .49	44	24.202	±.23	24.193	±.26	74	24.060	±.29	24.035	±.39
15	23.968	±.34	23.941	± .45	45	24.268	±.45	24.268	±.45	75	24.121	±.40	24.121	±.40
16	24.138	±.25	24.100	± .41	46	24.129	±.26	24.080	±.47	76	24.090	±.29	24.052	±.45
17	24.132	±.35	24.088	± .54	47	24.016	±.35	23.978	±.51	77	24.087	±.34	24.044	±.51
18	24.111	±.21	24.111	± .21	48	24.168	±.20	24.153	±.26	78	24.171	±.56	24.167	±.56
19	24.095	±.19	24.049	± .37	49	24.131	±.41	24.131	±.41	79	24.079	±.61	24.058	±.69
20	24.039	±.24	23.980	± .49	50	24.149	±.50	24.149	±.50	80	24.243	±.57	24.243	±.57
21	24.017	±.27	24.017	± .27	51	23.995	±.37	23.995	±.37	81	24.190	±.45	24.190	±.45
22	24.086	±.14	24.048	± .30	52	24.187	±.28	24.187	±.28	82	23.985	±.14	23.959	±.25
23	24.279	±.45	24.279	± .45	53	24.041	±.39	24.030	±.43	83	24.172	±.50	24.151	±.58
24	24.218	±.14	24.180	± .30	54	24.108	±.68	24.108	±.68	84	24.186	±.19	24.159	±.30
25	24.095	±.24	24.063	± .36	55	24.148	±.24	24.151	±.25	85	24.222	±.44	24.222	±.44
26	24.157	±.36	24.149	± .40	56	24.073	±.18	24.052	±.27	86	24.154	±.54	24.145	±.57
27	24.147	±.42	24.147	± .42	57	24.252	±.36	24.257	±.38	87	24.237	±.31	23.237	±.31
28	23.997	±.49	23.997	± .49	58	24.112	±.18	24.073	±.35	88	24.123	±.29	24.064	±.54
29	24.129	±.32	24.115	± .37	59	24.095	±.17	24.095	±.17	89	24.206	±.27	24.158	±.47
30	24.242	±.29	24.185	± .53	60	24.134	±.33	24.111	±.31	90	24.179	±.37	24.179	±.37

3" (80 MM)

	LINEAR RANGE					LINEAR RANGE					LINEAR RANGE			
	1-10 FT/SEC (.3 - 3 M/S)		1-20 FT/SEC (.3 - 6.1 M/S)			1-10 FT/SEC (.3 - 3 M/S)		1-20 FT/SEC (.3 - 6.1 M/S)			1-10 FT/SEC (.3 - 3 M/S)		1-20 FT/SEC (.3 - 6.1 M/S)	
NO.	MEAN K-FACTOR	LINEARITY	MEAN K-FACTOR	LINEARITY	NO.	MEAN K-FACTOR	LINEARITY	MEAN K-FACTOR	LINEARITY	NO.	MEAN K-FACTOR	LINEARITY	MEAN K-FACTOR	LINEARITY
1	8.709	±.45	8.709	±.45	27	8.696	±.49	8.696	±.49	1	3.964	±.13	3.952	±.43
2	8.676	±.63	8.676	±.63	28	8.685	±.44	8.685	±.44	2	3.957	±.38	3.950	±.54
3	8.674	±.51	8.674	±.51	29	8.677	±.49	8.677	±.49	3	3.964	±.27	3.950	±.62
4	8.683	±.37	8.684	±.38	30	8.706	±.44	8.706	±.44	4	3.966	±.37	3.956	±.65
5	8.688	±.50	8.688	±.50	31	8.703	±.52	8.703	±.52	5	3.949	±.12	3.936	±.45
6	8.690	±.66	8.690	±.66	32	8.711	±.29	8.703	±.37	6	3.947	±.34	3.933	±.71
7	8.703	±.38	8.703	±.38	33	8.705	±.30	8.699	±.37	7	3.952	±.14	3.938	±.49
8	8.686	±.51	8.686	±.51	34	8.695	±.28	8.689	±.36	8	3.955	±.35	3.942	±.69
9	8.725	±.41	8.725	±.41	35	8.726	±.32	8.726	±.32	9	3.960	±.21	3.949	±.49
10	8.713	±.14	8.701	±.28	36	8.696	±.59	8.696	±.59	10	3.945	±.32	3.928	±.75
11	8.702	±.49	8.702	±.49	37	8.673	±.51	8.673	±.51	11	3.953	±.43	3.943	±.69
12	8.713	±.39	8.713	±.39	38	8.702	±.47	8.702	±.47	12	3.958	±.14	3.946	±.43
13	8.688	±.44	8.688	±.44	39	8.690	±.35	8.690	±.35	13	3.945	±.48	3.931	±.83
14	8.698	±.50	8.698	±.50	40	8.707	±.34	8.706	±.35	14	3.950	±.26	3.938	±.58
15	8.705	±.36	8.705	±.36	41	8.695	±.41	8.695	±.41	15	3.950	±.15	3.939	±.43
16	8.670	±.50	8.670	±.50	42	8.713	±.27	8.713	±.27	16	3.958	±.17	3.950	±.38
17	8.695	±.38	8.695	±.38	43	8.682	±.27	8.678	±.31	17	3.954	±.31	3.938	±.72
18	8.685	±.41	8.685	±.41	44	8.720	±.34	8.720	±.34	18	3.952	±.31	3.942	±.58
19	8.697	±.47	8.697	±.47	45	8.675	±.36	8.675	±.36	19	3.955	±.39	3.938	±.81
20	8.678	±.56	8.678	±.56	46	8.691	±.51	8.691	±.51	20	3.953	±.31	3.939	±.64
21	8.700	±.32	8.700	±.32	47	8.730	±.27	8.730	±.27	21	3.956	±.26	3.945	±.53
22	8.705	±.50	8.705	±.50	48	8.640	±.60	8.640	±.60	22	3.958	±.24	3.947	±.51
23*	8.663	±.79	8.663	±.79	49	8.698	±.55	8.698	±.55	23	3.952	±.22	3.938	±.56
24	8.664	±.56	8.664	±.56	50	8.717	±.37	8.723	±.43	24	3.959	±.32	3.945	±.65
25	8.700	±.45	8.700	±.45	51	8.689	±.53	8.689	±.53	25	3.957	±.27	3.946	±.56
26	8.693	±.40	8.693	±.40						26	3.955	±.37	3.944	±.67

4" (100 MM)

K-Factor

Designated Linear Range

Line Size	1-10 ft./sec. (0.3-3 m/s) Meter Factor $\overline{K}$ (pulses/US GPM)	1-10 ft./sec. (0.3-3 m/s) Random Uncertainty (tS_K) (%)	1-20 ft./sec. (0.3-6 m/s) Meter Factor $\overline{K}$ (pulses/US GPM)	1-20 ft./sec. (0.3-6 m/s) Random Uncertainty (tS_K) (%)
2" (50 mm)	24.129	±0.77%	24.110	±0.85%
3" (75 mm)	8.6952	±0.39%	8.6946	±0.39%
4" (100 mm)	3.9548	±0.29%	3.9454	±0.35%

Linearity

Line Size	Mean Linearity $\overline{L}$ (%)	Random Uncertainty (tS_L) (%)	Mean Linearity $\overline{L}$ (%)	Random Uncertainty (tS_L) (%)
2" (50 mm)	±.32	±.27	±0.41	±0.24
3" (75 mm)	±.43	±.21	±0.44	±0.19
4" (100 mm)	±.28	±.20	±0.59	±0.25

Line Size	Flow Rate Range 1-10 ft./sec. (0.3-3 m/s)	1-20 ft./sec. (0.3-6 m/s)
2″ (50 mm)	±0.5%	±0.5%
3″ (75 mm)	±0.5%	±0.5%
4″ (100 mm)	±0.4%	±0.7%

TABLE 3. SUMMARY OF VORTEX FLOWMETER PERFORMANCE

TABLE 5. LIST OF FLUID APPLICATIONS

FLUID APPLICATION				
Control	Batching	Totalizing	Recording	Blending
Water	Ammonia	Acetic Acid	Amines	Diethylanaline
Kaprolactam	Vinyl Acetate	Diamine	Chlorine	Gasoline Blender
Sodium Sulfite	Butane	Milk	Bleaching Fluids	
Hypochlorite	Formaldehyde	Wine	Beer	
Urea Solution	Tetra-Methyl-Lead	Urea Solution	Green Liquor	
Phosphoric Acid	Isopropanol	Anhydrous Ammonia	Anhydrous Ammonia	
	Ethylene Oxide	Chlorinated Benzene		
	Platformate	Gasoline		
		Natural Gas Liquid		

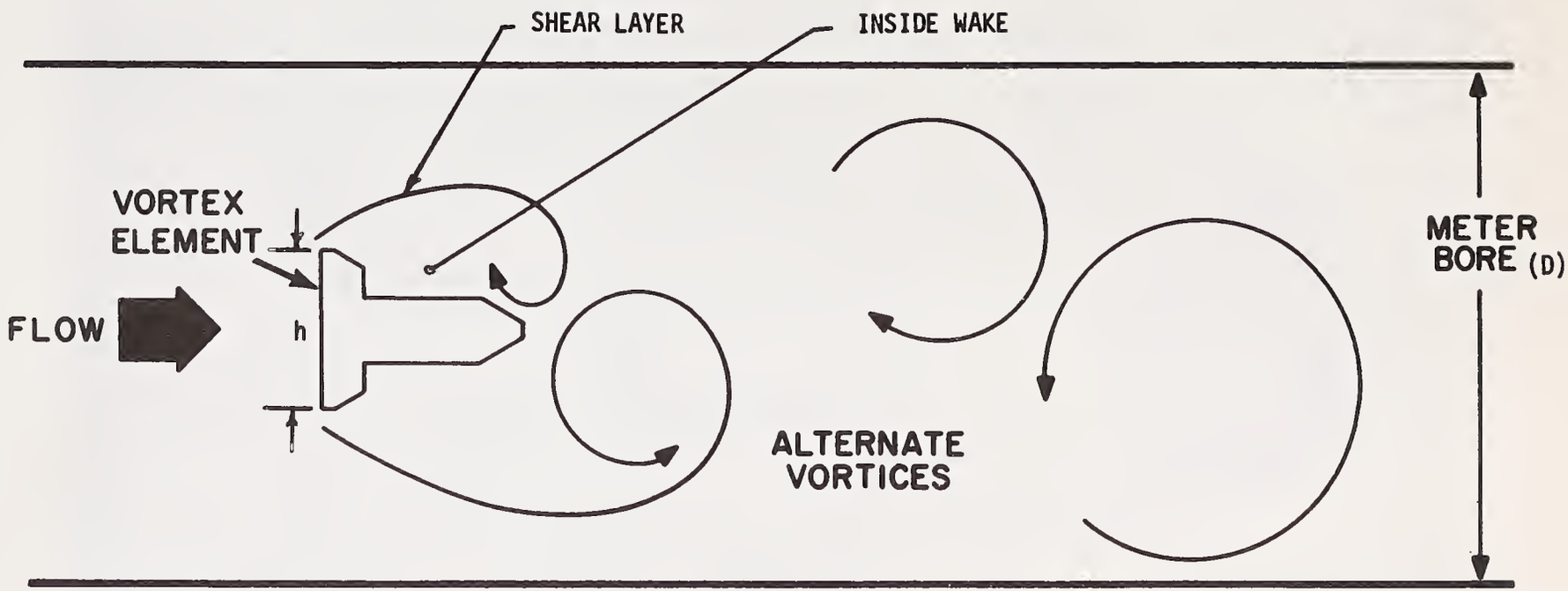

FIGURE 1. SCHEMATIC OF VORTEX FORMATION

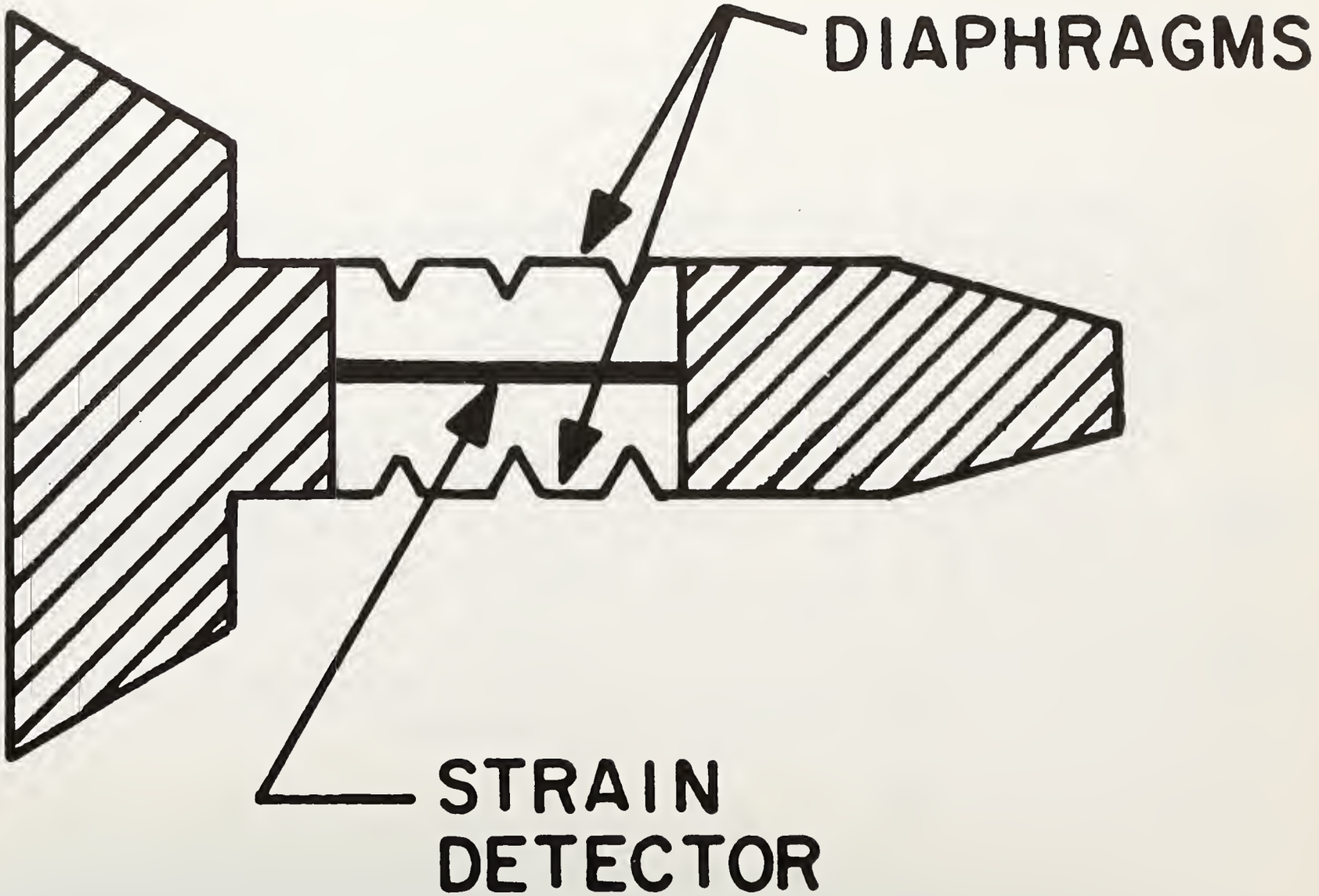

FIGURE 2. VORTEX ELEMENT AND SENSOR

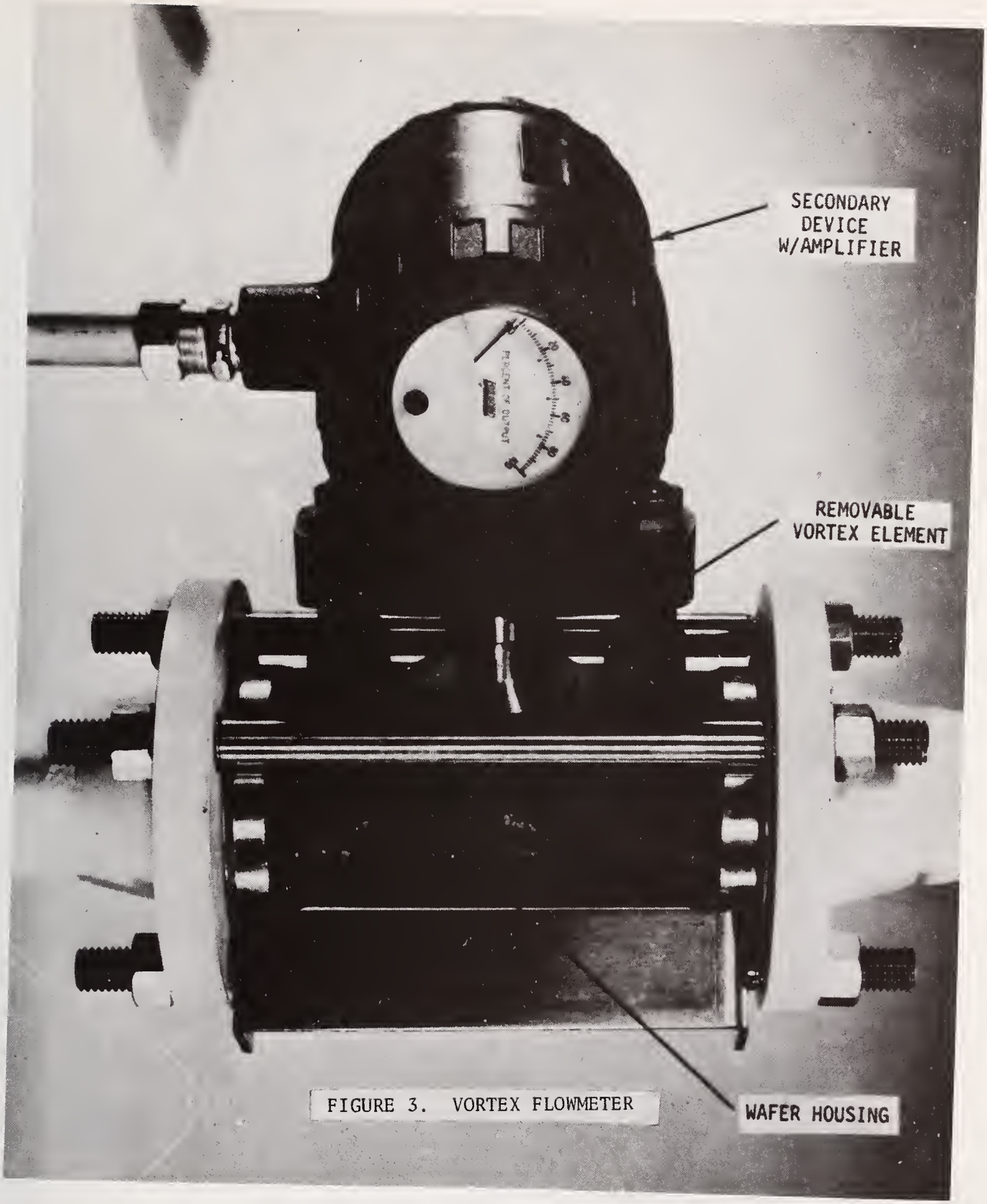

FIGURE 3. VORTEX FLOWMETER

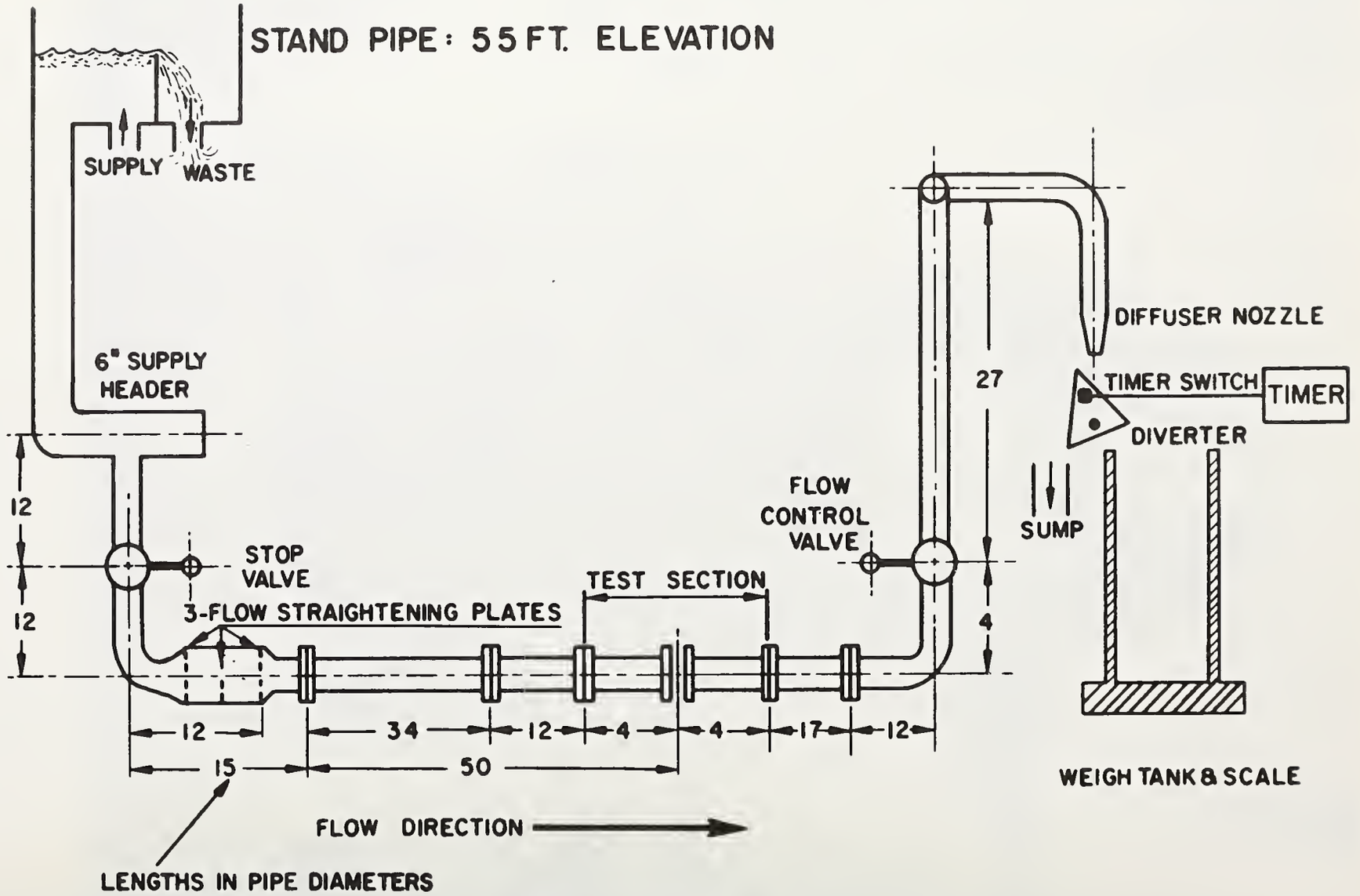

FIGURE 4. SCHEMATIC DIAGRAM OF FLOW LABORATORY

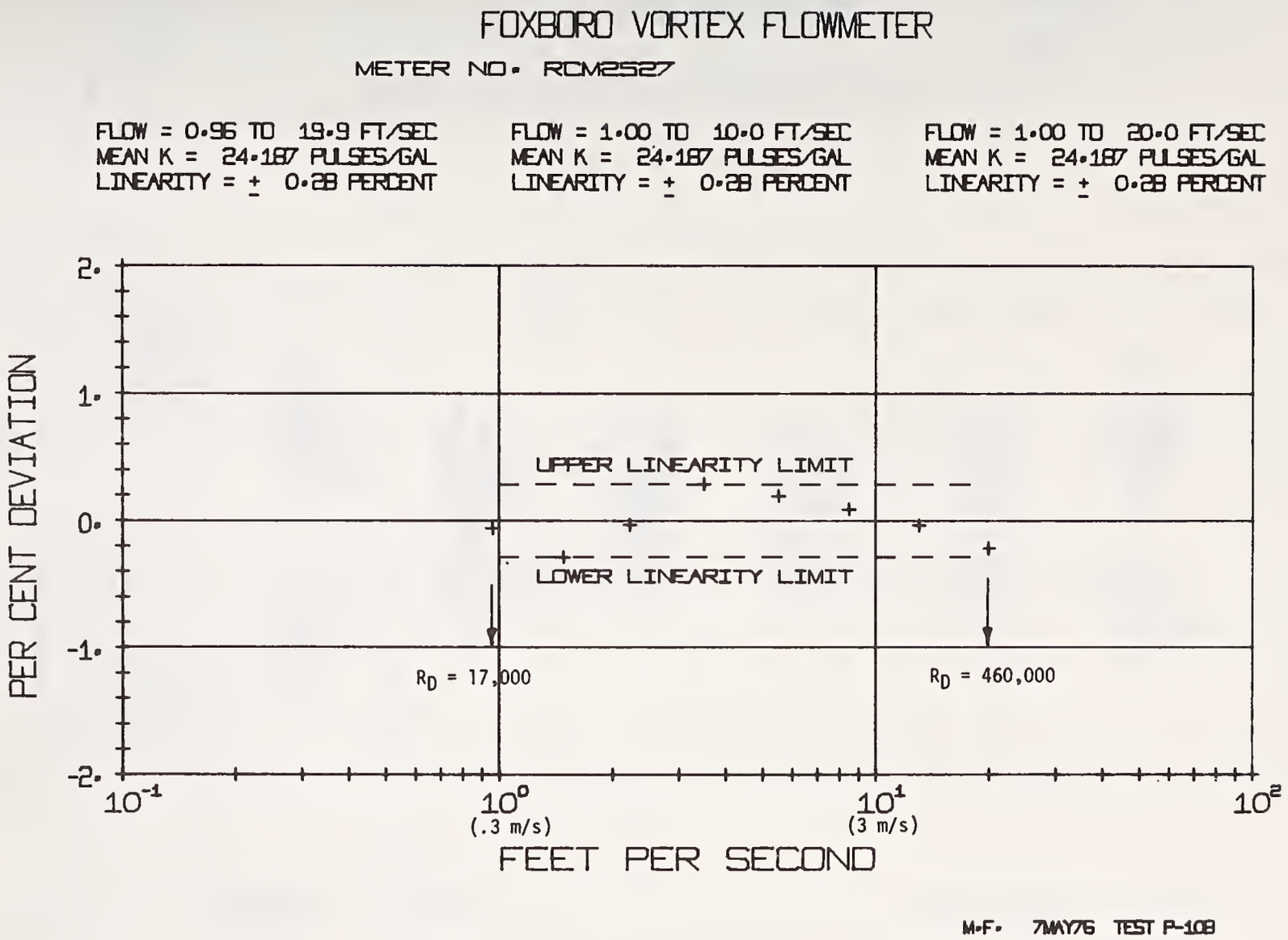

FIGURE 5. TYPICAL 2-INCH FLOWMETER CALIBRATION DATA

3-INCH STYLE A VORTEX METERS

K (PULSES PER GALLON)

P7 - P178

AVERAGE = 8.6946

TWO SIGMA = ± 0.710

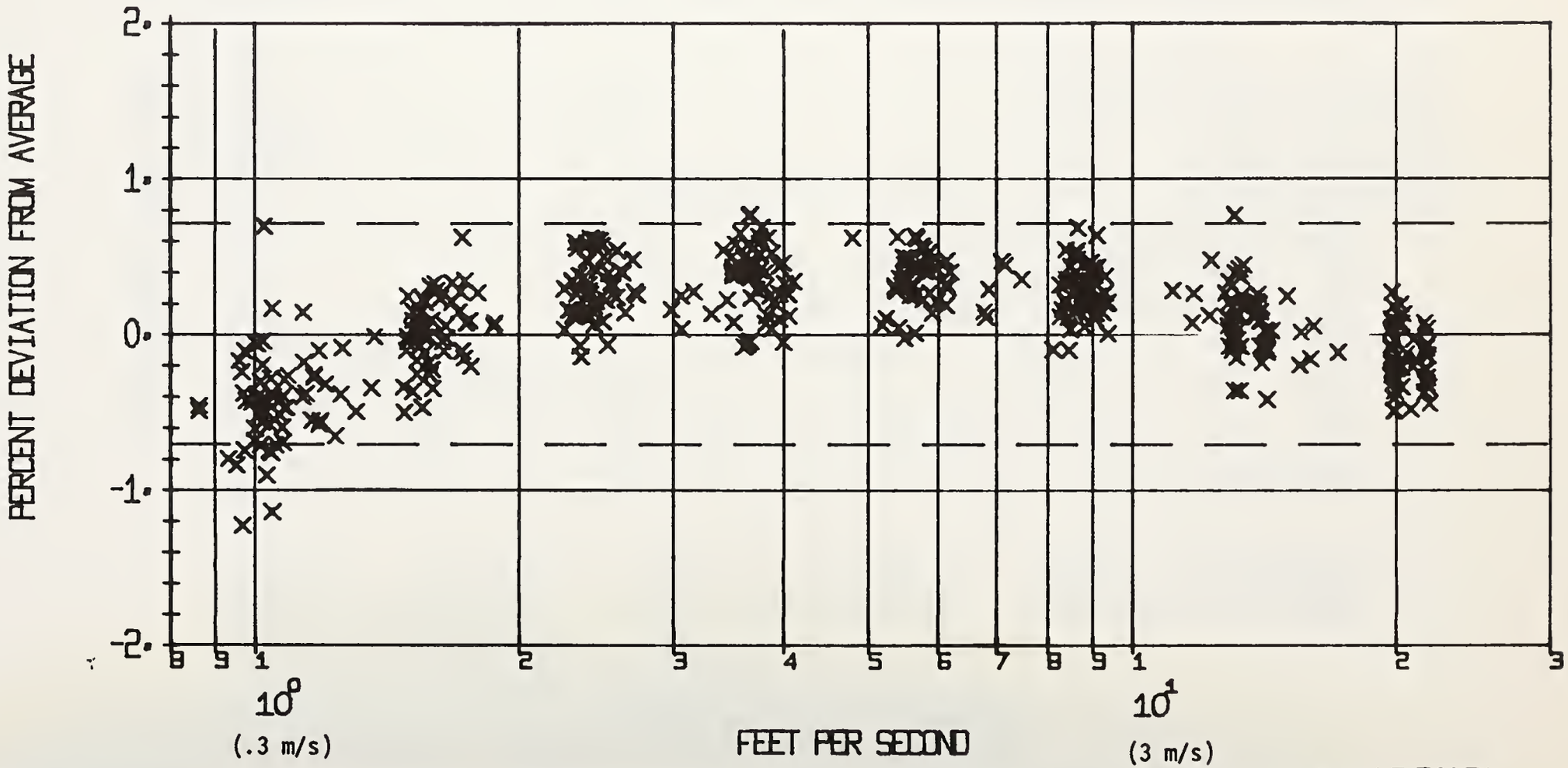

NO. OF DATA POINTS = 435

FIGURE 6. COMPOSITE PLOT INCLUDING METER FACTOR BIAS

BY J.T.OLLEN
DATE 11 OCT 76

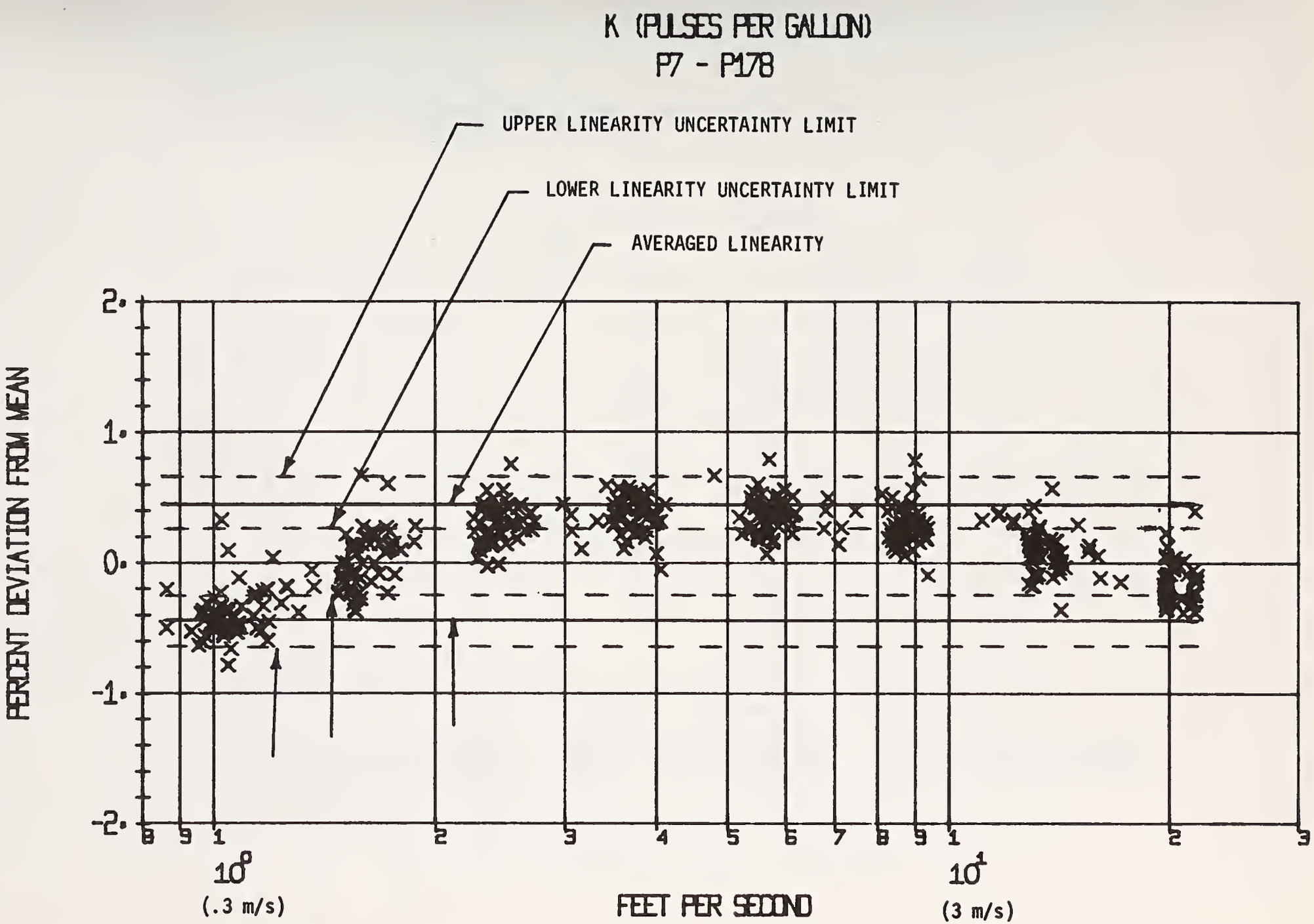

FIGURE 7. COMPOSITE PLOT EXCLUDING METER FACTOR BIAS

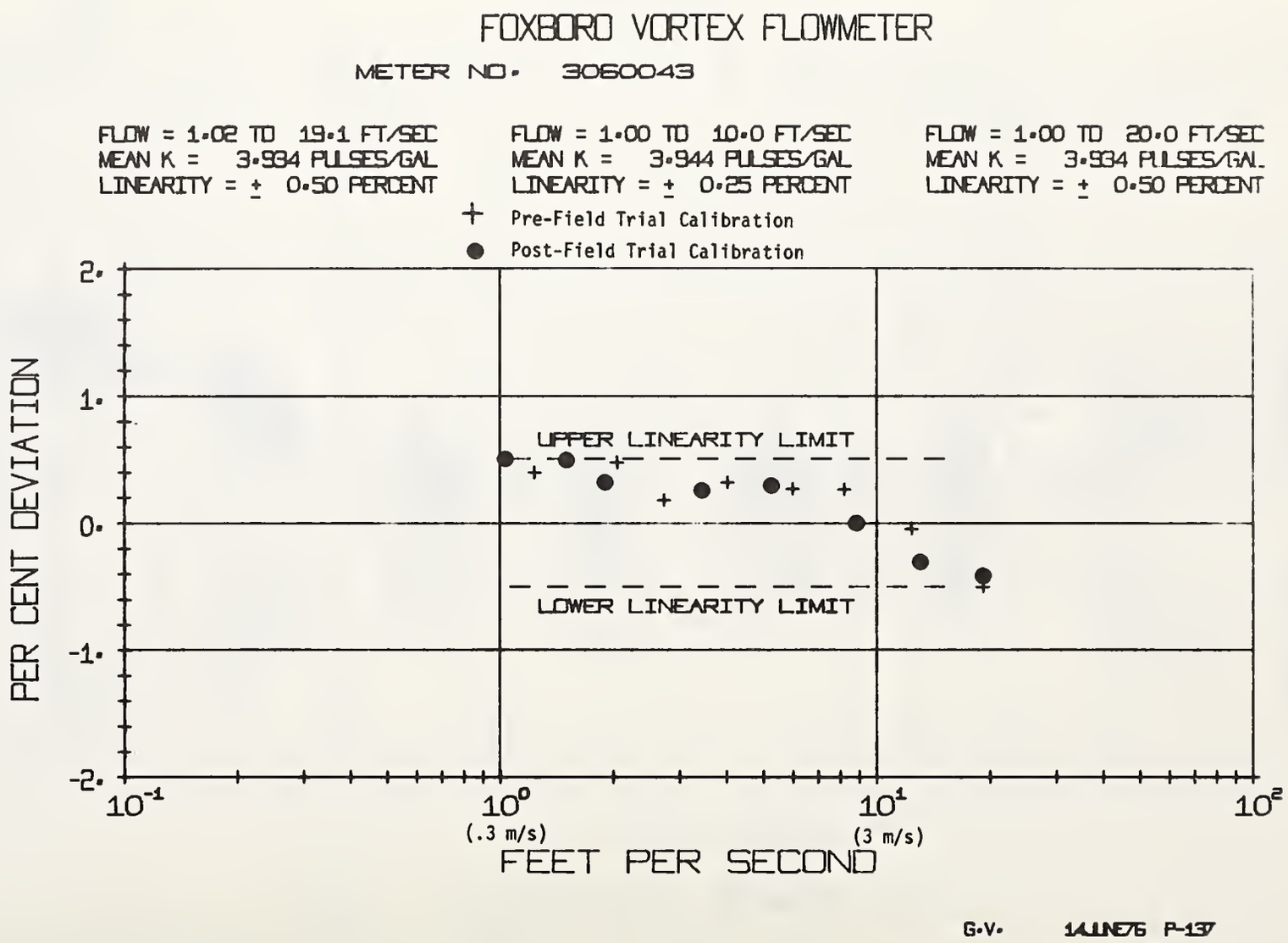

FIGURE 8. COMPARISON OF PRE- AND POST-FIELD TRIAL CALIBRATIONS

National Bureau of Standards Special Publication 484, Proceedings of the Symposium on Flow in Open Channels and Closed Conduits held at NBS, Gaithersburg, MD, February 23-25, 1977. .(Issued October 1977)

TEMPERATURE FIELD MEASUREMENTS IN TURBULENT THERMALS

Mohamed Gad-el-Hak

Flow Industries, Incorporated
Kent, Washington 98031

Laboratory studies of buoyant vortex bubbles and thermals in an unstratified atmosphere are presented. Thermals are generated by filling a soap bubble with a combustible mixture and igniting it with an electrical spark. These are compared to the thermals produced by igniting a similar mixture inside a cylindrical box with a sharp-edged orifice at its top. Detailed temperature field measurements are obtained using an array of hot-wire probes operating at low overheat. The temperature signals are digitized and different statistical quantities are obtained using an ensemble-conditional averaging technique. It is found that initial conditions do have a strong effect on the development and growth of a thermal, even for gross parameters such as the "entrainment coefficient."

Key Words: Buoyant thermals; entrainment coefficient; fireballs; turbulent thermals; vortex bubbles.

1. Introduction

The study of instantaneous and continuous sources of buoyancy[1] (thermals and plumes, respectively), is of great practical importance in various fields. In 1941, G. I. Taylor, in an unpublished report, studied the early stages of formation of a thermal which would be produced by a very intense (atomic) explosion. He later published his findings [1][2] regarding the formation of a blast wave and compared his results with photographic records of the first atomic explosion.[3]

[1]A fluid possessing a density difference with respect to its surroundings, whether as a result of differences in temperature, molecular weight (for gases), or concentration of a solute (liquids).

[2]Figures in brackets refer to literature references at the end of this paper.

[3]New Mexico, 1945.

Schmidt [2] considered what happens to the convection currents rising from heated bodies, at a distance above their source. He discussed the dynamics of turbulent plumes by supposing that the distribution of temperature and velocity can be found by balancing the horizontal turbulent transfer of heat and momentum against the vertical convective transfer. A simpler transfer assumption was made by Taylor [3], who related the inflow into a convective plume to its characteristic velocity. More theoretical and experimental studies were made for a body of fluid rising (or falling) through a uniform ambient [4-6], or through a stratified ambient with any vertical density distribution [7].

The motion of isolated buoyant thermals was also studied with a specific practical application in mind, such as the formation of cumulus clouds [8-10], the development of fireball in lighting [11], or the intermittent release of smoke from chimneys as a means of increasing the height attained [12].

In a series of studies [13-15], Wang, et al. tried to relate the turbulence intensity within the thermal to the entrainment parameter α.[4] Escudier and Maxworthy [16] presented an analysis for the motion of a turbulent thermal in an unstratified environment, based upon the entrainment hypothesis introduced by Taylor [7]. Their analysis is valid for any density difference between the thermal and its surroundings since they considered the influence of the "virtual mass" [17] of the unsteadily moving fluid.

Different investigators have used different techniques to generate identical thermals in laboratory studies. For example Morton, et al. [7], carried out their experiment in a stable stratified salt solution in which discrete clouds were released suddenly by removing the cover from the top of a small reservoir, which contained a known volume of light fluid. Fohl [18] burst helium filled soap bubbles at atmospheric pressure. Lin, et al. [14] produced relatively small but strongly heated thermal bubbles by pulsed arc discharges in otherwise undisturbed air. Haigh and Mantrom [19, 20], developed a system to remotely form and burst helium-filled soap bubbles in a high pressure tank filled with air. Shlien and Thompson [21] injected heat into a liquid by operating a conductivity probe at high power.

From these and other experiments one can deduce, among other things, a value for the entrainment coefficient α. It is found that α does not have a universal value, and changes over the range 0.01 - 0.35.

---

[4]Also called entrainment coefficient: the constant of proportionality in the mass conservation equation [16].

As Escudier and Maxworthy [16] have pointed out, it appears that α might be a function of the initial density difference, and also of the detailed nature of the initial conditions under which a given thermal is formed[5]. Fohl's [18] experiments ($\Delta_o \equiv 1$ - initial density/ambient density $\simeq 0.85$) gave a value $\alpha \cong 0.08$ for the best organized thermals, and $\alpha \simeq 0.17$ for the least organized ones. Experiments on less organized thermals [8] gave values of α in the range 0.2 - 0.35 ($\Delta_o \simeq -0.15$). Maxworthy [private communications] obtained $\alpha \simeq 0.01$ by giving a thermal an initial circulation.

The present study was motivated by these inconsistencies in previous measurements and a desire to understand the role played by initial conditions in forming a well organized thermal. As such it is only a preliminary effort which has, like so many, raised as many questions as it has answered. Thermals are generated by two new and distinctly different methods. In the first, a soap bubble is filled with a lean mixture of oxygen and propane and ignited with a spark. In this case, the thermal initially assumes the form of a smooth sphere. In the second, a cylindrical box with sharp-edged orifice at its top is filled with a similar mixture and then ignited. In this case, vorticity is not only produced by buoyancy effects, but also generated by viscous effects at the sharp-edged orifice; hence, different initial conditions are expected in the two cases. In both cases a structure like a vortex ring is observed to form at a later stage, particularly when a rich mixture is used and combustion continues as the thermal rises and mixes with ambient oxygen.

Detailed temperature field measurements are obtained using an array of hot wire probes operating at low overheat ratio. The temperature signals are digitized, and different statistical quantities are obtained using an ensemble-conditional averaging technique.

2. Experimental Equipment and Procedure

i. Generation of Turbulent Thermals

Preliminary calculations of the conditions to be expected in thermals produced in air, under various circumstances, showed that a most encouraging approach would be to fill a soap bubble with a combustible mixture and ignite it with a spark. Since the buoyancy of the initial mixture in air is amall, a large stable soap bubble can be produced initially while large buoyancy forces results after ignition. In the laboratory, Reynolds numbers of the order 10^4 - 10^5 can be attained by this method at atmospheric pressure, thus more closely simulating large scale thermals in the atmosphere.

---

[5]Hopefully, α is a constant for any given thermal. However, Dr. J.S. Turner (private communication) has suggested that α might be a running variable dependent upon the local density difference.

The soap bubble generator, figure 1(a), consists of a glass-blower's torch for mixing oxygen and propane, attached to a rotating funnel (diameter = 3.6 cm) for picking up a soap film (when in the downward position), and producing a stable soap bubble (when in the upward position). A special soap bubble solution was developed to produce large (10 cm diameter), long lived bubbles. It consists of 600 cc, commercially available, Jack dishwashing soap solution[6], 300 cc glycerol and 0.1 cc strong ammonia solution. A known flow rate of oxygen and propane is fed to the torch, from their respective tanks which are equipped with pressure regulators and needle valves. The mixture is lean (20% excess oxygen), and the theoretical energy released from an exothermic reaction inside a 10 cm diameter bubble is about 10^4 Joule.

Extreme care has to be taken to generate identical thermals each time. It is necessary to fill each soap bubble to the same desired diameter, with the same combustible mixture ratio. From an error analysis, visual observations using high speed photography, and examination of instantaneous temperature profiles, it is estimated that, in a series of experiments on any one day, the thermals are initially generated with a repeatability ± 5%.[7] However, the repeatability from day to day is within ± 10%, presumably due to changes in ambient conditions.

Thermals are also produced by filling the cylindrical box shown in, Figure 1(b), with the same volume of oxygen and propane used to fill a 10 cm diameter soap bubble. The (heavy) mixture enters the bottom of the box radially outwards to minimize or prevent escape. The box has a 10 cm diameter sharp-edged orifice on top, large enough to prevent a jet-like ejection of the combustion products after igniting the mixture. As the combustion products expand out of the box they roll up into a body of moving fluid which initially takes the form of an oblate spheroid [22], with considerable vorticity generated by viscous forces at the sharp edge.

Thermals are generally generated at the rate of two per minute. This would allow enough temporal separation to prevent interaction between two consecutive thermals. In the meantime, a large number of thermals could be produced before any appreciable drift in the ambient conditions would occur. To prevent external influences from interfering with the thermals (drafts in the room, etc.), they are generated inside a 120 x 120 cm plexiglass box 300 cm in height, with a fine screen on top to provide an exit for the rising gases. Near the ceiling, a typical thermal diameter is less than 80 cm or 35% of the cross-sectional area of the box.

---

[6]Proctor & Gamble Corporation.

[7]Range of variation of initial diameter and A/F ratios; hence, initial energy contained in a thermal.

ii. Flow Visualization

During the early stages of formation of a thermal, the temperature is high enough to cause strong visible radiation, which enables direct observation. A high-speed 16 mm movie camera (Fastax, category I, type WF3[8]), capable of attaining speeds as high as 8000 frames per second, is used to observe the initial 300 milliseconds of thermal formation and development. This high camera speed necessitated using high ASA rated film specially perforated on both edges to prevent tearing. At a later stage, the temperature inside a thermal is considerably lower due to energy loss by radiation and entrainment of colder ambient air, and, hence, it loses all its luminosity, with the result that conventional photography cannot be used. Shadowgraph movie films are taken at 64 frames per second, using a 500-watt mercury short arc lamp to project a shadowgraph image on screen. Because of the small density differences and low sensitivity of the shadowgraph method, no satisfactory pictures were obtained in these preliminary experiments.

Other flow visualization techniques are possible, such as holographic interferometry [19, 20], light scattering from small helium filled soap bubbles which are neutrally buoyant, or from dust particles, etc.

iii. Temperature Field Measurements

An array of four hot wire probes is used to obtain detailed information of the temperature field structure inside the turbulent thermals. Each probe is a straight wire mounted on jewelers' broaches (0.3 mm diameter) encased in epoxy resin, with 5 mm stainless steel tube for the main shaft. The sensitive part is 1.27 microns in diameter and 1 mm long, platinum - (10%) rhodium etched from Wollaston type after the silver coating has been soldered to the tips of the jewelers' broaches. A four channel constant current anemometer supplies about 1 mA current to each probe to maintain an overheat ratio of 0.8%. At this low overheat, the probe is essentially sensitive only to temperature fluctuations, and it can be shown that, under typical operating conditions, the sensitivity to temperature is about 100 times the sensitivity to velocity or concentration. Probe temperature (hence, resistance) follows closely changes in gas temperature, this unbalances the Wheatston bridge and the difference voltage is amplified in two stages by a factor of 6000. The first stage amplifier also serves as a low-pass filter to remove undesired high frequency noise above 3 kHz. The output voltage is proportional to the gas temperature above ambient.

The spatial resolution of a probe is of the order of the length of the sensitive part (1 mm), while the temporal resolution is governed by the diameter of the wire, overheat ratio and heat transfer coefficient [23].

[8] 3 M Company.

Direct sine-wave calibration gave a frequency response of about 1 kHz to the "3 db down point", which is satisfactory for our purposes. The temperature sensitivity is determined for each probe by direct calibration with a thermocouple in a heated oven. The response is found to be linear over the temperature range of interest (20 - 50° C).

The signal from the four channel anemometer is a.c. coupled and FM-recorded on a 3 M company wide band recording tape using a four channel Hewlett-Packard Instrumentation tape recorder, series 3960, at a recording speed of 3 ips. At this speed the frequency response of the recorder is flat up to 1 kHz, and the signal-to-noise ratio is 48 RMS/RMS (db). The analog signal is then digitized at a sampling rate of 4000 milliseconds per four words, and processed on a digital computer The hardware which performed the analog-to-digital conversions is a 12 bit 5 volt full conversion [24], providing a resolution of one part in 4096, or a digital signal-to-noise ratio of about 72 db. Digitized data are stored on a 9-track digital magnetic tape for processing by FORTRAN programs.

The four resistance thermometers are located at Z = 70, 124, 175 and 245 cm, above the initial position of a thermal center (Z = 0). The array is moved horizontally to measure the temperature fluctuations at six different locations across the thermal: X = 0, 6, 13, 25, 32 and 38 cm.

3. Formation of the Buoyant Thermals

Combustion inside a soap bubble has been used before in flame propagation research [25]. For the large diameter bubbles considered the internal pressure hardly changes as the diameter increases, hence approximately constant pressure combustion can be attained. For our air/fuel ratio and fuel types, the flame speed is about 350 cm/sec, so it takes about 14 milliseconds for the flame front to cross the region of fuel mixture. However, as the spherical combustion front advances, the burned gas being much hotter than the initial reactants occupies a larger volume. As a result, both the combustion front, the unburned reactants and the soap bubble interface are pushed outwards. In fact the combination of flame speed and expansion due to heating is so great that a weak spherical shock wave is formed. At some state during this process the soap bubble breaks probably before the flame front reaches it. When all of the combustible mixture has been consumed the diameter of the hot "fire ball" is approximately 23 cm. This has been deduced from photographic records, and also from thermodynamic calculations for the reacting mixture. At this state the temperature is estimated to be 2760° C ± 10%, and the density of the combustion products is 1.2×10^{-4} gm/cm^3. We arbitrarily choose this state to be the origin of time, since observations show that the combustion process is finished before the hot gas sphere starts to rise.

The important parameter "initial density difference" $\Delta_o = 1 - \rho_o/\rho_\infty$, where ρ_o is the (average) density of the combustion products at $t = 0$, and ρ_∞ is the ambient density, is then $0.9 \pm 2\%$.

Figure 2 shows a one second exposure picture immediately following the explosion of a soap bubble. The gas temperature is high enough to cause strong visible radiation. From such a picture, one might gain a qualitative idea about the large-scale structure responsible for entrainment, although as Lin, et al., [14] has pointed out, an inference of the temperature field structure from the luminous profile is difficult due to the nonuniform nature of the convective mixing process and the strong dependence of air emissivity on temperature. The increase in size with height is evident, and one might even attempt to compute very crudely an entrainment coefficient from such a picture, keeping in mind the limitations just mentioned.

A movie film is available for the early stages of formation of a thermal generated from the explosion inside a soap bubble. A camera speed of 3000 frames per second is used. Initially a smooth spherical fireball is observed, and a mushroom - like gas with vorticity generated by buoyancy effects is followed after about 60 milliseconds. The rotational motion causes the entrainment of colder ambient air with the gradual loss of luminosity particularly at the outer edges, and, hence, the thermal appears smaller than it actually is. The thermal accelerates upward to a maximum speed, then decelerates and eventually stops. The Reynolds number based on this maximum upward velocity and an "equivalent" diameter is calculated from the temperature field measurements to be about 3×10^4.

A second film taken at the same speed is also available for the early stages of formation of a thermal generated using the sharp-edged orifice. The viscous forces at the sharp edge generate vorticity, and as the combustion products expand out of the box, they roll up into a body which initially takes the form of an oblate spheroid. As in the previous case, the thermal entrains colder air from outside, and its size increases as it moves upward. Although approximately the same amount of energy is fed into thermals generated by the two methods, it is not expected that even gross parameters, such as the entrainment coefficient would be the same for the two cases.

4. Ensemble - Conditional Averaging

A typical signal from a resistance thermometer during the passage of a thermal is shown in figure 3. The probe is located 70 cm directly above the origin ($Z = 0$). The signal is obtained by playing back the analog tape into a Hewlett-Packard X-Y recorder model 7004B[9]

[9]The X-Y recorder has very limited frequency response which filters out the high frequency fluctuations.

The signal may be considered as representing (approximately[10]) an instantaneous temperature profile along a vertical cut in the center of the thermal. As in previous experiments [14], a sharp temperature interface at the top of the thermal is evident by the sudden rise in temperature as the thermal first touches the probe; also, a wake formation is suggested by the gradual decay near the end of the signal.

To extract useful statistical information from such a transient signal is a very difficult task. Time and space averages do not have any great physical significance, and only an ensemble average [26] would enable us to study the temperature field structure. This means an average taken over a "large" number of experiments that have the same initial conditions. In order to complete our task, we have to define the beginning of an event (or ensemble). Fortunately, in the problem at hand, the beginning of an event is very well defined by the sudden rise in temperature, hence a condition for the start of an event can easily be found.

If i indicates the event number, t the time measured from the beginning of that event, n total number of events, and $T_i(t)$ is the temperature (above ambient) at time t of the i^{th} event, then the ensemble average temperature is:

$$\overline{T}(t) \equiv \frac{1}{n} \sum_{i=1}^{n} T_i(t)$$

$$T_i(t) = \underbrace{\overline{T}(t)}_{\text{Average}} + \underbrace{T_i'(t)}_{\text{Fluctuation}}, \quad \sum_{i=1}^{n} T_i' \equiv 0$$

The average temperature is, of course, a function of time. The root-mean-square temperature fluctuations is given by:

$$\sqrt{\overline{T'^2}(t)} \equiv \sqrt{\frac{1}{n} \sum_{i=1}^{n} (T_i(t) - \overline{T}(t))^2}$$

$$= \left[\frac{1}{n} \sum_{i=1}^{n} T_i(t)^2 - \overline{T}^2(t)\right]^{\frac{1}{2}},$$

also a function of time. And so on for other statistical quantities.

---

[10] Since the thermal's characteristics vary slightly during the time of transient.

The spectrum[11] is rather more difficult to define for an ensemble of transient signals. For the much simpler case of a stationary random function, the spectrum can be obtained by Fourier transform, the two-point correlation function (mean-lagged product); or by calculating the Fourier coefficients of the (time) series, then the spectrum at any frequency f is $a^2 + b^2$, where a(f) + b(f) are the complex Fourier coefficients. For our transient signal, we divide the signal from each thermal into one second intervals, calculate the Fourier coefficients for each interval, and average the resulting spectra from corresponding time intervals over the whole ensemble. The resulting spectra is then a function of both time and frequency [S(f, t)], with a low cut-off frequency inversely proportional to the time interval (1 sec). To avoid aliasing in spectrum measurements, the sampling frequency should be at least twice the highest frequency of physical significance present in the data (the Nyquist folding frequency), and appropriate filtering is used when converting the analog data to digital. By definition, $\overline{T'^2} \equiv \int_0^\infty S(f, t)df$, and this can be used for checking the consistency of calculations.

The "integral scale" L is a measure of the longest connection, or correlation distance, between the temperature at two points of the temperature field. L can be computed by extrapolating the spectrum to zero frequency using the relation [26]

$$L(t) \doteq (\overline{U}/4\ \overline{T'^2})\, S\ (o,\ t),$$

where $\overline{U}$ is the average upward velocity at time t, and $\overline{T'^2}$ is the mean square temperature fluctuations at the same time.

5. Results

The time history of the ensemble averaged temperature $\overline{T}(t)$ for 262 thermals generated using the orifice method, at the four reference heights directly above the orifice center, is shown in figure 4. t = o indicates the arrival of a thermal at the nearest probe. The arrival time at the other three probes relative to this origin of time varies from thermal to another, and an arithmetic average over the whole ensemble for this time is shown on the abscissa. We note the strikingly smooth profiles, as compared to the (instantaneous) signal from one event (figure 3). This is a consequence of the loss of phase information in the ensemble average, and can be used to test the convergence of the averaging process. The averaging was also performed using 20 events only, and the resulting profiles are qualitatively similar, an indication of a

[11] The fluctuating temperature field may be assumed to be composed of fluctuations corresponding to different frequencies in a continuous frequency range. A spectral analysis of the temperature flucuations will show how the contributions are distributed over these frequencies.

good repeatability in initial conditions. As expected, a thermal cools as it moves upward; the temperature is highest at its top (about 17°C above ambient at Z = 70 cm), and approaches ambient conditions gradually, suggesting the existence of a thermal wake.

A similar set of curves is shown in figure 5 for 169 thermals generated using the soap bubble method. The temperature profiles have a similar form to the previous ones, except for the appearance of a second peak at Z = 70 and 124 cm. This might indicate that, at this relatively early stage of development, the mass entrainment process does not penetrate all the way into the core of a thermal, hence the "hot spot" which appears even after averaging over 169 different thermals. This might also indicate less efficient mixing for this kind of thermal, consistent with the lower vorticity levels as compared to thermals generated using the orifice method.

Figure 6 shows ensemble average temperature profile at different positions across 50 thermals generated using the orifice method. The probe is kept at constant altitude Z = 124 cm, but its horizontal position is changed as indicated. The "arrival time" (relative to the nearest probe, Z = 70 cm) as well as the peak temperature are slightly different for the different positions across the thermal. The differences are within the variations expected from an ensemble to another. The signal tail at x = o has the lowest temperature, perhaps an indication of greater amount of cold air entrainment at this position. Figure 7 is a similar one for 40 thermals generated using the soap bubble method. The probe height is the same as before, and the horizontal positions are x = 0, 6 and 13 cm. Again, a second peak appears in the average temperature profiles for this kind of thermal.

Figure 8 shows root-mean-square temperature profile [$\sqrt{T'^2}$] for 262 thermals generated using the orifice method, as computed using the ensemble-conditional averaging technique, at x = 0 and Z = 70, 124, 175 and 245 cm. As before, t = 0 indicates the arrival of a thermal at the nearest probe. We note that the turbulence intensity is higher at Z = 124 cm than at Z = 70 cm, an indication of continuing production of new turbulence energy between these two heights. The maximum rms value is about 7.5°C, almost 60% of the corresponding mean value! One can estimate the "noise leval" from the rms value at t = 0; in this case it is about 0.4°C or 5.3% of the maximum rms value. The profiles bear the same general characteristics as the average temperature profiles.

A similar set of profiles is shown in figure 9 for 169 thermals generated using the soap bubble method. The maximum rms value is about 8.5°C, almost 70% of the corresponding mean value.

The spectrum S(f, t) for different cases is computed using the fast-Fourier-transform routine. Figure 10 shows a semi-log plot of S(f, t) versus f, for four time intervals: Δt = 0-1, 1-2, 2-3 and 3-4 sec. The thermals are generated using the orifice method, and the probe height is 70 cm directly above the orifice center. Figure 11 is a similar one for thermal generated using the soap bubble method. The area under each curve (on a linear plot) should equal the corresponding mean square temperature.

The integral scale is computed from the formula

$$L(t) \doteq (\overline{U}/4\overline{T'^2})\, S(o,t),$$

where S(o,t) is obtained by extrapolating the spectrum to zero frequency (using a linear plot); $\overline{T'^2}$ is computed from the rms temperature profiles at the intermediate time for each interval.[12] Table 1 shows the integral scale L in cm at Z = 70 cm directly above center for both kinds of thermals, at different time intervals Δt. Table 2 shows the integral scale for both kinds of thermals at various heights but only for Δt = 2-3 sec. Thermals generated using the soap bubble method tend to have larger integral scales, perhaps an indication of the lesser degree of organization as compared to the thermals generated using the orifice method. Integral scale computations should be viewed with caution, due to the high degree of arbitrariness in choosing the time intervals, and in extrapolating the spectrum to zero frequency.

Δt (Sec)	0-1	1-2	2-3	3-4
Orifice method	8.5	3.3	3.6	4.5
Soap bubble method	31.8	10.7	8.0	5.7

Table 1 Integral Scale L cm; Z = 70 cm.

Z cm	70	124	175	245
Orifice method	3.6	7.6	3.7	3.1
Soap bubble method	8.0	8.5	2.6	2.4

Table 2 Integral Scale L cm; Δt = 2-3

[12] $\overline{U}$ will be computed later in this section.

More information on the dynamics and structure of the thermals can be extracted from the temperature records. For example, an average velocity for a rising thermal can be estimated by noting the time it takes to travel between several probes directly above each other,[13] and computing the local slope dZ(t)/dt. It should be noted that this would represent the average upward velocity of the highest point on the thermal interface, and that this is not necessarily equal for all points inside the thermal. Velocities calculated in this way are shown in figure 12 for both types of thermals. Evidently the data shown represent the deceleration phase of the thermal. Near the source, the orifice thermals are faster by about 50%, however both types reach the same speed as they approach the ceiling, perhaps an indication of the resistance due to the wire screen on top of the plexiglass box.

By finding the best fit to the present data using the analytical model presented by Escudier and Maxworthy [16], one can estimate a rough value for the entrainment coefficient. However, it should be noted that this does not prove the validity of the models, nor the accuracy of the present measurements. For the orifice thermals, $\alpha = 0.06 \pm 10\%$ and for the soap bubble thermals, $\alpha = 0.1 \pm 10\%$. This agrees qualitatively with the photographic records. An orifice thermal has strong initial vorticity, and may develop a core (ring) with fast rotation, which in turn may have a stabilizing effect on the turbulence field; this would limit the amount of air entrained - - - hence, the smaller entrainment coefficient. Detailed data on the turbulent velocity field are needed to verify this point, and hopefully to understand the dependence of α on the initial conditions quantitatively.

6. Concluding Remarks

Detailed temperature field measurements in thermals generated using two distinctly different methods are presented in this paper. First, by igniting a combustible mixture inside a soap bubble; second, by igniting a similar mixture inside a box with a sharp-edged orifice at its top. The second kind is initially more organized with strong circulation resulting from the roll-up at the sharp-edged orifice. Initial conditions are shown to have a strong effect on the development of a thermal, even for gross parameters such as the entrainment coefficient. It is shown that α is smaller for the more organized kind of thermal. A thermal produced more or less "cleanly",[14] as with the soap bubble method, moves slower initially, as compared to the initially organized one.

---

[13] Again, this is repeated over a large number of realizations, and the concept of an "average thermal" is invoked.

[14] For example, a perfectly smooth non-turbulent fluid sphere, with zero initial impulse.

Uniform ambient conditions are used throughout the present work. An obvious continuation of the present experiment would be the use of stratified surroundings; either linearly stratified (to stimulate motion in the stratosphere, for example), or with a discontinuity of density (e. g., simulation of the tropopause). Thermals moving in an atmosphere which has been stirred, by moving grids, so that they move in a field of almost isotropic turbulence, would be of great interest to Geophysical studies. Other types of atmospheric structures can also be considered.

Detailed measurements of the turbulent velocity field are obviously needed. A laser-Doppler velocimeter with a tracking-amplifier is needed to measure instantaneous velocity profiles at different positions, since hot wires would be very difficult to use because of the high temperature and concentration fluctuations present.

This work was supported by the National Science Foundation, under Grant GK 38147X, to the University of Southern California. The author is immensely grateful to Professor T. Maxworthy, the Principal Investigator for suggesting the problem, for his guidance in carrying out the investigations and for providing many fruitful discussions.

References

1. G. I. Taylor, *Proc. Roy. Soc. (London)*, A201, 159 and 175 (1950).

2. W. Schmidt, *Z. angew. Math. Mech.*, 21, 265 (1941).

3. G. I. Taylor, *U. S. Atomic Energy Commission*, MDDC 919, LADC 276 (1945).

4. C. S. Yih, *Proc. 1st Nat. Congr. Appl. Mech.*, 941 (1951).

5. H. Rouse, C.S. Yih and H. W. Humphreys, *Tellus*, 4, 201 (1952).

6. G. K. Batchelor, *Quart. J. R. Met. Soc.*, 80, 339 (1954).

7. B. R. Morton, G.I. Taylor and J.S. Morton, *Proc. Roy. Soc. (London)*, A234, 1 (1956).

8. R. S. Scorer, *J. Fluid Mech.*, 2, 583 (1957).

9. J. Levine, *J. Atmos. Sci.*, 16, 653 (1959).

10. J. S. Turner, *Annual Review of Fluid Mech.*, 1, 29 (1969).

11. Y. N. Zhivlyuk and S. L. Mandel'shtam, *Zh. Eksp. Teor. Fiz.*, 40, 483 (1969).

12. J. S. Turner, *J. Mech. Eng. Science,* 2, 97 (1960).

13. C. P. Wang, *Phys. Fluids,* 14, 1643 (1971).

14. S. C. Lin, L. Tsang and C. P. Wang, *Phys. Fluids,* 15, 2118 ((1972).

15. C. P. Wang. *Phys. Fluids,* 16, 744 (1973).

16. M. P. Escudier and T. Maxworthy, *J. Fluid Mech.,* 61, 541 (1973).

17. L. M. Milne-Thomson, *Theoretical Hydrodynamics,* Macmillan, p. 237 (1967).

18. T. Fohl, *J. Appl. Phys.,* 38, 4097 (1968).

19. W. W. Haigh and D.D. Mantrom, *TRW Report,* DNA 2981 Z (1973).

20. W. W. Haigh and D.D. Mantrom, *TRW Report,* DNA 3139 Z (1973).

21 D. J. Shlien and D. W. Thompson, Some fundamental buoyant convection experiments, Part I & II, submitted to *J. Fluid Mech.* (1975).

22. T. Maxworthy, *J. Fluid Mech.,* 51, 15 (1972).

23. J. C. Wyngaard, *J. Sci. Instrum.,* 1, 1105 (1968).

24. C. W. Van Atta, *Annual Review of Fluid Mech.,* 6, 75 (1974).

25. B. Lewis and G. Von Elbe, Combustion flames and explosions of gases, *Acad. Press,* p. 200 (1961).

26 J. O. Hinze, *Turbulence,* McGraw-Hill, p.4 (1975).

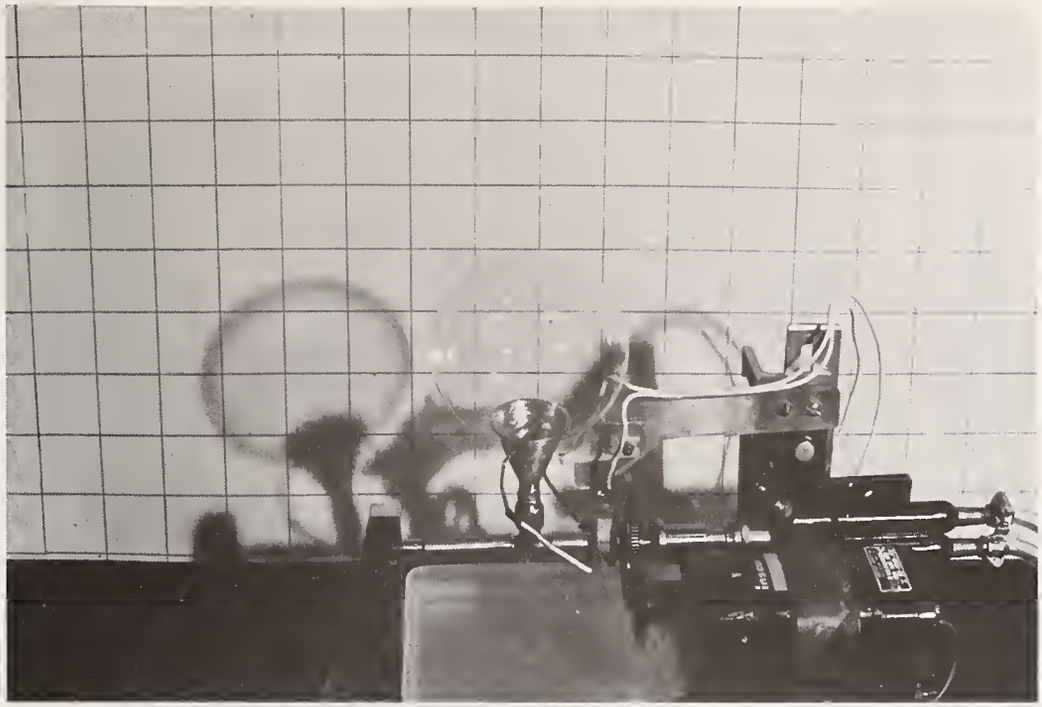

(a)

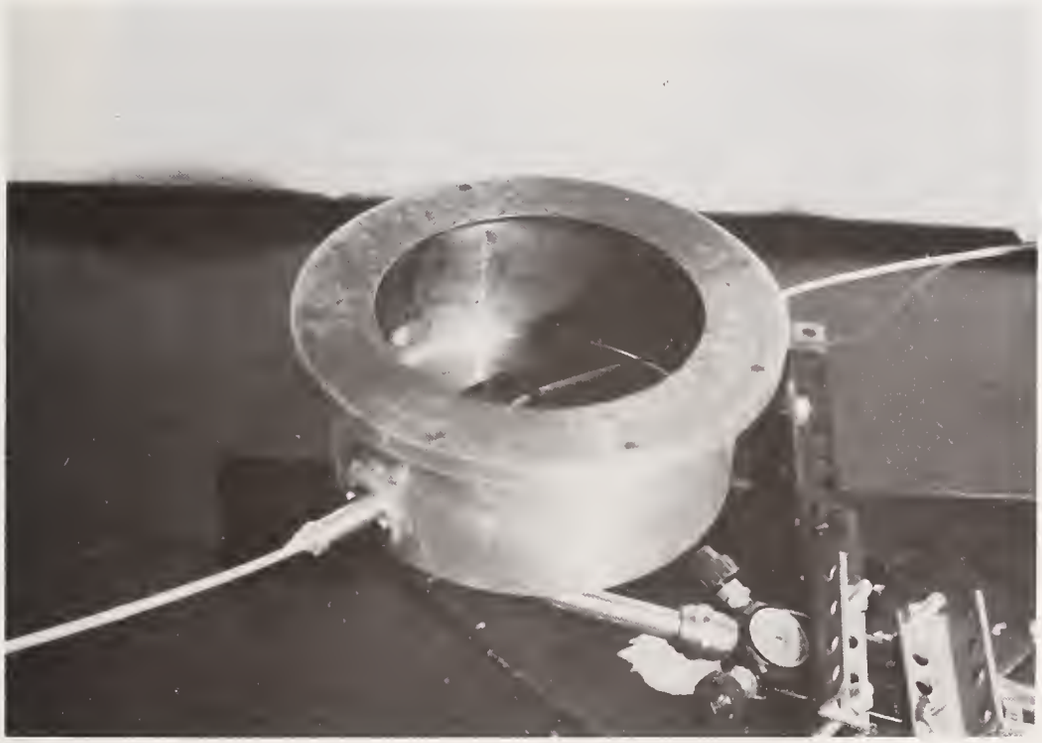

(b)

Figure 1. Thermal generators. (a) Soap bubble method (b) Orifice method.

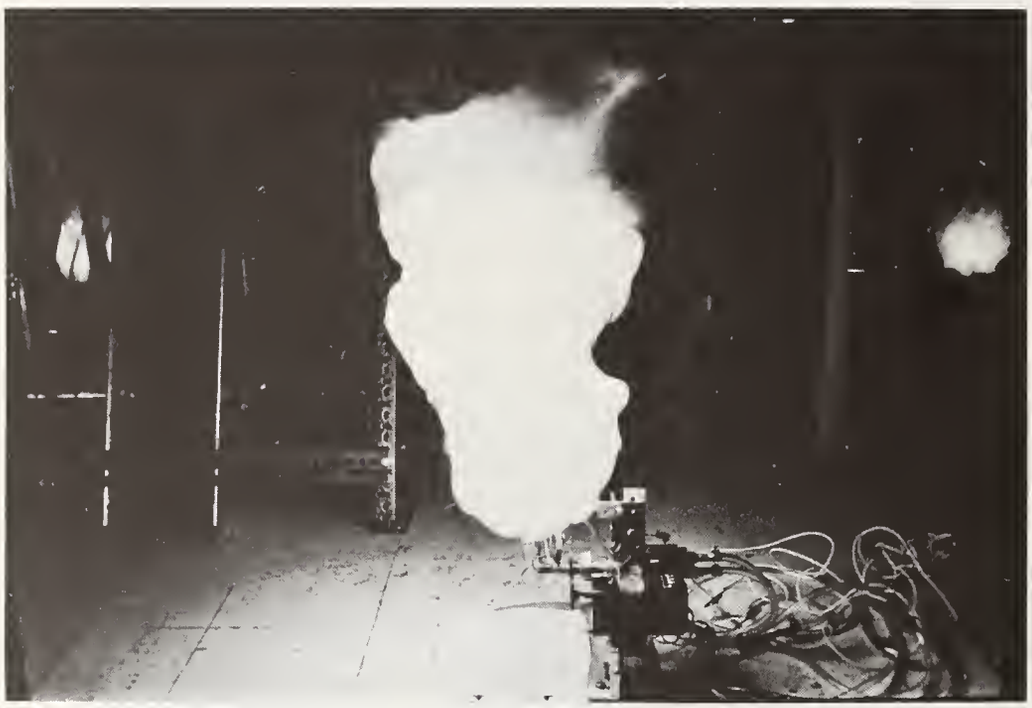

Figure 2. A one second exposure, showing the convolution of a thermal that resulted from an explosion of a soap bubble.

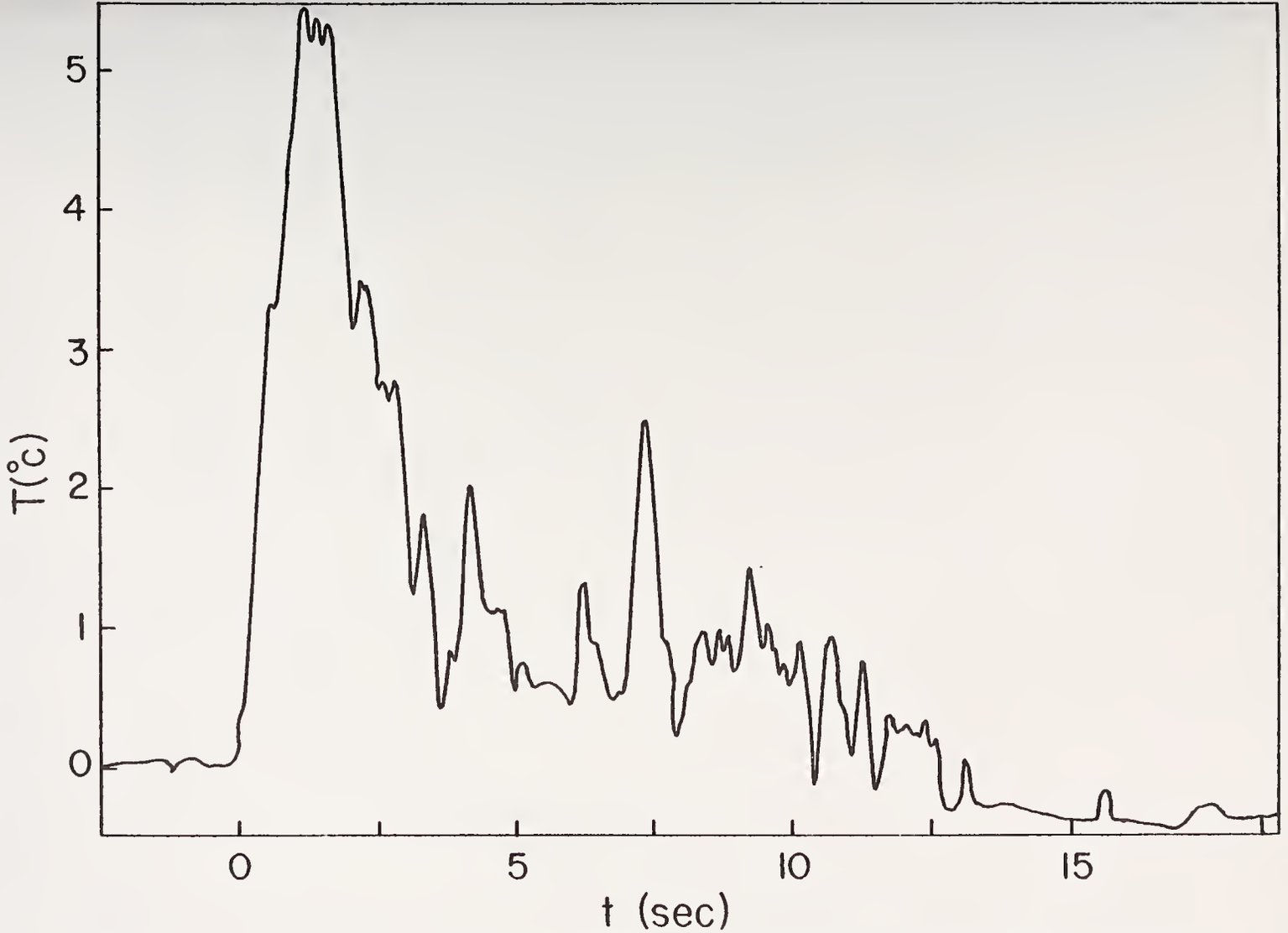

Figure 3. Typical signal from the resistance thermometer as one thermal passes by the probe: Orifice method; x=0 and z=70 cm.

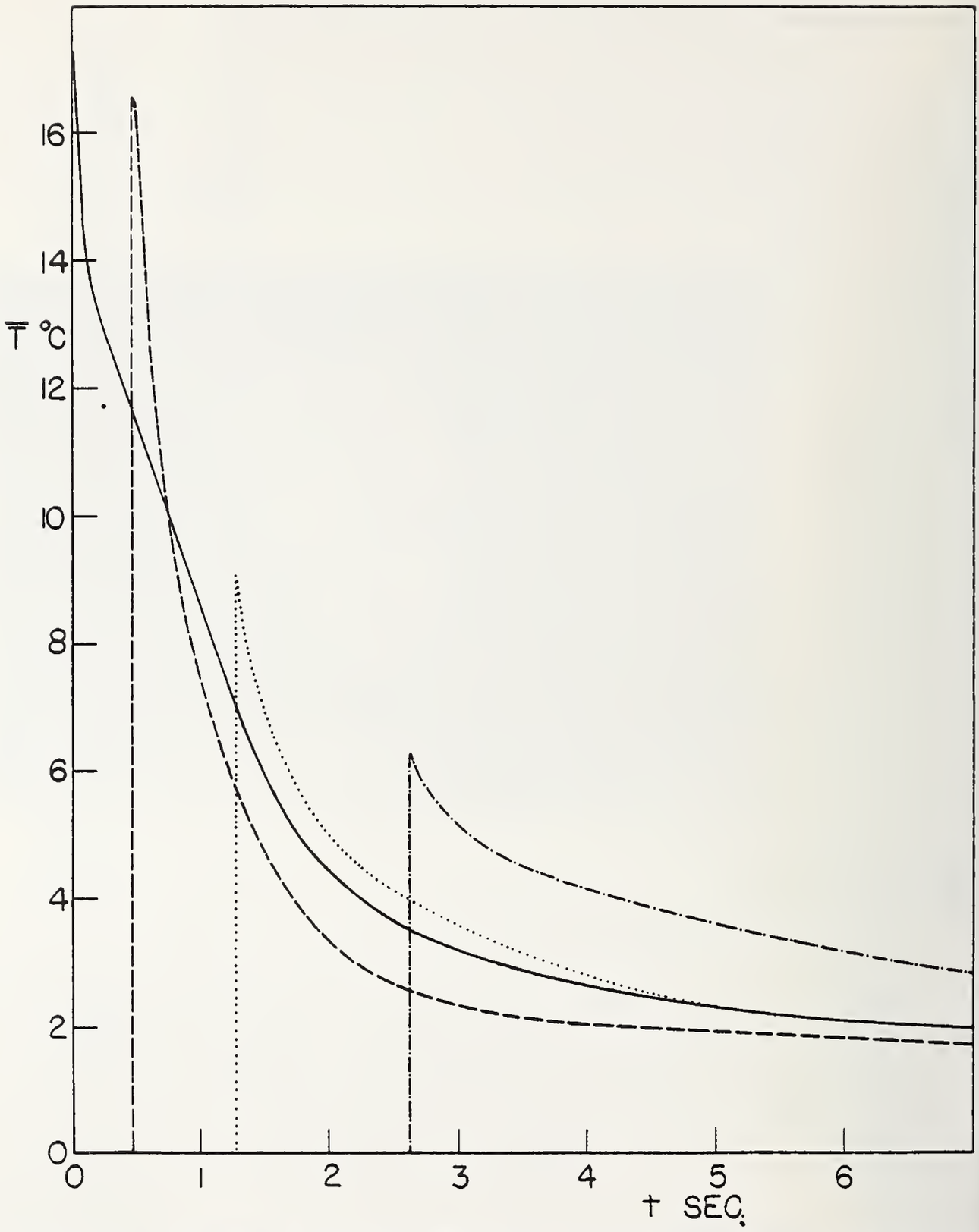

Figure 4. Ensemble average temperature: Orifice methods; x = 0._____ z = 70; ----, z = 124; ...., z = 175; .-.-.-, z = 245 cm.

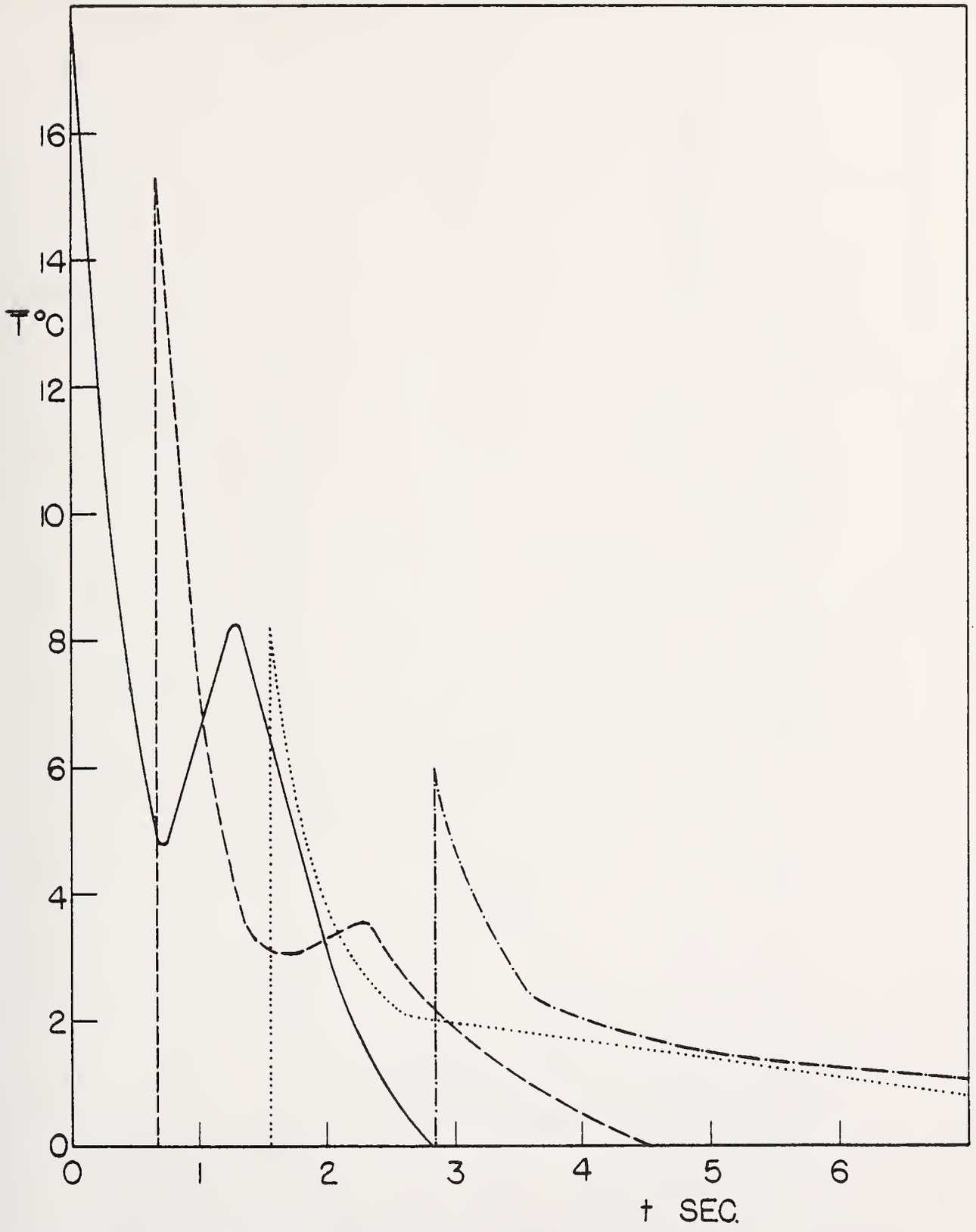

Figure 5. Ensemble average temperature: Soap bubble method; x = 0._____, z = 70; ----, z = 124; ...., z = 175; -.-.-, z = 245 cm.

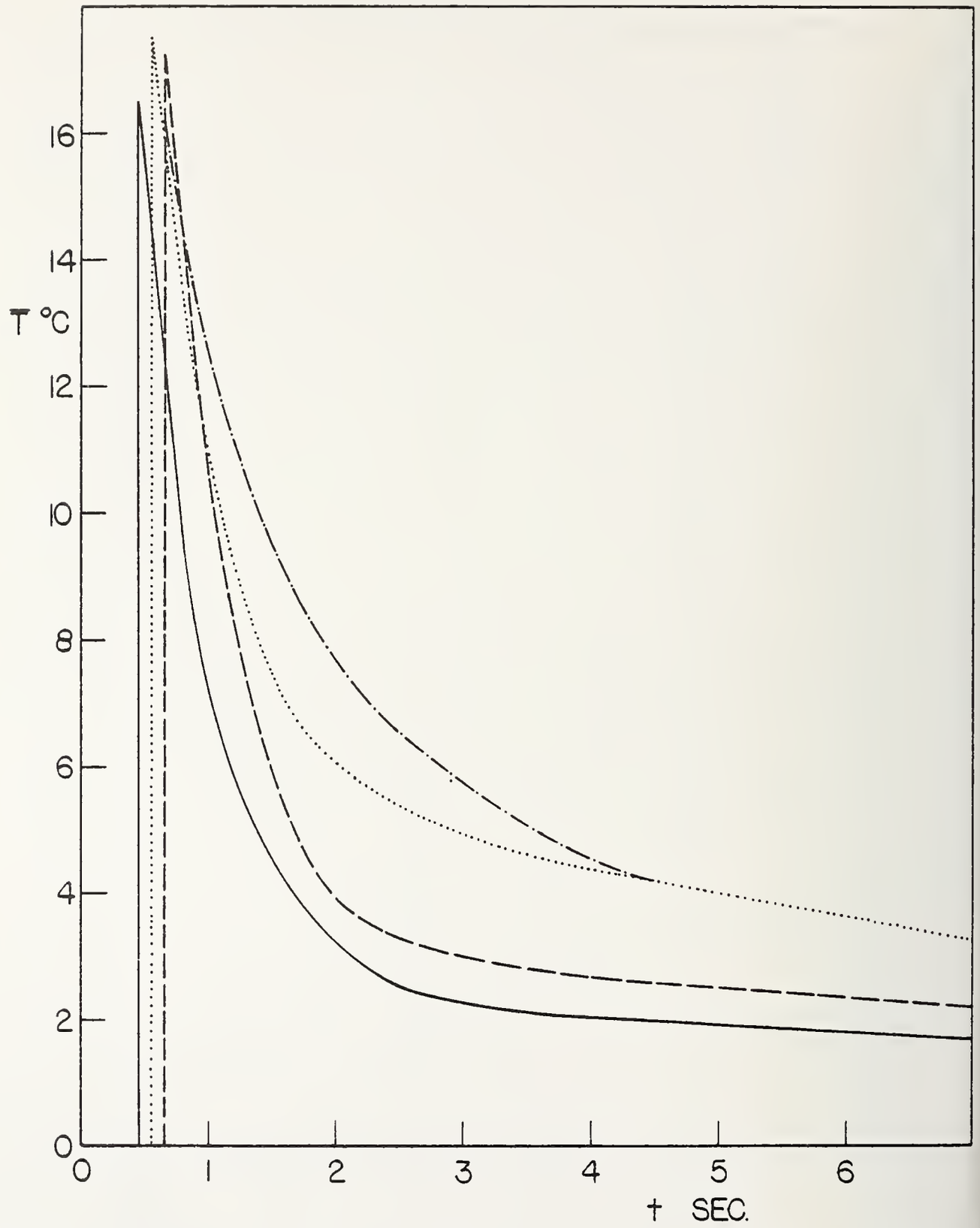

Figure 6. Ensemble average temperature: Orifice method; z = 124._____, x = 0; ----, x = 6; ...., x = 13; -.-.-, x = 25 cm.

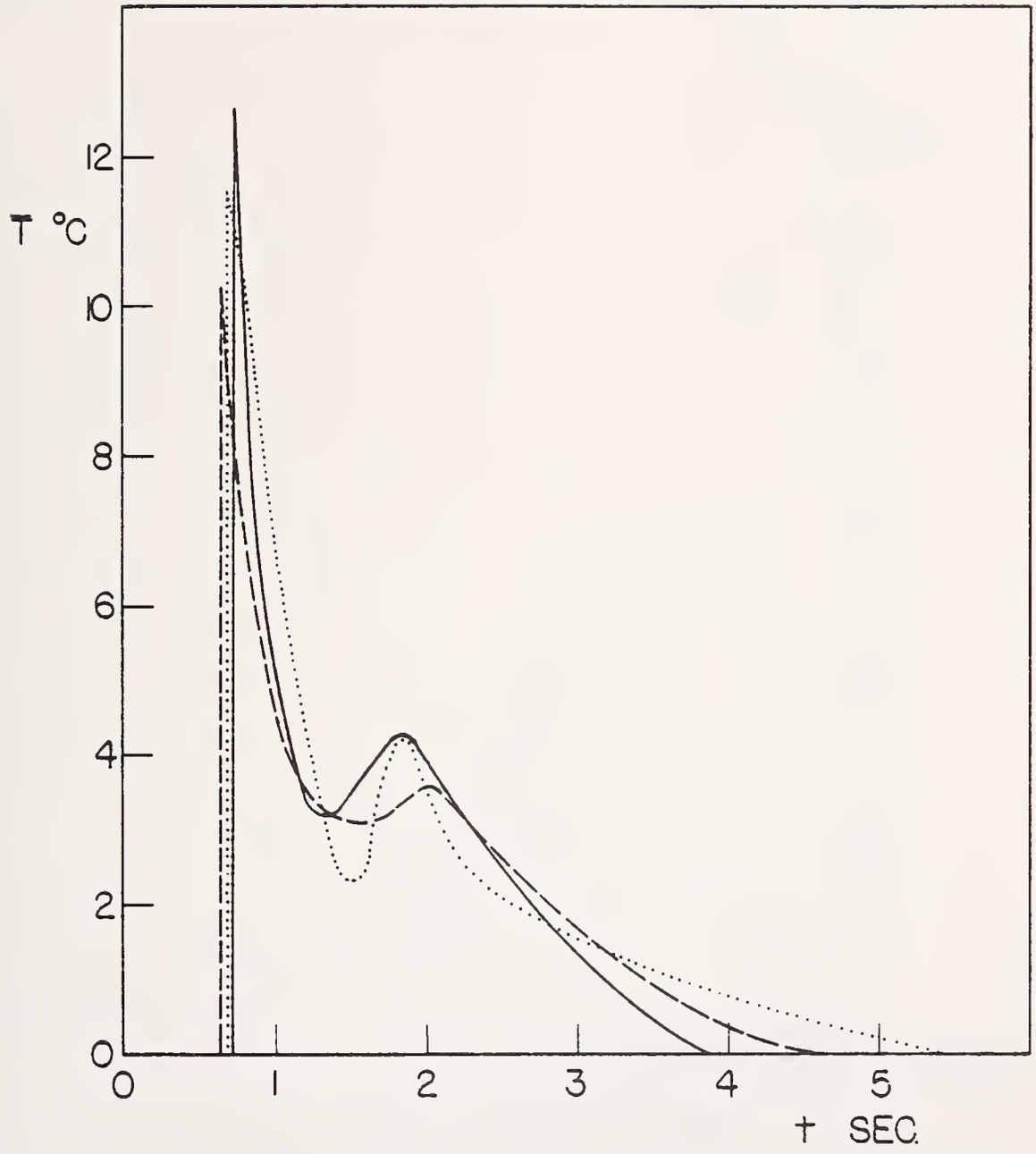

Figure 7. Ensemble average temperature: Soap bubble method; z = 124._____, x = 0; ----, x = 6; ...., x = 13 cm.

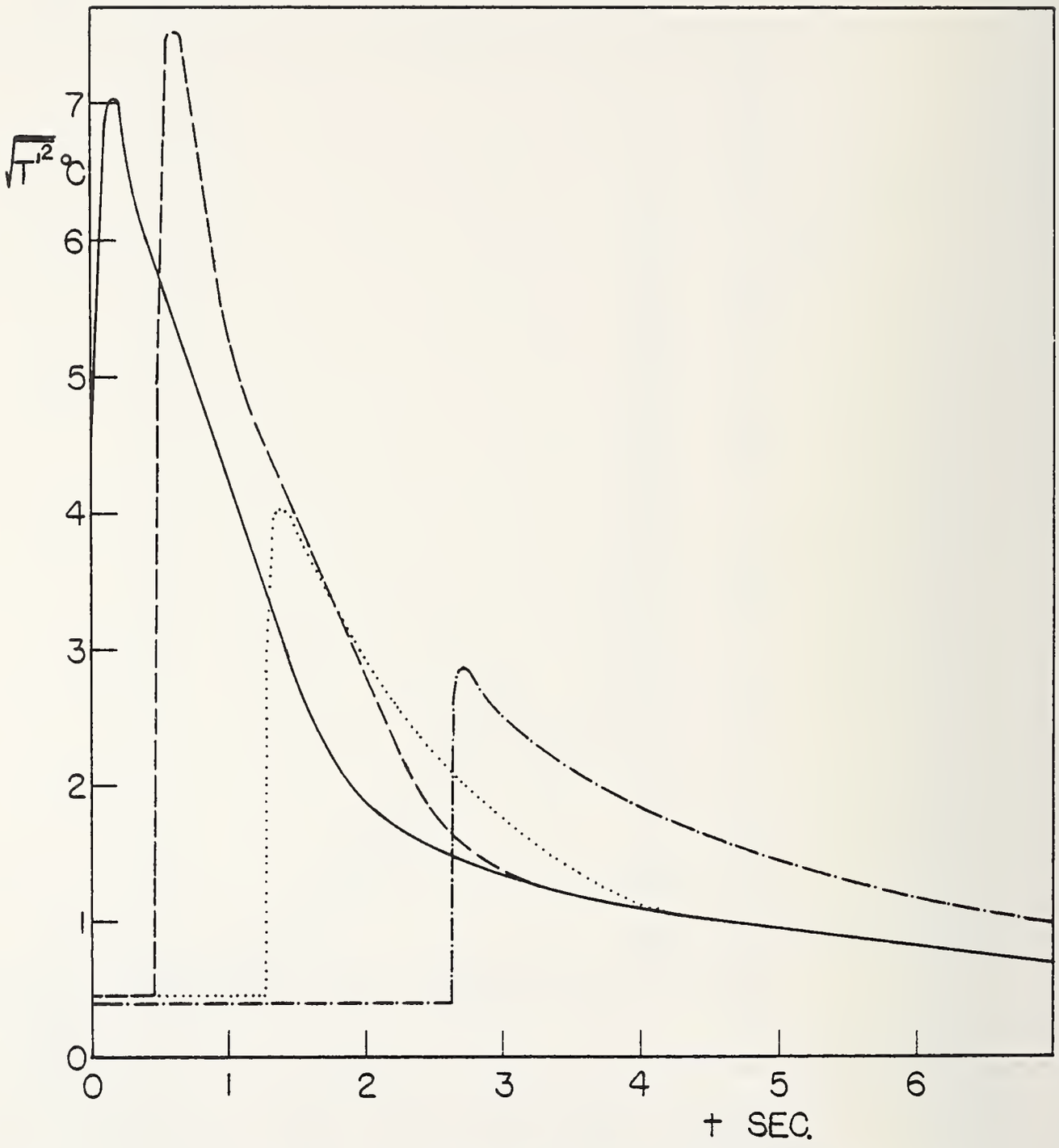

Figure 8. Root mean square temperature: Orifice method; x = 0._____, z = 70; ----, z = 124; ...., z = 175; ---, z = 245 cm.

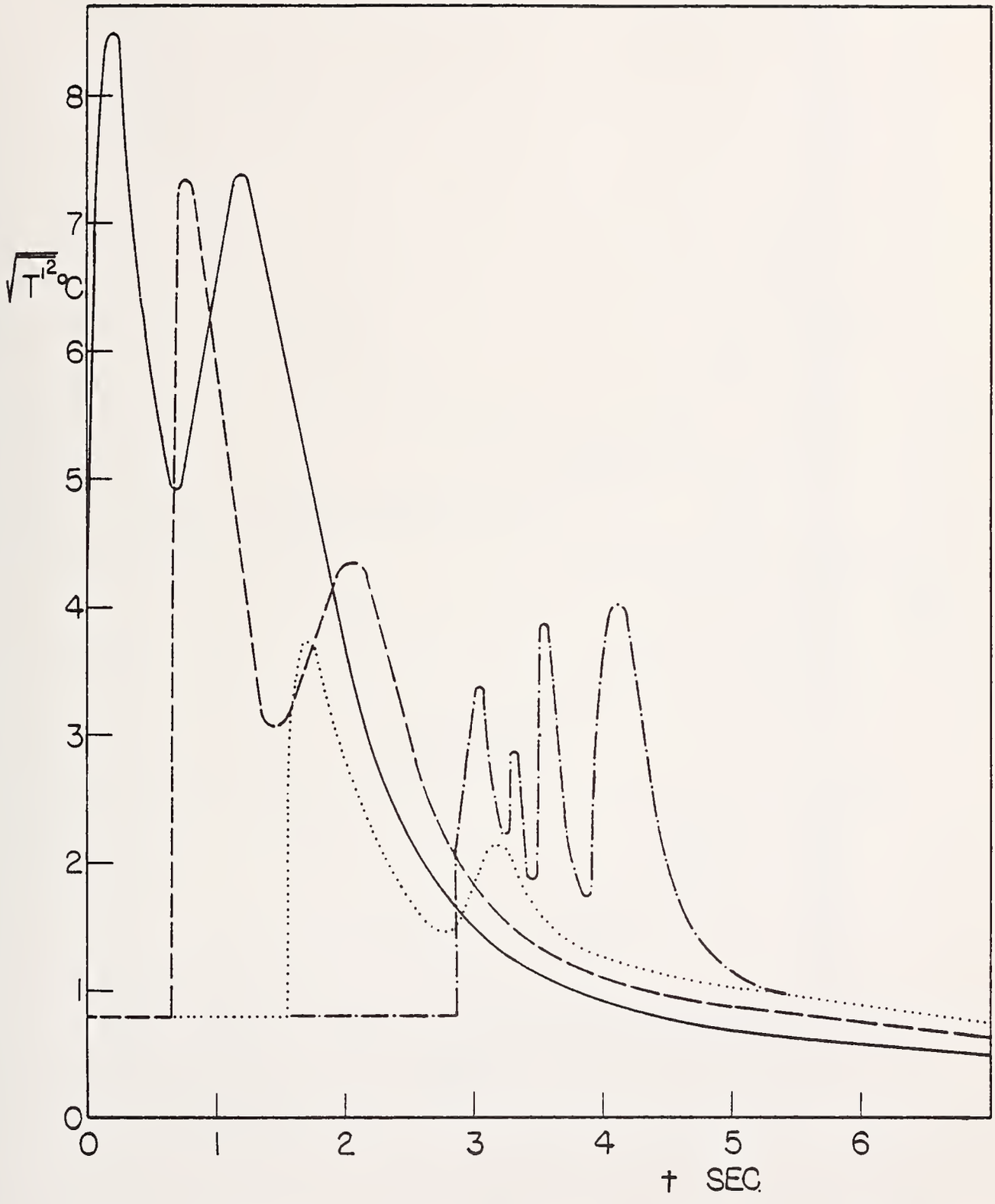

Figure 9. Root mean square temperature: Soap bubble method; x = 0._____, z = 70; ----, z = 124; ...., z = 175; -.-.-, z = 245 cm.

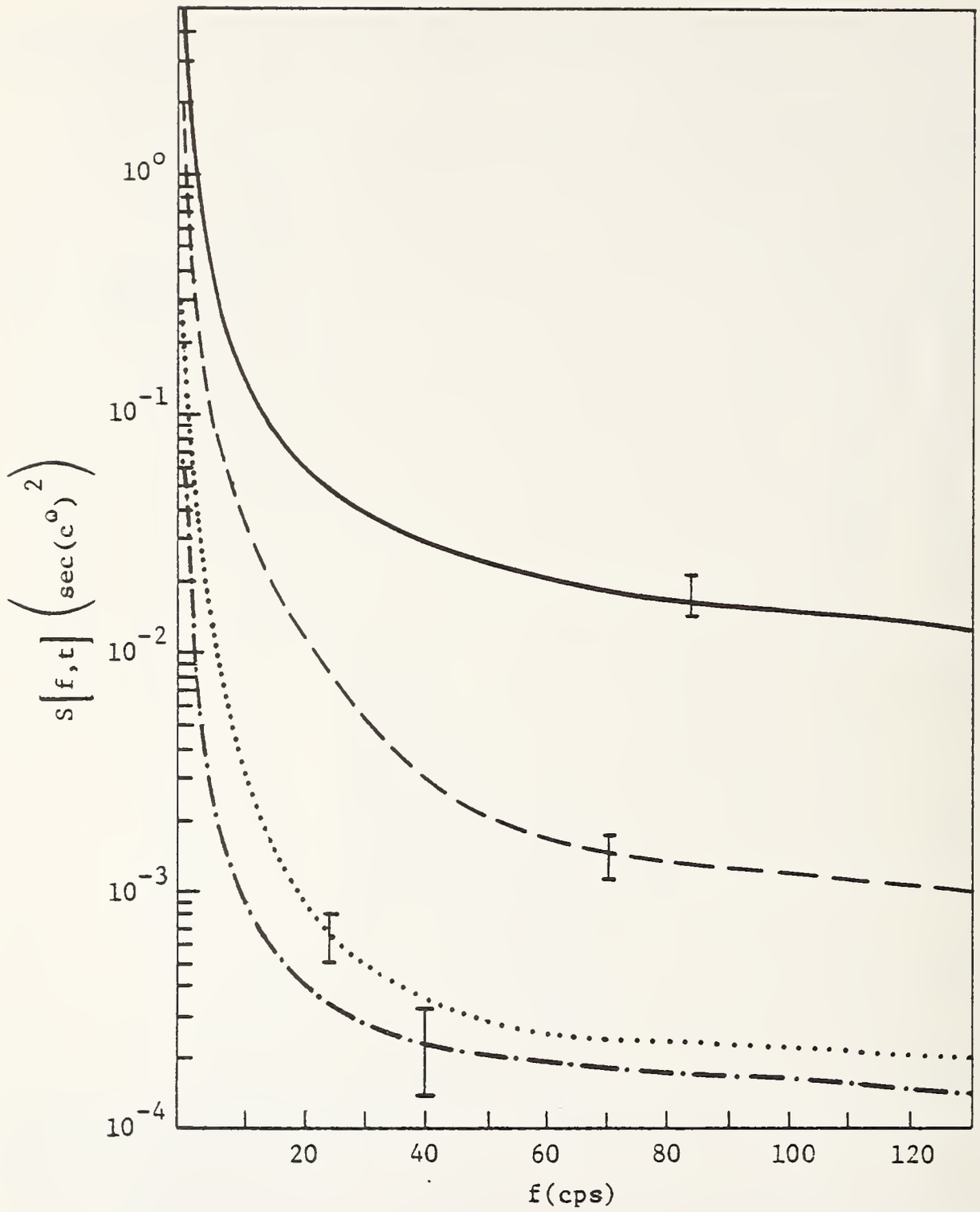

Figure 10 Spectrum: Orifice method; x = 0 & z = 70 cm. ——, Δt = 0 - 1; – – –, Δt = 1-2; ····, Δt = 2 - 3, —·—·—·; Δt = 3 - 4 sec.

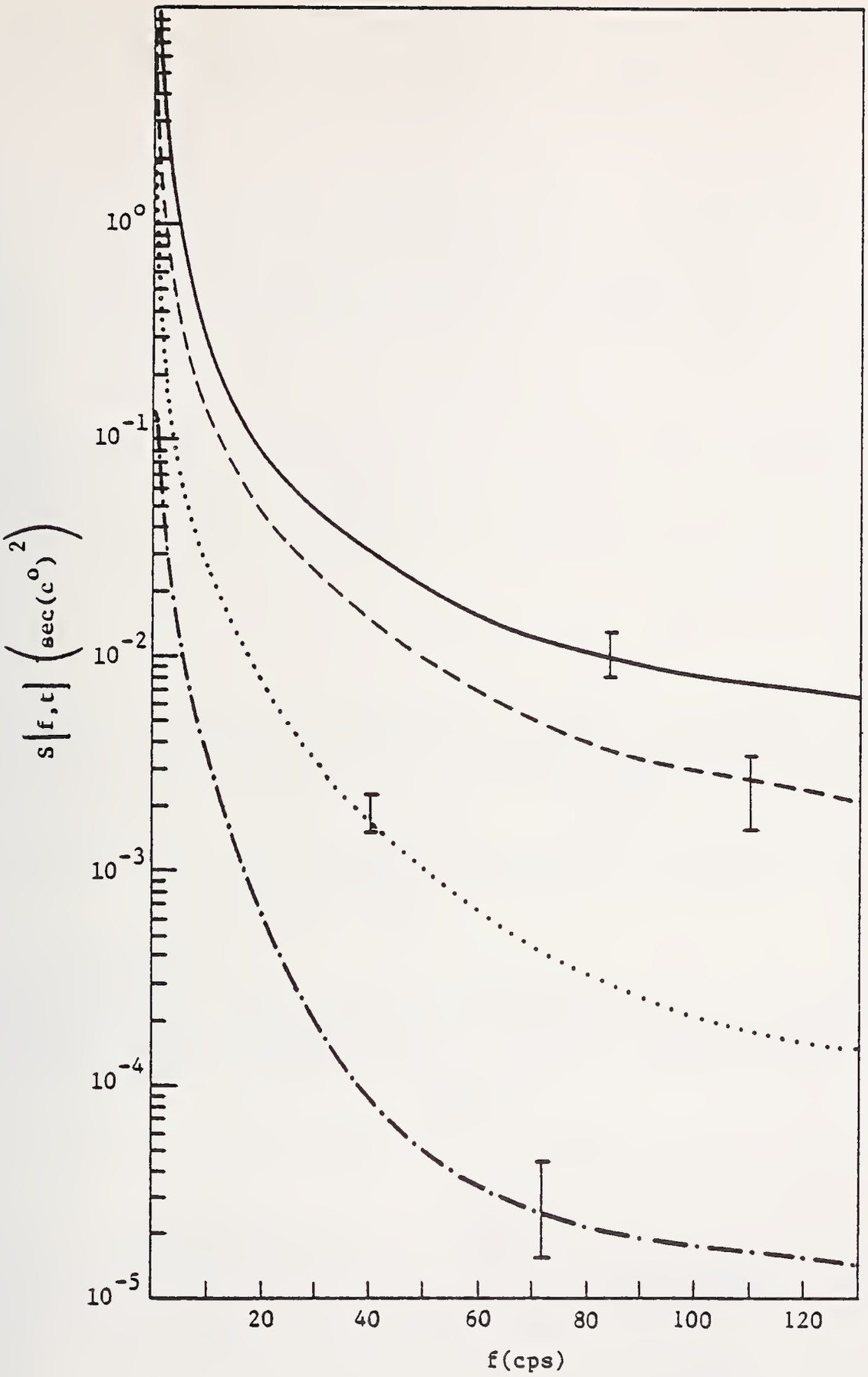

Figure 11 Spectrum: Soap bubble method; x = 0 & z = 70 cm. ——, Δt = 0 - 1; – – –, Δt = 1 - 2; ····, Δt = 2 - 3; —·—·—·—, Δt = 3 - 4 sec.

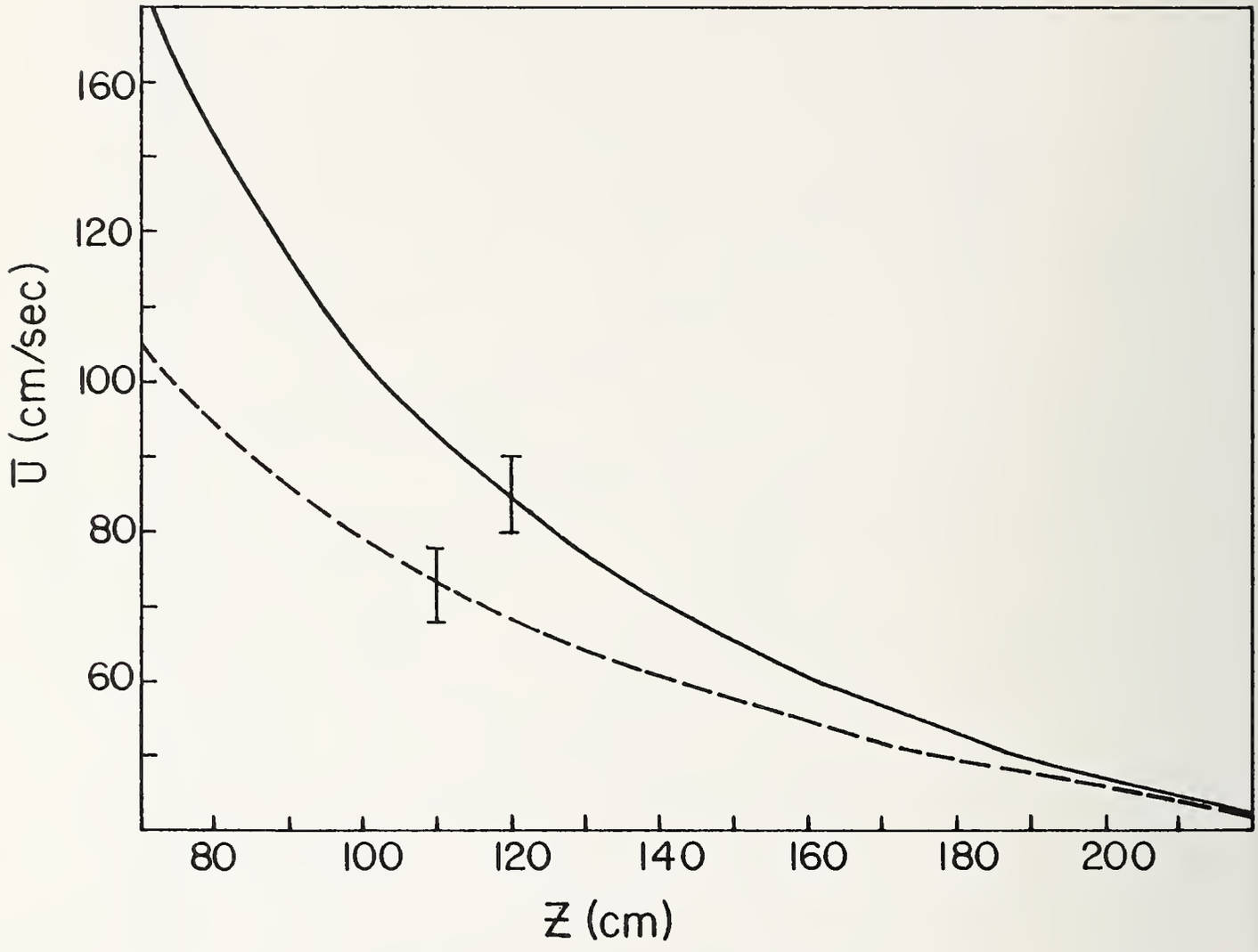

Figure 12. Average upward velocity;_____, Orifuce method;-----, Soap bubble method.

National Bureau of Standards Special Publication 484, Proceedings of the Symposium on Flow in Open Channels and Closed Conduits held at NBS, Gaithersburg, MD, February 23-25, 1977. (Issued October 1977)

FLOW MEASUREMENT UP-DATE

Robert B. Suhoke

Disa Electronics
779 Susquehanna Avenue
Franklin Lakes, N. J. 07417

1. INTRODUCTION

The intention of this paper is to provide insight into basically two flow measurement techniques. Consideration is given to the latest innovations in both the thermal and optical methods and the sources of possible error. Many of these error contributions can be reduced or eliminated by various techniques which will be explored and evaluated.

2. THERMAL METHODS

Thermal devices, more commonly referred to as hot-wire or film anemometers, have been in existence in various forms prior to this century and presently they remain employed in an extremely wide range of applications, the most predominant of course is flow measurement, Figure (1).

In 1914 L. V. King brought forth a solution for the heat transfer from an infinite cylinder in an incompressible flow written as:

$$Nu = A' + B' \ Re^{1/2} \tag{1}$$

This has survived in one form or another and is often used today to explain the basic related physics. Much of the early work and some of the initial apparatus developments occurred at the National Bureau of Standards [1].

Equation (1) can be expanded by writing:

$$\frac{Q}{lK\ (T-To)} = A' + B' \ \frac{(\rho U d)^{1/2}}{\mu} \tag{2}$$

Q, the heat loss, can be taken as equal to the electrical power delivered to the sensor and can be rewritten:

$$V^2 = A'RLK\ (T-To) = B'\ LKR\ (T-To)\ \frac{(\rho U d)^{1/2}}{\mu} \tag{3}$$

If the fluid temperature remains constant equation (3) becomes:

$$E^2 = A + BU^{1/2} \quad \text{or} \quad E = \sqrt{A + BU^n} \tag{4}$$

This response capability and small spacial probe size along with the continuous signal output are no doubt the most important reasons why this measurement technique was brought about and also why it is extensively used today.

If a close inspection of the circuit diagram is made one can readily see that if the bridge is to maintain balance and the probe is one leg of the bridge, and the decade or operating resistor is the balancing leg then the following will occur: The resistance of the probe sensor material will vary with ambient temperature changes in the flow channel while the resistance of the decade resistance or operating resistor leg remains constant. The system is calibrated at one given temperature (20°C) therefore the calibration is no longer an accurate presentation.

To circumvent this a film or wire coil with the same identical α (temperature coefficient of resistivity) can be made to replace the fixed leg of the bridge with the appropriate resistance (typically 60-80% above ambient for gases and 5-10% for liquids) and also placed into the flow environment. This allows the system to maintain a constant resistance ratio over the temperature range encountered. However, if the temperature is fluctuating at a frequency above approximately 2 Hertz this method is not compensating with fidelity due to the mass of the compensator.

For flows with slowly varying temperature this technique is ideal. However, for the high frequency case the bridge must be configured somewhat differently and the compensating leg replaced with a sensor similar to the velocity sensor with regard to geometry and materials. This method offers a relatively small mass to contend with and permits accurate velocity measurements irregardless of temperature fluctuation and fluid media.

These techniques may not be adaptable to all thermal-type devices, in which cases manual adjustment or correlation techniques must be employed. Also, simultaneous monitoring of temperature in combination with a family of calibration curves at a range of temperatures can be used to correct the data.

The next discussion point is the temperature distribution along the sensor itself. Knowledge of the detailed temperature distribution is not a requirement in most probe applications. The distribution is glossed over by the integrated mean temperature or resistance [2].

Much emphasis has been given to calibration technique and therefore the calibration method must also be explored and there are many. For gases most arrangements rely upon a pressure drop to determine the velocity using venturi sections, nozzles, pitot tubes, etc. If the device is not well defined one may be introducing inaccuracies into the experiment via the calibration obtained.

For liquids the method employed is more dependent upon the velocity range. Some typical systems most often used are tow tank, time/volume or weight collection, and standing tank with free jet exit nozzle, etc.

This leads directly to the first potential source of error. The value of the exponent n differs from sensor to sensor and also with velocity, Figure (2) along with the values of both A and B. It therefore becomes essential to calibrate each sensor/system individually and exercise periodic checks [2].

Although there has been extensive analysis on the subject of heat transfer applied to hot wires and films it has resisted all efforts to produce an accurate universal expression to describe it and to reiterate the only real method for interpretation of the results of thermal anemometry is direct calibration. A low turbulence flow of precisely known velocity is acceptable. One criteria is that the sensing probe must have the same orientation during calibration that which it will be mounted with regard to the velocity vector in the actual measurement. Typical directional sensitivity plots as shown in Figure (3) indicate the effect of yaw and pitch [3,4].

The probe geometry provides varied results [2]. For example, the prong spacing vs. sensor length for cylindrical types imparts noticeable changes. Figure (4). Proper probe design and precise calibration will reduce this contribution [4].

The temperature of the fluid must remain constant for the duration of the calibration measurement so that it will maintain accuracy. In the actual experiment this requirement may not always be satisfied, therefore, a method for compensation must be used. This can be accomplished via various techniques, however, before this can be intelligently discussed, a description of a typical electronic anemometer arrangement is required.

Hot-wire and hot-film anemometers are normally operated in the constant temperature (CTA) mode as shown in Figure (5). The resistance of the probe and, therefore, its temperature is maintained constant. The output bridge voltage is related to the heat transfer from the probe and this in turn is related to the fluid parameter under consideration (usually the velocity). The bridge is maintained in balance by a voltage from the servo-amplifier. Any change (ΔR) in the resistance of the probe resistance due to a change in the heat transfer will cause an unbalance in the bridge and simultaneously introduce an error voltage at the input to the servo-amplifier. This error voltage is highly amplified and fed back into the bridge to maintain balance via adjusted bridge voltage and sensor current. The probe temperature is thereby kept essentially constant and the thermal inertia of the probe is minimized. Due to the very high gain in the amplifier and the small mass of the sensor the system is capable of responding to very rapid fluctuations in velocity.

The present art of constant temperature anemometry is based on the design of a very stable servo-system with a very high closed loop gain and a well-balanced differential amplifier with a flat characteristic from DC to high frequencies. With the use of solid-state and integrated circuits these principles can and have been realized and extremely high feedback loop gains have been accomplished with stability thus allowing not only low noise but also the ability to correct for the frequency response of all types of probes including films.

These calibration schemes are static and an assumption must be made that the dynamic response is the same. Direct dynamic [5] schemes can be performed in a flow in which sinusoidal velocity variations are superimposed on a constant mean velocity.

Sensor contamination via the deposition of impurities present in the fluid can dramatically alter its heat transfer properties and subsequently the calibration. Cleaning and/or recalibration is required with the periodicty dependant upon the specific case. Additionally, in liquids dissolved gases can form bubbles on the sensor surface hence modifying the heat transfer and also the calibration [6]. The bubbles must be physically removed. To reduce this error contribution the sensor can be operated just slightly above the ambient temperature of the fluid and, if possible, precautions should be taken to reduce cascade effects and also implement deaeration processes in the case of supersaturated liquids.

Electronic drift in the past was a substantial contribution to measurement error but the latest technology in component design has reduced this problem by several magnitudes. Of course periodic stability checks enhance the virtue of the data obtained.

From a typical calibration as shown in Figure (2), it can be noted from the shape of the curve that the voltage resolution and thereby the velocity resolution can vary from volts to just a few millivolts over the range of, for example, 0-100 meter/sec. A high resolution voltmeter is then necessary to monitor the voltage for the velocity determination.

One solution is to provide a linearization circuit which matches the transfer function for a given probe velocity combination [7]. This can be accomplished by diode approximations, logrithmic and polynomial curve filtering and velocity controlled variable exponent techniques.

The benefits are twofold: higher accuracy is possible over the entire range and in the high turbulence case the non-linear distortion is eliminated. However, each additional electronic device included in the overall data producing system provides an additional drift potential which is additive.

For thermal anemometry it can be concluded that although there is an extremely wide range of differences of opinion in the extensive literature published to date, with regard to every facet, accurate measurements are obtainable with state of the art sensors and electronics. The overall accuracy result is in the hands of the end-user.

3. OPTICAL METHODS

Optical devices such as laser doppler anemometers or velocimeters are relatively new to the flow measurement field. In 1964 [23] it was demonstrated that coherent light sources could be used for the measurement of fluid velocities by observing the doppler shift in the frequency of light scattered from small particles moving with the fluid, Figure (6). In the

past few years the technique has expanded its capabilities immensely. Application demands have also moved with the same rapidity.

The laws of physics that apply can be expressed as follows: When two collimated beams of light intersect, they create a fringe pattern. A particle passing through this pattern causes a shift in the incident radiation. It can be shown that doppler frequency shift and particle velocity are related by:

$$f_d = \frac{2 \sin \frac{1}{2}\theta}{\lambda} U \qquad (5)$$

or:

$$U = \frac{\lambda}{2 \sin \frac{1}{2}\theta} f_d \qquad (6)$$

A laser doppler anemometer system is described in the block diagram of Figure (7). Typically most systems will follow this format or offer some small deviation. Each block will be discussed independantly with a brief explanation of its function and error contribution.

Radiation Source - The laser is monochromatic (single frequency) consisting of plane waves and the signal is both spatially and temporally coherent. Spatial coherence may be described by stating that all light waves in a cross-section of the beam are in phase with each other. This is accomplished in the laser cavity by suppressing the noncoherent modes of oscillation and placing a small aperture in the light path. Temporal coherence is present when the beam can interfere with itself over a considerable difference in path length. The light intensity follows a Gaussian distribution, Figure (8).

$$I = Io \exp - \frac{1}{2} \frac{x^2}{\sigma} \qquad I = 1/e^2 \text{ for } x = 25 \qquad (7)$$

corresponding to a beam diameter of 4 standard deviations. By integration of the intensity over the laser beam with a diameter of 4σ it can be demonstrated that 86.5% of the total emitted light is within the beam diameter.

Since the laser wavelength λ is a formidable part of the physical law of the doppler anemometer we must be concerned with multi-mode operation which is a primary cause of reduced effective coherence length which then places a requirement on the optical system with regard to equal path lengths. Path length differences can lead to a reduction in signal amplitude.

In high power lasers it is very easy to operate the laser in a mode other than TEM_{oo} (which is desired). The modes result in intensity profiles other than the Gaussian distribution and adjustment of the parameters of the laser cavity must be made. Also, laser oscillators normally operate at several optical frequencies simultaneously unless special single frequency techniques are used. When the multiple optical frequencies are combined on a square law detector such as a photomultiplier, the output contains

all possible difference frequencies between the optical frequencies. They may fall close to the doppler frequency making it impossible to differentiate one from the other. To limit this effect one can utilize short lasers which do not exhibit this effect or in the case of long lasers an etalon can be introduced into the cavity. It then selects one longitudinal mode thus eliminating the mode beating effect.

Transmitting Optics - The optical system transforms the input laser beam into an appropriate configuration for generating a doppler signal. This is normally accomplished with a beamsplitter (or bi-prism), mirrors and plano convex, a lens with a given focal length. There are three basic modes from which all other configurations are derived. They are: a) differential, b) reference beam, c) dual beam.

Criteria for measuring accuracy in the design of transmitting optics are that they be void of spherical and chromatic aberrations, have latitude for precise alignment adjustment [12]. In the differential mode, without alignment errors, the crossing of the beams takes place at their respective beam waists and the interference planes are approximately parallel with equal spacing. If the two beams intersect on the optical axis where they are not plane waves but contain a finite radius of curvature the fringe pattern will have an increasing spacing away from the transmitting lens. If particles with equal velocities move through the measuring volume perpendicular to the optical axis the doppler frequency generated will be dependent upon exactly where the particle physically passed through the measuring volume. If the two separated beams are parallel but do not encounter the lens perpendicularly the fringes are parallel but the separation increases perpendicular to the optical axis.

The Flow - The measuring volume is described as an ellipsoid of revolution of the two intersecting laser beams. Its dimensions are dependent upon:

a) Laser beam diameter - inversely proportional

b) Scattering angle θ - inversely proportional

c) Electronic level acceptance

When light falls upon a solid particle it will be scattered in every direction. The spatial scattering intensity distribution, i.e., the percentage of light going in certain directions in space will depend partly on the properties of the light itself (incident wavelength) and partly on the scattering particle (size, shape, refractive index). The intensity distribution for monchromatic light expressed as:

$$I = Io \frac{\lambda^2}{x^2 + y^2 + z^2} K (n,$$

when scattered from a single spherical particle with a diameter d, having a refractive index n relative to the surroundings.

The scattering function varies with particle diameter, the wavelength of the incident light and the refractive index of the particle. For given values of these parameters, the scattering function can be determined and the complete scattering picture mapped. The intensity of light radiated backward is very much lower than the intensity scattered forward.

In real cases, type and size of scattering particles will most often be restricted by the flow. For example, in very hot flows (a burning gas), only particles with a high melting point can be used. Furthermore, the particle must not be so large that its inertia prevents it from closely following turbulent variations in the flow, nor must it be so small that the amount of light scattered from the particles becomes too weak for detection.

The efficiency of the scattering process will be affected as the particle size changes from geometric to Mie to Raleigh scattering.

The interference fringe pattern in the measuring volume has a spacing given by:

$$dfr = \frac{\lambda}{2 \sin \theta/2} \tag{8}$$

As a particle passed through the fringes of the measuring volume, light will scatter from the bright fringes at a rate

$$f_d = \frac{U_x}{d} \tag{9}$$

If the fringes are aligned in the x-y plane and a particle with a velocity in the x direction passes through the fringes, the light reflected will have a frequency given by:

$$f_d = \frac{U_x \, 2 \sin \theta/2}{\lambda} \tag{10}$$

This frequency as given by equation (10) above bears a striking resemblance to that generated by doppler consideration.

The next consideration is the number of fringes in the measuring volume. This is essential for optimization with regard to signal quality, with regard to particle size, and also for the requirements of signal processing.

The number of fringes N_{fr} for a given optical system is given by:

$$N_{fr} = \frac{8 \, f_o \tan \theta/2}{\pi \, d_L} \tag{11}$$

Transfer Function vs. Index of Refraction - If the difference in index of refraction of the wall material is neglected and, considering water (the most commonly studied fluid with the exception of air), we can apply Snell's

Law to the situation indicated in Figure (9) and find that:

$$U = \frac{f_d}{2 \sin \theta/2} = \frac{f_{d,}}{2 \sin \theta_{,}/2} \tag{12}$$

The point of this result is that the transfer function remains unchanged when the laser beam passes from one medium to another. This is because index of refraction and wavelength form a ratio in the transfer function which remains constant, even though both change.

The offset in position of measuring volume within the flow can be calculated. Figure (10) indicates the effects on beams as they pass through different materials and thus the effect on the location of the measuring point.

The expressions for w and y may be derived as follows:

(i) From Snell's Law of Refraction -

$$n_w \sin \theta_w = n_p \sin \theta_p = n_a \sin \theta_a \quad (n_a = 1.00) \tag{13}$$

so θ_w, θ_p are

$$\theta_w = \sin^{-1} \frac{\sin \theta_a}{n_w}, \quad \theta_p = \sin^{-1} \frac{\sin \theta_a}{n_p}$$

since $\frac{f - a}{f} = \frac{x}{x/2} \rightarrow x = \frac{s}{2f} (f - a)$

$$y = x - p \tan \theta_p = \frac{s}{2f} (f - a) - p \tan \theta_p \tag{14}$$

$$w = \frac{y}{\tan \theta_w} = \frac{\frac{s}{2f} (f - a) - p \tan \theta_p}{\tan \theta_w} \tag{15}$$

(ii) From the above equation for w, we can get:

$$a = f \left[1 - \frac{2(p \tan \theta_p + w \tan \theta_w)}{s} \right] \tag{16}$$

where f = focal length of lens

s = separation distance of two beams

(iii) From above equation we can derive:

$$w = \frac{(f - a)\, s}{2f \tan \theta_w} - p \frac{\tan \theta_p}{\tan \theta_w} \tag{17}$$

If a is fixed and $p = p_o \pm x$, then $w = w_o \pm y$

$$\text{and } y = \frac{\tan \theta_p}{\tan \theta_w} x \tag{18}$$

It can be seen that the particles that are used for scattering purposes play a major part with regard to the accuracy of the measurement and that although an LDA is used to measure fluid velocities, the real measurement is the velocity of the scattering particles.

a) The largest particles contribute mostly to the light intensity so the velocities measured are weighted toward the largest particles in the distribution.

b) Particle sizes greater than 0.1 micron are required for LDA with the upper limit set at approximately 100 microns.

There are a number of effects that contribute to the relative motion with regard to the particle and the fluid, Figure (11). If a particle's density is different from the fluid medium, the particle velocity will not respond to the instantaneous velocity changes mainly because of inertia [19].

In air flows the particle density is very often much greater than that of the air which makes the effect more pronounced. An ideal situation is obtained when the density ratios are closely matched. Another effect of a density difference is the force of gravity inducing the particles to settle or drift up dependant upon densities greater or less than that of the fluid. Also, if a particle has rotation while moving with the fluid a force will be exerted on the particle in a direction which is perpendicular to the mean velocity vector and the axis of rotation. Another lifting effect can be found near the boundary where the velocity gradient is high.

Broadening of the doppler signal can take place if there is a strong velocity gradient across the measuring volume, velocity [10] fluctuations within the volume. Also finite transit time - random arrivals and departures of particles in and out of the volume can cause frequency and phase fluctuations in the doppler signal therefore presenting a finite width to the doppler spectrum. Signals from individual scattering particles last only for the time required to traverse the scattering volume. The frequency uncertainty is dependent on the scattering volume dimensions which are often controllable.

Receiver Optics - The measuring volume is brought into focus by a receiving lens, truncated by a fixed or adjustable field stop and then focused on a pinhole aperture. Finally, the light permitted to escape through the pinhole becomes slightly defocused so as to illuminate a large area of the photo cathode of photomultiplier. This basic geometry is used for all modes of operation including confocal backscatter.

Pinhole aperture size must be varied for optimization of signal-to-noise ratio. It is determined by:

$$d_p = \frac{f_t}{f_r} \cdot \frac{4 \lambda f_p}{\pi d_L} \qquad (19)$$

Signal Conversion - Signal conversion is effected by a photo detector; either a photomultiplier or photo diode. Each device simply changes light energy into electrical energy.

The principle for a typical PM are as follows: Radiant energy enters the evacuated enclosure through a "window" which has a semitransparent photocathode deposited upon its inner surface. The photocathode emits photoelectrons by the process of photoemission, i.e., by the interaction of the incident radiant energy with electrons in the photocathode material. Photoelectrons from all parts of the photocathode are accelerated by an electric field so as to strike a small area on the first dynode. Secondary electrons resulting from the process of secondary emission (i.e., from the impact of the photoelectrons on the first dynode) are accelerated toward the second dynolde by an electric field between dynodes No. 1 and No. 2 and impinge on the second dynode. The impact of the secondary electrons on dynode No. 2 results in the release of more secondary electrons which are then accelerated toward dynode No. 3. This process is repeated until the electrons leaving the last dynode are collected by the anode and leave the photomultiplier as the output signal.

The only possible degradation to the system would be additional noise and limited frequency response.

Signal Processing - The processing technique is a large contributor to the determination of the overall performance of an LDA system, particularly with regard to the magnitude and type of errors in the measurement. The first entry in the line of signal processing methods is the conventional spectrum analyzer with inherent measuring errors such as the skewness and broadening of the spectrum. A filter bank has basically the same constraints but improvement is obtained in that only the frequency range of interest is swept.

Another system which uses averaging is the photon correlation technique. This system construsts the time averaged autocorrelation frunction of the signal from the signal converter and becomes viable when the measurement offers only veryweak scattered light.

Time averaging methods are limited to long time history velocity measurements.

For real-time data the frequency tracker based on a phase or frequency locked loop can be considered. This method provides information relative to the flow fluctuations or short time history. It requires a continuous

or near continuous doppler signal to remain in lock. Since most signals are not entirely continuous due to phase reversal and periods when there are no particles in the measuring volume a tracker must be designed with a drop-out detector or hold circuit.

A counter-type processor is an alternative device for measurements where large drop-out periods are encountered. It is a measurement of the time of flight of a particle through a given number of fringes in the optical fringe or differential mode of operation.

The incoming signal which the electronic portion of the system must process has a given quality described ty the signal-to-noise ratio, ambiguity or broadening, and bias phenomena.

The acceptance level can be made adjustable by threshold levels and filtering techniques reducing the effect of noise and ambiguity by reducing the probe volume size. Window adjustments and validation by fringe count comparisons combined with amplitude level criteria serve to improve the overall accuracy.

4. CONCLUSION

The laser doppler anemometer on the surface appears to be the ideal method for flow measurement. It is inherently linear, requires no calibration (with the exception of standard electronics calibration checks), and does not provide any form of interference. However, it does provide a measurement of particle velocity which, with care, must then be related to the fluid velocity.

Hot-wire and film anemometry technique have been improved to the point where it can be considered a complimentary method when compared with the laser doppler anemometer.

Presently the LDA is well established as a useful measuring tool. It has already been subjected to a wide range of successful applications and a variety of flow problems. With future improvements with regard to operation and technique the LDA will undoubtedly become an important part of many additional measurement applications. We still require correction procedures for error and possibly the integration of them into the system would be an asset. A laser doppler anemometer justifiably is not a "point and measure" device. It does require sound judgment by the end-user.

NOMENCLATURE

Nu = Non-dimensional heat transfer coefficient

A = Constant determined by calibration

B = Constant determined by calibration

$R_e = \frac{\rho U d}{\mu}$

ρ = Density

U = Velocity

d = Wire diameter

μ = Viscosity

Q = Heat loss

l = Wire length

k = Thermal conductivity of fluid

T = Wire temperature

T_o = Fluid or ambient temperature

V = Voltage

R = Resistance

f_d = Doppler shifted frequency

λ = Laser wavelength

θ = Scattering angle of intersection

I = Light intensity

d = Distance between fringes

REFERENCES

[1] Schubauer, G. B., PROCEEDINGS OF THE INTERNATIONAL SYMPOSIUM ON HOT-WIRE ANEMOMETRY, March 1967, ed. by W. L. Melnik and J. R. Weske (AFOSR No. 68-1492, July 1968)

[2] Sandborn, RESISTANCE TEMPERATURE TRANSDUCERS, Metrology Press, Ft. Collins, Colorado, 1972

[3] Champagne, F. H., TURBULENCE MEASUREMENTS WITH INCLINED HOT WIRES, December 1965, Boeing Scientific Research Labs, Report #103

[4] Jorgensen, F. E., DIRECTIONAL SENSITIVITY OF WIRE & FIBER FILM PROBES, Disa Information #11

[5] Bechert, D., DYNAMIC CALIBRATION OF A HOT-WIRE ANEMOMETER USING A PULSATING NOZZLE FLOW, Euromech 63, (August 1975)

[6] Rasmussen, C. G., THE AIR BUBBLE PROBLEM IN WATER-FLOW HOT-WIRE ANEMOMETRY, Disa Information #5

[7] Comte-Bellot, G., ANNUAL REVIEW OF FLUID MECHANICS, Vol. 8, pp. 209-231 (1976)

[8] Nagib, H. M., Pluister, J. W., and Tan-Atichat, J., THE INTERPRETATION OF THE OUTPUT OF HOT-FILM ANEMOMETERS AND A SCHEME OF DYNAMIC COMPENSATION FOR WATER TEMPERATURE VARIATION, Proceedings of the Third Symposium on Turbulence in Liquids, University of Missouri at Rolla, (September 1973)

[9] Kovasznay, C. S. C., SHOULD WE STILL USE HOT WIRES?, Proceedings of the International Symposium on Hot-Wire Anemometry, W. L. Melnik and J. R. Weske, ed. (March 1967)

[10] George, W. K., LIMITATIONS TO MEASURING ACCURACY INHERENT IN THE LASER DOPPLER SIGNAL, Proceedings at LDA Symposium, Copenhagen (1975), p. 20, The Accuracy of Flow Measurements by Laser Doppler Methods

[11] Owen, J. M. and Rogers, R. H., VELOCITY BIASING IN LASER DOPPLER ANEMOMETERS, p. 89, Proceedings of LDA Symposium, Copenhagen (1975)

[12] Hanson, S., VISUALIZATION OF ALIGNMENT ERRORS AND HETERODYNING CONSTRAINTS IN LASER DOPPLER VELOCIMETERS, p. 176, Proceedings of LDA Symposium (1975)

[13] Melling, A. and Whitelaw, J. H., PROCEEDINGS OF THE THIRD BIENNIAL SYMPOSIUM ON TURBULENCE IN LIQUIDS, pp. 115-135

[14] McLaughlin, D. K. and Tiederman, W. G., STATISTICAL BIASING IN INDIVIDUAL REALIZATION LASER ANEMOMETRY, Workshop on Theory and Application of the LDA held at Oklahoma State University (June 11-13, 1973)

[15] Stevenson, W. H. and Thompson, H. D., THE USE OF THE LASER DOPPLER VELOCIMETER FOR FLOW MEASUREMENTS, Proceedings of a workshop co-sponsored by U. S. Naval Army Missile Command and Project Squid, Purdue University (March 9-10, 1972)

[16] Stevenson, W. H. and Thompson, H. D., PROCEEDINGS OF THE SECOND INTERNATIONAL WORKSHOP ON LASER VELOCIMETRY, Purdue University (March 27-29, 1974)

[17] Kreid, D. K., ERROR ESTIMATES FOR LASER DOPPLER VELOCIMETER MEASUREMENTS IN NON-UNIFORM FLOW, Proceedings of the Second International Workshop on Laser Velocimetry, p. 398-427, Purdue University (March 27-29, 1974)

[18] Love, T. J., A SIMPLIFIED SCHEME FOR ESTIMATE OF LIGHT SCATTERED BY A SINGLE PARTICLE IN THE DESIGN OF DETECTOR GEOMETRY FOR LASER ANEMOMETER APPLICATIONS, Laser Anemometer Workshop, Oklahoma State University, (June 11-13, 1973)

[19] Durrani, T. S. and Greated, C. A., LASER SYSTEMS IN FLOW MEASUREMENT, Plenum Press, N. Y. & London (1977)

[20] Bradshaw, P., AN INTRODUCTION TO TURBULENCE AND ITS MEASUREMENT, Pergamon Press (1971)

[21] Kristensen, H. S., HOT-WIRE MEASUREMENTS IN TURBULENT FLOWS, Disa Information Department, Disa Electronics (1973)

[22] Tennekes, H. and Lumley, J. L., A FIRST COURSE IN TURBULENCE, M.I.T. Press (1972)

[23] Yeh, Y. and Cummins, H. Z., LOCALIZED FLUID FLOW MEASUREMENTS WITH A HE-NE LASER SPECTROMETER, Applied Physics Letters, Vol. 4, No. 10, pp. 176-178 (1964)

[24] Yanta, W. J. and Smith, R. A., MEASUREMENTS OF TURBULENCE TRANSPORT PROPERTIES WITH A LASER DOPPLER VELOCIMETER, AIAA Paper, pp 73-169, AIAA 11th Aerospace Sciences Meeting, Washington, D. C. (January 10-12, 1973)

[25] Whitelaw, J. H. and Melling, A. M., MEASUREMENTS IN TURBULENT WATER FLOWS BY LASER ANEMOMETRY, Proceedings of the Third Symposium on Turbulence in Liquids, University of Missouri at Rolla, (September 1973)

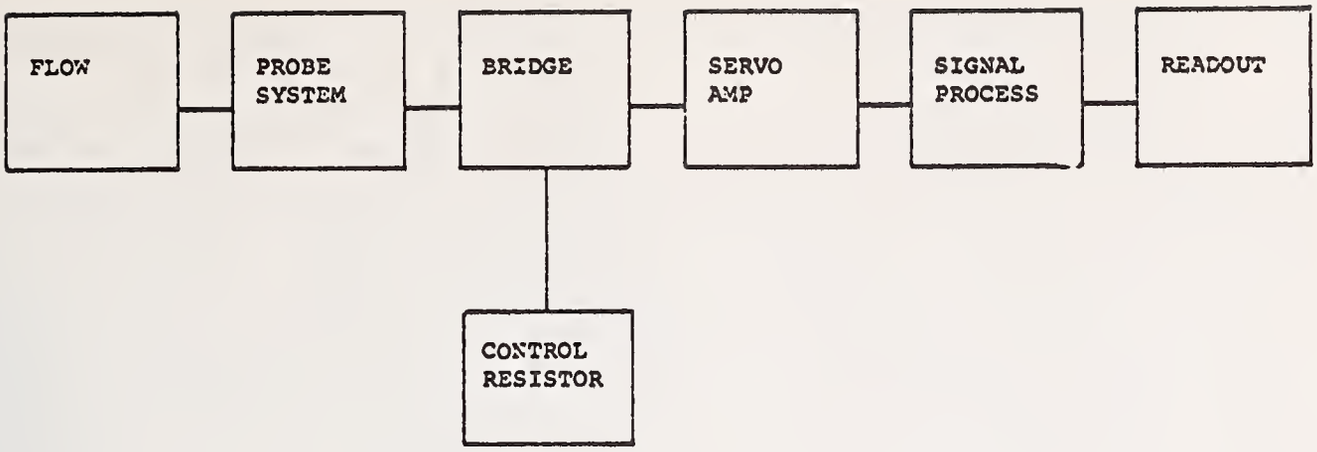

Figure 1. BASIC CTA THEORY

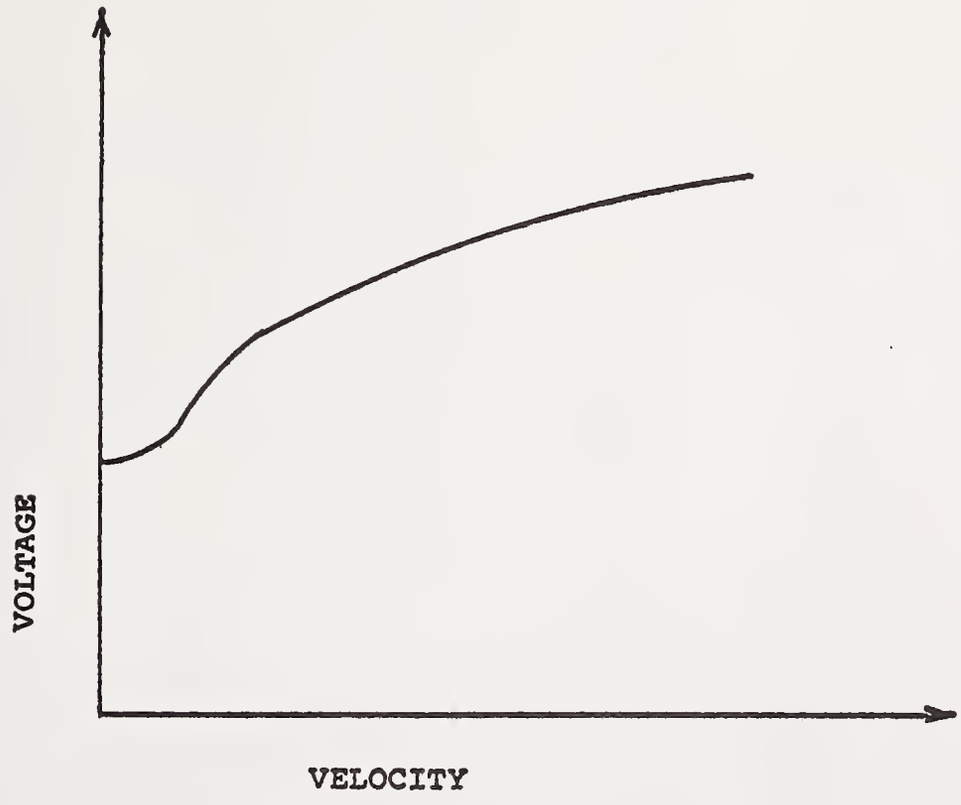

Figure 2. TYPICAL CALIBRATION CURVE

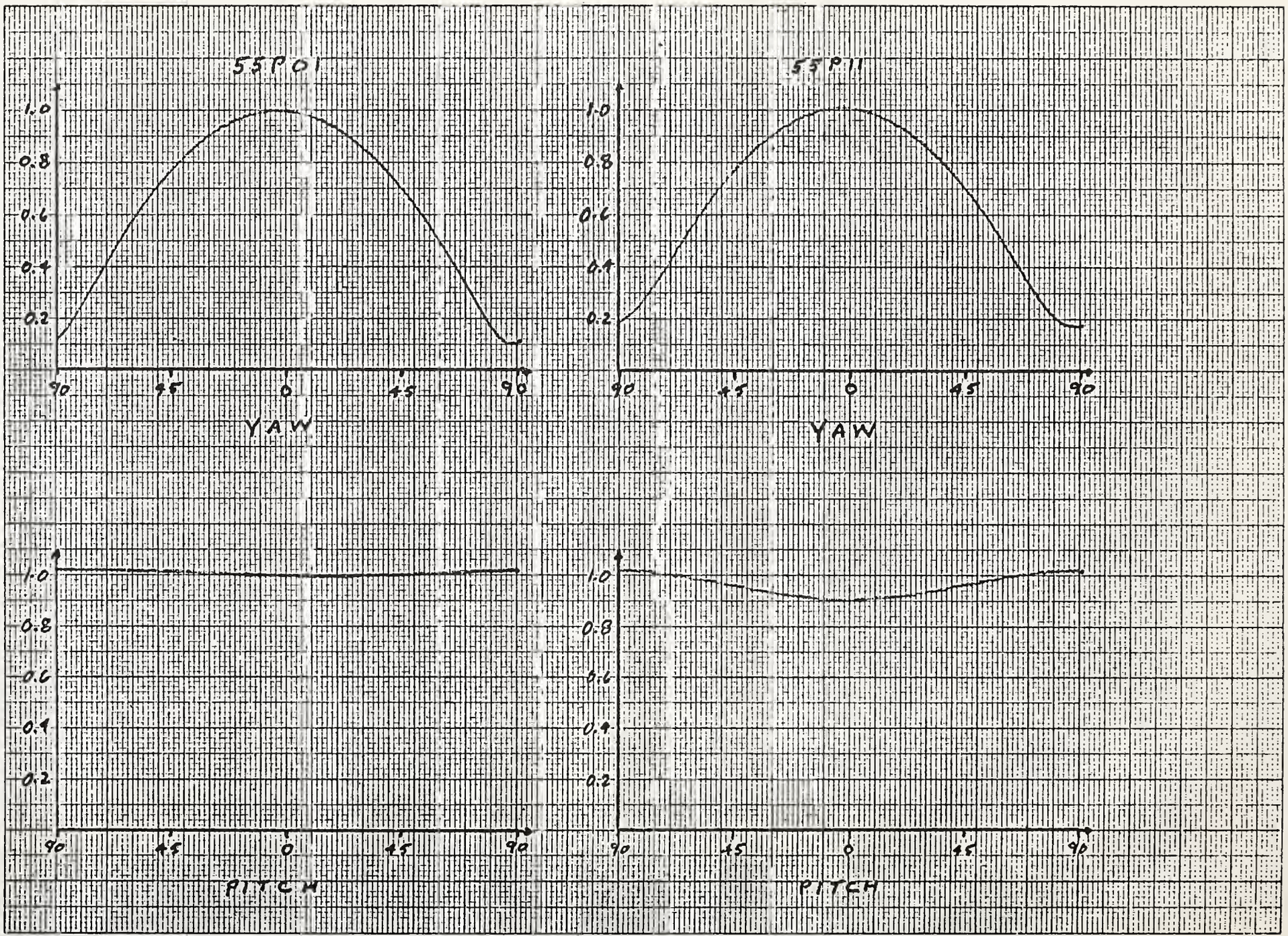

Figure 3. DIRECTIONAL SENSITIVITY

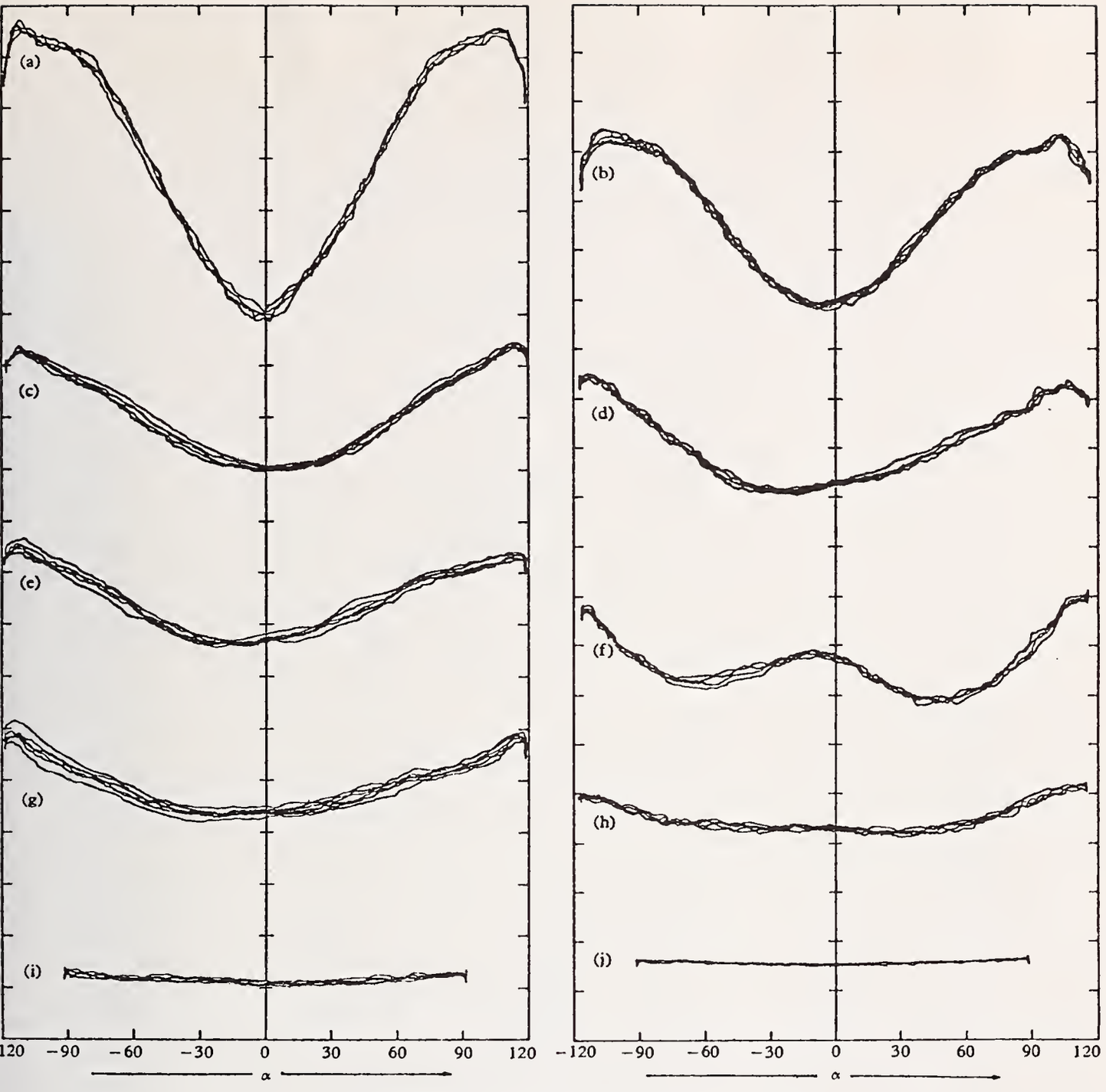

Directional characteristics of experimental probes with different prong lengths l and prong spacings s (with a constant sensory wire length of 1 mm).
The curves are related to the following probe and flow parameters:

Curve	Configuration of Hot-wire Probe (s, l)	Velocity Um/s	Linearizer output voltage for $\alpha = 0°$ in volts	Scale mV/DIV.
(a)	1, 9	11.3	3.28	100
(b)	1, 9	40.1	9.65	500
(c)	2, 6.5	11.1	2.58	100
(d)	2, 6.5	40.6	10.42	500
(e)	3, 8.8	10.1	2.78	100
(f)	3, 8.8	40.7	8.85	500
(g)	4, 7.6	9.9	3.10	100
(h)	4, 7.6	40.4	9.30	500
(i)	turntable	10.1	2.54	100
(j)	turntable	40.8	10.45	500

Figure 4. DIRECTIONAL CHARACTERISTICS OF PROBES

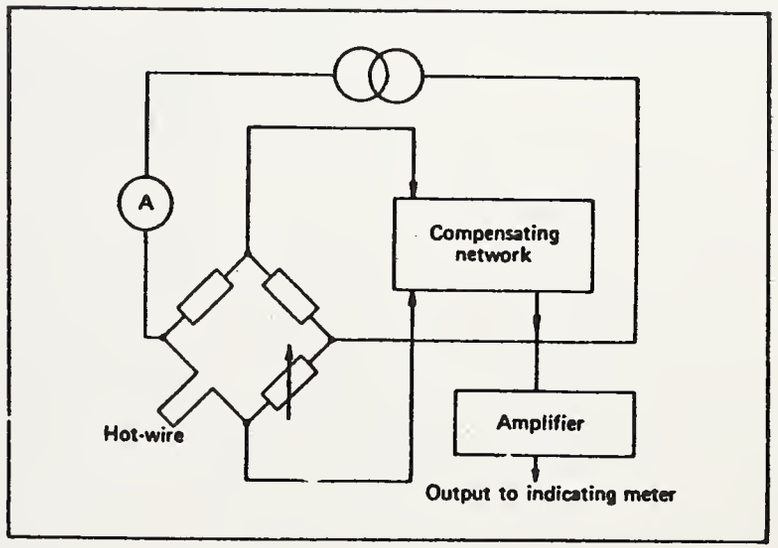

Constant-current anemometer.

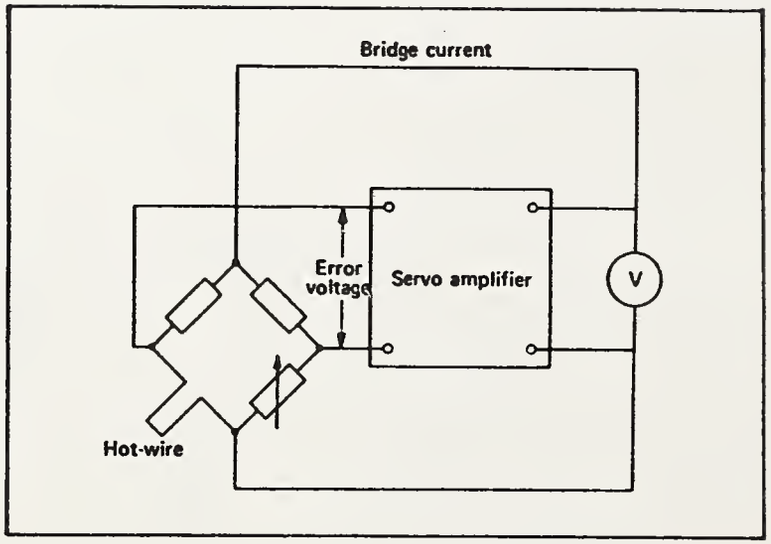

Constant-temperature anemometer.

Figure 5. SCHEMATIC DIAGRAMS OF CONSTANT-CURRENT AND CONSTANT-TEMPERATURE ANEMOMETERS

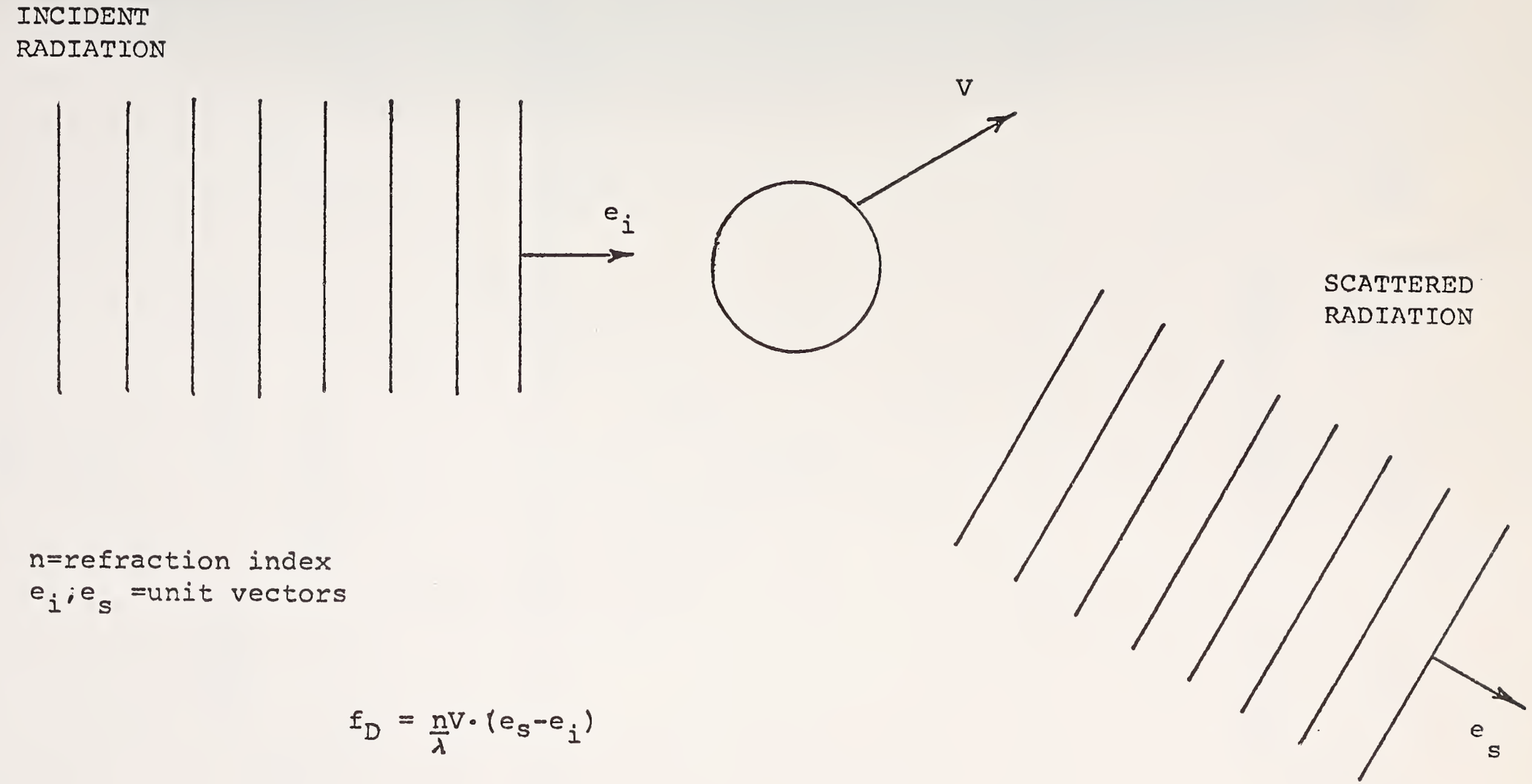

n=refraction index
e_i;e_s =unit vectors

$$f_D = \frac{n}{\lambda} V \cdot (e_s - e_i)$$

Figure 6. DOPPLER PRINCIPLE

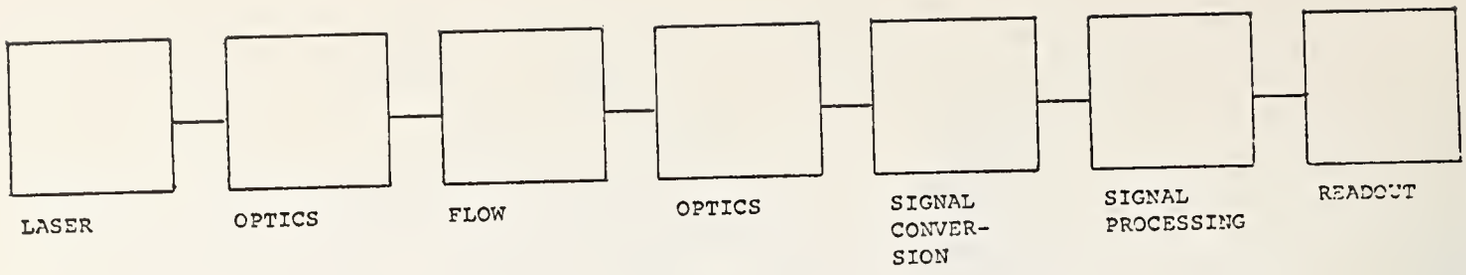

Figure 7. LDA BLOCK DIAGRAM

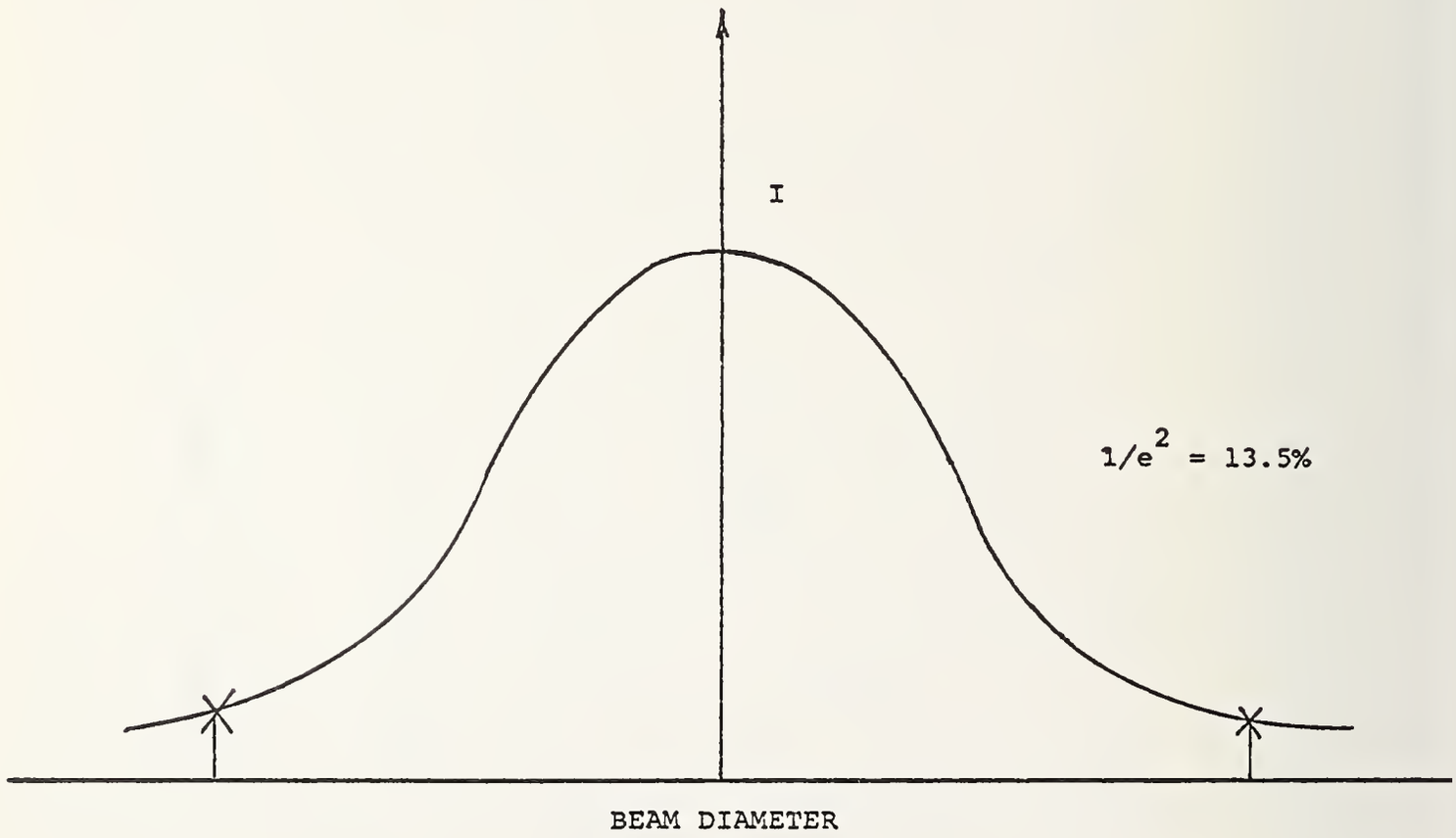

Figure 8. GAUSIAN BEAM

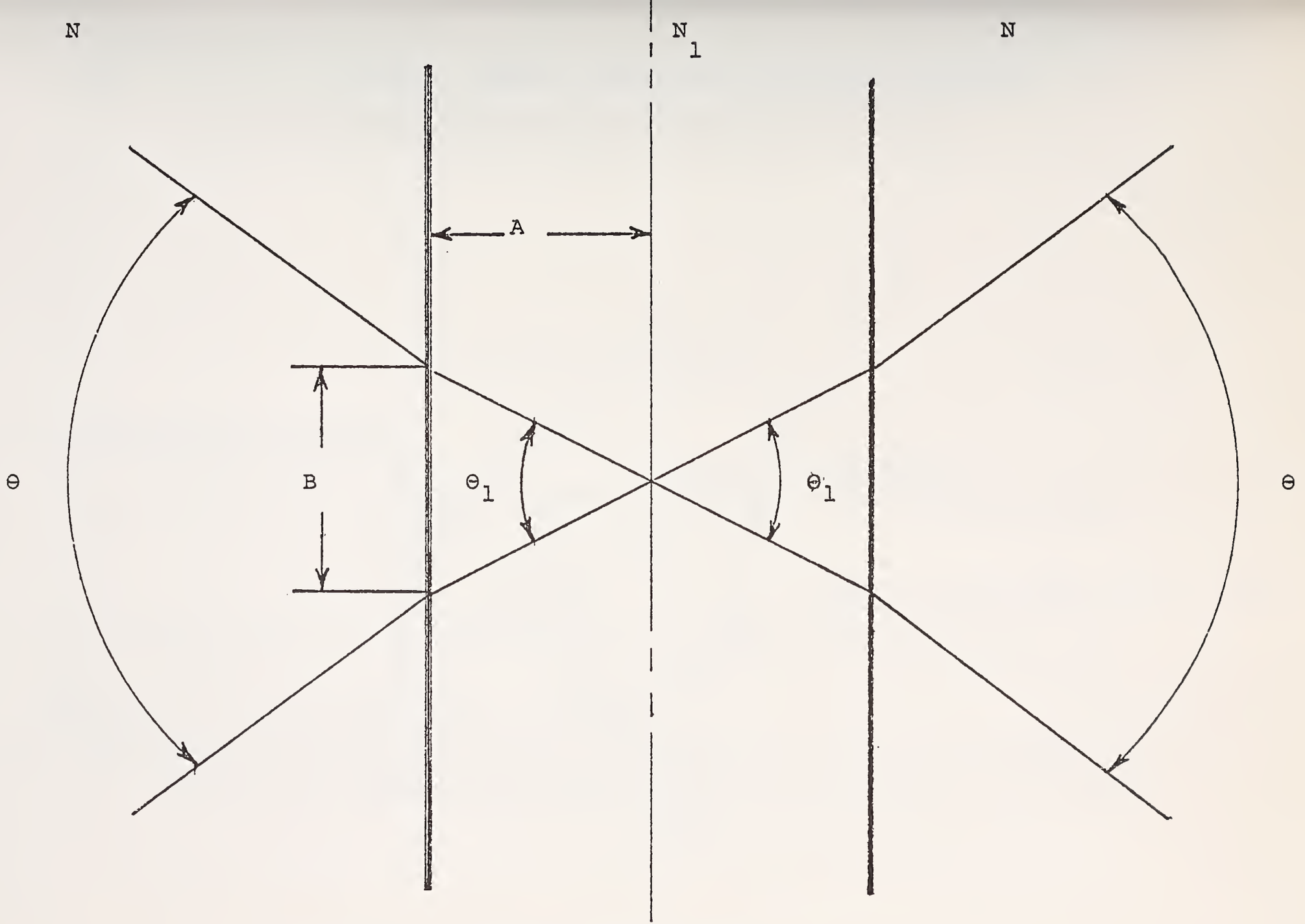

Figure 9. INDEX OF REFRACTION

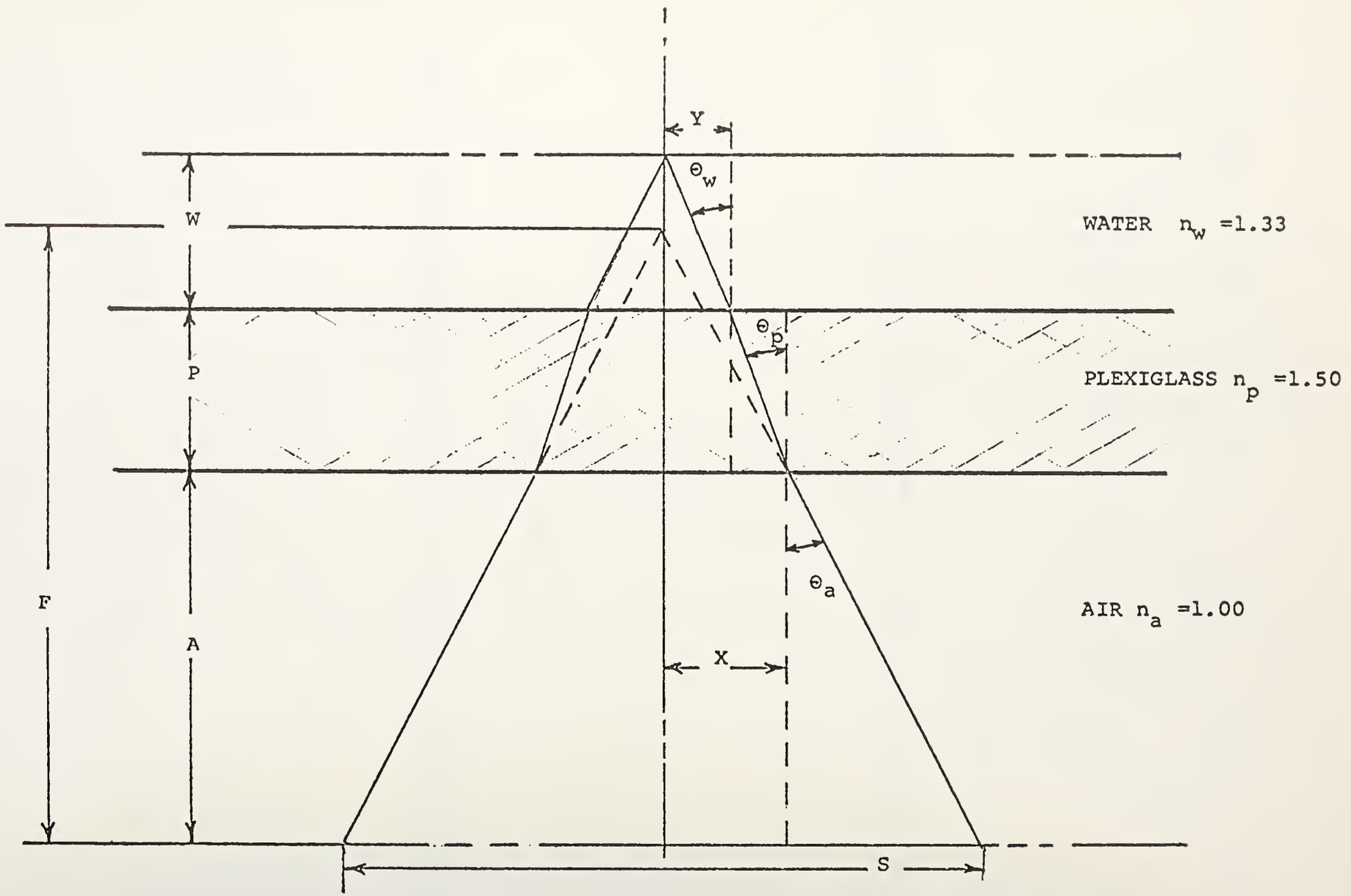

Figure 10. INDEX OF REFRACTION WITH VARIOUS INTERFACES

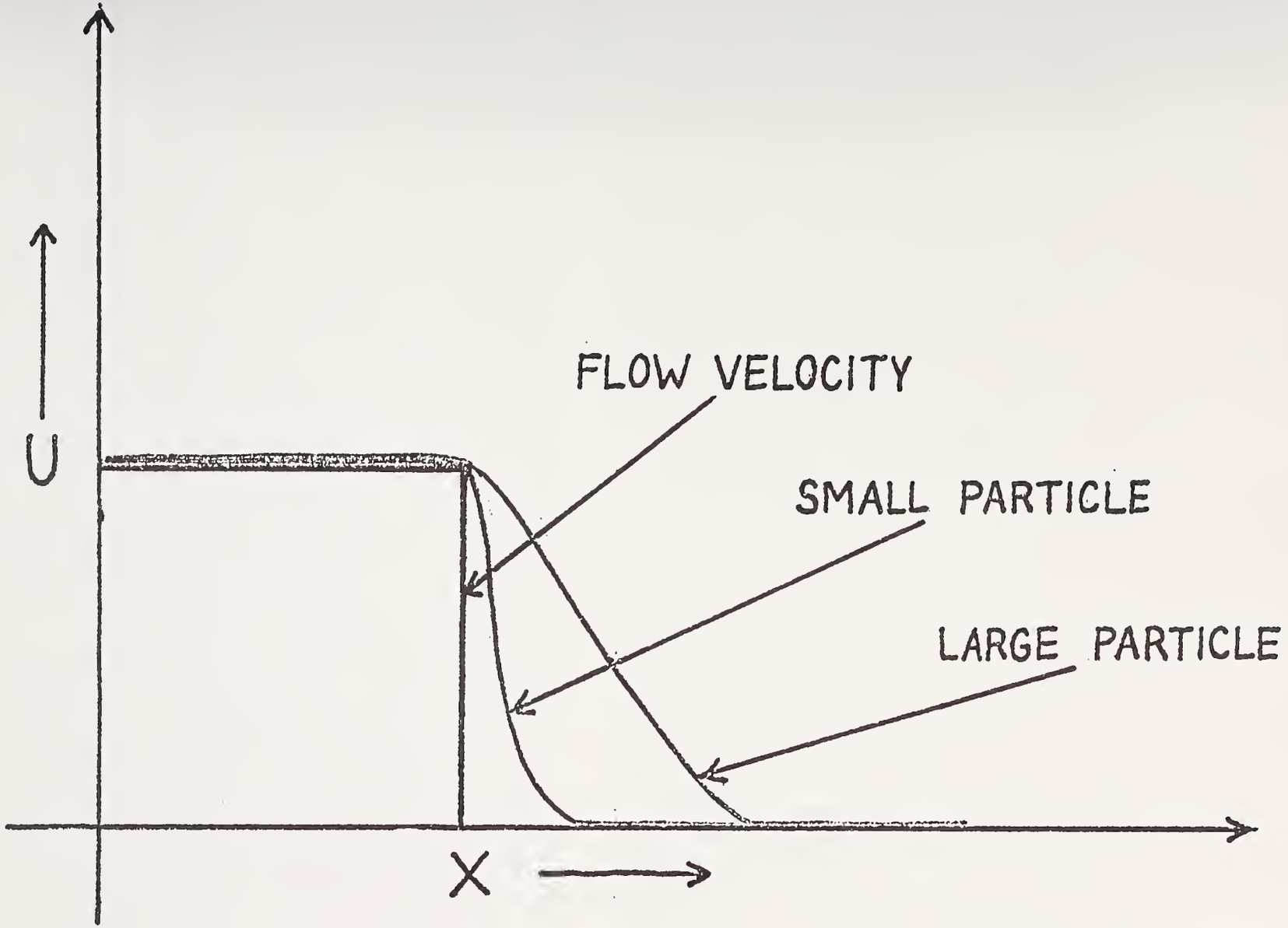

Figure 11. RELATIVE MOTION OF FLUID AND PARTICLES

National Bureau of Standards Special Publication 484, Proceedings of the Symposium on Flow in Open Channels and Closed Conduits held at NBS, Gaithersburg, MD, February 23-25, 1977. (Issued October 1977)

NEAR WALL VELOCITY MEASUREMENTS FOR WALL SHEAR INFERENCE IN TURBULENT FLOWS

F. J. Pierce
Professor of Mechanical Engineering
Virginia Polytechnic Institute
Blacksburg, Virginia

D. S. Gold, Engineer
E. I. Dupont
Waynesboro, Virginia

The existence of logarithmic near wall similarity for two-dimensional turbulent flows permits the inference of local wall shear stress from ordinary velocity profile data. In cases of minimal logarithmic similarity, it would be helpful to use the velocity measurements closer to the wall, in the 'very' near wall region. Regrettably, this data is all too often inconsistent, deviating considerably from the proposed similarity laws, and thus invalidating its use for wall shear inference. In an attempt to explain such inconsistent behavior, velocity profiles were systematically measured with four different probes under six different flow conditions. Additionally, classical displacement corrections were considered as was the effect of the choice of similarity laws and 'universal' law of the wall constants. While small, consistent differences were identified with different probes and different flow conditions, none of the probes or flow variations studied were able to explain the frequently encountered kind of inconsistency between measurements and proposed similarity laws in this very near wall flow.

INTRODUCTION

Evaluation of the local wall shear stress in a two-dimensional turbulent boundary layer or channel flow is important in estimating drag forces, pressure losses, and local heat transfer rates. Local wall shear stress can be evaluated by direct force measurements, but this method requires special instrumentation and is generally difficult. The existence of universal, near wall similarity allows for the indirect measurement of local wall shear stress with such devices as Preston tubes, Stanton tubes, rakes, fences, and heat meters. Yet an alternative method to infer local wall shear stress is to use ordinary near wall velocity data points such as are obtained in velocity profiles. This paper focuses on this last method.

Historically, in 1954 Clauser [1][1] first proposed using near wall similarity for inference of local wall shear stress. His method uses several near wall velocity points with a subjective estimate of a best fit with parametric skin friction or shear velocity lines. In 1959 Bradshaw [2] proposed an alternative method using fewer data points and somewhat more objective. Most recently, in 1965, Schraub and Kline [3] proposed another

[1]Figures in brackets indicate the literature references at the end of this paper.

variation which can be developed to give a more precise and even a statistical inference of the local wall shear stress.

All these indirect methods make use of the universal similarity described by the so called 'inner' or 'logarithmic' law, or 'law of the wall' written as

$$u^+ = \frac{1}{k} \ln y^+ + c \qquad (1)$$

Since this law does not correlate the velocity data right down to the wall through the usually designated buffer region and viscous sublayer, data points in these regions must be excluded in local wall shear stress inference methods using velocity profile data. The inclusion of a sublayer formula (and even a buffer region formula) gives an 'extended' law of the wall formulation made up of two (or three) formulas as

$$u^+ = y^+ \qquad (2)$$

$$u^+ = \frac{1}{k} \ln y^+ + c \qquad (1)$$

Alternatively, Spalding [4] and Kleinstein [5] have proposed the 'single formula' law of the wall which continuously covers near wall velocity data down through the viscous wall region. This relationship treats u^+ as the independent variable with

$$y^+ = u^+ + \exp(-kc) \left[\exp(ku^+) - 1 - (ku^+) - \frac{1}{2}(ku^+)^2 - \frac{1}{6}(ku^+)^3\right] \qquad (3)$$

A fourth order term, $-(ku^+)^4/4!$, can also be included above but its effect is relatively small and confined mainly to the so called buffer region. Equation 3 agrees well with the previous expressions and avoids the difficulty of manipulating two (or three) equations for each profile.

In the following, it is convenient to refer to the data correlated by the logarithmic law, Eq. 1, as the near wall data, and that yet closer to the wall as the very near wall data. This very near wall data would presumably correlate with the viscous sublayer relationship, Eq. 2, (and a buffer layer equation if one choses to use one) and the Spalding formula, Eq. 3, for small y^+. The division between the near wall and very near wall data is somewhat arbitrary as shown in Fig. 1.

In 1973, Pierce and Zimmerman [6] demonstrated how one could adopt the methods of Clauser or Schraub and Kline for local wall shear prediction to include all the near wall data through the buffer region and viscous sublayer. The inclusion of velocity data points nearer to the wall than included by Eq. 1 is of interest in flows with minimal logarithmic similarity as occurs in cases with severe pressure gradients or where sufficient flow time for the development of the logarithmic region is unavailable. In addition, speculating on the extension of such indirect methods to the case of three-dimensional flows, Pierce and Zimmerman observed that the usual pressure driven three-dimensional turbulent boundary layer has a minimum of logarithmic-like similarity for use in the possible inference of local wall shear stress for this more complex kind of flow.

Thus, the behavior of very near wall data becomes of stronger and more necessary interest.

The universality of a logarithmic near wall behavior of two-dimensional turbulent boundary layer and channel flows is reasonably well established (with the exception of extreme pressure gradients and flows with insufficient development distance). On the other hand, typical velocity data for two-dimensional turbulent flows nearer to the wall and in the so called buffer and viscous sublayer regions (the very near wall region) is noted for its inconsistency. While much of the velocity profile data for fully developed flows in pipes and channels does follow the viscous sublayer law and the corresponding portion of the Spalding single formula law, a very large number of boundary layer flows give velocity data points at significantly higher values in this very near wall region. It is often not so much a case of data being erratic in this very near wall region, as a case of the data seemingly wanting to follow a regular pattern, but well above that predicted by either Eq. 1 or the single formula law of the wall. The inconsistent behavior of this very near wall data is described in the reports of Coles [7] and Coles and Hirst [8] where over 400 profiles are considered in establishing law of the wall constants. Coles suggested that the discrepancies were not the fault of the formula, but assumed they were the result of experimental errors, and he chose to ignore the very near wall data points because of this inconsistent behavior.

Thus, while the techniques are available for the inference of local wall shear stress using the very near wall velocity profile data, the lack of well established and universal similarity for this very near wall data make suspect any inferred wall shear values using these techniques. This experiment attempted to provide some insight as to the behavior of very near wall velocity data in a low speed, incompressible, two-dimensional turbulent boundary layer in air by systematically changing the velocity measuring probe or the flow conditions. Consideration was also given to changes in the law of the wall constants, to systematic probe position errors, and to so called displacement corrections.

In the first series of experiments, velocity profiles were measured with

1. a gooseneck boundary layer probe (0.020-in. (0.5-mm) OD)
2. a small standard claw probe (0.020-in. (0.5-mm) OD)
3. a large standard claw probe (0.028-in. (0.7-mm) OD)
4. a standard, straight hot wire probe (0.0002-in. (0.005-mm) wire).

In a second series of experiments, profiles were measured for

5. a near zero pressure gradient
6. a mildly favorable pressure gradient
7. a mildly adverse pressure gradient
8. a slightly converging flow
9. a slightly diverging flow.

These last two cases were run in an attempt to determine if slight convergence or divergence in the flow would explain the inconsistent very near wall behavior. All of these flow conditions were run with a boundary layer trip well upstream of the test station. A final flow condition tested was with

10. a sharp leading edge for the floor of the channel.

This last case was to determine the effect of the boundary layer trip on the very near wall velocity measurements. All of the measurements were made at a fixed unit Reynolds number for the tunnel so that flow conditions were nominally constant. The pressure gradient flow cases and the converging-diverging flows had different local unit Reynolds numbers because of the area variations required to create these conditions. In all, thirty-nine velocity profiles were measured with four different probes and at six different nominal flow conditions.

EXPERIMENT AND APPARATUS

A schematic diagram of the apparatus is shown in Fig. 2. Air was drawn through 1.5-in. (3.8-cm) fiberglas filters into a plywood settling chamber, 49x54x50-in. (1.24x1.37x1.27-m). A louver damper regulated the flow velocity from 20 to 120-ft/sec (6.6 to 39.4-m/sec). A ten-horsepower, 60-hertz ILG Ventilating Company Size 300 centrifugal fan blew air into the test channel. A plywood diffuser connected the fan discharge to a rectangular 45x45x60-in. (1.1x1.1x1.5-m) plywood plenum containing a bundle of 1.5-in. (3.8-cm) diameter cardboard mailing tubes. Screens diminished the fan fluctuations and insured a moderate turbulence level in the test section air stream. A 4-ft (1.2-m) long plywood section followed by a sheet metal nozzle with a nine-to-one contraction ratio reduced the flow area to the 10x14-in. (25.4x35.6-cm) plexiglas walled tunnel cross section. A 1/4-in. (6.4-mm) gap between the nozzle and the tunnel filled with foam rubber minimized vibration transmission to the test channel.

Early turbulent transition was forced by 1/8-in. (3.2-mm) diameter rods across the four sides of the test channel inlet. The length of the two-dimensional test channel was 134-in. (3.4-m), and all velocity profiles were measured at a test station 84-in. (2.1-m) downstream of the test channel inlet. The rectangular test section served as the entrance section to a three-dimensional impinging jet geometry. Velocity profiles reported here were measured 50-in. (1.27-m) upstream of the jet entrance, and no three-dimensional effects were detected at this distance upstream. Four static pressure taps, 1/32-in. (0.8-mm) diameter, were placed in the tunnel roof at 2-in. (5.1-cm) intervals in the transverse direction with additional static pressure taps placed 2-3/4 in. (7-cm) upstream and downstream of the test station.

Small positive and negative pressure gradients were created by using a smoothly faired wooden wedge approximately 22-in. (56-cm) long having a shallow angle of 7 degrees. The pressure gradient was measured with three static pressure taps placed in the wedge, and spaced at 3-in. (7.6-cm) intervals in the streamwise direction. The wedge was attached to the tunnel roof so that it could easily be reversed providing the area variation for either rising or falling pressure. A pair of similar wedges were placed along the tunnel side walls to provide the small convergence or divergence in the flow on the floor. In this case it was not possible to separate the pressure gradient effect and the convergence (or divergence) in the flow. Inlet conditions in the test channel were altered by placing a flat plate with a sharp (45°) leading edge on the floor of the tunnel. When installed, the leading edge extended approximately 2-in. (5.1-cm) into the inlet flow nozzle, and all boundary layer trips were removed.

The vertical positioning of the various probes was obtained with a traversing mechanism. A dial indicator measured changes in distance from the tunnel floor to within ± 0.0005-in. (0.013-mm). A horizontal-vertical cathetometer was used to insure accurate vertical placement of the probe relative to the tunnel floor with the aid of a graduated metal gage block. After the probe was positioned correctly, the reading of the dial indicator was adjusted to correspond to the known distance above the tunnel floor. The estimated tolerance of the probe positioning procedure was ± 0.001-in. (0.025-mm).

The mean velocity profiles were measured by three different stagnation probes: (1) United Sensor, Model USC-E-101 gooseneck probe (.020-in. (0.5-mm) OD) with an offset radius of nominally one inch; (2) United Sensor, Model CA-120 claw probe (.020-in. (0.05-mm) OD); and, (3) United Sensor, Model CA-120-24-F-CD claw probe (.028-in. (0.7-mm) OD). The gooseneck probe was visually aligned with the tunnel centerline as this could be done easily within the ± 15° cited in [9] as critical for yaw errors less than ± 1% of the dynamic head. The claw probes were nulled for alignment, using the two outer orifices as is the usual procedure for such probes.

Additionally, a DISA straight hot wire probe type 55A22 (0.0002-in. (0.005-mm) wire), was also used for velocity measurements. This system was made up of an annemometer, a linearizer, a voltage divider, a VFC and an electronic counter. The hot wire was calibrated against a pitot-static probe in the tunnel free stream.

To insure similar tunnel flow conditions the tunnel unit Reynolds number as measured at a fixed location near the tunnel exit, was held at the nominal value of 5.8×10^5 per ft (1.9×10^6 per m). All pressure readings were made with micromanometers. Stagnation pressures were read at one minute intervals to allow for response time. Hot wire readings were averages of five readings each of which was averaged over ten seconds by the counter.

RESULTS

The 39 runs at six different flow conditions are coded in a four digit sequence as follows:

Tunnel geometry

- 1xxx constant area with trip wires
- 2xxx falling pressure (accelerating flow) with trip wires
- 3xxx rising pressure (decelerating flow) with trip wires
- 4xxx constant area with sharp leading edge
- 5xxx diverging floor flow with trip wires
- 6xxx converging floor flow with trip wires

Probe designation

- x1xx gooseneck boundary layer (0.020-in. (0.5-mm) OD)
- x2xx standard claw probe (0.020-in. (0.5-mm) OD)
- x3xx standard claw probe (0.028-in. (0.7-mm) OD)
- x4xx standard, straight hot wire probe (0.0002-in. (0.005-mm) wire)

The last two digits designate repeated profiles under any given probe/ flow conditions.

Space limitations do not allow a detailed discussion of individual profiles or data reduction options. The following discussion is intended to summarize and generalize the findings and interpretations. A detailed discussion of all aspects of the experiment and its results is contained in reference [10]. Table 1 summarizes the 39 runs made. The several repeated profiles in series 1100, 1200, and 1300 assured experimental technique and repeatability, and gave a good indication of the kind of experimental scatter to be expected with a given probe.

Before measured data can be expressed in similarity coordinates, the value of the shear velocity, or the wall shear stress, must be determined either by an indirect method based on near wall similarity or by direct force measurement. In this investigation the wall shear stress was inferred by the technique presented by Pierce and Zimmerman [6] which uses the method of Schraub and Kline [3] to infer a value of the shear velocity from each data point in the velocity profile. Since the shear velocity is a constant value for a given profile, the predictions from the individual data points were averaged to determine a unique value for the shear velocity. The data used in this prediction was limited to the range of data in the logarithmic region. Values of y^+ greater than 300 were excluded due to the presence of the wake region, and values less than 50 were excluded as in [7] and [8] for this is nominally the very near wall region (see Fig. 1) where inconsistent behavior is noted and to be examined here. The average value of the shear velocity was normally for six data points per profile. The cubic Spalding single formula, Eq. 3, was used to infer individual shear velocities and for comparison in u^+, y^+ plots.

Both the law of the wall and the Spalding single formula equation require two constants which must be evaluated experimentally. These constants are the same for both expressions, and they are generally accepted as being universally valid, yet there exists some substantial disagreement concerning the precise numerical values for them.

Table 2 summarizes a collection of these constants and Fig. 3 shows the effect on Eq. 1. These same constants appear in Eq. 3 with the same effect for $y^+ > 50$ and a similar spreading effect for $50 > y^+ > 0$ as shown in Fig. 4. The variation of these constants does affect the value of shear velocity calculated for a given profile and the 'goodness' of fit to the logarithmic region when plotted in u^+, y^+ coordinates. This variation does <u>not</u> appear to account for the erratic behavior of very near wall data. The Coles' values are judged to be based on the most exhaustive study of a very large collection of data. The Patel constants were used initially in this study because they are more recent and because they gave nearly identical results as suggested in Fig. 3 and 4. It is noteworthy that the Smith and Walker constants [11], sharply different from the above, are one of the few sets obtained from velocity and <u>direct</u> wall shear stress measurements.

Table 3 shows the range of physical wall distance, y, mean u/U, mean u^+ and y^+, and standard deviation of u/U and u^+ at corresponding y for the 20

profiles in the 1100, 1200, and 1300 series. The sample standard deviations in Table 3 indicate that the uncertainty involved with the velocity measurements nearest the wall for each of the probes was generally greater than the uncertainty for the remaining measurements. This type behavior is not surprising for the first data points due to their close proximity to the wall. For all three probes, the standard deviation of u^+ (excluding the data point nearest the wall) was well behaved through the logarithmic region of the profile. The largest value of the standard deviation in this region is 0.07 and this value corresponds to an approximate uncertainty of $\pm$ 0.3 ft/sec (0.09 m/sec) for the velocity measurements in the boundary layer and compares well with the expected uncertainty of the velocity based on a micromanometer uncertainty of $\pm$ 0.005 in. (0.13 mm) of water, or approximately $\pm$ 0.3 ft/sec. (0.09 m/sec). Experimental repeatability is also shown in Figs. 5 and 6 for the 1100 series runs. These figures show typical scatter for subsequent multiple run series.

Probe Effects

Figures 7 and 8 show the typical effects of the four probes used. In general, in the near wall region, the hot wire recorded highest velocities, followed by the large OD claw, the small OD claw, and the gooseneck (offset) boundary layer probe. The slightly higher near wall velocities measured with the large claw and wire predicted higher shear velocities, with the net effect of bringing the u^+, y^+ plots into closer agreement among the probes (higher local u divided by higher u^* tends to mask the physical velocity differences). An initial reaction is to identify the higher velocities of the large claw probe with so called displacement effects, but the even higher hot wire values question this conclusion and suggest probe stem interference effects. Heat loss to the wall would not be a likely explanation for the low overheat ratio and relatively large distances (for the hot wire) involved. These figures indicate that the hot wire probe has closer agreement with the claw probes than with the gooseneck probe, which suggests that the gooseneck geometry is a factor in the discernable differences in these near wall velocity measurements. Other factors considered on the readings of the stagnation type probes are discussed below.

Stagnation pressure is measured by an orifice at the stagnation point of a body. The presence of a probe will unquestionably disturb the flow to some extent, which can introduce systematic errors into the velocity measurements. Dean [9] notes that in the usual range of investigations, the total pressure probe is insensitive to Mach and Reynolds number effects and considerable misalignment. Errors resulting from viscous effects, normal velocity gradients, near wall effects, or stream turbulence could be significant in boundary layer velocity measurements. Various investigations cited by Dean indicate that the stagnation pressure is free of viscous effects for low velocity flows down to a Reynolds number of 30 based on the radius of the pressure orifice. For a probe with an inside diameter of 0.010-in. (0.25-mm), the critical Reynolds number corresponds to a velocity of 12-ft/sec (3.6-m/sec). Since flow velocities below 50-ft/sec. (15.2-m/sec) were never measured here, this effect does not appear to be significant.

When a stagnation probe is placed in a normal velocity gradient, there exists a gradient in stagnation pressure across the face of the probe orifice. The probe will not integrate this pressure gradient to give an indicated

pressure representative of the velocity at the geometric center of the orifice. Young and Maas [12] express this effect of the velocity gradient as a displacement of the 'effective center' of the probe from the geometric center toward the region of higher velocities by an amount equal to 0.18 times the external diameter of the probe. If this displacement correction was applied to the probes used in this experiment, the effect would be to lower the velocities nearest the wall, typically less than 2 per cent. Displacement corrections have also been discussed by Preston [13], Livesley [14], MacMillian [15] and Davies [16]. These authors discuss different factors affecting the measurements, and present varying numerical values for the displacement corrections. In fact, Davies suggest no correction be made for round probes in the diameter range of 0.031 to 0.48-inches (0.79 to 12.2-mm). Turbulence corrections suggested by Dean [9] for the normal Reynolds stress effect corrected the measured stagnation pressures by less than 1.2%.

The combined 'corrections' above were typically 3% at the wall, diminishing through the boundary layer. Such corrections were tried and while they tended to improve the appearance of the data, no such corrections were used in the results presented since 1) such corrections did not generally bring the measured data into 'agreement' with predicted similarity as Eq. 3; 2) such corrections could not be properly applied to the hot wire measurements which, though slightly higher, were in general agreement with the stagnation probe measurements; and 3) in his extensive study of such data, Coles [7] suggested the uncertainty of such corrections warranted their omission.

The assumption of a fixed error in probe vertical position would be the same as applying a displacement correction. Since such a correction did not generally retrofit the data to the expected u^+, y^+ form, it is assumed that such errors were not likely present.

While day to day variations in ambient pressure were nominally compensated for in setting the tunnel U/ν parameter to a constant value, there was some unavoidable variance in this parameter. To overcome this effect three sets of comparisons were made between the two claw probes and each claw probe and the gooseneck probe, each comparison at one time under essentially identical tunnel conditions to avoid any U/ν variances. The 1200, 1300 and 1400 series average behaviors were confirmed with the highest near wall velocities recorded by the large claw probe and the lowest by the gooseneck. Differences as large as 4% occurred between the two claw probes; of 6% between the large claw and the gooseneck; and of 4% between the small claw and the gooseneck. All probes agreed to less than 1% in the outer region of the boundary layer.

Flow Field Effects

All of the earlier results on the effects of different probes were for flow in a constant area channel of essentially zero pressure gradient. The effects of the flow field were considered in the following.

The effects due to mild negative and positive pressure gradients on the velocity profile were considered by placing the wooden wedge on the test tunnel roof as a converging or diverging section. The 22-in. (56-cm) wedge

provided a converging (or diverging) area variation over 16-in. (41-cm) by a 7° angle. Measurements were made at the center of this 16-in. (41-cm) length. The resulting pressure gradients were approximately -0.0025 lb/in.^{2}/in. (-6.79 Pa/cm) and 0.0023 lb/in.^{2}/in. (6.24 Pa/cm), respectively. Comparisons of profiles taken by the stagnation probes in the different pressure gradients are shown in Fig. 9.

Qualitatively, the relative differences in the profiles due to changes in static pressure behave as expected. The wake region for each probe was largest for the profile in the positive pressure gradient. Conversely, the negative pressure gradient produced the smallest wake region. Near the wall, there seems to be slight differences in the behavior of the velocity profiles due to variations in the pressure gradient, but these differences are consistent with the various probes in the constant area configuration. The pressure gradients do not appear to significantly alter the results in the near wall region but there is a tendency for the rising pressure field to lower the very near wall data points in the similarity coordinates, though not sufficiently. The question of the relatively short length of these pressure gradient flows was considered. It is recognized that the near wall flow has a much shorter memory than the wake flow, and the fact that Fig. 8 shows the wake responding to the effect of the local pressure gradient gives support to the assumption that the near wall flow did have sufficient flow time to respond as well.

Patel [17] predicts departures from the extended law of the wall due to pressure gradients with a pressure gradient parameter, α. Calculated values of approximately 0.004 and -0.004 were much too small to suggest significant departures from the extended law of the wall. Hence, the essentially consistent behavior of these profiles near the wall was expected. In these runs the tunnel parameter U/ν was held constant but the test section area variations to generate the local pressure gradients gave local U/ν values slightly higher than in the constant area flows.

The question of possible flow disturbance near the wall due to the presence of the upstream boundary layer trip wire was considered. A flat plate with a sharp leading edge was installed as the tunnel floor, and all boundary layer trips were removed to allow natural transition from laminar to turbulent flow. These two tunnel geometries are compared in Fig. 10. As shown, only small differences in the velocity profiles occur near the wall. The smaller wake for the sharp leading edge can be explained by the concept of an asymptotically developed wake function. Because the trip wires create an earlier transition to turbulent flow, the wake function has a longer distance to develop. Conversely, the sharp leading edge allows natural transition; hence turbulent flow develops farther downstream. Disregarding the changes in the wake region, the presence of the boundary layer trips has no discernible effect on the shape of the velocity profile in the similarity coordinates.

Finally, the effects of slight convergence or divergence at the test station were considered. A slight convergence and divergence was created (with accompanying unavoidable pressure gradients whose effects had already been considered) by placing smoothly faired wooden wedges of 7° on the tunnel

side walls. No graphical results are presented, but using the gooseneck probe (as in the other flow field comparisons) no near wall changes could be attributed to the convergence or divergence of the floor flow.

Effects of Formulas and Constants

In all of the earlier discussion, comparisons were made using the third-order Spalding equation and the constants suggested by Patel. The specific choice of formula and constants was a matter of convenience; however the consistent choice of the formula and constants was necessary to avoid ambiguous results created by varying selection of formulas and constants.

The effect on the prediction of the shear velocity due to the choice of the formula and constants is considered briefly here. Three formulas were compared; the Spalding third-order equation, Spalding fourth-order equation, and the two-formula law of the wall which is a combination of the viscous sublayer and the logarithmic region expressions. This version omits an expression for the transition or buffer region and tends to maximize differences with the other two versions. The constants suggested by Smith and Walker, Coles, and Patel were combined with each formula, resulting in nine combinations for predicting the shear velocity for any given velocity profile. The nine predictions of the shear velocities for several profiles were compared to show relative differences among the nine methods.

Velocity profiles were selected from various tunnel geometries, then the shear velocity for each profile was inferred for the nine methods. An average shear velocity was calculated for each run for the nine methods and differences relative to this average were calculated. A sample standard deviation was also calculated for each run. The combination of the Smith and Walker constants and the two-formula law of the wall always predicted the lowest value for the shear velocity. Values for the relative differences of the shear velocities are shown in Table 4, and comparisons of the formulas and constants were shown in Fig. 4 earlier.

Results in Table 4 indicate the relative differences for the various methods remain nearly constant for all profiles. When the method of wall shear stress inference from velocity profiles is applied to flows with a shear velocity in the range considered here, there will exist a systematic difference in the predicted value of the shear velocity due to the selection of the formula and constants. The question of which method is most accurate cannot be answered without direct measurement of the wall shear stress.

The following is judged worthy of consideration. All data was reduced using the combination of the Spalding third-order equation and the Patel constants. The Spalding formula is clearly in good agreement with the two- (or three) formula extended law of the wall, and the more recent Patel constants are in very close agreement with and nearly identical to the more heavily researched Coles constants. Not withstanding this, it is noted that in all the similarity plots, the agreement in the $50 < y^+ < 300$ range is not usually impressive. It can easily be shown that the agreement between these data and the theoretical curve varies with the selection of the formula and constants. For profiles in this report, best agreement resulted with the

two-formula law of the wall and the Smith and Walker constants. Typical profiles using this model are shown in Fig. 11. Comparisons between this figure and previous ones show improved agreement throughout the curve, particularly near the wall. The Smith and Walker work was considered by Coles but the effect of this one study, among so many others, was small in the definition of the Coles constants, k and c. It is noted that the Smith and Walker constants are possibly the only ones defined by direct force wall shear measurements for the determination of the nondimensionalizing shear velocity used in the similarity plots. Nearly all other studies determine this quantity indirectly.

CONCLUSIONS

The consistent behavior of the velocity measurements for each of the three stagnation probes indicated good experimental repeatability. Overlays of the velocity profiles for the probes illustrated the consistent results, and the standard deviations for the velocity measurements indicated low experimental scatter associated with the results. Similar consistency was noted for the hot wire probe as well.

Results from the comparisons of the four velocity probes indicated that velocity measurements in the boundary layer were affected differently by the presence of each of the probes. At a given nominal position in the near wall region, the highest velocities were recorded by the hot wire, next by the large claw, followed by the small claw, and lowest by the offset boundary layer probe. Good agreement for the velocity measurements in the free stream flow by the three probes inferred that the velocity discrepancies noted in the boundary layer were due, at least in part, to normal velocity gradients. Typical boundary layer displacement corrections did not bring the data into agreement with the near wall similarity law assumed and the highest velocities of the hot wire, for which there should be no displacement correction, suggested that such a correction was not appropriate. This is also supported by noting that different velocity measurements were reported for probes of equal tip diameter but of different geometry. It appears that the geometry of the probe (and the lower stem) in a shear gradient, does affect the probe response as typified by the large straight claw and straight hot wire giving similar high readings relative to the offset (gooseneck) boundary layer probe. None of these small systematic differences identified with each probe was of the order needed to bring the very near wall data into 'good' agreement with the assumed similarity law.

Flow field effects are summarized as follows. The presence of mild pressure gradients, approximately $\pm$ 0.0025 lb/in.^{2}/in. (6.79 Pa/cm), did not significantly affect the near wall data when plotted in similarity coordinates. There was noted a tendency for the rising pressure field to shift the very near wall data downward in the similarity figures. This was noted in different degrees for the three stagnation pressure probes. This shift while consistent, was not large enough to insure a 'good' fit with the similarity law assumed. No significant differences were noted in very near wall data when the boundary layer trips at tunnel entrance were removed and replaced by a sharp leading edge. Profiles were measured by two probes and the results

were consistent with those in the original geometry with boundary layer trips. No significant differences in very near wall data were noted with small convergence or divergence on the test floor and with the original constant area geometry. None of the flow field variations were of the order need to bring the very near wall data into 'good' agreement with the assumed similarity law.

For a given velocity profile, the specific choice of the similarity formulas and constants had significant effect on both the prediction of the shear velocity, and the differences between the velocity measurements and the similarity law chosen. Several profiles were compared using nine combinations of formulas and constants, and variations in the value for the inferred shear velocity of up to 3.7 per cent occurred. These differences can be attributed in large part to the near wall data not following the assumed similarity law in some cases as well as in others. No choice of similarity law or constants altered the behavior of the very near wall data as generalized for this experiment in Fig. 1. For all the profiles measured in this report, best agreement between the measured velocities and the similarity formula was achieved with the Smith and Walker constants and the two-formula law of the wall.

The results of the study indicate that small consistent changes in the very near wall velocity data can be identified with different measuring probes and different sizes and geometries of these probes, and small changes did exist for some of the singly different flow conditions. However, there is little doubt that none of the systematic variations made accounted for or produced the kind of inconsistency in very near wall velocity measurements that characterize a wide range of the well accepted data. In this sense, then, this work must report a negative result in that while we can state specifically what single variations in flow conditions and/or velocity probes did not account for this very near wall behavior, it cannot be stated positively what conditions must be met to insure agreement with the very near wall similarity formulas. Thus, in flows where a minimum of near wall similarity exists in the classic logarithmic region, one cannot yet use the very near wall velocity data with confidence even though techniques for the use of these data are available.

References

1. Clauser, F. H., "Turbulent Boundary Layer in Adverse Pressure Gradient," Journal of the Aeronautical Sciences, Vol. 21, February 1954.

2. Bradshaw, P., "A Simplified Method for Determining Turbulent Skin Friction from Velocity Profiles," Journal of the Aerospace Sciences, Vol. 26, December 1959.

3. Schraub, F. A., and S. J. Kline, "A Study of the Structure of the Turbulent Boundary Layer With and Without Longitudinal Pressure Gradient," Report MD-12, Thermosciences Division, Mechanical Engineering, Stanford University, 1965.

4. Spalding, D. B., "A Single Formula for the Law of the Wall," Journal of Applied Mechanics, Trans. ASME, Vol. 83, No. 3, 1961.

5. Kleinstein, G., "Generalized Law of the Wall and Eddy-Viscosity Model for Wall Boundary Layers," AIAA Journal, Vol. 5, No. 8, 1967.

6. Pierce, F. J., B. B. Zimmerman, "Wall Shear Stress Inference From Two- and Three-Dimensional Turbulent Boundary Layer Velocity Profiles," Journal of Fluids Engineering, Trans. ASME, Vol. 95, 1973.

7. Coles, D. E., The Turbulent Boundary Layer in a Compressible Fluid, USAF Project, Rand Corp., Report R-403-PR, 1962.

8. Coles, D. E., and E. A. Hirst, Computation of Turbulent Boundary Layer, 1968, AFOSR-IFP-Stanford Conference, Vol. 11, (Proceedings), Dept. of Mech. Engr., Stanford University, Calif., 1968.

9. Dean, R. C., Jr., Aerodynamics Measurements, Gas Turbine Laboratory, Massachusetts Institute of Technology, Eagle Enterprises, 1958.

10. Gold, D. S., "Near-Wall Velocity Measurements in Two-Dimensional Turbulent Boundary Layers," M. S. Thesis, Virginia Polytechnic Institute and State University, Blacksburg, Va., 1974.

11. Smith, D., and J. Walker, "Skin-Friction Measurements in Incompressible Flow," NASA RT R-26, 1959.

12. Young, A. D., and J. N. Maas, "The Behavior of a Pitot Tube in a Transverse Pressure Gradient," ARC R & M No. 1770, 1936.

13. Preston, J. H., "The Determination of Turbulent Skin-Friction by Means of Pitot Tubes," Journal of the Royal Aeronautical Society, Vol. 58, 1954.

14. Livesley, J. L., "The Behavior of Trasverse Cylindrical and Forward Facing Total Pressure Probes in Transverse Total Pressure Gradients," Journal of Aeronautical Sciences, Vol. 23, 1956.

15. MacMillan, F., "Experiments on Pitot Tubes in Shear Flow," ARC R & M No. 3028, 1956.

16. Davies, P. O. A. L., "The Behavior of a Pitot Tube in Transverse Shear," Journal of Fluid Mechanics, Vol. 3, 1958.

Table 1. Summary of Flow/Probe Configurations and Number of Runs

Flow/Probe	Runs	Flow/Probe	Runs
11xx	6	31xx	2
12xx	7	32xx	2
13xx	7	33xx	1
14xx	3	41xx	1
21xx	2	43xx	1
22xx	1	51xx	2
23xx	2	61xx	2

Table 2. Law of the Wall Constants

Investigator	k	c
Coles	0.41	5.0
Patel	0.42	5.45
Smith & Walker	0.46	7.15
Nikuradse	0.42	5.8
Clauser	0.41	4.4
Spalding	0.40	5.5
Laufer	0.40	7.2
Townsend	0.41	5.85
National Physical Laboratory	0.47	5.9

Table 3

Experimental Scatter for Stagnation Probes

Run Series: 1100

	Mean			Sample Standard Deviation	
Y (in.)	u^+	y^+	u/U	u^+	u/U
.013	13.84	24.58	.5585	.08	.0047
.015	14.06	28.38	.5670	.08	.0051
.017	14.28	32.17	.5762	.07	.0037
.020	14.54	37.87	.5865	.07	.0050
.025	14.93	47.33	.6022	.04	.0035
.030	15.24	56.80	.6147	.04	.0032
.040	15.72	75.72	.6341	.05	.0030
.050	16.17	94.65	.6522	.06	.0042
.100	17.62	189.30	.7105	.03	.0034
.150	18.56	283.93	.7483	.02	.0035
.200	19.24	378.57	.7758	.05	.0036
.300	20.35	567.90	.8207	.07	.0054

Run Series: 1200

	Mean			Sample Standard Deviation	
Y (in.)	u^+	y^+	u/U	u^+	u/U
.013	14.14	25.11	.5910	.23	.0074
.015	14.32	29.46	.5985	.14	.0056
.017	14.50	33.39	.6061	.10	.0045
.020	14.75	39.27	.6165	.08	.0038
.025	15.04	49.09	.6283	.06	.0041
.030	15.36	58.93	.6420	.04	.0026
.040	15.74	78.59	.6601	.03	.0019
.050	16.16	98.21	.6757	.04	.0015
.075	16.88	147.31	.7059	.03	.0025
.100	17.46	196.41	.7300	.03	.0034
.150	18.25	294.60	.7629	.05	.0037
.200	18.93	342.84	.7913	.06	.0037

1 in. = 2.54 cm

Table 3 (continued)

Run Series: 1300

	Mean			Sample Standard Deviation	
Y (in.)	u^+	y^+	u/U	u^+	u/U
.015	14.48	30.09	.6163	.15	.0077
.017	14.75	34.11	.6275	.11	.0066
.020	14.97	40.13	.6370	.09	.0055
.025	15.25	50.16	.6491	.07	.0048
.030	15.52	60.19	.6606	.04	.0048
.040	15.92	80.23	.6676	.03	.0039
.050	16.23	100.29	.6908	.03	.0037
.075	16.87	150.44	.7178	.04	.0042
.100	17.37	200.58	.7394	.05	.0051
.150	18.11	300.87	.7705	.05	.0043
.200	18.71	401.17	.7961	.06	.0038
.300	19.56	601.78	.8325	.09	.0037

1 in. = 2.54 cm

Table 4

Comparison of Law of the Wall Formulas and Constants

(Formula)			Spalding Third-Order			Spalding Fourth-Order			Law of the Wall Two-Formula		
(Constants)			Coles	Patel	Smith & Walker	Coles	Patel	Smith & Walker	Coles	Patel	Smith & Walker
Run No.	Mean u* (ft/sec)	Sample σ (ft/sec)	Per Cent Differences in Values for Shear Velocity								
1103	3.89	0.073	+2.37	+1.40	-1.60	+0.24	+1.01	-2.28	+1.50	+0.48	-3.06
1203	4.16	0.088	+2.72	+1.75	-1.83	-0.09	+1.27	-2.51	+1.75	+0.20	-3.28
1303	4.25	0.088	+2.56	+1.59	-1.58	+0.24	+1.11	-2.26	+1.59	+0.44	-3.70
1403	4.18	0.086	+2.53	+1.56	-1.52	+0.31	+1.08	-2.29	+1.56	+0.41	-3.64
2101	4.47	0.090	+2.52	+1.56	-1.63	+0.30	+1.07	-2.41	+1.56	+0.40	-3.37
2201	4.51	0.090	+2.56	+1.59	-1.60	+0.24	+1.01	-2.37	+1.59	+0.33	-3.34
2301	4.78	0.094	+2.46	+1.49	-1.60	+0.24	+1.01	-2.38	+1.59	+0.43	-3.25
3101	4.31	0.087	+2.67	+1.61	-1.58	+0.26	+1.13	-2.45	+1.32	+0.35	-3.32
3201	4.48	0.090	+2.53	+1.57	-1.62	+0.21	+1.08	-2.39	+1.57	+0.41	-3.36
3301	4.57	0.097	+2.61	+1.55	-1.55	+0.29	+1.06	-2.32	+1.64	+0.39	-3.29

1 ft/sec = 0.305 m/sec

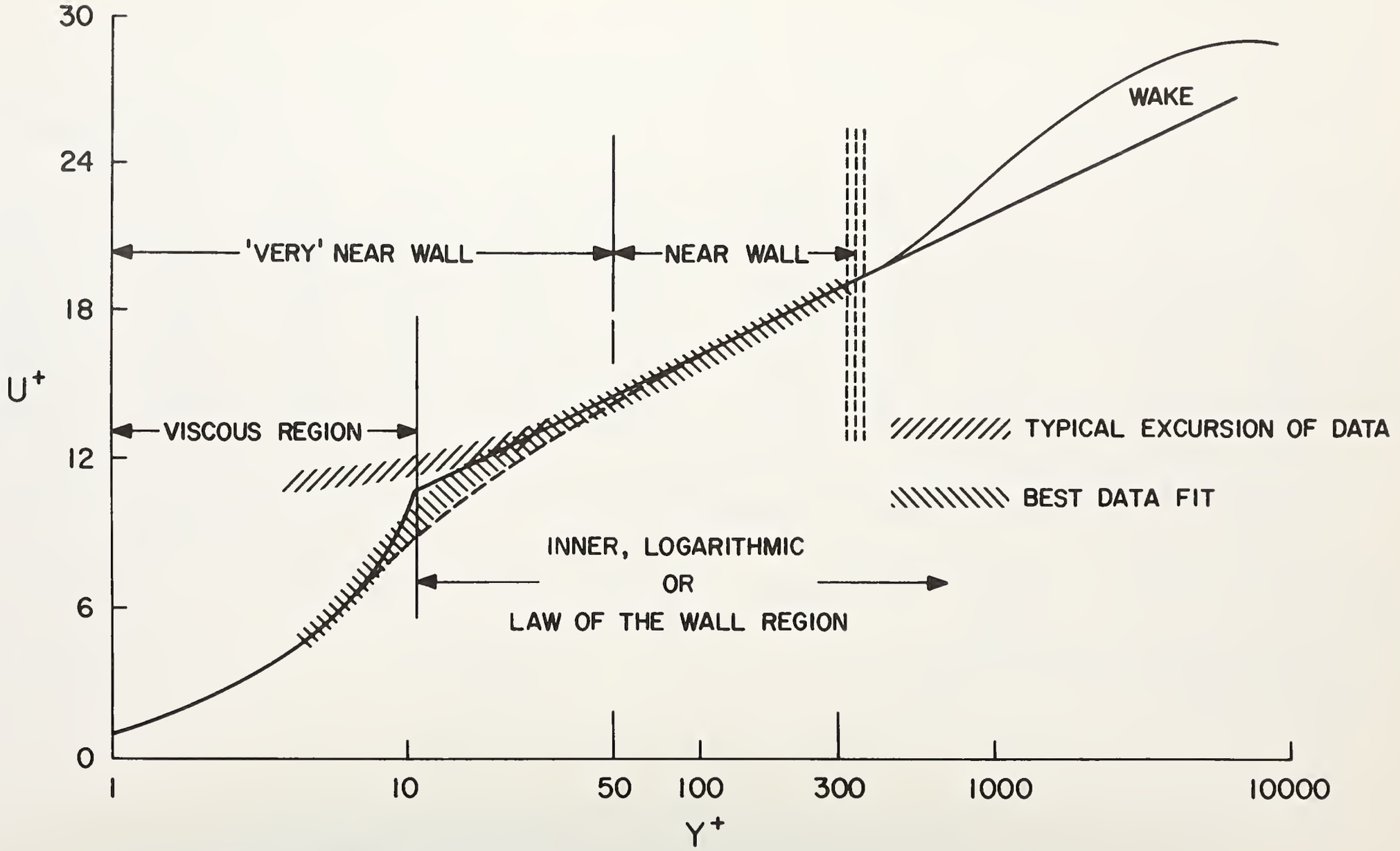

Fig. 1 Near wall similarity regions

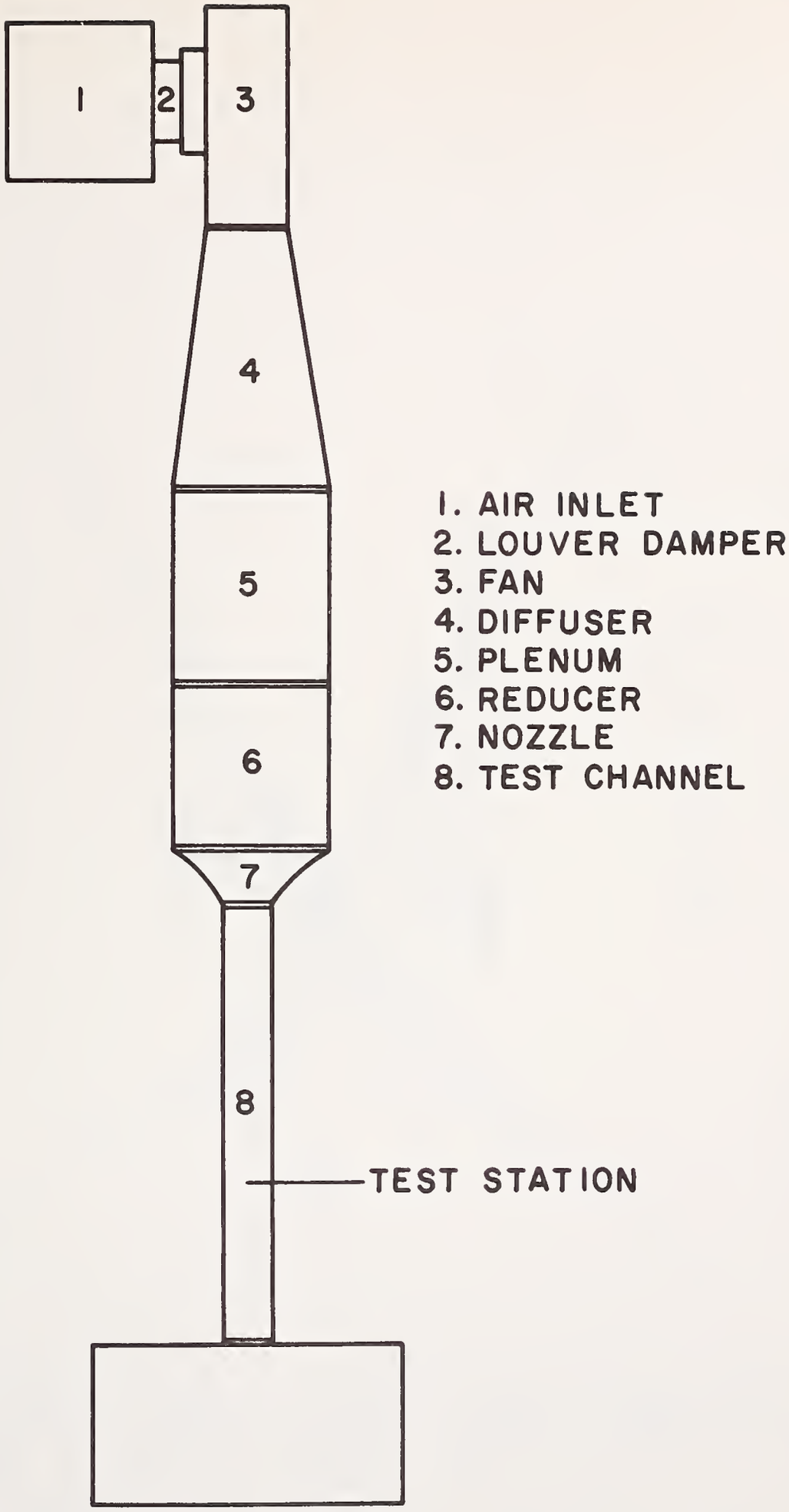

Fig. 2 Schematic diagram of apparatus

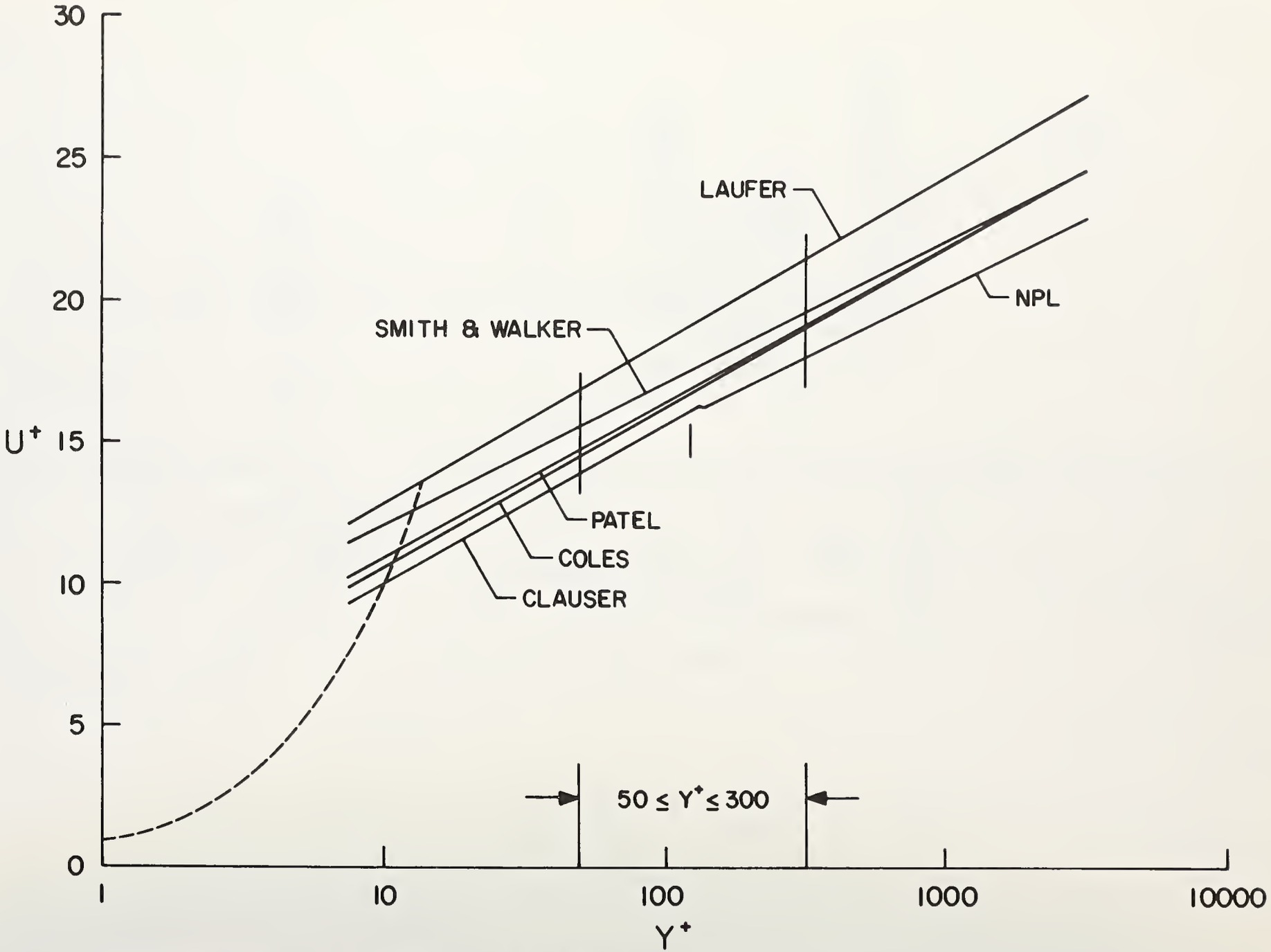

Fig. 3 Effect of k and c on logarithmic law

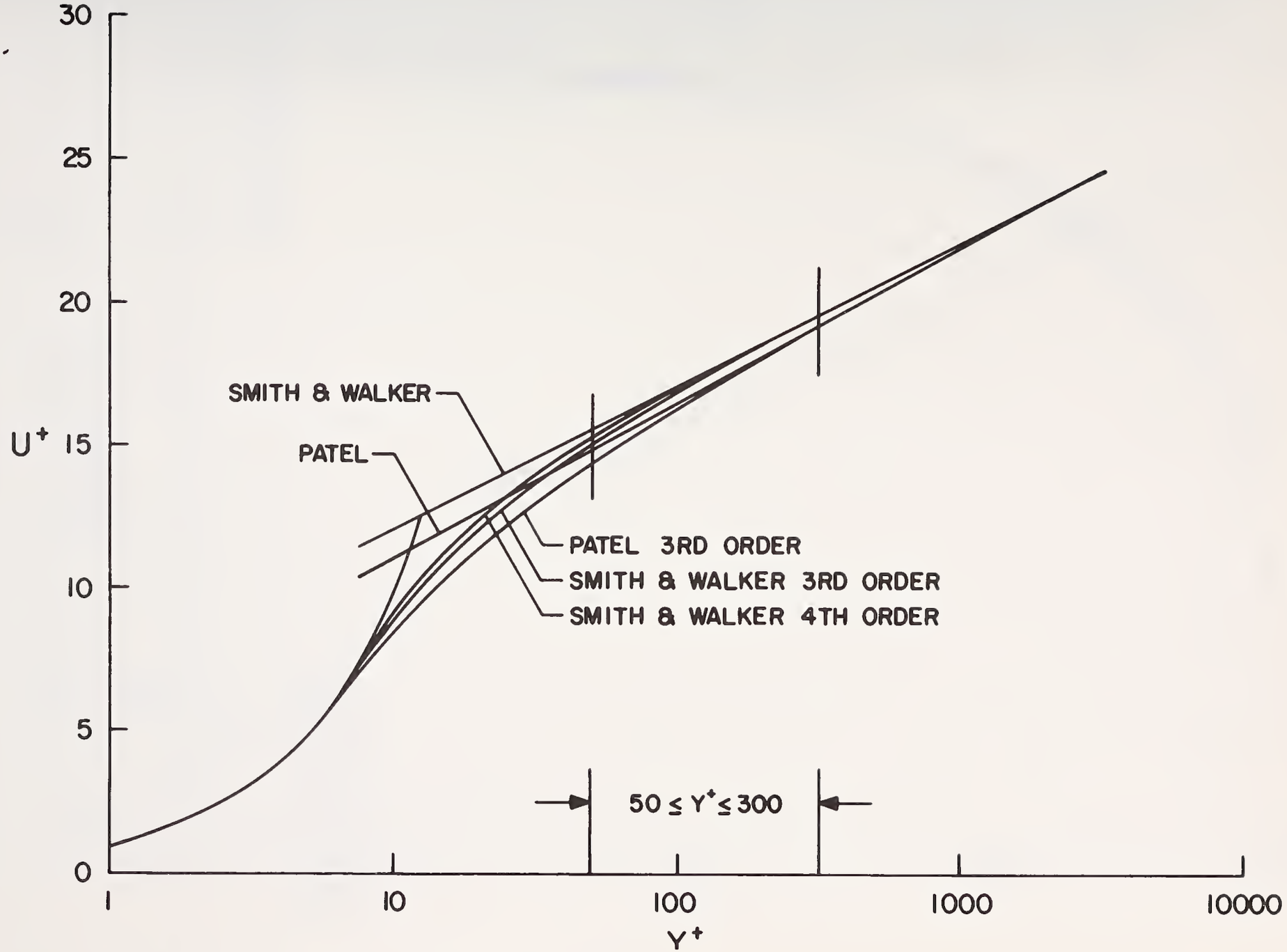

Fig. 4 Logarithmic and Spalding laws

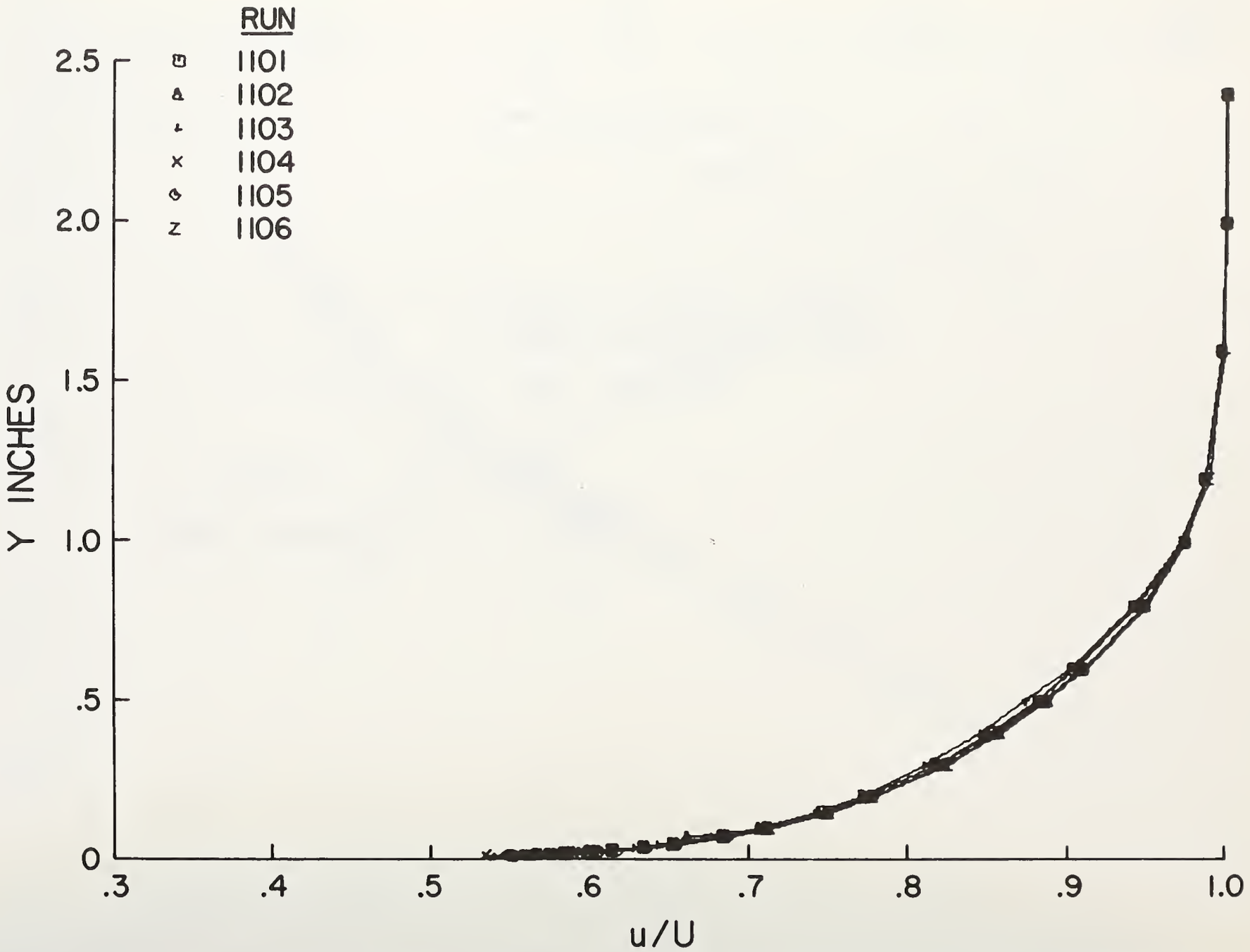

Fig. 5 Series 1xxx velocity profiles (1 in. = 2.54 cm)

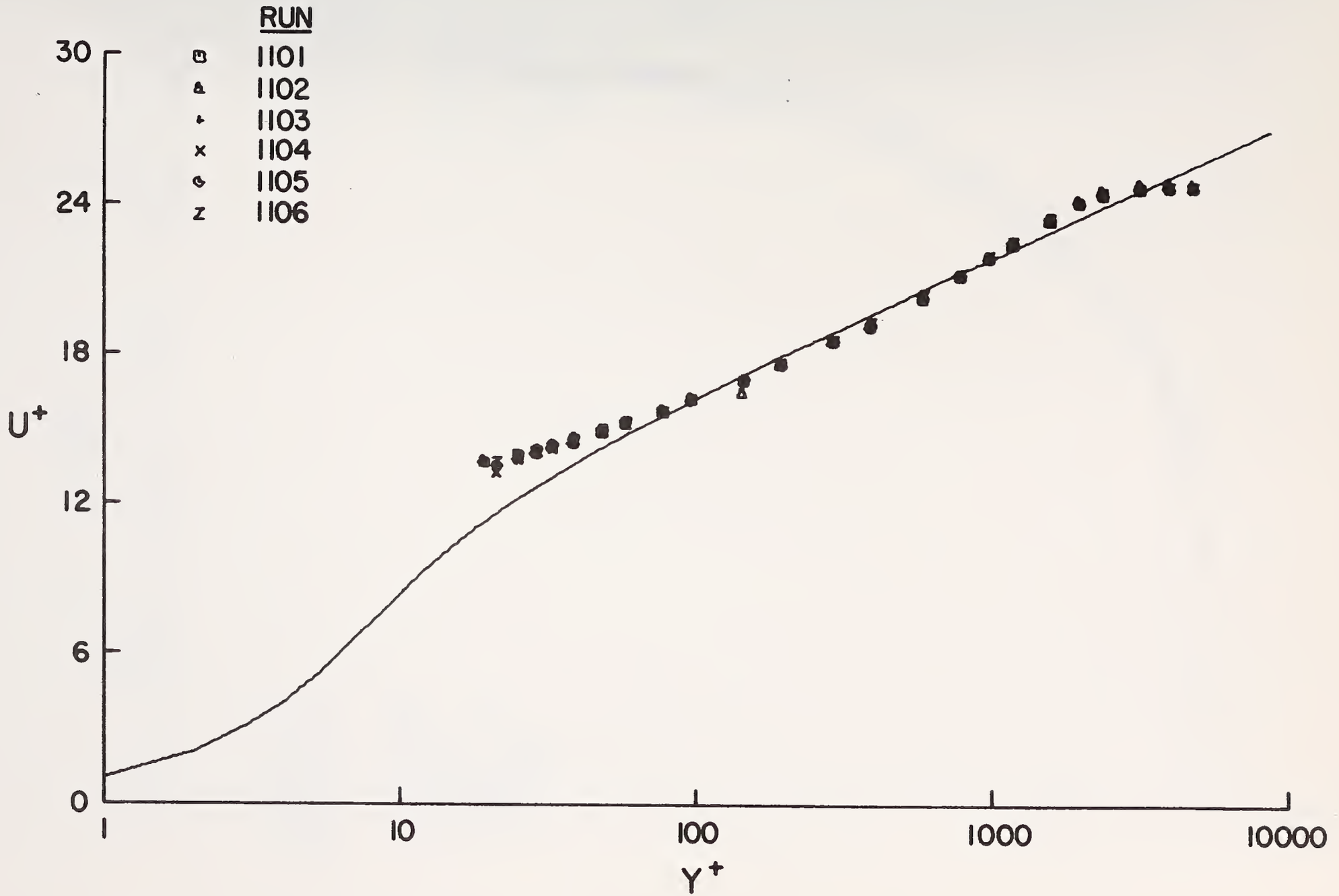

Fig. 6 Series 1xxx similarity profiles

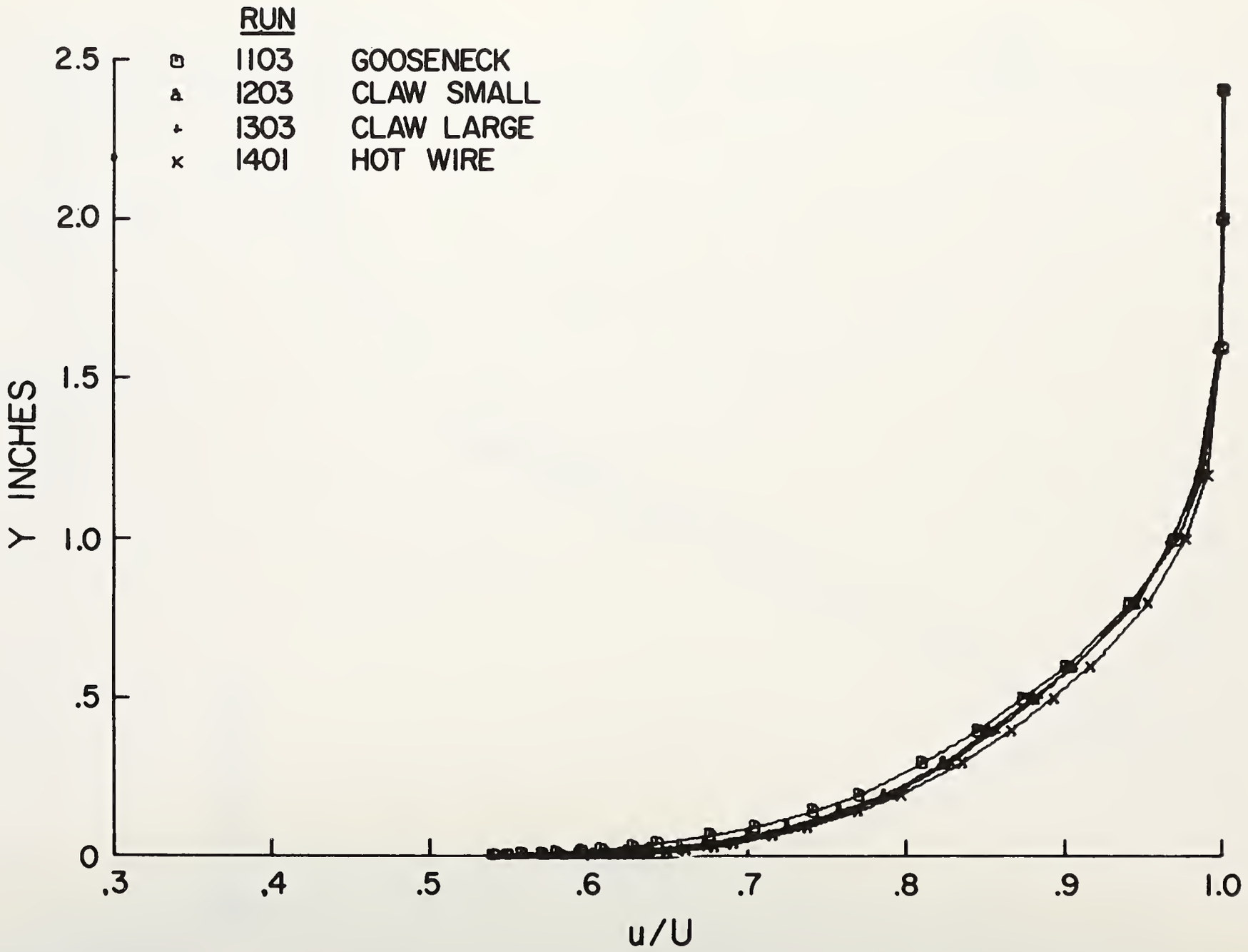

Fig. 7 Velocity profiles for different probes (1 in. = 2.54 cm)

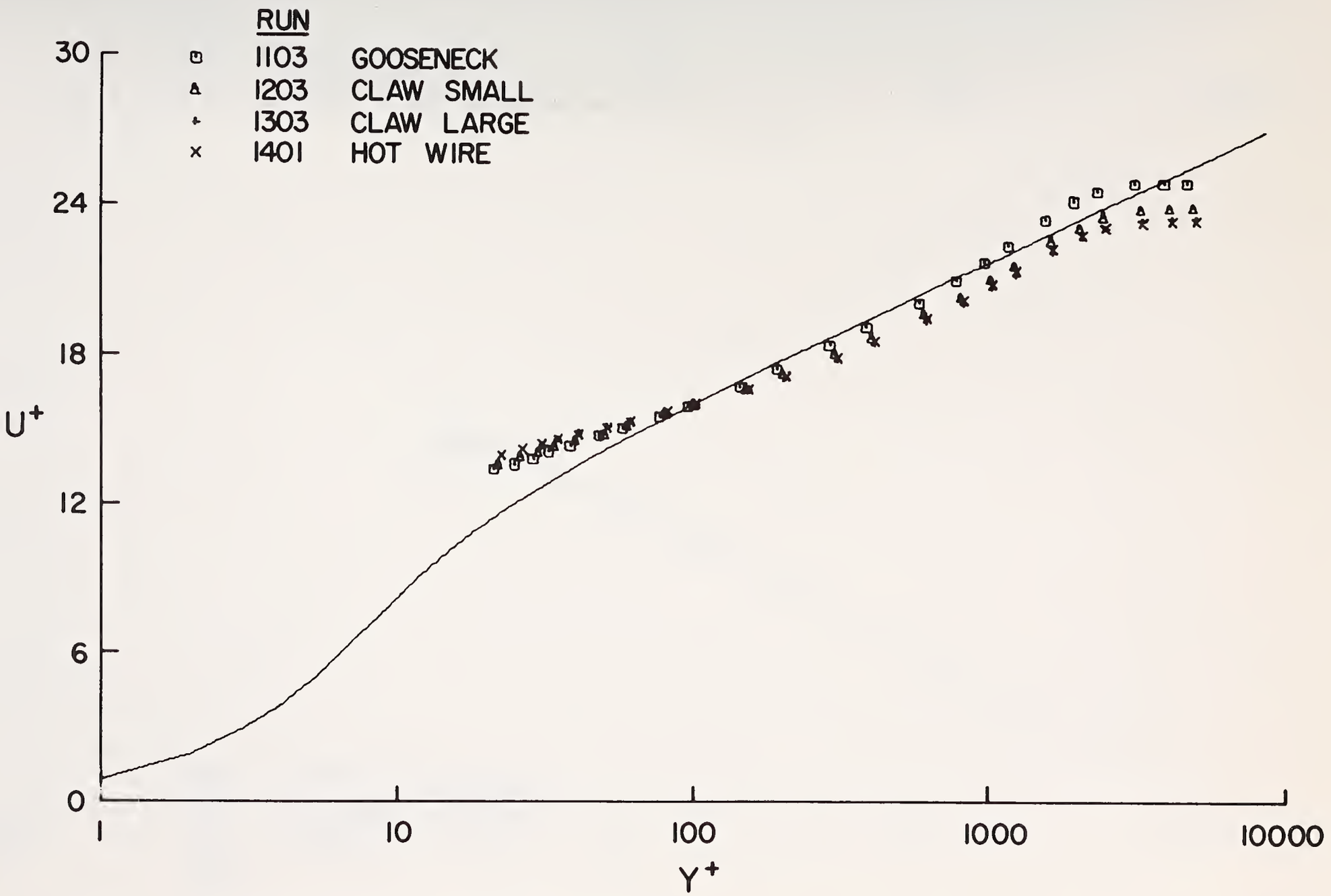

Fig. 8 Similarity profiles for different probes

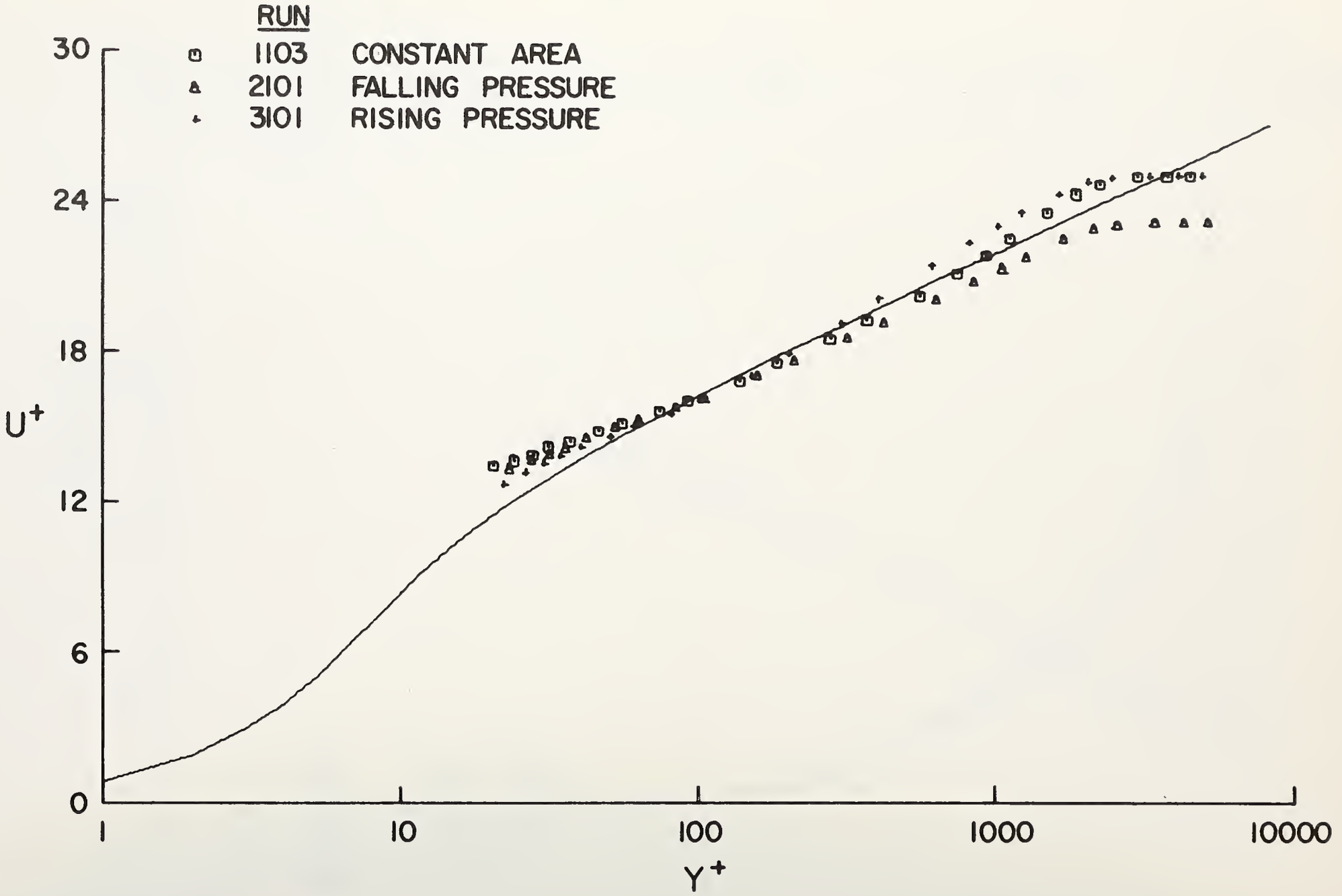

Fig. 9 Similarity profiles for pressure gradient flows

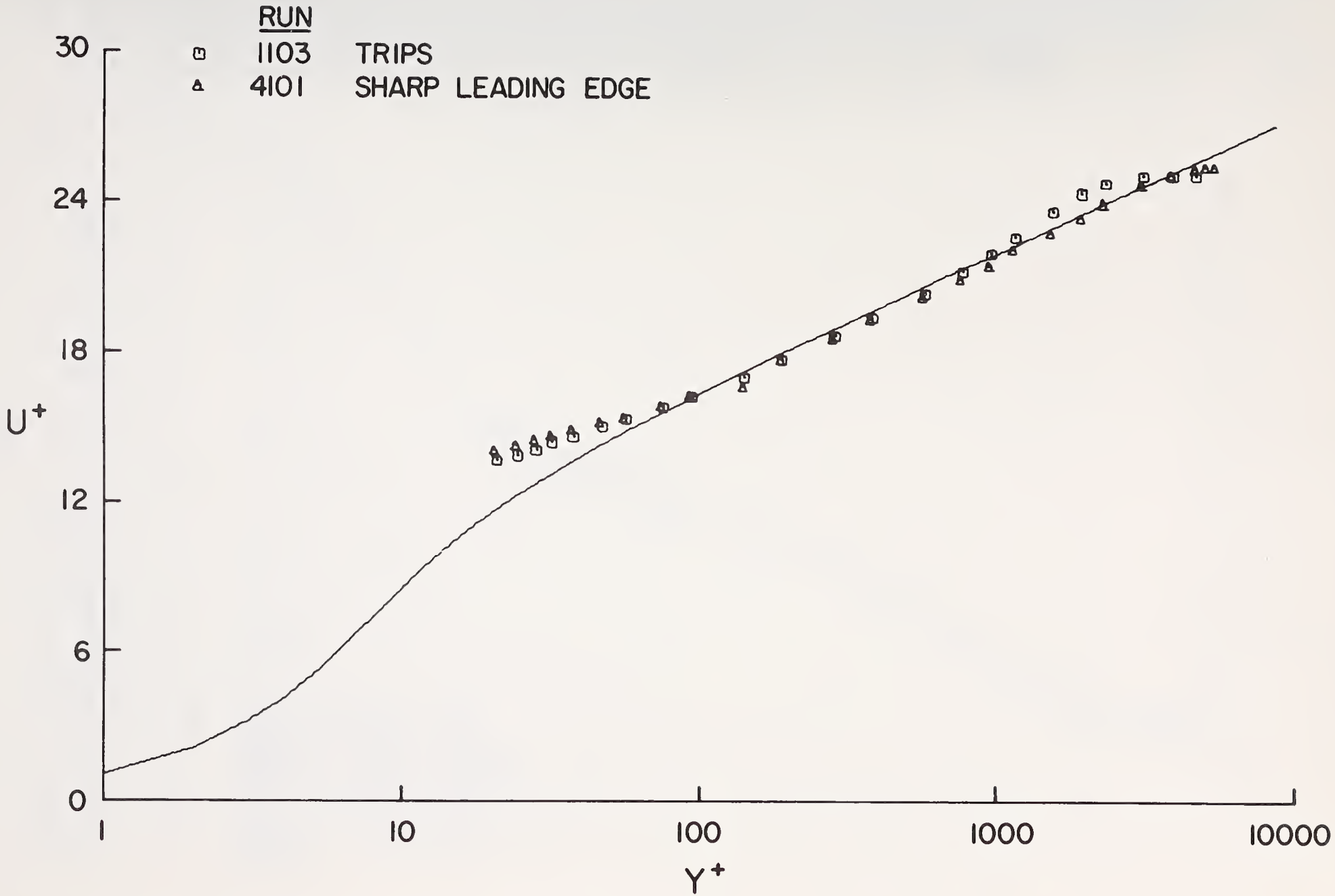

Fig. 10 Similarity profiles for tripped and sharp edge boundary layers

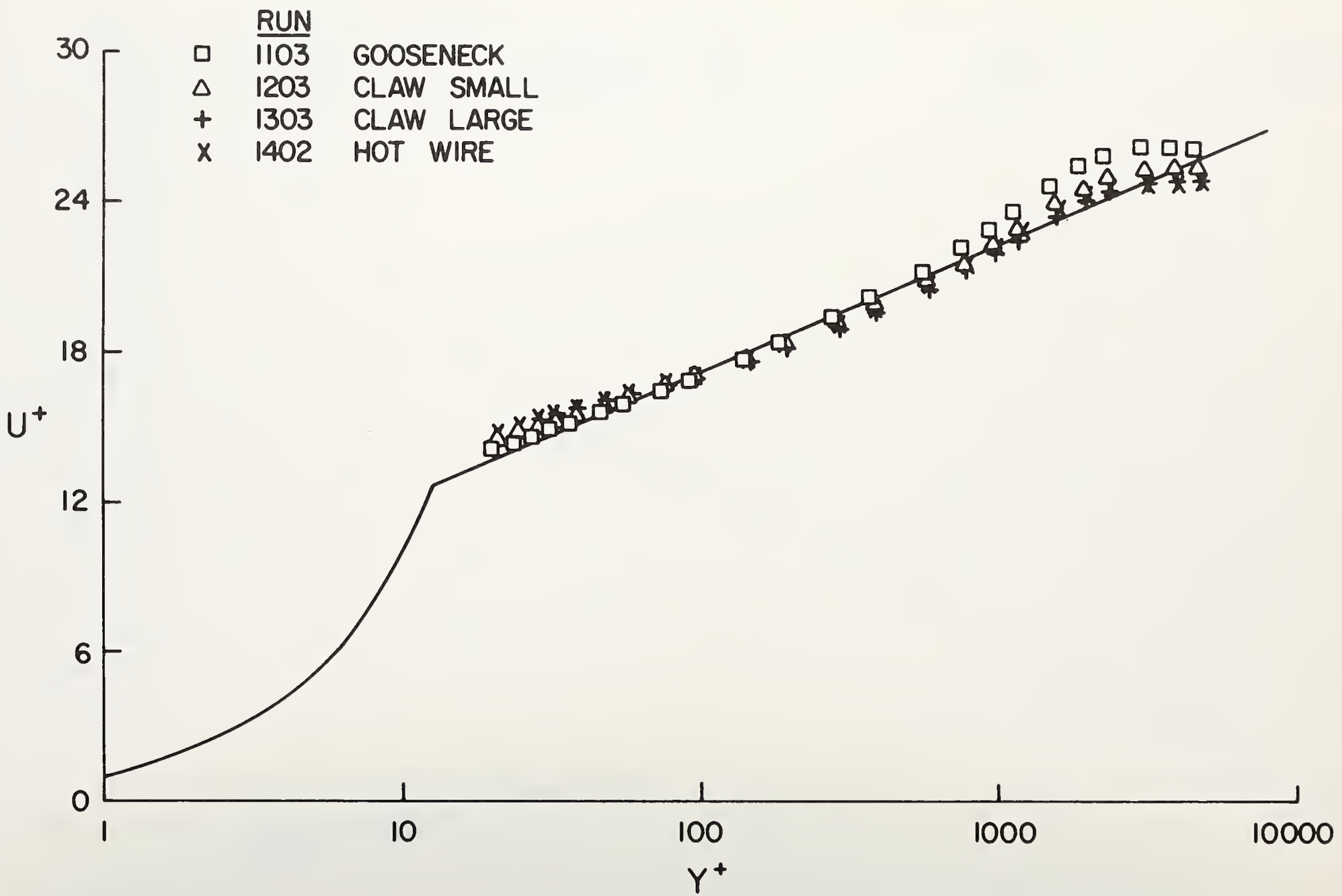

Fig. 11 Similarity profiles in Smith and Walker constants

National Bureau of Standards Special Publication 484, Proceedings of the Symposium on Flow in Open Channels and Closed Conduits held at NBS, Gaithersburg, MD, February 23-25, 1977. (Issued October 1977)

ON REDUCTION OF ERRORS ARISING IN HOT-WIRE ANEMOMETRY OF THIN TURBULENT SHEAR LAYERS

J. GAVIGLIO and J.P. DUSSAUGE
Institut de Mécanique Statistique de la Turbulence
12, avenue du Général Leclerc - 13003 MARSEILLE

1. INTRODUCTION

In supersonic flows, turbulent fluctuations can be classified (1) into vorticity, entropy and acoustic "modes". The first represents the vortical part of the fluctuating velocity field, which will be called "turbulent velocity field", or "turbulence field"; the second comes from turbulent heat transfers, involving non-isentropic temperature fluctuations; the latter expresses local pressure fluctuations, which in the case of waves radiated by the turbulent flow, is associated with irrotational and isentropic motions. Measurements of the level of theses modes are performed advantageously by using a constant-current type hot-wire anemometer (2). Only this type of instrument will be discussed in this paper. It is well known that, due to the imperfections of the anemometer, (3,4,5) the intensity of modes are often underestimated. In some cases this can be attributed to the low value of the impedance of the circuit feeding the hot-wire or to the nonlinear response of the associated amplifier; then the defects can be easily reduced or corrected.

Other sources of errors, which can be important, come from the upper bandwidth limit.This is particularly true for measurements made at supersonic speeds. An important source of errors is the attenuation of higher frequencies in the amplifier; a "truncation frequency" f_c of the uncompensated amplifier can be defined: for a sine wave signal, it corresponds to an attenuation of 50 % of the energy. The influence of the frequency response varies when the spectral distribution of the measured random signal depends on the temperature of the sensor. Additionally, important errors can also been induced by effect of the thermal lag of the hot-wire, which must be compensated by a network that at high frequencies gives only an approximate compensation, thus reducing the actual bandwidth.The two latter effects are coupled as described below. A correction is proposed which, in its form, differs from that given by Laderman and Demetriades (6). The errors depend both upon the characteristics of the amplifier, of the wire, but also on the flow characteristics. As it has been shown by Kistler (7), for a turbulent shear layer of thickness δ with a velocity u_∞ in the outer flow, the energy spectra largely extend over the characteristic frequency u_∞/δ which can exceed 10^5 hz in supersonic flows of moderate MACH number, $M_\infty < 5$. A method is proposed to correct for the errors, and to check the validity of the corrections.

2. METHOD OF CORRECTION FOR ERRORS INDUCED BY THE COMPENSATION CIRCUIT.

Because of the thermal lag of the wire, a sine wave signal of frequency n is reduced and phase shifted following the complex "ideal" law $\left(1+j\frac{\omega}{\omega_0}\right)^{-1}$; where $\omega = 2\pi n$ is the angular frequency and $\frac{1}{\omega_0}$

the "time constant" of the wire. For most compensation circuits, of which Kovasznay gives some examples (8), it has been verified that the transfer function can be written in the general form or "theoretical" form:

$$\mathfrak{C}_r = g_0\left(1+j\frac{\omega}{\omega_0}\right)\left(1+j\frac{g_0}{g_\infty}\frac{\omega}{\omega_0}\right)^{-1}$$

where g_0 and g_∞ are the gain of the amplifier for relatively low frequencies and for the higher respectively. Phase corrections must be applied in the case of double correlation function measurements performed with wires of differing or non-equalized time constants (9).

Here will be considered only the errors on the standard deviation of the signal which, after compensation, undergoes a residual attenuation. For a sine wave, the modulus of the transfer function of the compensating network alone reads:

$$\frac{1}{g_0}\left|\mathfrak{C}_r\right| = \frac{g_n}{g_0} = \left[1+\left(\frac{\omega}{\omega_0}\right)^2\right]^{1/2} \Big/ \left[1+\left(\frac{g_0}{g_\infty}\right)^2\left(\frac{\omega}{\omega_0}\right)^2\right]^{1/2} \qquad (1)$$

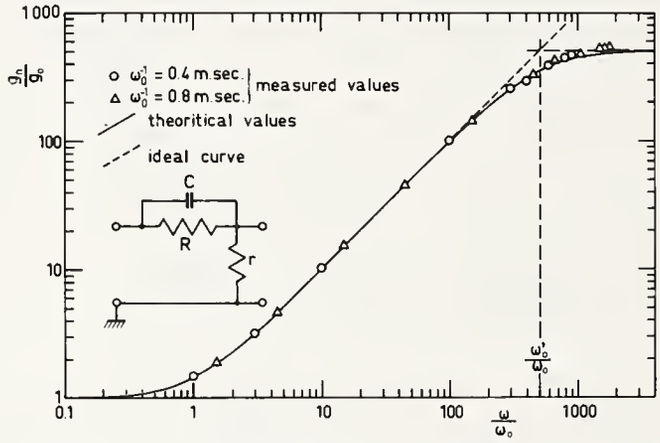

Fig. 1 - TRANSFER FUNCTION OF THE COMPENSATION NETWORK.

Fig. 1 shows an experimental verification of this law. The measured value compares favourably to the "theoretical values" computed from formula (1). The angular frequency ω'_0 is that for which the theoritical value of $|\mathfrak{C}_r|/g_0$ is $1/\sqrt{2}$ times the "ideal value". In the present case, $\frac{1}{\omega_0} = 0.4$ ms corresponds to $\frac{\omega'_0}{2\pi} \simeq 200$ khz and $\frac{1}{\omega_0} = 0.8$ ms corresponds to $\simeq 100$ khz.

This leads to the following correction:

let $F_m(n)$ and $F_c(n)$ be the power spectral density of the measured signal e'_m and of the corrected signal e'_c such as $\int_0^\infty F_m(n)\,dn = \int_0^\infty F_c(n)\,dn = 1$

they are related through the relation : $\overline{e'^2_c}\,F_c(n) = \overline{e'^2_m}\,F_m(n)\left[1+\left(\frac{g_0}{g_\infty}\right)^2\frac{(2\pi n)^2}{\omega_0^2}\right]$

Hence by integration : $\frac{\overline{e'^2_c}}{\overline{e'^2_m}} = 1+\left[4\pi^2\left(\frac{g_0}{g_\infty}\right)^2\frac{1}{\omega_0^2}\right]\int_0^\infty n^2 F(n)\,dn = 1+4\pi^2\left(\frac{g_0}{g_\infty}\right)^2 N^2\frac{1}{\omega_0^2}$ (2)

where N is an "equivalent frequency "defined (10) as $N^2 = \int_0^\infty n^2 F(n)\,dn$.

Introducing N helps to compute the corrections because its measurements does not require a complete spectral analysis. Indeed, N can be deduced in a simple manner from only the radius of curvature at the top of the auto-correlation curve, because the latter is the same as that of the sine wave of a frequency which can be determined as indicated on fig. 2.

N can also be obtained by using an appropriate passive filter network that produces the time derivative of the signal $\left(\overline{\frac{\partial e'}{\partial t}}\right)^2_m$ since $N^2 = \frac{1}{4\pi^2} \frac{\overline{(\partial e'/\partial t)^2_m}}{\overline{e'^2_m}}$

The correction related to the compensating network imperfections can be nearly exact when the signal energy lies in a frequency band much lower than the upper limiting frequency f_c. For example, in the case of Kistler's measurements (7) this condition seems to be practically verified when f_c is higher than four or five times u_∞/δ

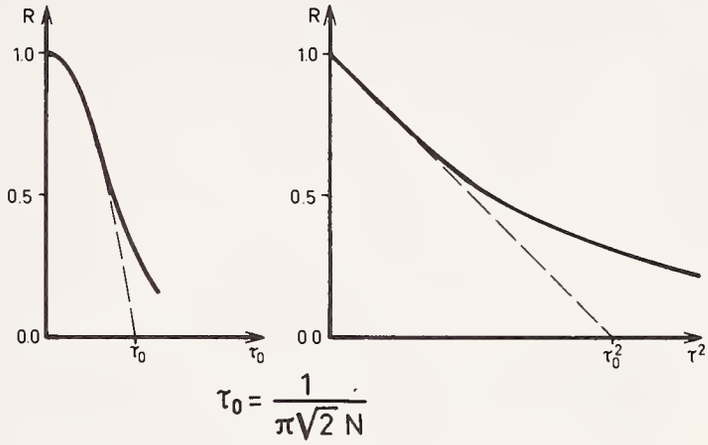

Fig. 2 - DETERMINATION OF N FROM AUTO - CORRELATION CURVES

N is characteristic of the dissipation range and, in an equilibrium boundary layer, increases when u_∞/δ increases. In such conditions, the analyzed shear layer will be called a "thick" shear layer. The definition depends upon the characteristics of the flow u_∞ and δ, and on the amplifier through the limiting frequency f_c. It corresponds to $u_\infty/\delta f_c \ll 1$, a condition which is easily satisfied in the case of subsonic flows. By contrast, when $u_\infty/\delta f_c$ is not negligible, the layer is called a "thin" layer. The higher the non-dimensional ratio, the thinner the layer. At supersonic speeds, this frequently occurs, because in most cases, f_c must be limited, to about two hundred kiloHertz for example, in order to avoid parasitic effects of a prohibitive background amplifier thermal noise, radio interference, etc....

Hence a compromise is looked for to choose f_c high enough to measure the main part of the signal energy, and low enough to avoid parasitic effects.

As for the corrections, they must be significant, easy to perform, and in addition their efficiency has to be checked. One can admit that each correction applied to a measured power spectral density is significant enough provided it does not much exceed approximately 100 percent. If several corrections are applied together, the rule is valid for the total correction.

The measured spectrum contains the errors due to noise, to the compensation circuit, and to the truncation in frequency. The first step in the correction procedure is to substract the noise from the measured spectrum. The second step is to correct for the errors introduced by the

compensation circuit, which are valid for frequencies that are not much greater than $\frac{\omega'_0}{2\pi}$. Fig. 3 shows an example; it corresponds to the experimental device indicated in §.3.1. The curve A represents the signal energy, corrected from noise. The curve B is deduced from A by applying the proposed correction for the compensation circuit distorsion. This is practically accurate enough for the whole bandwidth 0 to 210 khz since $\frac{1}{\omega_0}$ =0,57 ms.

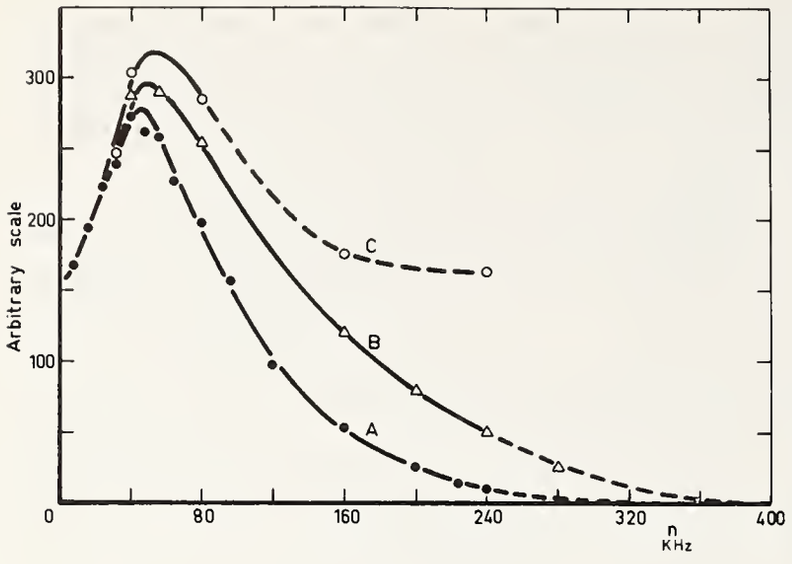

Fig. 3 - POWER SPECTRA (BOUNDARY LAYER)

One could attempt to correct the measured spectra for the effects of truncation for high frequencies, especially beyond the truncation limit f_c.

The total correction, being large, leads to significant distorsion, as shown by curve C. So only corrections related to noise and to compensation are retained. But the method is only valid under another condition , namely: f_c must be choosen high enough, if compared to N .

Otherwise, both the measured energy and the measured equivalent frequency would be reduced, and the proposed correction beeing decreased, would be insignificant. The example given in fig. 3, for which $f_c \simeq 210$ khz,

and N = 100 khz as deduced from auto-correlation measurements, seems to be a nearly critical one, for f_c is not very far from N. Nevertheless, the efficiency of the method has been checked, as shown in §.3, and the method remains still valid.

Formula (2) also needs verification, the time constant $\frac{1}{\omega_0}$ is

0.57 ms., the correction determined from the spectra is 46 %; that involving N reaches 53 %.

It may be noticed that the application of the correction method to a "thin" shear layer, as defined above, does not make it possible to measure the dissipation rate, since dissipation involves frequencies higher than f_c . Would the correction be possible, another limitation would arise because of the lack of spatial resolution of the wire.

A verification of the validity of the application method of the proposed correction is specified below.

3. EXPERIMENTAL CHECK OF THE EFFICIENCY OF THE METHOD

Experimental results obtained by hot-wire anemometry are used to check the efficiency of the method through comparisons with results obtained from

pressure measurements. Such comparisons have been done in a previous research, in the case of incompressible flows (9). Consider the ratio

$\overline{\rho u'^2} / \tau_0$; where ρ is the local density, u' the velocity fluctuation and τ_0 the friction at the wall. According to an hypothesis of Morkovin (11), which has been verified by many authors -see for instance Maise and Mc Donald (12) - the ratio is supposed not to be strongly dependant on MACH number. ρ and τ_0 are deduced from pressure and temperature measurements. In the present case, $\overline{u'^2}$ is measured with a tungsten-platinum hot-wire, the diameter of which is 3.8 microns. Ref.(13).

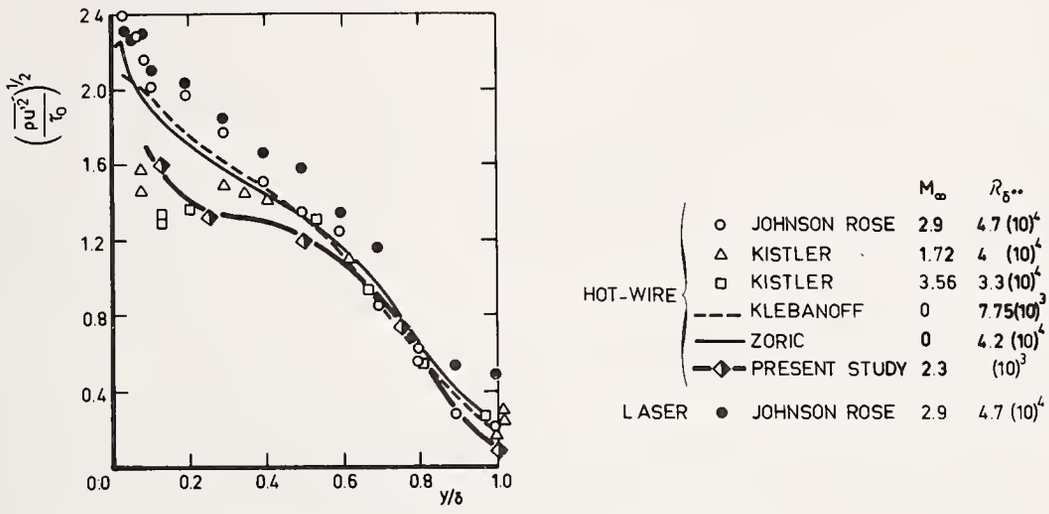

Fig. 4 - CHECKING OF CORRECTED RESULTS

Fig. 4 compares the corrected values of $\sqrt{\overline{\rho u'^2} / \tau_0}$, measured in a very "thin" turbulent boundary layer to results made in more favourable cases by other authors and recapitulated in ref.14. The layer under examination in the present case develops on the surface of a circular cylinder placed in a supersonic flow, with its axis aligned with the flow direction; the MACH number is 2.3, the thickness of the layer is 4mm. It has been verified that the approximation of thin shear layer is valid for the determination of the mean velocity field and of the wall friction. The momentum thickness Reynolds number $R_{\delta^{**}}$ is 1000, the friction coefficient is 2.88×10^{-3}. The present corrected results agree with others, although the corrections are large (in one case, they reach about 70 %).

Fig. 5 shows another comparison of velocity fluctuations between the present measurements and the results of ref. (7) and (15). As concerns the MACH number influence, the results obtained at I.M.S.T. are consistent with the results of Kistler.

In fig. 6, uncorrected and corrected values of the ratio $\sqrt{\frac{\tau_0}{\overline{\rho u'^2}}}$ measured at I.M.S.T., and compared to uncorrected values given by other authors (1, 7, 15, 16) in flows of thickness δ much larger than in the experiments performed at I.M.S.T. All the results are plotted together with Klebanoff's measurements, obtained in a "thick" boundary layer, i.e., free from bandwidth limitation and compensation errors.

The representation emphasizes the differences due to the parameter $u_\infty/\delta f_c$, since the MACH number influence is weak, as underlined by Morkovin (11); it indicates the general trend.

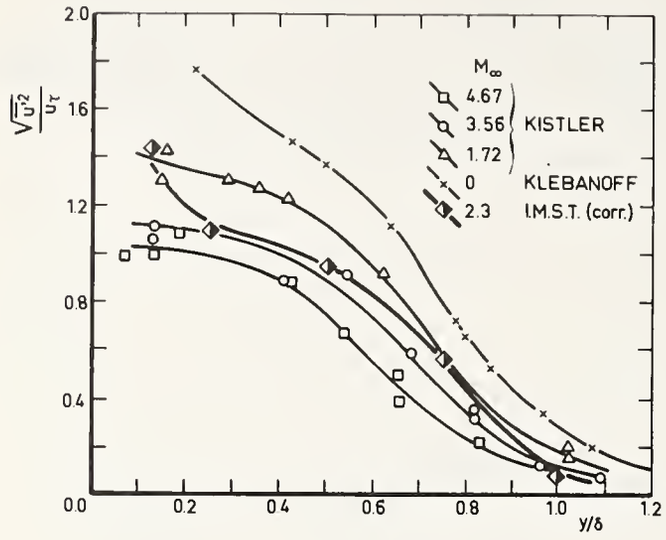

Fig. 5 - MEASUREMENTS CHECKING MACH NUMBER INFLUENCE.

Comparisons are made for different MACH numbers, and for distances to the wall of

$y/\delta = 1/8$ and $1/4$.

A more typical parameter would involve the influence of the time constant $\frac{1}{\omega_0}$ but its values are not published in the available literature, so that its influence cannot be rigourously determined. Uncorrected values of $\sqrt{\frac{\tau_0}{\rho u'^2}}$ largely increase with increasing $u_\infty/\delta f_c$, whatever M_∞.

This means that $\overline{\rho u'^2}$ is often underestimated. When the correction is applied - and this is the case for the measurements performed at I.M.S.T. in an unfavourable case - they strongly reduce the differences between the case of the "thin" supersonic shear layer and that of the "thick" subsonic layer used at a reference. The residual differences are attributable to both the residual error related to the compromise accepted in the determination of the bandwidth (§.2), and to the MACH number effect.

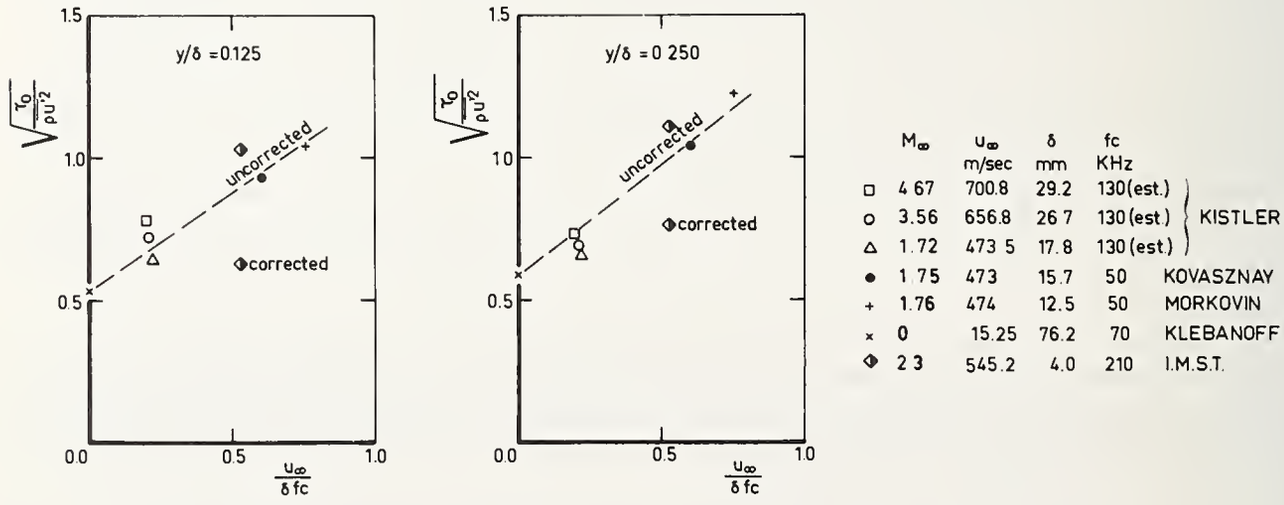

	M_∞	u_∞ m/sec	δ mm	fc KHz	
□	4 67	700.8	29.2	130(est.)	KISTLER
○	3.56	656.8	26 7	130(est.)	KISTLER
△	1.72	473 5	17.8	130(est.)	KISTLER
●	1 75	473	15.7	50	KOVASZNAY
+	1.76	474	12.5	50	MORKOVIN
×	0	15.25	76.2	70	KLEBANOFF
◈	2 3	545.2	4.0	210	I.M.S.T.

Fig. 6 - INFLUENCE OF THE NON-DIMENSIONAL FREQUENCY.

4. EXAMPLES OF MORE DETAILED ANALYSIS

Compensation errors vary with probe overheat. The errors reduce the

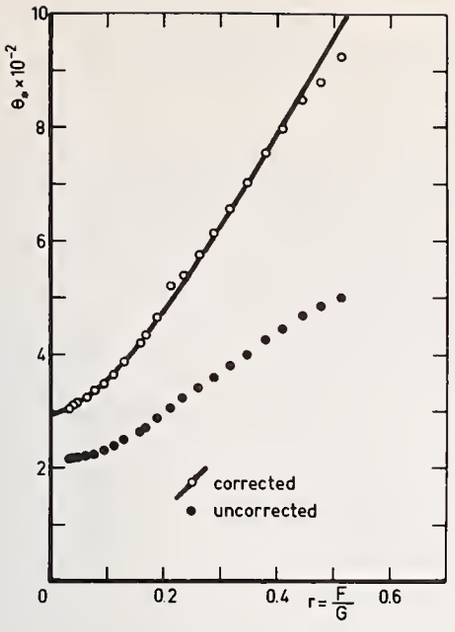

Fig. 7 - FLUCTUATION DIAGRAM
BOUNDARY LAYER
$y/\delta = 0{,}125$

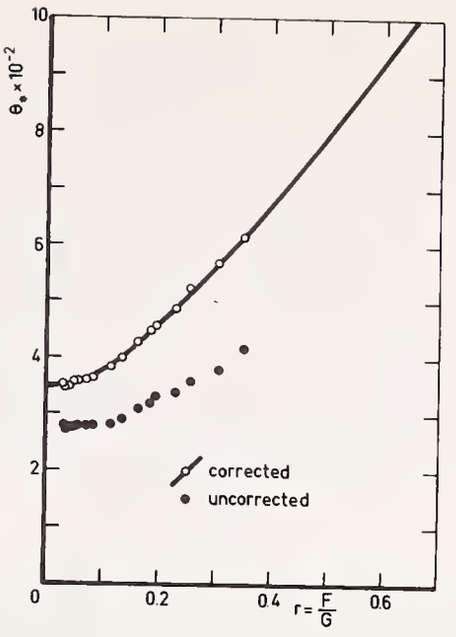

Fig. 8 - FLUCTUATION DIAGRAM
BOUNDARY LAYER
$y/\delta = 0{,}25$

level and distort the shape of the fluctuation diagram*, hence obscuring the physical meaning in terms of modes and correlation coefficients. This is illustrated by some typical examples given in fig. 7 to 9 for the case of the turbulent boundary layer described in §.3.1, and in fig. 10 for a wake**. All the experiments are performed at MACH number 2.3. It is recalled that the abcissa $r = F/G$ is the ratio of the hot-wire sentitivities, respectively to mass-flow and to local stagnation temperature. The ordinate $\theta_* = \frac{\sqrt{\overline{e'^2}}}{G\bar{e}}$ is obtained from the r.m.s. value of the voltage $\bar{e}$. The correction applies only to $\sqrt{\overline{e'^2}}$. Following Kovasznay (1) the curve $\theta_*(r)$ is an hyperbola.

This is verified through direct measurements if the correction $4\pi^2\left(\frac{g_0}{g_\infty}\right) N^2 \frac{1}{\omega_0^2}$ is negligible as compared to 1. Conversely, this is not the case of direct measurements when the error is large, whence a change in the curvature of $\theta_*(r)$.

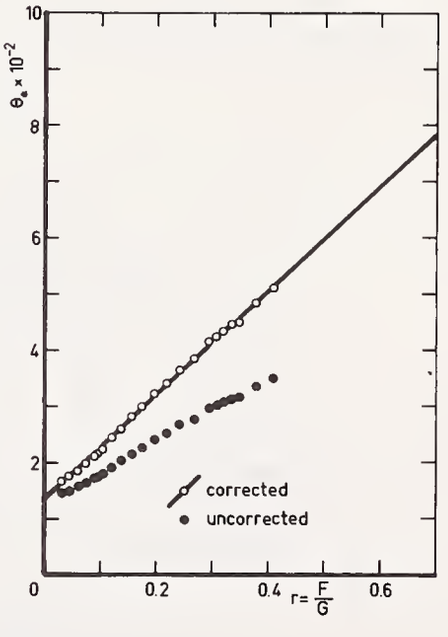

Fig. 9 - FLUCTUATION DIAGRAM.
SEPARATED BOUNDARY
LAYER, $y/\delta = 0{,}88$

In some limiting cases, the errors could transform the hyperbolic curve into a straight line, which characterizes either the pure entropy mode, or the acoustic mode: this is nearly the case for fig. 7. Applying the correction restores a convenient curvature except for high values of r, and suitably increases the level.

* The fluctuation diagram method has been extended to subsonic flows with heat transfer by E. Verollet (17).

**See Table 2.

Some indications can be given on the residual errors related to the correction method. Let us consider the formula

$$\sqrt{\frac{\overline{e_c'^2}}{\overline{e_m'^2}}} = \sqrt{1+4\pi^2\left(\frac{g_0}{g_\infty}\right)^2 N^2 \frac{1}{\omega_0^2}}$$

$\frac{g_0}{g_\infty}$ is a constant which depends only on the apparatus.

In unfavourable cases

$$\cdot 4\pi^2\left(\frac{g_0}{g_\infty}\right)^2 N^2 \frac{1}{\omega_0^2}$$

is about one. A rather pessimistic estimation of the possible errors in the determination of N^2 and $\frac{1}{\omega_0}$ gives the values 20 % an 10 % ; the resulting error on the expression contained under the square-root symbol is then about 15 % and the relative error on $\sqrt{\overline{e'^2}}$ about 8 %.

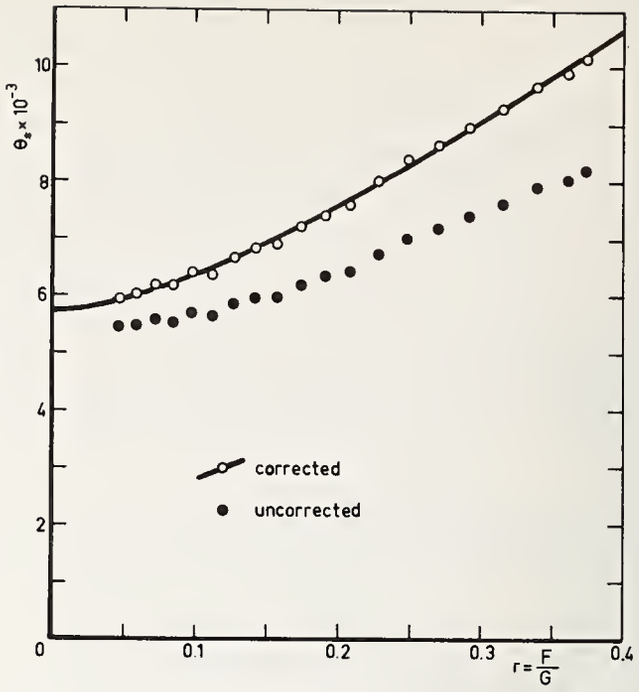

Fig. 10 - FLUCTUATION DIAGRAM . CENTERLINE OF A WAKE .

Therefore, even large corrections can be applied with some confidence, provided N^2 and $\frac{1}{\omega_0}$ are carefully measured.

TABLE 1 BOUNDARY LAYER

$\frac{y}{\delta}$	$\frac{\sqrt{\overline{u'^2}}}{\overline{u}}$ %		$\frac{\sqrt{\overline{\theta'^2}}}{\overline{\theta}}$ %		$r=\frac{\overline{u'\theta'}}{\sqrt{\overline{u'^2}}\ \sqrt{\overline{\theta'^2}}}$	
	uncorrected	corrected	uncorrected	corrected	uncorrected	corrected
0.125	5.65	9.46	5.06	8.94	- 0.81	- 0.88
0.250	4.63	6.88	5.59	8.13	- 0.70	- 0.77
0.500	4.17	5.45	6.53	9.04	- 0.78	- 0.85
0.750	2.54	3.02	6.11	8.06	- 0.83	- 0.89
1.00	0.31	0.44	1.62	2.35	- 0.40	- 0.80

TABLE 2 REFERENCE FIGURE 10

$\frac{\sqrt{\overline{u'^2}}}{\overline{u}}$ %		$\frac{\sqrt{\overline{\theta'^2}}}{\overline{\theta}}$ %		$r=\frac{\overline{u'\ \theta'}}{\sqrt{\overline{u'^2}}\ \sqrt{\overline{\theta'^2}}}$	
uncorrected	corrected	uncorrected	corrected	uncorrected	corrected
0.65	0.91	0.90	1.21	-0.51	-0.70

Numerical examples showing the importance of the compensation correction are given on tables 1 and 2, in terms of the vorticity mode, of the entropy mode, and correlation coefficient.

5. CONCLUSIONS

Errors arising in hot-wire measurements performed in thin turbulent shear layers are analyzed. It is shown how these errors increase with increasing the outer MACH number of the flow and decreasing the layer thickness. The analysis indicates that the errors could be reduced by enlarging the bandwidth of the amplifier and by reducing the time constant of the wire. A simple correction method is proposed to correct for these errors, it leads to a compromise for the choice of the bandwidth, and of the characteristics of the compensation circuit. The efficiency of the method is checked by comparing corrected results obtained in an unfavourable case with results deduced from mean pressure and temperature measurements. Moreover, the corrected results agree with direct measurements made in more favourable cases.

The analysis indicate how to find optimal conditions required to perform suitable measurements in supersonic turbulent layers. For a fixed MACH number, the correction can be lowered by thickenning the turbulent flow, for example by using wall roughness in the case of a boundary layer. Reducing the Reynolds number, provided the flow remains fully turbulent, also thickens the layer but this effect is moderate; on the other hand, it increases the time constant. Nevertheless, it diminishes the mechanical vibrations, strain gauge effects, deformations and risks of breakage of the wire, so that in some cases, the wire diameter can then be reduced. This in turn reduces the time constant value and consequently the corrections and the residual errors.

February 2d, 1977

I.M.S.T. - 12 Avenue Général Leclerc - 13003 MARSEILLE
FRANCE

and

O.N.E.R.A. - 29 Avenue de la Division Leclerc
92 CHATILLON SOUS BAGNEUX - FRANCE

R E F E R E N C E S

1. KOVASZNAY L.S.G. - Turbulence in supersonic flow J. Aero. Sc., 20, 10, 1953.

2. KOVASZNAY L.S.G. - Should we still use hot wires? Advances in hot-wire anemometry, A F O S R N° 68 - 1942,1968.

3. CORRSIN S. - Turbulence: Experimental methods. Handbuch der Physic Encyclopedia of Physics, Springer Verlag 1963.

4. BRADSHAW P. - An introdution to turbulence and its measurent.Aero. Dept, Imp. Coll. of Sc. and Techn., Pergamon Press 1971.

5. COMTE BELLOT G. - Hot-wire anemometry, Annual Review of Fluid Mechanics 8,1976.

6. LADERMAN A.J., DEMETRIADES A. - Mean and fluctuating flow measurements in the hypersonic boundary layer over a cooled wall; Journal of Fluid Mech. 63,1, 1974.

7. A.L. KISTLER - Fluctuation measurements in a supersonic turbulent boundary layer, The Physics of Fluids, 2,3, 1959.

8. KOVASZNAY L.S.G. - Development of turbulence measuring equipment. N.A.C.A. Rpt. 1209, 1954.

9. GAVIGLIO J. - Sur quelques problèmes de mesures de turbulence effectuées a l'aide de l'anemomètre a fils chauds parcourus par un courant d'intensité constante. Thèse doct. d'Etat,Marseille 1958 P.S.T. Minist. Air N° 385.

10. MARTINOT LAGARDE A. - Introduction au spectre de la turbulence, N.T. G.R.A. 55, Paris, 1946.

11. MORKOVIN M.V. - Effects of high acceleration on a turbulent supersonic shear layer 1957 Heat Transfert and Fluid Mechanics Institute, U.C.L.A. 1955.

12. MAISE G., Mc DONALD - Mixing length and kinematic eddy viscosity in a compressible boundary layer, AIAA Journal 6, 73, 1968.

13. GAVIGLIO J., DUSSAUGE J.P., DEBIEVE J.F., FAVRE A. - Behavior of a turbulent flow, strongly out of equilibrium at supersonic speed; I.U.T.A.M. symposium on structure of turbulence and drag reduction, Washington, D.C., 1977.

14. JOHNSON D.A., ROSE W.C. - Laser velocimeter and hot-wire anemometer comparison in a supersonic boundary layer. A.I.A.A. Journal, 13,4, 1975.

15. KLEBANOFF P.S. - Characteristics of turbulence in a boundary layer with zero pressure gradient - N.A.C.A. T.N. 3178, 1954.

16. MORKOVIN M.V. - Effects of high acceleration on a turbulent supersonic shear layer - 1957 Heat Transfert and Fluid Mechanics Institute, U.C.L.A. 1955.

17. VEROLLET E. - Contribution aux méthodes de mesures de turbulence de vitesse et de temperature par l'anémomètre à fil chaud. Thèse 3ème cycle d'Aérodynamique, Fac. des Sc. Marseille 1962.

°°°°°°°°°°°°°°°°

National Bureau of Standards Special Publication 484, Proceedings of the Symposium on Flow in Open Channels and Closed Conduits held at NBS, Gaithersburg, MD, February 23-25, 1977. (Issued October 1977)

PROBE AND METHOD FOR SIMULTANEOUS MEASUREMENTS OF "TRUE" INSTANTANEOUS TEMPERATURE AND THREE VELOCITY COMPONENTS IN TURBULENT FLOW

Gracio Fabris

Argonne National Laboratory

Need has always existed in the measurement of turbulent flows to obtain correct instantaneous values of temperature and three components of velocity at a particular point. Many proposed lengthy approximate correction methods, that attempt to account for "nonlinear" effects (cross contamination between different quantities) in hot-wire measurements, cannot be considered satisfactory.

The availability of powerful digital computers for theoretical and experimental studies has placed pressures on experimentalists to develop better probes and methods. This paper attempts to answer these pressures by describing the development of a special four wire probe and a method of processing the obtained signals. The use of four 0.000025 inch sensors makes the probe practically interference free. The processing method is based on the simultaneous solution of four complete nonlinear response equations for the sensors yielding in principle exact instantaneous values of velocity components and temperature. Additional features of the processing method include: instantaneous full correction for tunnel free stream velocity and temperature fluctuations, first order correction for DC drifts of the signals during data acquisition, subtraction of all 60 Hz related noise, correction for streamwise displacement of sensors based on instantaneous streamwise velocity.

1. Introduction

For well over a quarter of a century, hot-wire anemometry has been and re-ains the most significant experimental technique in single phase fluid echanics. It is used mostly for the measurements of instantaneous temperature r streamwise component of velocity.

Higher levels of turbulence, namely non-streamwise components of velocity luctuations, influence readings of a single hot-wire placed perpendicular to he mean flow. Such readings have to be corrected for the influence of two ther velocity components. See Klatt [1], Spencer [2] and Rodi [3].

An inclined single wire can be placed at different angles at a given point f turbulent flow, and levels of fluctuations $\overline{u^2}$, $\overline{v^2}$ and $\overline{w^2}$ and even six eynolds stresses as done by Hoffmeister [4] and by Mojola [5] may be determined

[1]Figures in brackets indicate the literature references at the end of this paper.

by taking at least nine measurements with the wire placed at different angles with respect to the main stream direction.

Papers that treat response of single hot-wire in three dimensional turbulence are numerous. One by Champagne, et al. [6] is often referred to. Others cited are those by Friehe and Schwartz [7], by Collis and Williams [8], Davies and Fisher [9], by Davis and Davies [10] and by Andrews, et al. [11].

Artt and Brown [12] operated a single hot wire at two different overheats and obtained approximate average streamwise velocity and temperature. However, a single wire cannot give instantaneous information about more than one component of velocity; and even that one is contaminated by the influence of other velocity components and possibly temperature.

By placing several hot-wires or hot-film sensors close to each other, it is possible to extract more information. "X-wire" was used repeatedly by many researchers to measure simultaneously u and v components of velocity as well as Reynolds stress.

The response of a wire in non-isothermal flow was considered by Corrsin [13], Rose [14], Araya and Plate [15] and others. Chevrey and Tutu [16] used two wires and an extensive analog scheme to measure simultaneously approximate temperature and streamwise components of velocity. Ali [17] has improved the Chevrey-Tutu's analog processing of two-wire signals. Sakao [18] used two hot-wires operated at two different temperatures to measure streamwise velocity in flow accompanied by temperature fluctuations. Mimaud-Lacoste [19] used constant current wire at low overheat and constant temperature wire at high overheat, similar to Chevrey and Tutu [16]. However, he used an analytical scheme for taking into account contamination by velocity on "temperature signal" and temperature contamination on "velocity signals."

Way and Libby [20,21] used a two sensor probe to measure streamwise velocity and concentration of a helium jet ejected into the air. By the addition of one more sensor Stanford and Libby [22] were able to measure the lateral component of velocity also. Corrsin and Kistler [23] developed a probe for the measurement of streamwise vorticity component. A similar probe was used by Coles and Van Atta [24] to measure mean velocity vector and six Reynolds stresses in swirling flow.

Spencer [2] used a three wire probe designed by him and made by Thermo-Systems Inc. He used digital processing of signals to obtain three instantaneous velocity components. However, these components were only approximate since complete response equations for sensors were not used. Computed time averaged velocity correlations were later corrected for the influence of the third velocity component on the sensors.

Lakshaminaraya and Poncet [25] placed a two sensor probe and a one

sensor probe placed closely together to measure three dimensional values. Simplified response equations were used and solved digitally.

Due to the tremendous advancement of computational techniques, predictive methods for turbulent flows are becoming more and more sophisticated trying to introduce more complicated "closure" equations hopefully based on the physics of turbulent flow. See Bradshaw [26], Hanjalic and Launder [27] and Morel [28]. The use of digital techniques in the processing of signals in turbulent flows is becoming more common nowadays, promising to bring significantly more insight into the nature of turbulent flow, and to close the gap that is developing between computational power and experimental facts available to prediction methodology.

In order to keep pace with the fortunate availability of digital computational power for experimental techniques, it is necessary to improve experimental probes and ways of processing their output signals. The development of probes and methods capable of yielding "true" instantaneous three velocity components and temperature values at one point is long overdue. It is certain that much more vital information about the structure of turbulent flow could be obtained by the simultaneous measurement of as many quantities as possible (Fabris [29]).

Tutu and Chevrey [30] have stated that to solve response equations for sensors linearly for second order correlations, it would be necessary to have a seven sensor probe to get correct instantaneous values of u and v. However, we will show that the number of sensors could be smaller when full nonlinear equations are solved simultaneously. Flow reversal is not considered since it cannot be measured due to prong interference.

The probe described in this paper was used by the author for conditional sampling in heated single turbulent wake and interacting heated-unheated wakes flow. Although that flow is not the object of this paper, occasional reference to it will be made insofar as it relates to the calibration of the probe and the method of processing of data.

2. Construction of the Probe

The probe as designed and made by the author at IIT is shown in Figure 1. For wire supports jeweler's broaches with a diameter at the tip of about 0.012 inches are used. The tips are bent inward in order to facilitate the soldering of the sensing wires. All four sensing wires consist of Wollaston-processed platinum-10% rhodium filaments. These are 0.000025 inches in diameter and are enclosed in a silver jacket 0.003 inches in diameter.

The distance between the wire support tips, measured in the plane x is constant, 7/32 inches, while the bare sensing lengths of the wires are 0.080 inches. Since the tip distance is two to three times larger than for standard commercial single wires, the interference of the probe tips with the flow at the sensing spot is minimal. Our diagnostic checks indicated interference of less than one percent. This finding is in agreement with that of Comte-Bellot, et al. [31]. The center of the sensing spot is about one inch upstream

of the root of the broaches. According to Dahm and Rasmussen [32] the 5/16 inch nose piece which held the broaches should have a negligible influence on the measurements. The sensing spot is six and a half inches upstream of the vertical stem of the probe support which has an airfoil like shape, in order to cut down on flow induced vibrations of the probe. The nose part of the probe has two hinges (indicated at lower left of Figure 1) and could therefore be rotated around two axes. Since the probe tip can be rotated around a third axis, parallel to the broaches, the sensing wires can assume any desired angle with respect to the flow direction. The sensors numbered one and two in Figure 1 are perpendicular to each other, forming a classical X-wire probe in the x-y plane. The shortest distance between them is approximately 0.03 inches (.01 is technically achievable). Sensor number three makes angles of approximately 45° with the x and z axes. Due to an error in assembling (interchange of supporting prongs), this sensor is 0.064 inches upstream of sensors one and two although it was designed to be only 0.020 inches upstream. The corresponding lag time is taken into account in the computer data processing. Sensor number four is parallel to the z-axis and is located 0.028 inches upstream of the c crossing of sensors one and two (see the side view in Figure 1).

If the above-mentioned error in fabrication had not occurred, the sensing lengths could have been shorter and all sensors could have been placed within a cube 0.04 inches per side.

Sensors 1, 2, and 3 are operated in constant temperature mode at high overheats while sensor 4 is operated in constant current mode at very low overheat.

In order for a four wire probe to yield reliable results, it is necessary that each of the quantities to be measured (u, v, w, θ) has a significant influence on the output signal of at least one of the sensors. As will be seen later, sensors 1 and 2 are primarily sensitive to u and v components of velocity, sensor 3 to u and w and sensor 4 to temperature θ.

3. Velocity Sensing

The velocities in the wake were sensed primarily by three inclined wires and the velocity in the free stream by a wire normal to the flow. All these wires were platinum--10% rhodium 0.000025 inches in diameter. Constant temperature DISA anemometers Model 55D01 were used with wires one and two at an overheat of 300°C and sensor number three at 150°C. DISA linearizers Model 55D10 and DISA filters Model 55D25 were used for all three channels.

Output signals of the anemometers raised to an exponents of 2.7 (experimentally determined) became linear functions of velocity. (Digital linearizati would be advantageous in terms of data processing.) These linearized outputs were passed through low-pass filters set at 2000 Hz. This number was chosen based on the highest frequency of interest in the wake investigation. Kolmogor frequencies are higher than this but their contributions to the turbulent chara teristics other than high frequency spectra are insignificant. However, even when short enough sensors are used to measure Kolmogoroff scales without

excessive length corrections (La Rue [33]), the spectral levels at these high frequencies usually fall below the electronic noise in the signal. Low-pass filtering avoids aliasing when power spectra are computed.

The output of the anemometry units often drifted for as long as two days when new wires were mounted. The cold wire resistance would drift and sometimes undergo even a step-wise change. Presumably these changes were due to the relaxing of internal stresses in the wires or due to oxidization as explained by Hassan and Dent [34]. All wires were, therefore, left to overheat for over 30 hours until the above-mentioned drift disappeared, before the experiments were performed.

4. Temperature Sensing

To measure temperature, the fourth sensor in the four-wire probe was principally used. The temperature in the free stream was also monitored. In both cases platinum-10% rhodium wires with diameters of 0.000025 inches were utilized. Resistances of these two wires were always matched to within ten percent. The cable leads from both wires, connected in the same "broken bridge" shown in Figure 2. A paper by Borchardt and Holland [35] explains features of the "broken bridge." A current of about 0.5 mA was passed through each wire. The function of this bridge was to subtract the temperature signal in the free stream from that in the wake and to amplify this difference approximately 8000 times. In this way any drift of the tunnel temperature was automatically cancelled at the bridge output. The bridge is significantly simpler than the circuits used by Ochs [36] and LaRue [33]. This is probably the reason for the lower noise level achieved in this study.

Grounding was extremely important for the temperature measurements. Most of the noise in the temperature signal consisted of the 60 Hz line frequency, its higher harmonics and some white noise. The stratagem of connecting the two wires in the same bridge resulted in the cancellation of most of the periodic noise. Proper grounding further decreased that part of the noise.

The output from the broken bridge and the amplifier was a linear function of temperature in the temperature range used in this study (the wake flow was overheated for only several degrees Celsius), a fact which made the processing easier. To determine its sensitivity to the temperature in the flow, it was necessary to determine the temperature resistivity coefficient. For one wire the change in the output signal from the "broken bridge" and amplifier unit was measured as a function of the change in the air temperature which was monitored by a precision mercury thermometer. During this process the temperature in the tunnel was varied by 5°C while the tunnel was operated at the standard speed of 21.2 ft/sec. From the initial resistance and the total amplification factor of the circuitry we obtained $\alpha = \Delta R_3/R_{30}\Delta\Theta = 0.001675$ per degree Celsius. This value falls squarely in the range reported by the wire manufacturer Sigmund and Cohn, namely from 0.0016 to 0.0017.

The sensitivity of the temperature measuring circuitry with both wires in place was determined by artificially decreasing a known wire resistance R_3 by known decrements ΔR_3. This was achieved simply by connecting a known resistor of high value (usually 1MΩ) in parallel with the wires. From the known temperature resistivity coefficient one easily determines what effective change in the air temperature is represented by $\Delta R_3/R_3$. From measurements of changes in the output voltage we found the sensitivity to be 6.98 V/°C.

In actual experiment, the wake temperature sensor had a resistance of $R_3 = 1358\Omega$, while free stream temperature sensor $R_1 = 1444\Omega$. The resistance of the bridge part of the broken bridge was

$$R_b = \frac{(R_3+R_4)^2(\frac{R_1}{R_3})}{(R_3+R_4)\ (1+\frac{R_1}{R_3})} \tag{1}$$

The voltage drop across the bridge part was

$$E = 15\ \frac{R_b}{R_b+R_0} \tag{2}$$

The output from the broken bridge was

$$e = \frac{R_4 - \frac{R_2}{R_1} R_{3_R}\ (1+\alpha\Delta T)}{R_4 + R_3}\ E\ , \tag{3}$$

since

$$\frac{R_2}{R_1} = \frac{R_4}{R_{3_0}} \tag{4}$$

we have

$$e = \frac{\frac{R_2}{R_1} R_{3_R}\ \alpha\Delta T}{R_4 + R_{3_R}}\ E \tag{5}$$

The output of the second unit was

$$e_2 = -e\ \frac{R_6}{R_5}\ . \tag{6}$$

Other resistances were R_0 = 5kΩ, R_4 = 25kΩ, R_2 = 50kΩ potentiometer, R_5 = 500Ω, R_5 = 200kΩ. Taking $\Delta T = 1^{o}C$, one obtains for this case, sensitivity to temperature

$$S = e_2\Big|_{\Delta T=1^{o}C} = 6.97\ V/^{o}C,$$

which agrees very well with the experimentally determined value of 6.98 $V/^{o}C$.

The time constant of the wire was measured by means of the square-wave test applying a current of 0.5 mA. Results given in Figure 3 indicate that the cut off frequency at 21.2 feet per second is 4500 Hz. This made compensation of temperature signals unnecessary. No significant decrease in this frequency, such as reported by La Rue [33] was observed even after several days of running.

5. Calibration of the Probe

As mentioned previously, sensor number four in Figure 1 was used primarily for temperature measurements while sensors one, two and three were used primarily for velocity measurements. No electronic interference between different sensor signals due to long cables running together through the probe supports was ever observed. Angular calibration tests for all three velocity sensors were performed. Linearized voltage outputs as functions of the yaw angle for sensors number one and two are displayed in Figure 4. It is apparent that the data can be successfully expressed by a cosine curve between the $\pm 30^{o}$ yaw angles.

The operating overheat of sensors one and two was $300^{o}C$, while sensor three was overheated to $150^{o}C$. When sensor three was not energized, calibration data for sensors one and two in Figure 4 moved upward by less than one percent. This mild temperature interference among previously used sensors is shown as dashed lines in Figure 4. These earlier velocity sensors were made of tungsten wire 0.00015 inches in diameter with a sensing length of 0.04 inches. Clearly, the thermal wake of sensor number three had significant adverse influence on signals from sensors one and two. Decreasing the overheat of sensor three in an attempt to restore the cosine law for sensors one and two did not solve the problem. Ultimately the offending tungsten sensor (number three) was replaced by a six times thinner wire made of platinum--10% rhodium. The cure, however, turned out to be short lived. During the etching of sensors number three and four, nitric acid vapors evidently caused unnoticeable damage which impaired the strength of the tungsten sensors one and two regardless of how carefully the etching process was performed. Later, usually after two or three hours of running, these two sensors would burn out. Finally the problem was solved by using Pt-10% Rh wires for all sensors, as described previously, with the satisfactory calibrations shown in Figure 4.

Since the development of interference-free multiple-wire probes with good

spatial resolution remains an art which is essential to investigations of turbulence structure, it is desirable to relate briefly the experiences of Spencer [2]. Spencer's sensor number three was downstream of sensors one and two. Also he reported that his experimental arrangement made the angular calibration of sensor three difficult. He reported a decrease in the linearized output of the third sensor of seven percent when his two upstream sensors were energized. He found no adverse effect on linearization, but he could not report on agreement or disagreement with the cosine law. Clearly the interference effects are rather subtle.

During our general yaw calibrations of sensor number three the outputs of sensors one and two, were monitored but disclosed only normal behavior up to $\pm 30^{o}$ yaw from the nominal position. Beyond these angles the silver jackets of sensors three and four apparently started to interfere with the flow sensed by wires one and two.

Calibrations preceding the final data taking and taping include the determination of the exact angles of the wires in the wind tunnel. This determination is subject to additional geometrical constraints associated with the utilization of the traversing mechanism. The head of the traversing mechanism was rotated in the free stream five degrees in the vertical plane for the determination of angles β_1 and β_2 and two degrees in the horizontal plane for β_3. The formula

$$\tan \beta_i = \frac{\frac{E_{2i}}{E_{1i}} - \cos \Delta\beta_i}{\text{sub } \Delta\beta_i}, \quad (i = 1, 2, 3) \tag{7}$$

based on the verified cosine law, was then used to compute the angles β_1, β_2, and β_3. Here E_{1i} and E_{2i} are measured linearized outputs of the corresponding channels before and after $\Delta\beta_i$ rotation. The sensitivity to errors in the determination of β_3 can be illustrated by noting that a one degree change in β_3 leads to a change of approximately ten percent in the inferred $\overline{w^2}$ value.

Because of the possibility of the impairment of accuracy in the determination of the angles due to the physical limitations on the motion of traversing mechanism the following additional procedures were used. Very careful measurements of u', v', and w' at the centerline of the cold wake were carried out with calibrated single-wire and X-wire probes which were not hampered by the constraints of the traversing mechanism. These measured values were used as "true" references for the measurement of the same quantities at the same position with the four-wire probe. These reference values were used to supplement the information from equation (7) for iterative determinations of "best" β_i values for the different runs with the aid of a computer data reduction program.

Angles β_1, β_2, and β_3, determined by the iterative process through comparison with the reference values, were always within less than one degree of the values obtained using equation (7).

6. The Data Processing Equipment

For the acquisition and digitizing of data mini-computer PDP-11/10 was used with auxiliary equipment including an analog-to-digital converter. The computer has sixteen channels, four of which are digitized simultaneously and the other twelve with minimal delay time. Figure 5 presents the block diagram of the complete data acquisition system as used by Fabris [29]. Other researchers may use different acquisition systems according to availability.

The outputs of the linearizers were adjusted to read approximately 10.5 volts for the probes in the free stream. The filters (auxiliary units) used with the velocity channels permitted amplification and DC offset. Thus the linearized signals were given a maximum amplification of approximately 3.5 and were then offset for -30 volts D.C.

Using an adjustable potentiometer in the "broken bridge" the temperature signal was set to approximately -3 volts when the temperature in the free stream was measured. The filter used with this signal restricted the output to a range from -6 to +6 volts.

Not more than 20 percent of the allowable range of the analog-to-digital converter (-10 to +10 volts) was used (of course, researchers should tend to use most of the allowable range). However, the quantizing errors were small so that the maximum errors incurred in computing instantaneous velocities and temperatures were less than 0.0015 feet per second and 0.00035^{o}C, respectively. These errors in instantaneous values can be positive or negative so that, in the computed averaged quantities, they are substantially cancelled out.

7. The Data Acquisition Program

The data acquisition program digitized five analog signals. The four signals coming from the four-wire probe (three velocity signals and the temperature difference between the wake and the free stream) were digitized simultaneously (the system did not allow for simultaneous digitization of more than four signals). The free stream velocity signal, which has a much lower frequency content, was digitized with a time delay of 0.115 ms. with respect to the first four signals. Figure 6 displays the scheme of data acquisition. The digitized discrete values were stored as sixteen-bit binary integer numbers on a nine-track magnetic tape. Actually, only the last 12 bits were used as data. The first four bits were used as complements since it was easier to handle 16-bit numbers.

8. The Wires Response Equations

Even though linearizers were used in the actual acquisition of data for the sake of simplicity and generality, raw output signals from the anemometry units will be treated in this section.

There exist many papers proposing different response equations for the constant temperature hot wires. Most generally accepted are those by King [37] and by Collis and Williams [8] for the response of hot wire to the normal component

of velocity and to ambient temperature. There are a number of works published later proposing somewhat different equations like those by Bruun [38] and by Siddall and Davies [39]. The relationship proposed by Mimaud-Lacoste [19] is algebraically simple and therefore convenient for digital processing.

There are also a number of papers dealing with the response of hot-wire to flow under different angles with respect to the wire. Champagne, Fleicher and Wehrmann [6] introduced the correction factor to account for deviation from the "cosine" law due to finite wire ratio 1/d. The paper by Friehe and Swartz [7] deals with the same matter, proposing a different correction scheme. In our case, since wires of the ratio 1/d > 600 were used, "perfect" agreement with the cosine curve had been expected. This was confirmed by the yaw calibration. Thus, for the wires used, outputs of the anemometry units become a straight forward function of the velocity perpendicular to a wire and of the temperature of the fluid. According to Morkovin [40]the effect of density fluctuations is negligible for low speed flows.

For a constant temperature anemometry unit

$$E_0^2 = (A+B(U_n)^{1/n})\left(1 - \frac{\theta}{Tw-Tref}\right) \tag{8}$$

or

$$E_0^2 = A\left(1 + \frac{B}{A}(U_n)^{1/n}\right)\left(1 - \frac{\theta}{Tw-Tref}\right) . \tag{9}$$

It is well known that A and B are functions of temperature only for a particular wire and a given ambient fluid at a constant pressure. It is best to experimentally determine the functional dependence of A and B on temperature, see Chevrey and Tutu [16] and substitute these formulae in the above equation. For relatively small values of θ a linear approximation may be used. It is generally accepted that the exponent 1/n is constant, though Elsner and Gundlach [41] proposed it to be a function of velocity. For wires used in this study calibration yielded n = 2.7. This was somewhat surprising at the outset. However, since the Reynolds numbers for the wire we used were smaller than those for the generally used 0.00015 inch tungsten wire, the above value for n does agree with the value inferred from Figure 2.9 of Sandborn's monograph [42].

U_n is the component of velocity perpendicular to a sensor. For sensors 1, 2, and 3 respectively,

$$U_{n_1}^2 = (U \cos \beta_1 + V \sin \beta_1)^2 + W^2 \tag{10}$$

$$U_{n_2}^2 = (U \cos \beta_2 + V \sin \beta_2)^2 + W^2 \tag{11}$$

$$U_{n_3}^2 = (U \cos \beta_3 + W \sin \beta_3)^2 + V^2 \tag{12}$$

Sensor four gives the output

$$E_4 = E_{4_0} + K_4\theta + K_U (\sqrt{U^2+V^2} - U_r) \tag{13}$$

where E_{4_0} is the output of the temperature measuring circuit for the probe in the free stream at reference temperature T_r and velocity U_r. K_4 and K_U are proportionality constants expressing output sensitivity to changes of temperature and of velocity. Linear dependence of constant current anemometry output on temperature is a well known fact. For relatively small currents the influence of a change in velocity is only a few percent at most. Accordingly the first order correction using K_U is justified.

Equations (8), (9), and (13) are really only sample formulae and a researcher can use different ones according to his preference and the conditions of his experiment. If less computation and simplified calibration is desired, simpler formulae should be used; if greater accuracy is desired in experiments involving extended velocity and temperature ranges, more sophisticated formulas should be used. The use of linearinesss is one possible way of cutting computational costs. In flows with low turbulence levels, equations (10), (11), and (12) could be simplified by dropping W in (10) and (11) and V in (12) with acceptable losses in accuracy.

Having voltage outputs from three CTA and one CCA circuits, it is best to write four corresponding equations with U, V, W and Θ as unknowns, and then to solve them simultaneously. The Newton-Raphson technique features the fastest convergence if the initial guess for unknowns is reasonable. Since velocities and temperature are changing only slightly from one time instant to the next, it is extremely convenient to take as the initial guess for one time constant values of U,V, W and Θ that are actual solutions for a previous time constant. Using this technique, accuracy of numerical solution better than 0.01 percent has been achieved by Fabris [29] with a single iteration. If a significantly higher accuracy is desired, it might prove beneficial to provide an initial guess of unknowns that would take in account trends in velocities and temperature in two previous consecutive instants, thus avoiding an excessive number of iterations.

9. Corrections

Digital processing permits a number of corrections to be made that would be almost impossible to make in analog processing. These corrections contribute greatly to the accuracy of flow measurements. Such corrections are of importance in many flows, for example in small deficit wake measurements.

9.1. Correction for DC Drifts

In any measurement, there is a finite time lag (often rather long) between the calibration of a probe and the electronics and the actual measurement. During that time there are inevitably some DC drifts (changes) in voltage outputs, decreasing the accuracy of measurement. The causes of these drifts are in the electronic instruments as well as in changes in ambient wind tunnel conditions, such as temperature, humidity and free stream velocity. It is virtually impossible to monitor drifts during the actual measurement, but one can find the total drift values in a given time interval by taking measurements in the reference flow before and after data acquisition. One cannot know which of the parameters has contributed most to the drift, but in the first approximation it can be assumed that the most significant part is or could be included in proportionality constant A in equation (9) (with the ratio B/A assumed to remain constant) or in the additive constant E_{4_0} in equation (13). Experience indicates that in practically all cases drifts are a continuous function in time and for reasonable short time intervals rather monotonic. So, lacking information on the actual nature of drift, it is justifiable to assume that drift is linear in time between the reference flow measurements made just before and just after measurements in the flow of interest.

In the case of measurements in the wake flow, or some other free stream turbulence flow, first reference measurements with the digital acquisition of data, are made in the undisturbed potential free stream. Then recordings are taken at desired number of lateral wake profile positions with the last measurements again in the original free stream reference position. During all these measurements time is noted when data at different wake positions are acquired. Now, assuming no change in ambient conditions, the computation of the above-mentioned constants is performed according to the linear interpolation formula

$$C_{i,j} = C_{i,\,\mathrm{ref.first}} + t_j \left(C_{i,\mathrm{ref.last}} - C_{i,\mathrm{ref.first}}\right)$$

$$(i=1,2,3,4,5),\ (j=1,\ldots,12) \qquad (14)$$

where i and j indicate the appropriate channel or wake positions.

Of course, the angles of the inclined wires with respect to the main stream have to be determined prior to the above calculation, so that the velocity normal to each wire is known for the probe in the free stream reference position. If one would like to increase accuracy and to correct for more than one constant per channel, one would have to perform additional reference measurements under different flow conditions. For example, it would be very convenient if there were a small still air chamber where the probe could be quickly placed and readings recorded before and after measurements in the flow to be studied. In such a way, additional reference values would be provided and interpolative correction for two constants per channel obtained, such as the constants A and B in equation (9).

9.2. Correction for Streamwise Displacement between Sensors

Inevitably there is some streamwise displacement between each of the sensors three and four and the (imaginary) crossing of sensors one and two. The four channels were sampled simultaneously which meant that at a given time the four wires did not sense the same fluid elements. This effect was taken into account as explained below.

It is known that in flows with lower turbulence such as the far wake Taylor's hypothesis is a good approximation to the physical process. This hypothesis simply states that the turbulent structure is convected past any point with the local mean velocity $\overline{U}(x,y)$ so that spatial and time derivatives are related

$$\overline{U} \frac{\partial}{\partial x} ( ) = \frac{\partial}{\partial t} ( ) \qquad (15)$$

This means that a fluid particle passing the first upstream sensors changes its temperature and velocity very little before it passes the downstream sensors. To estimate the error when the convection is not taken into account, we can use the spatial correlation measurements of Grant [43]. Judging by these correlations in a cylinder wake, we conclude that in our case the fluctuating properties would have changed only about two percent (correlation coefficient of 0.98) for a maximum wire displacement of 1.6 mm.

In our data reduction program, however, we can compensate for any displacement by effectively delaying the signals from the upstream wires for appropriate times using the instantaneous flow velocity in the x direction as the transport velocity for the signals. The conditions correspond then to the space-time correlations between two signals of turbulence at two streamwise locations studied by Favre [44]. Judging by his results when an optimal time delay would be applied for conditions of our flow, the correlation coefficient would be 0.997. Such an improvement was considered significant, and therefore all of our computations and results incorporated the optimum delay for channels three and four, see Figure 7. Optimum delay was always based on instantaneous streamwise velocity.

One minor complication arose in connection with the delay times: they did not correspond to the discrete time values at which our data were given and therefore interpolations were necessary. Study of Figure 7 should make the issues and procedures quite clear. The interpolation did degrade our corrections somewhat, especially when high-frequency components were present. To assess the degree of degradation, we computed the values of θ' over one record both for the original data and for the data obtained by interpolation at the delayed times. The latter was approximately 0.5 percent lower. This being an undesirable situation, we believe that the net gain in applying the optimal time delay is important and that the small degradation resulting from interpolation is negligible except perhaps in obtaining power spectra with high frequency content.

9.3. Corrections for Free Stream Velocity and Temperature Variations

Even though greatest care is taken, some velocity fluctuations remain in a free stream. Measuring the two point correlation function of the streamwise component of velocity in the free stream of the test section, Fabris [29] found that a major part of the streamwise velocity fluctuations is simultaneous at all points (pressure induced fluctuations) with a frequency range 0 to 10 Hz. Slow fluctuations of velocity (less than 1 Hz) had had a peak to peak amplitude of 0.015 U. Only 85 percent of these fluctuations could be averaged out using an averaging circuit with a time constant of ten seconds. Although these slow fluctuations do not influence the analog u' measurements (RMS meter filters out fluctuations with frequency of less than 1 Hz), they do influence U measurements. The RMS value of free stream velocity fluctuations measured by the analog RMS meter was 0.0035 U.

Using the fact of simultaneousness of free stream velocity fluctuations in the whole test section and the fact that in a small deficit wake only relatively small changes of streamwise velocity are encountered, one effective correction scheme was devised. Free stream streamwise velocity was monitored by a separate constant temperature anemometer probe. This velocity was subtracted by digital processing from the streamwise velocity simultaneously measured by the four-wire probe. In this manner, the instantaneous velocity defect in the wake with respect to instantaneous free stream velocity was obtained with the four-wire probe in the free stream (not close to the free stream probe). Digitally computed u' was 0.00055 U.

The free stream temperature did not show appreciable fluctuations except for quite slow variations which were of the order of 0.05°C during a 15 minute period. Such temperature drifts were compensated for by subtracting signals of the temperature sensor of the four wire probe from a reference temperature wire placed in the free stream.

After the above drift signals are eliminated, it is still difficult to judge the actual free stream temperature fluctuations. They are sufficiently small for possible false signals from the higher free-stream velocity fluctuations to creep in despite the very low overheat of the temperature wire sensor. Also, the noise level in the temperature signals is higher than that in the velocity signals. Be that as it may, θ' in the free stream thus obtained was 0.0014°C, which is considerably less than θ' inferred from a single wire uncompensated measurement.

9.4. Subtraction of the 60-Hz Conditioned Noise

At the outset most of the signal noise was 60-Hz conditioned regardless of how carefully grounding of the temperature probes and the bridge was effected. This created problems since the temperature signal was used for conditional discrimination. It forced us to carefully look for a solution. The combination of the stored information and the computer made it possible, as part of the data processing, to attempt to purge the periodic parts of this noise from the signal

The data acquisition program was written in such a way that all records were triggered at the same phase of the 60 Hz supply current. Since the sampling frequency was 4000 Hz, it meant that exactly 200 samples covered three cycles of the 60-Hz conditioned noise. Using the signals at the first and last reference recording per wake profile (i.e., free-stream position) each of these signals was "ensemble averaged" or "educted" in the data reduction program for 200 ordered samples within each interval of three cycles. There were seven three-cycle intervals used per record (1400 samples). In total 34 records were used. This simply meant making 200 separate sums each one composed of 238 summands. In this summation process the regular 60-Hz conditioned noise cumulated while the random part of the noise and the part of the signals due to velocity or temperature fluctuations in the flow cancelled out. Then the averages of these 200 sums were computed for each channel, subtracted from each of the sums and the result divided by 238, the number of summands.

In this manner three relatively clean cycles of 60-Hz conditioned noise were obtained for each channel. This repetitive "noise signal" was subtracted from all the digital data processed in our data reduction program to obtain what we call "cleaned" signals. Samples of the "educted" 60-Hz conditioned noise and of the corresponding "cleaned" signals are given in Figure 8 for channels three and four. The original signal was, of course, the sum of these two signals. The clear-cut improvement underscores the significance of our correction process, especially for measurement in low turbulence or in potential flow.

10. Conclusions

The availability of analog to digital conversion and digital processing of turbulence signals increases experimental possibilities greatly. The development of more sophisticated probes and methods of processing of their signals is necessary in order to more fully utilize the advantage of digital processing.

A four-wire probe and method capable of yielding "true" instantaneous values of temperature and three components of velocity at one point of turbulent flow has been developed. Due to the use of sensors 0.000025 inches in diameter, 0.012 inch diameter prongs, and with 7/32 inches the shortest distance between the prongs, the probe is practically interference free. All sensing wires can be placed within 1 mm^3 giving high spatial resolution. Table 1 compares this probe with the one used by Spencer [2]. The application of the probe and the method of processing of signals has been illustrated by measurements performed in small deficit, slightly heated, turbulent wake flow.

The method also includes corrections for DC drifts during measurement, for streamwise displacement between sensors, for instantaneous variations of the tunnel's free stream temperature and velocity as well as the subtraction of practically all 60 Hz related noise. Table 2 lists the types of corrections utilized.

These techniques resulted in high-accuracy measurement. Turbulence intensity in free stream was measured to be 0.055 percent of free stream velocity. Such low turbulence levels usually cannot be measured by CTA; see Corrsin and Kuo [45]. RMS noise level of processed temperature signal was determined to be only 0.0014°C. Such a low value, also, cannot be measured by previously available methods.

It is believed that the probe and the method developed would be of help i future turbulence research, especially when the technique of conditional samplin is used.

11. Acknowledgement

The author wishes to express his thankfulness to Drs. M. V. Morkovin and Y. L. Way, professors at Illinois Institute of Technology who were his Ph.D. thesis coadvisers. They have followed experimental work on this paper with keen interest and helped me with constant encouragements. Dr. Way has written the data acquisition program that digitized analog signals and stored them on magnetic tape. The research was supported under USAF OSR Grant No. AFOSR-73-2509.

TABLE 1. SINGLE-POINT MULTIWIRE PROBES

	Spencer [2]	Present
Number of Wires	3	4
Wire Material	tungsten	Pt-10% Rh
Diameter, inches (microns)	.00015 (3.75)	.000025 (.625)
Measurements	3 velocity components	3 velocity components and temperature
Made by	TSI	homemade (IIT)
Wire Interference	7%	1%
Cosine Law for Third Sensor	not reported	verified
Computed Instantaneous Velocities	approximate with correction of results	solutions of four simultaneous equations
Computed Instantaneous Temperature	not done	
Determination of Angles of Sensors	angular calibration	angular calibration and reference values

TABLE 2. CORRECTIONS

Type of Error	Way of Correction
Tunnel Velocity Variations	digital subtraction of free stream velocity signal
Tunnel Temperature Variations	analog subtraction of free stream temperature signal
Drifts of Instrumentation Signals	assumed linear in time between first and last reference measurements
60-Hz Conditioned Noise	calculated by education of records, then subtracted
Streamwise Displacement Between Sensors	signals delayed using instantaneous streamwise velocity

12. References

[1] F. Klatt, *Disa Information*, No. 14, March 1973.

[2] B. Spencer, *Ph.D. Thesis*, University of Illinois, 1970.

[3] W. Rodi, *Disa Information*, No. 17, February 1975.

[4] M. Hoffmeister, *Disa Information*, No. 13, May 1972.

[5] O. O. Mojola, *Disa Information*, No. 16, July 1974.

[6] F. H. Champagne, C. A. Fleicher, O. H. Wehrmann, *J. Fluid Mech.*, Vol. 28, Part 1, 1967.

[7] C. A. Friehe, W. H. Schwarz, *J. of Applied Mechanics*, December 1968.

[8] D. C. Collis and M. J. Williams, *J. of Fluid Mechanics*, Vol. 6, 1959.

[9] P.O.A.L. Davies, M. J. Fisher, *Proc. Roy. Soc.* A.V. 280, pp. 486-527, 1964.

[10] M. R. Davis, P.O.A.L. Davies, *Int. J. of Heat Mass and Mass Transfer*, V. 15 (1972).

[11] G. E. Andrews, D. Bradley, G. F. Hundy, *Int. J. of Heat and Mass Transfer*, V. 15 (1972).

[12] D. W. Artt and A. Brown, *Sci. Instrum.*, V. 4 (1971).

[13] S. Corrsin, *The Review of Scientific Instruments*, Vol. 18, No. 7, July 1947

[14] W. G. Rose, *J. of Applied Mechanics*, September, 1962.

[15] S.P.S. Arya, E. J. Plate, *Instruments & Control Systems*, March 1969.

[16] R. Chevrey, N. K. Tutu, *The Review of Scientific Instruments*, Vol. 43, No. 10, October 1972.

[17] S. F. Ali, *Rev. Sci. Instrum.*, Vol. 40, No. 2, February 1975.

[18] F. Sakao, *Scientific Instruments*, Vol. 6, No. 9, 1973.

[19] F. A. Mimaud-Lacoste, *M. S. Thesis*, Pennslyvania State University, 1972.

[20] J. L. Way, P. A. Libby, *AIAA Journal*, Vol 8, No. 5, May 1970.

[21] J. L. Way, P. A. Libby, *AIAA Journal*, Vol. 9, No. 8, August 1971.

[22] R. T. Stanford, P. A. Libby, *The Physics of Fluids*, Vol. 17, No. 7 (1974).

[23] S. Corrsin, A. L. Kistler, *NACA Rept 1244*, 1955.

[24] O. Coles, C. Van Atta, *AIAA Journal*, Vol. 4, No. 11, November 1966.

[25] B. Lakshaminaraya, A. Poncet, *J. of Fluids Engineering*, June 1974.

[26] P. Bradshaw, *Aeronautical Journal*, July 1972.

[27] K. Hanjalic, B. E. Launder, *J. of Fluid Mechanics*, V. 52, 1972.

[28] T. Morel, *Ph.D. Thesis*, Illinois Institute of Technology, Chicago, 1972.

[29] G. Fabris, *Ph.D. Thesis*, Illinois Institute of Technology, May 1974.

[30] N. K. Tutu, R. Chevrey, 1975. *J. Fluid Mech.*, V. 71, 785.

[31] G. Comte-Bellot, A. Strohl, E. Alcaraz, *J. of Applied Mechanics*, December 1971.

[32] M. Dahm, C. G. Rasmussen, *Disa Information*, No. 7, January 1967.

[33] J. C. LaRue, *Ph.D. Thesis*, University of California, San Diego, 1974.

[34] H. Hassan, J. C. Dent, *Brit. of Appl. Phys.*, Ser. 2, Vol., 1969.

[35] T. G. Borchardt, L. R. Holland, *Rev. Sci. Instrum.*, V. 40, No. 1, January 1975.

[36] G. R. Ochs, *ESSA Institutes for Environmental Research*, IER 47-ITSA-46 (1967).

[37] L. V. King, Phil. *Trans. R. Soc.*, 214A, 1914.

[38] H. H. Bruun, *Sci. Instrum.*, V. 4 (1971).

[39] R. G. Siddall, T. W. Davies, *Int. J. of Heat and Mass Transfer*, V. 15 (1972).

[40] M. V. Morkovin, *AGARDograph 24, NATO*, Paris, November 1956.

[41] J. Elsner, W. R. Gundlach, *Disa Information*, No. 14, March 1973.

[42] V. T. Sandborn, *Resistance Temperature Transducers*, Metrology Press, (1972).

[43] H. L. Grant, *J. Fluid Mechanics*, V. 4, 1958.

[44] S. J. Favre, *J. of Applied Mechanics*, June 1965.

[45] S. Corrsin, A. Y. Kuo, *J. Fluid Mechanics*, V. 56, Part 3, 1972.

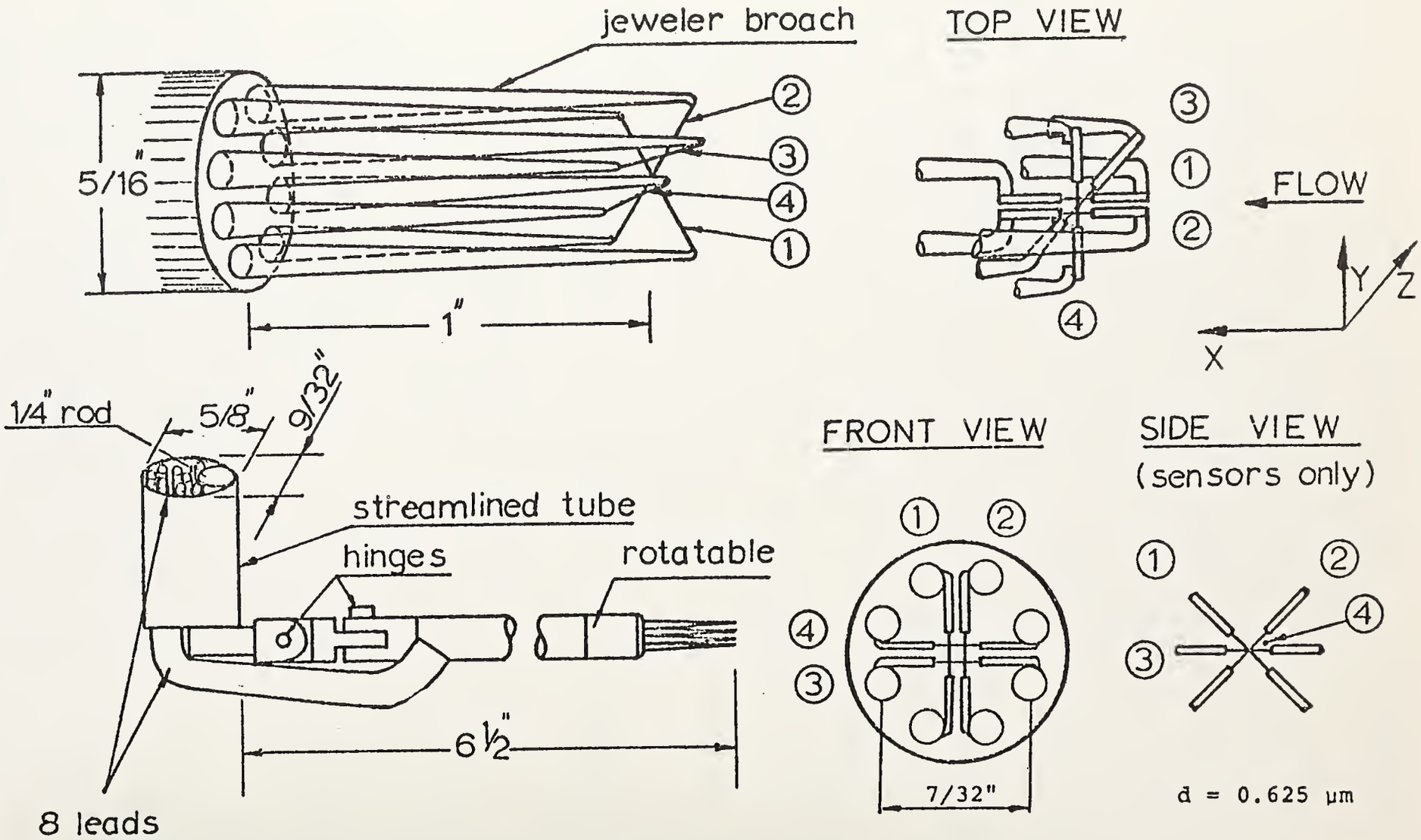

Figure 1. The Four-Wire Probe

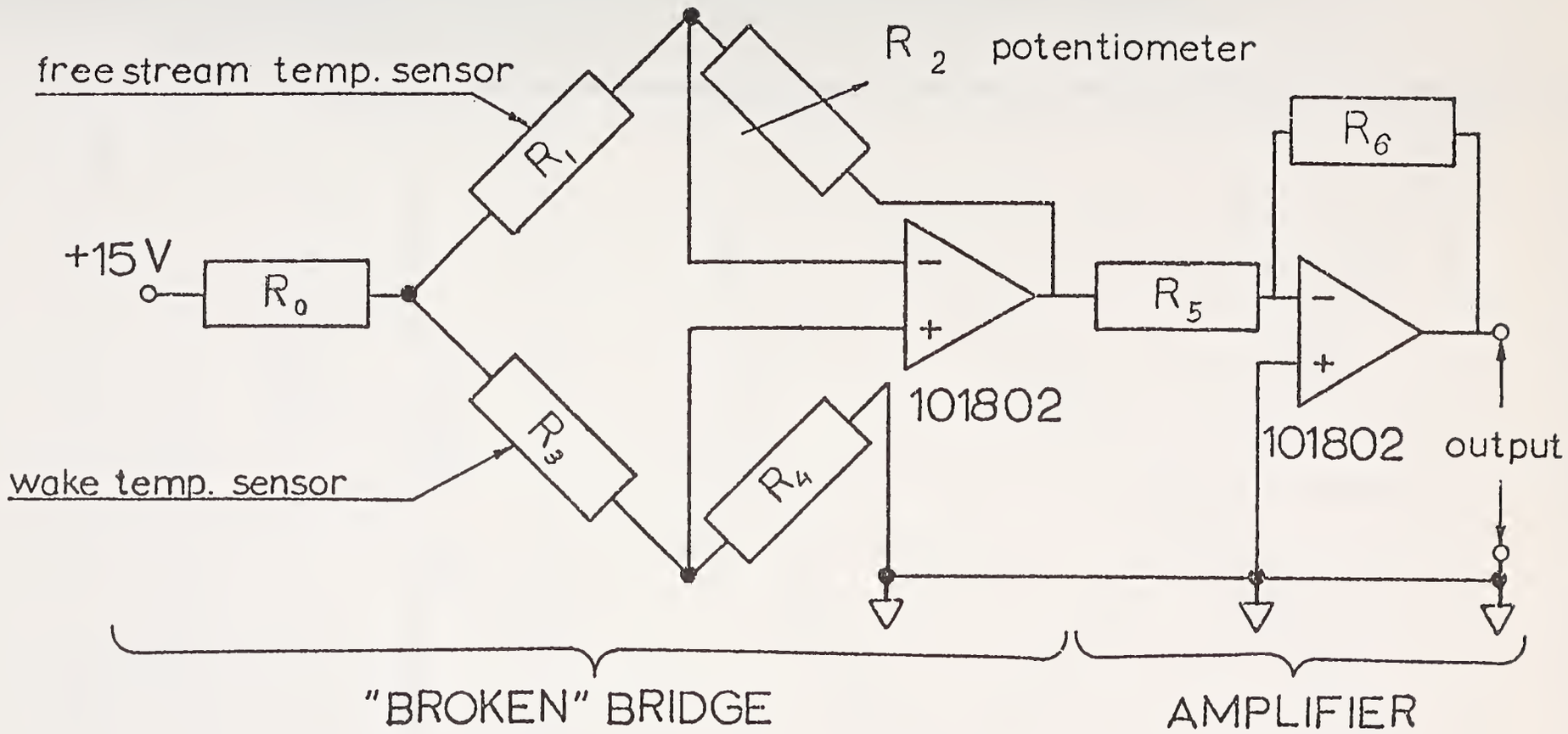

Figure 2. The Temperature Measuring Set-Up

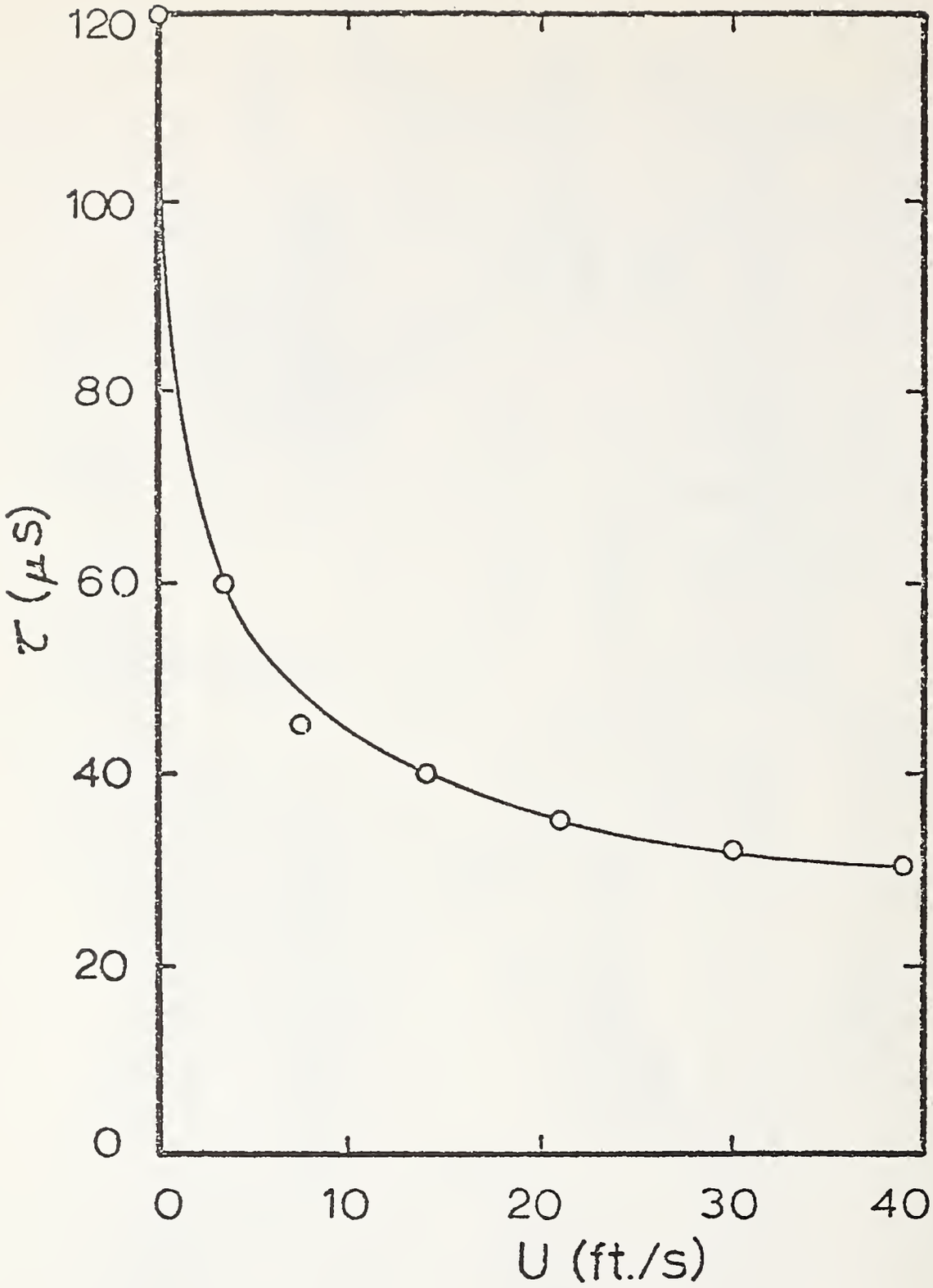

Pt-10% Rh, d = 0.000025 inches

Figure 3. The Wire Time Constant

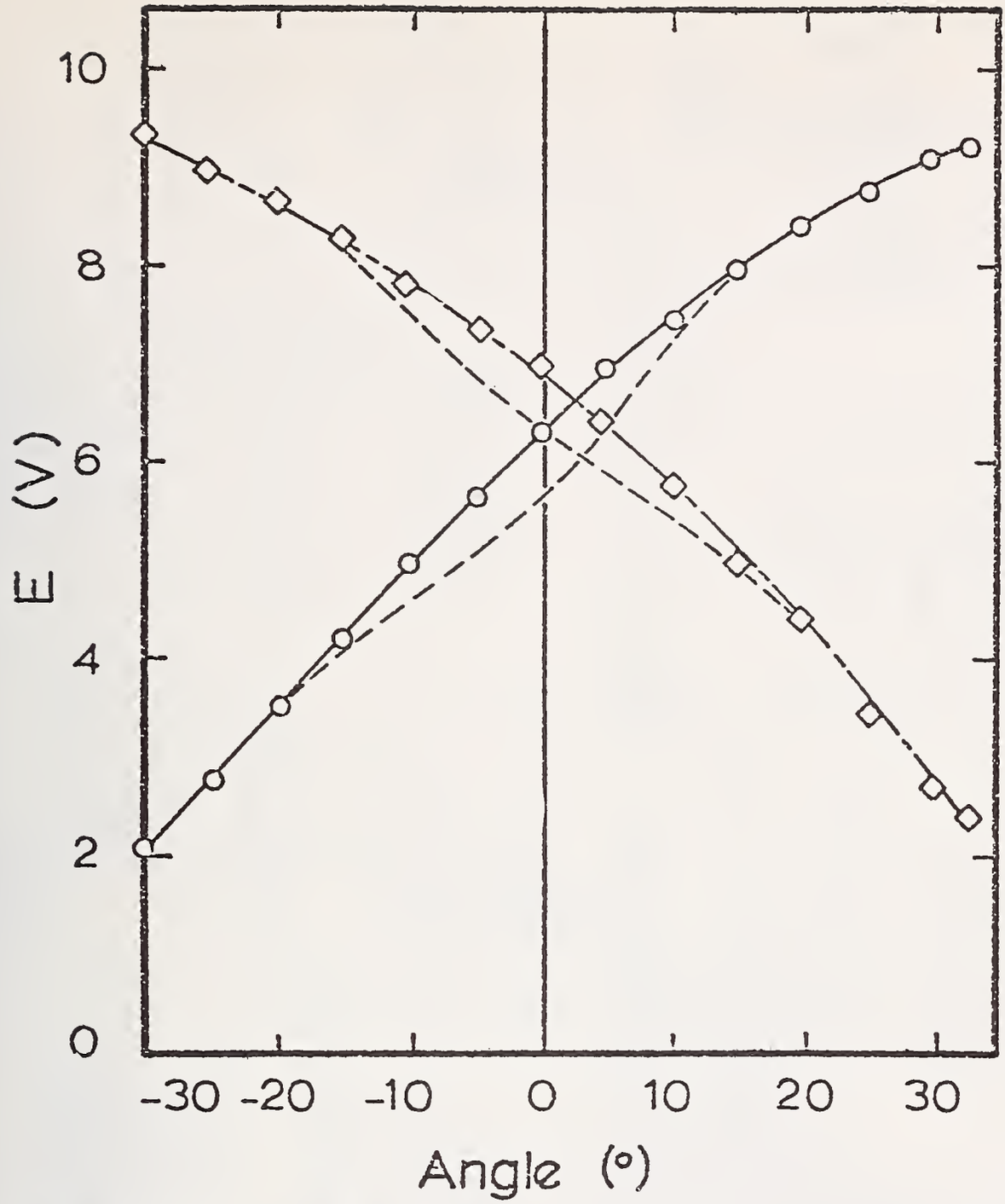

○ sensor 1 } overheats 300°C, sensor 3 overheats 150°C
◇ sensor 2 }
——"best fit" cosine curve,
---for sensors 1 and 2 when all three sensors were tungsten wires (d=0.00015") overheated to 240°C

Figure 4. Yaw Calibration of Wires

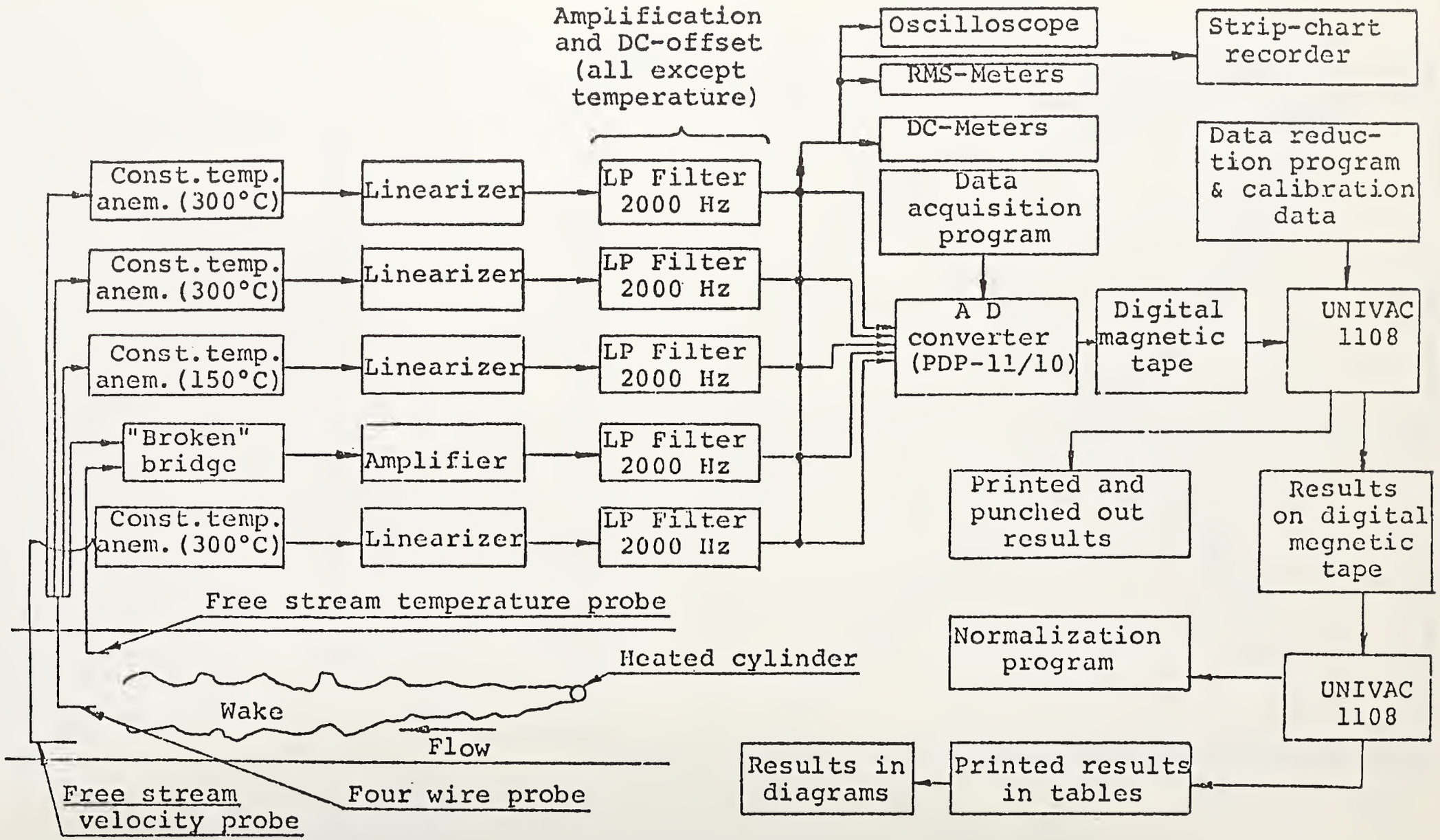

Figure 5. The Scheme for Data Processing

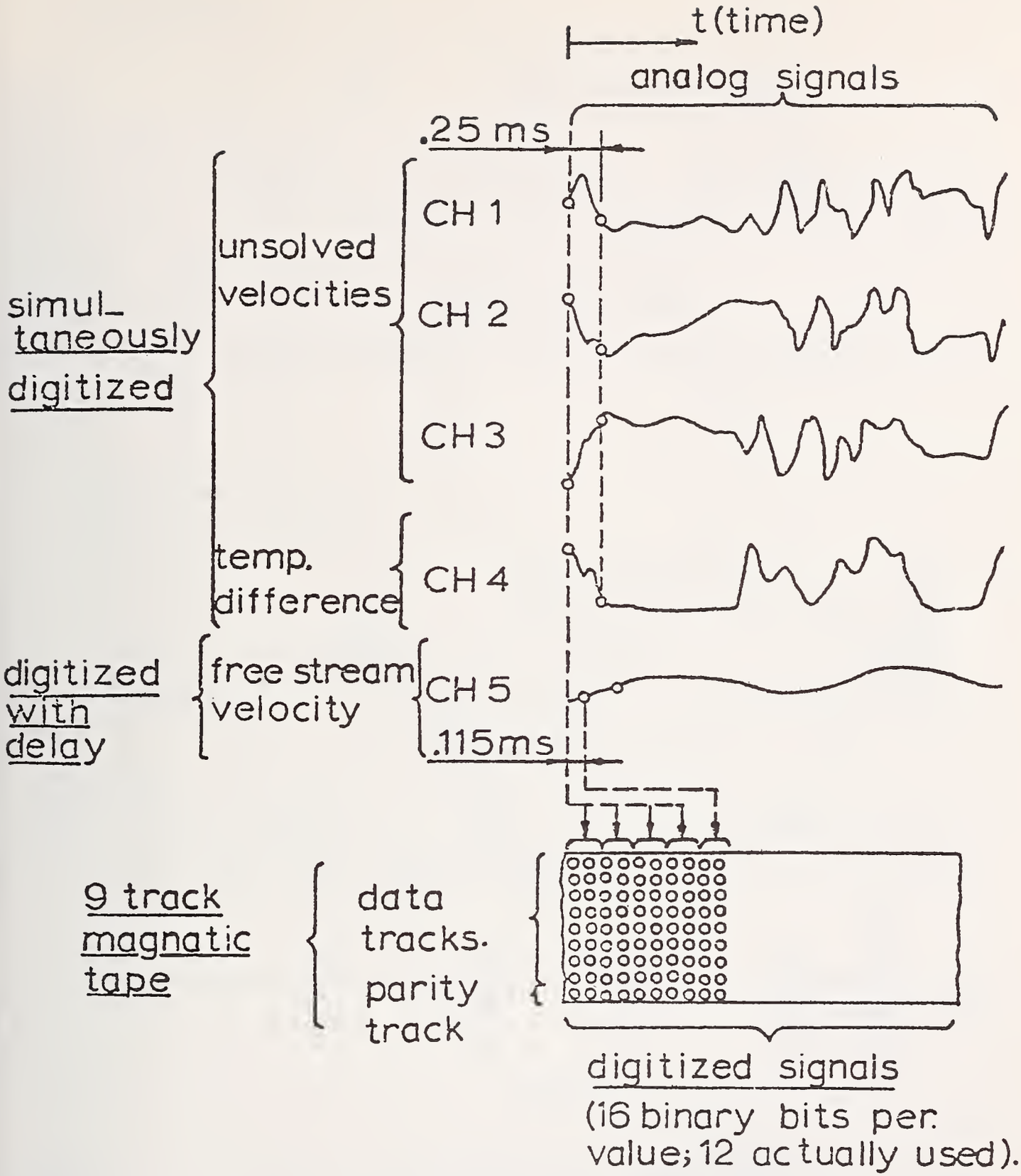

Figure 6. The Scheme for Data Acquisition

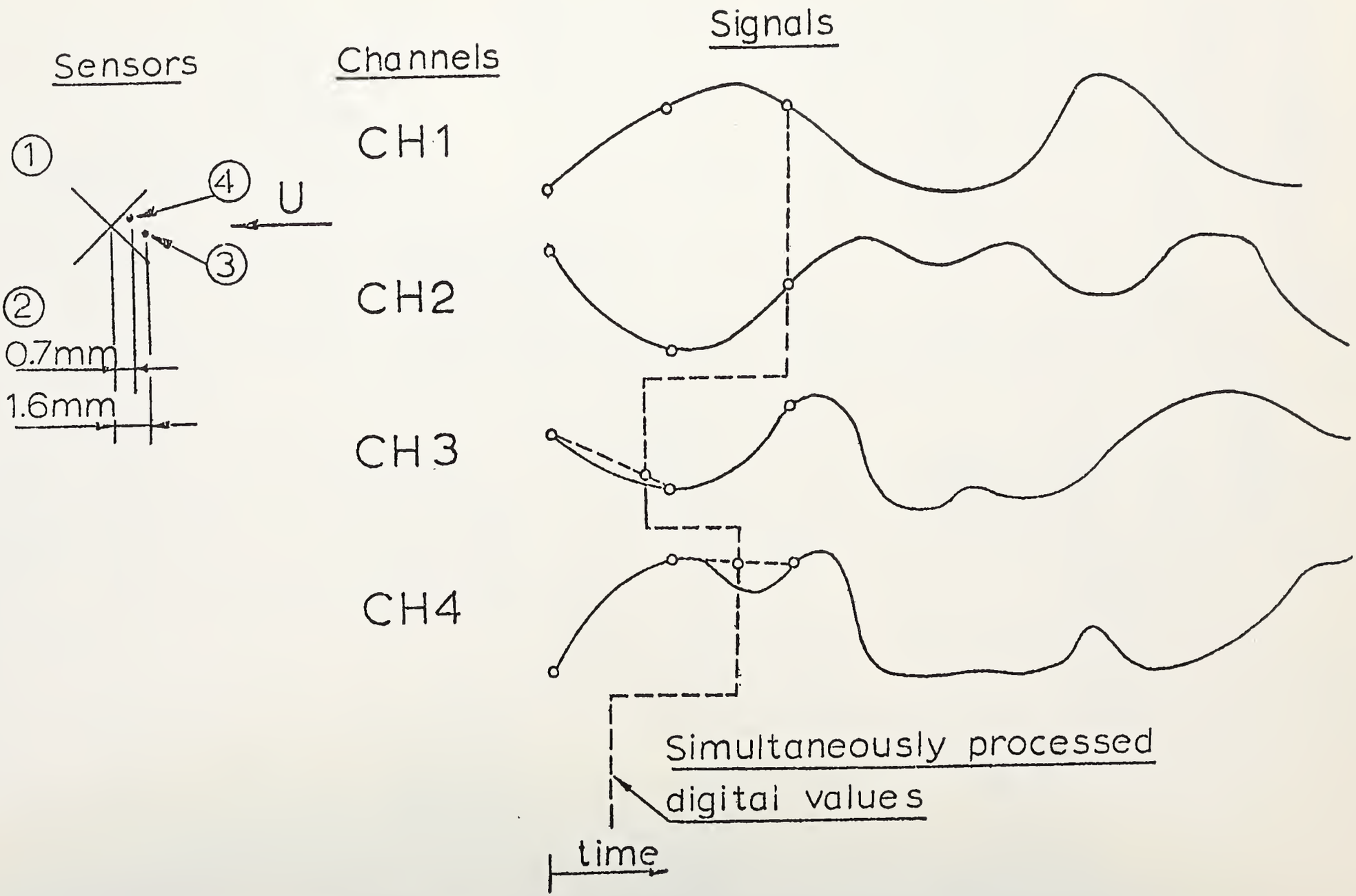

Figure 7. Scheme of Delay of Signals.

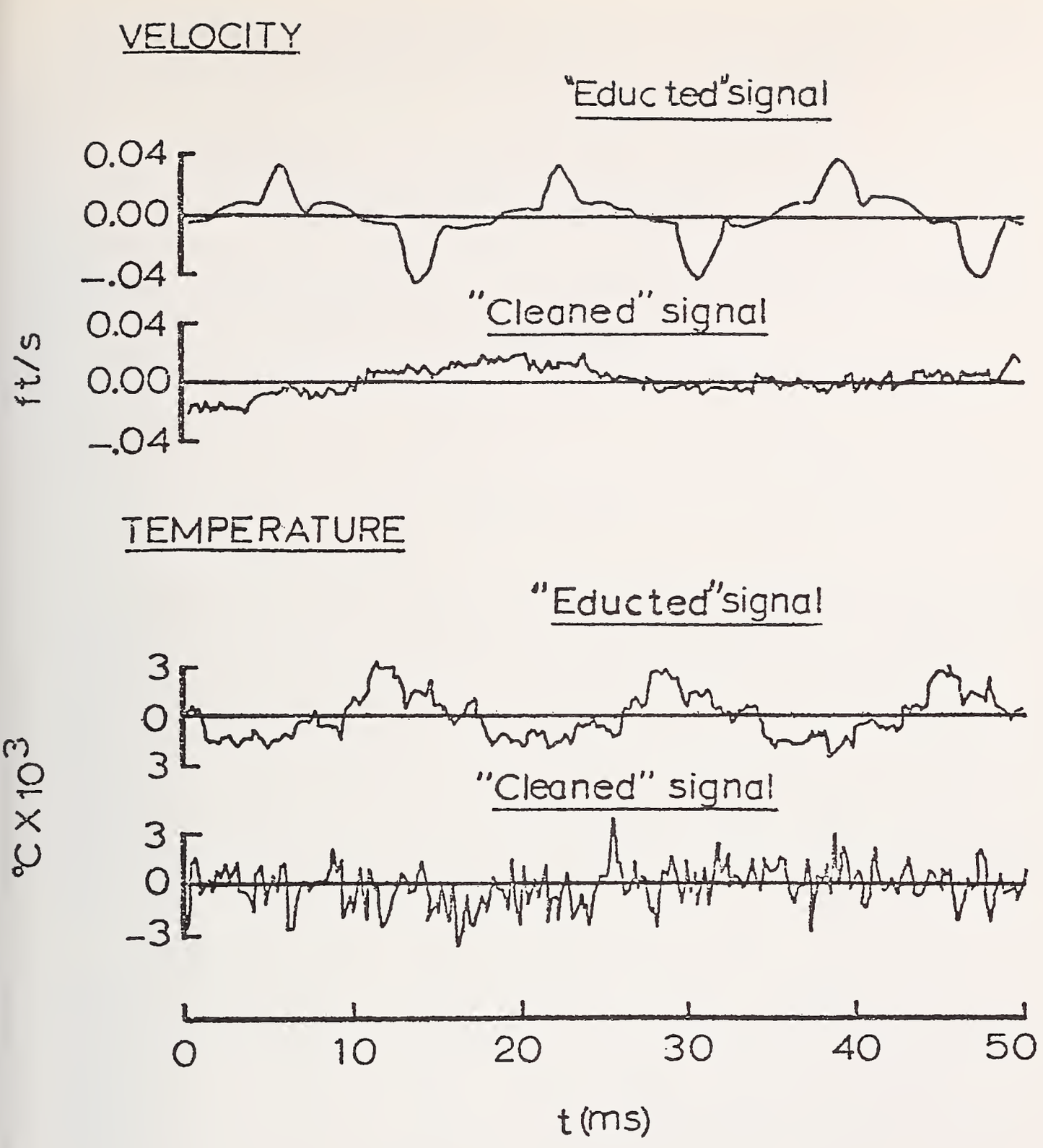

Figure 8. Educted and "Cleaned" Signals in Free Stream

National Bureau of Standards Special Publication 484, Proceedings of the Symposium on Flow in Open Channels and Closed Conduits held at NBS, Gaithersburg, MD, February 23-25, 1977. (Issued October 1977)

MEASUREMENT OF BOUNDARY LAYER TRANSITION USING ACOUSTIC TECHNIQUES

Donald C. Sachs, Thomas F. V. Meagher, and Vernon D. Peckham

Kaman Sciences Corporation
P. O. Box 7463
Colorado Springs, Colorado 80933

1. INTRODUCTION

The acoustical properties of boundary layers on the surface of bodies moving at hypersonic velocities have not been characterized fully by detailed measurements. It is known that boundary layer conditions (i.e., laminar, transitional, or turbulent) are dependent on a number of factors, including the Reynolds number of the flow, body orientation with respect to the flow, body geometry, et al. The essential acoustical parameters associated with boundary layers in general are well known to those who have worked in this field; among these parameters are pressure fluctuations in time which vary greatly with flow condition, spatial correlation of the fluctuations, and intermittency during marginal transition conditions(1-6)*.

A Boundary Layer Acoustic Monitor (BLAM) has been developed to take advantage of some of these acoustic properties to measure transition. In the design of this transducer, consideration has been given to measurand level, dynamic range, directionality, response frequency, packaging design for aerospace environments, installation requirements, and calibration techniques. Figures 1 and 2 are photographs of a monitor set; the set consists of a sensor connected with a cable to an electronics signal conditioning amplifier.

2. SENSOR DESIGN

The sensor depicted in Figure 1 utilizes an x-cut quartz crystal of round geometry operating in the thickness extensional mode between faces; its thickness is .63 cm and diameter is 2.54 cm. The crystal is mounted in a thin aluminum shell and

---

*Numbers in parentheses indicate the literature references at the end of paper.

is connected in such a way as to cause the external face to be at electrical ground potential. Isolation from system ground has been provided by thin epoxy-fiberglass laminate material on the external face which is placed in contact with the structure to be monitored.

Internally, the sensor also contains a very high input impedance pre-amplifier which interfaces to a cable transferring the signal to the signal conditioner amplifier; the coaxial cable also serves to provide d.c. power to the sensor.

In application, the sensor front surface is placed in direct acoustic contact with the rear surface of the wall over which the flow moves. A bonding epoxy has been used to provide both mechanical strength and to ensure good continuity for the acoustical waves to enter the sensor. The flange on the sensor which can be observed in Figure 1 is used for attachment in applications where the surface bonding material may be fluid.

The frequency response of the sensor extends from approximately 10 kHz up to over 500 kHz with resonance peaks occurring at intervals depending on individual system installations. In Figure 3 is shown a partial response spectrum of the 2.54 cm sensor installed on carbon-phenolic material 1.0 cm thick. A uniform surface peak pressure of 35 N/cm^2 (.005 psi) was applied to obtain the data shown.

3. ELECTRONICS SIGNAL CONDITIONER DESIGN

A functional block diagram of the signal conditioner is shown in Figure 4. The signal from the sensor is directed into an amplifier which has a non-linear feedback characteristic. After amplification, the signal is amplitude detected and further amplified to produce an output which ranges from 0 to 5 volts. The input-to-output characteristic of this amplifier is given in Figure 5. It can be noted that for very low input voltages the gain is several thousand whereas for the highest input signal, overall voltage gain is less than 1/2. Filtering is also accomplished in the signal path, both at the input to select the desired acoustical frequencies from the boundary layer and at the output to limit bandwidth as may be demanded by the application.

The circuit includes a voltage regulator and will accomodat input voltages from 24 to 32 vdc. Current input to the monitor set is 30 milliamperes maximum.

4. SPATIAL RESPONSE CHARACTERISTICS

When mounted on relatively thin-wall cylinders or on flat sheet material, the sensor is sensitive principally to waves which originate on the opposite surface within a sensor diameter distance. A measurement has been taken of the spatial selectivity of one installation; the resulting data are plotted in Figure 6 for one response frequency peak. The directionality is approximately equal to one gage diameter at the conditions specified in Figure 6.

5. FLIGHT TEST RESULTS

The sensor has been successfully flown on several reentry vehicles which were launched on ICBM trajectories. The sensor was attached to the inside of the heatshield surface as shown on Figure 7. Perturbations to the flow field due to the presence of the sensor are avoided by the back face mounting.

The flight monitors were placed near heating rate transducers so that a correlation of experimental results could be obtained. As turbulent flow begins and pressure fluctuations occur, the heat flow into the ablator increases. For the flight tests of interest, this heat flow was monitored by General Electric Corporation ΔT gages as depicted on Figure 8. The ΔT gage produces a signal proportional to the temperature difference between the forward and rear thermocouple junctions. During a rapid change in the heat flow into the heatshield, the thermocouples produce a signal proportional to the time dependent heating rate. The output of the ΔT gage should correlate with the BLAM response at the high altitude at which transition begins. Typical comparisons between the two types of transducers are shown in Figure 9. The BLAM data have been linearized such that the plotted analog trace is linearly proportional to the noise amplitude on the heatshield surface. These overplots show excellent agreement between the two transducer types during the onset (1697.3 seconds) of transition between laminar to turbulent flow. In addition, the BLAM sensor output indicates other significant boundary layer qualities. During the transition period (Figure 9, 1697.3 to 1698 seconds), the BLAM output indicates a peak in the amplitude of the fluctuating frequency components. It is also noted that the ΔT gage exhibits a similar characteristic during approximately the same time. This effect has been identified by several wind tunnel investigators as an occurrence of transition[7-9]. In each, the researchers have identified similar increases in either (or both) the fluctuating pressure or the heating rate during the time of transition.

Another significant finding in the data of Figure 9 is the presence of pulses in the BLAM output prior to the onset of transition. Identified as high altitude turbulent bursts occurring between 1693.5 and 1697.3 seconds, it is believed these are the first published records of this phenomenon from flight vehicles. Acquisition of these records was made possible by the wide dynamic range provided by the logarithmic amplifier. An as-recorded data plot from the flight test is presented in Figure 10; these data illustrate the emphasis on low amplitude signals if this plot is compared with the linear data in Figure 9.

6. WIND TUNNEL TEST RESULTS

As a part of the gage development work on the BLAM sensor, a series of wind tunnel tests were performed at the Naval Surface Weapons Center Tunnel No. 8. The test model used on these tests is shown in Figures 11 and 12; both BLAM and ΔT sensors were mounted, side-by-side, at six locations on the model, 3 stations on each of two meridians, as shown in Figure 12.

Representative wind tunnel test results are shown on Figures 13 and 14, which include data from the ΔT sensor and the BLAM. The reason that the indication of boundary layer transition on this BLAM record is not as pronounced as on the flight test results is because the noise level in the wind tunnel was very high. Therefore, the BLAM was required to measure a change in acoustic level (due to transition) which was superimposed upon a very intense tunnel noise level. In both cases shown here, the BLAM and ΔT data yield transition times which are comparable; the small differences are not considered significant.

It is evident that the BLAM sensor as applied to wind tunnel testing requires some additional development. Further work is contemplated in an effort to improve the quality of the wind tunnel data obtained.

7. NEW DEVELOPMENTS

A new sensor, the Acoustic-Pressure Transducer (APT), has been designed and built. This sensor is designed to measure, simultaneously, wall static pressure vs. time and acoustic noise pressure vs. time on hypersonic reentry vehicles. Body forces are exerted by slowly-varying static pressures whereas the presence (and history) of transition can best be determined by acoustic noise measurements.

The APT accomplishes this measurement by using a plug which penetrates the vehicle's heatshield and thereby transmits the pressure forces to the sensor diaphragm. The separate acoustic monitor is contained in the center of the pressure plug. Development tests on the APT are in progress and include tests in a 5-megawatt arc heater facility producing Mach 3 flows and surface heating rates of 300-1000 BTU/ft^2-sec.

8. CONCLUSION

A sensor has been developed which detects the presence of turbulent flow by means of sensing components of fluctuating pressure. Since the sensor is mounted on the inside of a wall or shield over which the boundary layer flows, it does not perturb the flow. Laboratory tests have been conducted to establish the directionality of the system. The measurement technique has been successfully demonstrated on several re-entry vehicle flights in which onset of turbulence was measured during hypersonic flow. Flight data verification was established by comparing the sensor with thermal monitors and correlating the acoustic data with flight dynamics data. This data evaluation has verified the measurement of high altitude turbulent bursts which demonstrates that the BLAM gage has a greater sensitivity than previous technology.

Wind tunnel tests using the BLAM gage reveal that tunnel noise partially masks the determination of transition. More work is required for this application. Some new developments are being pursued using the BLAM principle.

9. REFERENCES

1. Willmarth, William W., "Wall Pressure Fluctuations in a Turbulent Boundary Layer," NACA Technical Note 4139, Washington, D. C., March 1958.

2. Kistler, A. L. and Chen, W. S., "The Fluctuating Pressure Field in a Supersonic Turbulent Boundary Layer," *Journal of Fluid Mechanics*, Vol. 16, Part 1, May 1963, pp. 41-66.

3. Serafini, John S., "Wall Pressure Fluctuations and Pressure-Velocity Correlations in a Turbulent Boundary Layer," NASA TR R-165, Washington, D. C., December 1963.

4. Speaker, W. V. and Ailman, C. M., "Spectra and Space-Time Correlations of the Fluctuating Pressures at a Wall Beneath a Supersonic Turbulent Boundary Layer Perturbed by Steps and Shock Waves," NASA CR-486, Washington, D. C., May 1966.

5. Harvey, W. D., Bushnell, Dennis M., and Beckwith, Ivan E., "Fluctuating Properties of Turbulent Boundary Layers for Mach Numbers Up to 9," NASA TN D-5496, Washington, D. C., October 1969.

6. Raman, K. R., "A Study of Surface Pressure Fluctuations in Hypersonic Turbulent Boundary Layers," NASA CR-2386, Washington, D. C., February 1974.

7. Owen, F. K., et al, "Comparison of Wind Tunnel Transition and Frustum Disturbance Measurements," *AIAA Journal*, Vol. 13, No. 3, March 1975, p. 266.

8. Demetriades, A., "Hydrodynamic Stability and Transition to Turbulence in the Hypersonic Boundary Layer Over a Sharp Cone," Aeronutronic Ford Publication U-6139, Interim Progress Report, October 1975-March 1975, 15 April 1975.

9. Martellucci, A. and Neff, R. W., "Influence of Asymmetric Transition on Reentry Vehicle Characteristics," *Journal of Spacecraft*, Volume 8, No. 1, May 1971, p. 476.

FIGURE 1 BLAM SENSOR

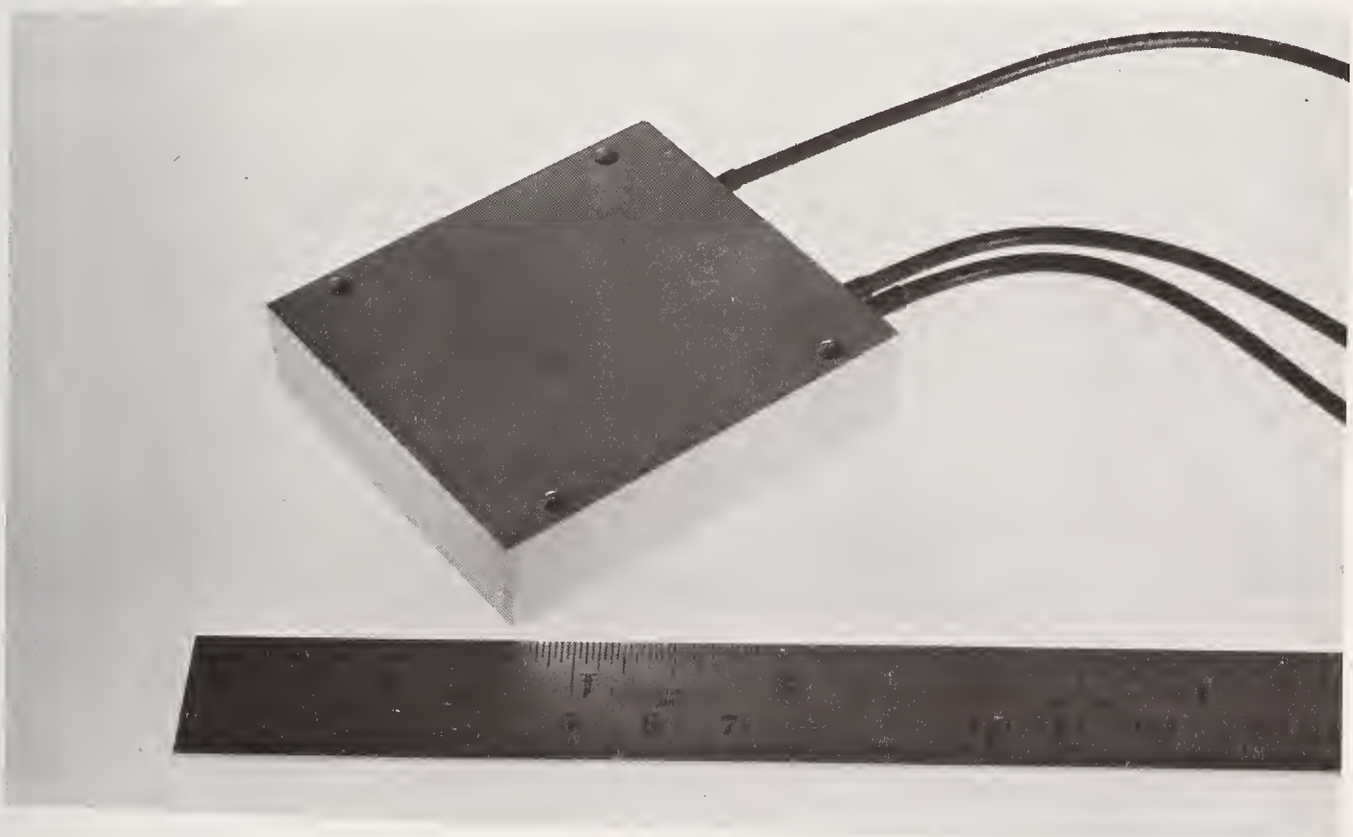

FIGURE 2 BLAM ELECTRONICS

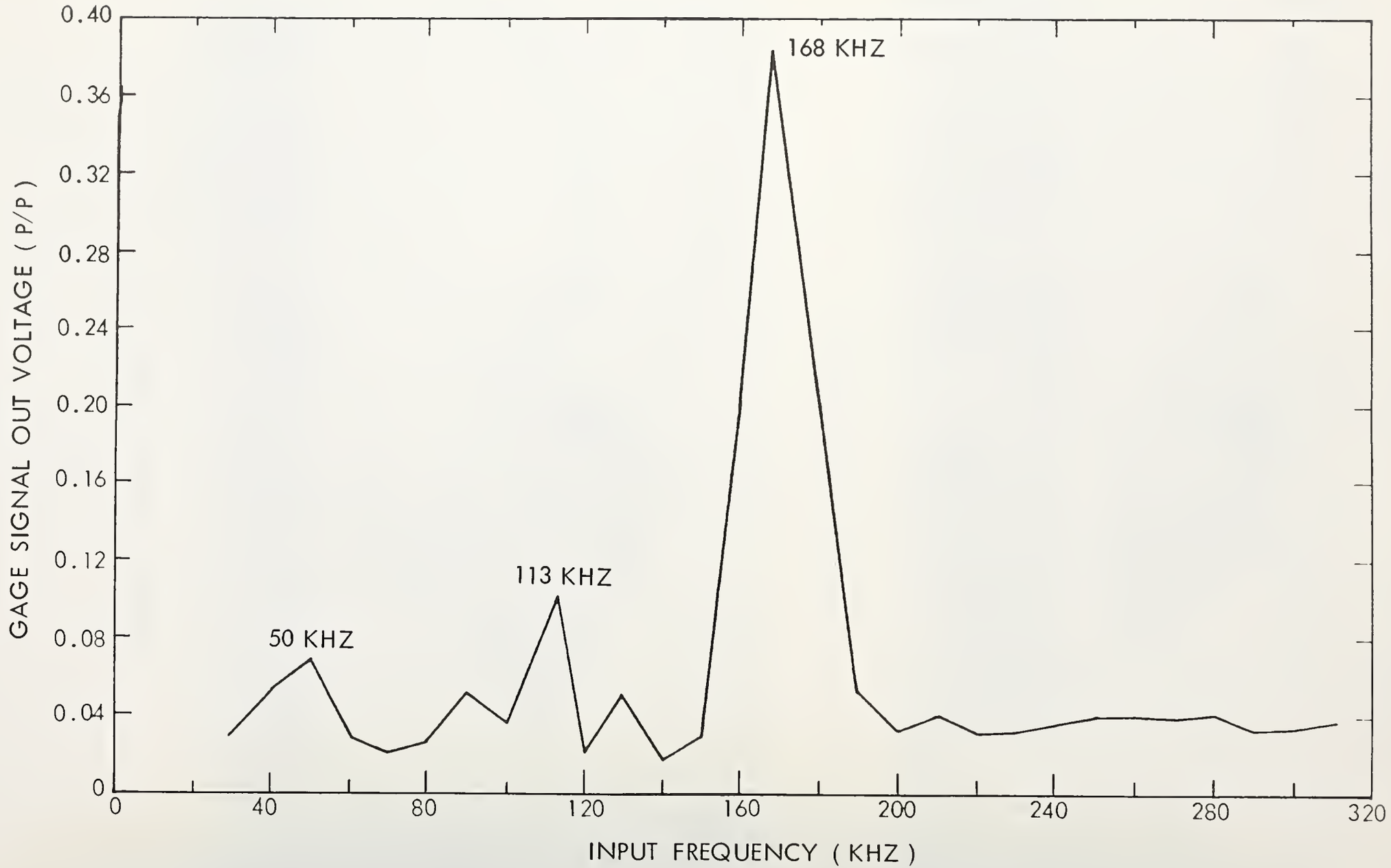

FIGURE 3 ACOUSTIC MONITOR RESPONSE

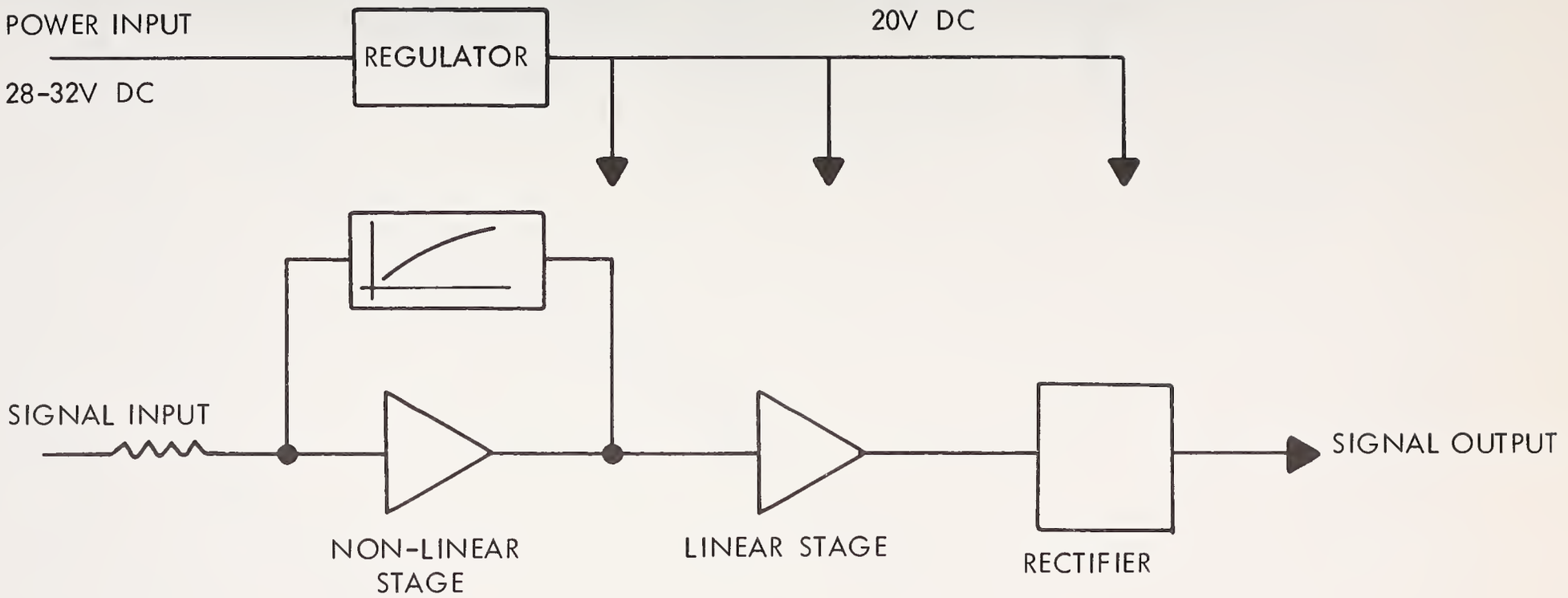

FIGURE 4

ELECTRONICS BLOCK DIAGRAM

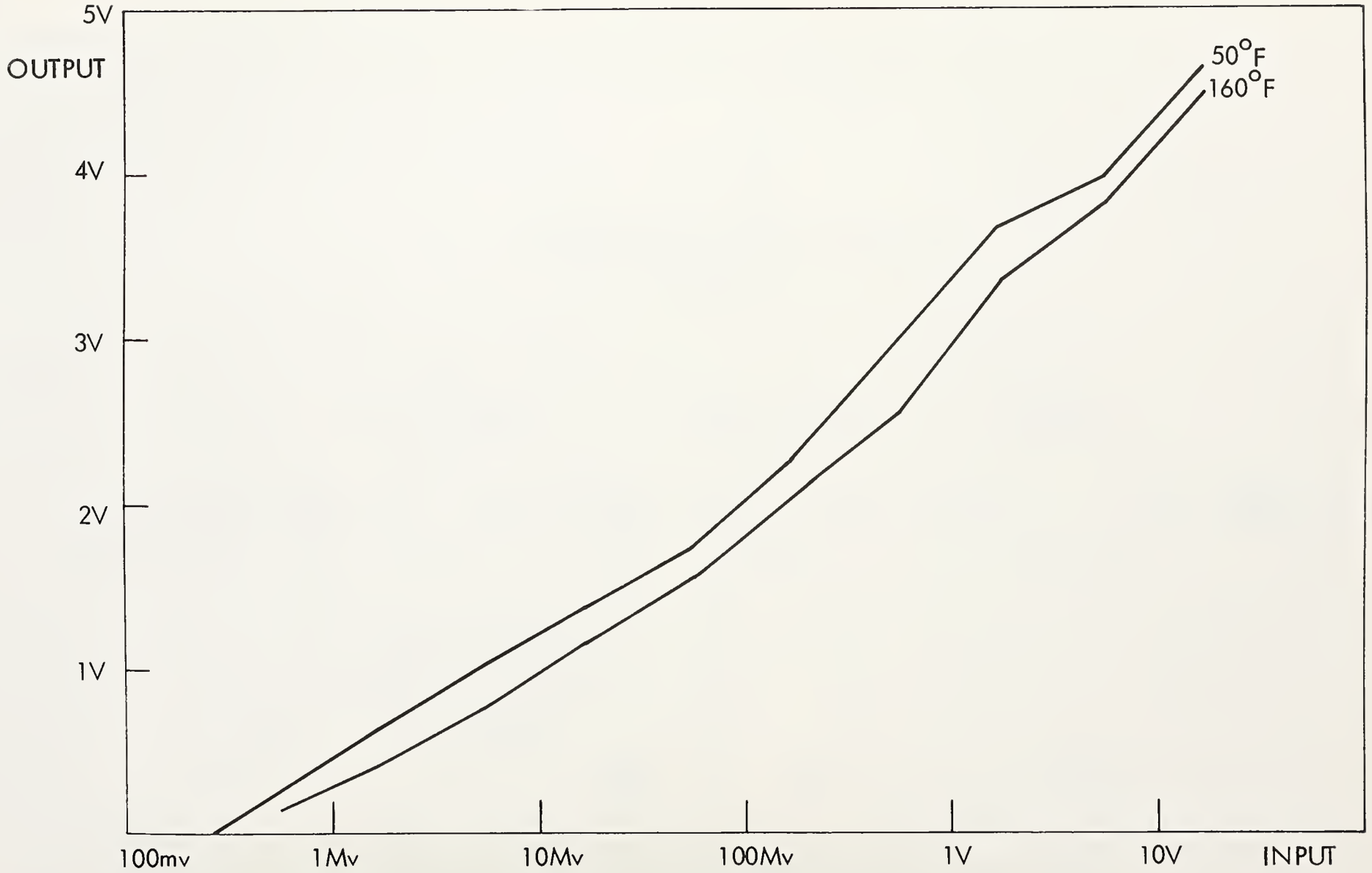

969

FIGURE 5 ACOUSTIC MONITOR AMPLIFIER CHARACTERISTICS

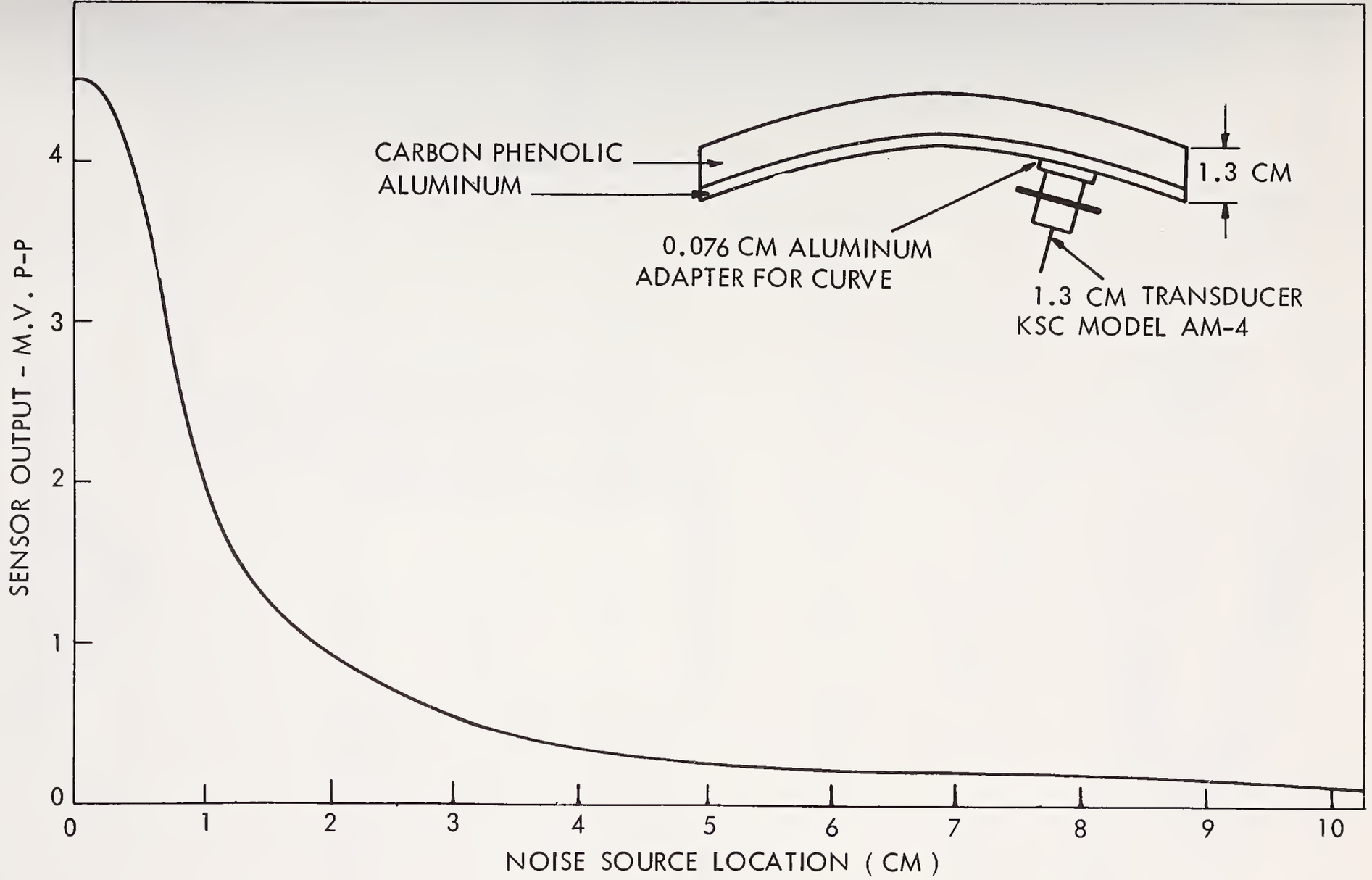

FIGURE 6 SPATIAL SELECTIVITY AT 280 KHZ

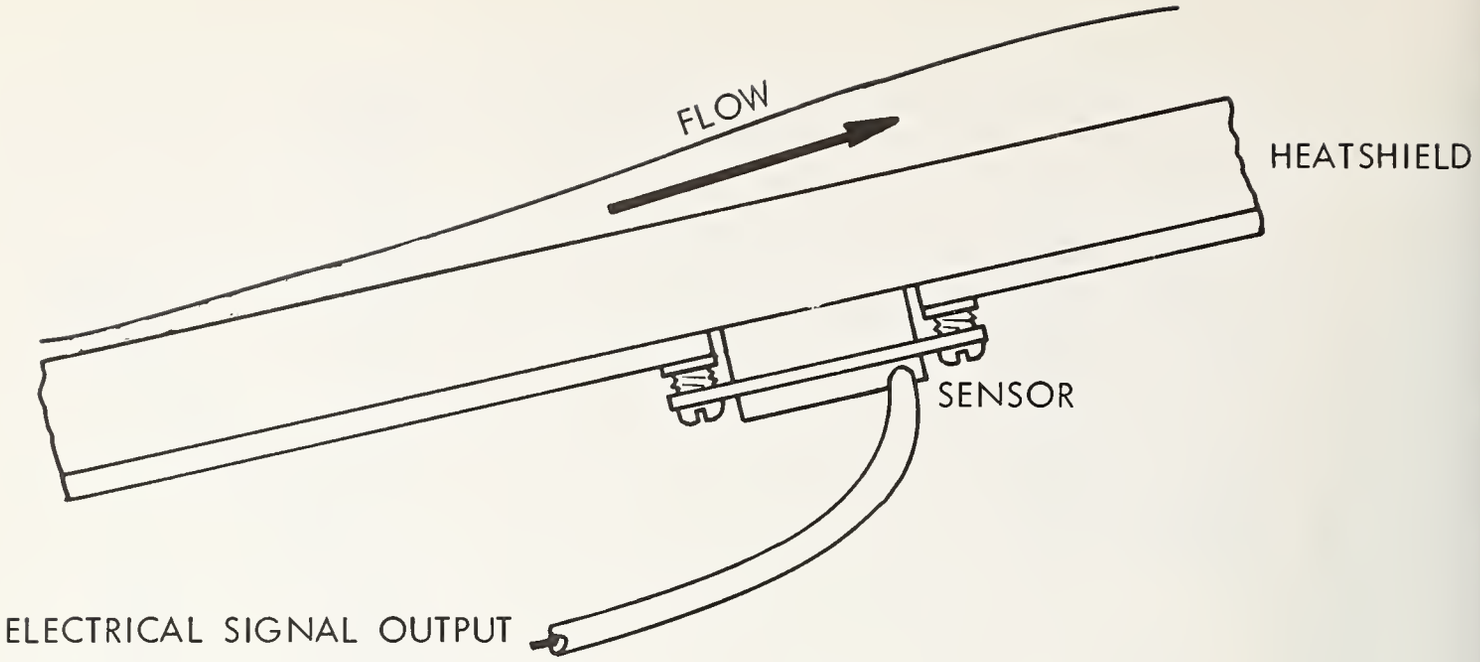

FIGURE 7 BLAM SENSOR INSTALLATION

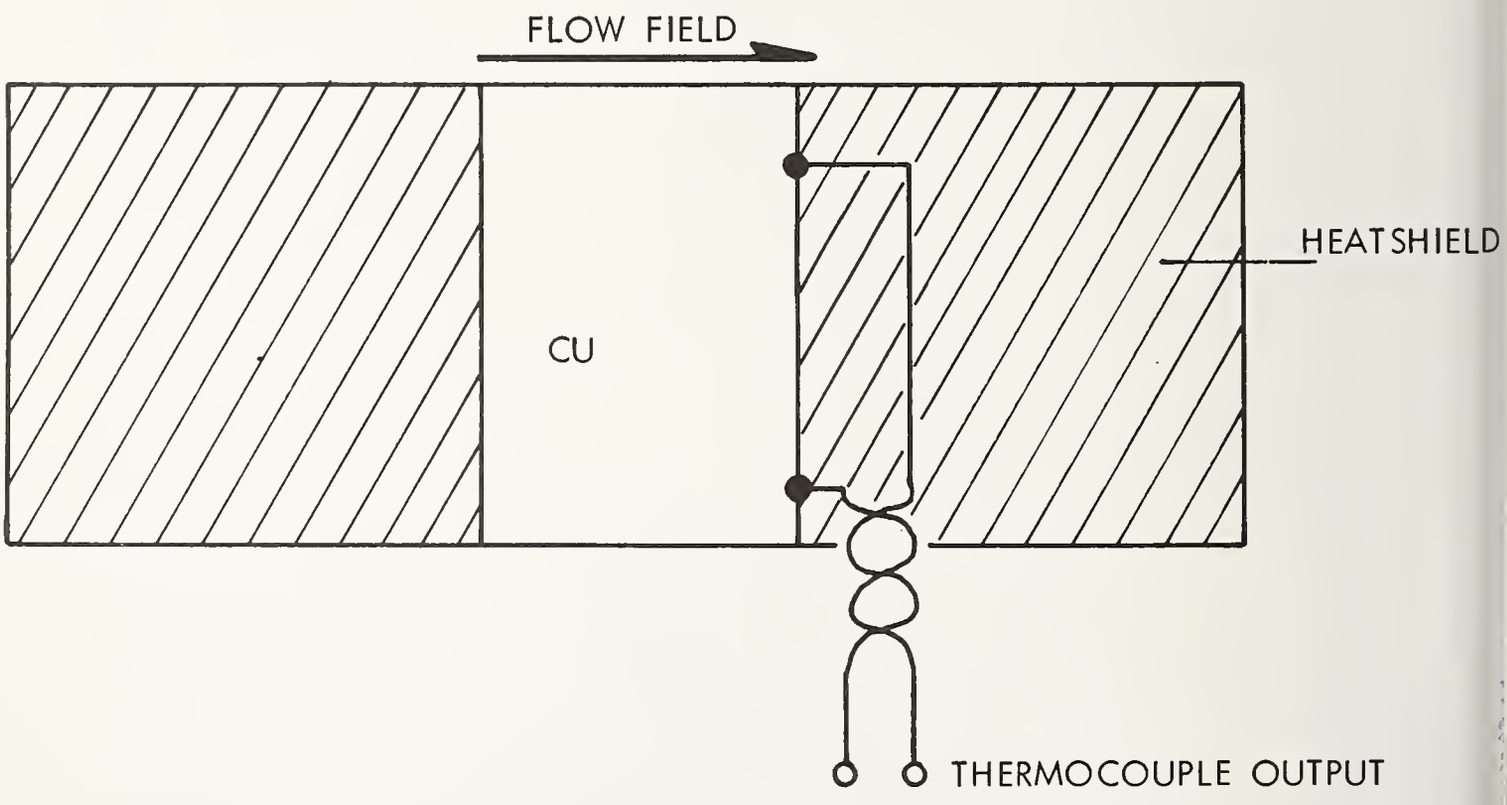

FIGURE 8

GE ΔT GAGE

(SCHEMATIC REPRESENTATION)

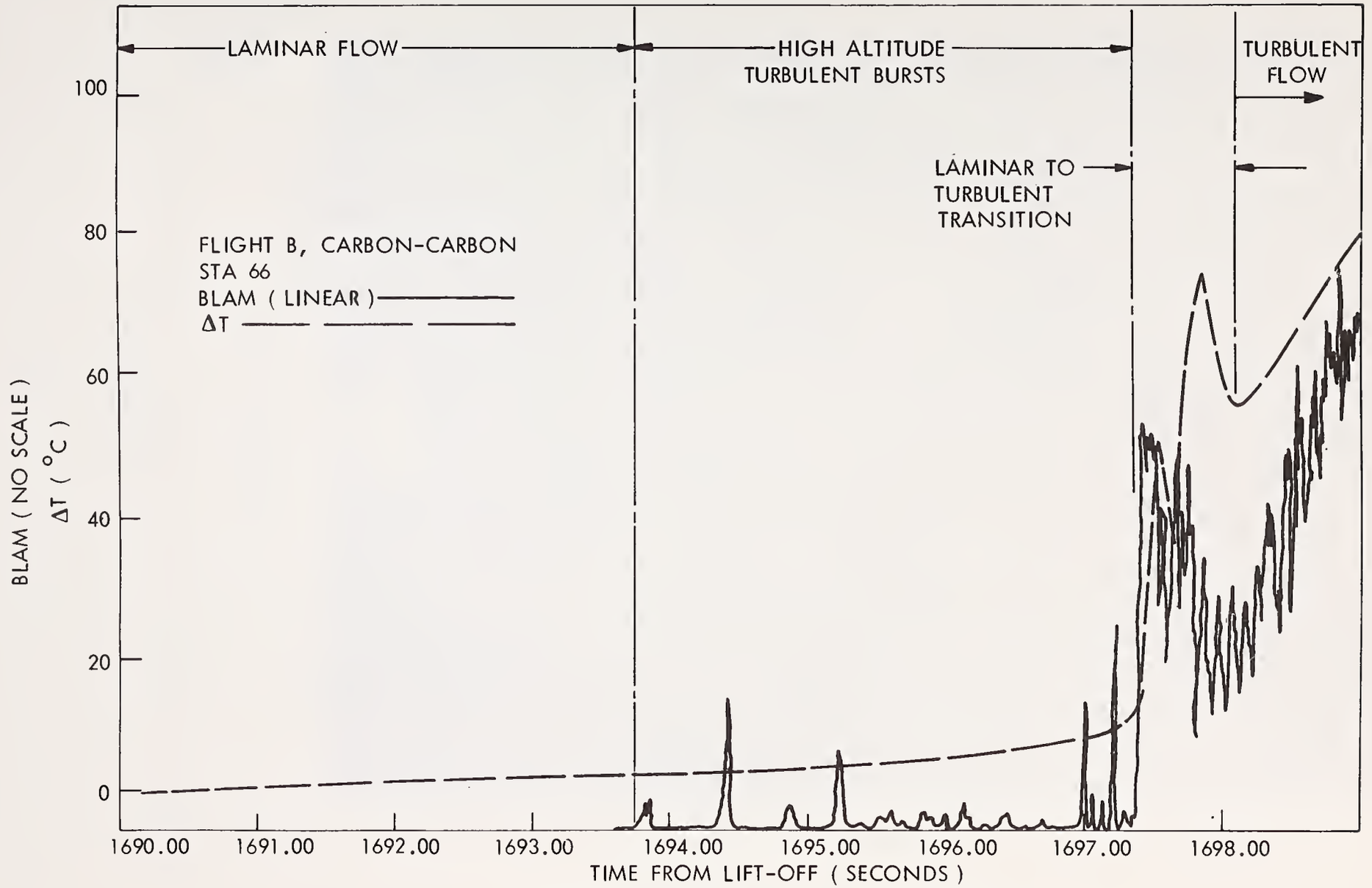

FIGURE 9 BLAM VERSUS ΔT COMPARISON

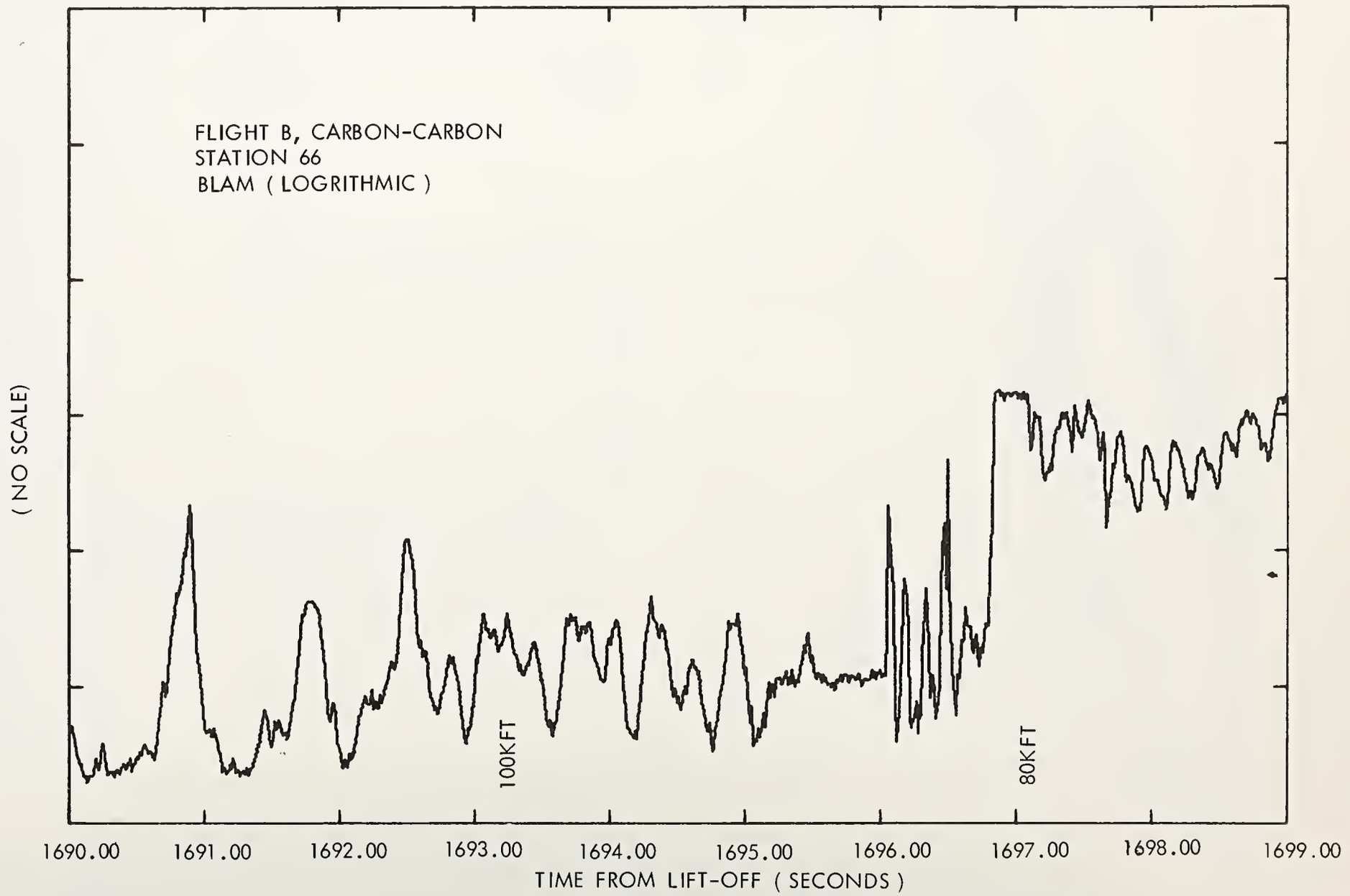

FIGURE 10 BLAM OUTPUT

FIGURE 11 WIND TUNNEL TEST MODEL,
Δt AND BLAM SENSORS

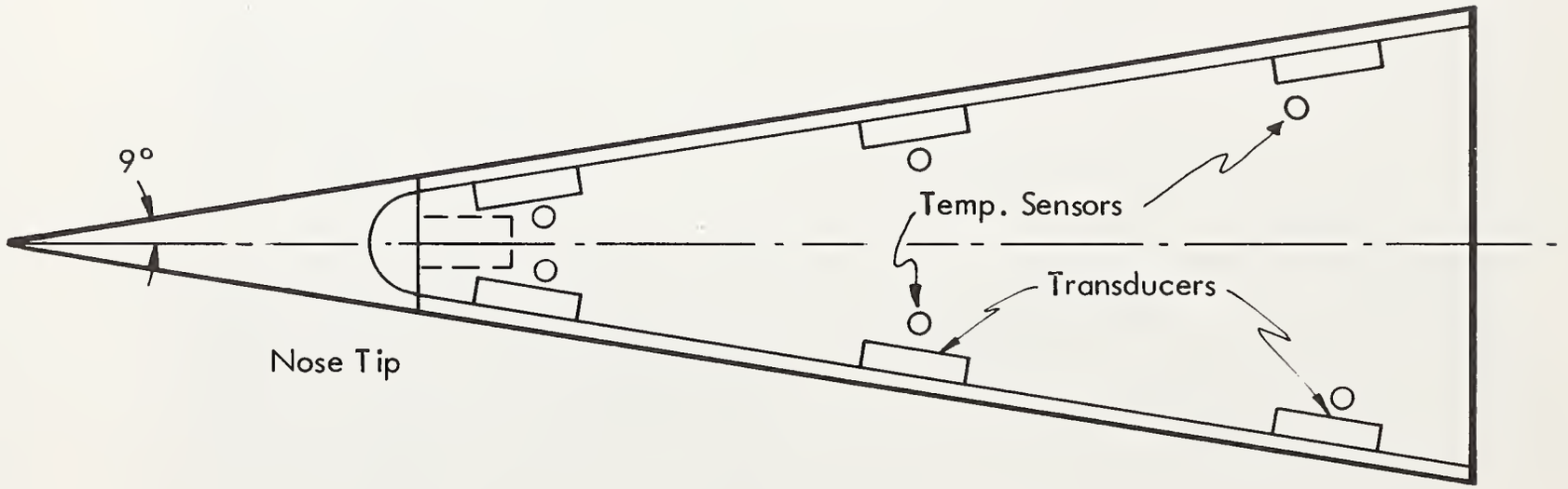

FIGURE 12 WIND TUNNEL TEST MODEL,
Δt AND BLAM SENSORS MOUNTED

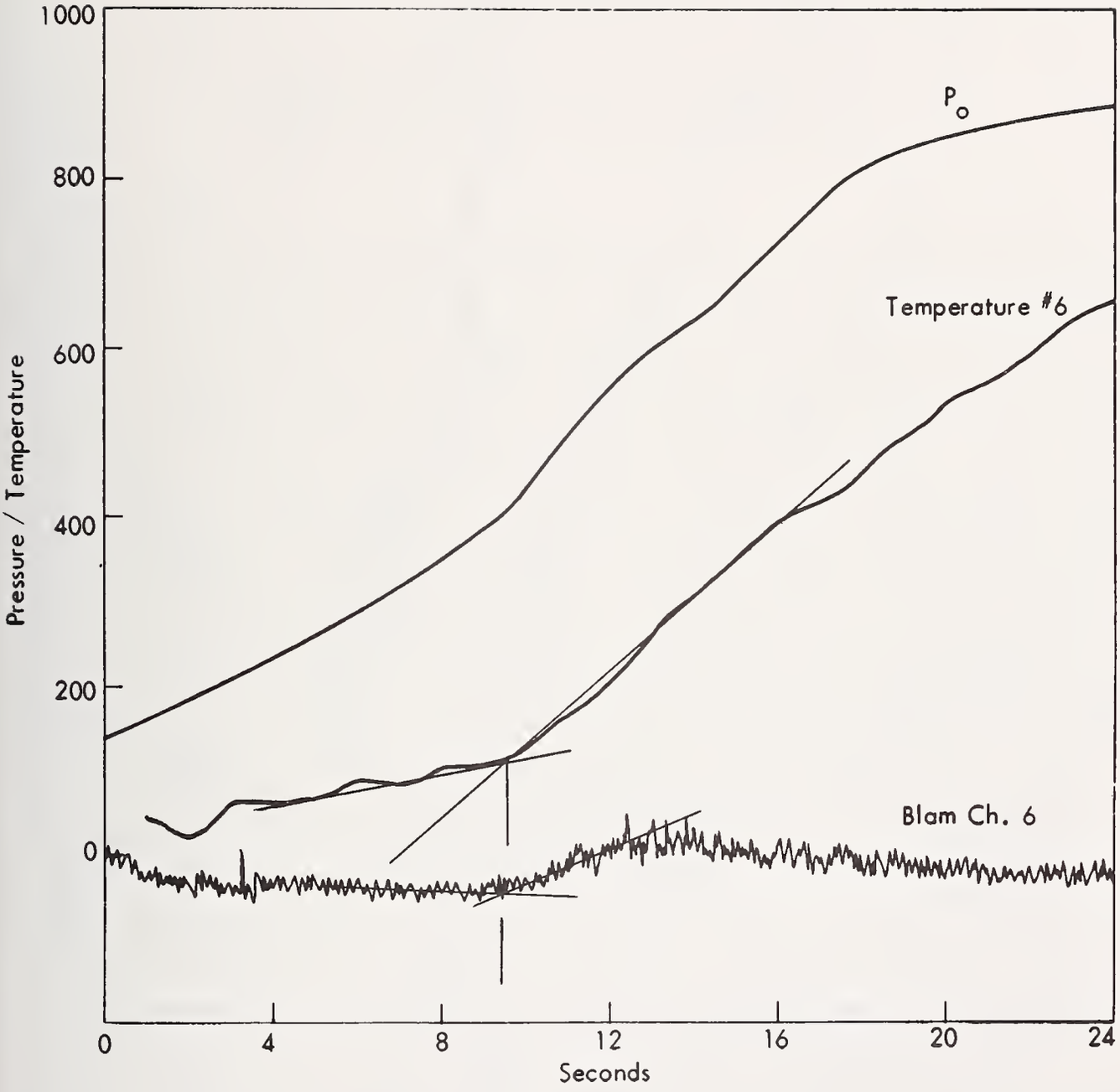

FIGURE 13 WIND TUNNEL MODEL TRANSITION RESULTS, Δt AND BLAM SENSORS, RUN NO. 2

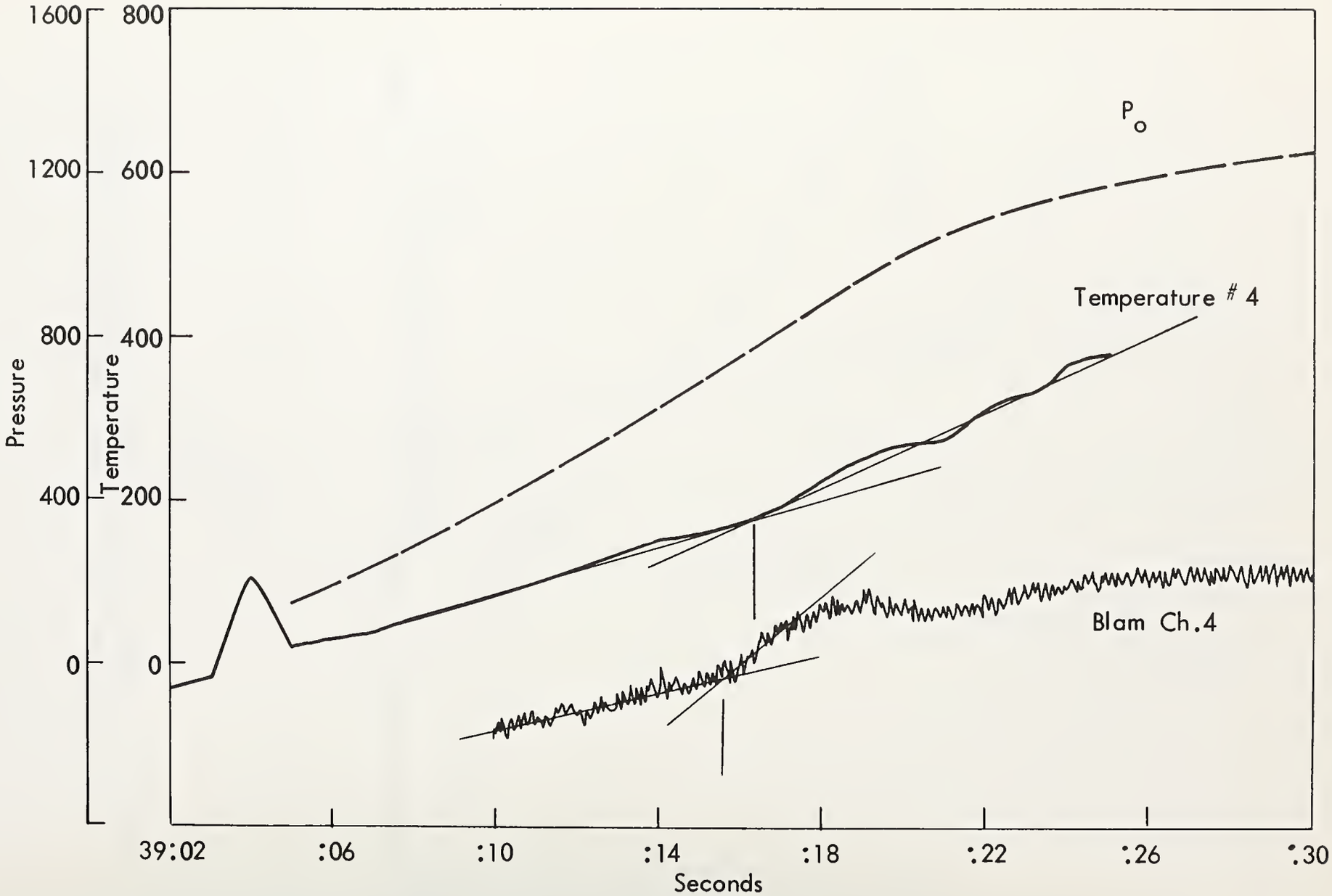

FIGURE 14 WIND TUNNEL MODEL TRANSITION RESULTS,
Δt AND BLAM SENSORS, RUN NO. 3

National Bureau of Standards Special Publication 484, Proceedings of the Symposium on Flow in Open Channels and Closed Conduits held at NBS, Gaithersburg, MD, February 23-25, 1977. (Issued October 1977)

MEASUREMENT OF RECIRCULATING FLOW BEHIND A CYLINDER WITH SPRAY COOLING

R. S. Rudland

Westinghouse Electric Corporation
Bettis Atomic Power Laboratory
West Mifflin, Pennsylvania 15122

A hot-film anemometer was used to measure the recirculating flow behind a heated cylinder which was cooled with spray water. The anemometer was electrically insulated from the water by a thin quartz film which was heated by the anemometer to help keep it dry. To measure air velocity in an air stream containing water droplets requires a sturdy anemometer which can withstand the droplet impact without breaking. The anemomust also be able to measure the air velocity in less than a millisecond in the presence of water droplets. The hot-film anemometer was selected because it is a sturdy, fast response instrument which detects changes in heat transfer related to changes in fluid velocity. Since the heat transfer to water and to air are quite different, it is necessary to keep the anemometer dry when measuring air velocity. When the anemometer was calibrated it was found that the anemometer could dry itself in about a millisecond. This meant that the anemometer could measure air velocities with as many as a thousand drops a second hitting the anemometer. Also, the calibration revealed that the calibration curve shifted upward in proportion to the amount of spray present due to the heat loss at the probe support.

Once the anemometer was calibrated it was used to measure air flow patterns behind a cylinder. These measurements helped evaluate the change in vortex patterns due to the spray. The test results indicated that the vortex shedding pattern was noticeably changed by the spray. The shedding frequency increased about 20% when the spray was present and the recirculating flow over the trailing surface was also increased. This improvement in flow over the trailing surface is expected to improve the heat transfer from the cylinder noticeably.

Key Words: Anemometer; Wake flow; Cylinder; Frequency; Vortex street; Spray; Two component flow; Hot film anemometer; Recirculating flow.

Introduction

In the study of compact heat exchangers, one promising approach has been found in the use of spray water-in-air to increase the heat transfer rate. Tests on single cylinders have shown that the heat transfer rate can be increased as much as thirty times that of air alone [1][1]. As a step towards extending the single tube results to the more general case with multiple rows of tubes, the trailing (wake) flow behind the cylinder was examined in detail since the interaction of the trailing flow behind the cylinder with succeeding rows of tubes is important in the overall heat transfer properties of the heat exchanger. A measuring technique was developed to measure the air velocity in the wake when spray water was present. The anemometer selected for these measurements was a sturdy, fast response, cylindrical, hot-film anemometer described by Thermo Systems Inc. [2]. The sturdyness of this anemometer was necessary to withstand impacts from the spray water and the fast response was needed to be able to detect the rapidly changing flow behind the cylinder.

Anemometer Description

The hot-film anemometer shown in Figure 1 was selected for measurement of spray water and air flow in the wake of a cylinder where large scale turbulence is present. This anemometer is constructed of a tough glass fiber supported between two probes and plated with a thin platinum film which has electrical properties similar to that of a platinum hot-wire anemometer. When the thin film of platinum is coated with a thin film of quartz the sensor becomes electrically isolated from the conducting fluid but is still sensitive to changes in fluid velocity. The basis for selection of this anemometer depends on the following test conditions:

1. Large scale turbulence was present in the flow at frequencies up to 7000 cycles per second.
2. Spray water droplets of about 200 microns in diameter were present in the water at velocities up to 25 meters per second (80 feet/sec.).
3. Air velocity measurements were needed to determine the heat transfer properties over the trailing surface of the cylinder.

The advantages of the hot-film anemometer over other types of anemometers can be summarized as follows:

1. The hot-film anemometer is small enough to respond rapidly to changes in velocity even with spray present.
2. The anemometer is sturdy enough to withstand impacts from large, high velocity, water droplets without damage to the sensor.
3. The anemometer can dry itself off in approximately one millisecond after becoming wet. This allows accurate velocity measurements of air for droplet

[1] Numbers in brackets refer to references in the bibliography.

impacts up to 1000 times per second.

This instrument measures the current required to hold the resistance constant on the sensor. This is proportional to the square root of the power going to the sensor [3]. This power is converted to heat in the sensor resistance and is transferred to the fluid. Heat transferred from the sensor to the fluid is proportional to the square root of velocity plus a zero velocity heat load. This can be written as:

$$Q = I^2 R_o \qquad \text{(Power to the sensor)}$$

$$Q = Q_o + C_o \sqrt{V} \qquad \text{(Heat loss} \propto \text{velocity)}$$

$$\therefore\ V = (I^2 - I_o^2)^2 / I_o^4 \times C_1 \qquad (1)$$

where; Q is the power to the sensor
Q_o is the power at zero flow
C_o is a constant determined experimentally
C_1 is a calibration constant
R_o is the sensor resistance at reference temperature
I_o is the current to the sensor at zero velocity
I^o is the sensor current at velocity V
V is the measured velocity

This derivation assumes that the temperature of the fluid does not change from the calibration to the time of measurement since C_o and Q_o depend on the difference in temperature between the sensor and the fluid. If there is a question about the temperature remaining constant, a compensating sensor can be added to the probe with a control circuit to hold the temperature difference at a constant value. The anemometer sensing element can also be used to measure the fluid temperature by turning off the power to the sensor and measuring the sensor resistance at zero power. The electronic circuit for the anemometer is shown in schematic form in Figure 2. It is seen that the sensor is part of a Whetstone bridge having an operational amplifier across the bridge to provide a feedback signal which adjusts the power to the sensor thereby balancing the bridge. By setting the gain on the bridge amplifier as high as possible without producing oscillations in the output, the frquency response of the system can be made to respond to frequencies as high as 20,000 cycles per second.

Calibration of the Anemometer

When using hot-film anemometers, each application requires provisions in the test for a calibration [4]. In this case the anemometer was calibrated in a wind tunnel by first measuring the air velocity with a NPL approved modified Prandtl pitot-static probe connected to a micromanometer and then measuring the same flow with the hot-film anemometer. Studies performed

on this wind tunnel (See Figure 3) have indicated that the spray water does not change the air velocity [1]. This allows the spray to be turned on at each setting of velocity to calibrate the anemometer for changing spray flow rate. The results of this calibration are shown in Figure 4 where a typical oscilliscope display is shown to illustrate how the air velocity was measured when spray was present. The air velocity corresponds to the lowest level of the voltage-level (which corresponds to the sensor current) on the oscilliscope display since this indicates that the sensor has dried off after being hit by a water droplet. This sensor is connected to a high power circuit which can produce large surges in current in response to sudden changes in sensor temperature which shortens the drying time of the sensor. It takes about one millisecond for the sensor to dry itself off after an impact which means that the sensor can make useful measurements up to one thousand impacts per second. It is also seen in Figure 4 that the curve shifts upward as the spray flow rate increases. This is due to the heat loss from the supports which are cooled by the water but are not able to dry off as fast as the sensor element. This heat loss can be accounted for as an extra heat load which is dependent on water flow rate rather than velocity. Taking this into account in Equation 1 produces the following equation for velocity:

$$V = C_2 \left[\frac{(I - I_w)^2 - I_o^2}{I_o^2} \right]^2 \qquad (2)$$

where; I_w is the increment of current needed to offset the heat loss to the supports as a function of water flow rate
C_2 is a calibration constant

From Figure 4 it is seen that current I_w is directly proportional to the mass flow rate of the spray. This is replotted in Figure 5 to show the linear behavior of the calibration curve. In this figure the heat loss due to water is:

$$I_w = C_3 \times \dot{m}_w$$

where; C_3 is the calibration constant
$\dot{m}_w$ is the mass flow rate of water per unit cross sectional area

Test Description

The measurement of flow past a cylinder with spray water was performed in a closed loop wind tunnel shown in Figure 3. The test section was made of plexiglass with a .305 meter by .305 meter flow area (12 in. sq.). The test cylinder was 7.62 cm. in diadeter (3 in.) and could be heated with electric heaters. Spray water was introduced through a Delavan SQ-10

square spray nozzle. The mean droplet size varied with the water flow rate from about 100 microns at low flows to about 300 microns at high flows. High speed photographs have shown that the droplets move at the air velocity by the time they reach the cylinder. Similar studies have shown that the air velocity is not altered by the introduction of the spray into the air [1]. Visual observations of the cylinder with an air-water spray flowing past it have revealed that the flow seperated from the cylinder over a range from 92^{o} to 108^{o} measured from the forward stagnation point. According to Schlichting [5] a seperation point near 70^{o} is associated with laminar flow while a seperation point near 100^{o} is associated with turbulent flow. Laminar seperation has lower pressures over the trailing surface while turbulent seperation has higher pressures. Hodgson [1] measured the pressure around the cylinder and found that the flow was laminar up to 16 meter per second (50 ft/sec) and turbulent above that with air flow. Measurements of specific pressure gave values near -2.0 for laminar flow and -1.3 for turbulent flow where specific pressure is defined as:

$$C_p = (P - P_o)/(\tfrac{1}{2}\rho_a V_o^2) \qquad (3)$$

where; P is the pressure over the trailing surface
P_o is the static pressure upstream of the cylinder
ρ_a is the density of air
V_o is the velocity of air upstream of the cylinder

Rudland [6] measured the pressure in the wake close to the cylinder and found that the specific pressure varied from -1.8 to -3.0 for air but stayed constant when water spray was present. This suggests that the spray produces turbulent flow which moves the seperation point back to 100^{o} and raises the back pressure in the wake. The hot-film anemometer measured sinusoidal flow patterns in the wake region which corresponded to the von-Karmen vortex streets which shed periodically from the back of the cylinder. If we define Strouhal number as:

$$St = V/(f \times d) \qquad (4)$$

where; f is the shedding frequency
d is the cylinder diameter

then a value of .21 was determined for air flow which was lowered to .18 when spray was added. This reduction in Strouhal number corresponds to an increase in shedding frequency of nearly 20%. This increase in frequency is caused by the change from laminar to turbulent flow which pushes the vortices closer together thereby increasing the rate of shedding. Marris [7] described a similar effect which showed how the frequency goes up when the vortices are forced closer together behind a cylinder.

Results

Using the hot-film anemometer, the air velocity as well as the temperature and number of droplets hitting the probe was measured at various elevation behind the cylinder. These measurements were made in conjunction with measurements of the mass flow rate of spray. Turbulence measurements of the air were included in these measurements as well as vortex shedding frequencies. The turbulence measurements and vortex shedding measurements were used to help understand the nature of the flow in conjunction with the pressure measurements. Having established that the spray caused the flow to become turbulent, it is anticipated that the wake flow will be more active which will cause the heat transfer over the trailing surface to increase. Mixing of the spray with the air behind the cylinder is expected to be more intense for turbulent flow than for laminar flow. Comparisons of laminar air flow and turbulent spray flow at the same velocity are plotted in Figure 6 to illustrate that turbulent mixing is more active than laminar mixing. It can be seen that the velocity profile for turbulent flow becomes uniform in only a few diameters downstream while the laminar flow takes longer. Figure 7 attempts to show how the spray is mixed in the wake by the large scale vortex motion and small scale turbulence. Within five diameters downstream the spray is very well mixed. This is faster than would be expected to occur in a turbulent flow without the vortex shedding.

Conclusions

Use of the hot-film anemometer to measure air flow in an air-water mixed flow has demonstrated that this anemometer is a sturdy instrument which is capable of being used for a wide variety of flow measurement applications. A calibration of this instrument in the spray flow revealed that the sensor was suitable for mixed flow applications with only minor adjustments to the governing equations. This instrument was able to measure the flow pattern behind a cylinder with water present thereby demonstrating that the wake flow provided good mixing of the spray due to the turbulent seperation caused by the water on the cylinder. Future efforts to study tube bundles should concentrate on the mixing pattern of the air and water behind the cylinders in the tube bundle.

Bibliography

1. Hodgson,J.W.,R.T.Saterbak,and J.E.Sunderland,"An Experimental Investigation of Heat Transfer from a Spray Cooled Isothermal Cylinder",AIChE-ASME Heat Transfer Conference,Philadelphia,Pa., August 11-14,1968.

2.Thermo Systems Inc.,"Hot Film and Hot Wire Anemometry-Theory and Application" Bulletin TB5.

3.Flow Corporation,"Series 900 Application Notes", Bulletin 901.

4.Disa Information,"Measurement and Analysis",No. 10,October 1970.

5.Schlichting,h.,Boundary Layer Theory , McGraw Hill,6th Ed, 1968.

6.Rudland,R.S.,"Convective Heat and Mass Transfer from a Horizontol Cylinder to an Air-Water Spray in Cross Flow", PhD Thesis,Georgia Institute of Technology,Atlanta,Ga. September,1968.

7.Marris,A.W.,"A Review on Vortex Streets, Periodic Wakes, and Induced Vibration Phenomena",Transactions of the ASME,Journal of Basic Engineering,June,1964.

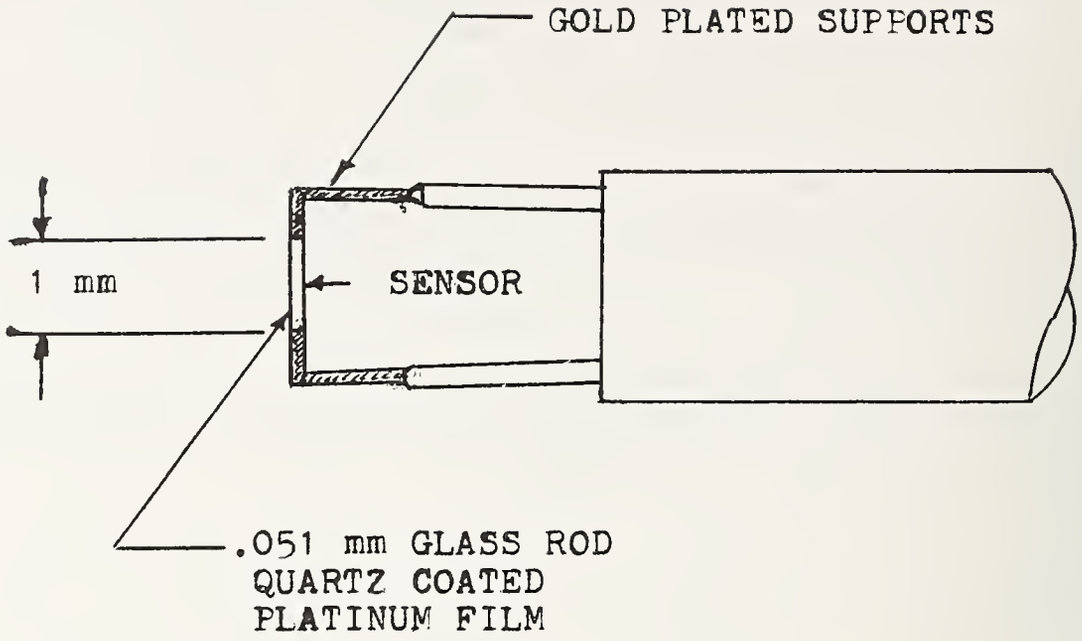

Figure 1 Schematic of Hot-Film Anemometer

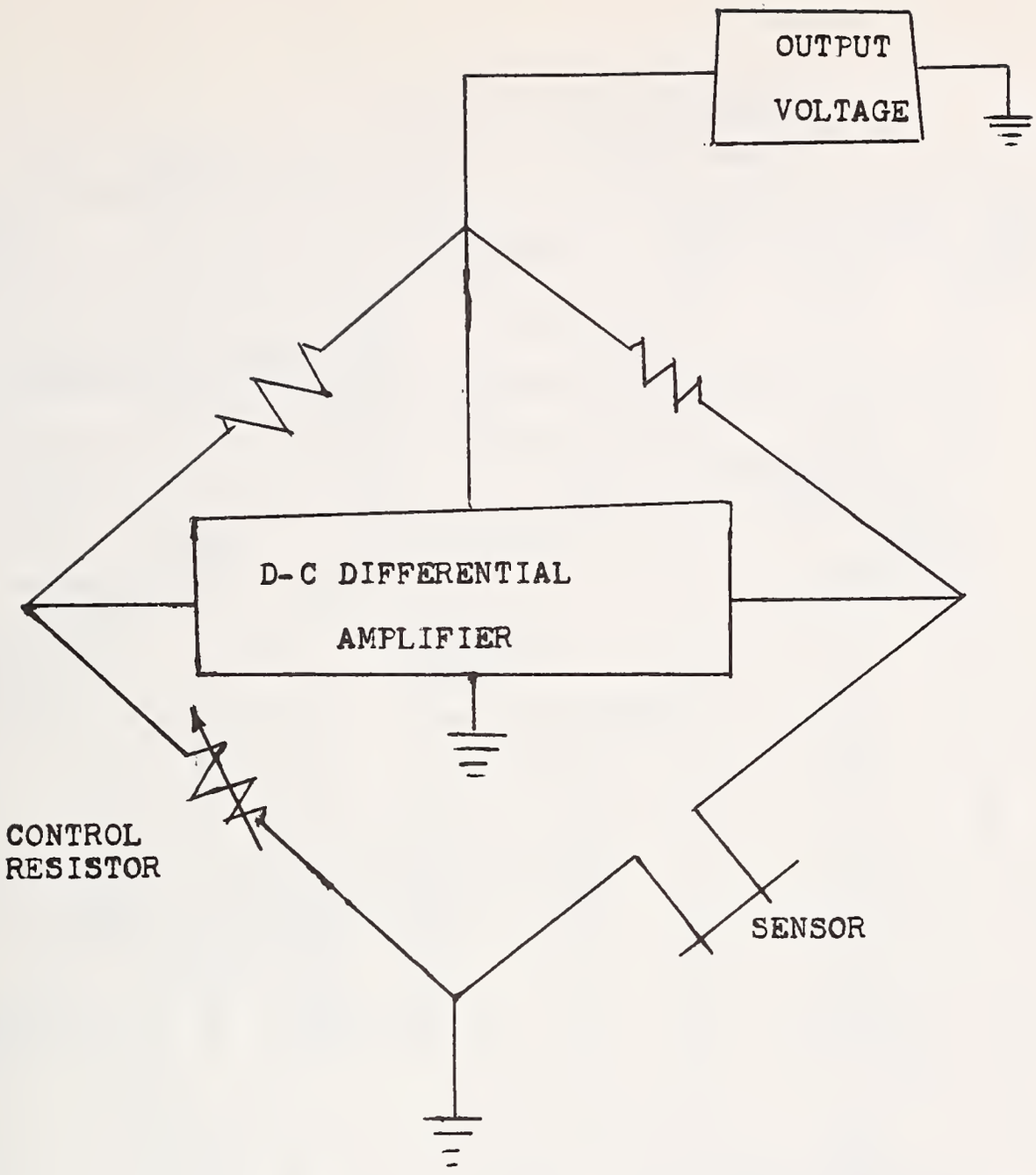

Figure 2 Electronic Arrangement for Anemometer Operation

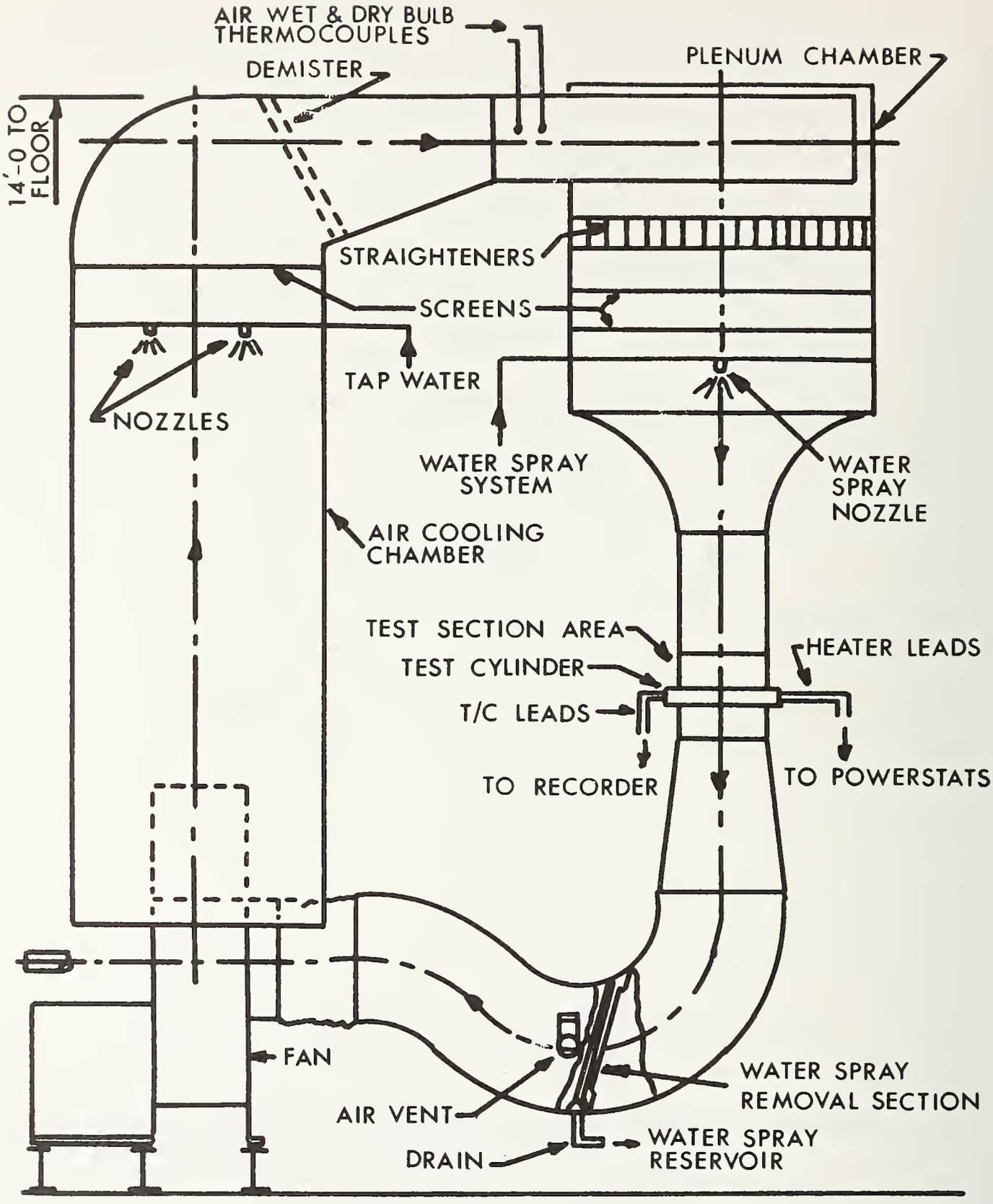

Figure 3 Wind Tunnel Test Facility

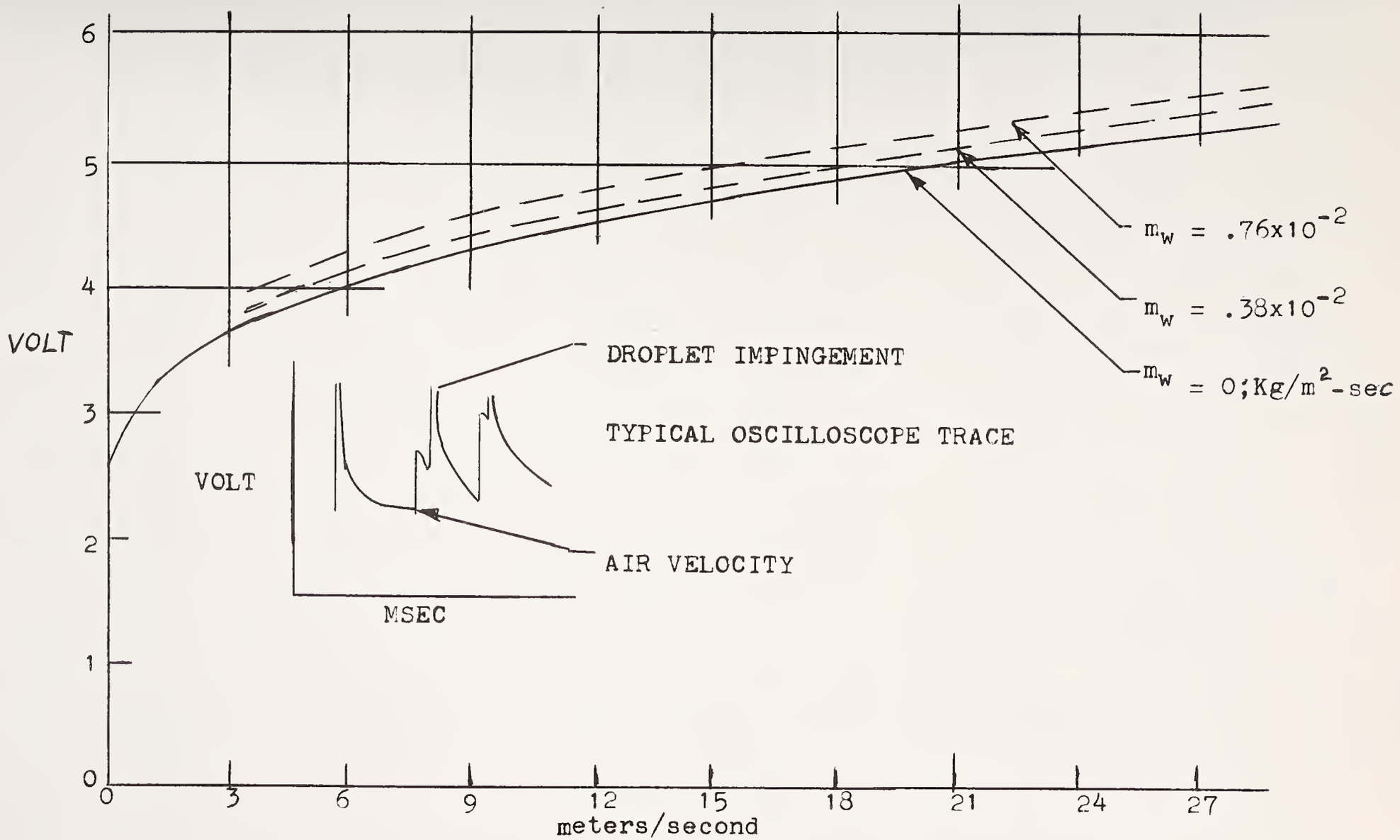

Figure 4 Anemometer Calibration and Oscilloscope Display

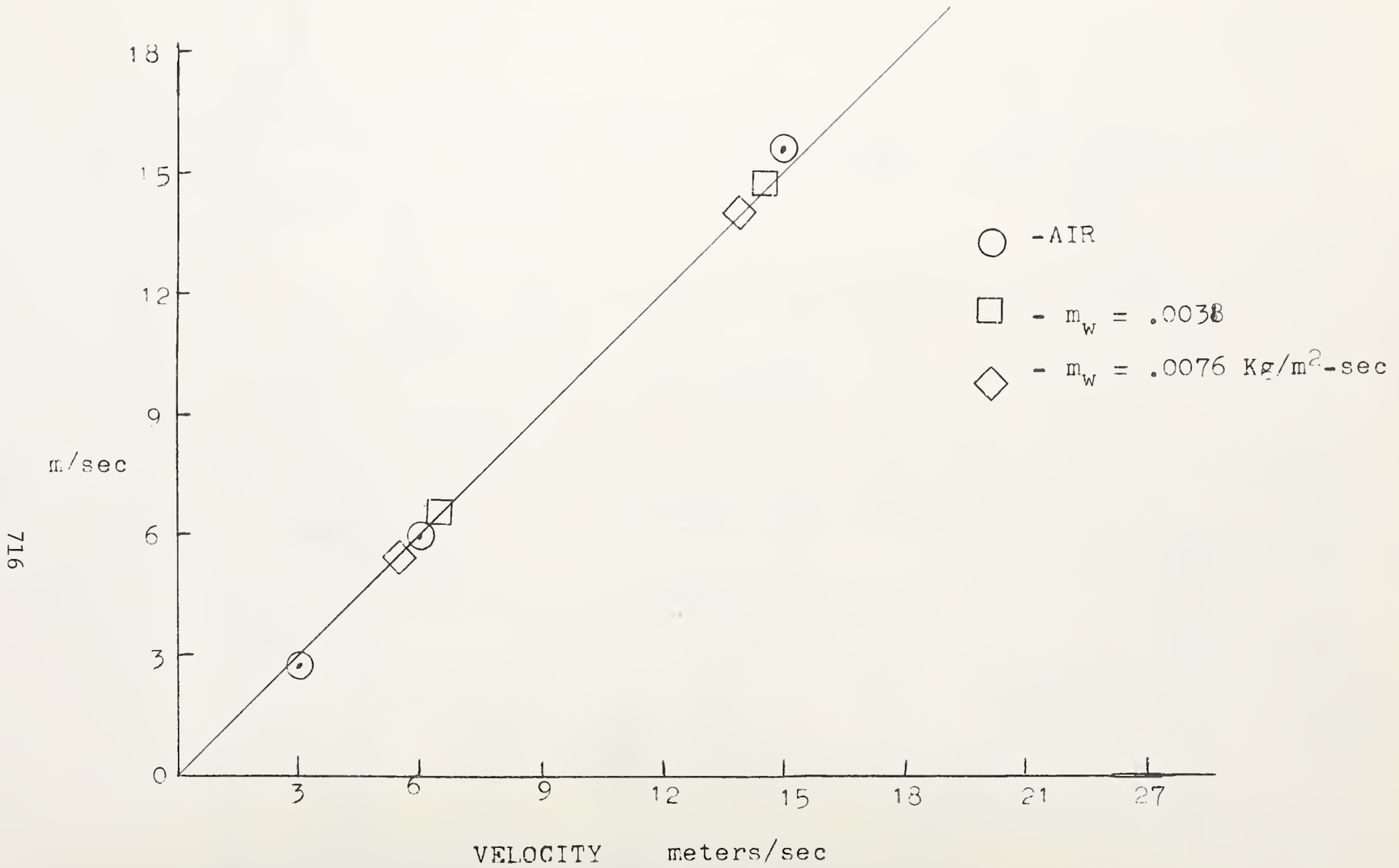

716

Figure 5 Anemometer Calibration Accounting for Spray Flow

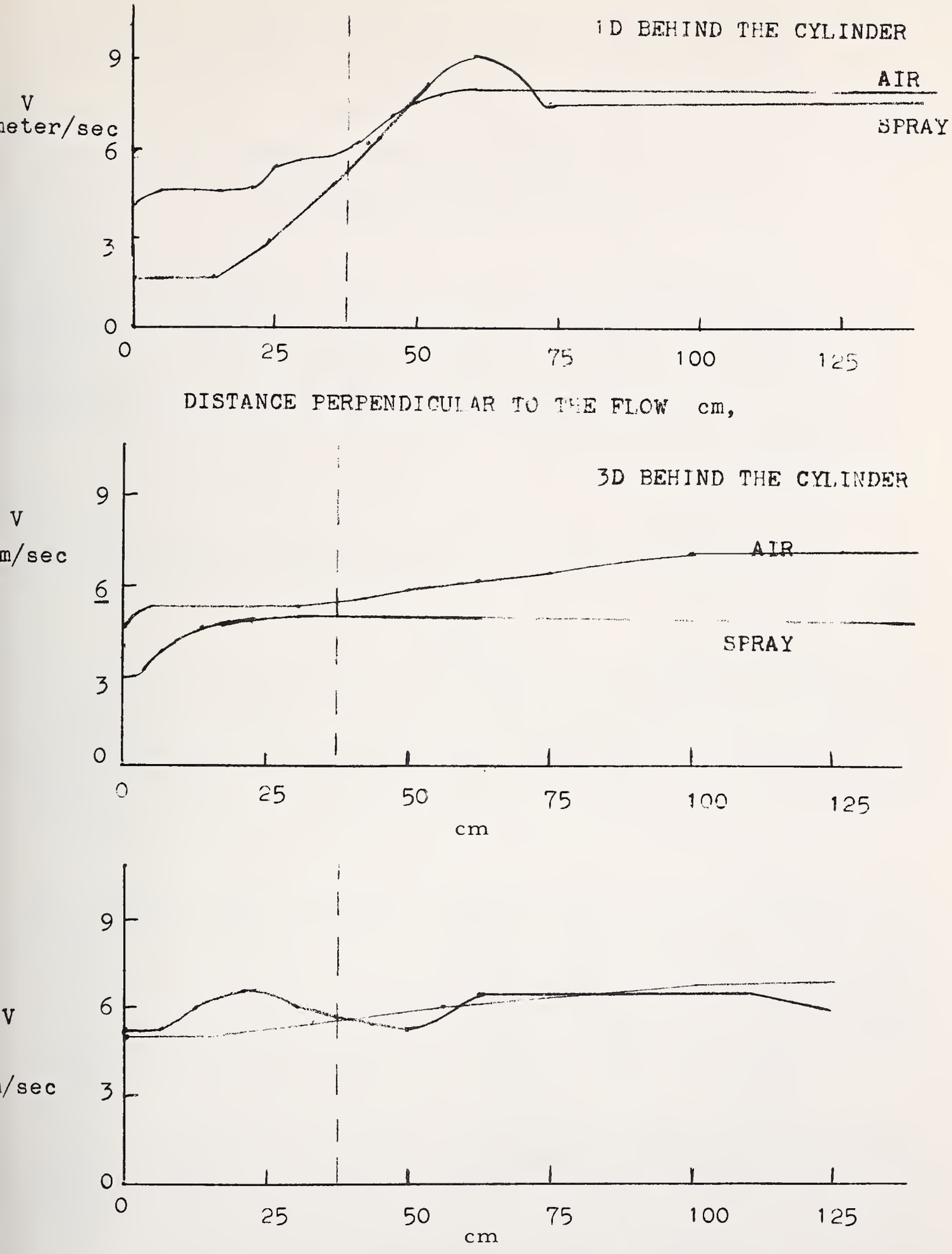

Figure 6 Velocity Profile in Wake Behind the Cylinder

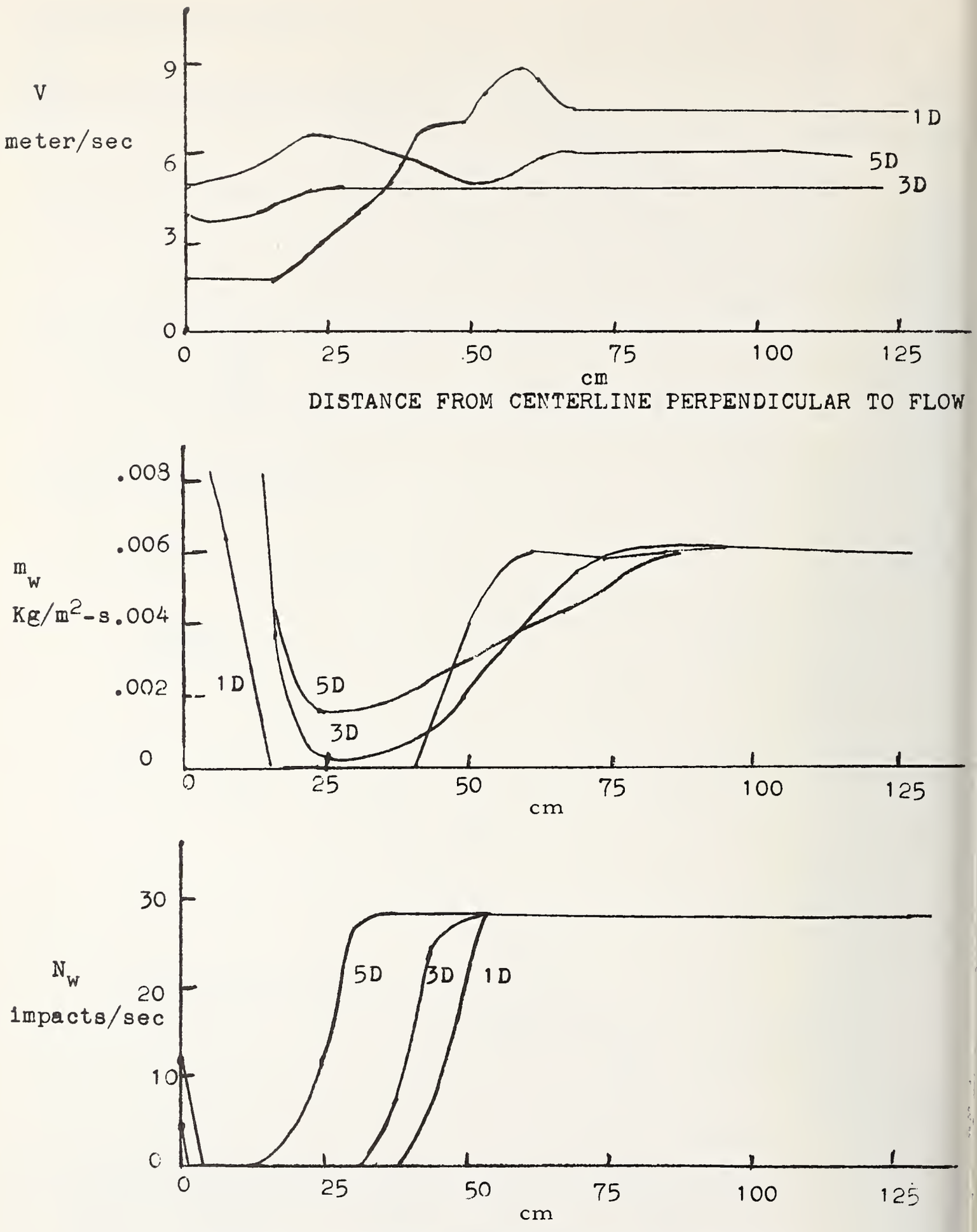

Figure 7 Measurement Behind the Cylinder

National Bureau of Standards Special Publication 484, Proceedings of the Symposium on Flow in Open Channels and Closed Conduits held at NBS, Gaithersburg, MD, February 23-25, 1977. (Issued October 1977)

A NEW TYPE OF VELOCITY PROBE

William B. Brower, Jr. and Alan Servoz

Rensselaer Polytechnic Institute
Troy, N.Y. 12181

A trip-wire velocity probe has been designed and tested which employs a sphere as the mechanism for producing a pressure difference. To render this pressure difference independent of Reynolds number a trip-wire is placed on the upstream side of the sphere, which trips the boundary layer to turbulent flow. The resulting design has greater sensitivity than the Pitot-static tube, and can fit through smaller openings than a comparable Pitot-static tube. The dimensions of a typical probe are given, as are the results of a series of wind-tunnel tests at "low" Reynolds numbers.

Key Words: Calibration; Pitot-static tube; transition; trip-wire probe; turbulent boundary layer; sphere flow; Reynolds number.

1. Introduction

Along with the need for monitoring stack-gas flows for purposes of pollution control, the need for accurate knowledge of stack-gas velocity distribution has increased. The conventional instrument for making gas-flow velocity measurements is the Pitot-static tube in conjunction with a manometer to pick up the difference between the probe stagnation and static pressures which, according to Bernoulli's equation, is equal to the dynamic pressure, i.e. $p^o-p = \frac{1}{2}\rho U^2 \equiv q$. The velocity, of course, is proportional to $h^{\frac{1}{2}}$, where $\underline{h}$ is the manometer reading.

For the stated purpose, a Pitot-static probe has a few difficulties. In the first place access ports to stacks are the order of 4 inches in diameter. The length of the port duct may be the order of 8-12 inches. Thus if the outside diameter of a Pitot-static tube were D=0.5 in., the length of the tube from tip to stem would be the order of 7-9 inches, making it impossible to insert the probe straight into the hole, or even to insert it by cocking it. On a large-diameter stack where the length of the probe support-arm might be up to 20 feet, a probe which cannot fit straight into the port would be an especial inconvenience.

In addition, in a "dirty" flow, particles suspended in the stack gas have a tendency to impinge upon and perhaps enter either the stagnation-pressure tap or the static-pressure tap, or both. Since in a typical probe these holes may be the order of 0.1D there is a real danger that the capture of a few large particles may result in the clogging of one or more taps, thereby producing erroneous readings. A probe which utilizes large-diameter pressure taps would be relatively insensitive to accumulations of particles. Moreover, it could be routinely cleaned.

A final problem with the Pitot-static tube is that at low free-stream speeds its sensitivity (i.e. the pressure difference Δp) is low, resulting in small manometer deflections. For example, at standard atmospheric pressure and a stack temperature of 300°F, a flow velocity of U=20 ft/sec will produce a manometer deflection of h=0.062 in. H_2O. Field measurements of such low pressures are more prone to error than in a laboratory. Thus it would be useful to have available a probe which generates a larger pressure drop for a given flow speed than is furnished by a Pitot-static tube.

One ordinarily expects that in a stack the turbulence level of the main flow would be high, due to its previous history involving combustion, heat transfer, etc. Since knowledge of the actual turbulence level is not usually available, it is desirable to utilize a probe which produces readings which are independent of the actual turbulence level - that is, its reading at a given flow speed should be the same whether the flow is laminar or turbulent. A Pitot-static tube possesses this quality and, ideally, so should any substitute.

The object of the current investigation is to design and test a new type of probe which meets the following specifications:

1) It should be constructed so that it can be inserted through a 4-inch diameter hole and be readily aligned with the flow direction.

2) It should be insensitive to capture of particles and should have relatively large-diameter pressure taps to allow for easy cleaning.

3) It should produce a pressure reading which is independent of the state of free-stream turbulence.

4) It should produce a pressure drop significantly greater than that provided by a Pitot-static tube for a given flow speed.

5) It should have accuracies of the same order as the Pitot-static tube, where a possible error of 0.5% is typical.

It is further noted that a probe may have other requirements such as the ability to allow tapping off a gas sample, or to verify flow direction, or to withstand high temperatures. Although the current study is not directed at these objectives, we believe the resulting design can be modified to accommodate them.

2. Preliminary Design Considerations

In order to achieve a pressure-difference Δp, larger than realized with a Pitot-static tube, one is quickly led to the use of a sphere, for the following reasons:

1) As is well-known, the theoretical, potential-flow, surface-velocity distribution on a sphere is given by $u_s = (3/2)U\sin\phi$. Thus the maximum pressure drop below stagnation occurs at $\phi = 90°$:

$$\Delta p\Big|_{\phi=90°} = \tfrac{1}{2}\rho u_s^2\Big|_{\phi=90°} = \frac{9}{4}q.$$

If a practical device could be designed to achieve this pressure drop, its sensitivity would be 2.25 times that of the Pitot-static tube.

2) Since the flow around a sphere is essentially axi-symmetric the effect of probe misalignment can be minimized by "averaging" the static-pressure values from several taps at the equatorial station.

3) Furthermore, effects of free-stream turbulence are diminished since, as the flow accelerates over the front surface, the local turbulence intensity actually decreases, and reaches a minimum near $\phi = 90^{o}$.

4) Finally, since the sphere is supported by a sting from the rear, interference effects can be kept small if the sting diameter is significantly less than that of the sphere.

The most comprehensive data available on sphere flow appear in a recent paper by Achenbach [1].[1] We summarize below some of his principal findings:[2]

1) As Eiffel discovered, and Prandtl gave the explanation therefore, the flow over a sphere can be divided into several régimes.[3] As shown in Figure 1, the dependence of the drag coefficient on the Reynolds number Re provides an excellent delineator. The régimes are:

   - Subcritical, or laminar boundary layer, $Re < 2.5 \times 10^{5}$.

   - Transcritical, or transition to turbulence, $2.5 \times 10^{5} < Re < 4 \times 10^{5}$.

   - Supercritical, or turbulent boundary layer, $Re > 4 \times 10^{5}$.

2) Transition occurs at $Re \approx 3.5 \times 10^{5}$, although other experimenters find that this value will vary over a small range, depending on the state of the free-stream turbulence.

3) On a smooth sphere, transition from laminar-to-turbulent boundary layer is first observed at values of $\phi_t = 90^{o}$ to 100^{o}, starting at $Re \approx 3.5 \times 10^{5}$. As the Reynolds number is increased the transition point moves continuously upstream until $\phi_t = 60^{o}$ at $Re = 5 \times 10^{6}$, the highest value for which this measurement was made. See Figure 2.

4) In the subcritical régime laminar separation occurs at $\phi_s = 82^{o}$. As shown in Figure 3, as the Reynolds number is increased through transition, the separation point moves sharply downstream, stabilizing in the vicinity of $\phi_s = 120^{o}$ for supercritical flow.

---

[1] Figures in brackets indicate the literature references at the end of this paper.

[2] Appreciation is expressed to Dr. E. Achenbach for permission to reproduce four of his figures which appear in this paper as Figures 1 through 4.

[3] Achenbach distinguishes a total of four by subdividing the transcritical régime into two. In addition, in this paper we have interchanged Achenbach's use of transcritical and supercritical in keeping with the conventional uses of the terms.

5) At transition there is also a drastic shift in the pressure-coefficient distribution as shown in Figure 4. It is this change which is primarily responsible for the drop in C_D in supercritical flow. Figure 4 gives plots of C_p for two different Reynolds numbers in the supercritical régime which are nearly coincident in the range - $0 \leq \phi < 105^o$. The minimum reading of C_p = -1.15 to -1.20 occurs just upstream of the equatorial station of $\phi = 90^o$. This corresponds to a value of $\Delta p/q$ = 2.15 to 2.20 versus the envisioned upper limit of $\Delta p/q|_{\phi=90^o} = 2.25$. Obviously, for a turbulent boundary layer, the maximum pressure-drop is greater than for the laminar case. Furthermore, the pressure distribution for turbulent boundary layer appears to be relatively insensitive to the value of Re.

3. The Trip-Wire Probe

Taking into account the preceding it was decided to use a sphere of 1.25 in. in diameter. This would give a fairly large body in which to fit ducting, allow for a sting of "reasonable" length, yet keep within the 4-in. over-all requirement.

However, in standard air, a 1.25 in. sphere at Re = 10^5 corresponds to a flow speed of 160 ft/sec, which is higher than we ordinarily expect in typical stack measurements. That is, in most cases a sphere of this size would be operating in the lower range of subcritical flows where we expect laminar separation and a pressure distribution which is Reynolds-number-dependent.

To get around this anticipated difficulty it was decided to investigate the possibility of using a trip-wire to force transition to turbulent boundary layer. This technique, conceived by Prandtl, was shown by Wieselberger [2] to have the desired effect. Schlichting [3], p. 40, reproduces Wieselberger's photographs, clearly demonstrating that installation of a trip-wire on the nose of the sphere induces transition to turbulence, as is shown by the delay in separation compared to the same flow without a trip-wire. Wieselberger placed the ring trip-wire at the station $\phi = 82^o$. The diameter of the wire was chosen to be equal to the theoretical laminar-boundary-layer thickness for the experimental flow speed.

The laminar-boundary-layer thickness can be calculated from [3], Table 11.2, p. 227. For a sphere of D = 1.25 in. the boundary-layer thickness is plotted as a function of U for various values of ϕ in Figure 5, for air at standard atmospheric conditions.

4. Experimental Procedure

Measurements were made on two models. The first consisted of a 1.25-in. diameter plexiglass sphere supported from a 0.75-in. diameter sting 6.25-in. long, to reduce support interference but large enough to pass all the required pressure tubes. In addition to the total-pressure tap on the ℄ two sets of 6 taps were located in spiral patterns at angles of $\phi = 15^o, 30^o, 45^o, 60^o, 75^o$, and 90^o to allow for verification of flow symmetry. A United Sensor Corporation type-PA Pitot-static probe was used for calibration. Micromanometers were used to measure pressure differences at all times.

Pressure-distribution measurements were made over a range of Reynolds numbers in the RPI indraft tunnel which has a diameter of 12.4 in. The model was then successively modified by installation of several trip-wires of varying diameter at the $\phi = 82.5^{o}$ station and additional runs were made.

Based on these results a final model of the trip-wire probe was designed which is shown in Figure 6. A brass sphere was used, 1.25-in. in diameter, supported from a 0.5-in. diameter sting 2.00 in. long, giving a longitudinal length (which is the transverse dimension for probe insertion purposes) of 3.25 in. All pressure taps are 0.125-in. in diameter allowing for easy clean-out. The four static-pressure taps are spaced at 90^{o} intervals and at 45^{o} from the supporting arm to reduce interference effects. The four taps are joined internally to allow "averaging" of the static pressure.

Because of a troublesome flow instability in the indraft tunnel which could not be completely eliminated, measurements on the final trip-wire probe were made in the RPI 4x6-foot-test-section wind tunnel and calibrated as before.

5. Results

Figure 7 shows the pressure distribution over the sphere front face without the presence of a trip-wire. Since the asymmetry was not severe the data shown are the average of those of the two pressure taps for each value of ϕ. The pressure distribution is as expected, remaining close to the inviscid theory up to $\phi \approx 50^{o}$, then reaching a minimum near $\phi = 75^{o}$ where the magnitude of the minimum depends on Re.

A 0.020-in. diameter trip-wire was then placed in a groove at $\phi = 82.5^{o}$. A micrometer measurement showed that the effective diameter was actually 0.015 in. This corresponds to the boundary-layer thickness on a 1.25-in. diameter sphere at U = 102 ft/sec. On this configuration the trip-wire alters the pressure distribution substantially, as shown in Figure 8. In fact, the pressure distribution becomes almost flat over the range $60^{o} < \phi < 90^{o}$, with the magnitude depending on the Reynolds number. At speeds below 102 ft/sec, the trip-wire is completely immersed in the boundary-layer and its effectiveness is reduced.

In order to reduce Reynolds-number dependence a second set of runs was made with a 0.026 in.-diameter trip-wire (effective diameter 0.020 in.). Figure 9 shows the results. Less Re-dependence is obtained but the pressure variation near $75^{o} < \phi < 90^{o}$ is distorted by the presence of the trip-wire.

To minimize effects of local pressure-distortion, the trip-wire location in the final probe was moved forward to $\phi = 75^{o}$. Results for this model, incorporating data for several runs which are shown in Figure 10, are gratifying. An almost Re-independent variation of the pressure coefficient was obtained; i.e.

$$C_{p}\Big|_{\phi=90^{o}} = -0.375 \pm 0.02, \quad 2\times10^{4} \leq Re \leq 10^{5},$$

where most deviations are, in fact, much smaller. The corresponding flow speed range is $31 \leq U \leq 162$ ft/sec.

This value of C_p, converted to a pressure difference[4], gives $\Delta p=1.375q$ which represents an increase in the sensitivity of almost 40% over the Pitot-static tube, although it is well below the theoretical maximum $\Delta p=2.25q$.

Below Re = $2x10^4$ the test-data scatter increases erratically. Although some of this may be attributable to the difficulty of getting reliable readings, the more likely cause is that at Re = $2.7x10^4$ the boundary layer thickness is the same as that of the effective trip-wire diameter. At the lowest values of the test Reynolds number, the trip-wire is completely immersed in the boundary layer and we speculate that the transition from laminar-to-turbulent boundary layer becomes unstable over a small range of Reynolds number.

It is apparent that the Reynolds number above which turbulent-boundary-layer is maintained, and the value of the probe calibration constant, are both functions of the trip-wire thickness -- more precisely of the ratio of the trip-wire effective diameter to the sphere diameter. The dramatic effect of the change in both the transition Re and the calibration constant are demonstrated by Figure 11. This test employed the final probe model with a 0.020 in. trip-wire (0.015 in. effective) at the $\phi = 75^o$ station. In this configuration transition occurs at Re $\approx 5.5x10^6$ such that in the fully turbulent regime $C_p = -0.86$ or, equivalently, $\Delta p/q = 1.86$.

This latter value is much closer to the optimum value of 2.25, but the lower limit of the useful velocity range (for constant calibration factor) is drastically increased. Depending on the application it should be possible to modify both the sphere diameter and the trip-wire effective thickness for optimal characteristics. Thus it would be useful to have available results of a systematic experimental study of the effect of trip-wire thickness on these two parameters.

6. References

[1] Achenbach, E., Experiments on Flow Past Spheres At Very High Reynolds Numbers. J. Fluid Mechanics, 54, pt. 3, 656 (1975).

[2] Wieselberger, C., Der Luft widerstand von Kugeln. AFMS, 5, 140 (1914).

[3] Schlichting, H., Boundary Layer Theory, 6th ed, McGraw-Hill Book Co., (1968).

[4] McCaffrey, B.J. and Hekestad, G., A Robust Bidirectional Low-Velocity Probe for Flame and Fire Application. Brief Communications, Combustion and Flame, 26, 125 (1976).

[4]The reader's attention is directed to another new probe design [4] which is intended for the use in fire and flame studies. Experimental data are given for a range of velocities an order of magnitude lower than presented herein. In the other design it is essential to employ the calibration curve which is highly dependent on Re.

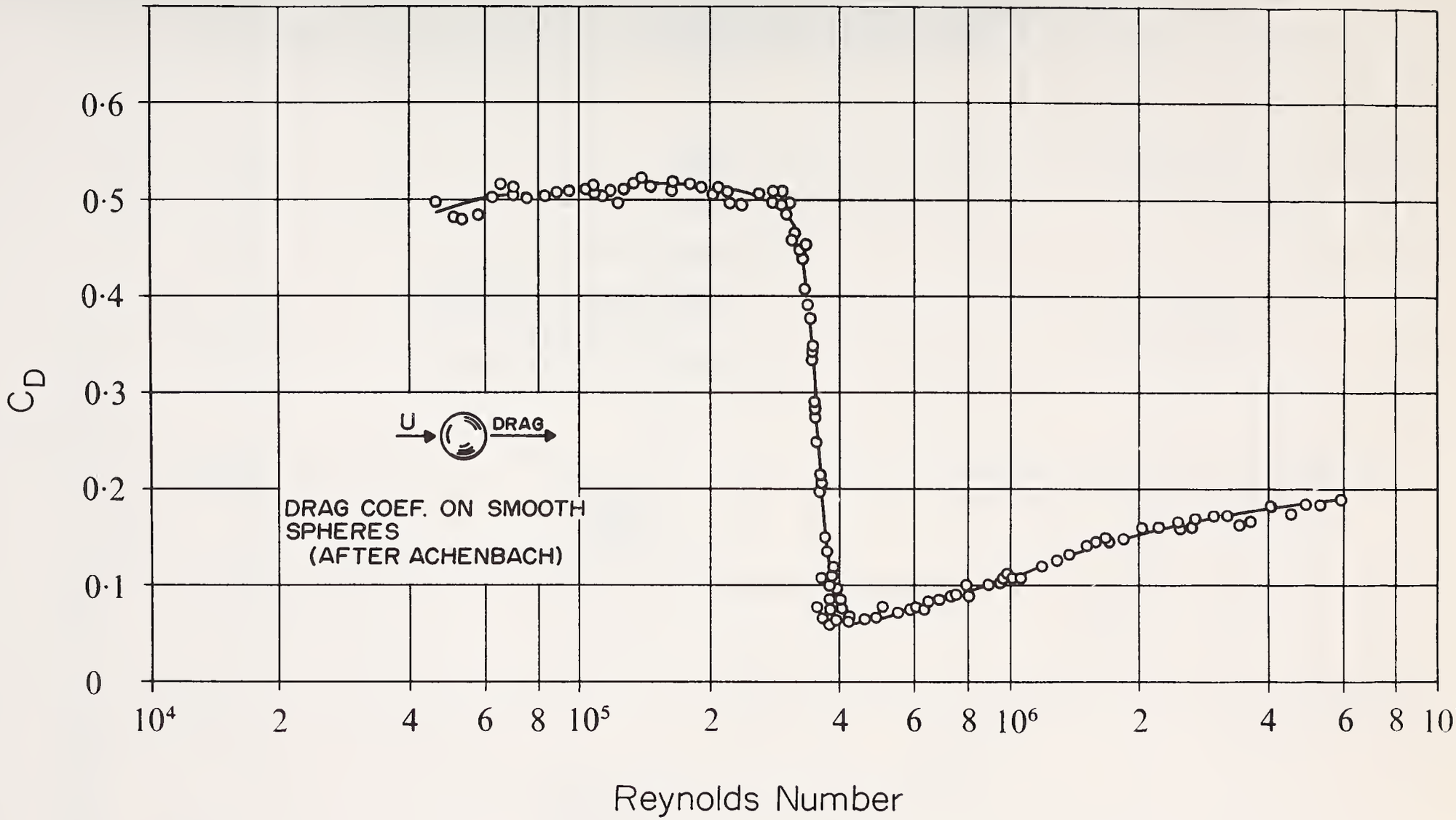

FIGURE 1. DRAG COEFFICIENT ON A SMOOTH SPHERE AS A FUNCTION OF REYNOLDS NUMBER; FROM [1].

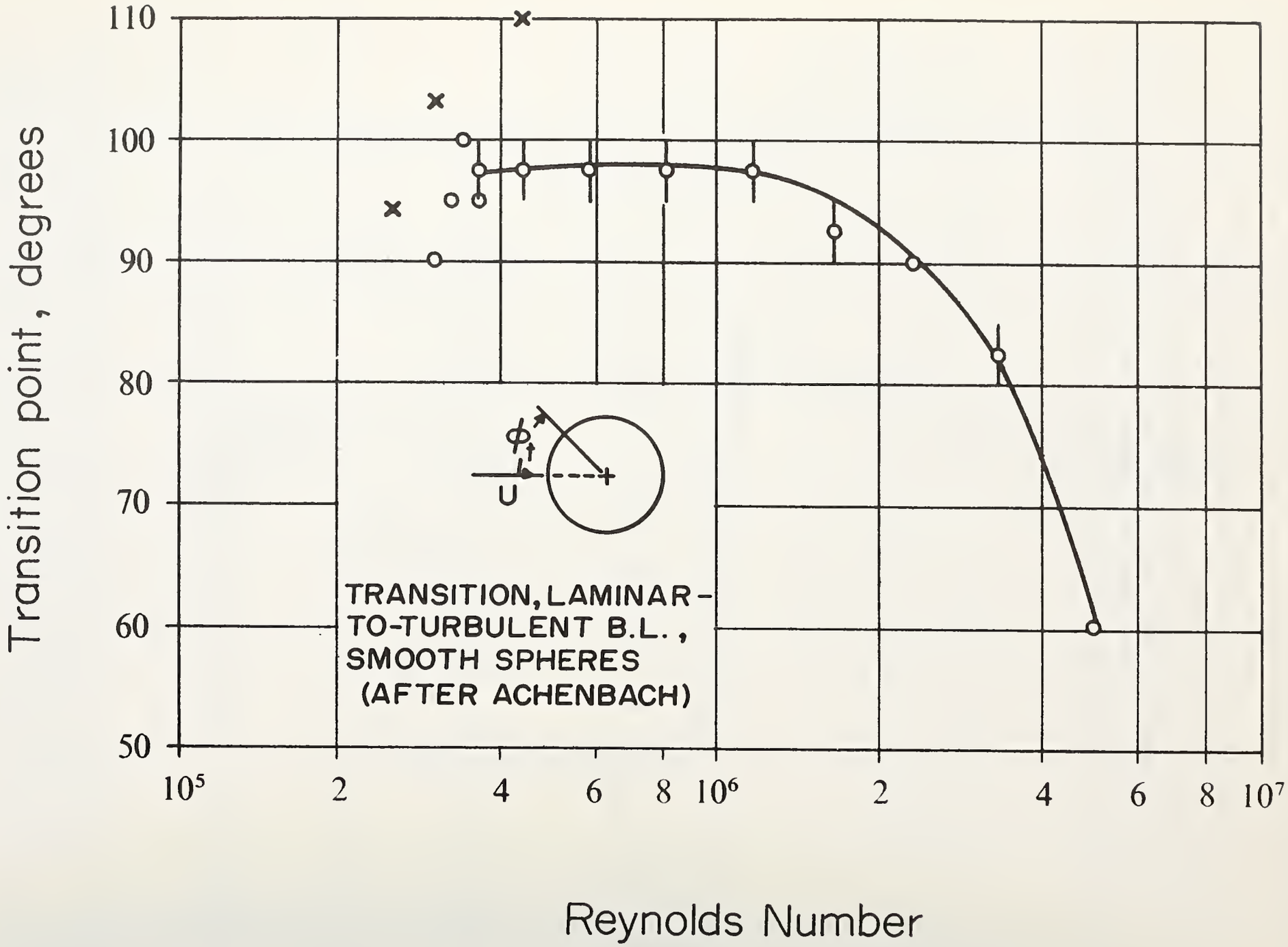

FIGURE 2. POSITION OF TRANSITION FROM LAMINAR-TO-TURBULENT BOUNDARY-LAYER FLOW FOR SMOOTH SPHERES; FROM [1].

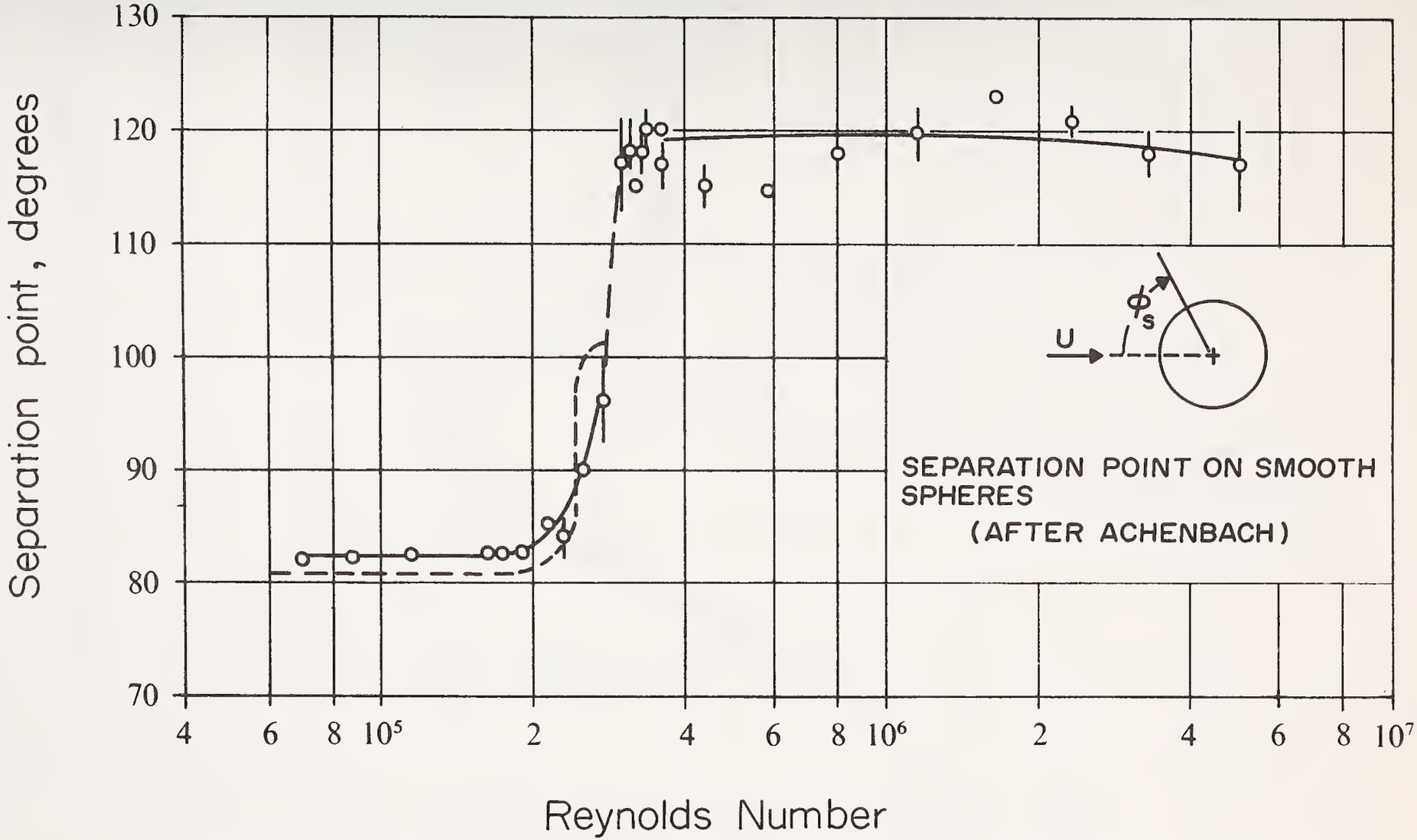

FIGURE 3. POSITION OF BOUNDARY-LAYER SEPARATION FOR SMOOTH SPHERES; FROM [1].

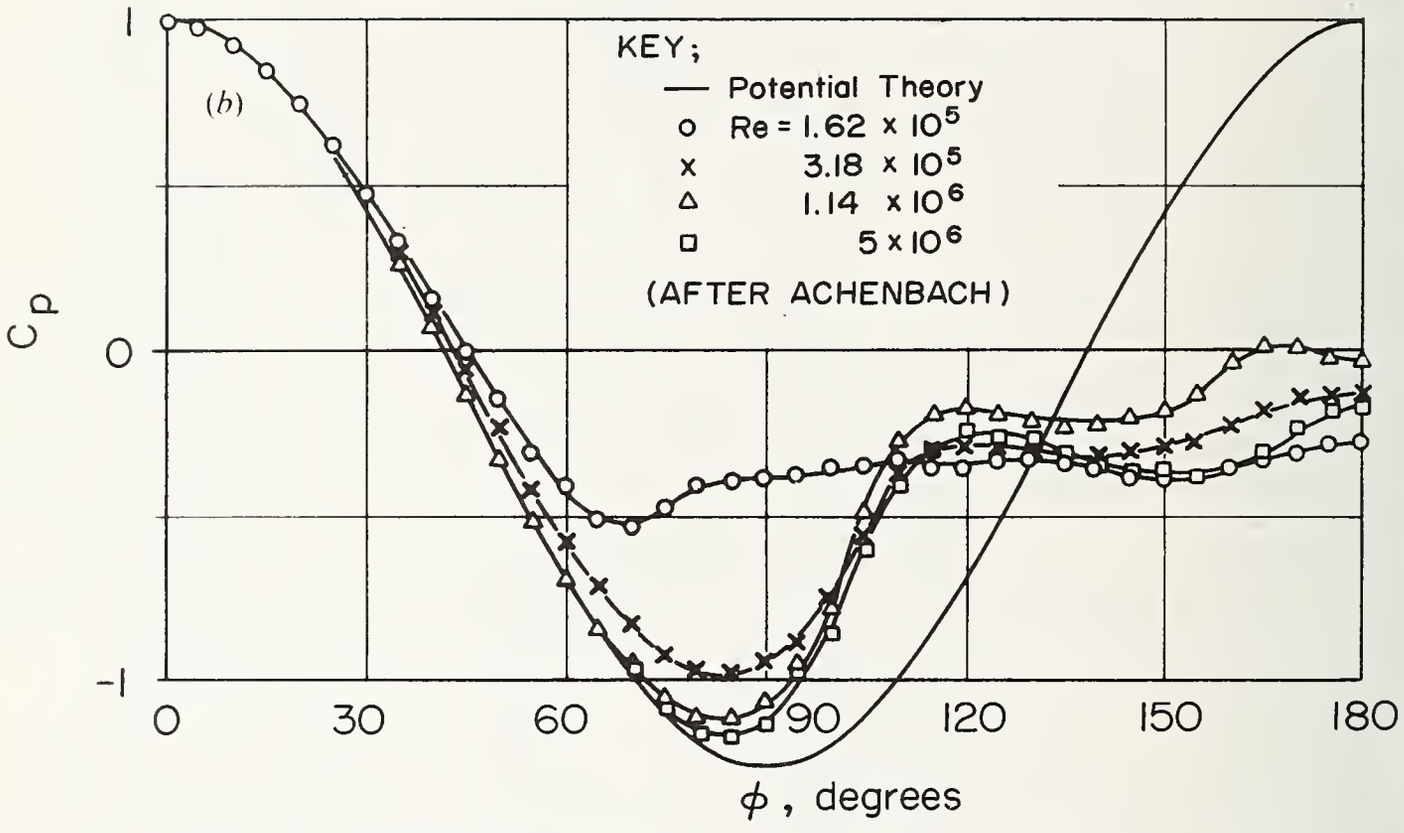

FIGURE 4. PRESSURE-COEFFICIENT DISTRIBUTION FOR A SMOOTH SPHERE AT VARIOUS REYNOLDS NUMBER; FROM [1].

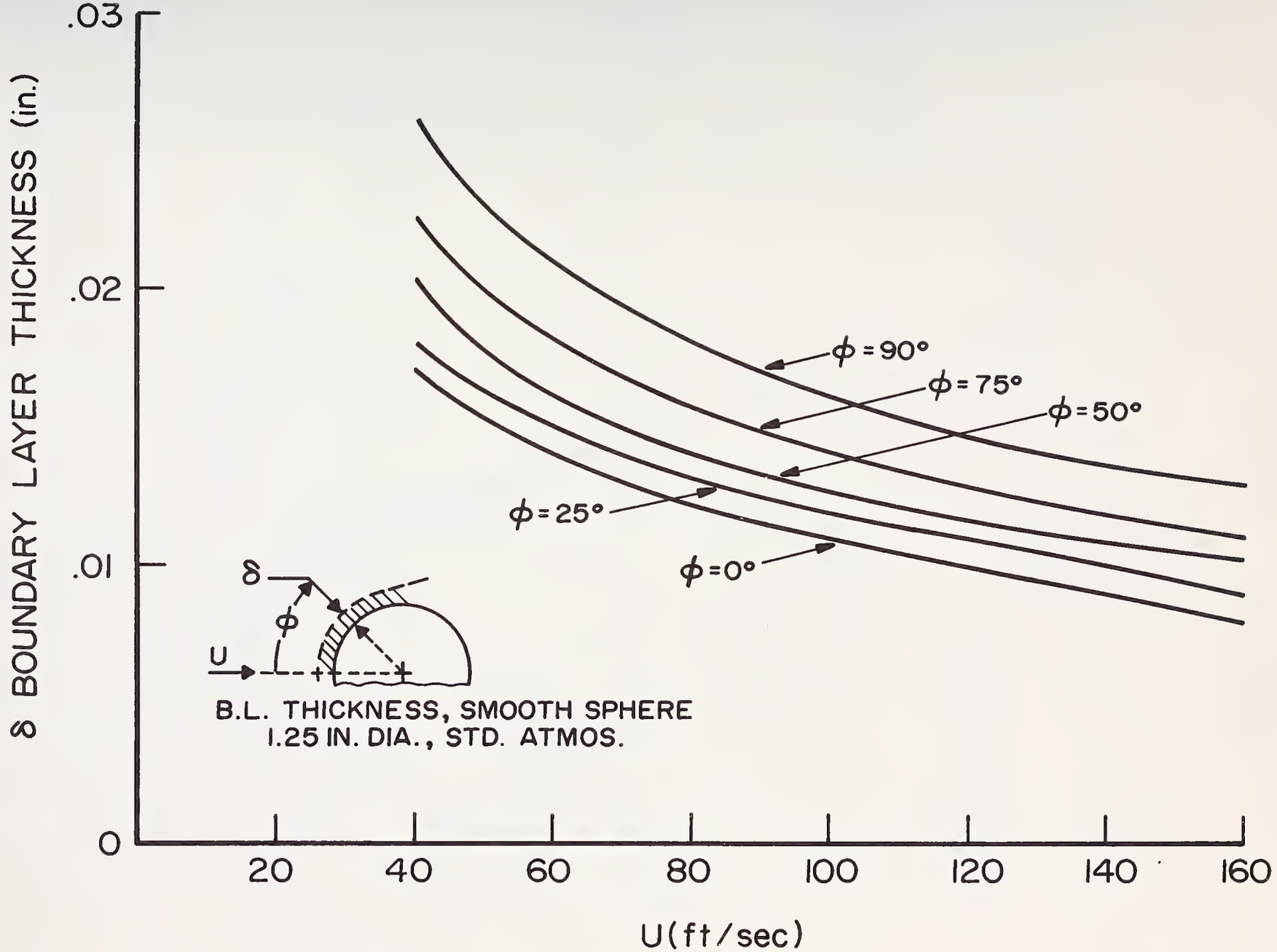

FIGURE 5. THEORETICAL LAMINAR-BOUNDARY-LAYER THICKNESS ON A 1.25-IN. DIAMETER SPHERE VERSUS FREE-STREAM VELOCITY, AT STANDARD ATMOSPHERIC CONDITIONS.

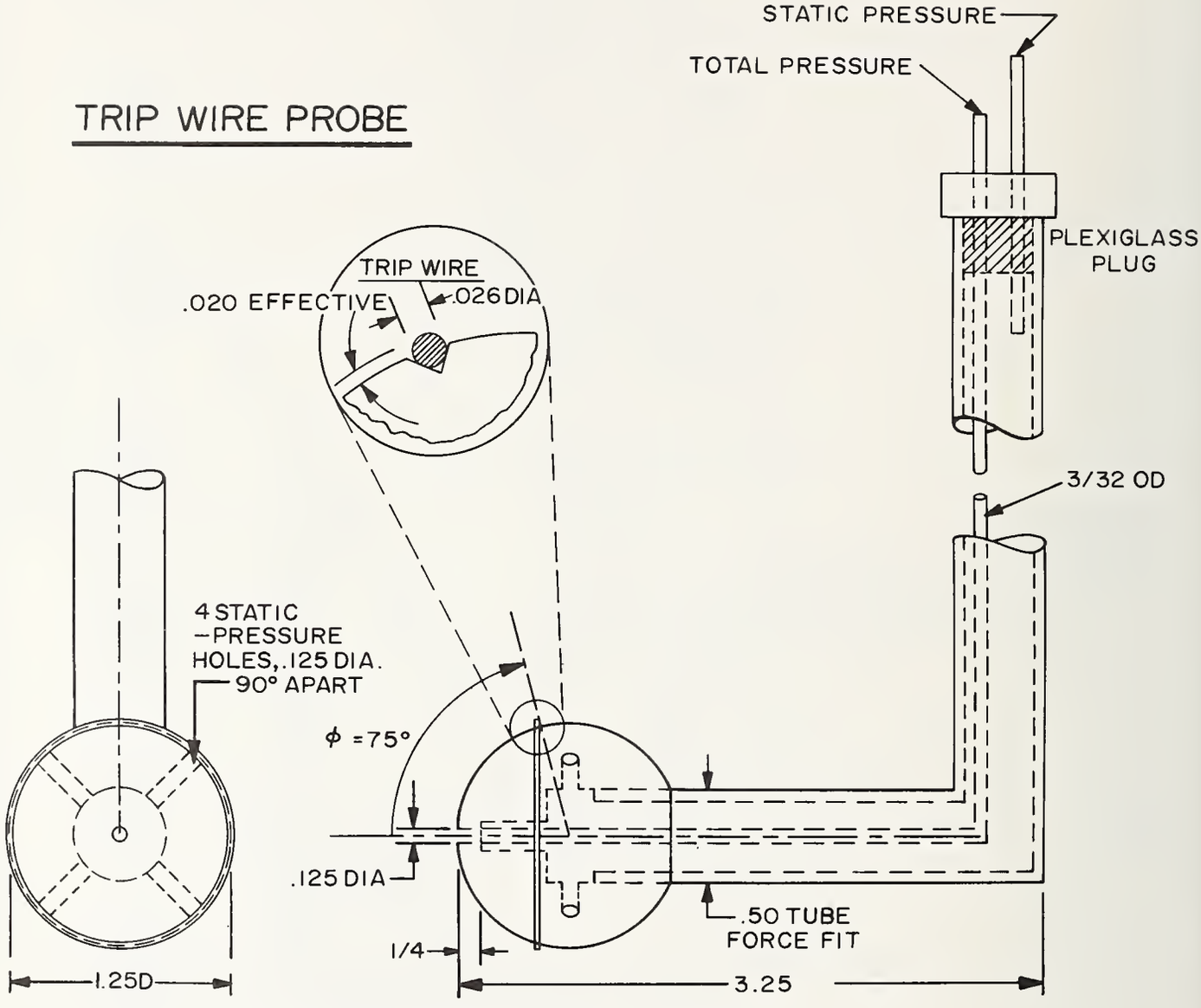

FIGURE 6. THE TRIP-WIRE VELOCITY PROBE.

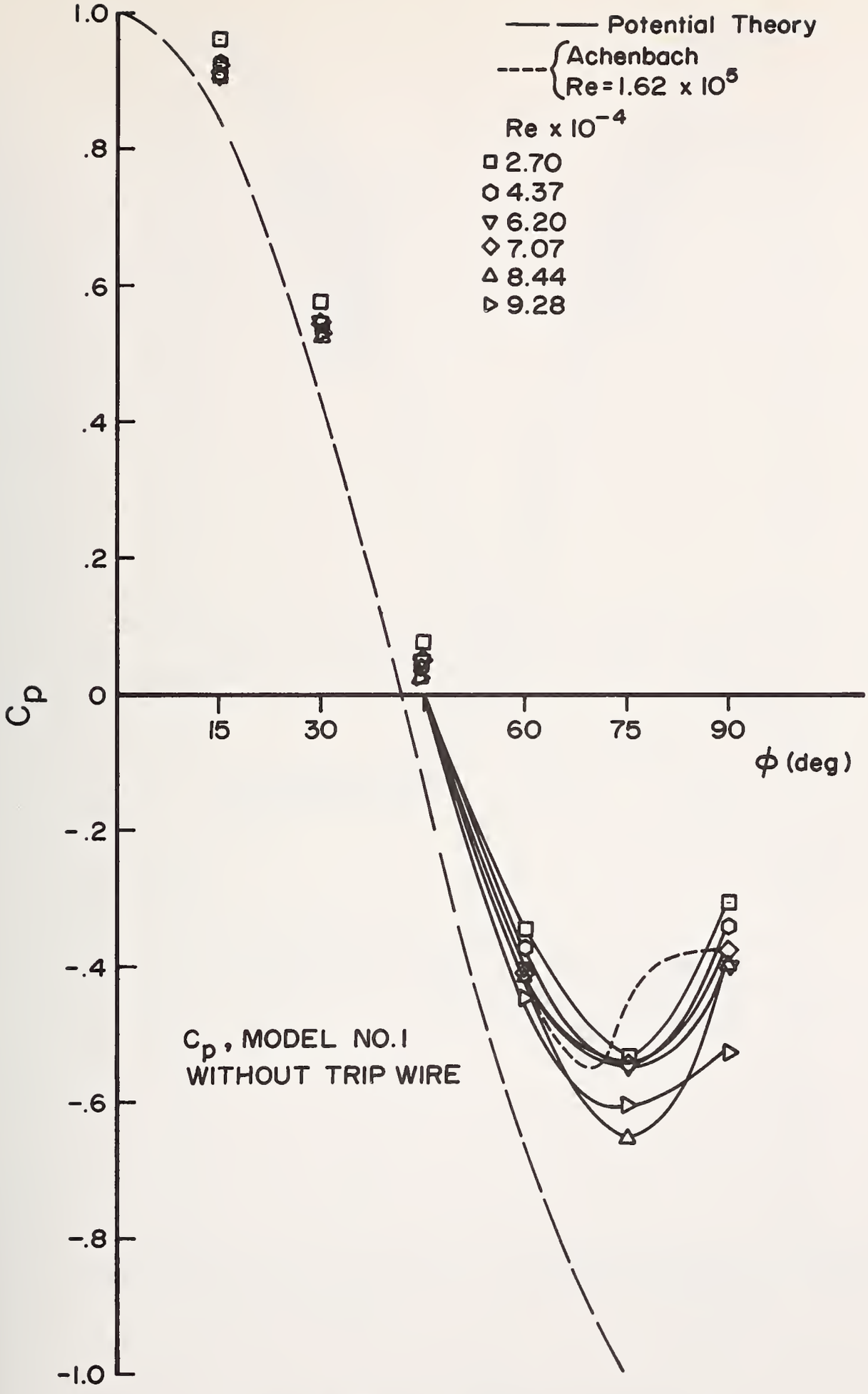

FIGURE 7. C_p vs ϕ ON MODEL NO. 1 WITHOUT TRIP-WIRE.

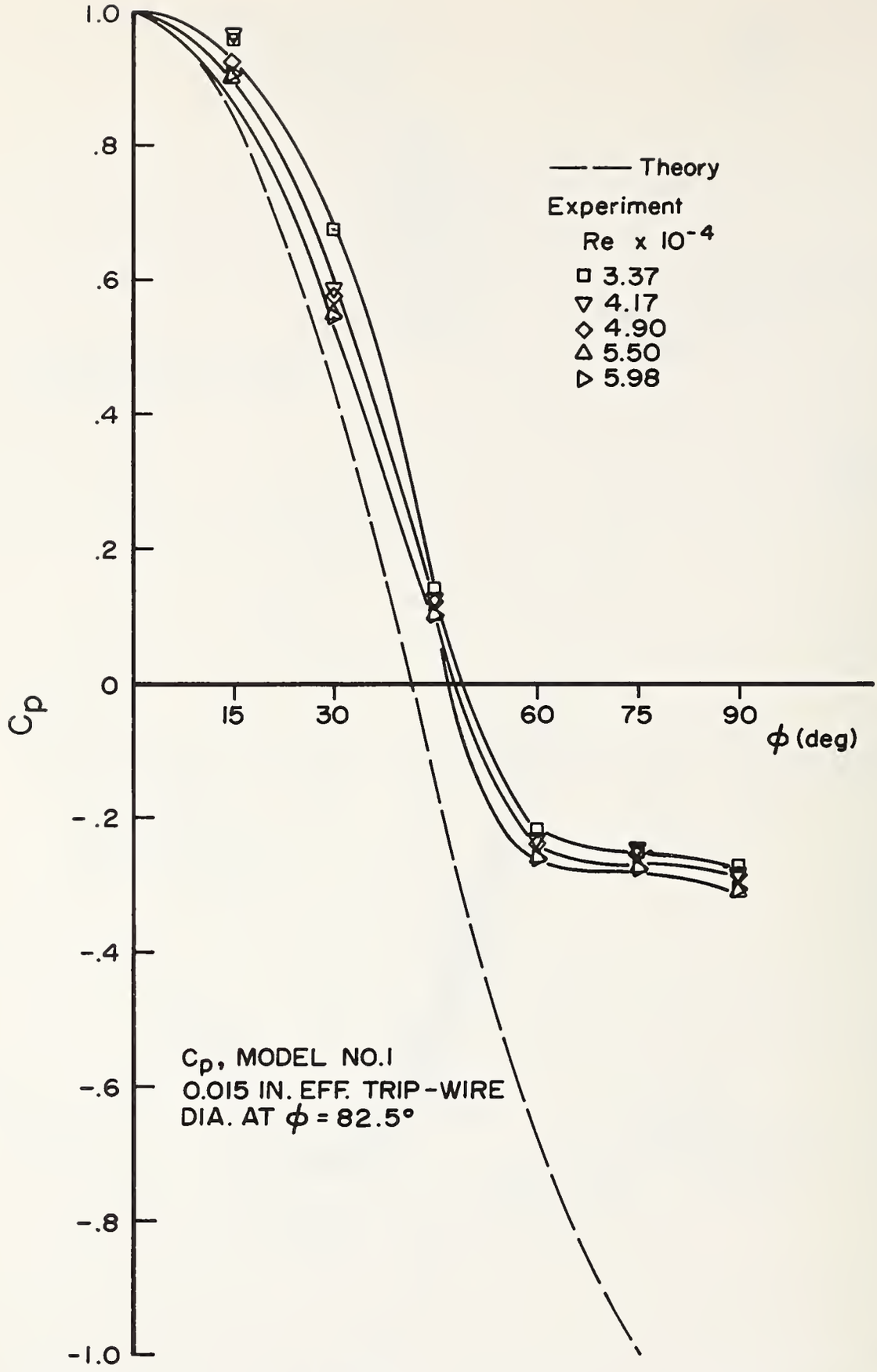

FIGURE 8. C_p vs ϕ ON MODEL NO. 1, 0.020 IN. (0.015 IN. EFFECTIVE) TRIP-WIRE.

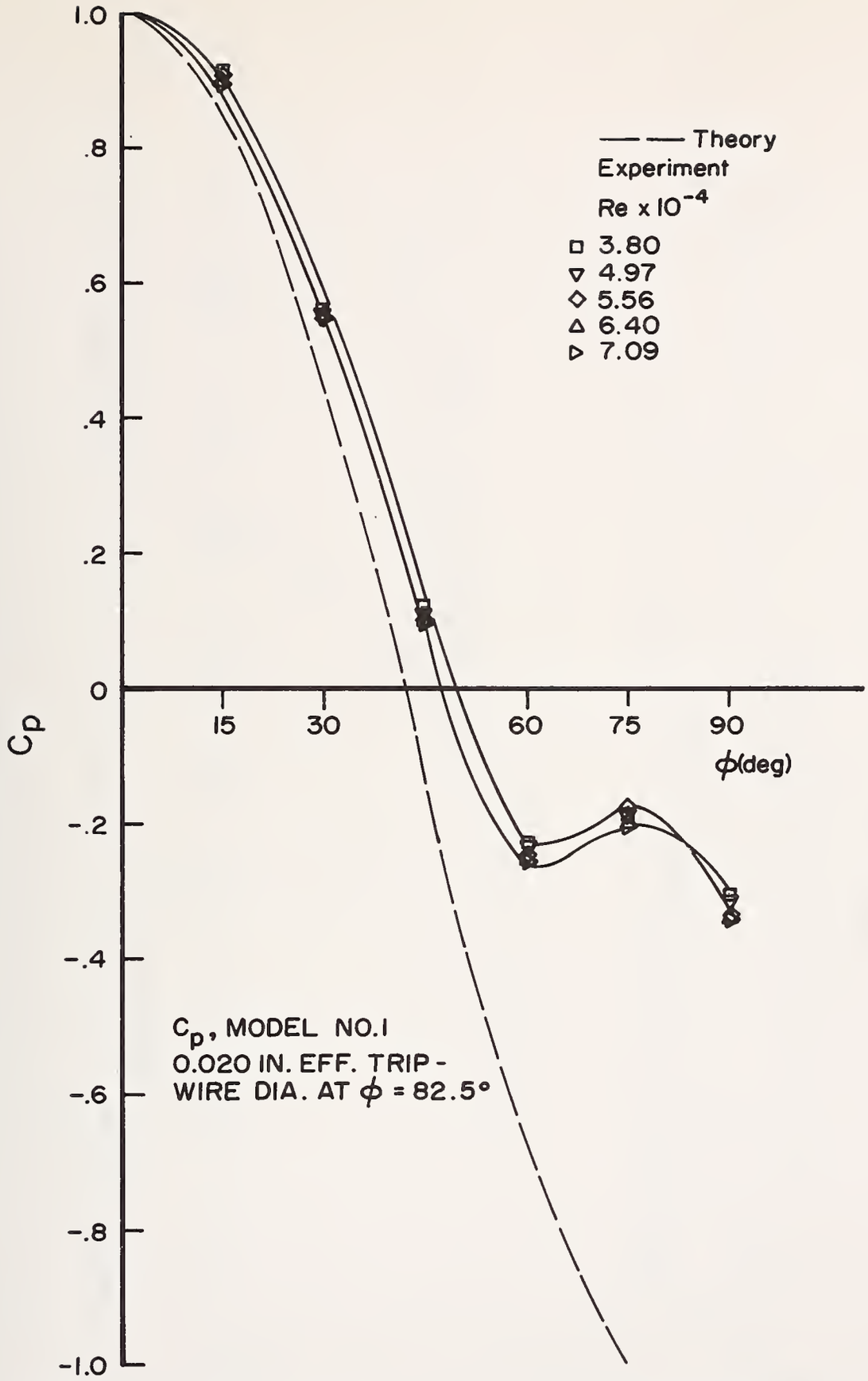

FIGURE 9. C_p VS ϕ ON MODEL NO. 1, 0.026 IN. (0.020 IN. EFFECTIVE) TRIP-WIRE.

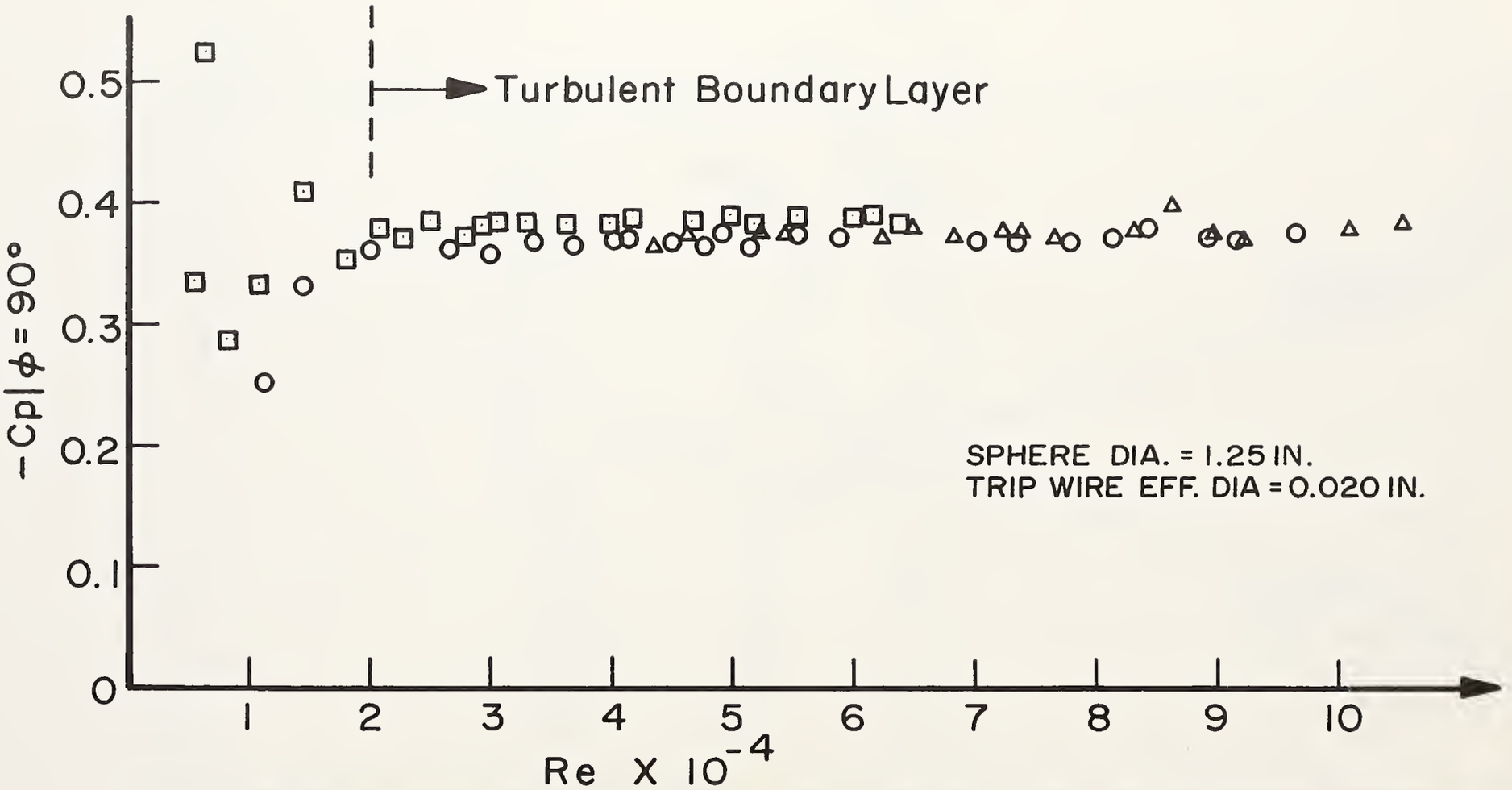

FIGURE 10. FINAL MODEL, C_p AT ϕ = 90° VS RE, 0.026 IN. (0.020 IN. EFFECTIVE) TRIP-WIRE.

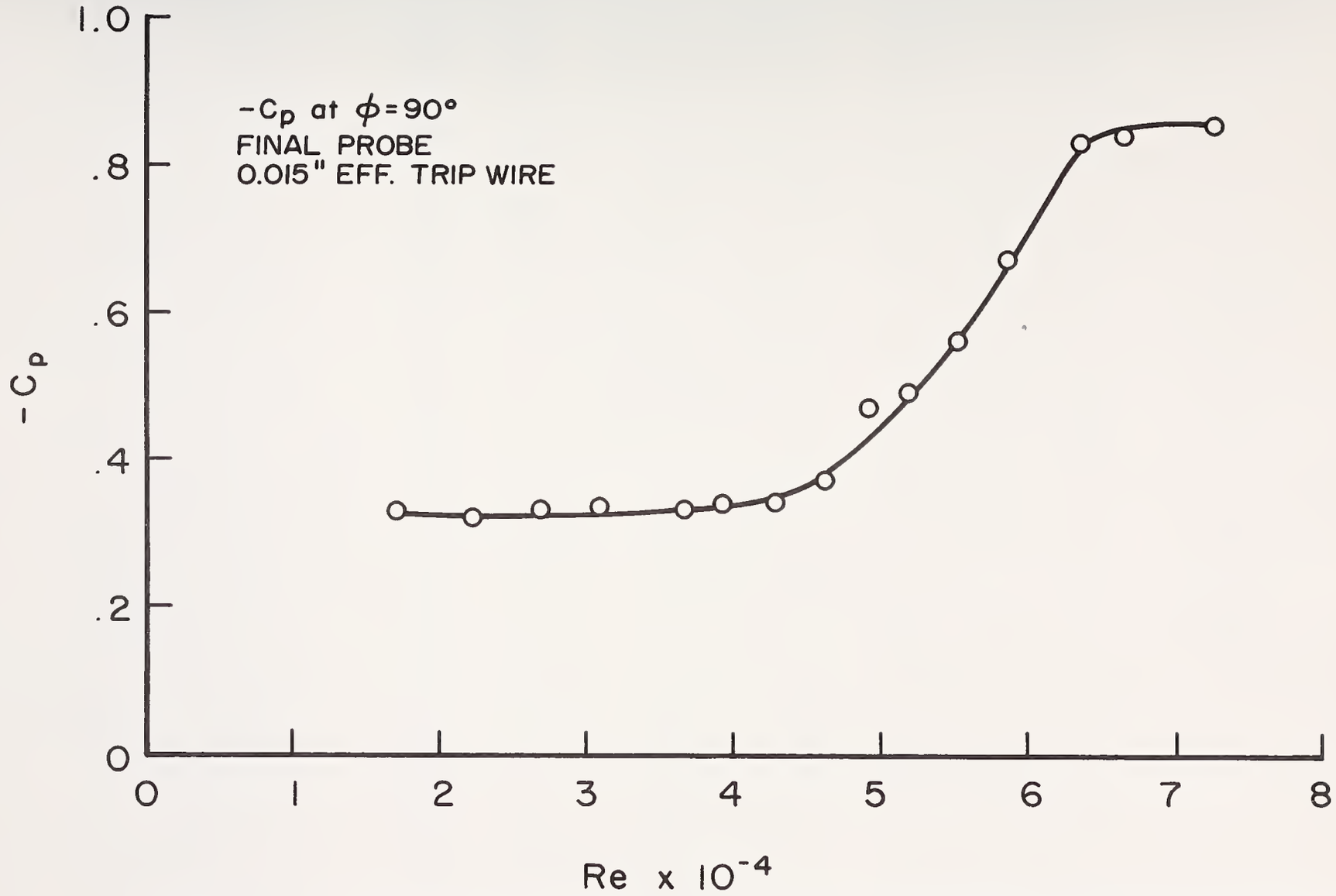

FIGURE 11. C_p AT ϕ = 90° VS RE, 0.026 IN. (0.015 EFFECTIVE) TRIP-WIRE ON FINAL MODEL.

National Bureau of Standards Special Publication 484, Proceedings of the Symposium on Flow in Open Channels and Closed Conduits held at NBS, Gaithersburg, MD, February 23-25, 1977. (Issued October 1977)

THE INFLUENCE OF TURBULENCE ON STATIC AND TOTAL PRESSURE PROBES

V. E. Scottron

Institute of Water Resources
University of Connecticut
Storrs, Connecticut 06268

In the course of studying boundary layer flows over a rough boundary in an adverse pressure gradient in a wind tunnel, measurements of mean and turbulent velocities were taken using a hot-wire anemometer. Comparative velocity measurements were taken with static and impact probes attached to a micromanometer. Attempts have been made to determine the influence of the turbulence components on the readings obtained by these probes. Also comparisons have been made with the results of similar studies made by other investigators, such as Toomre, Bradshaw and de Haan.

The probes used in these tests were 1/16 and 1/8 inch diameter separated probes. Combined probes could not be used near the wall due to the local pressure disturbances caused by the roughness. The boundary layer thicknesses were large, of the order of 10 to 12 inches so that it was possible to obtain a wide variation of turbulence levels by positioning of the probes. Pressure differences were referenced to a fixed static probe outside the boundary layer in a very low turbulence region.

Pressure indications were sufficiently large that it was possible to obtain reasonable verification of the theoretical estimates obtained by Toomre.

Key Words: Pitot tubes, static pressure probe, impact pressure probe, turbulence, turbulent boundary layers, velocity measurement.

1. Introduction

Investigation into the effects of turbulence on the behavior of static and total pressure probes was started as a part of a major study on boundary layer flows over a rough wall in an adverse pressure gradient [1]. Recent studies [2] on the detailed behavior of flow in open-channel junctions and side-channel spillways have continued this interest in instrumentation problems. The experimental objectives always require the measurement of mean velocities within a reasonable degree of accuracy, often in the presence of very intense, large-scale turbulence.

Clearly, the conditions are far from ideal for measurement of either mean velocities or turbulence intensities. In order to establish even a first-order correction for the effect of high level turbulence, it is first necessary to have available an approximation of the turbulence for at least two components. Hinze [3] presents a very discouraging summary of the problems involved in using the hot-wire anemometer for velocity measurements under such conditions. Becker and Brown [4] indicate a good reliability of total pressure up to about

$$w^2 \equiv \overline{U_n^2}/\overline{U^2} = 0.2$$

Let us return to the experiment which initiated the studies on static and total pressure probes. An attempt was made to determine the role of wall roughness in the development of the boundary layer in a strongly adverse pressure gradient approaching separation [1]. Local turbulence levels turned out to be extremely high throughout much of the boundary layer. In addition to the eddies generated by the wall roughnesses, the square screen mesh, which was used to create the roughness, also produced sizeable pressure disturbances. Since the free-stream turbulence levels remained quite low at 0.3% or less, both hot-wires and pressure probes could be used effectively outside of the boundary layer. Within the boundary layer, it was necessary to use static pressure probes that were separated from the total pressure probe because of the variation of the static pressure near the rough wall. This wall-generated pressure fluctuation also prevented the use of wall taps in determining static pressure. Static pressure distributions along the flow path were checked by means of surface taps located outside of the rough wall boundary layer in the plane smooth wall which formed the floor of the wind tunnel and also by static probes in the central free stream region.

A number of schemes were tried to produce reasonable agreement between hot-wire and pressure probe readings. A method which combined the suggestions of Hinze [5], Toomre [6] and Siao [7] was adopted since it seemed to produce the closest agreement. At that time, the behavior of the static pressure probes was assumed to follow the first-order corrections given by Toomre [6] and Strasberg [8]. Subsequent experimental results which seem to verify these corrections are reported in this paper.

2. Equipment and Instrumentation

a. THE WIND TUNNEL

The wind tunnel test section is approximately 2 feet wide and 4 feet high with flexible side walls 15 feet long. One wall was kept plane and covered with square mesh screen of 0.500 inch spacing and 0.105 inch diameter wire. The opposite wall was smooth and positioned to control the longitudinal velocity and pressure distribution. It was thus possible to

obtain extremely thick boundary layers with free stream velocities approximating 70 feet/second. Variations in static pressure across the boundary layer were thus large enough to be measured in this situation.

b. PITOT TUBES AND STATIC PROBES

Three pitot tubes were used to make the velocity measurements: All had separate impact and static elements. The small pitot tube had a geometrical construction that permitted measurements near the wall. The impact element was square-nosed hypodermic tubing, 0.025 in. outside diameter and 0.016 in. inside diameter, shaped so that it could be placed tangent to the wall. The static element was 1/16-in.-diameter tubing with four holes of 0.016 inch spaced at 90-degree intervals around the tube at a distance of approximately 10 diameters from the leading edge. These holes were in the same plane normal to the flow direction as the opening of the impact element. The static element was located 1/2 inch farther out in the boundary layer and 1/2 inch below the impact element during the measurements. This geometry ensured that, for all pitot tube positions, the static element would not be affected by the strong local static pressure variations caused by the rough wall. These pressure disturbances did not appear to extend over 0.3 inches into the boundary layer. Careful calibration of this pitot tube under low turbulence conditions in the free stream showed no appreciable error in comparison with large diameter tubes.

Where the boundary layer was over 7 inches thick, another pitot tube was used to traverse the boundary layer from about 4 inches from the wall out to the free stream. This pitot tube overlapped the range of the smaller tube for a distance of 3 inches and permitted a comparison of data obtained in this region. Both impact and static tubes were 1/16 inch in diameter. The static tube was identical to the static tube of the smaller pitot tube and was located 1 inch out from the impact tube. The tip of the impact tube had an internal diameter of 0.052 inches.

A pitot tube similar to the 1/16-inch probe, but having 1/8-inch-diameter impact and static tubes, was used as a free stream reference and, when it would not disturb the flow at a measuring station, for monitoring the steadiness of the flow. This pitot tube was fixed in position for a given set of measurements. The standard reference velocity for the wind tunnel was obtained by calibrating the pressure difference between a fixed impact tube at the entrance to the tunnel contraction and a static (smooth wall) tap at the beginning of the test section against the pressure differences across the 1/8-inch pitot tube at fixed locations in the free stream.

c. HOT WIRES

The hot-wire probes were standard Flow Corporation 0.00015-inch-diameter copper-plated tungsten wire having an active length of about 1 mm. These were set with the wire vertical and parallel to the wall at a

longitudinal location identical to that of the pressure probes. The hot-wire anemometer was a constant temperature type of instrument which provided a linear relation between mean velocity and d-c amperage measurements.

d. PRESSURE MEASUREMENTS

A sensitive micromanometer, [9] which could be read to the nearest 0.0002 inch, was used to measure pressures at the lower velocities. This gave excellent results in regions of low turbulence but proved overly sensitive and difficult to read in regions of high turbulence. Most of the pressure readings were taken on precision inclined manometers which had slope settings from 1:10 up to 1:4. Reproducibility of readings proved quite satisfactory with these manometers. The manometer fluid for all the units was Dow Corning Silicone 200 (specific gravity of 0.817), which has properties highly suitable for this use.

e. MEAN VELOCITY MEASUREMENTS

During the tests extremely high levels of turbulence intensity were encountered close to the wall. Here the rms values of u were from 40 to 50 percent of the local mean velocity. This gave rise to sizeable errors in the measurement of both mean velocity and turbulent intensity. Figure 1 illustrates a typical comparison of hot wire and pitot tube uncorrected mean velocity readings. It was apparent right from the start that the correction of instrument readings would constitute one of the key problems in these tests.

3. Hot Wire Anemometer

The measurement of mean velocities and longitudinal turbulence intensities where the intensities are low is a fairly straightforward matter. A small low-turbulence wind-tunnel was used for calibration of hot wires and pressure probes with consistently reproducible results. All measurements of $\bar{U}$ and u were based on such low-turbulence calibrations. It is also possible to use carefully matched anemometer circuits and hot wire elements to determine the cross-components of turbulence v and w as well as the Reynolds Stress and a variety of correlations where the turbulence levels are low.

Unfortunately, as turbulence levels increase to values of $\overline{u^2}/\bar{U}^2$ exceeding 0.10, it is necessary to apply a variety of corrections to measured values of $\bar{U}$ and u . In addition, data collected on the matched linearized anomometer circuits become completely unacceptable due to lack of reproducibility. Since $\overline{v^2}$ and $\overline{w^2}$ enter the computation of the turbulence corrections and they can not be measured reliably, it becomes necessary to estimate these. The evaluation of higher correlations within a high

intensity turbulent shear flow becomes an impossibility. Another factor of great significance is the inability of the hot wire to distinguish between + and - on an instantaneous basis.

In an earlier paper [1], it was shown that by ignoring the effect of higher correlations and assuming a Gaussian distribution within the turbulence in order to develop a correction for local velocity reversal [7], the following corrections could be applied to the hot wire readings:

$$\frac{\overline{U}}{\overline{U}_w} = \frac{\left[1 - \frac{1}{2}\frac{\overline{v^2}}{\overline{U^2}} + \cdots\right]}{[\text{erf}\ (\eta) + e^{-\eta^2}/\sqrt{\pi}\eta]} = \frac{f_3(\eta, v/u)}{f_1(\eta)} \tag{1}$$

$$= \left[\ 1 - \eta^2\left(\frac{1}{2}\ v/u\right)^2\ \right] /\ f_1(\eta) \tag{2}$$

where:

$$\eta = \overline{U}/\sqrt{2\overline{u^2}}$$

$\overline{U}$ = corrected mean velocity

$\overline{U}_w$ = measured mean velocity

and for the intensity:

$$\frac{u}{u_w} = \frac{1}{\sqrt{1 - 2\eta^2[\{f_1(\eta)\}^2 - 1]}} = \frac{1}{f_2(\eta)} \tag{3}$$

combining Equations 2 and 3, we get:

$$\left(\frac{u}{\overline{U}}\right)\frac{f_3\ (\eta, v/u)\ f_2(\eta)}{f_1(\eta)} = \left(\frac{u}{\overline{U}}\right)_w \tag{4}$$

Once the corrected value of $u/\overline{U}$ is known, it is possible to obtain correct values of U/U_1 from equation (2).

$$\frac{\overline{U}}{\overline{U}_w} = \frac{\overline{U}}{\overline{U}_1}\frac{\overline{U}_1}{\overline{U}_w} = \frac{f_3(\eta, v/u)}{f_1(\eta)} \tag{5}$$

or $$\frac{\overline{U}}{\overline{U}_1} = \frac{\overline{U}_w}{\overline{U}_1} \frac{f_3(\eta, v/u)}{f_1(\eta)} = \frac{\overline{U}_w}{\overline{U}_1} F_h (\eta, v/u) \qquad (6)$$

It should be noted here that $\overline{U}_1$, the free-stream velocity exists in a low-turbulence region and was used as a reference calibration value at each test station. $\overline{U}_1$ is therefore presumably free from error, at least, free of those errors which have just been discussed, and may be moved into and out of equations as a true constant.

The ratio of $u/\overline{U}_1$ involves only the single correction factor $f_2(\eta)$ to modify $u_w/\overline{U}_1$, but the local intensity ratio of $u/\overline{U}$ is of more significance in evaluating the corrections for mean velocity. Typical values of the mean velocity factor, F_h, are shown in Table 1 for two stations in the boundary layer.

4. Static Pressure Probes

Before attempting to evaluate the influence of turbulence on the measurements sensed by static pressure probes, it is necessary to determine the way in which the pressure varies across the boundary layer. The equation which applies in this case for the y component normal to the wall will be:

$$\frac{\partial \overline{uv}}{\partial x} + \frac{\partial \overline{v^2}}{\partial y} = -\frac{1}{\rho} \frac{\partial p}{\partial y} \qquad (7)$$

where $\overline{uv} = -\tau/\rho$

on integration from y to δ, this becomes:

$$\overline{P} = \overline{P}_o - \rho\overline{v^2} - \int_y^\delta \frac{\partial \overline{uv}}{\partial x} dy \qquad (8)$$

where $\overline{P}_o$ = free stream static reference pressure.

The ratio of the integral term is small compared to $\overline{v^2}$, about ± 0.10 for the tests described here. A good approximation for the static pressure is therefore $\rho\overline{v^2}$ below the free stream pressure on a line normal to the wall.

b. EXPERIMENTAL PROCEDURE

In order to estimate the corrections for the static probes, two standard static probes as described in Section 2b were used. One of these was 1/16 inch diameter and the other 1/8 inch diameter. One of these would be placed outside of the boundary layer for reference and the other traversed essentially normal to the wall. The micromanometer described in Section 2d was used to read the differences in pressure between two probes. If no corrections were needed, the difference should correspond to $\overline{v^2}$. As has been noted previously, however, it was necessary to estimate values of $\overline{v^2}$ and $\overline{w^2}$ so that results are presented in terms of these estimates in comparison to measured pressure differences.

c. ANALYSIS AND OTHER EXPERIMENTS

In 1936, Goldstein [10] and Fage [11] concluded from both theory and experiment that:

$$\overline{P}_m = \overline{P} + C\rho(\overline{v^2} + \overline{w^2}) \tag{9}$$

$$= \overline{P} + C\rho\overline{u_n^2} \tag{10}$$

where C = constant, $0<C<1/3$

Toomre [6] later demonstrated that this relationship was correct for random eddies that were smaller than the probe, but that if the probe were considerably smaller than the typical eddy size, the probe would sense a yawed flow and a reduction in pressure.

For the large eddy case, Toomre calculated:

$$\overline{P_m} = \overline{P} - A\rho\overline{u_n^2}/2 \tag{11}$$

where A is a constant having a limiting value of unity.

Hinze [5] estimated $A>1/2$

A variety of experimental values have been obtained. Strasberg [8] obtained A=-1, but did not attempt to verify the algebraic sign. Siddon [12] obtained $+0.6<A<+1.0$ depending on the flow conditions. DeHaan [13] showed similar values by oscillating a static pressure probe in yaw under controlled turbulence conditions. Bradshaw [14] on the other hand, found values of A=0 for tests run in a free jet.

d. RESULTS

For convenience, all pressure measurements were reduced to non-dimensional form by dividing by $\rho\bar{U}_1^2$. The pressure differences then became proportional to $\overline{v^2}/\bar{U}_1^2$ or $\overline{u_n^2}/\bar{U}_1^2$. If the value of A=1 in the Toomre equation (11), then:

$$\bar{P}_o - \bar{P}_m/\rho\bar{U}_1^2 = \overline{v^2}/\bar{U}_1^2 + \overline{u_n^2}/2\bar{U}_1^2 = F_V \qquad (12)$$

Since actual values of $\overline{v^2}$ and $\overline{w^2}$ are not known, these have been estimated from other boundary layer data, particularly that of Schubauer and Klebanoff [15] where there were certain similarities in the boundary layer behavior. The estimate was based on the assumption that values of $\overline{v^2}/\overline{u^2}$ and $\overline{w^2}/\overline{u^2}$ would be the same for corresponding values of y/δ as the flows approached separation.

Three sets of curves have been plotted using these data:

Figure 2. Station 9, showing the traverses for both the 1/16 inch and 1/8 inch diameter probes versus estimated corrections where A=1 and A=0.

Figure 3. Station 13, using 1/16 inch diameter probe only.

Figure 4. Station 13, using 1/8 inch diameter probe only.

Two facts are immediately clear on examining these curves. The first is that the estimates are poor. The second is that the correction favors the upper estimate or that A=1 is the more acceptable value. It is thus concluded that the Toomre analysis gives acceptable results.

5. Total Pressure Probes

The square-nosed impact probe is subject to a variety of corrections such as those due to its own Reynolds Number, wall proximity, compressibility, etc. These may be eliminated by proper size of probe, flow speed and position so that only the question of the influence of turbulent flow characteristics need be considered. A carefully made square-nosed pitot tube will have a coefficient approximating unity. Assuming a coefficient of unity, the effect of turbulence may then be represented by:

$$(\bar{P}_{tot})_{meas} = \bar{P} + \frac{1}{2}\rho\bar{U}^2\left[1 + \frac{\overline{u^2} + (1-B)\overline{u_n^2}}{\bar{U}^2}\right] \qquad (13)$$

as given by Hinze [3]. The value of B may be based on an approximate fit to the directional calibration of the impact tube, or it may be evaluated by fitting corrected hot-wire data. In general, the effect of the transverse components of turbulence yields values of B greater than unity and possibly higher than the 1.5 which was estimated in these experiments.

Siao [7] considers the effect of instantaneous velocity reversals ($\overline{U}+u<o$) on the pitot tube. His conclusion is that this is extremely small even for values of $\overline{u^2}/\overline{U}^2 = 0.40$, where the correction is about 1%. The key problem then would seem to be that of evaluating B within a reasonable degree of accuracy.

Part of the difficulty for the experimental case cited is that the impact tube and the static probe are not located at the same distance from the wall. As a consequence, the corrections for the static probe and impact probe must be applied separately when a differential pressure reading is used to evaluate the mean velocity. The form of equation becomes:

$$(\overline{P}_t - \overline{P})_{meas} = \rho\frac{\overline{U}^2}{2}\left[1 + \frac{\overline{u^2} + (1-B)\overline{u_n^2}}{\overline{U}^2}\right] + A\rho\overline{u_{ns}^2}/2 + \rho\overline{v_s^2} - \rho\overline{v^2} \qquad (14)$$

where subscript s is at location of static probe and other values are taken at impact probe location. Then since the desired correction is to be used to modify $\overline{U}_m/\overline{U}_1$ to the form $\overline{U}/\overline{U}_1$ and $(\overline{P}_t-\overline{P})_m = \rho\overline{U}_m^2/2$, the "pitot" function for mean velocity corrections will have the form:

$$\frac{\overline{U}}{\overline{U}_1} = \left(\frac{\overline{U}_m}{\overline{U}_1}\right)F_p \qquad \text{and} \qquad (15)$$

$$F_p = \frac{1}{\sqrt{1 + \left(\frac{\overline{U}_1}{\overline{U}}\right)^2\left[\frac{\overline{u^2}}{\overline{U}_1^2} - \frac{1}{2}\left(\frac{\overline{u_{ii}^2}}{\overline{U}_1^2}\right) + \left(\frac{\overline{u_n^2}_s}{\overline{U}_1^2}\right) + 2\left(\frac{\overline{v_s^2} - \overline{v^2}}{U_1^2}\right)\right]}} \qquad (16)$$

where $\overline{U}_1$ is the free-stream velocity. A=1 and B=1.5 have been substituted.

Values of this function are given in Table 1 for Stations 9 and 11. Figure 5 shows a plot of the corrected values of the mean velocity for Station 11 to indicate the comparison between hot-wire and pressure probe measurements.

6. Discussion

Subsequent to the development of the corrections indicated, Hinze [3] on pages 109 and 110 develops a relatively complex correction for the longitudinal turbulence intensity as measured by a constant temperature anemometer using a linearizing circuit. The interesting effect which this produces is a reduction from the measured intensity. The correcting function due to the instantaneous reversals of velocity as developed in Section 3 shows an increase from the measured intensity. There is thus a tendency for these two effects to cancel each other. Unfortunately, the terms in the "amplifier" correction proposed by Hinze are not readily evaluated in a shear flow, so it is not known whether the intensity, $u/\bar{U}$, is larger or smaller than that shown by the measured value.

The mean velocity correction for hot-wire measurements is quite small as may be seen in Table 1. F_h is thus not particularly sensitive to turbulence intensity variation from the measured values. Even so, it is probable that the hot-wire mean velocities are somewhat overcorrected.

A careful look at the results shown in Table 1 suggests that the pitot tube data are also somewhat overcorrected. Study of equations (14) and (16) seems to leave only the adjustable constant B available for changing the corrections. To reduce the correction requires an increase in B from the estimated value of 1.5. Fortunately, the necessary increase does not appear to be very great, otherwise there would be disagreement with the published figures of 1.2 and 1.5 obtained by Hinze, although he also indicates that higher values of B are possible.

For people working primarily in hydraulic flows there continues to be a need to obtain fairly reliable data on turbulence intensities since these enter into the calculation of the probe corrections. Becker and Brown [4] have indicated some success in making these measurements and it is to be hoped that this activity will be pursued.

7. Acknowledgments

The author gratefully acknowledges the assistance which he has received from the Naval Ship Research and Development Center, Washington, D. C. 20007 in conducting this research. The assistance of Mr. John L. Power and Mr. Edwin P. Rood is especially acknowledged.

8. References

[1] Scottron, V.E., Turbulent Boundary Layer Characteristics over a Rough Surface in an Adverse Pressure Gradient, Naval Ship Research and Development Center Report, 2659, (1967).

[2] Lin, J.D., Scottron, V.E., Soong, H.K., Friction Effects on Spatially Varied Open Channel Flows with Increasing Discharge, Am. Soc. of Civil Engrs., Waterways Division, (Aug. 1976).

[3] Hinze, J.D., Turbulence, 2nd Ed., McGraw-Hill Book Co. (1975).

[4] Becker, H.A. and Brown, A.P.G., Response of Pitot Probes in Turbulent Streams, J. Fluid Mech., 62, 85 (1974).

[5] Hinze, J.P., Turbulence, McGraw-Hill Book Co. (1959).

[6] Toomre, A., The Effect of Turbulence on Static Pressure Measurements, Aero. Research Council, England, F.M. 2972 (June 1960).

[7] Siao, T-T., Correction for Mean-Velocity and Turbulence Measurements for High Turbulence Levels, Scientia Sinica, Vol. VIII, No. 12, p. 1558 (1959).

[8] Strasberg, M., Measurements of the Fluctuating Static and Total-Head Pressures in a Turbulent Wake, David Taylor Model Basin Report 1779, (Dec. 1963).

[9] Smith, A.M.O., and Murphy, J.S., Micromanometer for Measuring Boundary Layer Profiles, Rev. of Scientific Instruments, 26, 8 (Aug. 1955).

[10] Goldstein, S., A Note on the Measurement of Total-Head and Static Pressure in a Turbulent Stream, Proc. Roy. Society, London, A Vol. CLV, p. 570 (1936).

[11] Fage, A., On the Static Pressure in a Fully Developed Turbulent Flow, Proc. Roy. Society, London, A Vol. CLV, p. 576 (1936).

[12] Siddon, Th.E., On the Response of Pressure Measuring Instrumentation in Unsteady Flow, Inst. Aero. Studies, Univ. Toronto, UTIAS Rep. No. 136 (1969).

[13] DeHaan, R.E., Design of a Probe Microphone, App. Sci. Res., 22, 306 (1970).

[14] Bradshaw, P. and Goodman, D.G., The Effect of Turbulence on Static-Pressure Tubes, Aero. Res. Council, London, R. and M. No. 3527 (1966).

[15] Schubauer, G.B., and Klebanoff, P.S., Investigation of Separation of the Turbulent Boundary Layer, Nat. Adv. Comm. for Aero., Report 1030 (1951).

TABLE 1

Comparison of Hot-Wire and Pitot-Tube Corrections

Station 9

	Corrected	Hot-Wire		Pitot-Tube		$\Delta\overline{U}/\overline{U}_1$
y'	$u/\overline{U}$	F_h	$\overline{U}/\overline{U}_1$	F_p	$\overline{U}/\overline{U}_1$	%
0.130	0.626	0.925	0.151	0.710	0.156	+ 3.3
0.160	0.573	0.945	0.171	0.750	0.171	0.0
0.205	0.565	0.948	0.189	0.779	0.190	+ 0.5
0.250	0.515	0.958	0.212	0.809	0.210	- 0.9
0.325	0.503	0.960	0.232	0.829	0.232	0.0
0.400	0.484	0.965	0.262	0.854	0.258	- 1.5
0.550	0.416	0.976	0.306	0.883	0.295	- 3.6
0.700	0.366	0.980	0.352	0.906	0.340	- 3.4
1.000	0.326	0.984	0.416	0.931	0.410	- 1.4
1.300	0.280	0.987	0.486	0.948	0.488	+ 0.4
1.600	0.239	0.990	0.556	0.965	0.561	+ 0.9
1.900	0.208	0.992	0.615	0.977	0.637	+ 3.6
2.200	0.165	0.994	0.708	0.987	0.708	0.0
2.650	0.122	0.997	0.821	0.993	0.785	- 4.4
3.100	0.085	0.998	0.904	0.997	0.892	- 1.3
3.550	0.052	0.999	0.942	0.999	0.951	+ 1.0
4.000	0.027	1.000	0.984	1.000	0.984	0.0

Station 11

0.130	0.386	0.982	0.111	0.792	0.113	+ 1.8
0.160	0.412	0.978	0.114	0.784	0.107	- 6.1
0.205	0.441	0.974	0.117	0.781	0.112	- 4.3
0.250	0.457	0.971	0.123	0.791	0.118	- 4.1
0.325	0.512	0.957	0.122	0.778	0.119	- 2.5
0.400	0.470	0.968	0.136	0.805	0.129	- 5.1
0.550	0.474	0.967	0.150	0.817	0.145	- 3.3
0.700	0.540	0.950	0.154	0.801	0.152	- 1.3
1.000	0.467	0.965	0.190	0.828	0.180	- 5.3
1.300	0.495	0.958	0.209	0.829	0.207	- 1.0
1.600	0.470	0.961	0.236	0.831	0.230	- 2.5
1.900	0.450	0.964	0.272	0.851	0.270	- 0.7
2.200	0.446	0.963	0.308	0.869	0.307	- 0.3
2.650	0.373	0.974	0.384	0.901	0.372	- 3.1
3.100	0.335	0.978	0.448	0.930	0.446	- 0.4
3.550	0.286	0.983	0.512	0.946	0.518	+ 1.2
4.000	0.247	0.987	0.593	0.960	0.594	+ 0.2
4.600	0.195	0.991	0.701	0.979	0.697	- 0.6
5.100	0.149	0.994	0.798	0.988	0.793	- 0.6
5.600	0.121	0.996	0.855	0.995	0.855	0.0

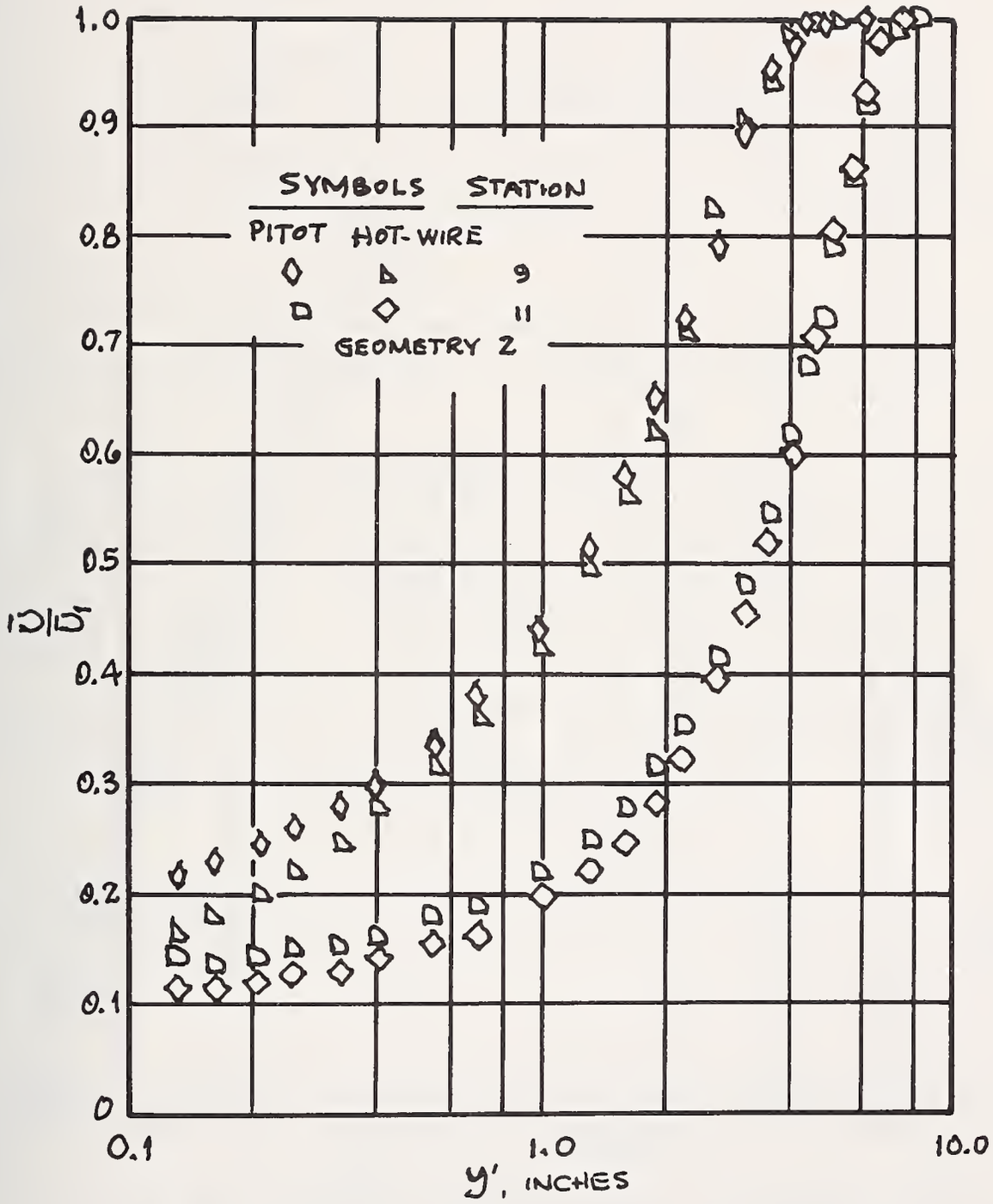

FIGURE 1 - HOT-WIRE AND PITOT TUBE MEAN VELOCITIES

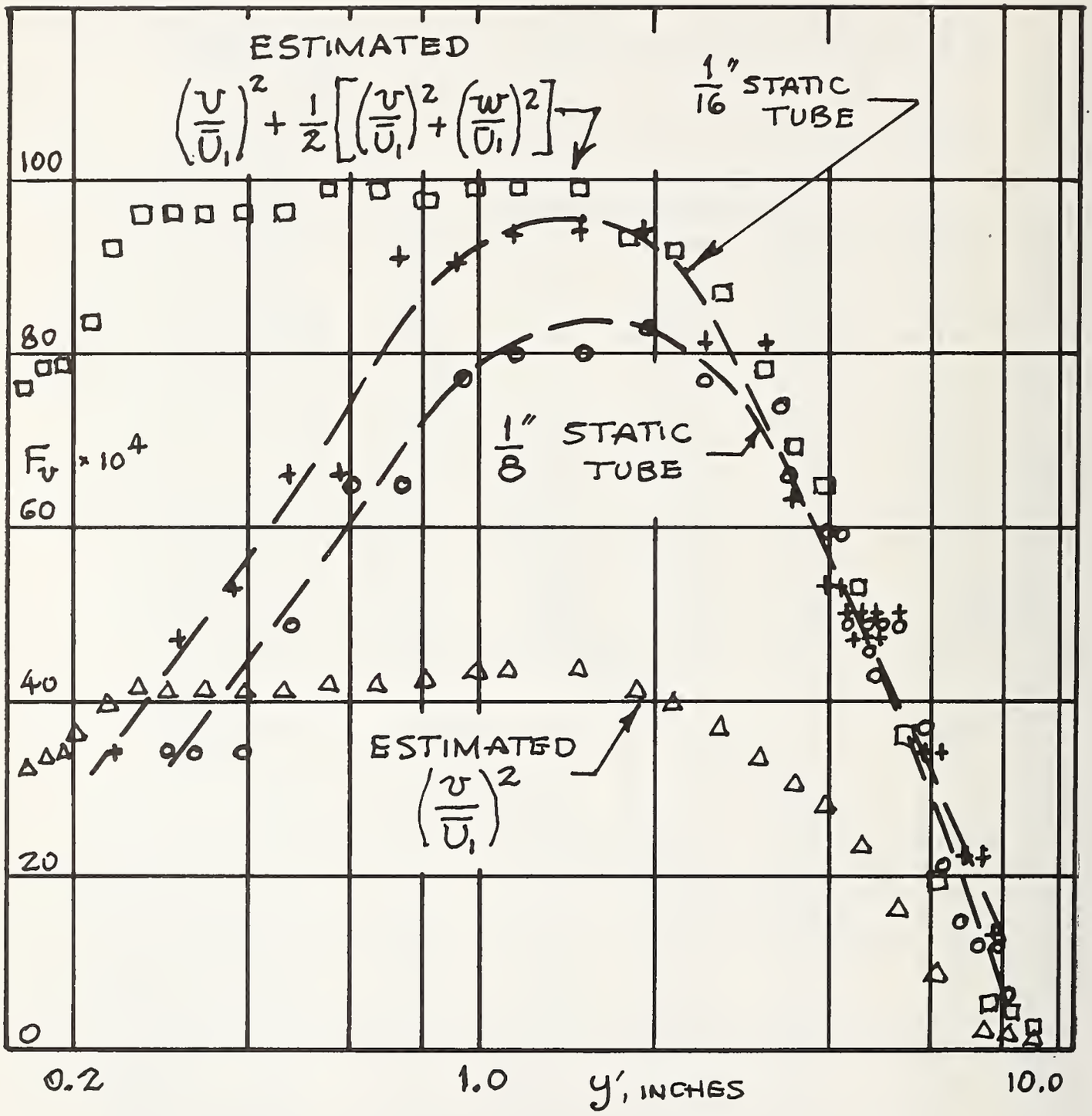

FIGURE 2 - PRESSURE GRADIENT 4, STATION 9
STATIC PRESSURE VARIATION

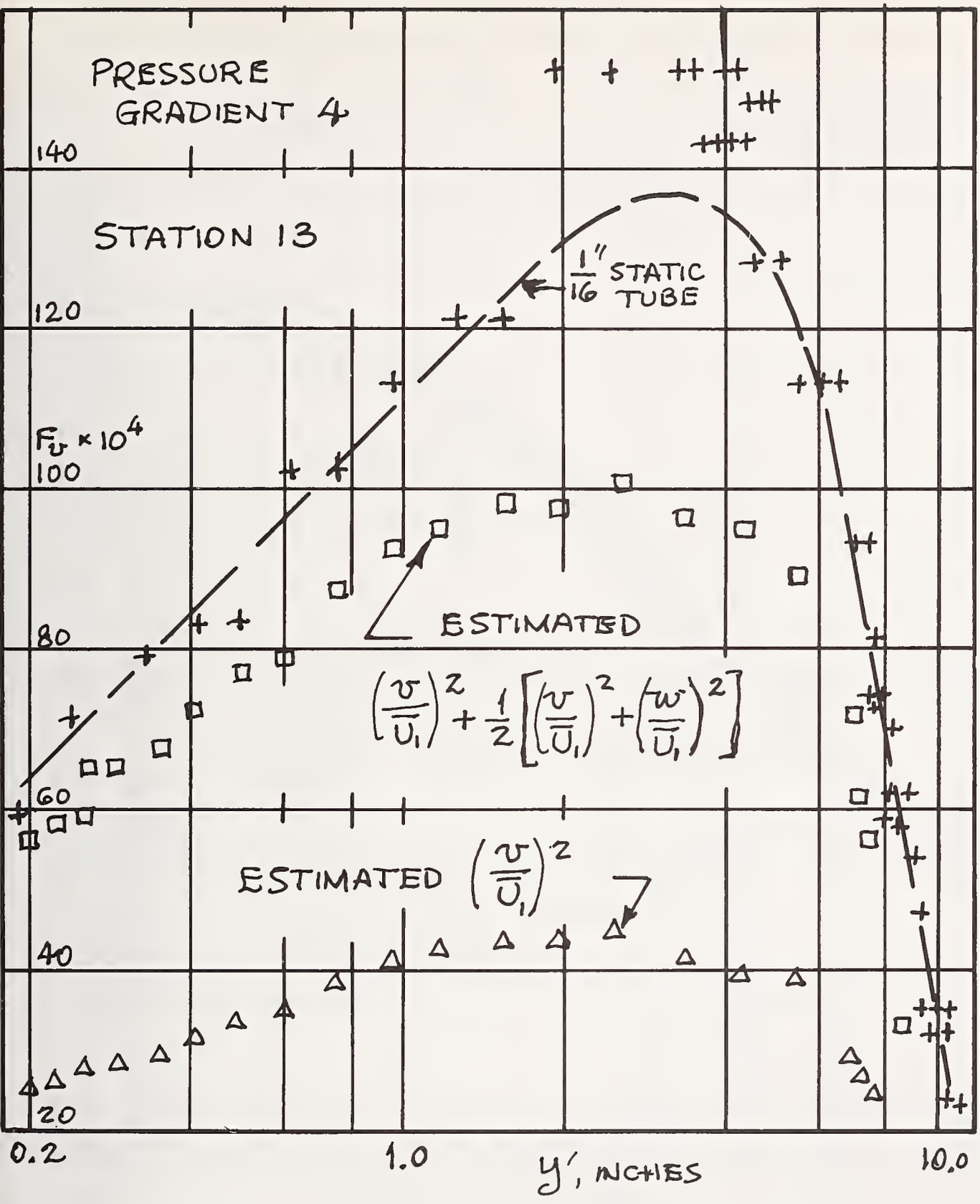

FIGURE 3 · PRESSURE GRADIENT 4, STATION 13
STATIC PRESSURE VARIATION

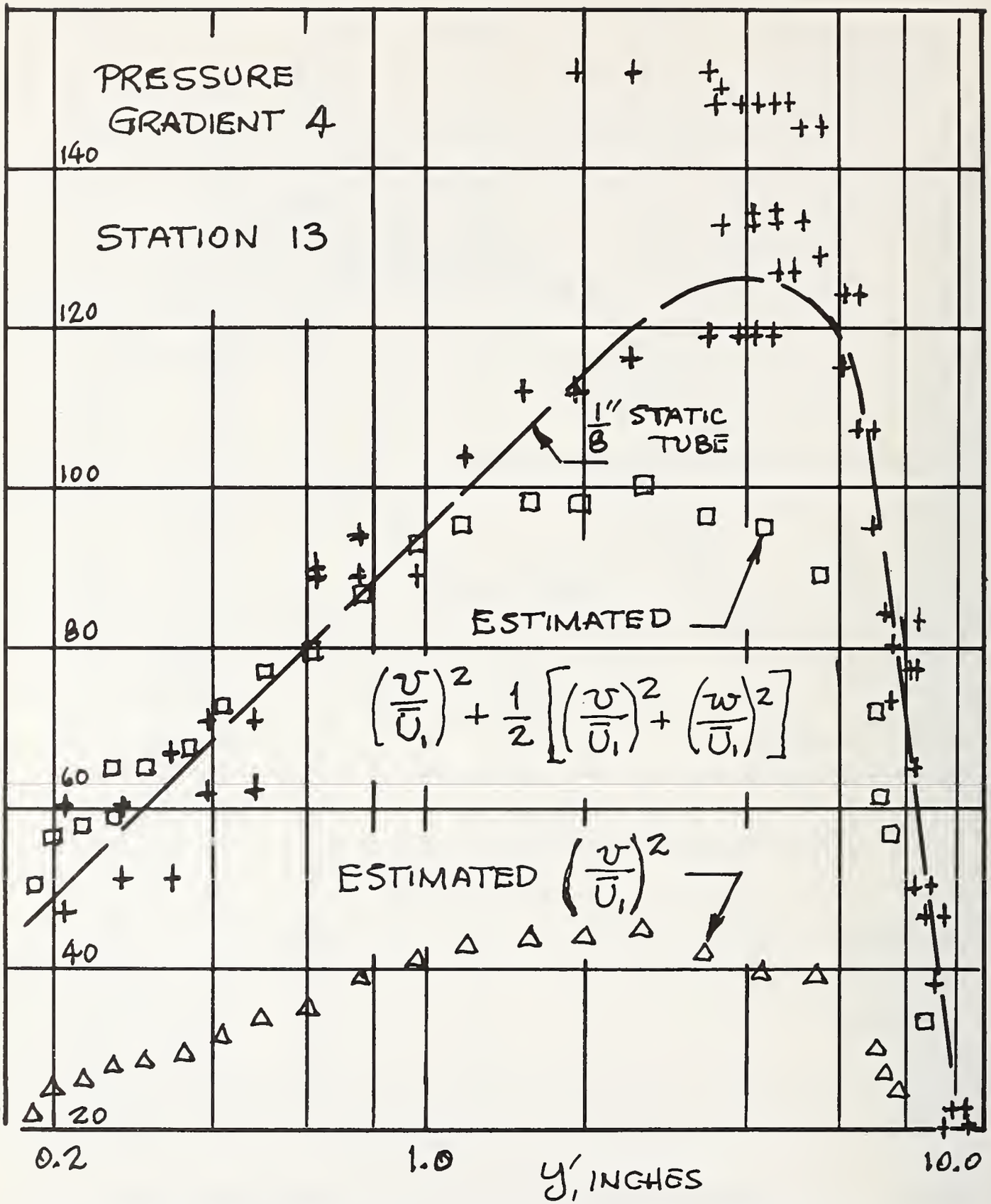

FIGURE 4 - PRESSURE GRADIENT 4, STATION 13
STATIC PRESSURE VARIATION

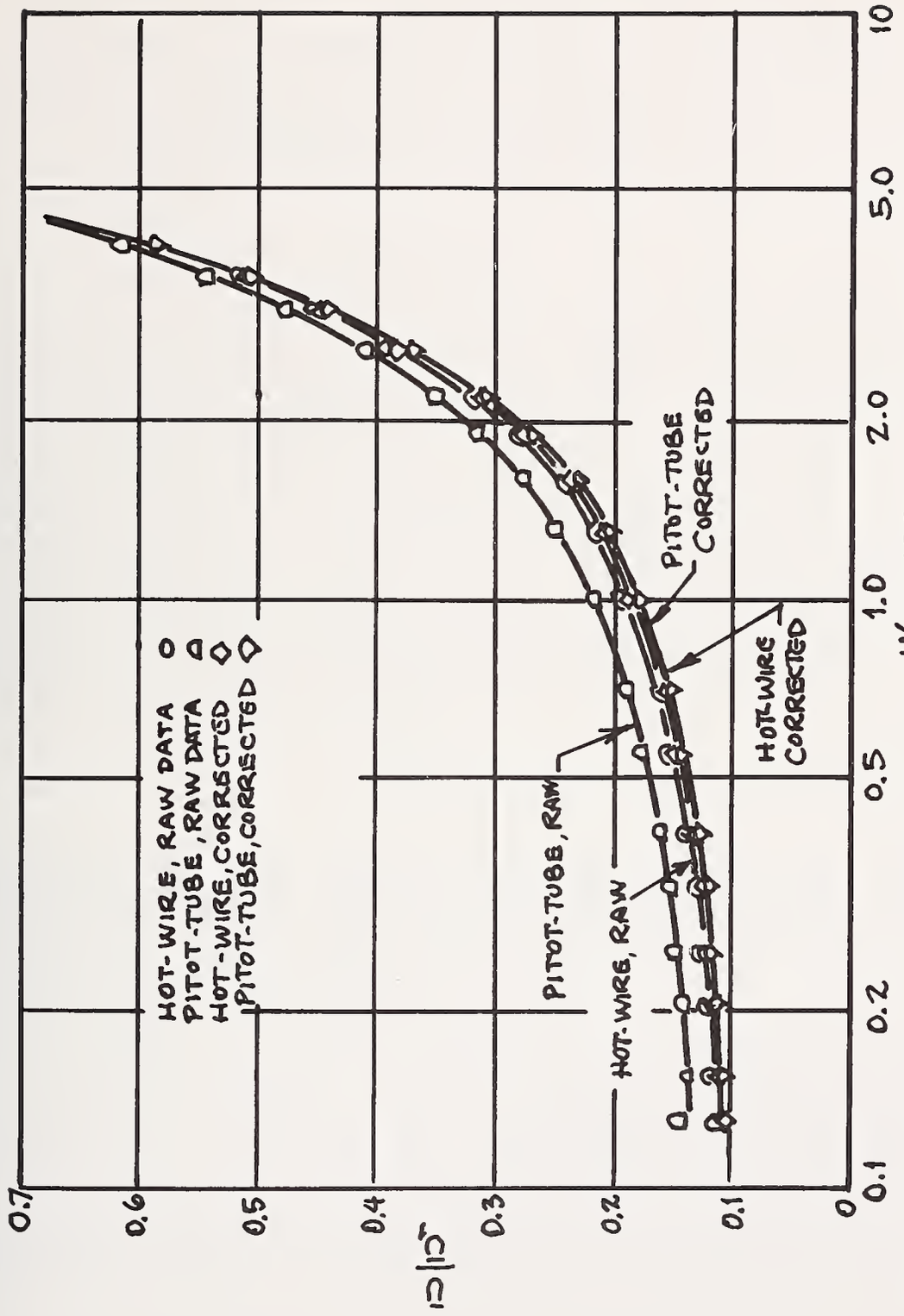

FIGURE 5. PRESSURE GRADIENT 2, STATION 11

National Bureau of Standards Special Publication 484, Proceedings of the Symposium on Flow in Open Channels and Closed Conduits held at NBS, Gaithersburg, MD, February 23-25, 1977. (Issued October 1977)

DETERMINATION AND ELIMINATION OF ERRORS IN VELOCITY READINGS AT VENTILATION TUBING INLETS

Robert A. Haney

Mining Enforcement and Safety Administration
Pittsburgh, Pennsylvania

1. Abstract

Accurate air velocity measurements have been obtained by applying a methods factor to vane anemometer readings at the inlet of an exhaust tubing installation. Methods factors were determined by comparing simultaneous 4-inch rotating vane anemometer readings at the centerline of the tubing inlet to a Pitot-static tube traverse of the duct. Test velocities ranged from approximately 600 to 8,600 fpm. Methods factors were independent of velocity but dependent on tubing diameter and tubing entrance configurations. For straight unflanged tubing, the methods factors for 12-, 14-, 16-, 18-, and 20-inch diameter rigid tubing and 24-inch diameter spiral reinforced tubing were 0.69, 0.68, 0.66, 0.74, 0.75 and 0.72, respectively.

2. Introduction

Underground coal mine ventilation networks consist of a primary ventilation system and a secondary or face ventilation system. The primary ventilation system delivers fresh air to the last open crosscut of each working section and the face ventilation system moves the air from the last open crosscut to the working faces.

Primary airflow or main mine ventilation is induced by fans ranging from 4 to 10 feet in diameter. Separate intake and return openings to the surface are required. Main fans are installed on the surface and generally exhaust air from the return openings. Multiple intake and return openings with multiple fans are common in modern coal mines. Fan capacities of 200,000 to 500,000 cfm are common, and the total air volume in a ventilation system may reach a million cfm. Fans generally operate at 4 to 8 inches of water gage.

Air entering the mine is directed to the working places through the use of stoppings or walls built in the crosscuts that separate the intake and return airways. In this manner, the entire mine entry is utilized as an air duct. Mine entries are typically 3 to 7 feet high and 15 to 20 feet wide. Because of the great distance the air must travel, leakage or airflow from intake to return before it reaches the working face is usually high. Generally less than 50 percent of the air that enters the mine eventually reaches the last open crosscuts.

Statutory provisions of Public Law 91-173, the Federal Coal Mine Health and Safety Act of 1969 require that:

> the minimum quantity of air reaching the last open crosscut in any pair or set of developing entries and the last open crosscut in any pair or set of rooms shall be nine thousand cubic feet a minute, and the minimum quantity of air reaching the intake end of a pillar line shall be nine thousand cubic feet a minute. The minimum quantity of air in any coal mine reaching each working face shall be three thousand cubic feet a minute.

In addition, Title 30, Code of Federal Regulations, Part 75.301-4 requires that except where blowing face ventilation is used ".... the minimum mean entry air velocity shall be 60 feet a minute..." In order to determine compliance with these standards, air velocity and air quantity measurements must be taken by mine officials and mine inspectors.

Face ventilation which is an extension of the primary ventilation can be either an exhaust or blow system. However, since good exhaust ventilation is currently the best means to control air borne dust in the face area, most coal mines utilize the exhaust method of face ventilation.

Air is carried from the last open crosscut to the face by either a line brattice or an auxiliary fan and tubing system. Line brattice is a jute or plastic material extending from the last open crosscut to the face and separates the face entry into an intake and return side. As the working face advances, the face ventilation system also advances. Federal regulations require the face ventilation system to be maintained not greater than ten feet from the point of deepest penetration of the face.

In auxiliary fan installations, a fan is placed in the last open crosscut and is used to induce airflow through tubing that has been extended into the face area.

While fan and tubing systems can be designed to provide sufficient airflow in the face area, circumstances may occur which would result in an insufficient air quantity in the face area. Lumps of coal or debris in the fan inlet could restrict the fan airflow. Cracks or holes in the tubing could short circuit air from the face, or the fan and tubing system may be improperly designed and may not be capable of delivering sufficient air volume to the working face.

The measurement of air quantities in underground auxiliary ventilation tubing is necessary to determine the air volume being delivered through the tubing and to assure that fan and tubing systems are performing properly. The standard method of air quantity determination employs a Pitot-static tube traverse of the ventilation duct to determine the average air velocity through the duct. This technique is time-consuming and the required instrumentation is cumbersome to handle and transport underground. A Pitot-static tube traverse and the resulting calculations may take as long

as 20 to 30 minutes where as a single vane anemometer reading and calculations can be made in less than 2 minutes. While standard rotating vane anemometers are commonly used to determine air velocities in mine entries, they have not been used to determine air velocities at the inlet of auxiliary tubing because tubing entrance configurations and tubing diameters create conditions that give anemometer readings other than true air velocities.

While ventilation tubing diameter varies with the requirements of individual mines, the tubing inlet configuration is generally a straight unflanged or unbelled opening. It was, therefore, desirable to know what factor should be applied to a centerline 4-inch rotating vane anemometer reading at the inlet of different sized tubing with a straight inlet so that the actual air velocity in the tubing could be determined.

3. Testing Procedure

The testing procedure adopted was one which would allow centerline anemometer readings to be taken at the duct inlet while Pitot-static tube traverse readings are being taken in the duct itself. Approximately 50 feet of tubing was used for each test setup. Airflow during the study was induced by an axial flow fan. A 16- by 18-mesh screen straightener was inserted 10 feet downstream of the tubing inlet and perpendicular to the direction of airflow. This reduced the turbulence and established a more uniform velocity profile at the point of the Pitot-static tube traverse, five diameters downstream from the straightener. An illustration of the general test setup is shown in figure 1.

During the tests, the tubing was supported approximately 8 inches off the ground on concrete blocks. The supports were maintained at least 4 feet away from the tubing inlet. No other obstructions or surfaces were near the tubing inlet.

Because air velocities at the tubing inlet were often above the range of the standard 4-inch 8-vane anemometers, 4-inch 4-vane high speed anemometers were used. While running tests with these anemometers, care was taken to avoid placing the anemometer in an air velocity that was above the range of the instrument thus preventing damage to the instrument.

Anemometer readings were taken at the centerline of the tubing inlet. To avoid damage, the anemometer was moved slowly into the airstream. The anemometer was supported on a 5/16-inch diameter rod that was 2 feet long, and, except for starting and stopping the instrument, the operator's hands were out of the airstream. The rod was physically held against the duct so the inlet plane of the duct approximately bisected the anemometer frame. This method of positioning the anemometer permitted little or no movement of the instrument during the tests and was easily repeated. Since no simple and compact attachment could be devised to positively centralize the anemometer in all sizes of the duct it was decided that the axial position would be estimated by the aid of a scale located on the rod. Effects due to positioning or variation of the instrument are included in the experimental error. The actual air velocity in the duct was determined by a 20-point Pitot-static tube traverse (four readings at right angles at the centroid of each of five equal area concentric circles). Figure 2 illustrates the technique adopted at both the inlet of the duct and the Pitot-static tube traverse location.

FIGURE 1. - GENERAL TEST SETUP.

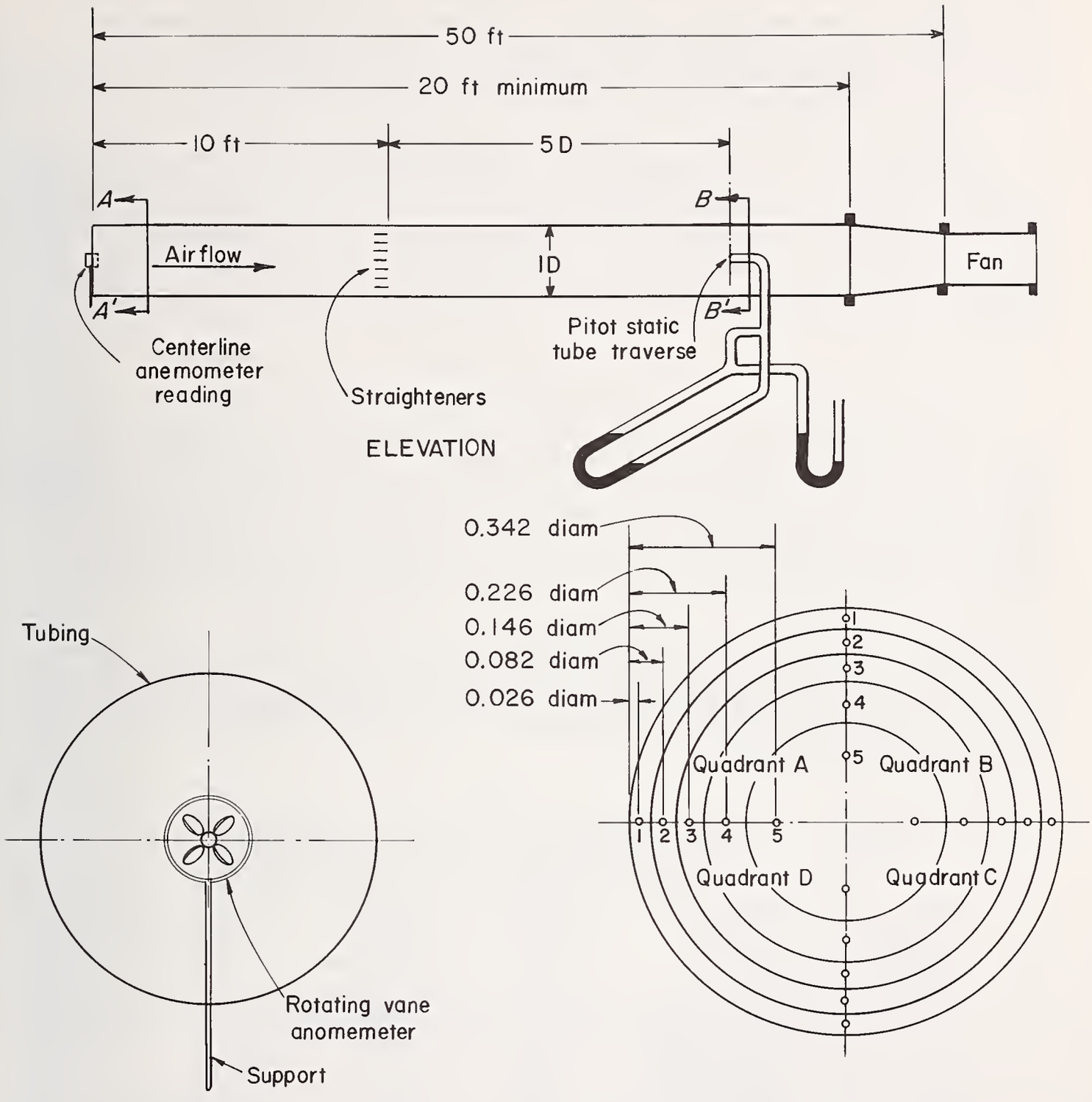

FIGURE 2. AIR VELOCITY MEASUREMENTS AT THE TUBING INLET AND INSIDE THE TUBING.

Tubing sizes used in this investigation were 12-, 14-, and 16-inch polyvinyl chloride (PVC); 18- and 20-inch fiber glass; and 24-inch spiral reinforced tubing. For each tubing size, three to five velocity levels were tested. At each velocity level, five groups of readings were taken. Each group consisted of five 1-minute anemometer readings and a concurrent Pitot-static tube velocity traverse of the duct. Indicated anemometer readings were corrected by application of a calibration curve and Pitot-static tube readings were corrected to ambient air density. In all, approximate 160 tests were made over a velocity range of 600 to 8,600 fpm.

Recognizing that inlet configurations could be critical in establishing a methods factor, several additional tests were performed to determine the effect of changes in inlet configuration. For this series of tests, readings were taken with a 1-1/2-inch wide flange attached to the entrance of a 14-inch diameter duct. Readings were taken at the inlet with a rotating vane anemometer and inside the duct with a Pitot-static tube as in the other tests.

4. Test Results

The methods factor to be applied to field anemometer readings was obtained by taking the ratio of the average velocity in the duct as determined from the 20-point Pitot-static tube traverse to the average of the corrected anemometer readings concurrently taken at the centerline of the duct inlet. By examination of figure 3, it was found that the methods factor showed little, if any, dependence on velocity for a given tubing size; however, the factor did change as the diameter of the tubing changed.

Table 1 gives the average methods factors determined for each size of tubing for high speed anemometers. The table also shows the range of velocities and the standard deviation from the average methods factor for each set of tests. The average methods factor ranged from 0.66 to 0.75 for the high speed anemometers.

TABLE 1. - Methods factors for centerline anemometer readings at the inlet to exhaust tubing

Tubing diameter, inches	Velocity range, ft/min	Average methods factor	Standard deviation	Type of tubing
HIGH SPEED 4-INCH, 4-VANE ANEMOMETER				
12	1,000-4,300	0.69	±0.01	PVC
14	1,000-8,600	.68	±.02	PVC
16	1,100-6,900	.66	±.03	PVC
18	1,200-5,000	.74	±.03	Fiber glass
20	1,000-4,400	.75	±.04	Fiber glass
24	600-1,800	.72	±.07	Spiral reinforced

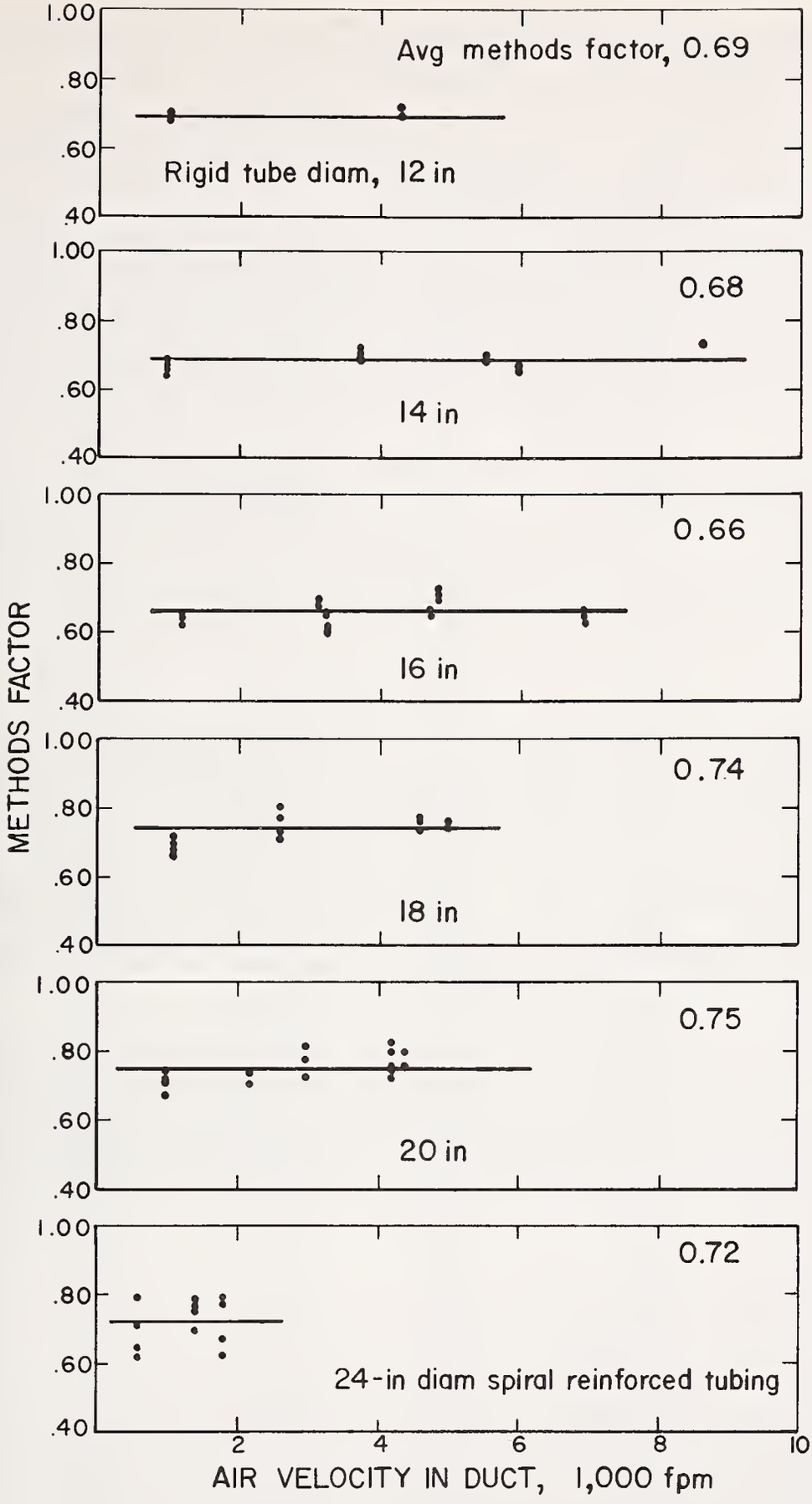

FIGURE 3. METHODS FACTORS VERSUS AIR VELOCITY FOR VARIOUS DIAMETER TUBING.

The largest standard deviations occurred during the tests where the velocities in the tubing were the lowest. This corresponds to the velocity range where Pitot-static tube readings are the least accurate. At higher velocities, the largest standard deviation was ±0.04, corresponding to ±5 percent of the mean. This indicates very little fluctuation in the methods factor and a high degree of confidence in the average methods factor.

Table 2 gives a compilation of the air quantity that would be present for various anemometer readings at the inlet of different diameter tubing. In each case, the methods factor is applied to the corrected anemometer reading and the air quantity is computed from the formula: air quantity (cfm) equals corrected anemometer reading (fpm) times methods factor times area (ft^2). This table is compiled to reduce field calculations.

When a 1-1/2-inch flange was attached to the inlet of the 14-inch tubing, the methods factor for velocities between 4,000 and 6,000 were determined to be 0.80 with a standard deviation of ±0.02, as opposed to the unflanged inlet system having a methods factor of 0.68 for similar velocities. This shows that any change in the inlet configuration of the duct system may change the established methods factors.

5. Conclusions

For routine air measurements in exhaust auxiliary mine ventilation systems, a methods factor dependent on tubing diameter can be applied to centerline 4-inch rotating vane anemometer readings at the tubing inlet to determine the air velocity through the tubing. Accuracy of ±10 percent is easily obtained by this method. If a higher degree of accuracy is desired, air velocity measurements should be made using a Pitot-static tube traverse.

While the methods factors showed a dependence on tubing diameter, they showed little, if any, dependence on air velocity.

The factors determined by this investigation and shown in table 1 apply only to readings taken at the inlet of a straight unflanged duct. These factors should not be used when other inlet configurations exist as tests have shown that the addition of a 1-1/2-inch wide flange at the inlet of 14-inch diameter tubing increases the factor from 0.69 to 0.80.

TABLE 2. - Air quantity for vane anemometer readings at the inlet of different diameter tubing (extrapolated to 10,000 fpm)

(Air quantity = corrected anemometer reading x methods factor x area)

Corrected anemometer reading, fpm	Air quantity--cfm					
	Tubing diameter, inches					
	12	14	16	18	20	24
	Methods factor					
	0.69	0.68	0.66	0.74	0.75	0.72
1,000	540	730	920	1,310	1,640	2,260
1,200	650	870	1,110	1,570	1,960	2,710
1,400	760	1,020	1,290	1,830	2,290	3,170
1,600	870	1,160	1,470	2,090	2,620	3,620
1,800	980	1,310	1,660	2,350	2,950	4,070
2,000	1,080	1,450	1,840	2,620	3,270	4,520
2,200	1,190	1,600	2,030	2,880	3,600	4,980
2,400	1,300	1,740	2,210	3,140	3,930	5,430
2,600	1,410	1,890	2,400	3,400	4,250	5,880
2,800	1,520	2,040	2,580	3,660	4,580	6,330
3,000	1,630	2,180	2,760	3,920	4,910	6,790
3,200	1,730	2,330	2,950	4,180	5,240	7,240
3,400	1,840	2,470	3,130	4,450	5,560	7,690
3,600	1,950	2,620	3,320	4,710	5,890	8,140
3,800	2,060	2,760	3,500	4,970	6,220	8,600
4,000	2,170	2,910	3,690	5,230	6,550	9,050
4,200	2,280	3,050	3,870	5,490	6,870	9,500
4,400	2,380	3,200	4,050	5,750	7,200	9,950
4,600	2,490	3,340	4,240	6,010	7,530	10,400
4,800	2,600	3,490	4,420	6,280	7,860	10,860
5,000	2,710	3,630	4,610	6,540	8,180	11,310
5,200	2,820	3,780	4,790	6,800	8,510	11,760
5,400	2,930	3,930	4,980	7,060	8,840	12,210
5,600	3,030	4,070	5,160	7,320	9,160	12,670
5,800	3,140	4,220	5,340	7,580	9,490	13,120
6,000	3,250	4,360	5,530	7,850	9,820	13,570
6,200	3,360	4,510	5,710	8,110	10,150	14,020
6,400	3,470	4,650	5,900	8,370	10,470	14,480
6,600	3,580	4,800	6,080	8,630	10,800	14,930
6,800	3,690	4,940	6,270	8,890	11,130	15,380
7,000	3,790	5,090	6,450	9,150	11,460	15,830
7,200	3,900	5,230	6,630	9,410	11,780	16,290
7,400	4,010	5,380	6,820	9,680	12,110	16,740
7,600	4,120	5,520	7,000	9,940	12,440	17,190
7,800	4,230	5,670	7,190	10,200	12,760	17,640
8,000	4,340	5,820	7,370	10,460	13,090	18,100
8,200	4,440	5,960	7,560	10,720	13,420	18,550
8,400	4,550	6,110	7,740	10,980	13,750	19,000
8,600	4,660	6,250	7,920	11,250	14,070	19,450
8,800	4,770	6,400	8,110	11,510	14,400	19,910
9,000	4,880	6,540	8,290	11,770	14,730	20,360
9,200	4,990	6,690	8,480	12,030	15,060	20,810
9,400	5,090	6,830	8,660	12,290	15,380	21,260
9,600	5,200	6,980	8,850	12,550	15,710	21,710
9,800	5,310	7,120	9,030	12,810	16,040	22,170
10,000	5,420	7,270	9,210	13,080	16,370	22,620

National Bureau of Standards Special Publication 484, Proceedings of the Symposium on Flow in Open Channels and Closed Conduits held at NBS, Gaithersburg, MD, February 23-25, 1977. (Issued October 1977)

INDIRECT TWO-PHASE FLOW MEASUREMENT: ANALYSIS AND REDUCTION OF METHODS ERRORS

N. N. Kondic
Industrial Systems Engineering
University of South Florida
Tampa, Florida 33620

- Abstract -

Flow measurement is systems characterized by adverse features (high temperature and/or pressure, aggressive fluids, chemically reacting materials, vibrations, etc.) often require the application of indirect methods. Although more complex, due to instrumentation and data processing involved, such methods sometimes offer an additional advantage, when they are devised to be contactless (i.e. when pick-up probes and similar flow-field disturbing elements are eliminated). This family of methods introduces either tracers (chemical, radioactive, colorimetric, etc.) within the flow, or wave-transmitting and receiving devices (sound, ultra-sound, photons of various wavelength). Tracer concentration and wave-field characteristics (energy, flux) are functionally dependent on the characteristics of the original flow-field (velocity, gas fraction, particle concentration, etc.). This functional dependence, i.e. its accuracy (which depends on the assumptions and approximation in the mathematical analysis of all phenomena involved) is an important component of the overall method's accuracy. In addition, statistical fluctuations within the basic flow-field (turbulent in most practical cases) are generally independent of statistical fluctuations which are often inherent with the measurement method employed: fluctuations of tracer density or of the radioactive decay rate or other wave-source intensity variations. An appropriate analysis of these sources of errors-- which are different from the usually listed errors when direct-reporting instrumentation is being utilized -- can give an assessment of their magnitudes and indicate approaches to reduce them, including experimental procedures and data analysis improvements.

1. Introduction

In elementary, straightforward measurements, a strictly defined function correlates the basic measured property (e.g. temperature) and the registered one (length of mercury column); in this case the function is linear, expressing proportionality. Fluctuating temperature, use of thermocouples or pyrometers etc. introduce the need for a phenomenological-mathematical analysis to obtain the correlation between the basic and the measured property (magnitude).

In turbulent two-phase flows, which are inherently fluctuating, the phases' concentration and/or temperature represent important measurement goals in various disciplines of applied sciences, especially in thermal (power) engineering, the chemical industry and bio-medical applications. The measurement task is much more involved when it is necessary to meet the requirement of using exclusively external (contactless) devices to determine the properties of a turbulent multiphase system. Such experimental approaches exclude insertion of any sensors ("pick-up") into the fluid, to prevent the possibility of a chemical or flow-desturbing interaction between the inserted device and the fluid. Also, in numerous systems, any addition of tracers is strictly forbidden. The measurement problems already encountered, caused by these restrictions, become extremely complex when the measurement objectives are the local values of properties, i.e. their spatial distribution within the system, which can be in the shape of a 2- or 3-dimensional field.

This report deals with two-phase flow concentration (defined conventionally as the mass- or volume ratio of the denser phase or component to the total mass or volume) as the measured property, but the general considerations can be applied to others (e.g. temperature). A comparative analysis as well as experience proves that with an increased complexity of measurement methods the errors are augmented in two ways; new causes of errors appear and the quantitative effect of old and new errors increase.

2. Literature survey

Since the time when radiation-attenuation usage for determination of the average void fraction along a beam started, the geometry related source of errors has been noticed and assessed, first in a simplified way, /1/. This source of errors, pertaining to the two-phase system pattern (i.e. arrangement of phases) was later statistically treated, analytically in /2/ and analytically-experimentally in /3/ and /4/ . Nearly in the same time, a different approach to resolve the same problem analyzed the effects of shape, size and relative position of bubbles (voids) along the radiation beam. This was reported in /5/, /6/ and /7/. The results emerging from Ref's /2/ through /7/ help enhance the accuracy of line-average void fraction measurements and they point out to the researcher how to design and better tuilize an experimental facility and the data it renders.

As the next step, two advanced, more recent methods, able to measure indirectly local values in any system where a 2- or 3-dimensional concentration field exists, are reported in /8/, /9/ and /10/. These methods employ gamma (or X-ray) sources and detectors (standard commercial equipment), all of them located externally, i.e. at the outer side of boundaries which enclose a 2-phase system. Three unique characteristics of electro-megnetic radiation are utilized; (a) its exponential attenuation along the propagation path, (b) initiating of secondary radiation "sources" along the primary beam due to scattering, and (c) the dependence of the scattered photons' energy and radiation absorption coefficient on the scattering angle. Fluctuations inherent with radioactive (and some other) sources of penetrating radiation are treated in /11/, while statistical fluctuations of turbulent flows are extensively dealt with in /12/ and /13/. The dynamics of multiphase systems and those with flowing suspensions are subjects of /14/ and /15/, while for useful probabilistic criteria and statistical formulae /16/ was used.

3. Components of indirect methods' errors

Mathematical derivations of functions which correlate registered signals with concentration values are based on true, i.e. representative values of magnitudes involved (pertaining to steady state), such as radiation source intensity, fluid velocity, concentration, detector efficiency etc. For sake of brevity, this report will not elaborate on the so-called standard sources of errors (individual, instrumental, systematic, external -- such as mechanical vibrations, supply voltage or pressure variations --etc.) and will focus on the specific family of methods' errors. The following analysis will be performed in regard to the most complex of the methods listed, described in /10/, and a special emphasis will be put on the influence of random fluctuations of various origin and character. The only assumption is that these random phenomena can be expressed in terms of statistical probability functions. This assumption is well supported by /11/ and /12/. The application of the analysis which follows to simpler methods involving similar phenomena in the measured and measuring system is straightforward.

Users of many indirect measurement methods, which are applied to systems with time-fluctuating properties should be cautioned that simple (linear) time-averaging of registered signals within an interval of time "larger than the system's characteristic time" is generally far from a cure-all of the fluctuation-caused effects. This remark is true also in respect to systems without fluctuations in the wave-source of the measuring device, which can be closely achieved when light or (ultra-) sound is used. Only in very special cases can simple time-averaging properly compensate for the distortions due to random phenomena occuring during the measurement period. The first reason which supports this warning statement lies in the existence of a multitude of available averaging functions (linear, square, reciprocal, log etc.), thus, the best one has to be selected, if possible. The second reason, which can be considered as the dominant one, emerges from the closer analysis to follow. It pertains to a general situation represented by an example, illustrated by Fig 1 and explained by a condensed description of several phenomena occuring and thus enabling the method from /10/ to be successfully implemented on two-phase (even multiphase) systems. These phenomena are:

A. The source emits radiation in a random fashion, with which a probability function P_s can be associated. For some non-radioactive sources P_s is a uniform function in time, equal to 1 when normalized.

B. The photons emitted by the source traverse an average linear density (integral of density versus length) of atoms interacting with the oncoming radiation (photons) in the two-phase system. This integration is performed along Z_{si} from the inner system wall at the source side up to the beam-intersection point (subscript ip), defined as the location where the longitudinal axes of the source-collimator (z) and detector-collimator (y) intersect. Those two axes form an angle ranging between 0^o and 180^o, as shown in /9/ and /10/. This angle is 90^o on Fig. 2.

The time-fluctuations of the above defined length-average linear density are described by a probability function, P_{si}.

C. Analogous to B., a probability function P_{id} pertains to the average linear density along the path of scattered photons from the intersection point up to the inner wall of the system at the detector, i.e. along y-axis distance Y_{id}.

D. At the beam-intersection point, P_{ip} is the probability of scattering atoms presence. Normally, a finite volume exists physically there, and the intersection point is merely the center of that volume.

It should be noted that each of the three probabilities explained (P_{si}, P_{id}, P_{ip}) is a function -- with a good approximation a product -- of two sub-probabilities: P_{ph} (different in si, id and ip regions), which is mass-concentration related, i.e. pertains to the presence of denser phase (according to the convention adopted) in the respective region. The second probability is P_{sa} (which is practically equal for regions si and id, but generally different from the one at location ip), describing the chance of the presence of scattering atoms in the paths of arriving photons in the volumes considered (microscopically, the atoms density is not uniform, and, on the other hand, the arriving photon is hitting or missing a moving target). The three P_{sa} functions are also temperature-dependent, but they differ noticeably from uniformity (= 1 when normalized) only for weak radiation sources and/or when extremely narrow beams are utilized, when the equalizing effects of large numbers of events decrease.

E. The radiation detector efficiency is assumed constant, resulting in P_{de}= 1 (when normalized). This is because, as already mentioned, the instrumental and external sources of errors (mechanical vibrations, pressure and voltage fluctuations etc.) are disregarded here.

Taking in consideration the above listed probabilities, the following equation can be written. It describes what happens with any photon (gamma quant) to be generated by a spontaneously emitting radioactive source, which photon moves initially (prior to scattering) in a desired direction, which is axis z. The equation, as well as the analysis outlined, neglects the evaluation of straightforward calculable phenomena (which can be associated with fully uniform probabilities), such as radiation attenuation in system walls, scattering in surrounding air and present objects, as well as in the source - and detector hardware. All these probabilities are lumped in the term P_{lu} of the following equation, expressing the total resulting probability for the above defined photon to reach the detector:

$$P_{to} = (P_{lu})\,(P_s)\left[RA(P_c, Z_{si})\right](P_{si})\left[c_{rip}\,(Z_{si})\right](P_{ip})\left[RA(P_c, Y_{id})\right](P_{id}) \qquad (1)$$

$c_{rip}\,(Z_{si})$ is the simple time-averaged dimensionless (relative) concentration of the denser phase, i.e. matter at the intersection point. "Simple time-averaged value" means the one resulting from a direct, linear intergration in time. Any other average concentration can be (arbitrarily) defined and used, only then, the probability function P_{ip} and others have to be redefined, but all already said remains valid. RA are radiation attenuation functions (negative exponential), which include the radiation scattering and absorption coefficients k_o and k_1 and Z_{si}. The latter is the distance along z-axis from the inner wall surface at the radiation source along the initial beam up to the beam-intersection point. Y_{id} is analogous to Z_{si}, but along axis y. In the detailed mathematical expressions the power of the exponential attenuation functions (RA) contains also integrals with Z_{si} and Y_{id} as their upper limits, as well as the probability P_{ip} (as shown in section 4.3.) P_c is related to P_{ip} and explained in section 4. 2.

The described complex shape of functions within the expression for P_{to} renders it obvious that it is not possible to perform any simplified association, e.g. a multiplication of the probability functions involved. This rules out a simplistic forming of a joint product-probability function (in addition, the average product ≠ product of average factors). The listed probability functions are mathematically different due to their different physical origin; P_s is ruled by nuclear processes, next three P-functions with 2nd subscript ph are consequences of hydrodynamic phenomena; finally, the corresponding three P-functions with sa as the 2nd subscript depend on molecular mechanisms in fluids and are temperature dependent.

The given equation makes it clear that none of the time-averaged detector signals (i.e. using any function for the time-intergration cannot be equal to the true steady state signal, which is defined as follows: it would result from the simple time-averaged source intensity (flux), attenuated by the (simple) time-averaged concentration field, which is the measurement goal(simple time-averaging is equivalent to the steady state). The here formulated exclusion of direct averaged signals use is not a dead-end negative statement. On the contrary, the task is now clearly formulated. It is necessary to find (evaluate, derive, assess, etc.) all the probability functions playing the role (as described) in the detector reading, which reports the counting of events characterized by probability P_{to} (see equation). Once the probabilities involved are described (as analytical functions, graphs or tabulated data), the representative signal, emerging from measured data processed by these functions, can be further used. This is done by proper implementation of the representative signal as explained in the analysis /10/ of data interpretation and final results derivation, which are the local values of the concentration field. /10/ also explains the mathematical procedures to be performed with the values of representative detector readings.

Next chapter elaborates more closely on the analytical procedures necessary to implement in order to achieve the reduction of several among the five listed kinds of methods' errors.

4. Analysis to reduce indirect methods' errors.

4. 1. General

The contents of this chapter will concentrate on error sources listed under phenomena B, C, and D, in chapter 3. The corresponding probability functions needed for the concrete application of the analysis to follow have been at least partially explored in particular disciplines. To phenomenon A. corresponds probability P_s, which is the subject of numerous works dealing with nuclear physics, such as /11/, while P_{de} (related to phenomenon E.) is either constant or defined by detector design. P_{si}, P_{id} and P_{ip} are first of all inter-related functions, obeying the laws of constrained random statistical behavior /15/, /16/. Second, for many systems in practical application, tubulent fluctuations - which

are the ultimate physical cause of these functions, have been successfully measured and thoroughly analyzed: classical work /12/, further on /13/, /14/ and /15/, as well as a number of volumes of N.A.S.A. reports (especially between years 1940 and 1970) can serve as a valuable source of pertinent data.

Concerning the two sub-probabilities, P_{ph} (describing mass concentration, i.e. mixture density) and P_{sa} (describing atoms density fluctuations within the phases), the latter one will be considered constant and equal to one when normalized. This will result in $P_{si} = (P_{si})$ etc. In special cases, when $P_{sa} \neq 1$, which warrants a closer micro-study, classical textbooks on Kinetic Fluid Theory, Statistical Physics and Thermodynamics or similar works give sufficient material for evaluating the probability function P_{sa}. The outcome of such a study can be easily introduced into this report's results.

4. 2. Probabilities P_c and P_{ip}

Before evaluating the integral probabilities P_{si} and P_{id}, attention should be focused on the local probability, P_c , which is greatly affecting P_{si} and P_{id}.

For systems where an analogy between temperature and concentration holds at least qualitatively, the results of turbulent temperature fluctuation analysis. /13/, could be used, but with due caution, or they may be properly adapted to two-phase systems. Results pertaining directly to particulate (or bubble-containing) systems are definitely more desired for application in this study. Diffusion of discrete particles in homogeneous turbulence represents a topic in /12/; it seems closer applicable to this report's goals, despite certain restricting assumptions listed in /12/, which idealize the system. Also, /12/ deals mostly in terms of the widely used velocity-defined correlation coefficients (C_c) and intensity of turbulence (I_t). These parameters are consequences of local properties' fluctuations, but the time-dependence and the spectral (probability) distribution of these fluctuations themselves cannot be derived in the reversed direction, i.e. from C_c and I_t which parameters are in essence integrated time-averaged values.

The analysis and results from /15/ are more suited for the flowing 2-phase system from /10/, which is under closer consideration in chapters 3. and 4. of this report and shown in Fig. 2.

Utilizing the more familiar notations from /12/, in a turbulent 2-phase fluid, with fluid velocities (U_i, u_i) along three Cartesian axes (i=1 for x, i=2 for y and i=3 for z) and mass concentrations (C, c), it holds:

$$U_i = \bar{U}_i + u_i \qquad (2)$$

$$C = \bar{C} + c \qquad (3)$$

Eq. (3) holds also for volumetric concentration of the denser phase, as this convention has been adopted in this report. Being a scalar property, concentration does not carry the axes' subscript.

The normalized probability function, describing the fluctuating component of the velocity, u (omitting from now on the axis' subscript), defining the chance of u to be in the interval u ± du, is, according to /15/:

$$P = (1/\sqrt{2\pi}) \exp(-a/2) \tag{4}$$

This is the Gaussian probability law, with the exponent:

$$a = u^2/(u')^2 \tag{5}$$

The denominator in the last equation is the mean-root-square value, defined on p. 4 of /12/ as:

$$u' = I_t \bar{U} \tag{6}$$

Using Eq. (6), the exponent a is more conveniently expressed as the ratio of two relative magnitudes:

$$a = (u/\bar{U})/I_t \tag{7}$$

$\bar{U}$ is the time-averaged, linear mean value of velocity and it is known for the flow under consideration, while I_t can be measured /12/, or estimated based on published data pertaining to similar systems.

It should be noted that, according to /15/, the dimensionless exponent a depends on five dimensionless parameters: (1) Reynolds number, (2) Froude number (velocity/((grav. acceler.)·(duct diam.))$^{0.5}$), (3) quotient of representative particle diameter/duct diameter, (4) ratio of densities of two phases and (5) dimensionless concentration of the mixture, denoted as c_r in Eq. (1).

In order to find the probability P_c, which is defined similarly to P_u, but it pertains to concentration fluctuations, a different coefficient, b, has to be used instead of a. The following Gaussian law is applicable for a scalar property in free turbulence, according to /12/ , pp. 292, 311, without a condition of velocity/concentration analogy in the system.

$$P_c = (1/\sqrt{2\pi}) \exp(-b/2) \tag{8}$$

$$b = c^2/(c')^2 \tag{9}$$

P_c pertains to any location, or $P_c(z)$ or $P_c(y)$, because b is position dependent. In the special case, when $z = Z_{si}$, P_c represents in fact the previously introduced and defined P_{ip}. $(c')^2$ is the average square concentration fluctuation.

A possibility to express c' in terms of known magnitudes is to utilize in some way Fick's laws of diffusion. This is done in /12/, p. 311, where the compliance of these laws with the Gaussian probability for a particle to advance over a certain distance is proven. The exponent of that Gaussian probability is defined analogously to a and b, only with Lagrangian distances replacing velocities respectively concentrations.

All of this encourages the use of eq's (8) and (9), although neither /12/ nor /15/ relates c' to some known or numerically available parameter, analogous to I_t. This leaves c' as the only unknown magnitude. In the absence of available experimental data, c' can be measured by an appropriate data interpretation procedure in two-phase systems (using specialized anemometers). On the other hand, c' can be expressed through a ratio which corresponds to I_t - - see Eq. (6), and available values for I_t can be utilized for the first approaches, i.e. computer runs. A subsequent calibration (assumption checking) procedure, using an integral function of P_c, i.e. a special case of P_{si}, which covers the whole region from wall-to-wall of the system, can be easily included in a feedback-iterative process. The aim of such a process would be to verify and/or ultimately establish the best usable value of c' or $(c'/\overline{C})$, the latter being a kind of "intensity of concentration turbulence".

The following two sections will explain the previously introduced notion of constrained, or rather inter-related random behavior of some properties within the system under consideration.

4.3. Probability P_{si}

It is obvious that at any instant (time, t) at different locations along z axis, the values of P_c will be different, or, a more general functional dependence has to be taken in consideration: $P_{cz} = P_{cz}(z, t, b)$. As time fluctuations, i.e. its influence will be taken care of by the integration of detector signals in time, and b is already a function of z (but not a pronounced one, as will be discussed later), the length-integrated probability, P_{si}, involves the proper probabilistic use of P_c from Eq. (8). The problem of application of that equation to an interval along z-axis emerges from the fact that in the same moment, at various locations along any axis, the fluctuating components of concentration, c, assume different, random values, but, with a probability P_c.

P_{si} will be derived in continuation, based on the original interpretation of the radiation attenuation formula. In this formula, /10/, the absolute value of the negative exponent with e for the path Z_{si} as the interval in question along z-axis, can be expressed either as a sum or as an integral:

$$k_o \Delta z \left[(\overline{C} + c)_{z_1} + (\overline{C} + c)_{z_2} + \ldots\ldots + (\overline{C} + c)_{Z_{si}} \right] =$$

$$k_o \left[\int_0^{Z_{si}} \overline{C}\,(z)\, dz + \int_0^{Z_{si}} c\,(z)\, dz \right] = E_{sa} + E_{sf} = E_s \qquad (10)$$

k_o is the linear attenuation coefficient for the initial, primary radiation, (unscattered, originated by the source).

It has to be stressed that mathematical derivations and results in works dealing with radiation attenuation methods' application to density/concentration measurements -- including ref's /1/ through /4/, /8/, /9/ and /10/, introduce only the first, ideally averaged (i.e. steady state corresponding) part of the exponent, E_{sa}. The second exponent, E_{sf}, which is a consequence of fluctuating concentrations, can be calculated as follows. At any point in time, at various values of z along the interval Z_{si}, c has different values. Although they are random, they can range only between c_{mi} and c_{mx}. These extreme values of concentration fluctuations are calculable for any system under consideration: they correspond to the limiting cases of C: all gas or all liquid, or liquid and solid etc. Generally, the limiting values of C (i.e. of c) are independent of location, i.e. of coordinates z or y. According to Eq. (3), c can assume positive and negative values, and in each point along Z_{si} , a probability P_c, Eq. (8), will be associated with any value of c. Therefore. E_{sf} from Eq. (10) would be more precisely expressed as (with the subscript f for "fluctuating"):

$$E_{sf} = k_o \int_0^{Z_{si}} (c_f P_c)_z \, dz \qquad (11)$$

But, the following equation, which is the finite form version of the above one is more realistic. Such a form is needed in order to correctly interpret the physically existing statistical nature of the phenomena involved:

$$E_{sf} = k_o \Delta z \sum_{i=1}^{i=N_z} \left[c_f P_c(c_f) \right]_i = k_o \Delta z\, \overline{c}_{sf} \qquad (12)$$

$$\Delta z = Z_{si}/N_z \qquad (13)$$

N_z is the average number of discontinuities (bubbles, particles etc.) along Z_{si}, which number is directly calculable form the average linear numerical concentration between z=0 and $z=Z_{si}$.

It should be noted that P_c is a function of c', through b -- see Eq. (9) -- and therefore it depends on z, i.e. on the subscript i, but from /12/ , p. 521-523, the following is obvious: for all practical purposes, I_t changes very little with the distance from the wall (z or y), and since $c'/\overline{c}$ is analogous to I_t, the same can be expected. Therefore, the work with an average c' (resulting in an average b) along Z_{si} and Y_{id} can be

deemed satisfactory accurate.

Each time Eq. (12) is implemented, a set of N random numbers (generated) defines N values of fluctuating concentrations, c. This should be done in the following way. The maximal random number in the group (RN) will be associated with c_{mx}, and the minimal RN with c_{mi}. In this way a scale is established between the RN's and c's. Any c which corresponds to a RN > $\overline{RN}$ will be interpreted in Eq. (12) as positive, while any c corresponding to a RN < $\overline{RN}$ will be treated as negative. $\overline{RN}$ corresponds to $\bar{C}$, and that, average random number emerges from the explained scaling procedure; an analogous procedure is to be used when calculating b and P_{ip} from Eq. (8). Finally, based on the steps outlined and equations listed, one obtains the needed probability, P_{si}:

$$P_{si} = e^{-E_{sf}} \qquad (14)$$

This equation has to be implemented M times, and from these results a linear average P_{si} is then to be calculated. Such an averaging corresponds to a uniform probability for each group of random numbers to show up (or, for each composite event to occur), while the probability function P_c has taken care of the effects and proper application (such as occurence chance) for each of the random numbers in the group. M is the number of "changed situations" along the length Z_{si} during the total measurement time, t_m. M can differ somewhat along z and y axes, but it is calculable from system parameters, such as fluid velocity, concentration etc. One can realize that the concentration, which is built into M and N, has to be initially assumed or assessed and that feedback iterative loops will be generally included into the final numerical data interpretation, which procedure is a routine when computers are utilized.

Eq. (14) can be used without joining P_{si} with P_{id} and P_{ip} only when Z_{si} represents the total length of the system. This would be the case when the detector is aligned along z-axis, receiving the non-attenuated portion of the original radiation. Otherwise, when the detector is aligned with y-axis, receiving the radiation scattered from the "ip" point (where z and y axes intersect), as is the case in system from /10/, Eq. (14) has to be used in such a way that the magnitudes it contains have to be evaluated simultaneously with the ones built into the probabilities P_{id} and P_{ip}, as explained in next section.

4. 4. Probability P_{id}

Based on identical considerations of random phenomena involved, as done in section 4.3., one obtains the following final results:

$$E_{df} = k_1 \Delta y \sum_{j=1}^{j=N_y} \left[c_f P_c(c_f) \right]_j = k_1 \Delta y \, \bar{c}_{df} \qquad (15)$$

$$\Delta y = Y_{id}/N_y \qquad (16)$$

$$P_{id} = e^{-E_{df}} \qquad (17)$$

k_1 is the linear attenuation coefficient for the scattered (secondary) radiation. Concerning its application, there are hardly any situations where Eq. (17) would be used alone, i.e. without Eq's (8) and (14). The procedure for the joint usage of eq's (8) and (14) and (17) is as follows:

Two groups of random numbers, one of them containing N_z and the other N_y random numbers will be generated (or selected from tables) and these two groups will be "paired" or associated with each other also in a random manner; a third, independent random number will be used to calculate b. Now, for each of these pairs, the following probability will be calculated:

$$P_{sd} = P_{si} \quad P_{id} \quad P_{ip} = \left[e^{-(E_{sf} + E_{df} + b/2)} \right] / \sqrt{2\pi} \qquad (18)$$

Finally, a linear average of P_{sd} will be calculated, after Eq. (18) was M time used. If $M \neq M_z \neq M_y$, one can either work with a value of $M = (M_z + M_y)/2$ or do as follows: two groups of random numbers can be paired and used as explained M_{mi} times (where M_{mi} is the smaller value, say M_z); then E_{df} (i.e. P_{id}) will be calculated $(M_y - M_z)$ times more using the remaining groups of N_y random numbers. At the end a proper averaging, including P_{ip}, needed to calculate the such combined P_{sd} will be performed. The simultaneous calculations of components within P_{sd} represents a certain constraint in the analysis of the composite random phenomenon, occuring along axes z and y.

Looking at the exponent of Eq. (18),

$$E_{sd} = E_{sf} + E_{df} + (b/2) = (k_o \Delta z)\, \bar{c}_{sf} + (k_1 \Delta y)\, \bar{c}_{df} + (b/2) \qquad (19)$$

the following could be observed: if c values are randomly distributed about c=0 (where $C=\bar{C}$). for very large values of M, N_z and N_y, both average values $\bar{c}_{sf}$ and $\bar{c}_{df}$ will approach zero, which would render $P_{sd} = 1$ (because $b \rightarrow 0$ in that case too), but as long as they differ from 0, the non-zero positive multipliers in parentheses -- see Eq. (19) -- keep $E_{sd} \neq 0$. Also, three additive terms forming E_{sd} can have various signs at each of the M implementations of eq's (18) and (19). Further on, the averaging of P_{sd} is done by powers of E_{sd}, which is different than averaging E_{sd} themselves. Finally, looking deeper into the analysis, it could be anticipated that generally, even for M, N_z and N_y as large as desired, it has to be $P_{sd} \neq 1$. Explanation for this is as follows. The spectral distribution of c, Eq. (8), based on the philosophy which in /15/ renders Eq. (4) for velocities, assumes the time-average value, $\bar{C}$, as the most probable value in the same time, which could be a matter for discussion. Obviously, the following holds for the statistical (weighted) average: $C_{av} > \bar{C}$. If this would be taken in account when performing an improved scaling of random numbers with fluctuating concentrations, c, a shift would appear in final numerical results. In other

words, a bias would show up, resulting in a compulsory $E_{sd} \neq 0$ (and $P_{sd} \neq 1$) for any desired large values (even for infinitely large) of M, N_z and N_y. But, even if accepting the spectral situation for concentrations as given in /15/ for velocities, since generally $\overline{C} - 0 \neq C_{mx} - \overline{C}$, a skewing of the probability spectrum exists due to the asymetry of its cutt-off points. Therefore, the outlined probabilistic random number interpretation (which is in no jeopardy because of this explanation) will again result in the condition $P_{sd} \neq 0$ for any duration of measurements. Concerning the estimate whether P_{sd} is $\gtrless 1$, the following holds: $P_{sd} > 1$ if $\overline{C} > C_m$ and $P_{sd} < 1$ if $\overline{C} < C_m$, where $C_m = (C_{mi} + C_{mx})/2$. This criterion emerges from a quantitative discussion of the cut-offs in the Gaussian probability curve.

4. 5. Procedural remarks

Based on the analysis performed, it is evident that for finite, even very long measurement times, the simple (linear) time-averaged detector signals should not be directly implemented, i.e. used in equations derived for ideal steady states. This holds for all systems where fluctuations of any measurable property occurs with non-uniform probability. Recording and a general statistical processing (seeking mean values, deviations etc.) as thorough as possible of the signals should be performed during various lengths of measuring intervals. This would at least provide indications of various phenomena occuring in the system under consideration. Very often, interpretation of signals' behavior in time can directly or rather indirectly yield information needed in performing measurement error reduction, such as the one which is the subject of this report.

The analysis outlined in previous sections, especially eq's (1), (3), (8), (9), (12), (13), (15) through (18) represent all the essentials necessary for a precise measurements interpretation procedure, which can take care of those random phenomena which do not possess a self-compensating feature in time. These phenomena, if not properly taken in account, can represent a significant contribution to the measurements errors. This kind of error would show up when direct, simple interpretation of recorded data is done, when these data are directly caused by non-uniform random phenomena. Errors of this sort can exist for any desired duration of experiments.

A complex algorithm, which represents the data interpretation/ measurement errors reduction procedure consists of the equations listed in the previous paragraph, together with the analytical results of the basic (steady state) phenomena innerent in the system under consideration. These results, as derived in /8/, /9/ and /10/, pertain to a generalized, more complex situation, where local values of concentration are measured, having the entire instrumentation placed externally to the system. Further on, the algorithm contains the assumptions - checking formulae (for concentrations etc.), which represent self-correcting feedback inputs built in corresponding iteration loops. A program corresponding to such an

algorithm is applicable to a variety of systems and can be executed in a straightforward way on commercially available digital computers*.

5. Conclusion

In order to reduce measurement errors, particularly when employing advanced indirect (contactless) methods needed for aggressive, or high pressure/temperature/velocity multi-phase turbulent flows, it is necessary to go beyond standard avenues and procedures of improving hardware, instrumentation, recording techniques etc. It is important to take in account properly and as accurately as possible all the phenomena taking place in the physical macro- and micro-system under consideration, which is the measured system, as well as those taking place in the measureing system. This system is to be selected carefully and attached to the original, existing system with the purpose to render usable and reliable data, which can be successfully processed to finally yield the desired results. The necessary correcting functions, based on a probabilistic analysis of all statistically occuring phenomena during the measurement are evaluated, their influence demonstrated and a general accuracy-improving data interpretation procedure presented.

---

* The assistance of Ms. H. Wilson, Tampa, in the technical preparation of this report is greatly appreciated.

References

1. Hooker, H. H. and Popper, G.F., A Gamma-Ray Attenuation Method for Void Fraction Determination ... ANL-5766, Nov. 1958.

2. Kondic, N.N., A Contribution to the Analysis of Real Attenuation of the Penetrating Radiation Depending on the Elements of the Measured and Measuring System, Colloque Euromech No. 7 sur la Mécanique des Liquides Contenant des Bulles, April 23-26, 1968, Grenoble, France.

3. Sudhakar, N., Statistical Improvement in the Void Fraction Determination with Nuclear Radiation , Thesis, Graduate School, Univers. of Kentucky, Lexington (Mechan. Eng. College), 1970.

4. Sudhakar, N., Hahn, O. J. and Kondic, N., Channeling Correction for Void Fraction Measurements, American Nucl. Society Meeting, Nov. 1972, Washington, D.C.

5. Harms, A.A., Lo, S. and Hancox, W.T., Measurement of Time-Averaged Voids by Neutron Diagnostics:, J. of Applied Physics, Vol. 42, No. 10, Sept. 1971.

6. Harms, A.A., Dynamic Effects in Radiation Diagnosis of Fluctuating Voids, Nuclear Science and Engineering, 46, 1971.

7. Harms, A.A. and Laratta, F.A.R., The Dynamic-Bias in Radiation Interrogation of Two-Phase Flow, Internat. J. Heat & Mass Transfer, Vol. 16, 1973.

8. Kondic, N. and Hahn, O.J., Theory and Application of the Simultaneous Parallel and Diverging Radiation Beam Method in Two-Phase Systems, Paper No. Mt.1.5., International Heat Transfer Conf., Versailles-Paris, France, 1970.

9. Kondic, N.N., Contactless Methods for Measuring Local Values of Concentration and Temperature in One- or Multiphase Systems, International Congress CHISA, Sept. 1972, Prague, Czechoslovakia.

10. McAdams, V.D., Kondic, N.N. and Baldwin, M.N., Determination of Local Density by Gamma-Scattering Using External Means, American Nuclear Society Meeting, June 1973, Chicago, Illinois.

11. Lapp, R.E. and Andrews, H.L., Nuclear Radiation Physics (Englewood Cliffs, N.J., Prentice Hall, Inc. 1963).

12. Hinze, J.O, Turbulence (McGraw Hill Book Comp. New York, 1959).

13. Lin, C.C., Statistical Theories of Turbulence (Princeton University Press, Princeton, N. Jersey, 1961).

14. Soo, S.L., Fluid Dynamics of Multiphase Systems (Blaisdel Publishing Corp., Waltham, Massachusetts, 1967).

15. Fortier, A., Mécanque des Suspensions (Masson et Corp., Paris, France, 1967).

16. Sokolnikoff, I.S. and Sokolnikoff, E.S., Higher Mathematics for Engineers and Physicists (McGraw-Hill Book Corp., New York & London 1941).

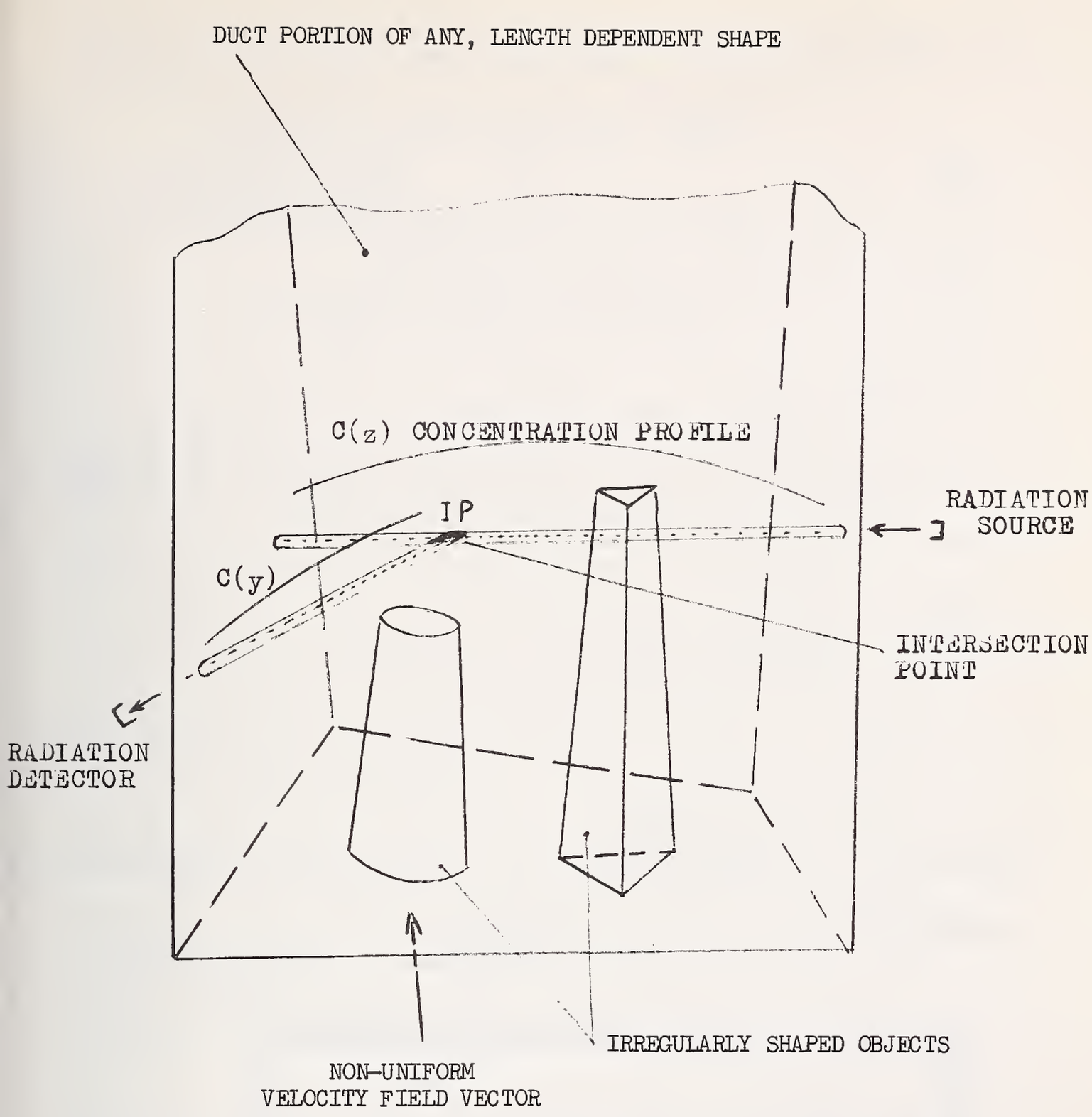

FIGURE 1

GENERAL 3-DIMENSIONAL FLOWING CONCENTRATION FIELD SITUATION

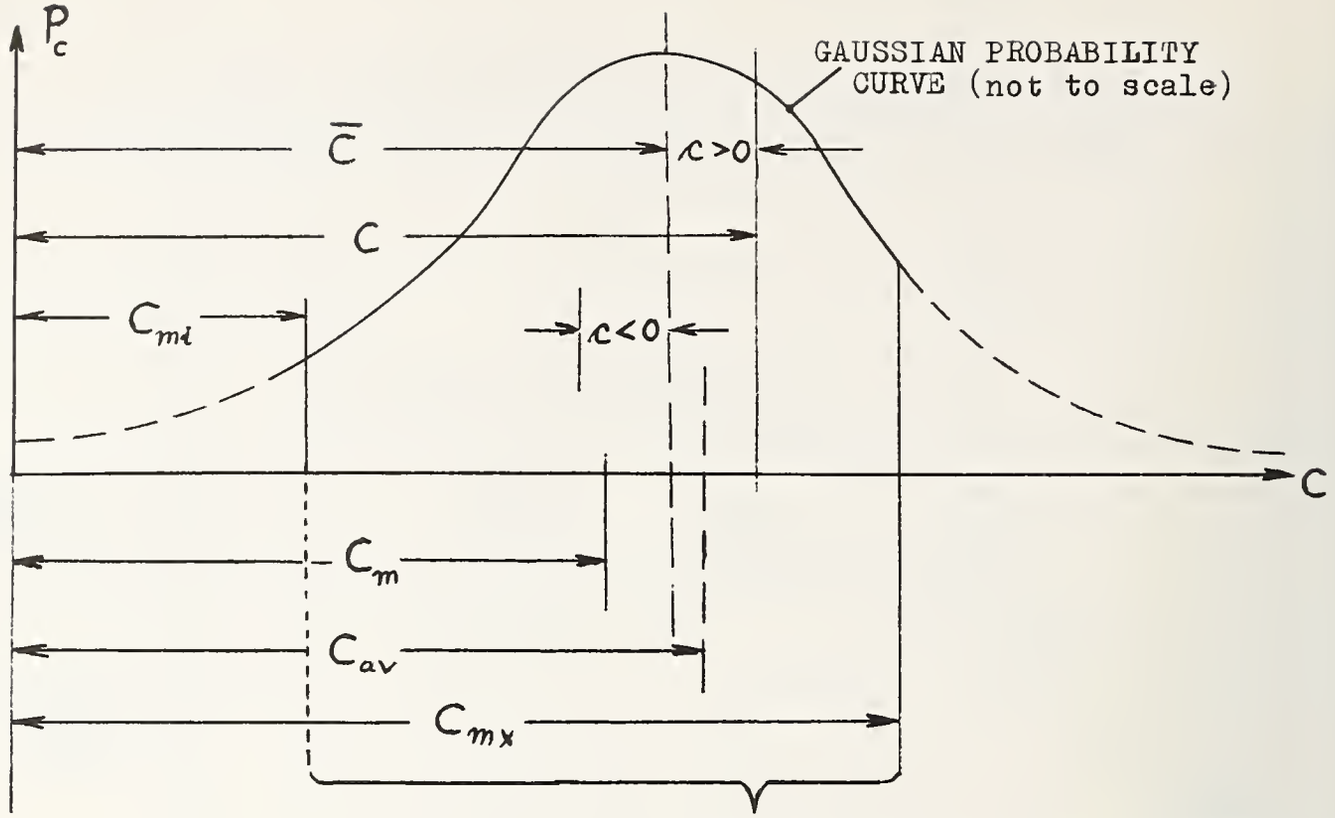

FIGURE 2

APPLICATION TO A CONCRETE SYSTEM (below) and STATISTICAL REPRESENTATION (up)

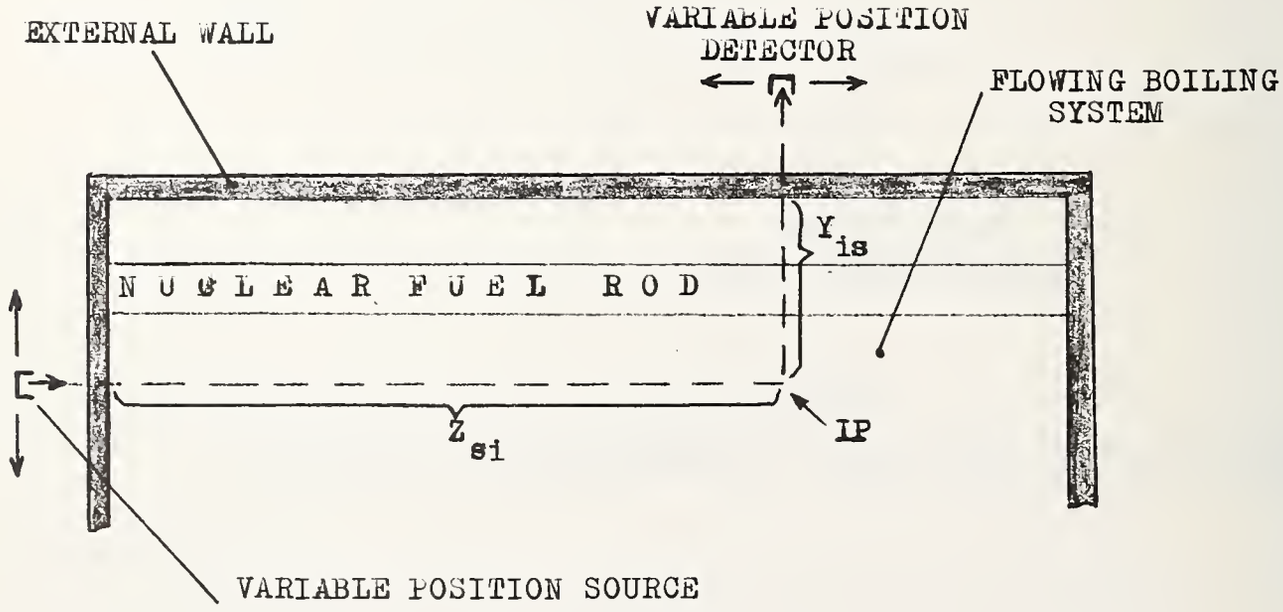

National Bureau of Standards Special Publication 484, Proceedings of the Symposium on Flow in Open Channels and Closed Conduits held at NBS, Gaithersburg, MD, February 23-25, 1977. (Issued October 1977)

MEASUREMENTS OF DENSITY AND DENSITY GRADIENT WITH AN OSCILLATING CONDUCTIVITY PROBE

Donald P. Delisi and Robert H. Kirchhoff*

Flow Research Company
A Division of Flow Industries, Inc.
Kent, Washington 98031

Density measurements obtained using single-electrode conductivity probes in a stratified salt solution are reported. A comparison of vertical density profiles obtained from upward and downward traversing probes show that measurement errors take the form of a hysteresis loop. Non-dimensional plots of these measurements characterize probe performance in terms of the size of the hysteresis loop as a function of the parameters in the experiment.

A series of experiments were performed with vertically oscillating conductivity probes to decrease the hysteresis effect in the density measurements. Typically, a probe was oscillated at a peak-to-peak amplitude of 1 mm at a frequency of 20 Hz. Analysis of the data yields, for a single dimensionless parameter, a range of values over which the hysteresis effect is negligible. This parameter is a simple combination of the probe dimensions, gravity, and the oscillation characteristics. The data indicate that, above a certain value of the parameter, the hysteresis effect is negligible regardless of the local density gradient.

Also reported are a theoretical development and results of additional experiments, in which the oscillating conductivity probe signal is analyzed to calculate the local density gradient. It is shown that phase synchronous detection of the probe signal can result in the direct measurement of the local density gradient. Experimental data showing satisfactory agreement with the theoretical results are reported.

Key Words: Conductivity probe; density; density gradient; stratified flow; oscillating probe; experimental; laboratory; internal wave.

1. Introduction

Conductivity probes measure the electrical conductance between two sensing elements. If the sensing elements are far from each other and if one element is much smaller than the other, the probes are called single electrode conductivity probes, and the measured conductance is essentially the conductance of the fluid around the smaller element [1].** With one

---

*Consultant, Associate Professor of Mechanical Engineering, University of Massachusetts, Amherst, Mass.

**Figures in brackets indicate the literature references at the end of the paper.

sensing element much smaller than the other, the probes measure the conductance in a very small volume of fluid, and the conductivity measurements become essentially point measurements.

In laboratory experiments investigating stratified fluids in water tanks and water tunnels, it is common to use salt water as the working fluid. In this case, varying the salt concentration changes the density of the water and varies the stratification. Conductivity probes measure the conductance of the saline solution, and, using a prior calibration, we can obtain the local density of the solution at a point. Errors in measuring the conductivity of the fluid reflect as errors in determining the density of the solution. Conductivity probes have been used as a laboratory tool for the diagnosis of a variety of problems, including studies of internal gravity waves [2,3], measurements of concentration profiles in reverse osmosis [4], investigations of momentumless wakes [5], and studies of the properties of turbulent flows [6].

In this paper we report density and density gradient measurements that are obtained with single-electrode conductivity probes in a non-flowing, stratified salt solution. We characterize the errors associated with measuring density and density gradient with the macroscopic parameters of the conductivity probe, as distinguished from the microscopic electrokinetics of the probe. In section 2 we discuss the operating characteristics of conductivity probes and the nature of the associated error. The reduction of the probe error by forced oscillation of the conductivity probe is examined in section 3, and the technique of oscillating the conductivity probe is extended to measurements of the density gradient in section 4. In section 5 we give a summary and conclusions.

2. Operating Characteristics of Conductivity Probes

The experiments reported in this paper were performed with cylindrical, single-electrode conductivity probes of characteristic probe-tip dimension a, operating in a non-flowing, stratified tank of saline solution. A schematic drawing of a typical probe tip is shown in figure 1. The sensing element in the probes is platinum wire. The exposed tip of the wire is covered with a platinum black coating by using a commercial platinizing solution.

In this study we used two probe tip designs. In the first design, the exposed wire tip is flush with the glass surface at the probe tip. In the second design, the wire extends 1-1½ wire diameters beyond the glass surface. We found that this second design yields probes with a higher signal-to-noise ratio than probes of the first design. The characteristic probe-tip dimension a is taken as the arithmetic average of the wire diameter and the probe-tip body diameter.

Seven different conductivity probes were used in this study. Six of the probes had glass tips and were similar in design to either the probes of Gibson and Schwarz [1] or the probes of Mied and Merceret [7]. The tip of the seventh probe was made of ADAPTIC, a commercial dental restorative manufactured by Johnson and Johnson. In this study, the characteristic tip dimension a ranged from 0.31 mm to 3.05 mm, and the diameter of the platinum-wire sensing elements ranged from 0.05 mm to 0.81 mm.

Figure 2 is a schematic drawing of the experimental apparatus. The experiments were conducted in a salt water tank measuring 150 cm long, 89 cm deep, and 28 cm wide. A typical density-versus-depth profile used in these experiments is also shown in figure 2. The profile consists of a linearly

stratified region at the top of the tank, with a density jump and a constant density region at the bottom of the tank, below the stratified region. The density gradient in the top region and the magnitude of the density jump were varied in these studies. The conductivity probe was attached to a traverse, which moved the probe vertically through the fluid.

We calibrated the probes by immersing them in salt water solutions of known density and measuring the output voltage of the conductivity gauge (Flow Research Model 1104). From this calibration, we determined the transfer function $e = f(\rho)$, where e is the measured voltage at the output of the conductivity gauge and $\rho = \rho(z)$ is the density of the salt water, where z is the depth of the probe. For a given range of densities, the transfer function is linear, and $e = k\rho(z)$, where k is a constant. The value of k varies with the conductivity probe and the conductivity gauge. Typically, for these experiments, k was approximately 250 volts $cm^3 gm^{-1}$, and the measured voltage was linear with density between 1.008 and 1.023 gm cm^{-3}.

A single-electrode conductivity probe measures the electrical conductance of the fluid near the probe tip. Ideally, if the probe moves into a region of different conductance or, alternately, if fluid of different conductance moves past the probe tip, the probe measures the conductance of the new fluid. If the working fluid were inviscid and if the probe worked ideally, the probe would always measure the conductance of the new fluid. In reality, however, some old fluid is always carried with the probe, with the result that the probe reading is in error.

Conductivity probes are often used to measure internal wave motions in stratified salt solutions [2,3]. In many applications, the conductivity probes are stationary in laboratory coordinates, and the internal waves propagate past the probes. In this study, we simulated this situation by moving a conductivity probe vertically through a tank of stratified salt water which was at rest in laboratory coordinates.

A comparison of vertical density profiles obtained from upward and downward traversing probes show that measurement errors take the form of a hysteresis loop. A typical density profile is shown in figure 3. In this figure, the dashed line represents the true density profile. Assume a conductivity probe is positioned at depth Z_1 and is allowed to reach equilibrium at that depth. Now, we move the probe vertically downward through the fluid at a constant speed U. At the depth Z_2, we reverse the probe motion and the probe moves upward through the fluid at the same velocity U. At the depth Z_1, we again reverse the motion of the probe, and the probe traverses downward through the fluid. The density (inferred from the conductance) profile measured by this probe is shown by the solid line in figure 3. Initially, the probe measures a density ρ_1 at the depth Z_1. As the probe traverses vertically downward through the fluid, the density measured by the probe at a given depth is different from the true density at that depth. This density difference reflects the fact that some fluid from higher levels has been dragged to lower levels with the probe. When the probe reaches the depth Z_2, the motion of the probe is reversed, the probe now drags fluid from lower levels to higher levels, and, at a given depth, the probe measures a density that is the true density at a lower level. At the depth Z_1, the probe again reverses direction with similar results. Thus, we see that the measurement error takes the form of a hysteresis loop in a depth-versus-density profile. Here, we define the hysteresis loop error $\Delta\rho_{HL}$ as the density difference between an upward and downward traverse.

Measured density profiles are shown in figure 4 for several traversing speeds. In this figure, the true density profile (inferred from careful static measurements of the density) has a constant gradient with depth, and the Brunt-Vaisala frequency, defined as $N = (-\, g/\rho\, d\rho/dz)^{\frac{1}{2}}$ is constant, where g is the acceleration due to gravity. The data in figure 4 show that the hysteresis loop error decreases as the traversing speed decreases. This decrease in $\Delta\rho_{HL}$ occurs because the traversing time between two levels is approaching the diffusion time of the fluid. Thus, for an infinitely slow traverse speed, the fluid carried with the probe from another level will have an infinite amount of time to diffuse away from the measuring volume of the probe, and the probe will measure the correct density.

A dimensional analysis of the significant probe parameters yields three independent, non-dimensional groups:

$$\text{a Froude number} = \frac{U}{\sqrt{ag}}\ ,$$

$$\text{a Reynolds number} = \frac{Ua}{\nu}\ , \text{ and}$$

$$\text{a dimensionless number characterizing the hysteresis loop error} = \frac{\Delta\rho_{HL}}{\frac{U^2}{g}\,\frac{d\rho}{dz}}$$

where ν is the kinematic viscosity of the fluid. In these experiments, the Reynolds number was varied between 0.2 and 5.3, and the Froude number was varied from 1.9×10^{-3} to 8.8×10^{-2}.

Experimental measurements for four probes of different probe diameter are shown in figure 5 for a variety of operating conditions. Figure 5 shows that, for a given probe in a given density gradient, an increase in the traverse speed produces an increase in $\Delta\rho_{HL}$. Cross plots of this and other, more extensive data show that, for a given probe and a fixed traverse speed, an increase in the local density gradient will increase $\Delta\rho_{HL}$. Also, for a fixed probe traverse speed and a fixed density gradient, an increase in the probe diameter will increase $\Delta\rho_{HL}$. These results are summarized in table 1.

The results shown in table 1 indicate that, to reduce $\Delta\rho_{HL}$, we must make the probe as small as possible and the traverse speed as slow as possible, and the density gradient should be weak. Thus, decreasing the probe size not only increases the resolution of the probe, but also decreases the density measurement error.

An immediate application of these results is that, for a stationary probe that is measuring internal waves in a given density gradient, high-frequency wave oscillations (corresponding to a large traverse speed) will have a larger error in the measured amplitude than will low-frequency wave oscillations. We can also use the data shown in figure 5 to estimate $\Delta\rho_{HL}$ for a given probe moving in a given density gradient with a given traverse speed. We can then use $\Delta\rho_{HL}$ to estimate the error in the measured amplitude of an internal wave of a given frequency of oscillation.

3. Density Measurements With Oscillating Conductivity Probes

Using oscillating conductivity probes, we conducted a series of experiments aimed at reducing the hysteresis loop error. A schematic drawing of the oscillating probe system is shown in figure 6, and a block diagram of

the associated electronics is given in figure 7. In this study the probes were oscillated vertically by using a solenoid, which was driven by a low-frequency signal generator. The probe and oscillating system were driven at the resonant frequency to achieve sufficiently large amplitudes. Typical, maximum peak-to-peak amplitudes were 1 mm at a frequency of 20 Hz. The vertical motions of the probes were measured with a Linear Variable Differential Transformer (LVDT). The oscillating system was attached to the traversing mechanism by thin, stainless-steel strips. A linear potentiometer was also attached to the traverse for measuring the mean depth of the probe.

Figure 8 shows typical results of density measurements made with the oscillating probes, for a linear density profile. In the case shown in this figure, the traverse was run at its maximum speed, and the measurements shown are for several amplitudes of oscillation A. The data shows that, for a given traverse speed and a given density gradient, increasing the oscillation amplitude decreases $\Delta\rho_{HL}$.

Oscillating the probe introduces two new parameters into the dimensional analysis: the amplitude of oscillation A, and the frequency of oscillation ω. The result is that there are now the following five non-dimensional groups to be considered:

$$\text{a Froude number} = \frac{A\omega}{\sqrt{ag}},$$

$$\text{a Reynolds number} = \frac{(A\omega)a}{\nu},$$

$$\text{an error parameter} = \frac{\Delta\rho_{HL}\,\omega^2}{g\,d\rho/dz},$$

$$\text{a velocity ratio} = \frac{A\omega}{U}, \text{ and}$$

$$\text{a geometric ratio} = \frac{A}{a}.$$

Note that the Froude number defined here is appropriate for the oscillating case and is the Froude number defined in section 2 times the velocity ratio. For these experiments, the velocity ratio is always greater than ten, the Reynolds number spans the range between 55 and 440, and the frequency of oscillation of the probe ω is always considerably greater than the Brunt-Vaisala frequency N, the ratio having values of $62 \leq \omega/N \leq 184$.

Density measurements from an extensive set of experiments are shown in figure 9. This figure plots the error parameter defined above versus the Froude number squared. Data for seven different probes are shown for a variety of operating conditions. The data show that the measurements from all the probes collapse reasonably well onto one curve. The initial effect of increasing the amplitude of oscillation while a given probe is traversing a given density gradient is a decrease in $\Delta\rho_{HL}$. If the amplitude of oscillation is increased, $\Delta\rho_{HL}$ decreases, and the measured density approaches the true density. The data shown in figure 9 are essentially independent of the velocity ratio $A\omega/U$. We conjecture that local mixing generated by the forced oscillation of the probe is responsible for the decrease of $\Delta\rho_{HL}$ as the amplitude of oscillation increases. We discuss the effects of this local mixing on the flow in section 4.

The data shown in figure 9 indicate that for all probes there is a single value of the square of the Froude number $(A\omega)^2/ag \approx 0.6$ above which the magnitude of the hysteresis loop is negligible. In figure 10 we plot the amplitude of oscillation necessary to decrease $\Delta\rho_{HL}$ to zero versus density gradient. This figure shows that the amplitude of oscillation for $\Delta\rho_{HL} = 0$ is independent of the value of the local density gradient. The data shown in figures 9 and 10 are significant because they imply that the errors in measuring density can be reduced for a given probe by a judicious choice of the amplitude and frequency of oscillation and that these errors will be independent of the density gradient. These results differ from the non-oscillating probe results shown in table 1, where we saw that increasing the density gradient increases the hysteresis loop error. Thus, an experiment performed with oscillating conductivity probes can be designed a priori for a single value of $(A\omega)^2/ag \geq 0.6$, independent of the local value of the density gradient, and the hysteresis loop error will effectively be reduced to a negligible value.

4. Density Gradient Measurements With Oscillating Conductivity Probes

By oscillating conductivity probes in the vertical direction, we can also measure the local density gradient. This technique is an extension of a similar technique used to measure local velocity gradients in air with hot-wire probes [8,9].

We expand $\rho(z)$ in a Taylor series about z_o to get

$$\rho(z) = \rho(z_o) + \frac{\partial\rho}{\partial z}\bigg|_{z_o} \Delta z + \frac{1}{2}\frac{\partial^2\rho}{\partial z^2}\bigg|_{z_o} \Delta z^2 + \frac{1}{6}\frac{\partial^3\rho}{\partial z^3}\bigg|_{z_o} \Delta z^3 + \cdots .$$

If we assume that the transfer function between the measured voltage at the output of the conductivity gauge and the density of the salt water is linear and of the form $e = k\rho(z)$ (section 2), and if we introduce a small-amplitude harmonic perturbation $\Delta z = A \sin \omega t$, we may write the transfer function as

$$e(t) = k\left[\rho(z_o) + A\frac{d\rho(z_o)}{dz}\sin \omega t + \cdots + \theta(A^n, n\omega)\right], \qquad (1)$$

where θ indicates higher order terms. In eq. (1), we assume that the amplitude of oscillation A is small compared to the characteristic length scale of the change in density gradient.

We have performed experiments where phase-synchronous detection is used to measure the coefficient of the first harmonic in eq. (1). The voltage signal at the output of the conductivity gauge along with the signal from the LVDT is fed into a Princeton Applied Research Model 129A lock-in amplifier. The lock-in amplifier yields the rms amplitude of the coefficient of $\sin \omega t$ in eq. (1), and a direct measurement of the local density gradient $d\rho(z_o)/dz$ is obtained. In the experiments, the densities were in the linear range of the conductivity gauge, and the amplitudes of oscillation were small compared to the thickness of an interface.

Typical density gradient measurements are shown in figure 11 for a density profile that is linear on top, constant on the bottom, and has a

density jump centered at $z = 70$ cm . In this figure, the solid line indicates the density gradient, which was inferred from careful static measurements of the density profile. The density gradient measurements obtained directly from eq. (1) are shown for three amplitudes of oscillation for a single probe. The results show that the measured density gradient approaches the inferred density gradient as the amplitude of oscillation increases.

Figure 12 shows density gradient measurements from several experiments using an oscillating conductivity probe. In this figure we plot the ratio of the density gradient measured with phase-synchronous detection (eq. 1) to the density gradient inferred from careful, static measurements of the density profile versus the ratio of the amplitude of probe oscillation to the characteristic probe-tip dimension. Two sets of data are plotted in figure 12. We obtained the stationary measurements by positioning the probe at a given depth and oscillating the probe with different amplitudes of oscillation. For these measurements, the mean depth of the probe was constant with time. We obtained the moving measurements in figure 12 by oscillating the conductivity probe as it slowly traversed vertically through the fluid. Thus, the mean depth of the probes was slowly changing with time during these measurements.

The measurements in figure 12 show that the ratio of the measured density gradient to the inferred density gradient approaches unity as A/a approaches approximately 1.5. The moving measurements have a slightly larger error than the stationary measurements.

The results shown in figures 11 and 12 are encouraging because they show that local density gradient measurements can be obtained at a point without either moving the probe or using two probes, which involves double calibrations.

We examined the effect on the fluid of oscillating the probe to determine if the mixing generated by the oscillations is significant. To determine the effect of oscillating the probe, we monitored the stationary density gradient measurements as a function of time. (The density gradient measurements were monitored since we believed that mixing effects would show up in measurements of the density gradient more rapidly than in measurements of the density itself.) The results of the preliminary measurements indicate that mixing does not affect the measurements of the density gradient until at least three to five minutes after the oscillation of the probe has started. We therefore believe that oscillating conductivity probes initially have very little effect on the structure of the local density field.

5. Summary and Conclusions

This paper illustrates some of the errors in measuring density in non-flowing, stratified salt solutions. The errors take the form of a hysteresis loop in profiles of density versus height. The error in the hysteresis loop is a function of the probe, the density gradient, and the speed of traverse, or, alternately, in the case of a probe fixed in laboratory coordinates, the frequency and amplitude of internal waves passing by the probe.

The hysteresis loop error can be significantly reduced by oscillating the probe. We present measurements which show that the hysteresis loop error can be effectively reduced to a negligible value if the square of the Froude number is approximately 0.6 or larger. This result is substantiated for several different probes and is independent of the local value of the

density gradient. The result is significant since it allows investigators to design an experiment with a priori knowledge of the errors that will be associated with the measurements of density and permits the design of experiments with reduction of this error.

By properly analyzing the signal from a vertically oscillating conductivity probe, we can also obtain a direct measurement of the local density gradient. Our measurements show that the measured density gradient approaches the inferred density gradient obtained from static measurements of the density profile as the ratio of the amplitude of the probe oscillation to the characteristic probe tip dimension approaches 1.5. This method offers a unique technique of directly measuring the local density gradient in stratified salt-water solutions.

Acknowledgments

The authors would like to express appreciation to the Geophysical Fluid Dynamics Laboratory/NOAA at Princeton University, where the experiments were performed. We would also like to thank Princeton Applied Research Corp. for the use of a lock-in amplifier during the course of these measurements. The first author would like to express his appreciation to the National Research Council for the support of an NRC/NOAA Resident Research Associateship during part of this investigation. Part of the analysis of this data was supported by Flow Research IR&D funds.

References

[1] Gibson, C. H. and Schwarz, W. H., Detection of conductivity fluctuations in a turbulent flow field, J. Fluid Mech. 16, 357-364 (1963).

[2] Delisi, D. P. and Orlanski, I., On the role of density jumps in the reflexion and breaking of internal gravity waves, J. Fluid Mech. 69, 445-464 (1975).

[3] Martin, S., Simmons, W., and Wunsch, C., The excitation of resonant triads by single internal waves, J. Fluid Mech. 53, 17-44 (1972).

[4] Hendricks, T. J. and Williams, F. A., Boundary layer flow problems in desalination by reverse osmosis, Dept. of the Interior, Office of Saline Water, Grant No. 14-01-0001-951, Final Report (1970).

[5] Stockhausen, P. J., Clark, C. B., and Kennedy, J. F., Three dimensional momentumless wakes in density stratified liquids, MIT Hydrodynamics Laboratory Report No. 93 (1970).

[6] Gibson, C. H. and Schwarz, W. H., The universal equilibrium spectra of turbulent velocity and scalar fields, J. Fluid Mech. 16, 365-384 (1963).

[7] Mied, R. P. and Merceret, F. J., The construction of a simple conductivity probe, Johns Hopkins University Report, Department of Mechanics (1970).

[3] Kirchhoff, R. H. and Voci, E. K., Direct measurement of the velocity gradient in a fluid flow, AIAA J. 10, 1119-1120 (1972).

[9] Kirchhoff, R. H. and Burbank, R. A., Response of a hot wire oscillating in a shear flow, AIAA J. 12, 96-98 (1974).

Table I Probe Response Functional Relation

DEP VAR.	INDEPENDENT VARIABLES		
$\Delta\varrho_{HL}$	U	a	$d\varrho/dz$
INC	INC	FIX	FIX
INC	FIX	INC	FIX
INC	FIX	FIX	INC

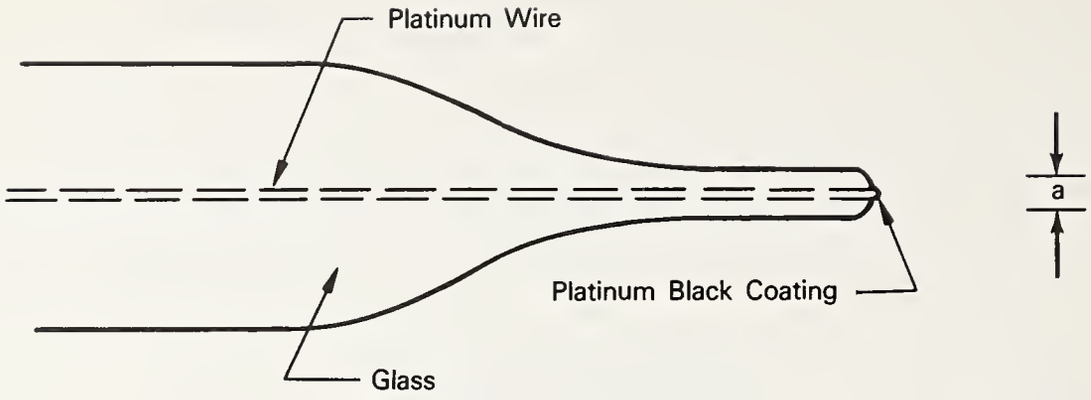

Figure 1 Schematic Drawing of Conductivity Probe Tip

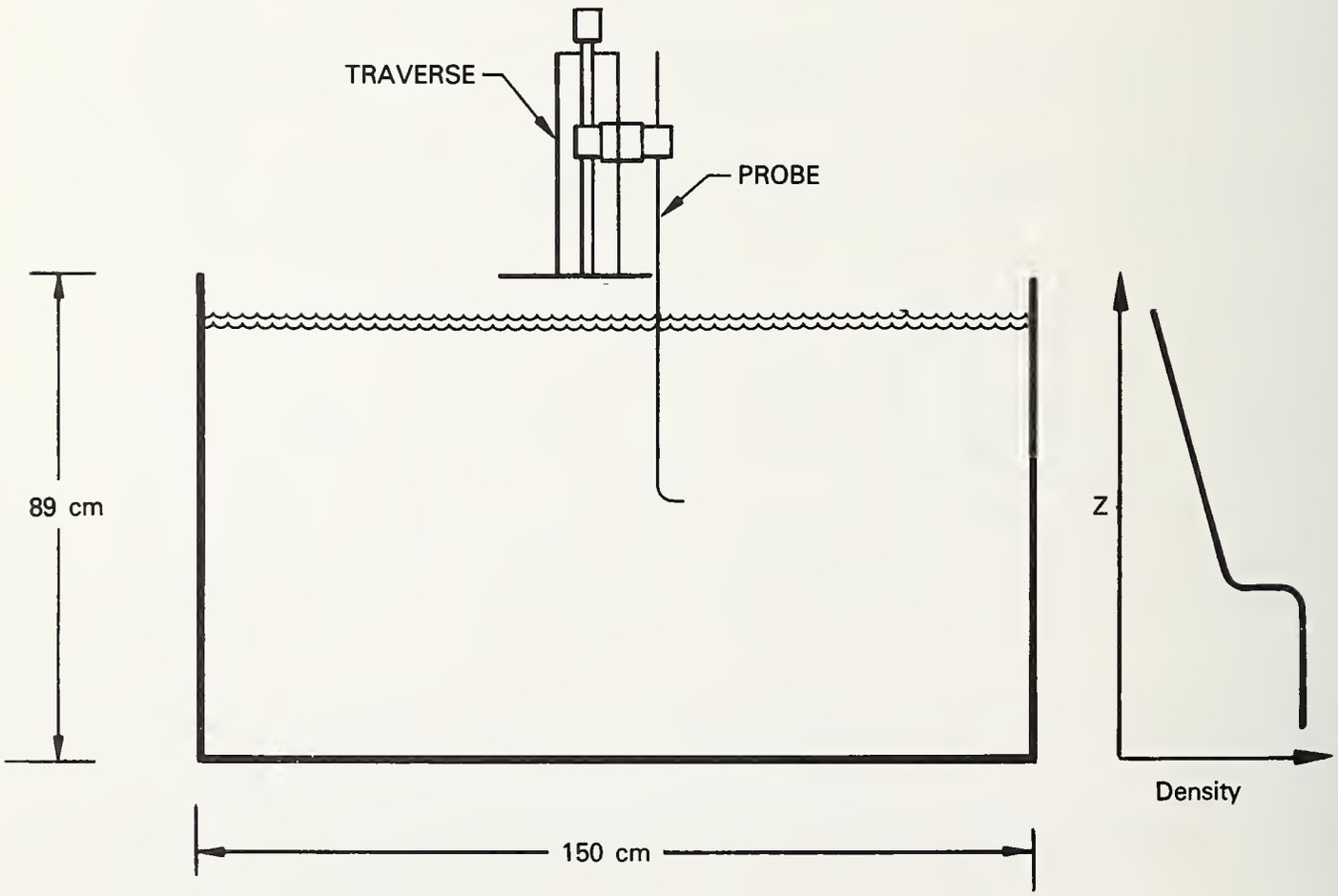

Figure 2 Schematic of the Experimental Apparatus

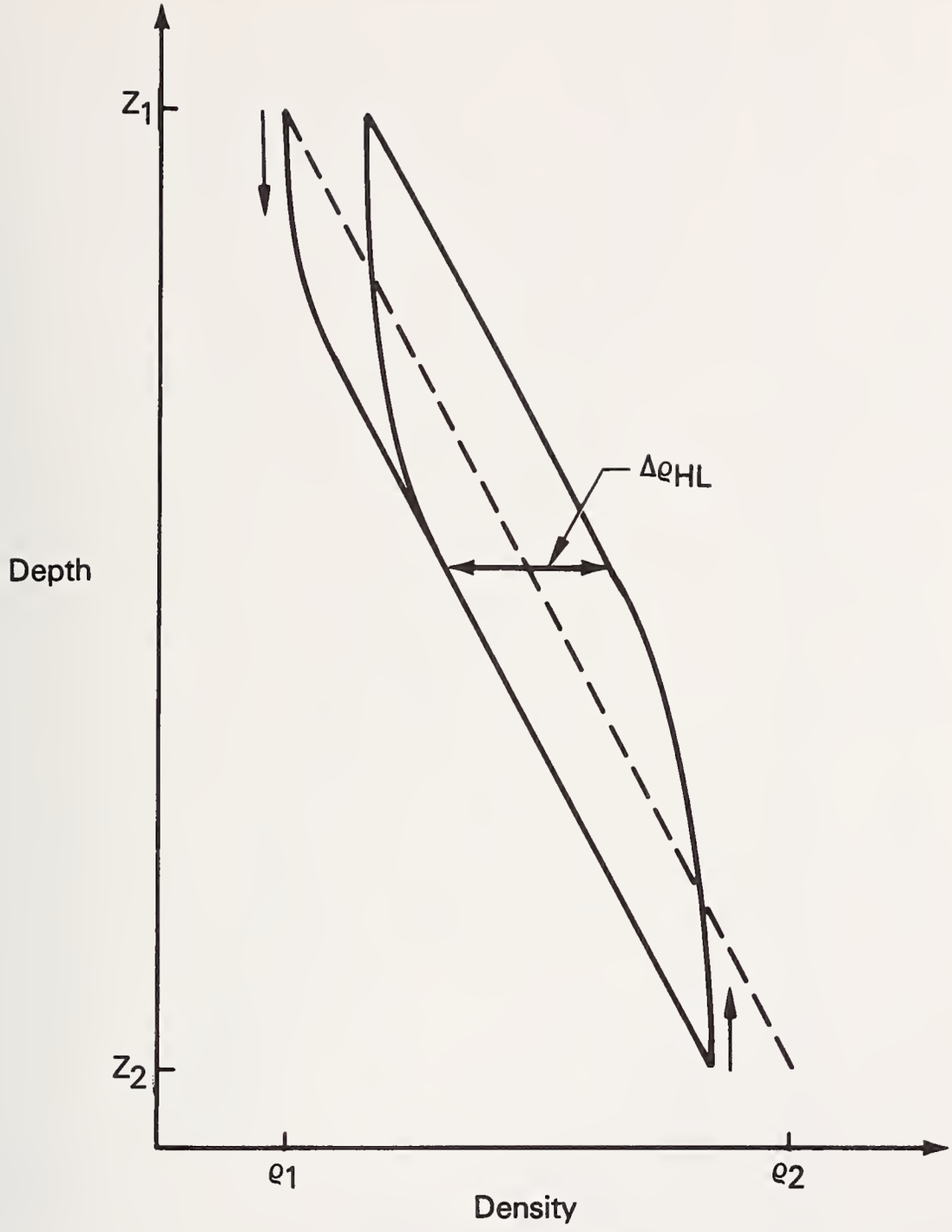

Figure 3 Schematic of a Typical Depth-Versus-Density Profile for a Traversing Conductivity Probe. The True Density Profile is shown by the Dashed Line; the Measured Profile is shown by the Solid Line. $\Delta\varrho_{HL}$ is the Hysteresis Loop Error.

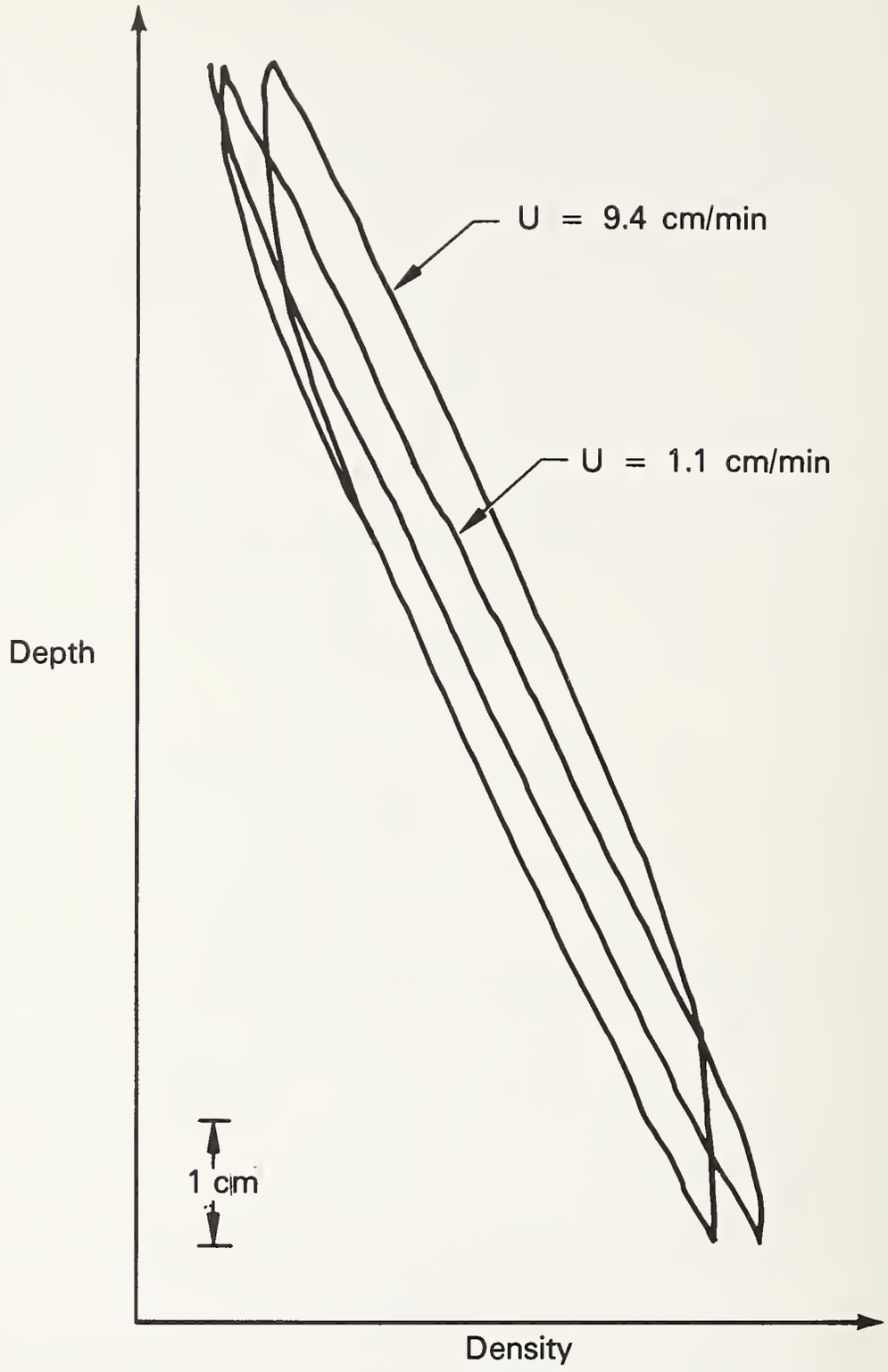

Figure 4 Measured Density-Versus-Depth Profiles for Two Traversing Speeds; $d\varrho/dz = 4.4 \times 10^{-4}$ gm/cm^4

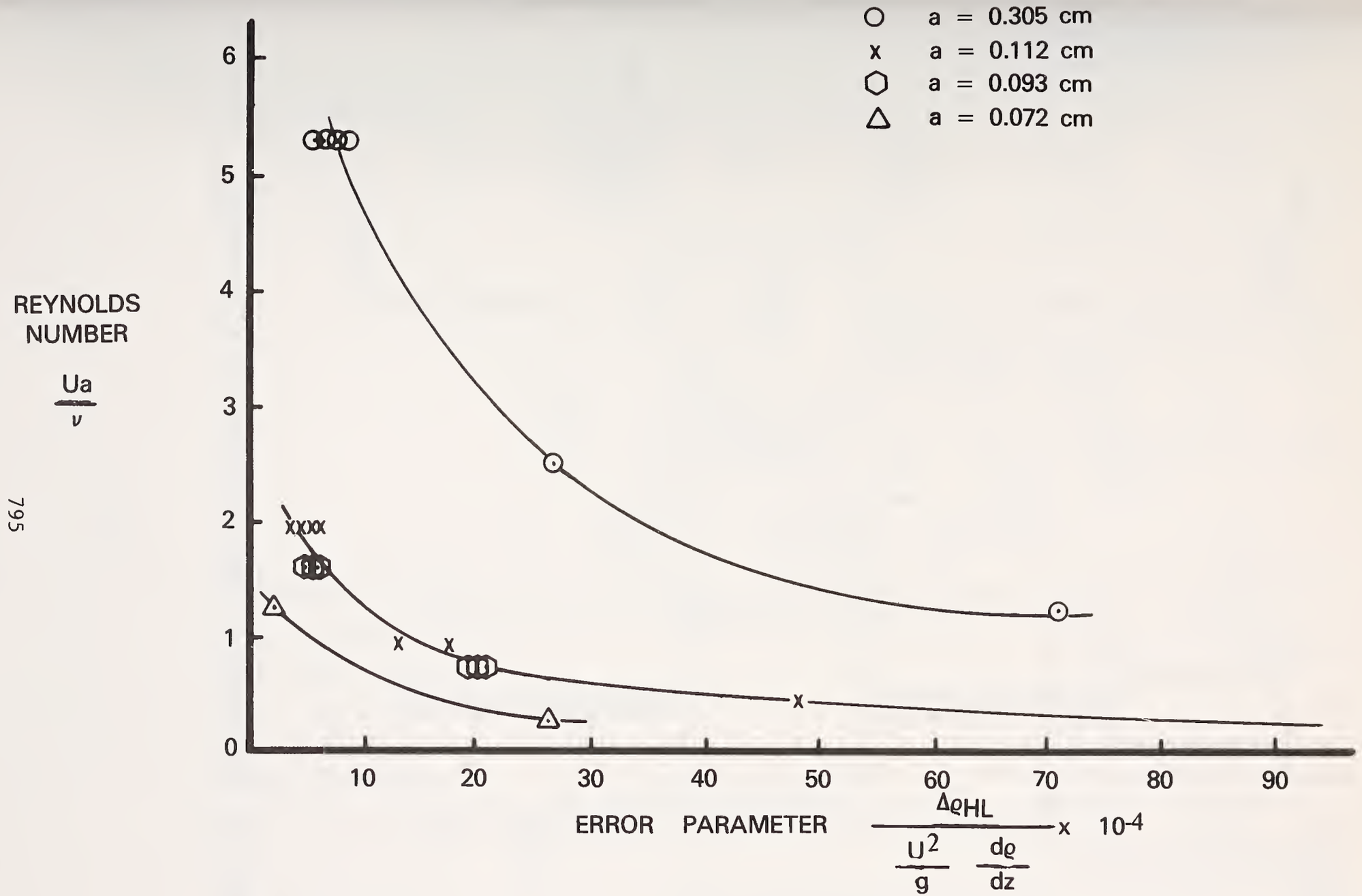

Figure 5 Reynolds Number Versus Error Parameter For Non-Oscillating Probes

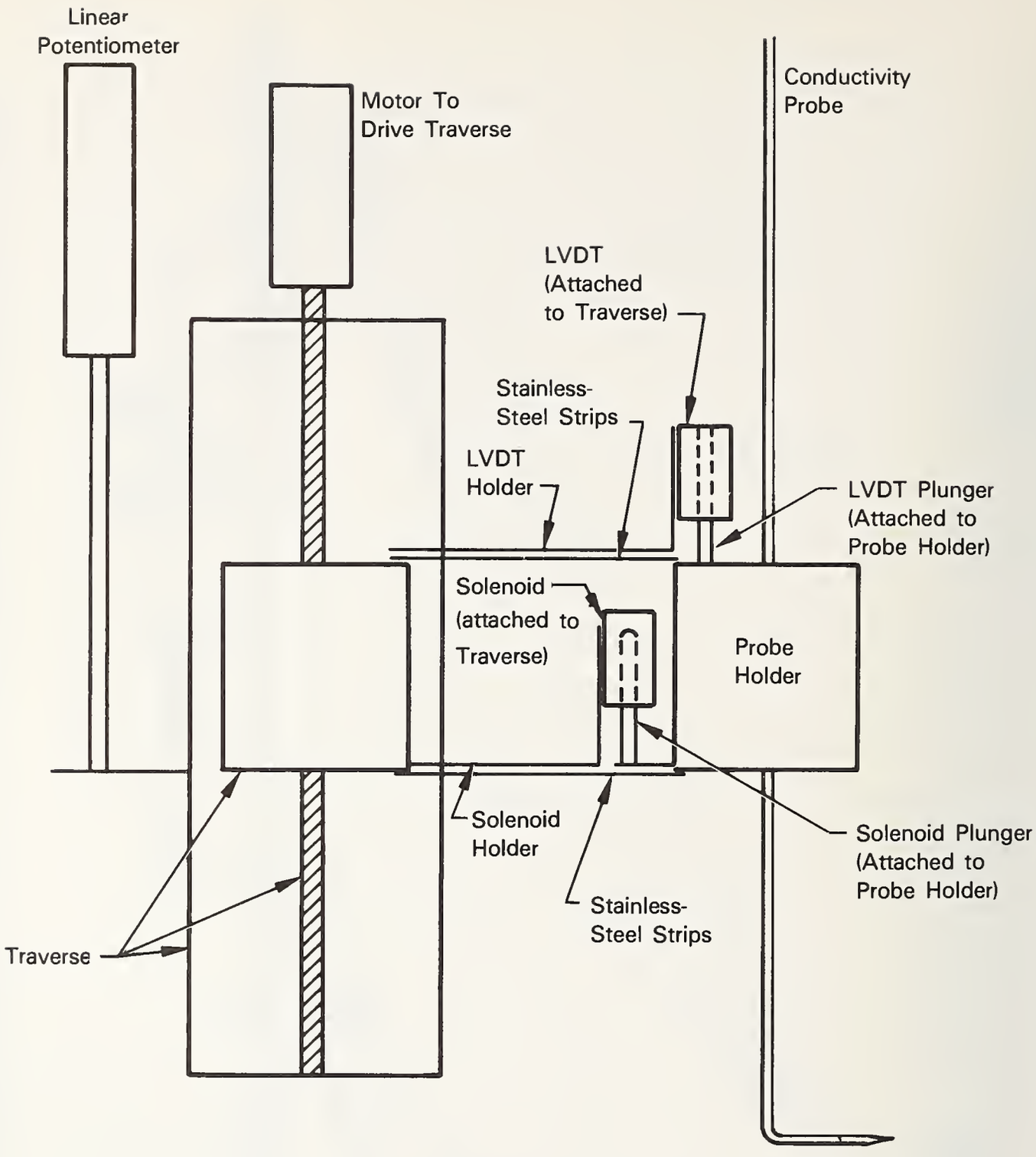

Figure 6 Schematic of the Oscillating Probe System

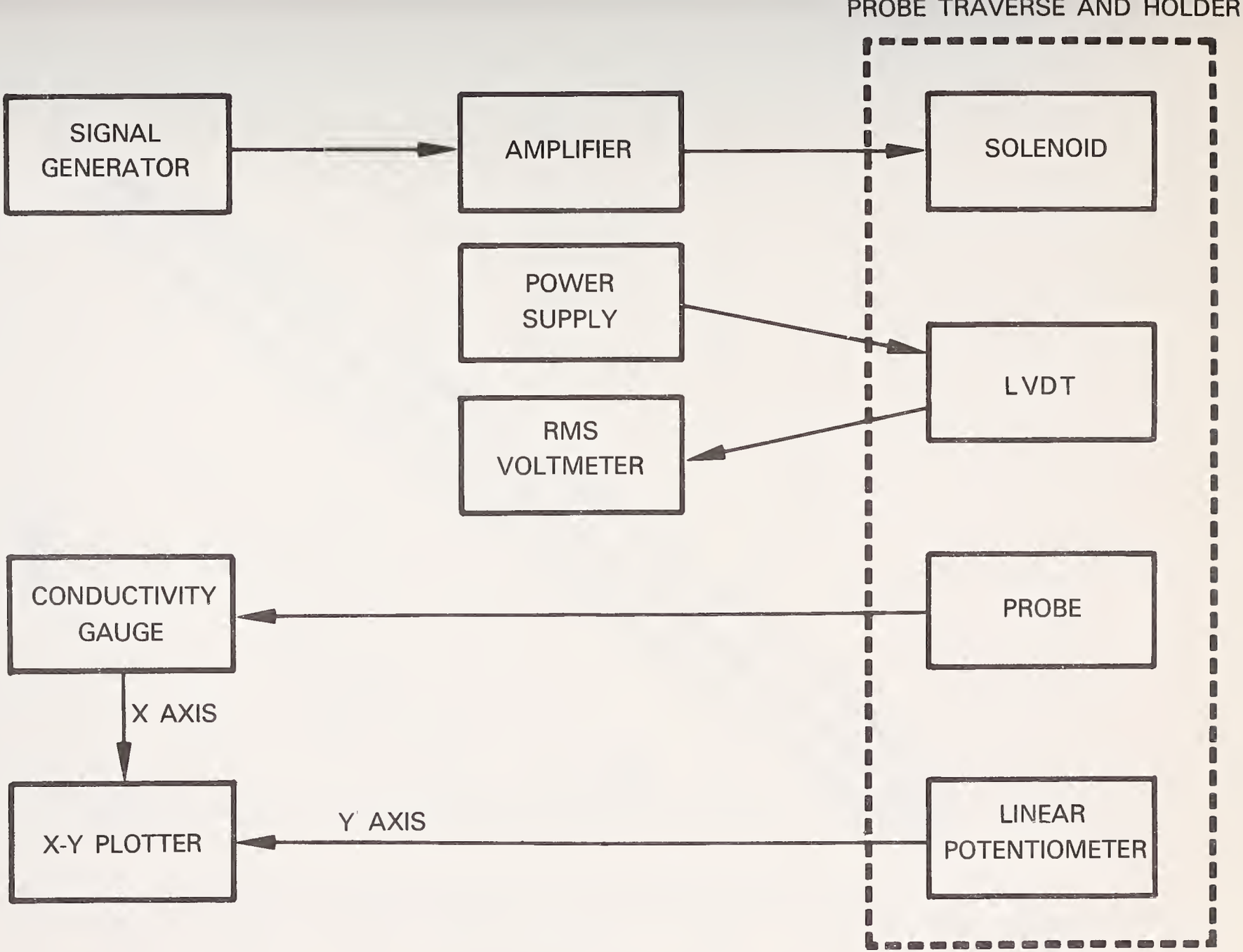

Figure 7 Block Diagram of the Electrical Circuit

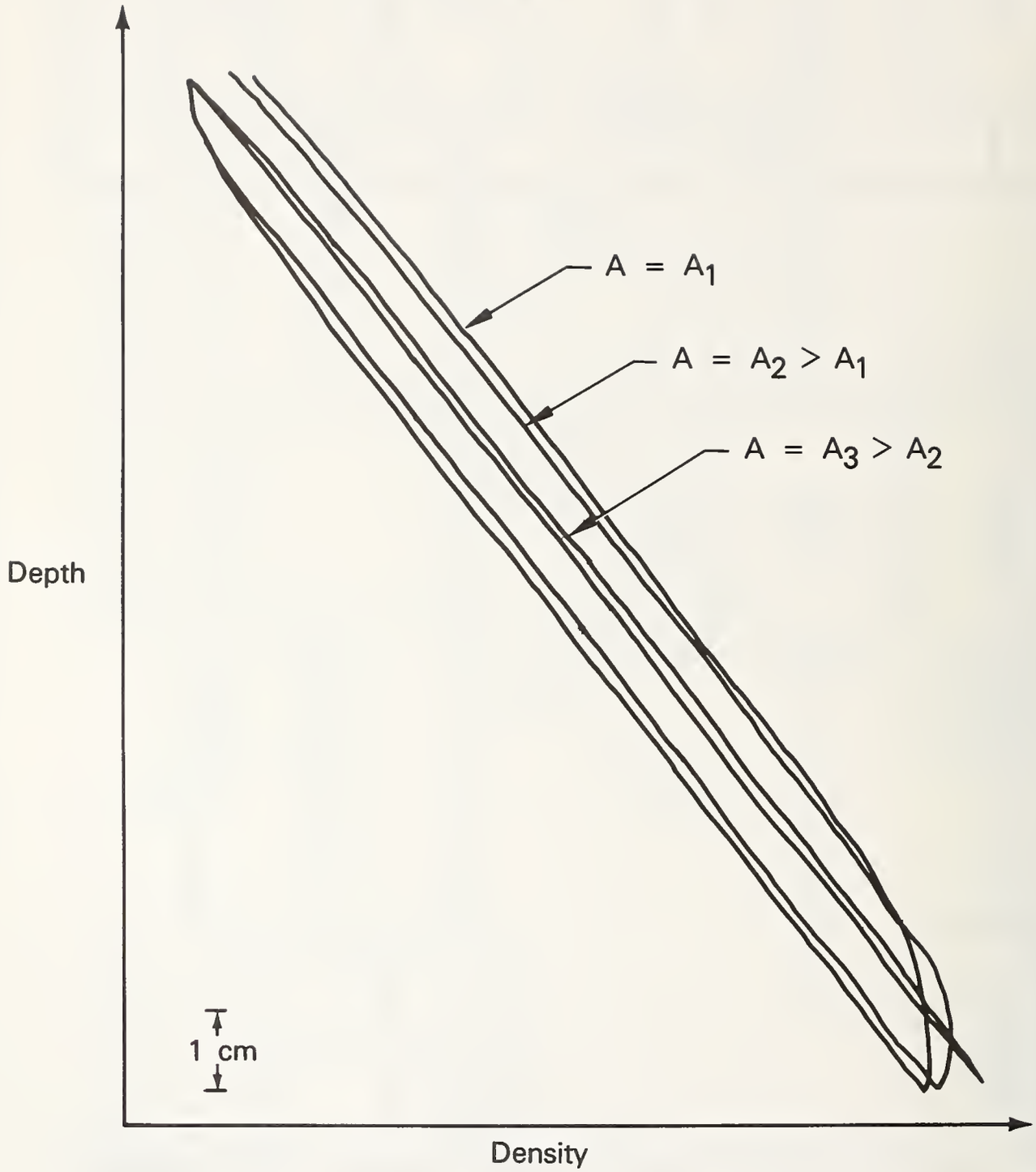

Figure 8. **Measured Density Versus Depth Profiles For An Oscillating Probe; a = 0.305 cm, U = 9.4 cm/min, $d\varrho/dz = 4 \times 10^{-4}$ gm/cm^4**

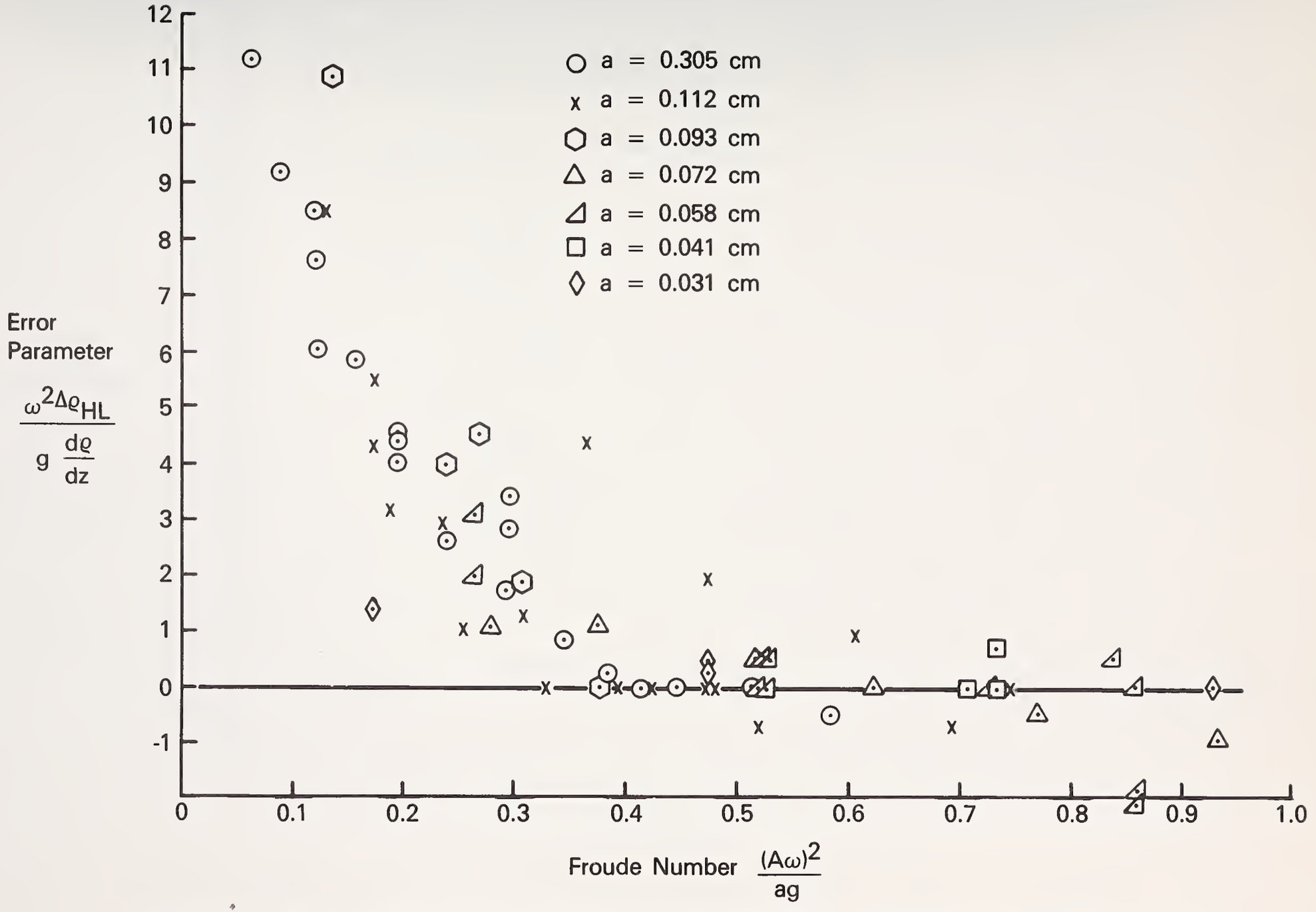

Figure 9 Error Parameter Versus Froude Number for Oscillating Probe Data

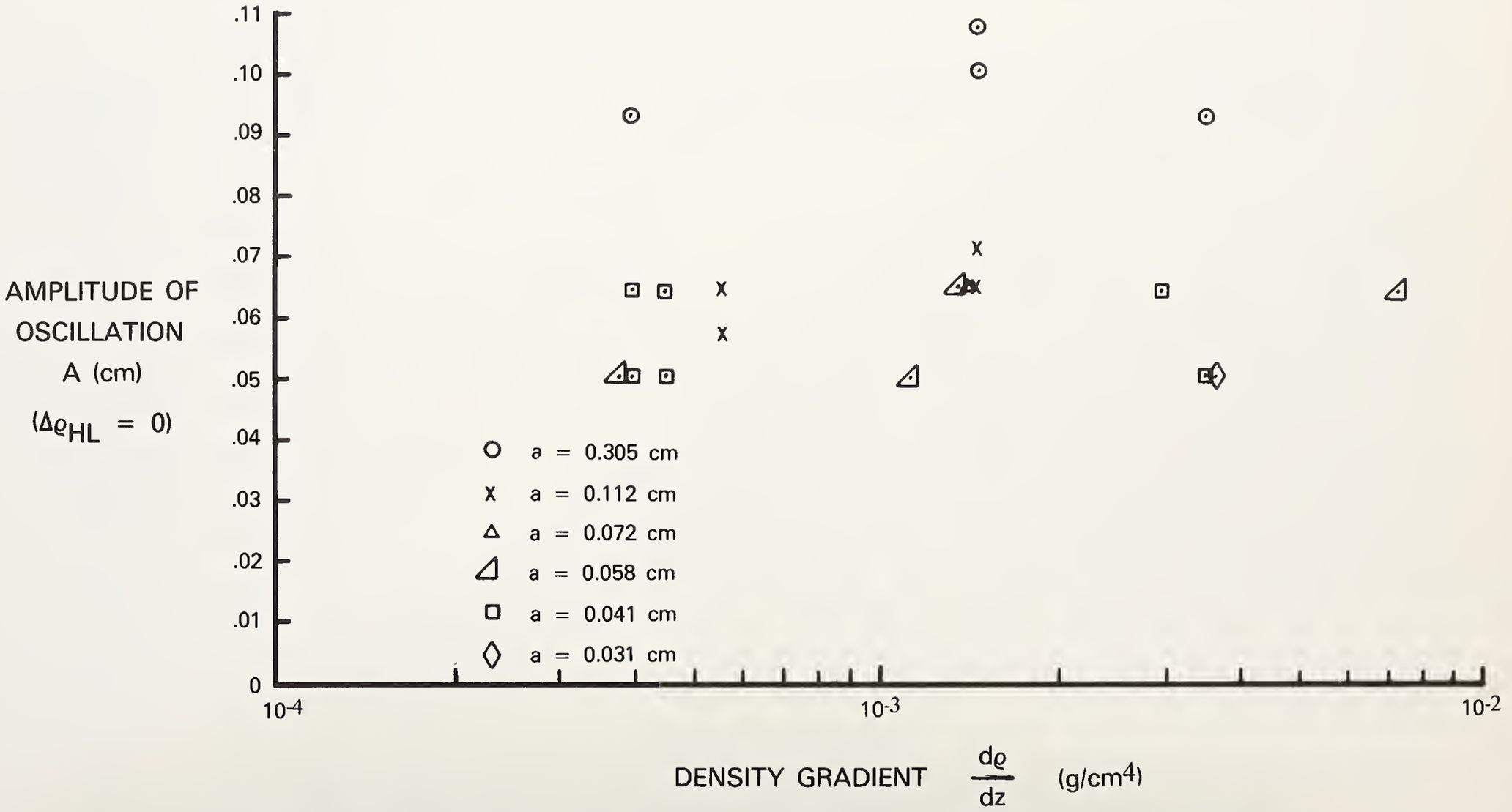

Figure 10 Amplitude of Oscillation For $\Delta\varrho_{HL}$=0 Versus Density Gradient, U = 9.4 cm/min

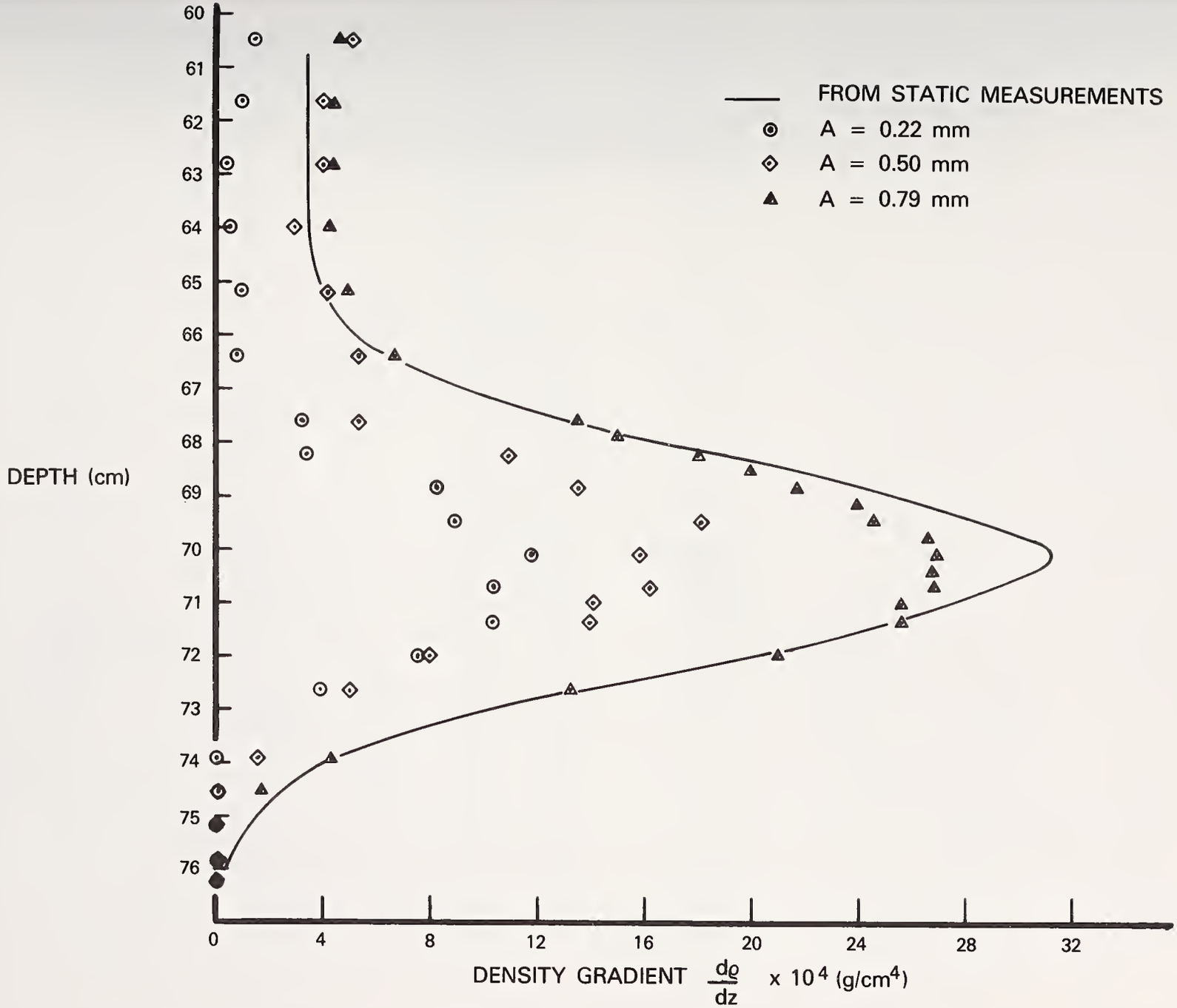

Figure 11 Measurements of Density Gradient With an Oscillating Probe, a = 0.058 cm

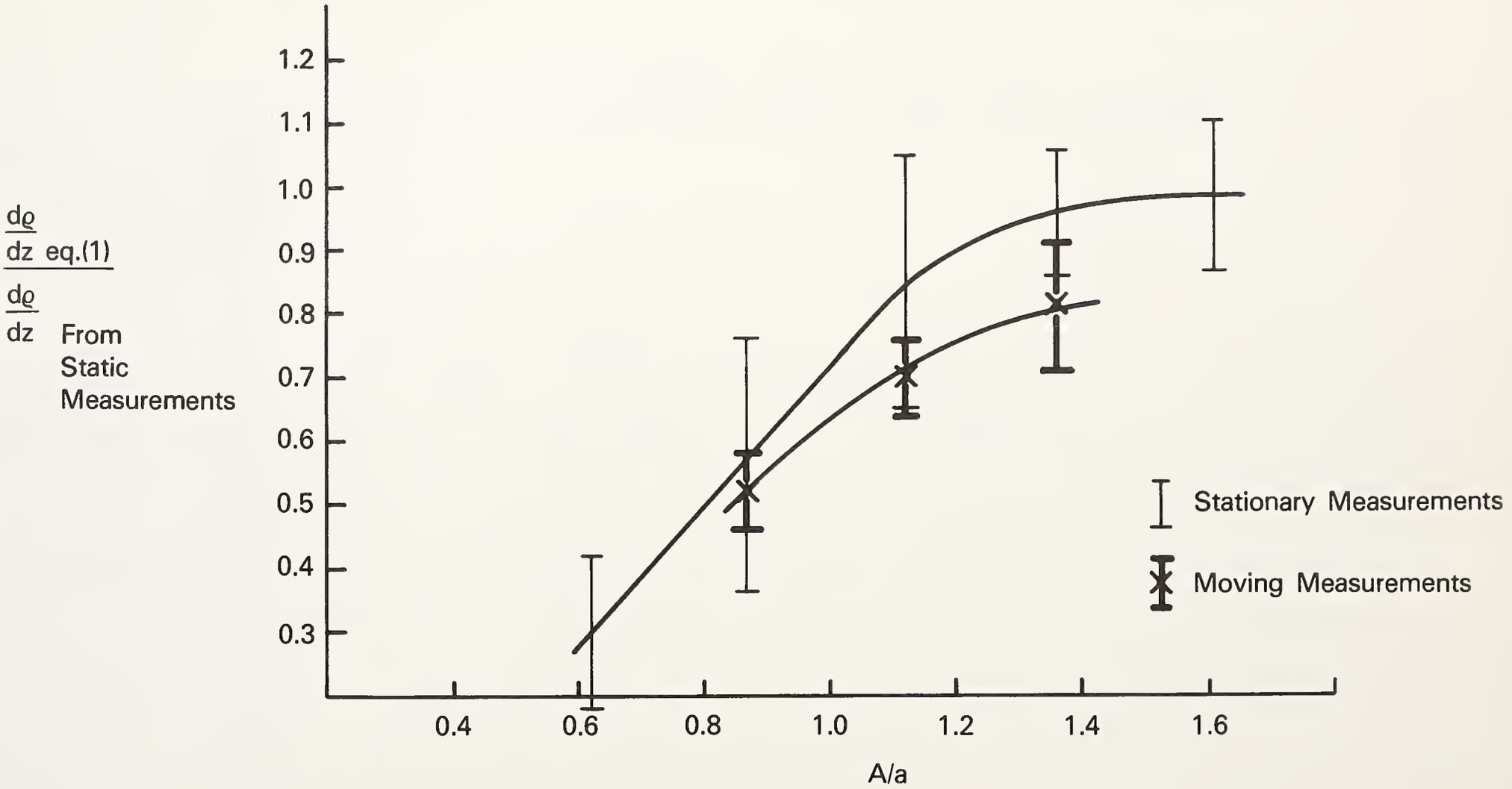

Figure 12 Density Gradient Measurements with an Oscillating Conductivity Probe , a = 0.058 cm

National Bureau of Standards Special Publication 484, Proceedings of the Symposium on Flow in Open Channels and Closed Conduits held at NBS, Gaithersburg, MD, February 23-25, 1977. (Issued October 1977)

NEW TECHNIQUES FOR AUTOMOTIVE FUEL FLOW MEASUREMENTS

Milton Baker

General Motors Proving Ground
Milford, Michigan 48042

1. Introduction

This paper discusses techniques for making accurate automotive fuel economy measurements using an in-line flow transducer and an electronic display unit. The paper reviews the fuel delivery system of a conventionally carbureted vehicle and describes some of the sources of flow measurement errors this system introduces. Design requirements for automotive fuel flow measurement instrumentation are developed and techniques are presented for making accurate flow measurements in the presence of these error conditions.

The descriptive material presented is general in format as each vehicle manufacturer has different design requirements for the fuel delivery system. Testing, however, has shown this information applicable to vehicles from a number of different vehicle manufacturers.

2. Fuel Delivery System - Conventionally Carbureted Vehicle

The fuel delivery system of a conventionally carbureted vehicle shown in Figure 1 consists of three major elements: the fuel tank, the fuel pump, and the carburetor.

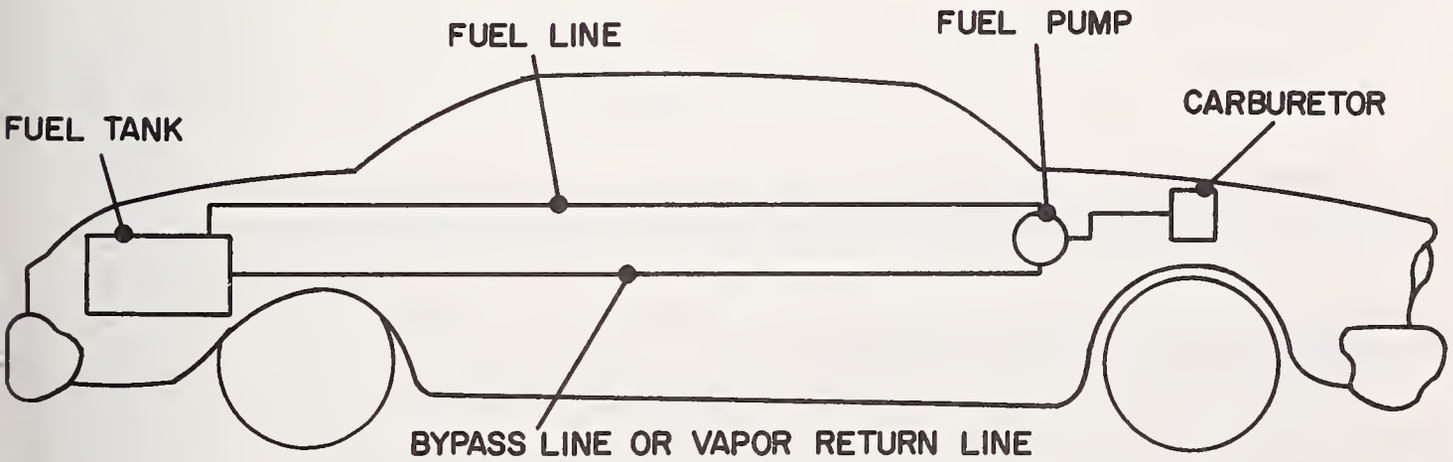

FIGURE 1. SIMPLIFIED FUEL DELIVERY SYSTEM DIAGRAM - CONVENTIONAL CARBURETOR

The fuel tank functions as the primary fuel reservoir for the vehicle. The fuel pump draws fuel from the tank and supplies it under pressure to the carburetor for metering into the engine.

Many vehicles contain fuel pumps with a bypass or vapor return line. On each output stroke of the pump, fuel is delivered primarily to the carburetor with a portion returned to the fuel tank. Orifices in the fuel pump outlet line and bypass line determine the flow rate ratio between fuel flow to the carburetor and return flow to the fuel tank.

The function of the circulating fuel loop between the fuel tank and fuel pump is to assure that cool, liquid fuel is supplied to the carburetor. This eliminates adverse vehicle performance due to vapor formation in the fuel line.

Fuel from the fuel pump outlet is delivered to a secondary fuel reservoir in the carburetor called the float bowl. A needle valve and float system maintain a predetermined level in the float bowl to assure adequate fuel delivery to the engine during transient conditions. When the level in the float bowl falls, the needle valve opens admitting fuel to the chamber until the predetermined fuel level is again reached.

It should be noted that the float bowl reservoir acts as a buffer accumulator between the fuel line and fuel consumed by the engine. During transient operations, fuel will begin flowing into the engine before the float level drops enough to admit fuel from the fuel line. Virtually all types of transducers which measure fuel flow into the float bowl will produce flow data which lags actual consumption during transient operation.

3. Potential Sources of Flow Measurement Errors in the Fuel Delivery System

Extensive study of the conventional vehicle fuel delivery system has isolated three major sources of error-producing flow conditions: reverse fuel flow, pulsating fuel flow, and fuel vapor.

A. Reverse Fuel Flow

Reverse fuel flow is a condition where fuel flows from the carburetor back to the fuel pump or tank during normal steady-state or transient driving conditions.

In order to understand the cause of reverse fuel flow, it is necessary to examine the vehicle's fuel pump shown in Figure 2.

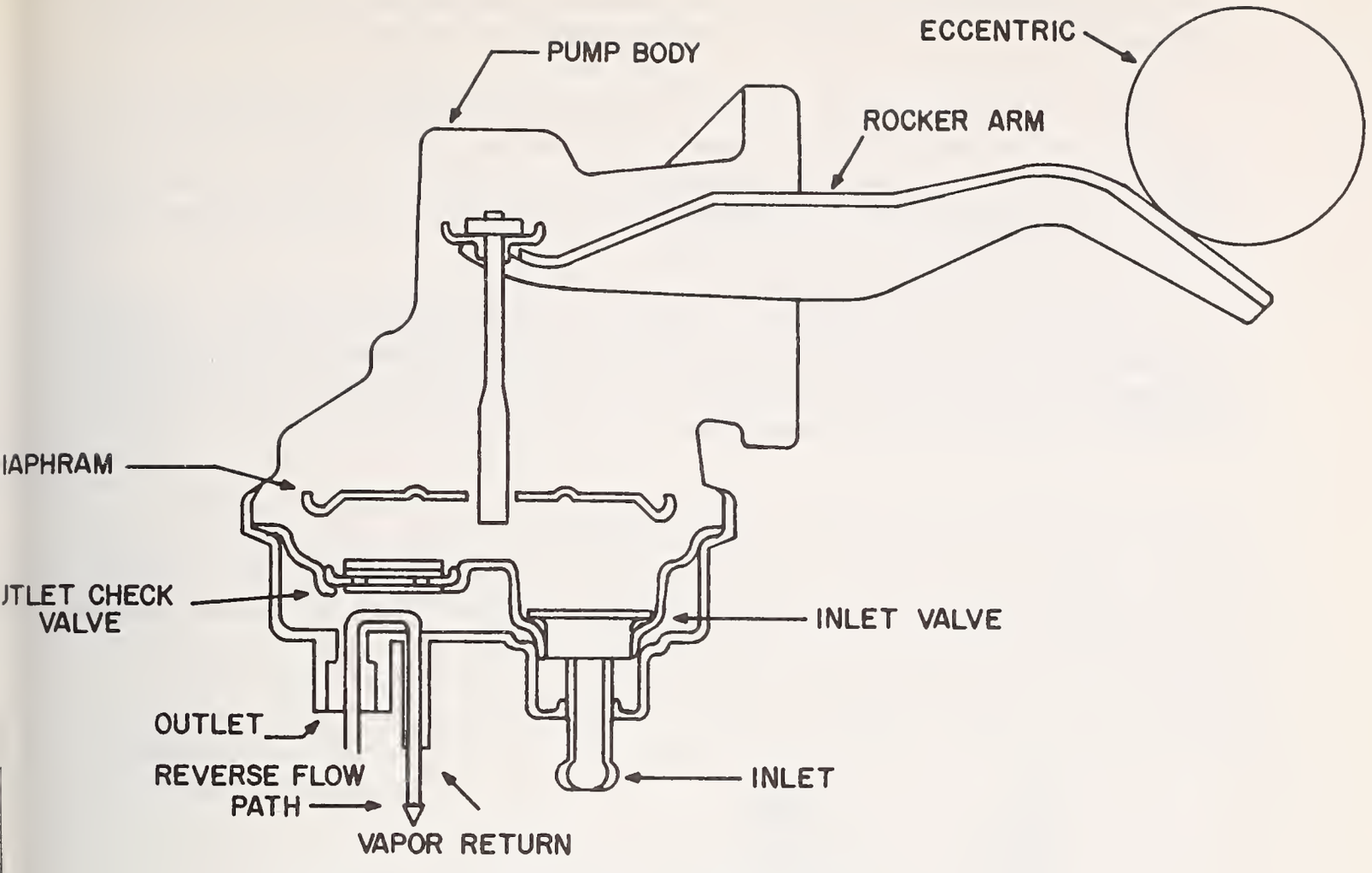

FIGURE 2. MECHANICAL FUEL PUMP

The fuel pump is a mechanically driven diaphram device. In operation, as the rocker arm driven by the engine camshaft moves down, fuel is drawn into the pump through the inlet valve. A check valve prevents any fuel from being expelled at the outlet. As the rocker arm moves up, fuel is displaced out of the pump chamber through the outlet line to the carburetor.

It can be seen that on the positive stroke of the fuel pump, when the outlet check valve is closed, a common chamber is formed between the outlet line and bypass line. Fuel from the carburetor at a higher pressure can flow through the outlet orifice to the fuel tank via the bypass line orifice.

Any element of compliance in the fuel line, such as vapor, exaggerates this condition. Large relative forward and reverse fuel displacements cause errors in in-line flow transducers.

This condition was first observed using high-speed motion picture photography with a turbine-type in-line flow transducer. Reverse flow produces large errors in transducers which are unable to determine fuel flow direction. Most transducers used in fuel consumption measurements cannot distinguish forward and reverse flow. Any flow, regardless of direction, causes the transducer to indicate fuel consumed. Without flow magnitude and direction sensing, in-line flow transducers have been observed to indicate as much as 100% higher than actual fuel consumption.

Another situation where reverse fuel flow is a serious error contributor is during long-term tests where the vehicle is turned off and then restarted.

When the vehicle is turned off, the fuel line will eventually drain from the carburetor to the fuel tank through the bypass line or system check valves. This fuel must be subtracted from the total; otherwise, when the vehicle is restarted, fuel necessary to charge the lines will be counted as fuel consumed. This can produce errors as large as 100-200 cm^3 of fuel consumed.

Because of errors contributed by reverse flow during vehicle operation, a design requirement for any in-line flow transducer is the ability to sense flow magnitude and direction. In addition, dither conditions where fuel is oscillating in the fuel line must produce a zero net flow indication.

B. Pulsating Fuel Flow

A second source of measurement error is pulsating fuel flow. The output pressure waveform from a mechanical fuel pump is shown in Figure 3.

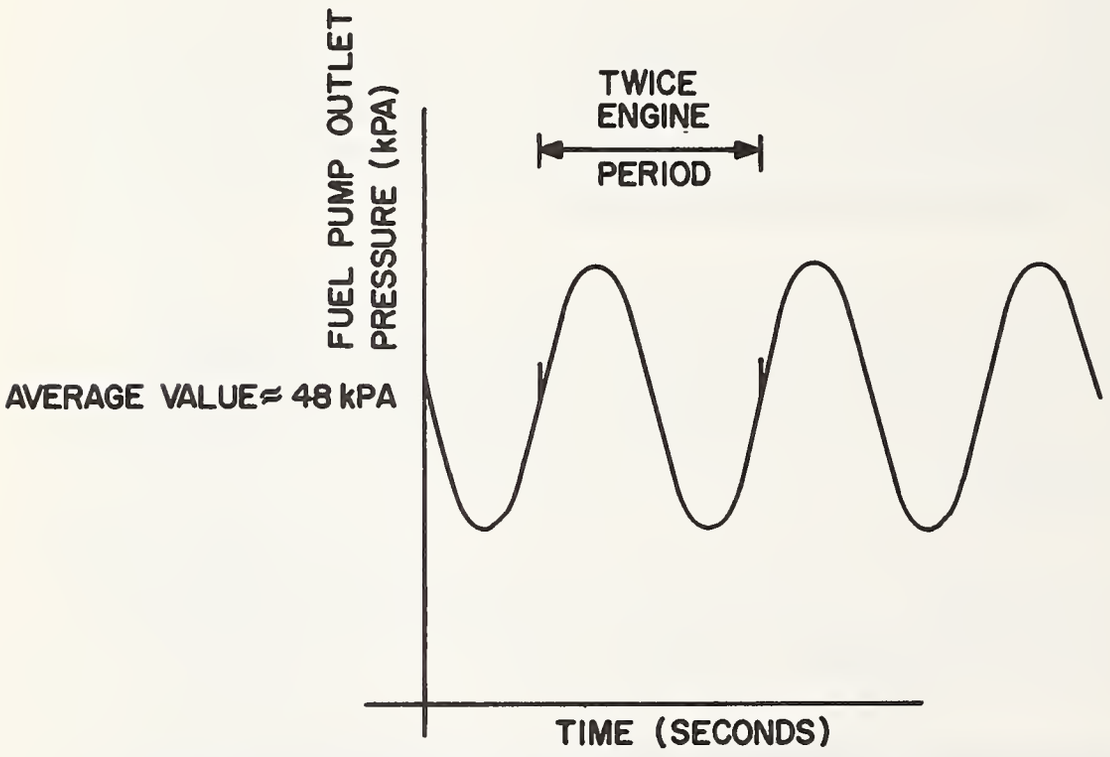

FIGURE 3. PRESSURE VS. TIME WAVEFORM FOR AUTOMOTIVE FUEL PUMPS

The superimposed time varying portion of the waveform, together with fuel line resonances, produces pulsating flow. In addition, the needle valve opens and closes periodically allowing fuel to surge into the float bowl. As with reverse flow, any element of line compliance magnifies the effect. These pulsating conditions can produce a water hammer effect causing the transducer to move in response to pressure pulsations.

Certain types of transducers, such as the turbine type, when excited by a pressure pulse continue to rotate due to paddle wheel inertia after fuel has stopped flowing. This "overcoasting" response to fluctuating pressure conditions in the fuel line can produce large errors in flow measurements.

C. Fuel Vapor

A third error source in automotive in-line fuel flow measurement is from fuel line vapor. Vapor is usually formed by excessive temperature conditions somewhere in the fuel line. The Reid Vapor Pressure (RVP) of fuel is an indication of the temperature at which fuel will vaporize. Different RVP fuels are used by customers in different ambient environment operating conditions to minimize the problem of engine vapor lock.

Volumetric transducers are very susceptible to vapor-induced measurement errors, due to the volumetric difference between a quantity of fuel in the liquid or vapor state. If the transducer rotating element is displaced by fuel vapor instead of liquid fuel, the transducer will indicate much higher flow rates than are actually encountered.

Transducers which operate with differential pressure across an orifice will produce erroneous outputs when vapor is present in the flow orifices. Vapor collecting within a transducer may cause the transducer to cease functioning as no fuel is present to make the transducer rotate.

4. Criteria for Automotive Fuel Measurement Systems

Many types of fuel transducing devices exist today employing a wide range of physical principles to produce outputs proportional to fuel flow rate.

The choice of a transducing technique is often dictated by practical considerations. The automobile manufacturers, United States Government agencies, and independent testing organizations perform fuel economy measurements on large vehicle fleets, using short-term, high-resolution tests run by unsophisticated test personnel.

These considerations dictate an easily installed and easily operated device capable of producing high-resolution measurements. Generally in-line flow transducers tend to fulfill these design requirements.

Other techniques such as gravametric and carbon balance measurements tend to be much more difficult to install and require sophisticated test personnel. These techniques are generally not applicable to vehicles operating on road test schedules and are usually confined to laboratory environments.

The in-line flow transducer element is compatible with testing goals of multiple, short-term, high-resolution automotive fuel flow measurements.

1. In-Line Flow Transducer Specifications

a. Flow Rate Range

A practical system must be capable of covering the .5 cm^3/s-20 cm^3/s flow rate range in order to be able to measure idle fuel flow on subcompact vehicles and wide open throttle conditions on large vehicles.

b. Linearity

The device should produce indicated readings which are within ±1% of actual readings over the .5 cm^3/s-20 cm^3/s flow rate range. Society of Automotive Engineers' specification J1082 calls for cumulative fuel consumption readings to be within .5% of actual values. A device with a ±1% of reading error versus flow rate curve situated symmetrically around the zero error line can meet this specification.

c. Resolution

With emphasis on vehicle fuel economy and projections for more fuel-efficient vehicles, resolution becomes important. A practical cumulative fuel measurement resolution is .1 cm^3.

The Society of Automotive Engineers' J1082 specification requires 3.785 cm^3 resolution (.001 gallons); however, for many test schedules, this resolution is too course to resolve the .5% of reading accuracy specification.

d. Pressure Drop

For any in-line transducer, pressure drop is an important consideration. Too large a pressure drop can affect vehicle performance. A specification of 14 kPa maximum pressure drop at 20 cm^3/s has been found to have minimal effect on vehicle operation.

e. Bidirectionality

A transducer must maintain the same pressure drop and "K" factor (fuel displacement/revolution) in both directions so that reverse flow may be measured and accounted for.

f. Safety

Transducers which mount in the passenger compartment without outside venting, or have glass burettes which could become broken in the passenger compartment, could pose a safety hazzard. Any electrical wiring should be explosion-proof.

g. Ease of Installation

As previously mentioned, the ability to mount the transducer quickly on board the vehicle greatly facilitates testing programs.

A wide variety of commercially available transducers have been evaluated against these design specifications at General Motors Proving Ground. Devices which perform flow filtering, use auxiliary fuel pumps, pressure regulators and pulsation dampers have been found unacceptable because of alterations to the vehicle fuel delivery system. Devices which consume large amounts of electrical power, such as electrically driven pumps, may also influence fuel economy.

Turbine type flow meters can meet pressure specifications, but are subject to reverse flow and pressure pulsation errors associated with the dynamics of the internal paddle wheel.

Differential pressure drop across an orifice devices seldom can meet dynamic range specifications without multiple orifices and a complicated hysteresis switching system. The problem of orifice switching in the presence of dynamically changing flow conditions produces errors.

Vane type transducers are sensitive to pressure pulsation and reverse flow conditions. Multiple chamber reservoir systems where fuel fills one reservoir while the vehicle runs on the other reservoir have high pressure drops and leakage associated with solenoid switching times.

Testing has shown the positive displacement transducer the best choice. Positive displacement transducers are affected by reverse flow and vapor; however, are not subjected to inertial coasting effects. Only fuel moving through the transducer will cause the device to rotate. Fuel present at the outlet will inhibit further rotation.

A positive displacement transducer can be made bidirectional so that fuel displacement/revolution is the same in either direction.

The important characteristic of the positive displacement device is that barring vapor and leakage only precise quantities of fuel through the measurement element will cause the device to rotate.

Positive displacement transducers are subject to leakage errors through the device which are usually prevalent at low flow rates. Vapor causes large errors in positive displacement systems. No positive displacement transducer is capable of accurate flow measurements without external electronic hardware to recognize and correct for various error conditions.

2. Electronic Specifications

The previous sections discussed sources of error and the selection of a positive displacement flow transducer as a best choice. No positive displacement transducer evaluated was capable of eliminating error source contributions.

A strategy was adopted employing a four-piston positive displacement transducer with an integrated electronics unit to recognize error producing flow conditions and to correct for them. The concept of an underhood mounting transducer and manifold assembly and a dashboard mounting electronics signal conditioning and display unit forms the basis for a General Motors-designed precision fuel measurement system shown in Figure 4. This section describes the design of the electronics unit. These techniques have general application in flow measurement systems.

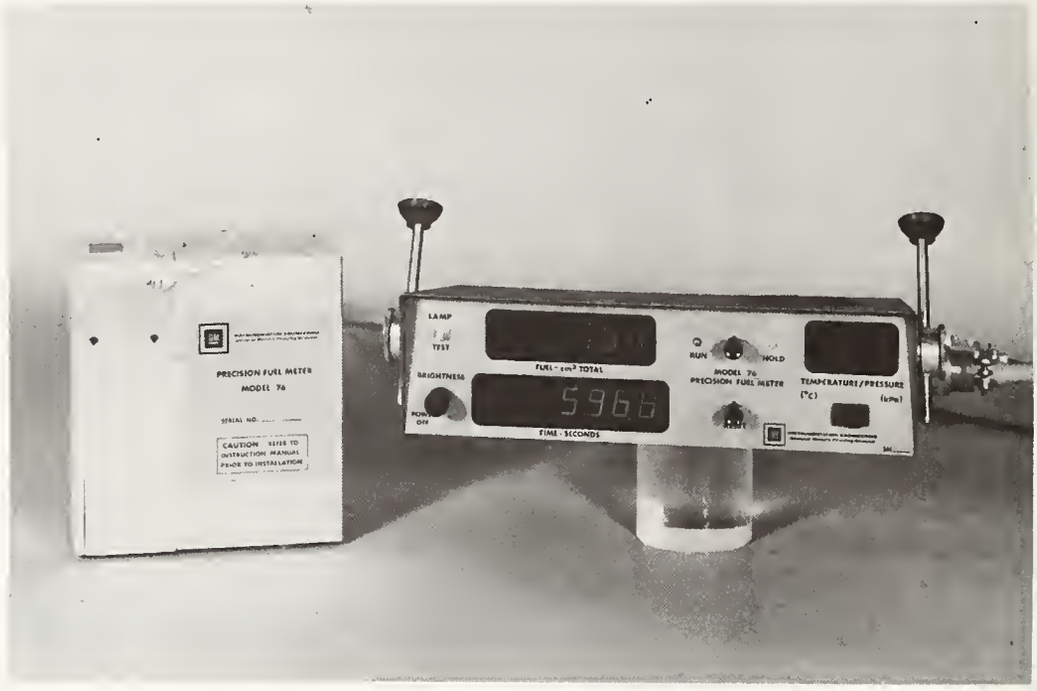

FIGURE 4. MODEL 76 PRECISION FUEL METER

5. Techniques For Reducing Contributions From Sources of Error

A. Reverse Flow Errors

A primary error contributor is reverse fuel flow, where fuel is flowing from the carburetor to the fuel tank during normal vehicle operation. To make accurate flow measurements with reverse flow present, fuel flow magnitude and direction must be sensed.

Most all in-line positive displacement flow transducers convert rotational motion of the transducer element to an electronic signal with optical electronics, hall effect switches, reed switches, etc.

A way to produce flow magnitude and direction signals is to place two pick-up devices 45° apart so that a quadrature phase signal is produced. This is shown schematically using an optical technique in Figure 5.

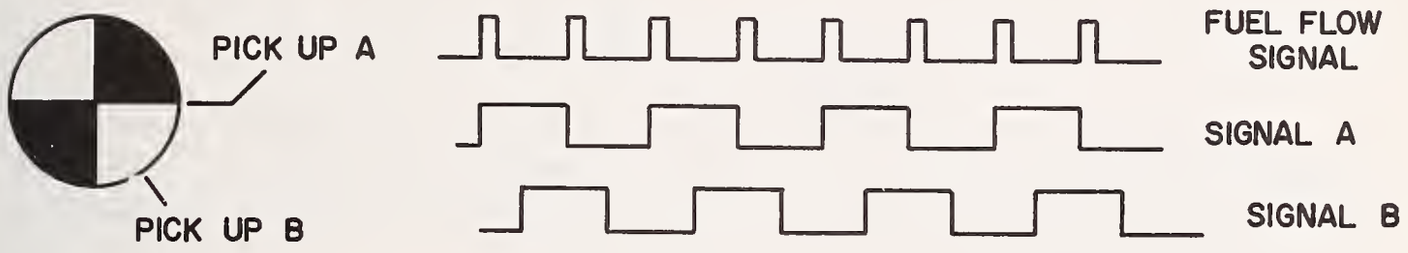

FIGURE 5. QUADRATURE SYSTEM

Each edge of the signal A represents a quantity of fuel flowing. Signals A and B are sent to an electronic circuit which differentiates signal A to produce fuel flow magnitude and uses signals A and B to decode fuel direction, using the algorithm shown in Figure 6.

TRANSITION OF A	STATE OF B	DIRECTION
⌐	LOW	FORWARD
¬	HIGH	FORWARD
⌐	HIGH	REVERSE
¬	LOW	REVERSE

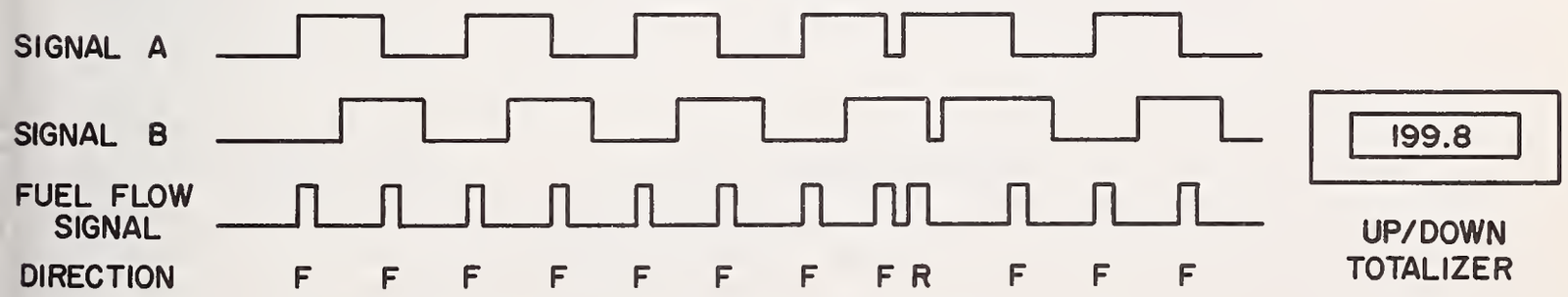

FIGURE 6. QUADRATURE ALGORITHM AND ILLUSTRATION

The flow magnitude and direction information signals are sent to an up/down fuel flow counter. Magnitude pulses with forward direction information cause the counter to increment; magnitude pulses with reverse direction information cause the counter to decrement.

With this technique, all forward and reverse fuel flow is accounted for. This technique has been found very effective in reducing reverse flow errors.

B. Pulsating Fuel Flow Errors

As shown in the quadrature phasing diagram of Figure 6, should the transducer dither (oscillate forward and backward a short distance) at a pick-up site, forward and reverse counts are added and subtracted with a zero net flow indication. This technique is effective in eliminating pulsating flow errors.

C. Vapor Induced Errors

A major source of measurement error affecting in-line flow transducers is fuel vapor. Vapor conditions are primarily the result of excessive temperature conditions.

Vapor induced errors can be controlled in a number of ways. Since vapor is primarily produced by high temperature, the transducer should be located where it will remain cool.

As previously mentioned, using a fuel with a lower Reid Vapor Pressure will help eliminate any temperature problems.

With many installations, however, alternative techniques must be used. Two effective techniques are vapor elimination and optical vapor detection.

Vapor Elimination

A vapor eliminator at the inlet to the transducer has been effective in eliminating system vapor. Although this vapor represents fuel lost, it is eliminated prior to the transducer so that vapor loss is not a source of measurement error.

An effective vapor eliminator is shown in Figure 7.

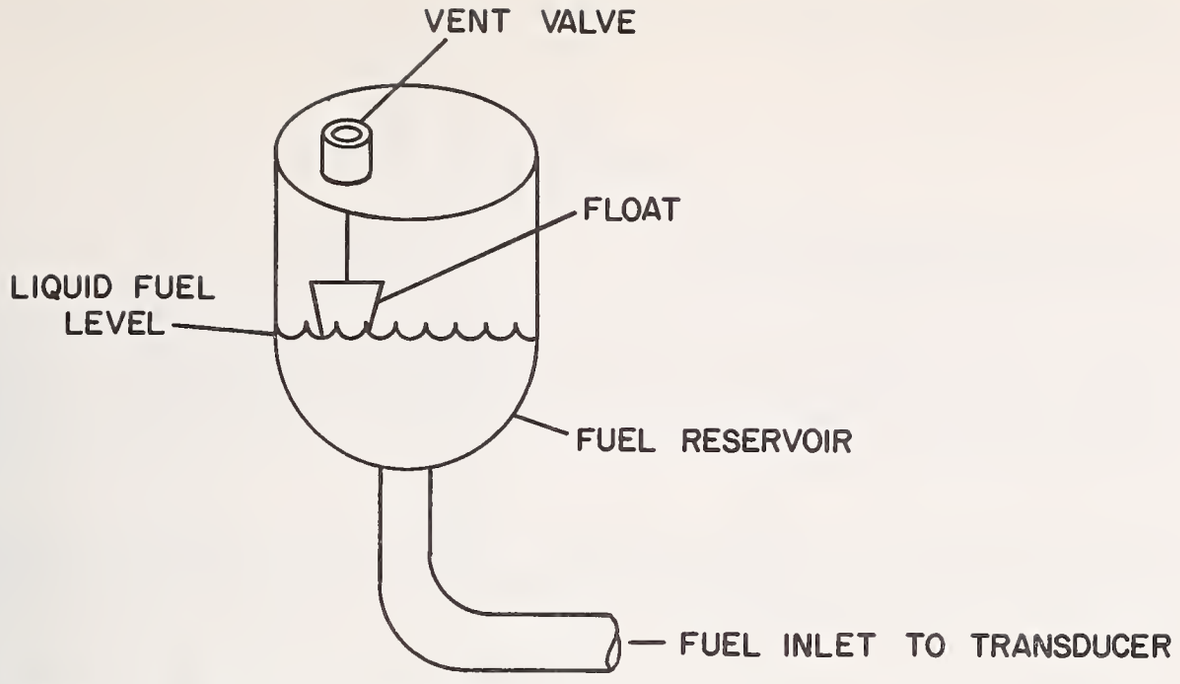

FIGURE 7. VAPOR ELIMINATOR DETAIL

Vapor which is lighter than liquid fuel rises as liquid fuel moves down toward the transducer inlet. As more vapor and less fuel enter the chamber, the float falls allowing the vapor to vent to atmosphere. When the fuel becomes almost totally vapor, the vapor eliminator may become ineffective and vapor will move into the transducer producing measurement errors.

Optical Vapor Detector

To warn the operator that vapor is passing through the transducer, an optical vapor detector can be incorporated in the transducer manifold.

The optical vapor detector contains a light emitting diode and phototransistor focused across a clear glass tube in which fuel is flowing.

Normally, the fuel maintains a clear optical path allowing the light emitting diode to sustain the phototransistor in a saturated state. When a bubble is present, an optical distortion is produced at the liquid-vapor interface (meniscus) which momentarily upsets the optical path and turns off the phototransistor. Phototransistor turnoff is connected to an audible warning device indicating the presence of vapor. The unit is shown schematically in Figure 8.

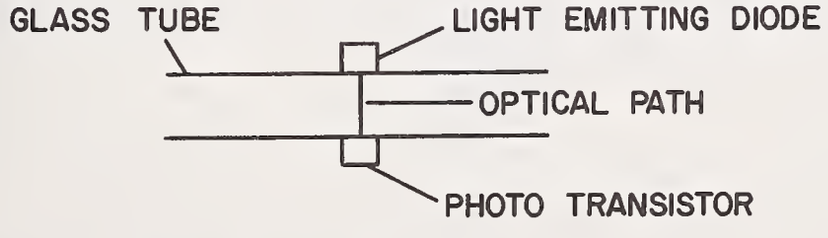

FIGURE 8. OPTICAL VAPOR DETECTOR - SIDE VIEW

Vapor elimination and optical vapor detection have been found effective in reducing vapor induced errors.

D. Additional Considerations

1. Conversion to Engineering Units

Each transducer element is configured to produce electronic pulses to indicate the number of times the transducing element was rotated. Each transducer will have a slightly different fuel displacement/revolution or "K" factor due to machining and assembly tolerances.

Precision fuel measurement requires each transducer to be individually calibrated and its "K" factor used to generate a conversion from transducer rotations to engineering units (cm^3 of fuel).

A technique which has been incorporated in the General Motors Precision Fuel Meter is to store an 8-bit binary representation of the "K" factor for each transducer in the transducer manifold. This binary word programs the electronics display unit to correctly convert transducer pulses to engineering units. This technique permits transducers to be used interchangeably with electronics display units.

As an example of how this works, consider a transducer which displaces 10.8 cm^3 of fuel per revolution. If there are ten evenly spaced electronic pulses generated for each transducer revolution, each electronic pulse represents 1.08 cm^3 of fuel. For this transducer, the number 108 would be stored in the transducer manifold.

The electronics uses the binary number representing 108 to cause exactly 108 high-frequency pulses to be generated for each electronic pulse from the transducer (effectively multiplying the number of input pulses by 108). The high-frequency pulses are divided by 100 so that the first pulse from the transducer produces 1 pulse output from the divide-by-100 circuit with a residual of 8 left in the divider.

The first 12 transducer pulses produce 12 output pulses from the divider with a residual of 96, and the display will read 12. When the next pulse from the transducer is received, 108 pulses are produced by the high-frequency clock and the display increments by 2 (96 residual plus 108 divided by 100 equals 2.04) and indicates 14 correcting the display since each transducer pulse represents 1.08 cm^3 of fuel. The electronics will continue to correct throughout the measurement period. Figure 9 shows in detail the quadrature detector integrated with the engineering unit converter and totalizer.

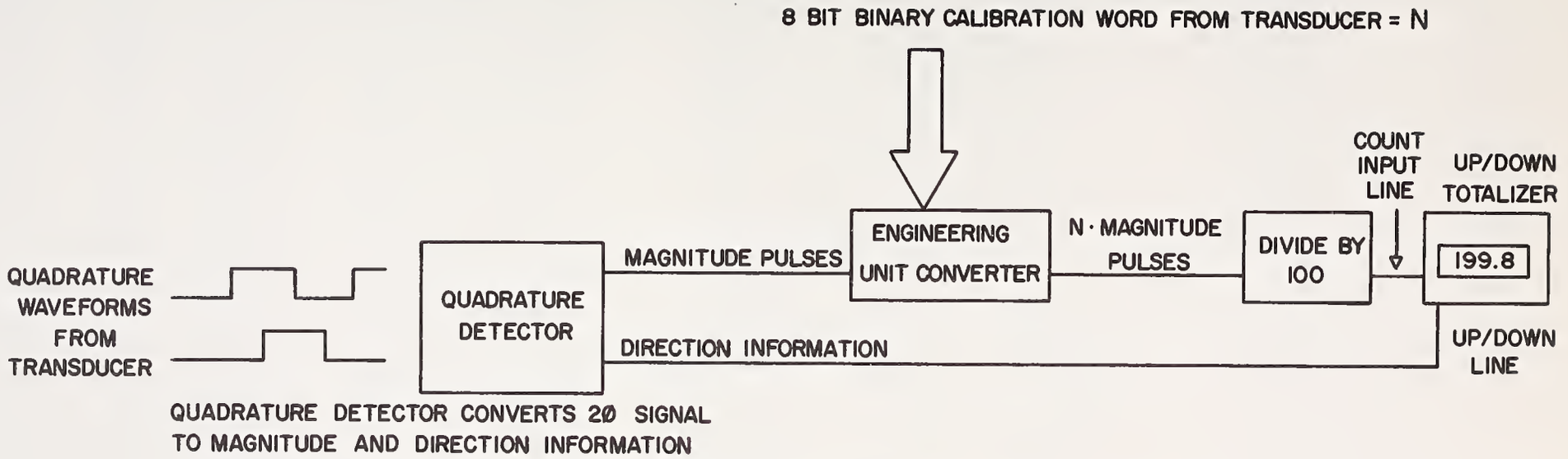

FIGURE 9. QUADRATURE DETECTOR INTEGRATED WITH ENGINEERING UNIT CONVERTER.

2. Electrical Noise Immunity

Many fuel-measuring devices are connected to the vehicle electrical system and therefore are subject to a very noisy, poorly regulated power source. Care must be taken to ensure that data is actual and not the result of transient electrical noise produced by the vehicle electrical system.

Techniques which increase system noise immunity including isolating power supplies, high noise margin logic such as CMOS, shielding, transient suppression, and extensive filtering at high and low frequencies should be incorporated. It is also recommended that test instrumentation be shielded from sources of Radio Frequency Interference.

3. Data Displays

Three basic display parameters are desirable in an automotive fuel measurement device: cumulative cm^3 of fuel, elapsed test time, and fuel temperature.

Cumulative fuel measurements with elapsed time information can be used for totalized fuel measurements or flow rate information. Fuel temperature information is required for volumetric temperature corrections. One degree celcius readout accuracy allows volumetric correction to within .1%.

In addition, a display of transducer outlet gauge pressure is often desirable to ensure correct operation of the transducer element. Low outlet pressure (with respect to atmospheric pressure) indicates incorrect operation of the transducer element.

4. Display Technology

A wide range of display technologies are available to designer. Analog meters for flow rate measurement can generally become damaged in the vibratory automotive environment.

Digital displays for automotive use require high intensity for readability on high ambient light days and low ambient light levels for nighttime viewing.

Planar gas discharge displays have been found to be intense enough for daytime viewing and with a dimming circuit acceptable for nighttime use. No other type of display appears to provide this much dynamic intensity.

6. Calibration And In-Vehicle Accuracy Verification

Two types of testing are required to assure the accuracy of instrumentation used for precision automotive fuel flow measurements. Laboratory calibration is used for setting "K" factor and checking the operational accuracy of the device.

In-vehicle accuracy verification is used to assure that the device works correctly in the actual measurement environment (the automotive fuel system). A large number of devices advertised as fuel economy measurement instruments have never been accuracy tested on an operating vehicle.

A. Laboratory Calibration Techniques

A laboratory calibration facility should be capable of producing accurate, repeatable fuel flow while simulating conditions encountered in the vehicle fuel delivery system. The calibration facility in Figure 10 meets these design requirements.

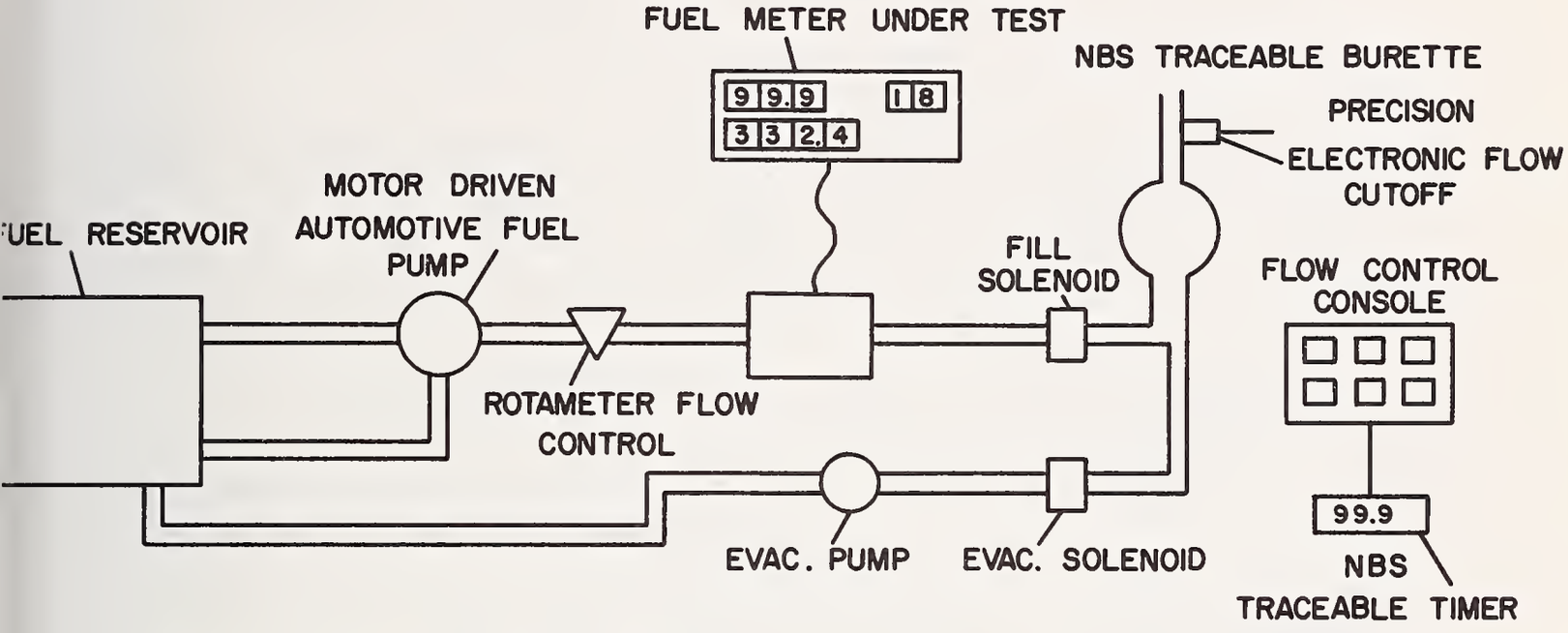

FIGURE 10. PRECISION FUEL METER CALIBRATION FACILITY

A fuel reservoir is used to store calibration fuel. The mechanical fuel pump driven by an electric motor causes fuel to flow through the fuel meter under test into a National Bureau of Standards traceable burette system. Calibration fuel should be of the type the fuel meter is to be used with so that viscosity induced errors show up during calibration.

In operation, a console starts fuel flowing through the fuel meter into the burette system. The rotameter is set for an approximate flow rate. The exact flow is determined at the end of the test. The console control will then evacuate fuel to the zero line on the burette. An electronic shutoff closes the evacuate solenoid precisely when the zero line is reached.

In the run condition, fuel flows through the fuel meter into the burette. When a precise fuel level is reached, the electronics simultaneously shuts off the fuel meter under test, the burette fill solenoid, and a National Bureau of Standards traceable timer.

Three numbers are obtained at the conclusion of the test: cm^3 of fuel in the burette, indicated cm^3 from the fuel meter under test, and test time from the precision timer.

Burette cm^3 divided by test time produces test flow rate. Percentage error is computed by comparing burette cm^3 and indicated cm^3 from the fuel meter.

A graph can be plotted expressing percentage error versus flow rate for the fuel meter under test. Figure 11 shows a sample data table and graph.

BURETTE cm^3	METER cm^3	Δ cm^3	TIME (s)	FLOW RATE	PERCENT ERROR
1000.0	999.0	-1.0	322.87	3.097	-.1
1000.0	998.0	-2.0	500.0	2.00	-.2

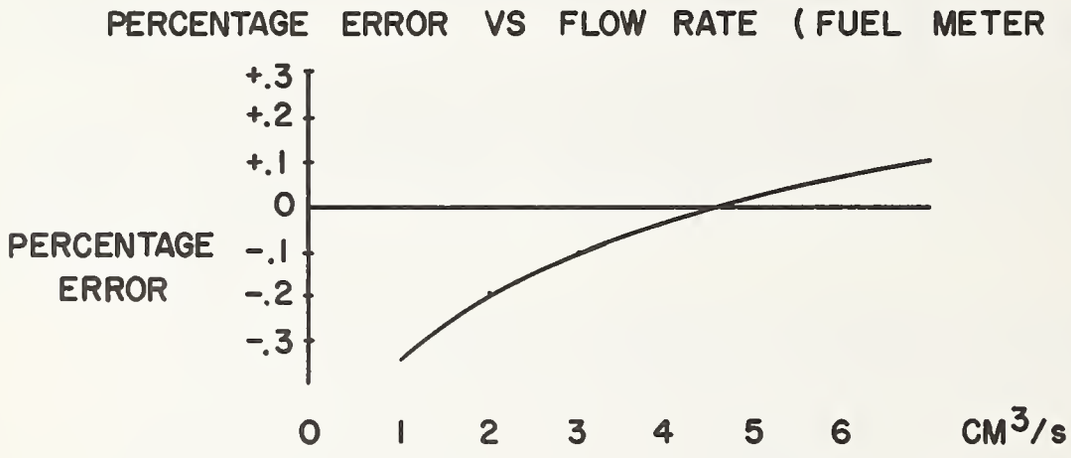

FIGURE 11. SAMPLE CALIBRATION DATA

B. In-Vehicle Accuracy Testing

Any on-board fuel measurement system must be tested for accuracy on an operating vehicle. A technique has been developed using a small, light, aluminum alternate source fuel tank for in-vehicle testing.

A test system is shown in Figure 12. The alternate source fuel tank is closely coupled to the fuel pump to minimize non-repeatable line initialization problems. The fuel tank is connected to the fuel pump with quick disconnect type fittings.

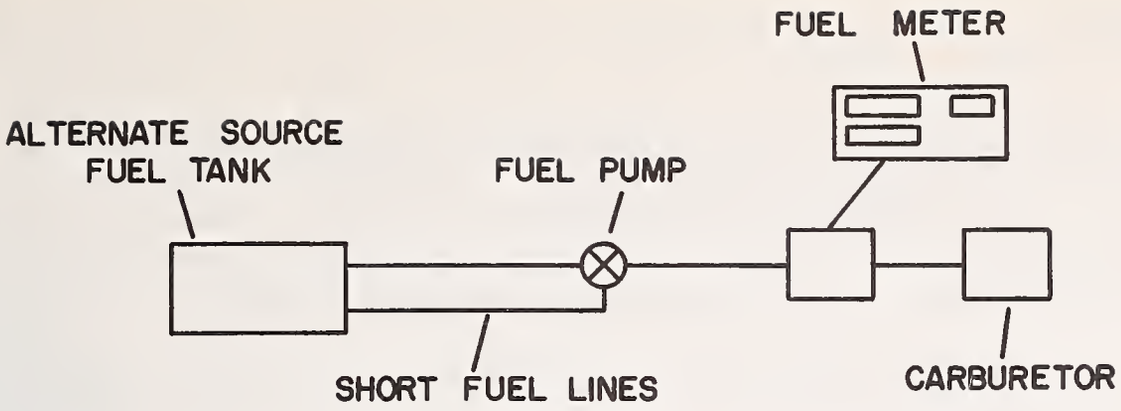

FIGURE 12. IN-VEHICLE TEST INSTALLATION

The tank is weighted prior to connection to the fuel pump. When the test commences, the fuel meter is actuated and the vehicle driven in a dynamometer. Temperature conditions can be varied within the dynamometer cell.

Fuel temperatures should be sampled and logged during vehicle operation.

At the conclusion of the test, the tank is uncoupled from the vehicle and weighted. Knowing the fuel density accurately for the test conditions, calculated fuel consumption can be obtained from the following formula:

$$\frac{\text{initial weight (grams)} - \text{final weight (grams)}}{\text{density at test conditions}} = \text{cm}^3 \text{ of fuel consumed}$$

This number can be compared with measured fuel consumption data from the fuel meter with volumetric corrections made for temperature changes. Using this technique, a percentage error can be calculated for a fuel meter installed on an operating vehicle.

7. Conclusion

The techniques presented in this paper of bidirectional counting, vapor elimination and optical vapor detection, individual transducer calibration and digital conversion of data to engineering units, electronic noise suppression, precision calibration techniques and the use of a positive displacement fuel transducer have been found effective in reducing the sources of error on fuel measuring systems.

These techniques have been incorporated in a precision fuel measurement system designed by General Motors Corporation.

Although the paper focuses on techniques for reducing fuel flow measurement errors on conventionally carbureted vehicles, many of these techniques are directly applicable to fuel economy measurements on fuel injected vehicles, diesel engine vehicles and vehicles with non-standard fuel delivery systems. Further information on application of these techniques to any of these vehicles may be obtained by contacting the author at General Motors Proving Ground.

National Bureau of Standards Special Publication 484, Proceedings of the Symposium on Flow in Open Channels and Closed Conduits held at NBS, Gaithersburg, MD, February 23-25, 1977. (Issued October 1977)

DIGITAL COMPENSATION TECHNIQUES FOR POSITIVE-DISPLACEMENT AND TURBINE FLOWMETERS

Roger Jennings
Fluidyne Instrumentation
Oakland, California 94612

INTRODUCTION

Limitations in the availability of fossil fuels, natural gas, and other energy resources due to physical and geopolitical factors have, in recent years, increased the price of these products by as much as a factor of five. During the next 20 years, prices of both petroleum and natural gas are expected to increase at a rate substantially in excess of, and will thus contribute greatly to, the rate of inflation. While conservation of these resources by the fundamental laws of economics combined with government intervention in the production and consuming segments of the economy will undoubtedly result in improved conservation practices, virtually all projections show increasing usage of these vital raw materials through at least the year 2000.

The first step in any conservation program must be the accurate determination of production and consumption quantities. For conservation programs to be effective, these measurements must be made with sufficient accuracy and resolution to allow the determination of the effects of incremental conservation measures. Further, because of increasing cost of petroleum-based fuels and their petrochemical derivatives, accurate measurement of product delivery and consumption, whether in pipelines, tank trucks, rail cars or ships, as well as within energy and raw material consuming processes themselves, must be made to assure proper billing for these products or to allocate their costs for accounting purposes.

Transportation vehicles, of course, constitute one of the major sources of fossil-fuel consumption in all developed countries. Industry-sponsored and governmentally-imposed fuel economy improvement programs are designed toward the goal of resource conservation. Here again, accurate measurement of fuel consumption under both test-stand and in-vehicle conditions must be obtained. Rationalization of present dynamometer data obtained under simulating driving cycles with that achieved by normal users of the vehicle must occur if meaningful fuel economy data for consumer guidance is to be prepared. For instance, current consumer fuel consumption data prepared by the Environmental Protection Agency differs

substantially from that obtained by in-vehicle measurement of fuel consumption with professional drivers under simulated normal-use conditions [1].[1]

Measurement of consumption of petroleum products and petrochemicals is determined primarily by flow transducers. These range from simple orifice or venturi devices to highly sophisticated positive-displacement meters. Turbine, gear and piston-type positive-displacement, and vortex-shedding flowmeters are most often used where accurate flow measurement under a wide range of operating conditions is required. The electrical output of both turbine and vortex-shedding flowmeters is inherently digital in nature, while positive-displacement flowmeters are available with both pulse and digital outputs. The introduction of digital integrated circuits, and particularly large-scale integration (LSI) techniques has reduced the cost of digital electronic systems to the point where they are used on virtually an exclusive basis in instruments for the determination of volumetric flow.

Petroleum products are universally sold on a volumetric basis (gallons, cubic meters, etc.), however their fuel value is related to weight (btu/pound, calorie/gram, etc.). The determination of flow rates in continuous operations or charge quantities in batch processes in the chemical or petrochemical industry is also based on weight. For this reason, conversion of the output of the flow transducer, basically a volumetric device, must be made to gravimetric or standard volumetric units (related to a specific reference temperature) to provide meaningful data. Mechanical temperature-compensation methods for positive-displacement flowmeters (such as ball and disk integrators or gear-changing devices) and electronic systems for turbine and vortex-shedding flowmeters have been developed with widely-varying cost/accuracy relationships. Compensation for fluids having non-linear specific gravity change with temperature have been difficult, if not impossible to achieve at reasonable cost using techniques employed to date.

This paper outlines a new technique for both linear and non-linear specific gravity compensation of both positive-displacement and turbine flowmeters. As a byproduct of methods developed for this purpose, simplified compensation systems for changes in turbine meter output frequency with fluids of varying viscosity as well as compensation for the non-linear portion of the flow rate-versus-output frequency curve for turbine transducers used under widely-ranging flow conditions are now commercially available.

---

[1]Figures in brackets indicate the literature references at the end of this paper.

DIGITAL FLOW TRANSDUCER COMPENSATION TECHNIQUES

The development of the flow transducer compensation technique described in this paper was brought about by the search for improved accuracy in the determination of automotive and industrial engine fuel economy. Studies made at the proving ground of a large U.S. automobile manufacturer [2] indicated that a precision, four-piston positive-displacement flowmeter represented the most accurate transducer for in-vehicle fuel economy tests. These transducers are characterized by slight variations in K-factor (pulses/gallon) from unit-to-unit as a result of manufacturing tolerances. To obtain display of fuel consumption in engineering units (in this case cubic centimeters of fuel consumed) as well as interchangeability of transducer and display units, a digital compensation method was developed wherein the transducer assembly itself provided information to the display electronics identifying the K-factor of the particular meter connected.

As the resolution required for fuel economy measurement (0.1 or 1 cc) and the K-factor of the meter was very close to the required resolution, conventional variable-time base division circuits used to normalize flowmeter outputs were not practical. Further, because reverse flow regularly occurs in the fuel systems of spark-ignition engines, up-down counting techniques were required to provide net fuel consumption information. This led to the development of the unique pulse multiplication/division system which forms the basis of the compensation techniques described below. Adding test time and fuel temperature to the display resulted in conformance to the requirements of an industry-standard road test procedure [3].

As shown in figure 1, a two-phase flow transmitter comprising an optical disk driven through a magnetic coupling by the flow transducer interrupts the flow of infra-red energy from a pair of light-emitting diode (LED)/phototransistor couples located such that their outputs are in phase quadrature relationship. The square wave outputs of the two LED/phototransistor pairs are amplified and applied to the input of a quadrature detector circuit which determines the direction of flow (FOR/REV) and in addition provides a pulse output multiplied by a factor of two. In the example shown, the transducer has a K-factor of 1.07 cc/pulse.

Count pulses from the quadrature detector circuit are applied to the set input of a flip-flop which allows clock pulses at a high repetition frequency to be gated to the count input of an 8-bit down counter which has been previously preset to the desired K-factor. In this case, the K-factor is derived from jumpers internal to the transducer assembly which have been factory-installed to correspond to the K-factor of the

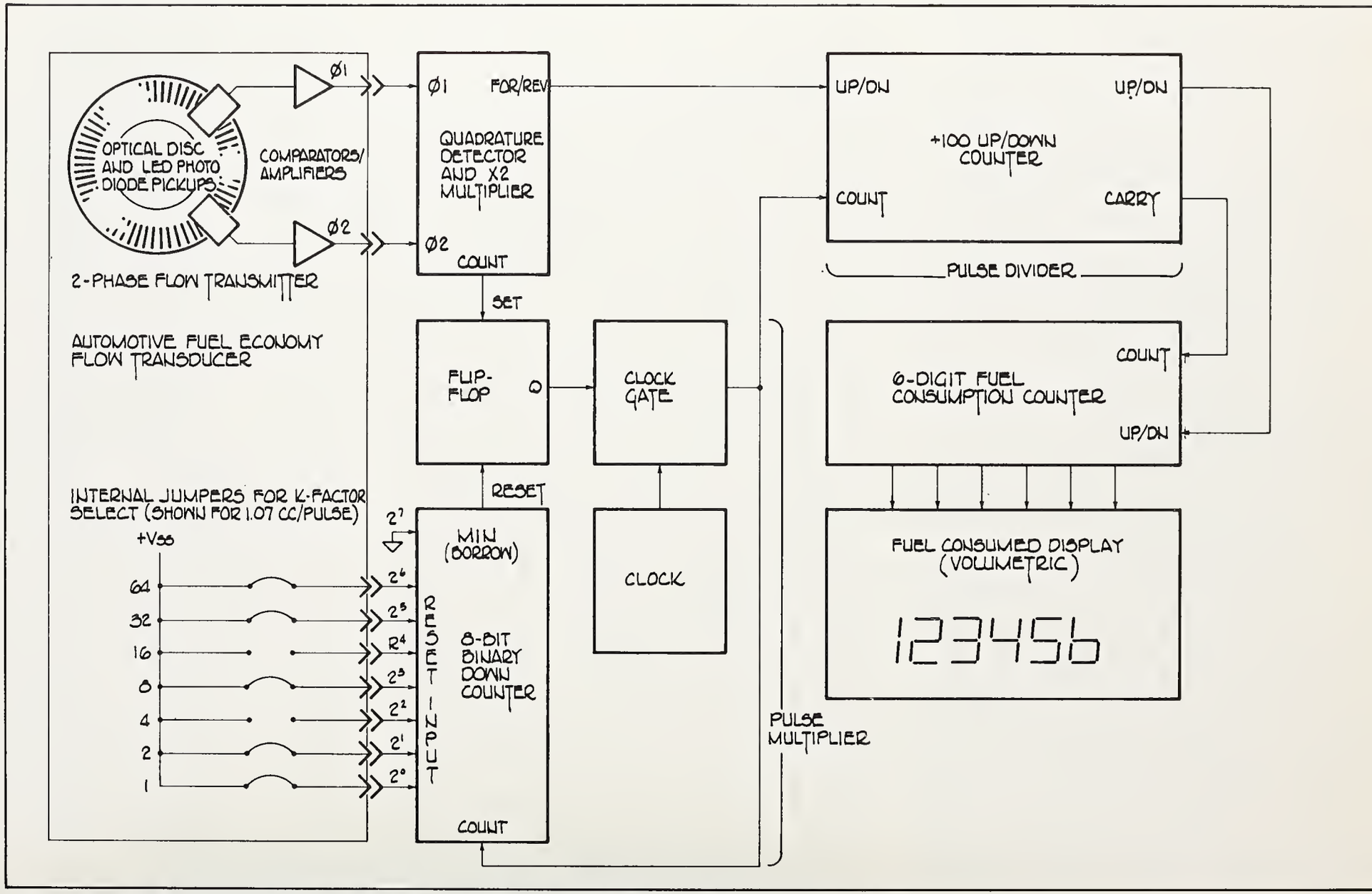

FIG. 1. PRECISION AUTOMOTIVE FUEL ECONOMY MEASUREMENT SYSTEM (GASOLINE).

flowmeter as determined by calibration procedures. When the counter reaches zero (min or borrow), the flip-flop is reset, opening the clock gate. The 107 output pulses are input to a divide-by-100 up/down counter, the output of which is directed to the six-digit display. It can thus be seen that for every input pulse from the flowmeter, 1.07 counts will be registered. If the display is calibrated in cubic centimeters, it will appear to count normally for the 13 pulses from the flowmeter. The fourteenth pulse from the flowmeter will cause the display to increment by two. If the K-factor of the meter is less than one cc/pulse, the display will always increment by one. Systems utilizing the above technique have met with wide acceptance in precision automotive fuel economy measurement [3] and several hundred of these devices are now in use throughout the United States, Europe and Asia.

For industrial applications, K-factor resolution in excess of the approximate ±0.5% achievable with the system shown in figure 1 is required. In this case, the length of the multiplier and divider chains is simply increased. Further, since transducers are seldom interchanged in industrial applications, it is more convenient to use a conventional thumbwheel switch to set the flowmeter K-factor. Thus binary-coded decimal (BCD) rather than binary counters are preferred. By suitable setting of the K-factor thumbwheel switches, output pulses equal to volumetric flow in any desired engineering units may be achieved with the degree of resolution limited only by the number of stages of multiplication and division.

If the system is designed such that the multiplier is always less than the divider, pulse multiplier/divider circuits may be cascaded, each performing an individual correction function. If the output of the first correction stage is volumetric units, and the K-factor switches of the successive stage set to the specific gravity (in lbs/gal, gm/cc, etc.), gravimetric engineering units can be obtained. Although the meter K-factor can be set to take into account specific gravity, it is usually more convenient for the operator to set both meter factor and specific gravity in meaningful engineering units.

Linear Specific Gravity Compensation Techniques

In diesel engine applications, for instance, fuel consumption measurements are made in gravimetric units as fuel efficiency is expressed as brake specific fuel consumption (BSFC), lbs/horsepower-hour or kilogram/kilowatt-hour [4]. As fuel temperature is difficult or impossible to control under normal vehicle operating conditions, measurement of the fuel economy of diesel-powered vehicles requires specific gravity correction to the appropriate reference temperature (60°F or 28°C) for accurate results. The compound correction system shown in figure 2 incorporates this feature.

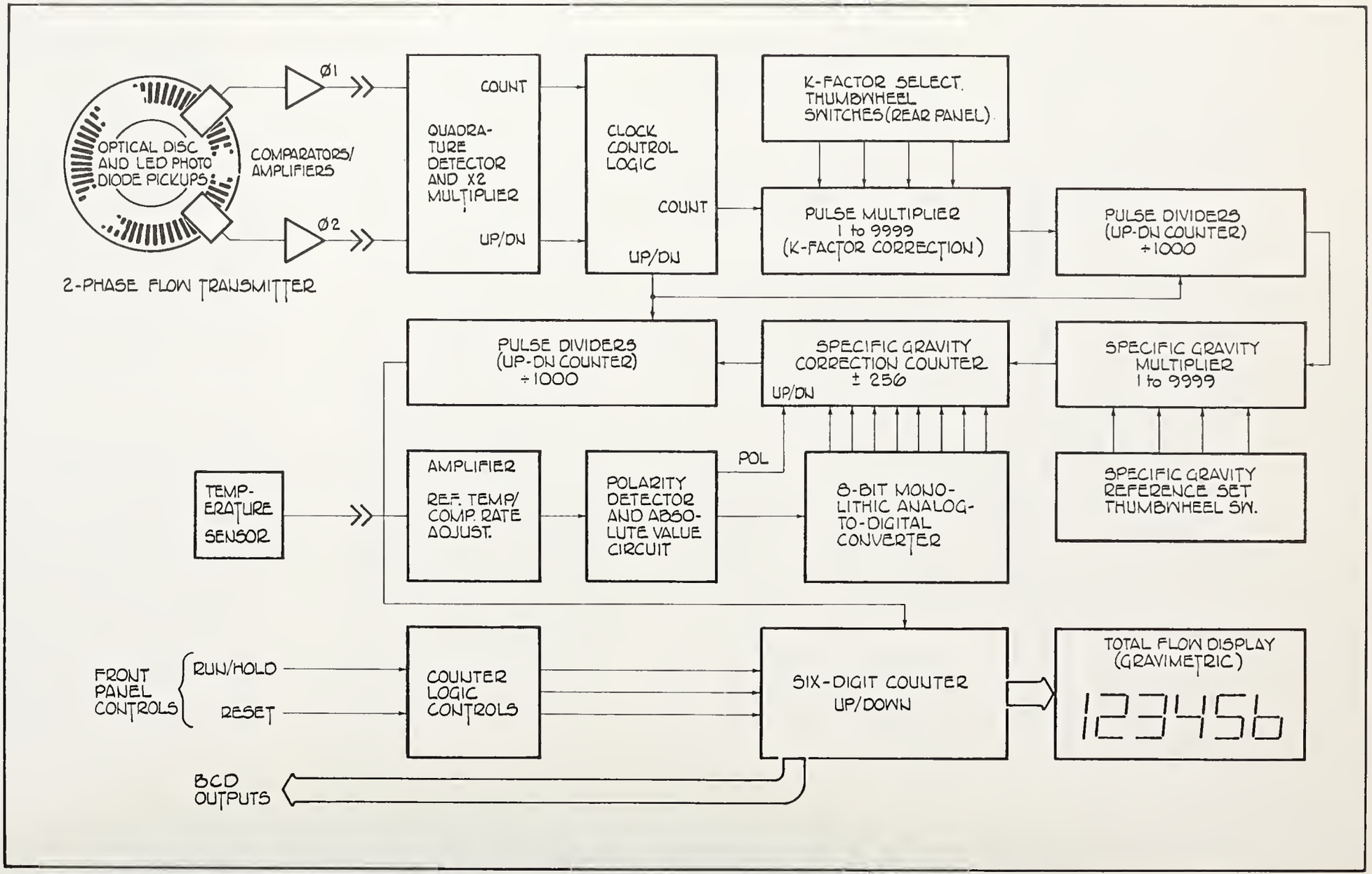

FIG. 2. LINEAR SPECIFIC GRAVITY COMPENSATION FOR POSITIVE-DISPLACEMENT FLOW TRANSDUCERS

Digital specific gravity compensation techniques require an accurate temperature sensor located immediately up or downstream of the flow rate transducer. The output of the sensor is amplified and scaled in accordance with the coefficient of thermal expansion of the fluid. This amplified output is applied to an absolute value circuit which provides a unipolar output to an 8-bit analog-to-digital converter as well as a deviation-direction (polarity) signal to the clock control circuit. The output of the analog-to-digital converter is used to preset a specific gravity correction counter in a fashion similar to that for the K-factor correction counter of figure 1.

For each pulse output by the K-factor multiplier/divider circuit, a pre-selected number of pulses are output from the fluid specific gravity multiplier. If the fluid temperature is above the reference temperature, the number of pulses preset in the specific gravity correction counter is subtracted from the resulting pulse burst output to the specific gravity pulse divider circuit. Conversely, if the fluid temperature is below the reference temperature, the appropriate number of pulses are added to that from the specific gravity multiplier.

Assuming a specific gravity of 1.000, this technique can provide specific gravity correction of $\pm$25.6%, more than adequate for most industrial applications. Using a pulse addition and subtraction technique, rather than direct multiplication/division by temperature data, provides increased resolution and minimizes the accuracy requirement of the analog-to-digital converter. This reduces system cost and complexity.

Non-Linear Specific Gravity Compensation

Many fluids such as fluorocarbons, light hydrocarbons, etc., exhibit highly non-linear coefficients of thermal expansion. Prior to the development of the digital correction system described herein, the only practical technique for non-linear flow transducer compensation involved the use of multi-segment analog arbitrary function generators. These devices consist of an operational amplifier with a number of diodes connected in its feedback loop which create, through adjustment of an equal number of potentiometers, a transfer function approximating the specific gravity versus temperature curve of the fluid. Analog arbitrary function generators are difficult to adjust and are subject to the well-known vagaries of analog circuits in general - time and temperature-induced drift, offset errors, etc.

Using the digital specific gravity correction technique, shown in figure 3, an electrically eraseable and reprogrammable read-only memory (EPROM) organized as 256 words of 8-bits can be inserted between the analog-to-digital converter and the specific gravity correction counter. In this case, the output of the analog-to-digital converter provides the address to the EPROM. The corresponding data pre-programmed from the specific gravity-versus-temperature curve of the liquid is used to preset the specific gravity correction counter.

Due to their widespread use in microprocessor-based systems, 256 x 8 EPROMs and their required programming equipment are available from a number of sources at relatively low cost. Two 256 x 8 EPROMs, as shown in figure 3, one for temperature excursions above and one for those below the reference temperature represent the equivalent of a 512-segment arbitrary function generator, an obviously impractical device to construct or calibrate. As the outputs of each EPROM are open collector and may be bussed, other sets of EPROMs may be included in the system and automatically or manually brought into play if a variety of fluids are to be metered by an individual transducer.

TURBINE FLOW TRANSDUCER COMPENSATION TECHNIQUES

The K-factor and specific gravity compensation techniques described for positive-displacement flow transducers are equally applicable to turbine flowmeters. Where bi-directional flow is expected, turbine flow transducers with dual magnetic pickups, located such that their outputs are in phase quadrature relationship, may be utilized to supply signals identical to those of the optical disk transmitter associated with positive-displacement meters. Although divider circuits are often used for K-factor compensation of turbine flow transducers, the pulse multiplication/division circuitry described provides a scaled and compensated output which may be used not only for totalizing purposes, but also for flow rate indication through the use of frequency-to-voltage conversion techniques or fixed time-base counters.

A more interesting extension of the K-factor multiplier/divider technique allows the usable range of turbine flowmeters to be extended from the normal linear area within a 10:1 ratio of minimum to maximum flow (turn-down ratio). Figure 4 shows the performance characteristics of a typical turbine flowmeter in both its linear and non-linear areas. Non-linearity at lower flow rates is due to viscosity versus momentum (Reynolds' number) characteristics of the flow as well as drag effects in the bearings. Although simple ana-

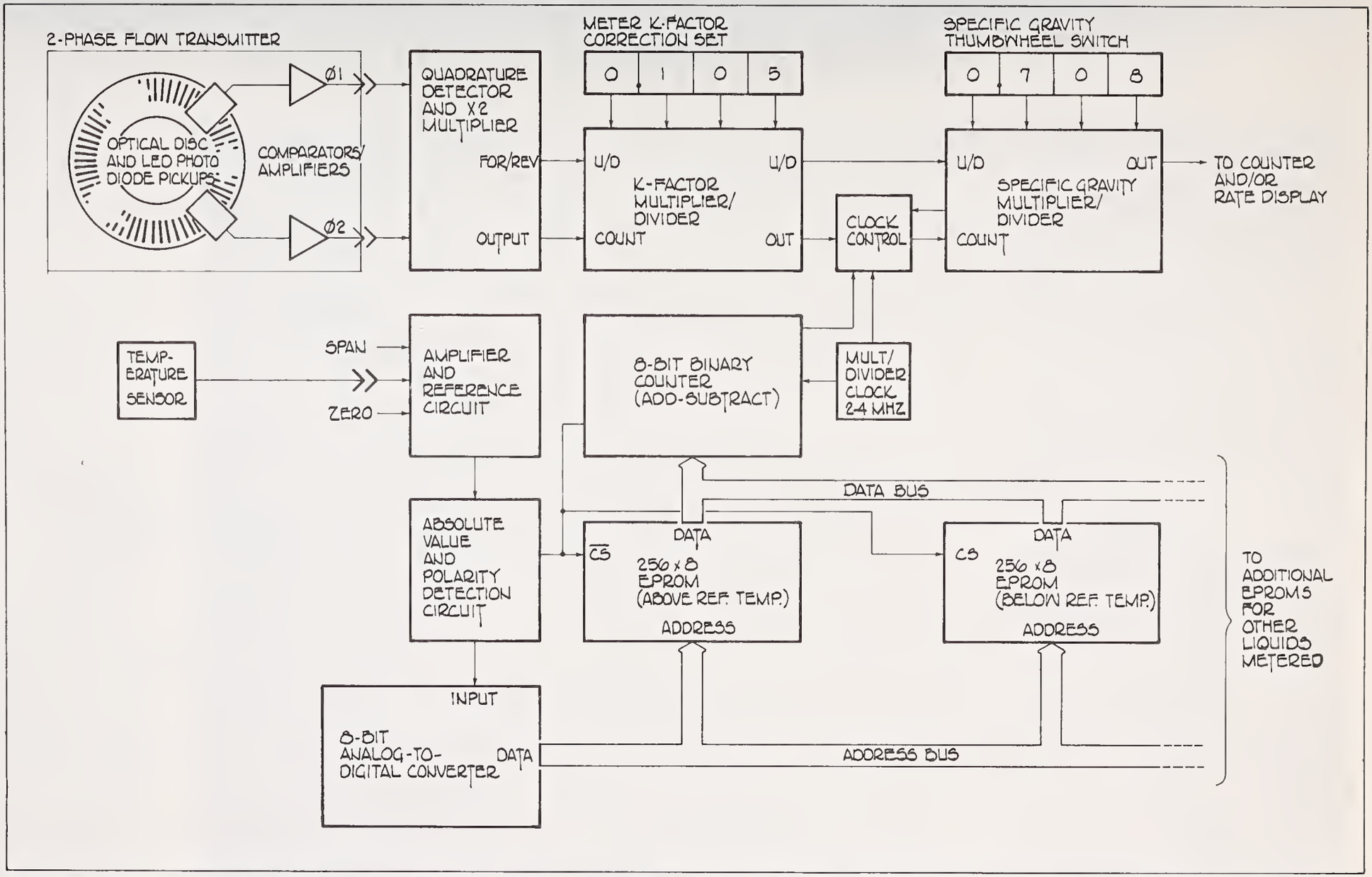

FIG. 3 512-POINT NON-LINEAR SPECIFIC GRAVITY COMPENSATION SYSTEM FOR POSITIVE-DISPLACEMENT FLOW TRANSDUCERS

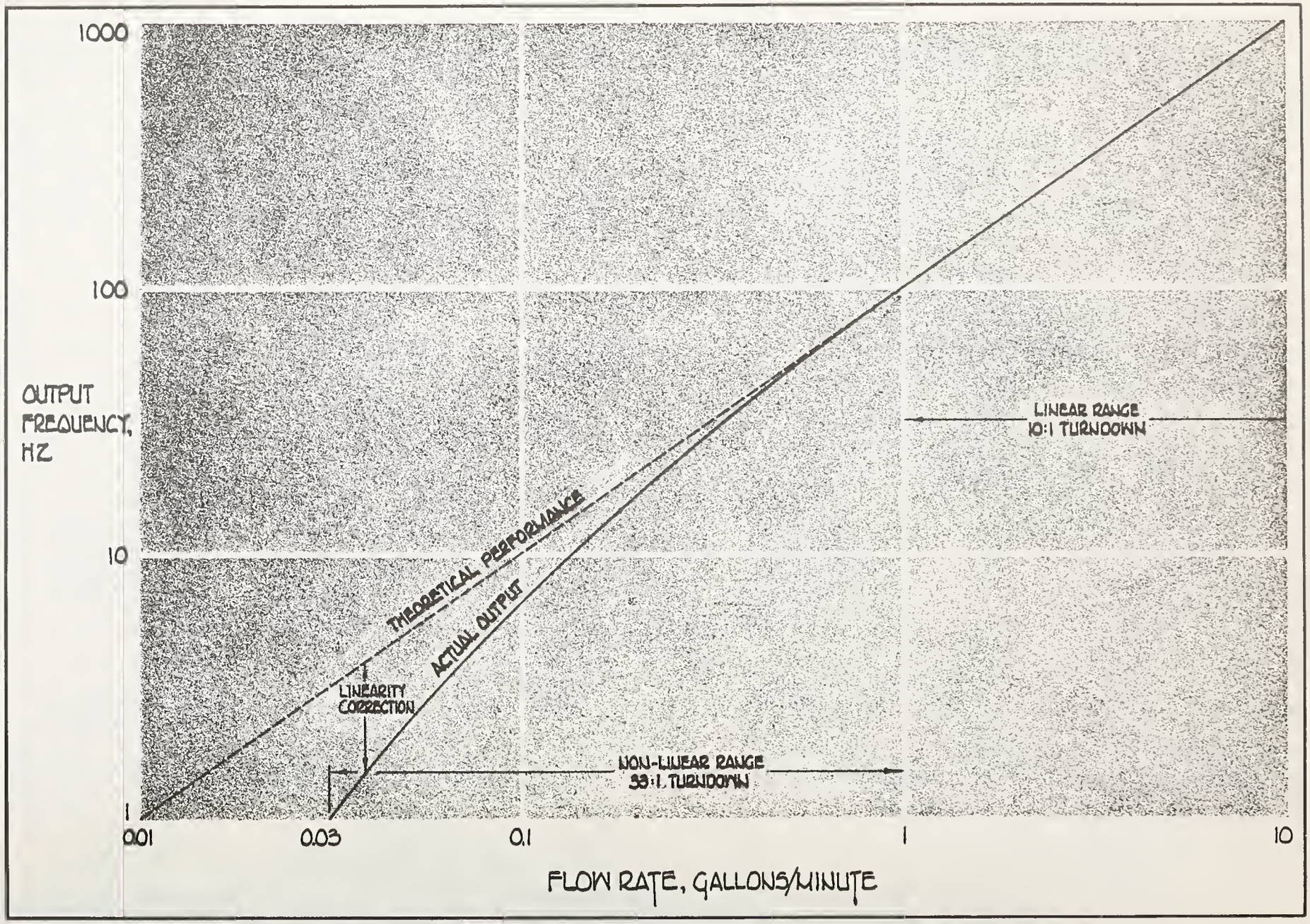

FIG. 4 TYPICAL LINEARITY CURVE, FLOW RATE VS. OUTPUT FREQUENCY, FOR TURBINE FLOWMETER (330:1 TURNDOWN)

log or digital offset techniques have been used to approximate non-linearity at low flow rates, these methods cannot be optimized for the individual characteristics of turbine flow transducers.

Figure 5 depicts a fully-digital flow linearization technique which can greatly extend the turn-down ratio of conventional turbine flow transducers. By multi-point calibration of the transducer, the K-factor versus flow rate curve can be determined with any degree of resolution necessary. This data is then programmed into an EPROM which provides the correction data to the meter K-factor multiplier/divider circuit, in similar fashion to specific gravity correction techniques.

In this case, the address of the EPROM is derived from a time period measurement of the interval between successive pulses from the transducer's magnetic pickup. Assuming that the blades of the transducer are totally symmetrical and evenly spaced, the time period from pulse-to-pulse will be proportional to the reciprocal of flow rate. If such symmetry cannot be guaranteed, the input divider and count logic system can be organized such that the interval required for one complete revolution of the rotor is used to provide the time base. Clock pulses are gated into an 8-bit binary counter/latch combination, the output of which is proportional to the reciprocal of flow rate and which is used to provide the address to the EPROM. If the counter overflows, this signal can be used as an underflow alarm or count inhibit signal to indicate "no-flow" or a flow condition below that which may be compensated by the system.

Using the reciprocal of the flow rate to provide the address to the EPROM simultaneously accomplishes two objectives. At the point where the flow rate reaches the linear portion of the curve, the output of the 8-bit binary counter and thus the EPROM address becomes zero for all higher flow rates. Thus, appropriately, no correction is applied to the K-factor multiplier/divider system. In addition, the resolution of the system is greatest at that point on the K-factor/flow rate diagram (figure 4) at which curvature is maximum. This provides a "data compression" function which increases the effective resolution of the system in that area in which it is most needed.

As no analog components are included in this system, its overall accuracy is solely a function of the frequency stability of the correction clock and the resolution of the EPROM and K-factor setting system. The use of multiplication/division circuits provides an output which is compatible with conventional turbine flow transducer instrumentation systems. This allows the correction device to be easily inserted between the transducer and existing display or process control equipment at minimum incremental cost.

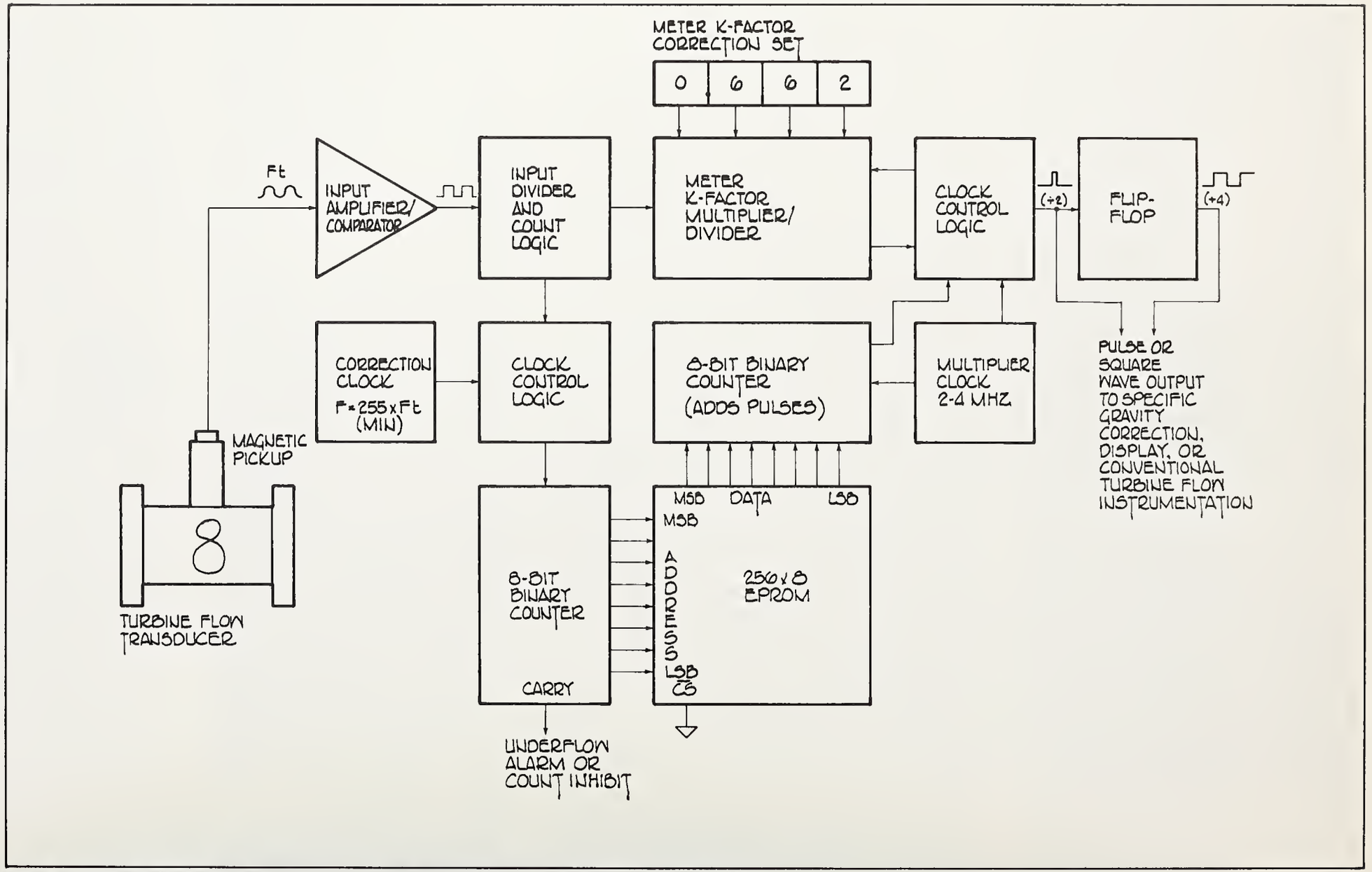

FIG. 5 WIDE-RANGE TURBINE FLOW TRANSDUCER LINEARIZATION SYSTEM.

Viscosity Compensation of Turbine Flow Transducers

Although the relationship between K-factor and viscosity is more accurately expressed as a function of Reynolds number (R_e), over a relatively limited flow rate range characteristic of many process control applications the K-factor-versus-viscosity characteristics of a typical turbine flow transducer will be represented by figure 6. The data shown in figure 6 is derived from multiple measurements at the expected flow rate with fluids having viscosities selected to duplicate the range expected in service.

The viscosity compensation technique as shown in figure 7 is similar to that used for specific gravity compensation. Since temperature is a very much simpler value to measure than viscosity, the EPROM contains temperature versus K-factor correction values derived from the combination of a temperature/viscosity curve for the liquid and the K-factor/viscosity curve for the transducer. As the K-factor set in the basic multiplier/divider system is the maximum (normally at approximately one centipoise), the K-factor correction counter need only add pulses to compensate for the reduced K-factor resulting from viscous drag.

If substantial changes in the K-factor/viscosity characteristics are expected over the normal flow rate range of the meter, additional EPROMs can be prepared and selected by means of a flow rate detection circuit similar to that of figure 5.

Reynolds' Number Compensation for Turbine Flow Transducers

A more elegant solution to viscosity compensation of turbine flow transducers over a wide range of flow and viscosity conditions takes into account Reynolds' number effects on turbine transducer K-factor. This technique uses a "universal viscosity curve"[5] developed for a specific flow transducer by multipoint calibration over the expected flow rate range with fluids of different viscosities. The results of the calibration procedure are plotted in terms of K-factor (pulses/gallon) versus Reynolds' number, R_e. Reynolds' number represents the ratio between the inertial and frictional forces of a fluid and thus effectively determines, along with mechanical design characteristics, the speed of rotation of the turbine element.

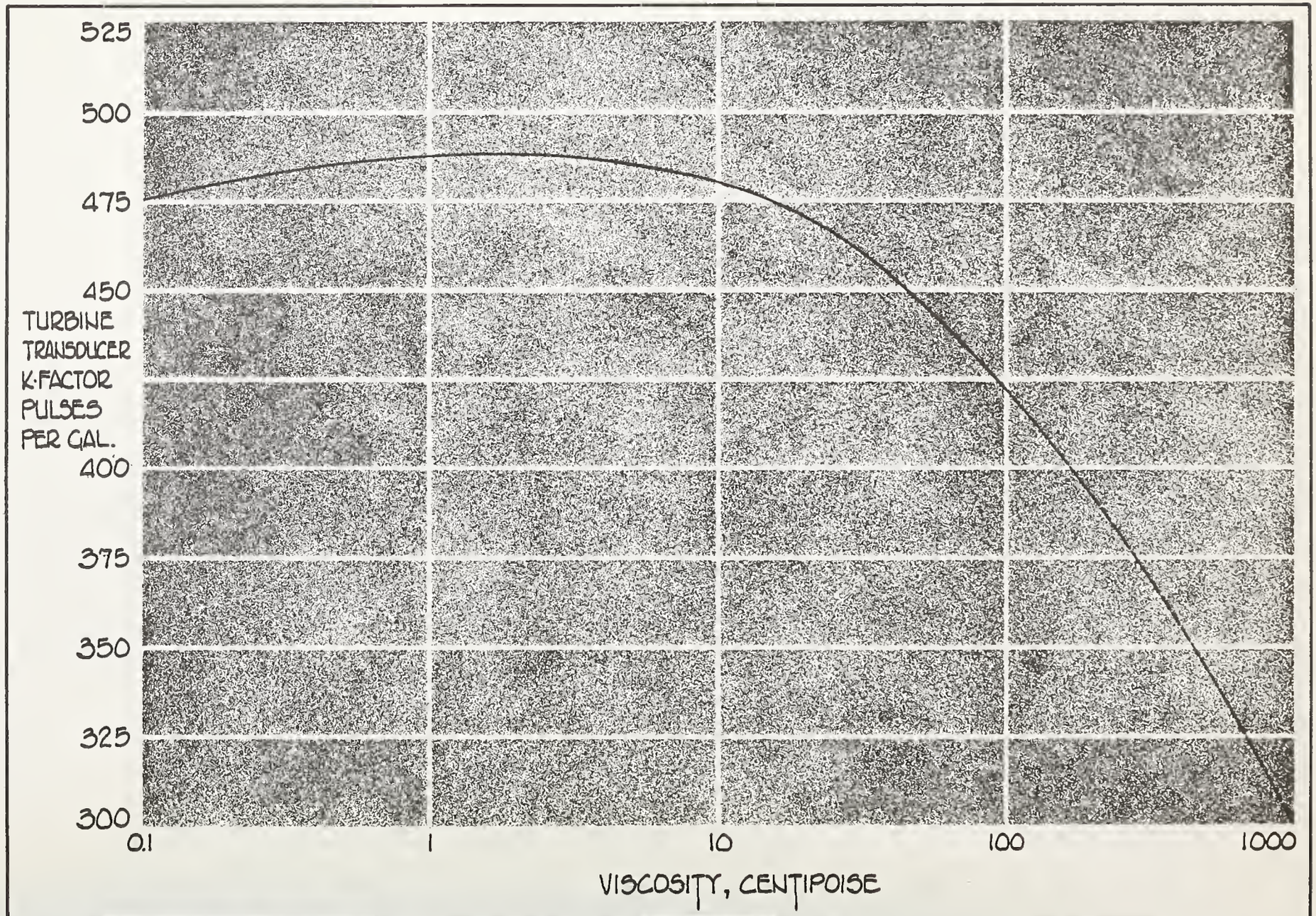

FIG. 6. TYPICAL LINEARITY CURVE, VISCOSITY VS. K-FACTOR, FOR TURBINE FLOW TRANSDUCERS (FLOW=K).

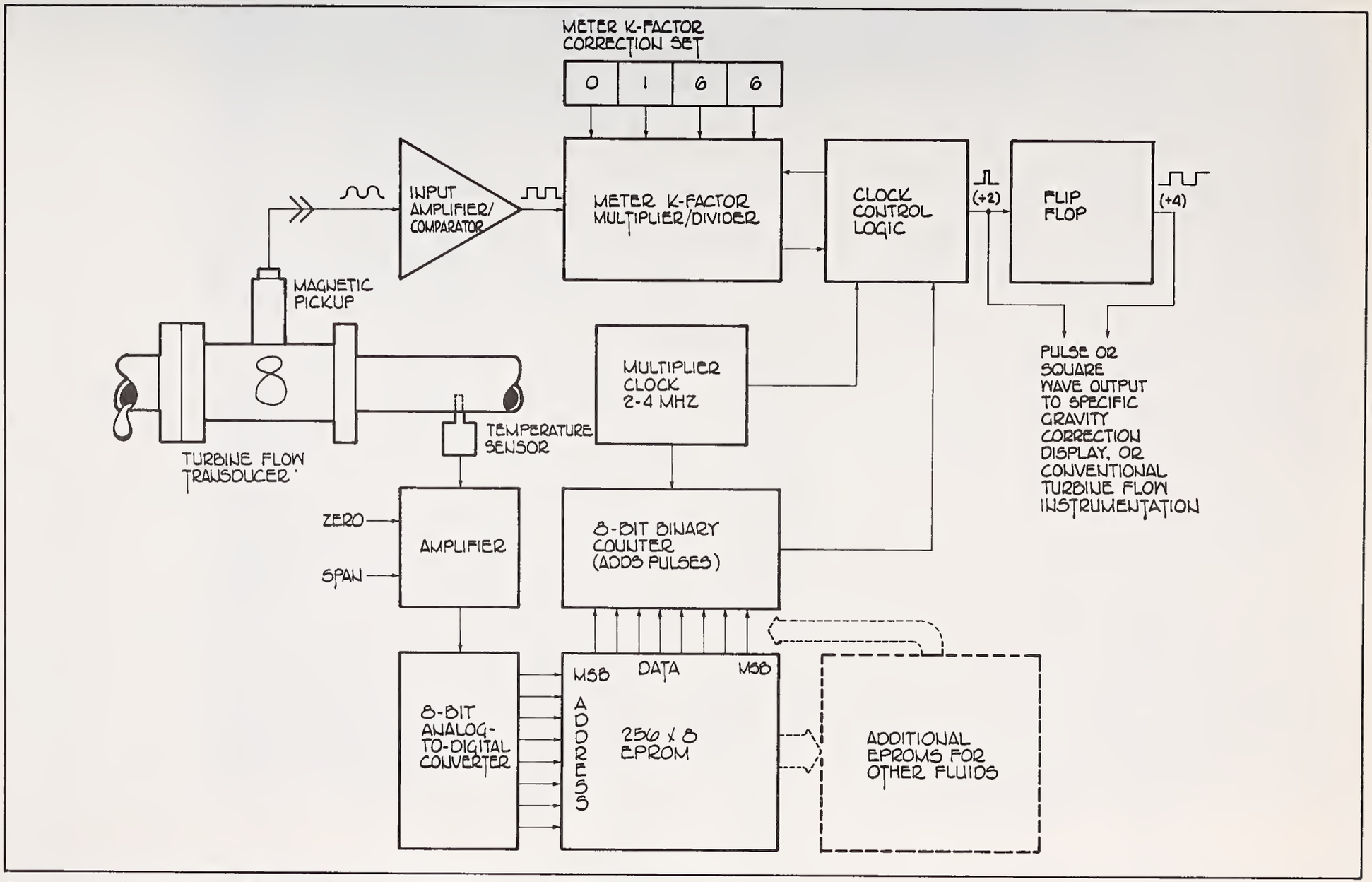

FIG. 7. TURBINE FLOW TRANSDUCER VISCOSITY COMPENSATION SYSTEM.

Numerically, Reynolds' number is expressed as:

$$R_e = VD/v \quad (3)$$

where: R_e = Reynolds' number (dimensionless)
V = fluid velocity
D = pipe or flowmeter diameter
v = kinematic viscosity

As: $$V = \frac{Q}{A} = \frac{4Q}{\pi D^2} \quad (4)$$

where: Q = flow rate, volume/time
A = flowmeter cross-sectional area

$$R_e = \frac{4Q}{\pi Dv} = c\,\frac{Q}{v} \quad (5)$$

where: c = units constant (including diameter)

And: $$F_t = KQ \quad (6)$$

where: F_t = turbine flowmeter frequency, Hz
K = flowmeter K-factor

Thus: $$R_e = \frac{c}{K} \cdot \frac{F_t}{v} \quad (7)$$

Since both c and K are constants under given conditions, the actual K-factor (pulses/gallon) may be plotted as a function of Reynolds' number or F_t/v. Such a plot is shown in figure 8.

By the Hagan-Poiseuille expression, the viscosity of a fluid in a laminar flow element may be described by the following equation:

$$v = \frac{\Delta P g D^2}{32 d L V} \quad (8)$$

where: ΔP = pressure drop through flow element
g = gravitational acceleration
d = fluid density
L = length of flow element
D = diameter of flow element

Substituting Q for V as above and eliminating constants:

$$v = n\,\frac{\Delta P}{dQ} \quad (9)$$

where: n = units constant (including length and diameter)

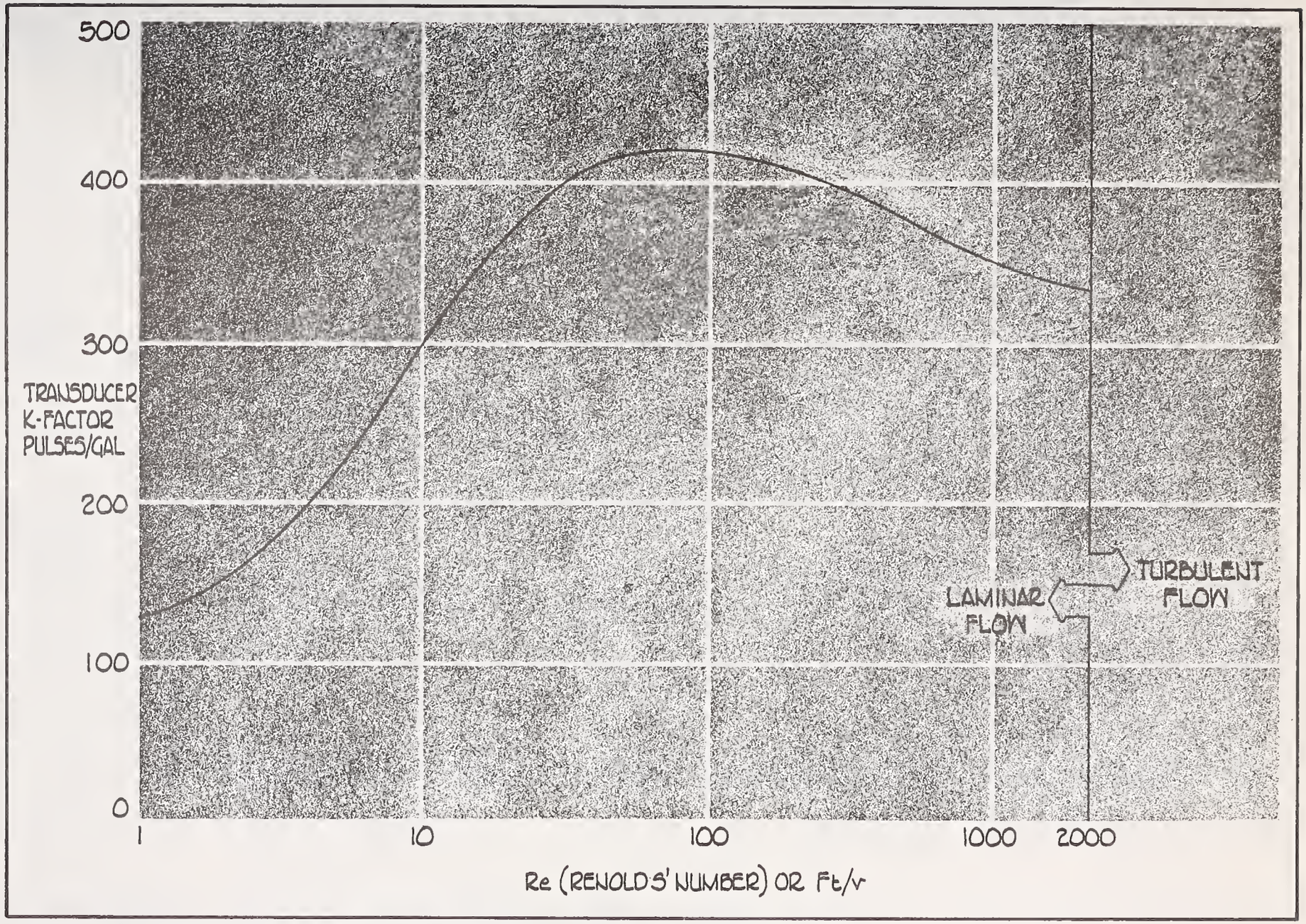

FIG. 8. "UNIVERSAL VISCOSITY CURVE" FOR TURBINE FLOW TRANSDUCERS.

Thus the instantaneous viscosity of the fluid can be determined by measuring the pressure drop through a laminar flow element (which may consist of nothing more than a length of pipe of accurately-known dimension) or the flow transducer itself), knowing the fluid flow rate and density. In this case, however, the fluid flow rate, Q, must be the true, corrected flow rate, rather than the flow rate directly indicated by the pulse output frequency of the flow transducer.

The compensation system shown in diagramatic form in figure 9 is designed to determine viscosity and to divide this value into the pulse output frequency (F_t) of the turbine meter. The resultant value is used as the address for a read-only memory in which the "universal viscosity curve" for the meter is stored. Data stored in the EPROM adjusts the pulse output frequency to its corrected value, F_c. This corrected value is multiplied by the turbine pulse output frequency, F_t, and then divided by the pressure drop through the flow element (measured by a differential pressure sensor) to obtain the memory address.

It will be noted that the Reynolds' number data lags the measurement interval by one second. This time constant will ordinarily be acceptable as viscosity changes are a function of temperature variation, the rate of which will be determined by the thermal inertia of the flowing product. The time delay also provides the system stability required by the feedback loop from the corrected flow rate output through the frequency divider to the loop-up table address.

One of the interesting features of the compensation system shown in figure 9 is the ability to perform a relatively simple calibration procedure on the combination of the turbine flow transducer and laminar flow element to obtain the "universal viscosity curve" look-up table in the EPROM without the necessity of calculating Reynolds' number or knowing the instantaneous viscosity of the fluid. In this case, the span of the input amplifier to the analog-to-digital converter is adjusted to provide full-scale output at the maximum expected pressure drop. This value can be calculated or determined experimentally from the maximum expected combination of flow and viscosity.

If a positive-displacement or previously-calibrated turbine meter is available to determine the true volumetric flow rate, flow transmitter pulses, suitably scaled, are applied to the input of the frequency multiplier in lieu of the self-generated corrected flow rate. By the use of a microprocessor or a minicomputer, each time a new look-up table address is generated by the counter/latch combination, the instantaneous frequency of the flow transducer can be determined and stored in a random-access memory for subsequent processing to generate the complete look-up table.

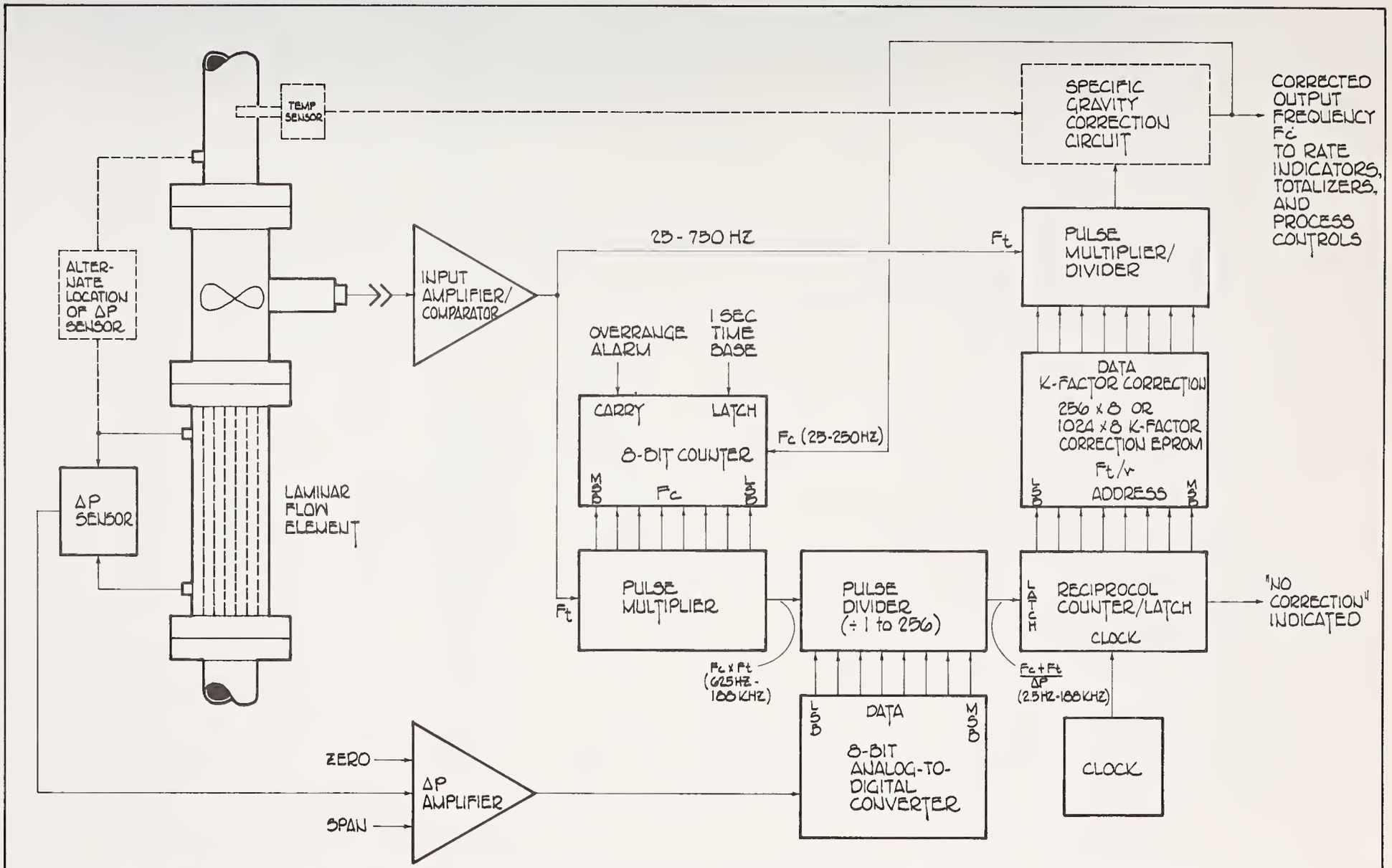

FIG. 9 REYNOLDS' NUMBER COMPENSATION OF TURBINE FLOW TRANSDUCERS.

Turbine flow transducer calibration is, however, most often accomplished with ballistic calibrators which do not provide rate information. Assuming that the flow rate through the ballistic calibrator can be maintained at a constant rate during the test, integration techniques can be used to provide the look-up table data. In this case, an arbitrary but accurately-known frequency, F_i, is injected into the F_c input of the frequency multiplier, not shown. The output of the multiplier/divider is applied to a totalizer actuated by the position indication switches of the ballistic calibrator. Similarly, pulses from the flow transducer under test are accumulated in a second counter. The time for the displacement of a given volume of fluid is simultaneously determined.

The basic equations associated with ballistic calibrators for flow transducers having pulse outputs are as follows:

$$Q = \frac{V}{t} \quad (10)$$

where: Q = flow rate, gpm
V = ballistic calibrator volume, gallons
t = calibration period, minutes

$$K_t = \frac{N_t}{V} \quad (11)$$

where: K_t = meter K-factor, pulses/gallon
N_t = number of flowmeter pulses counted during calibration

$$F_t = \frac{K_t Q}{60} = \frac{N_t}{60t} \quad (12)$$

where: F_t = flowmeter output frequency, Hz

The output of the pulse multiplier/divider, N_v, is integrated over the time of the test. With F_i, the injection frequency, held constant:

$$N_v = \int_o^t \frac{F_i F_t}{K\Delta P} = \frac{F_i}{K} \int_o^t \frac{F_t}{\Delta P} \quad (13)$$

where: N_v = number of pulses output from multiplier/divider
F_i = injection frequency, Hz (a constant)

$K\Delta P$ = frequency divisor (proportional to ΔP)

Thus the ordinate of the curve is given by:

$$\frac{F_t}{V} = \frac{N_v}{60_t} \cdot \frac{F_c}{F_i} \quad (14)$$

where: F_c = corrected output frequency at flow rate Q (see text)

And the abcissa is given by (11) above.

The corrected output frequency, F_c, may be established with reference to the maximum K-factor of the meter under test. This value will ordinarily be obtained at viscosities between 1 and 2 centipoise and flow rates in the mid- or upper range of the capacity of the meter. F_c for the particular test is calculated by the following formula:

$$F_c = \frac{F_{t(max)}}{t} \cdot \frac{V}{Q_{(max)}} \quad (15)$$

where: $F_{t(max)}$ = frequency obtained from conventional calibration at $Q_{(max)}$ pulses/gallon

$Q_{(max)}$ = flow rate at maximum K-factor

Alternately, any reasonable arbitrary value may be assigned to $F_{t(max)}$ and all measurements throughout the curve related by (15) above.

As the greatest resolution is obtained by the correction-addition method, the data to be stored in the EPROM as a result of the test is derived from the difference of F_c and F_t. Because of the inversion of the expression F_t/V for improved resolution at lower Reynolds' numbers, the reciprocal of the result obtained in (14) above is used to generate the numeric value of the EPROM address.

Values intermediate between points determined by the technique described can be generated by the computer system through linear interpolation or conventional curve-fitting techniques, depending upon the number of data points obtained. As the system requires calibration at a substantial number of flow points with liquids of several different viscosities, a considerable improvement in efficiency over manual calibration techniques is achieved.

Compensation of Turbine Flow Transducers in Gas Service

In the previous discussions, it has been assumed that the turbine and positive-displacement flow transducers have been used with liquids having densities varying only with temperature and not with pressure - that is, incompressible fluids. When gases are measured with turbine flow transducers, their electrical output must be normalized to standard conditions of both temperature and pressure. This is done in accordance with the relationships established by Boyle's Law and Charles' Law, respectively.

Turbine flowmeters measure the flow rate of gases in actual cubic feet/minute (ACFM) or actual cubic meters/minute (ACMM). For data to be meaningful, it must be expressed in standard cubic feet/minute (SCFM) or standard cubic meters/minute (SCMM). This is achieved by the following equation:

$$Q_s = \frac{Q_a \times P_a \times T_s}{P_s \times T_a} \quad (16)$$

where (in English units):

Q_s = standard gas flow rate (SCFM)
Q_a = actual gas flow rate (ACFM) measured by flow transducer
P_a = actual gas pressure at flowmeter, psia
P_s = 1 atmosphere, 14.7 psia
T_a = actual gas temperature, °R (°F + 460)
T_s = 520°R (60°F reference temperature + 460°R)

Thus: $$Q_s = \frac{Q_a \times P_a \times 520}{14.7 \times T_a} = 33.7\, Q_a \frac{P_a}{T_a} \quad (17)$$

The above equations, of course, require that the gas behave in "perfect" fashion and that viscosity effects be negligible. If this is assumed to be the case, the modified multiplication/division system shown in figure 10 can be used. If not, the EPROM linearization technique may be used as previously described.

Output pulses from the turbine flow transducer are amplified and converted to square waves by the input comparator. The square wave output is applied to an 8-bit pulse multiplier which provides a burst of pulses for each input pulse numerically equal to the output of an 8-bit analog-to-digital converter representing actual gas pressure (P_a). For simplicity it is assumed that the least significant bit (LSB) of the analog-to-digital converter for pressure is equal to 1 psi, thus the pressure range of the system is 0 to 256 psia.

Pulse bursts from the pressure multiplier are applied to a 12-bit divider for temperature compensation. Again, for simplicity, we assume that the least significant bit of the analog-to-digital converter represents 1°F. If an acceptable temperature range for the system is 52°F (512°R) to 307°F (767°R), the offset adjust switch for the 512-bit would be opened presetting the divider to 512. The output of the amplifier for the temperature sensor would be adjusted to zero at 52°F and to the full-scale input voltage of the analog-to-digital converter at 308°F.

The output of the multiplier/divider chain thus represents the ratio P_a/T_a of equation (2) above, requiring only that the pulse train be divided by the K-factor of the meter (in pulses/ACFM) to obtain one pulse/SCFM.

Again, the output of the multiplier/divider may be a signal compatible with existing instrumentation or process control systems minimizing the incremental cost of the compensation system.

Such a system can be cascaded with the rate-related compensation system of figure 5 to remove linearity errors as a function of flow rate. If the principle source of linearity error is related to the actual velocity of the turbine rotor, the rate linearization system can be inserted between the transducer and the gas-law compensation system. If rate-induced linearity errors are expressed in relation to SCFM, the rate-based correction system would be added after gas-law compensation.

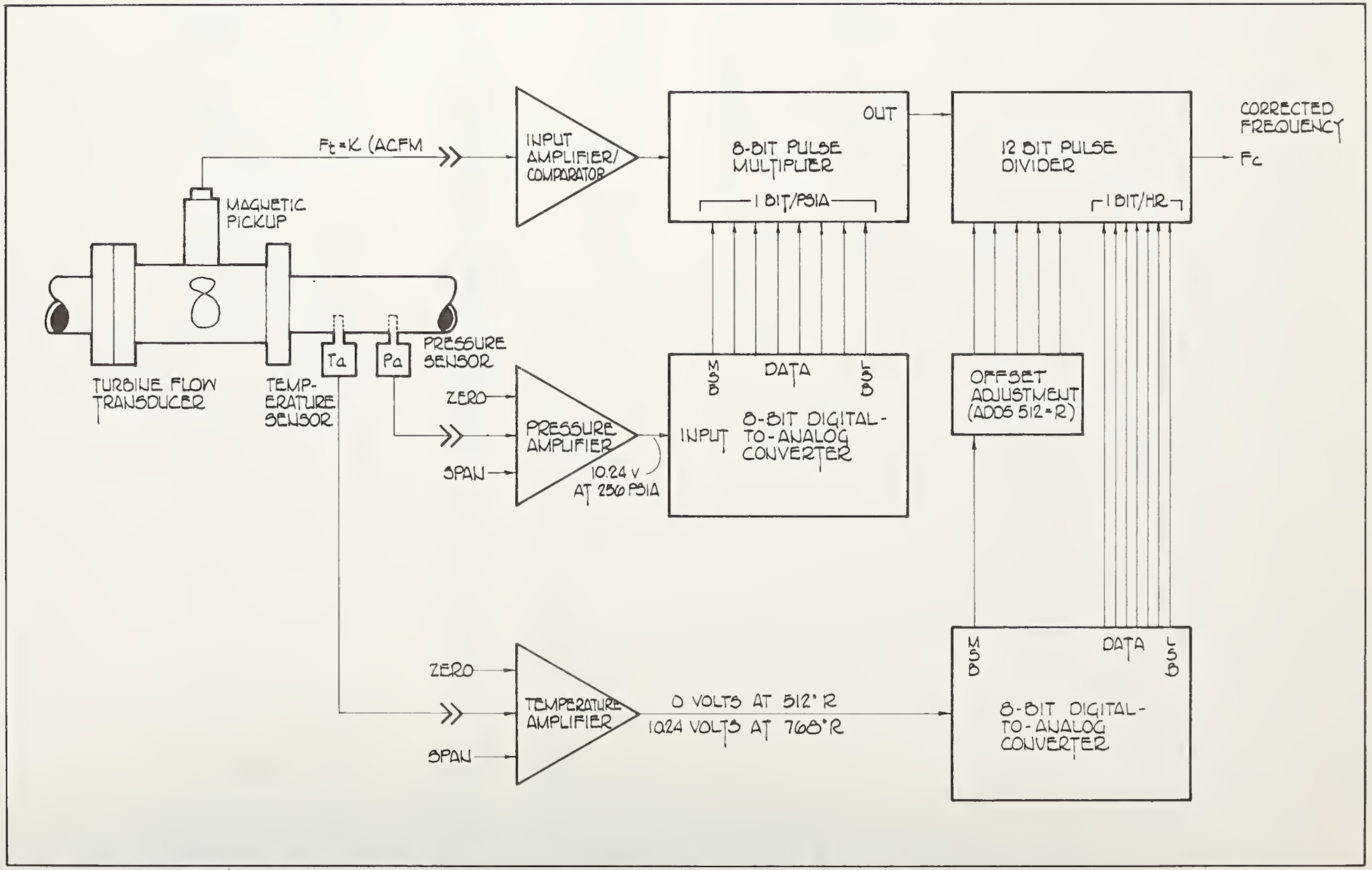

FIG. 10 "PERFECT" GAS LAW COMPENSATION OF TURBINE FLOW TRANSDUCERS.

COMMERCIAL SYSTEM IMPLEMENTATION

The systems described above hsve been implemented commercially using standard CMOS logic for all components other than analog-to-digital conversion and EPROMs. Converters and EPROMs used are PMOS with CMOS output compatibility. This results in high noise immunity (a 12-volt power source is used) combined with low internal heat dissipation and power requirement.

Throughout the systems described, 8-bit analog-to-digital converters and EPROMs have been used. With polarity sensing techniques for specific gravity correction, 9-bit accuracy (1 part in 512) can be achieved. Although 10- and 12-bit converters are available from a number of sources, their accuracy is substantially in excess of the associated transducer. In the case of specific gravity compensation, the deviation from the reference temperature is measured and, at a specific gravity of 1.000, 0.1% compensation resolution and 0.2% accuracy may be achieved. As analog transducers become available with greater accuracy, it is expected that converters of higher resolution and EPROMs of greater word length will be warranted.

The use of microprocessors, of course, was considered during the early phases of the development program for the various compensation systems. Although microprocessors are well suited for mathematic operations of the type discussed above, an excessive number of peripheral components (in excess of the total number of components used to implement the above designs) was required to perform an identical function. Microprocessors appear better suited for more sophisticated compensation techniques such as inclusion of second order deviations from the perfect gas laws, effects of gas viscosity and density on transducer output, etc.

On the other hand, the use of discreet logic allows compensation for metering errors with an accuracy and resolution approximately equivalent to that of the transducer itself (0.25 to 0.5%) which is felt to be adequate. To attempt compensation with resolution beyond the precision of measurement of the primary transducer element is a violation of the laws of information theory. Finally, the discrete-component approach to the compensation techniques achieves a high cost/benefit ratio. This allows a sufficiently rapid recovery of initial investment to warrant inclusion in the vast majority of industrial and scientific flow measurement systems.

SUMMARY

Linear and non-linear compensation of positive-displacement and turbine flow transducers for the coefficient of thermal expansion of the liquid being measured, as well as correction for Reynolds' number effects on turbine flowmeter accuracy can be achieved by the digital techniques described. Compound correction systems for turbine meter gas-law compensation may also be implemented using these methods.

Using digital techniques, non-linear compensation can be obtained through the use of programmable read-only memories (PROMs). If erasable and reprogrammable PROMs (EPROMs) are used, the compensation system may be periodically recalibrated along with the flow transducer and revised compensation look-up tables created at minimum cost. Although some techniques such as multiplication and division may be accomplished with analog circuit modules with somewhat less circuit complexity, digital techniques eliminate the time and temperature-induced drift associated with analog components.

Evolutionary improvement in the accuracy and dependability of both positive-displacement and turbine flow transducers combined with accurate compensation techniques for those sources of error which cannot be conveniently overcome mechanically will provide the process industries with the instrumentation systems necessary to meet the conservation challenges of the 1980s.

REFERENCES

1. West, D. T., et al, "A Technical Report of the 1975 Union 76 Fuel Economy Tests," publication 750670, Society of Automotive Engineers, Pittsburgh, PA. (1975).

2. Baker, Milton, "New Techniques for Automotive Fuel Economy Measurement," Flow Measurement Symposium, National Bureau of Standards, Gaithersburg, MD. (1977).

3. Fuel Economy Procedures Task Force, "Fuel Economy Measurement - Road Test Procedures - SAE J1082," SAE RECOMMENDED PRACTICES, Society of Automotive Engineers, Pittsburgh, PA. (1974).

4. Jennings, Roger, "Fuel Economy Measurement using Positive-Displacement Flow Rate Transducers," Instrument Society of America, 22nd International Instrumentation Symposium, Pittsburgh, PA. (1976).

5. Stine, G. Harry, Ed., "Calibration in Liquids, The Flow Factor," vol. 3, no. 4, Flow Technology, incorporated, Phoenix, AR. (1975).

National Bureau of Standards Special Publication 484, Proceedings of the Symposium on Flow in Open Channels and Closed Conduits held at NBS, Gaithersburg, MD, February 23-25, 1977. (Issued October 1977)

VISCOSITY EFFECTS ON THE TURBINE FLOWMETER

J. M. Ball, Physicist

Flow & Pressure Group
US Army Metrology & Calibration Center
DRSMI-MSP
Redstone Arsenal, AL 35809

ABSTRACT: The so called universal viscosity curve has been a common medium for the presentation of turbine flowmeter performance characteristics for some time. This paper shows that the most common types of turbine flowmeters do not usually perform according to a single curve when the viscosity is changed. We also present data which demonstrates that certain modulated carrier type turbine flowmeters do respond predictably when the fluid properties change. Errors produced by the misuse of the universal curve are demonstrated, and errors in the characteristic value (K factor or C factor) due to fluid property measurement errors are described.

Key Words: Accuracy; calibration; characteristic factor (K or C); curve fitting; pickoffs (magnetic and RF); turbine flowmeter; universal curve; viscosity measurement.

1. Introduction

For the past several years there has been discussion and disagreement among turbine meter users and makers concerning the so called "universal viscosity curve" (See Figure 1). Most often the questions raised concern the accuracy with which one can expect to use such a curve. Some recent studies have indicated that either such universal curves do not exist, or that they cannot be used to the accuracies desired (less than 1/2% of reading).

There are numerous turbine flowmeters in the US Army system, and this laboratory has received several requests from customers for universal curves - most of which could not be supplied due to inadequacies in the turbine meter's performance. Cases have occurred in laboratory applications where a "universal" curve based upon a single fluid calibration was being used for multiple fluid applications.

The widespread use (and misuse) of the universal curve for turbine flowmeters prompted this paper. The test data and results which follow were obtained in the US Army Standards Laboratory (USASL), the primary standards laboratory for the US Army.

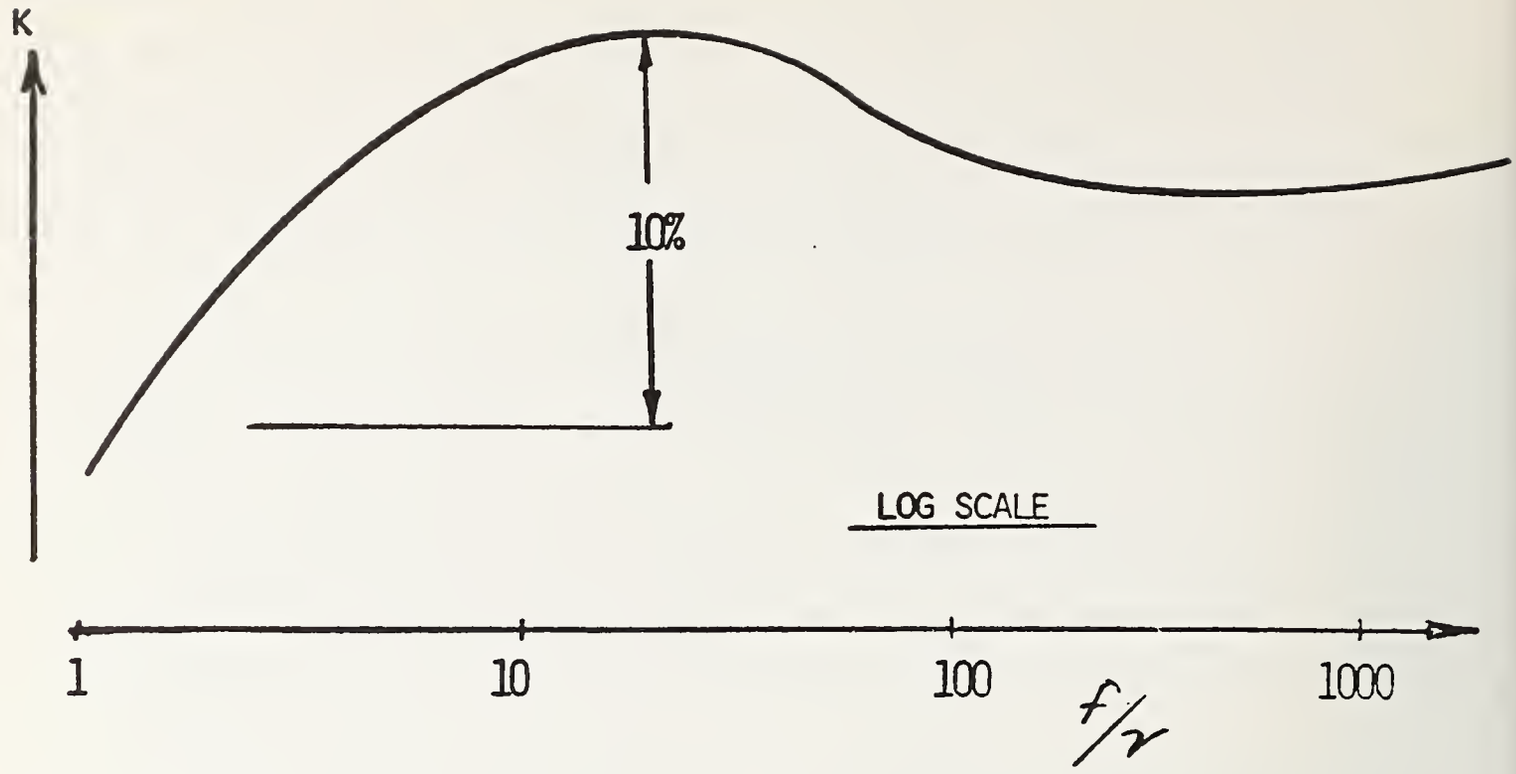

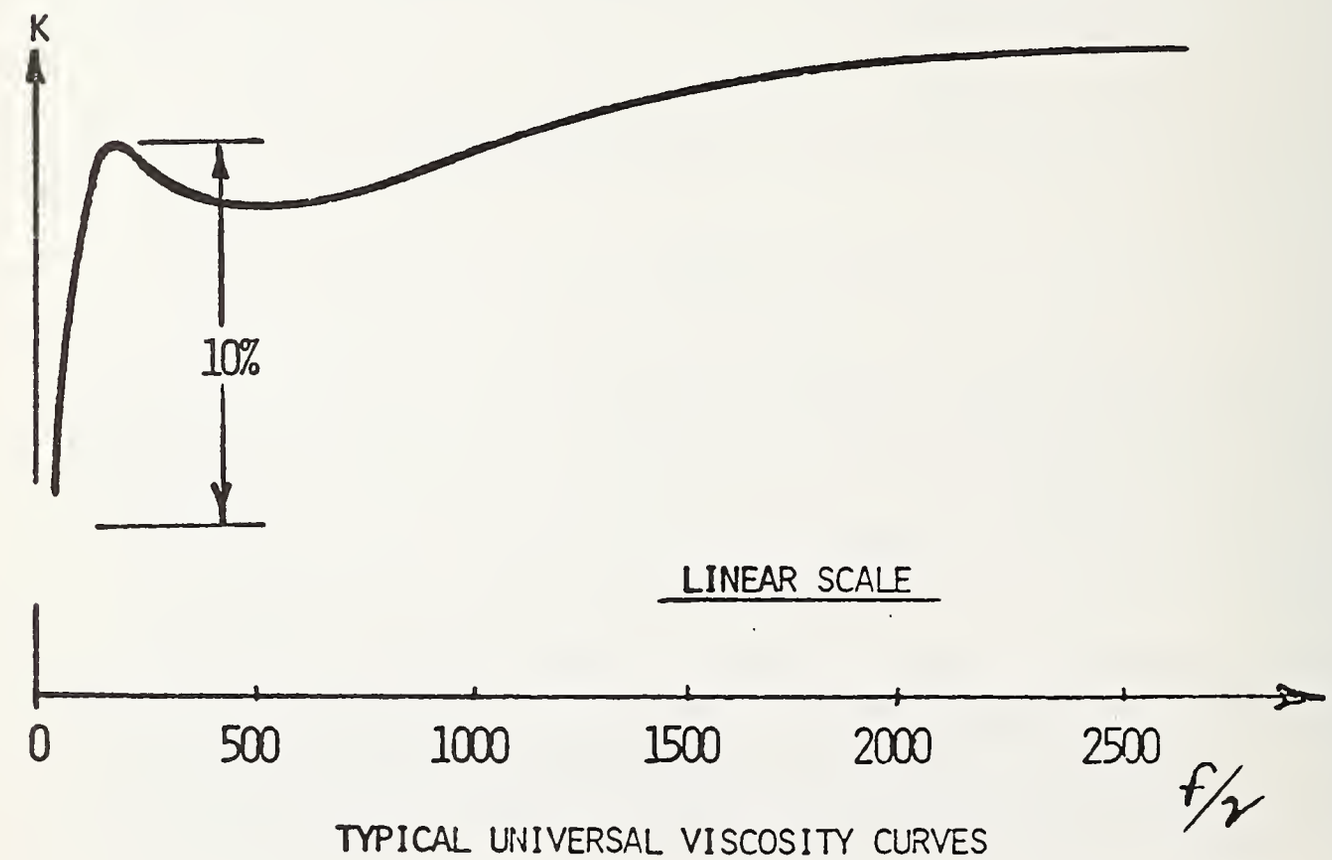

TYPICAL UNIVERSAL VISCOSITY CURVES

Figure 1

2. The Turbine Meter

Throughout this paper the term "turbine meter" will mean a propellor-type flow transducer which has the turbine mounted with the axis parallel to the direction of flow. The electrical output is produced by a pick off coil (inductance, variable reluctance, or modulated carrier (RF)) mounted upon the body of the meter. The meters considered are constructed of steel. Figure 2 shows this type of turbine meter, which is the most common design in use today in the US Army system.

3. Description of Calibrators

As a primary liquid flowmeter calibrator the USASL uses a volumetric displacement device which is basically a large cylinder within which a piston moves due to pneumatic pressure (See Figure 3). The moving piston displaces liquid through the turbine flowmeter being tested. This primary system uses an optical/electrical encoding system to produce pulses proportional to the volume displaced during a period determined by the output frequency of the turbine meter being calibrated.

Using this calibrator (which is temperature and pressure controlled) the calibration of turbine meters is reduced to counting the number of encoder counts and the number of turbine meter pulses generated during a timed interval. All data reduction is performed by computer (Figure 4 shows a typical data list). By nature the calibrator is unaffected by fluid density or viscosity.

The USASL also has gravimetric calibrators which determine flowrate through the weight of fluid displaced during a timed period (See Figure 5). These machines have a systematic error of approximately twice that of the volumetric device (.1% volumetric, .2% gravimetric), but are still suitable for turbine meter study.

4. Description of Method

The data which follows was produced by the USASL calibrators when testing turbine flowmeters. The viscosity of the flowing fluid was determined through frequent calibrations of the fluid viscosities versus temperature and continual monitoring and control of the operating temperature.

5. Characteristic Factor

For turbine meters the most common method of relating the flowmeter output frequency to the flowrate is through the "K-factor" (number of pulses per gallon). Another form in common use in the Army is the "C-factor" (C-factor x frequency = GPM) which is used as a frequency meter preset value. Functionally, the C-factor looks like the inverse of the K-factor (See Figure 6).

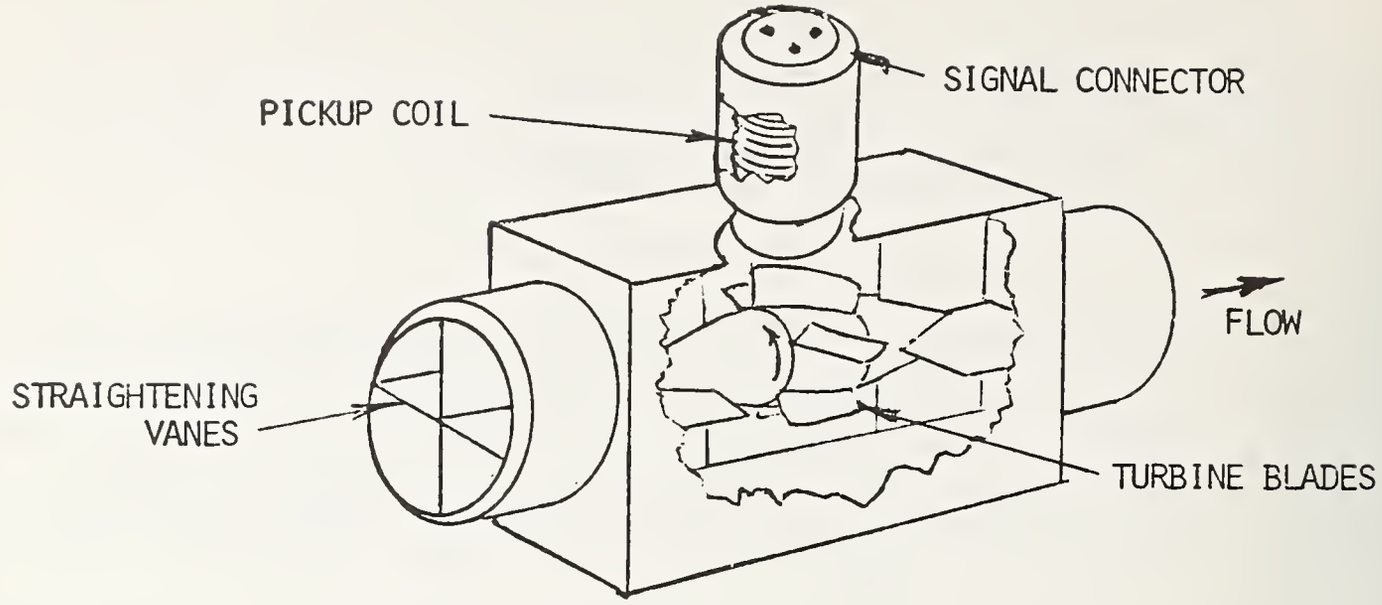

TYPICAL TURBINE FLOWMETER

Figure 2

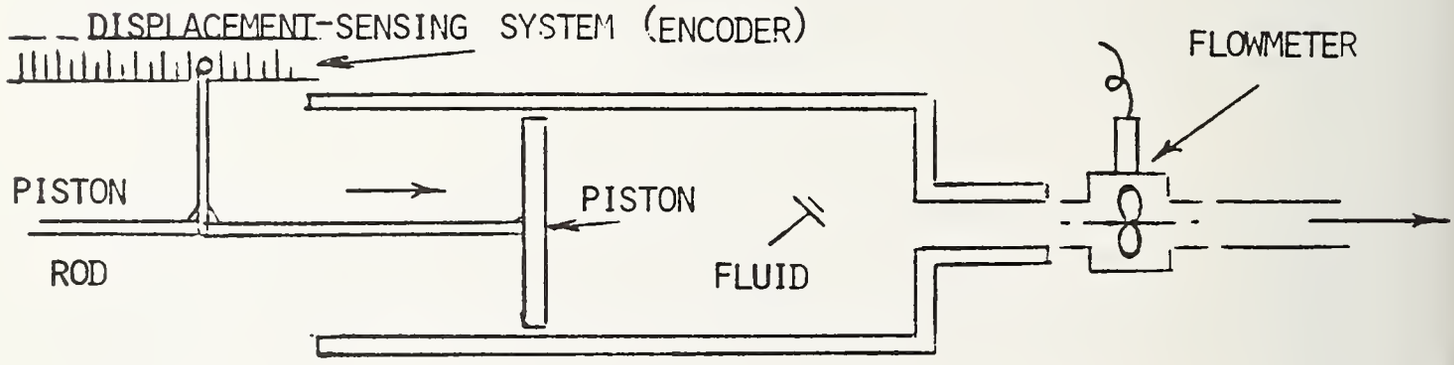

VOLUMETRIC DISPLACEMENT CALIBRATOR

Figure 3

TOTAL FLOWMETER PULSES	FLOWCAL COUNTER READING	TIME (SEC)	FREQUENCY (CPS)	FLOWRATE (GPM)	CYCLES PER GALLON	C
5400.	56100.	2.69140	2006.3937	10.41306	11560.8128	.51899465E-02
5400.	56100.	2.68890	2008.2562	10.42274	11560.8128	.51899465E-02
5401.	56087.	2.68480	2011.6955	10.43624	11565.6338	.51877831E-02
5400.	56132.	2.97870	1812.8714	9.41407	11554.2222	.51929069E-02
5400.	56113.	2.97540	1814.8820	9.42132	11558.1345	.51911492E-02
5401.	56108.	2.97000	1818.1818	9.43761	11559.1645	.51906866E-02
5400.	56103.	2.96890	1818.8555	9.44027	11560.1945	.51902240E-02
5401.	56152.	3.33950	1617.3080	8.39997	11552.2458	.51937953E-02
5401.	56146.	3.33940	1617.3564	8.39932	11553.4803	.51932404E-02
5401.	56137.	3.33500	1619.4903	8.40905	11555.3326	.51924079E-02
5401.	56179.	3.71970	1451.9988	7.54501	11546.6937	.51962927E-02
5402.	56165.	3.72080	1451.8333	7.54090	11551.7103	.51940361E-02
5402.	56157.	3.71280	1454.9656	7.55607	11553.3559	.51932963E-02
5404.	56216.	4.48100	1205.9808	6.26728	11545.5033	.51968284E-02
5403.	56196.	4.43020	1219.5838	6.33689	11547.4751	.51959410E-02
5402.	56197.	4.42580	1220.5703	6.34330	11545.1324	.51969954E-02
5402.	56188.	4.42030	1222.0890	6.35017	11546.9817	.51961631E-02
5404.	56230.	5.14570	1050.1973	5.45905	11542.6238	.51981226E-02
5404.	56225.	5.13410	1052.5701	5.47090	11543.6552	.51976604E-02
5403.	56214.	5.13220	1052.7649	5.47186	11543.7775	.51976053E-02
5404.	56248.	5.90820	914.6610	4.75604	11538.9350	.51997866E-02
5403.	56237.	5.90730	914.6310	4.75584	11539.0564	.51997320E-02
5403.	56246.	5.90350	915.2198	4.75966	11537.2100	.52005641E-02
5404.	56238.	5.89990	915.9477	4.76189	11540.9858	.51988622E-02
5404.	56274.	6.73160	802.7809	4.17622	11533.6037	.52021902E-02
5403.	56257.	6.73560	802.1557	4.17248	11534.9541	.52015812E-02
5403.	56238.	6.72300	803.6591	4.17889	11538.8512	.51998244E-02
5403.	56270.	6.77470	797.5261	4.14936	11532.2892	.52027832E-02
5403.	56254.	6.77230	797.8087	4.14965	11535.5692	.52013038E-02
5402.	56252.	7.62810	708.1711	3.68396	11533.8443	.52020817E-02
5402.	56255.	7.62480	708.4776	3.68575	11533.2292	.52023591E-02
5402.	56249.	7.63160	707.8463	3.68208	11534.4594	.52018042E-02
5398.	56240.	9.08590	594.1074	3.09223	11527.7630	.52048259E-02
5398.	56219.	9.09160	593.7349	3.08913	11532.0691	.52028825E-02
5397.	56229.	9.08390	594.1281	3.09230	11527.8822	.52047721E-02
5399.	56227.	9.07520	594.9180	3.09516	11532.5644	.52026590E-02
5400.	56249.	8.19050	659.3004	3.43082	11530.1890	.52037308E-02
5401.	56257.	8.19410	659.1328	3.42980	11530.6843	.52035073E-02
5402.	56253.	8.20350	658.4994	3.42563	11533.6392	.52021742E-02
5401.	56247.	8.19100	659.3822	3.43049	11532.7343	.52025824E-02
5396.	56217.	10.05640	536.5737	2.79267	11529.2065	.52046257E-02
5396.	56235.	10.06340	536.2005	2.79162	11524.5165	.52062922E-02
5396.	56215.	10.06990	535.8544	2.78882	11528.6166	.52044406E-02
5396.	56215.	10.06690	536.0141	2.78965	11528.6166	.52044406E-02
5395.	56208.	10.52380	512.6475	2.66821	11527.9156	.52047571E-02
5394.	56192.	10.53250	512.1291	2.66524	11529.0606	.52042401E-02
5394.	56201.	10.52780	512.3578	2.66686	11527.2144	.52050737E-02
5387.	56136.	13.76860	391.2526	2.03679	11525.5852	.52058094E-02
5387.	56125.	13.77970	390.9374	2.03475	11527.8441	.52047893E-02
5387.	56112.	13.76470	391.3634	2.03649	11530.5148	.52035838E-02
5379.	56046.	19.07640	281.9714	1.46772	11526.9496	.52051932E-02
5379.	56027.	19.07630	281.9729	1.46723	11530.8586	.52034286E-02
5379.	56027.	19.08960	281.7765	1.46620	11530.8586	.52034286E-02
5356.	55726.	26.59250	201.4102	1.04687	11543.5708	.51976965E-02
5365.	55958.	56.52190	94.9190	.49458	11515.0284	.52105820E-02

Figure 4

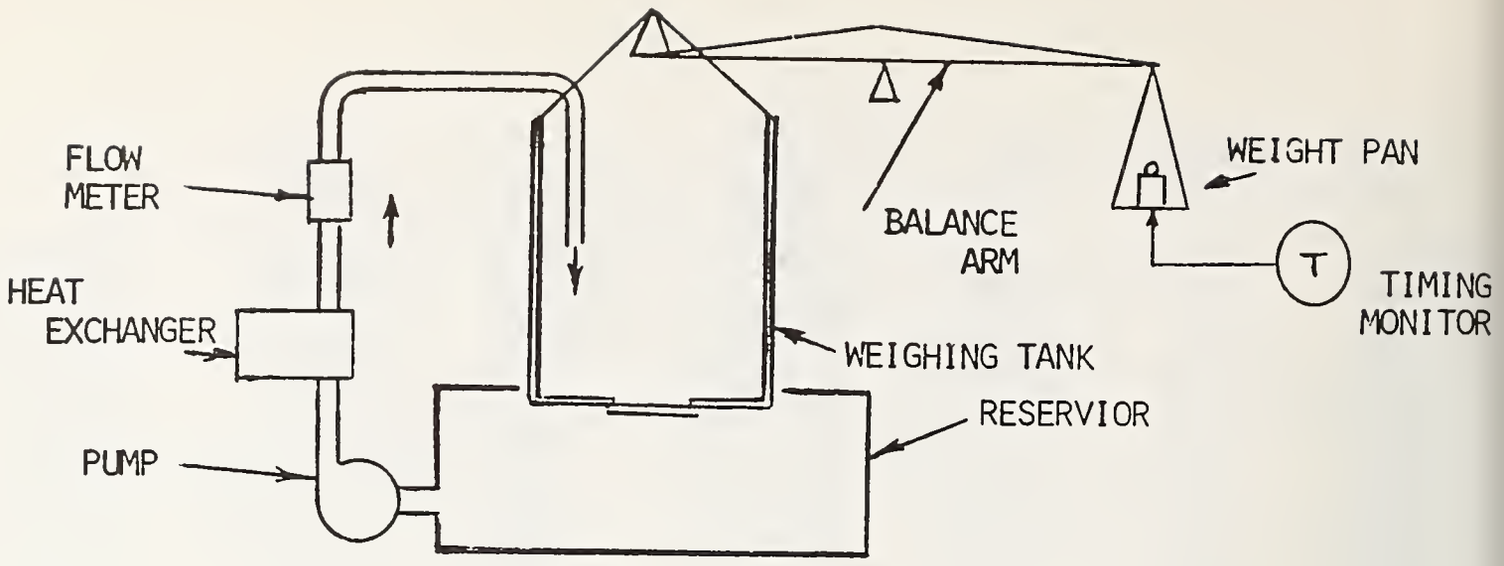

SCHEMATIC OF WEIGHT-MEASURING FLOW CALIBRATOR

Figure 5

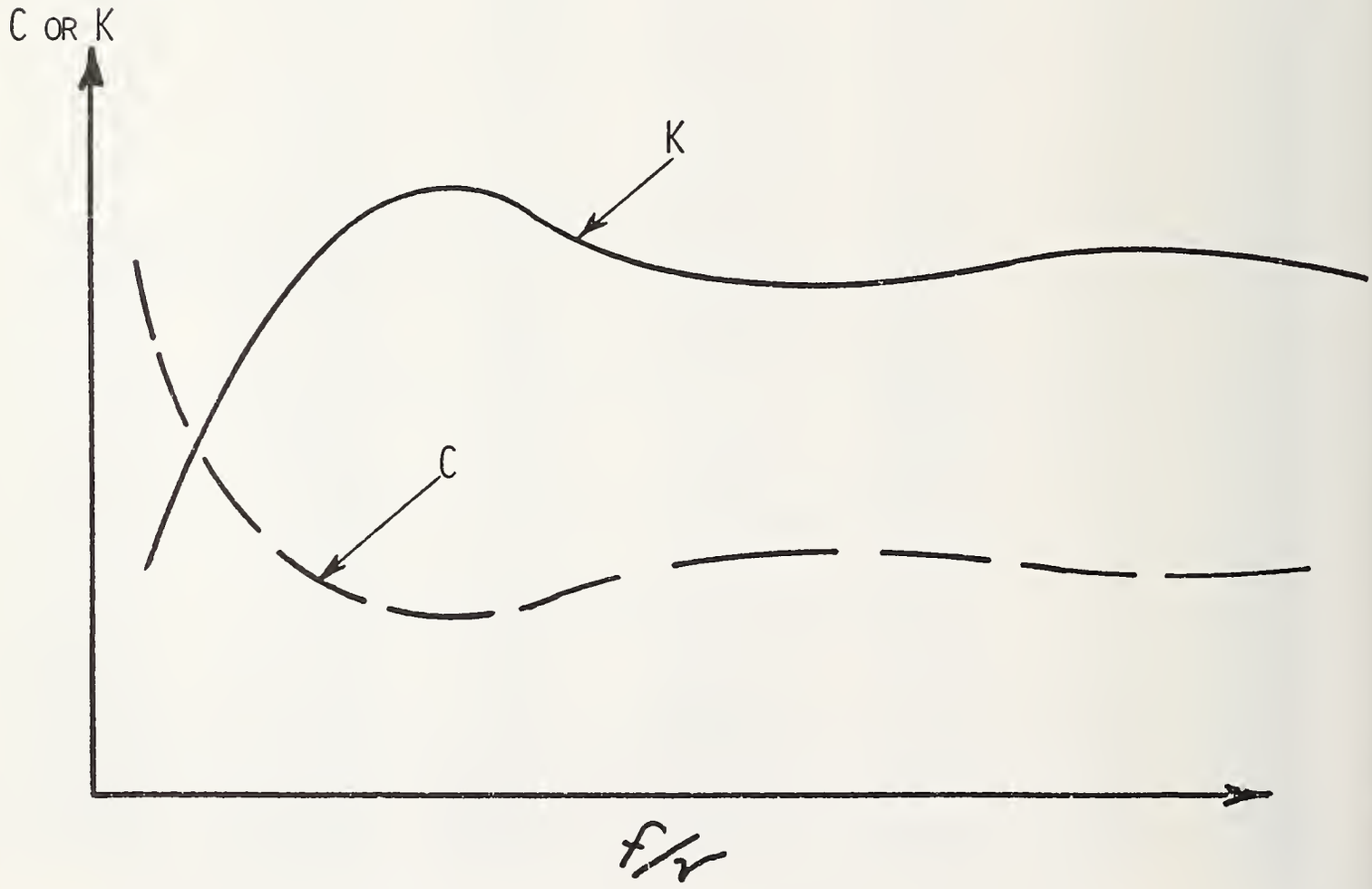

COMPARISON OF C- AND K-FACTOR CURVES

Figure 6

$$K = \frac{\text{counts}}{\text{gallon}} \qquad C = \frac{\text{GPM}}{\text{Hz}}$$

6. Universal Curve

In 1961 the relationship of H. M. Hochreiter

$$\frac{Q}{nD^3} = \phi \left(\frac{nD^2}{\nu}, \frac{F}{\rho n^2 D^4}, \frac{E}{\rho n^2 D^2}, \frac{d_1}{D}, - - - - \right)$$

was used by R. Shafer to describe for one particular meter geometry the function ϕ_1.

$$\frac{f}{Q} = \phi_1 \quad (f/\nu)$$

f = frequency, Q = flowrate, ν = kinematic viscosity

Shafer's data indicated that no single form of the function ϕ_1 describes the performance of a turbine meter. He also noted that this form of data presentation (the universal curve) is often used by meter manufacturers (See Figure 7). L. O. Olsen's technical note from NBS in 1974 restated some of these conclusions.

Other researchers have concluded that the universal curve is only useful at high Reynolds Numbers (note the response of J. Grey to the Hoscheiter article). Since f/ν is similar to Re (if $Q \simeq Af$ where A is a constant, then $Re \simeq B\ f/\nu$, where B is constant), high Reynolds Numbers mean either high frequency or low viscosity operation (See Figure 6).

Three researchers, V. R. Withers, F. A. Inkley, and D. A. Chesters in a paper presented at a flow measurement conference in 1971 found differences of one percent and more in the turbine meter characteristic factor in the same fluid at different temperatures (i.e. different viscosities) (See Figure 8).

7. Magnetic Flowmeter Data

Following (Figures 9A, 9B, & 9C) are curves showing the results obtained from typical multiple fluid calibrations of high quality variable reluctance or inductance type turbine meters ("magnetic" turbine meters). In those figures which show a "universal curve" sketched in, note the percentage spread. Most manufacturers clain $\pm$ .5% or less uncertainty for their instruments, and our results show that such expectations, while reasonable for a single fluid curve over a small temperature band, are unrealistic in a universal curve. We have also observed that only meters larger than 1/2" show good (near 1% overlap) performance.

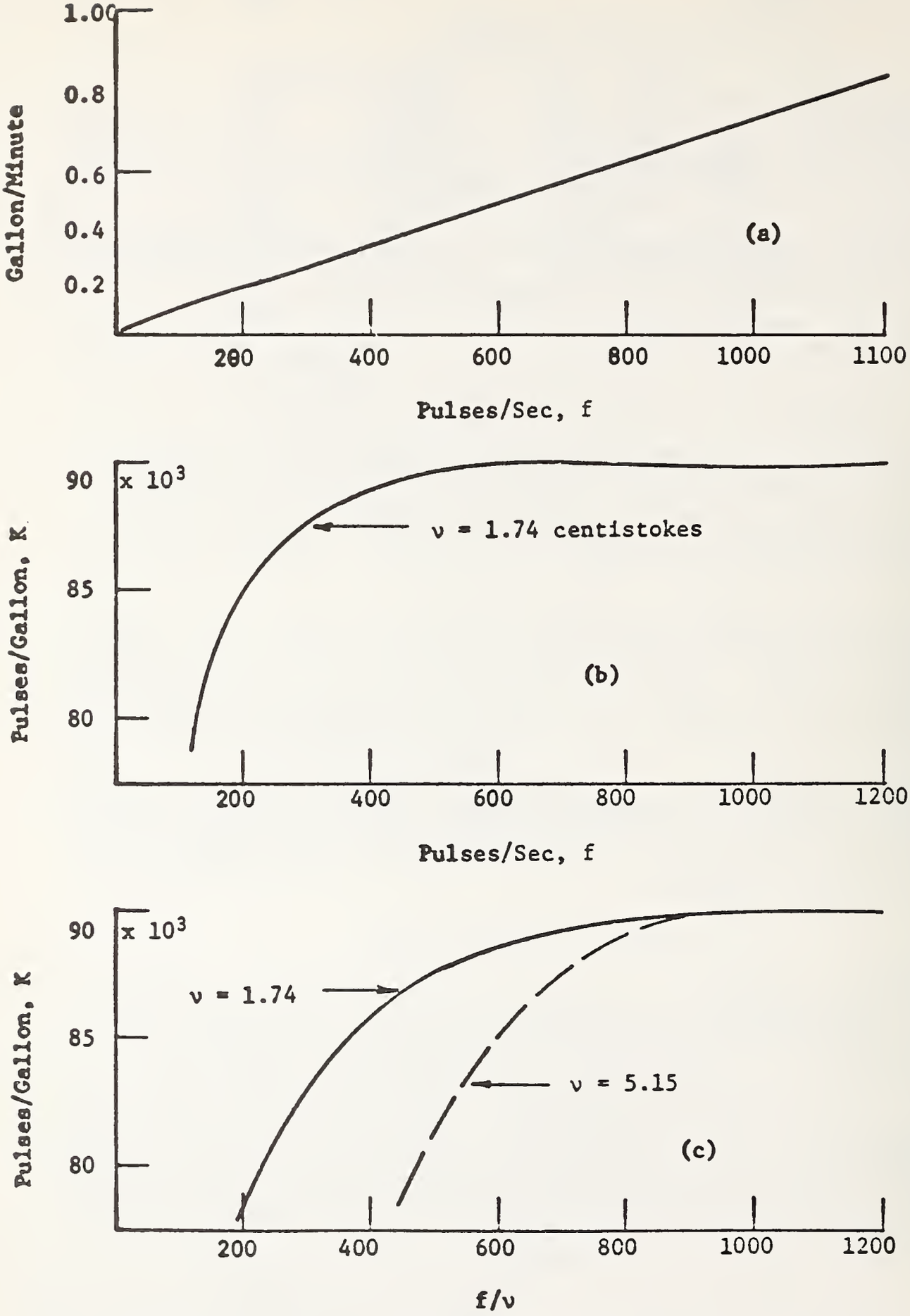
1.00
0.8
0.6
0.4
0.2
Gallon/Minute
(a)
200
400
600
800
1000
1100
Pulses/Sec, f
90
x 10³
85
80
Pulses/Gallon, K
ν = 1.74 centistokes
(b)
200
400
600
800
1000
1200
Pulses/Sec, f
90
x 10³
85
80
Pulses/Gallon, K
ν = 1.74
ν = 5.15
(c)
200
400
600
800
1000
1200
f/ν

Figure 7

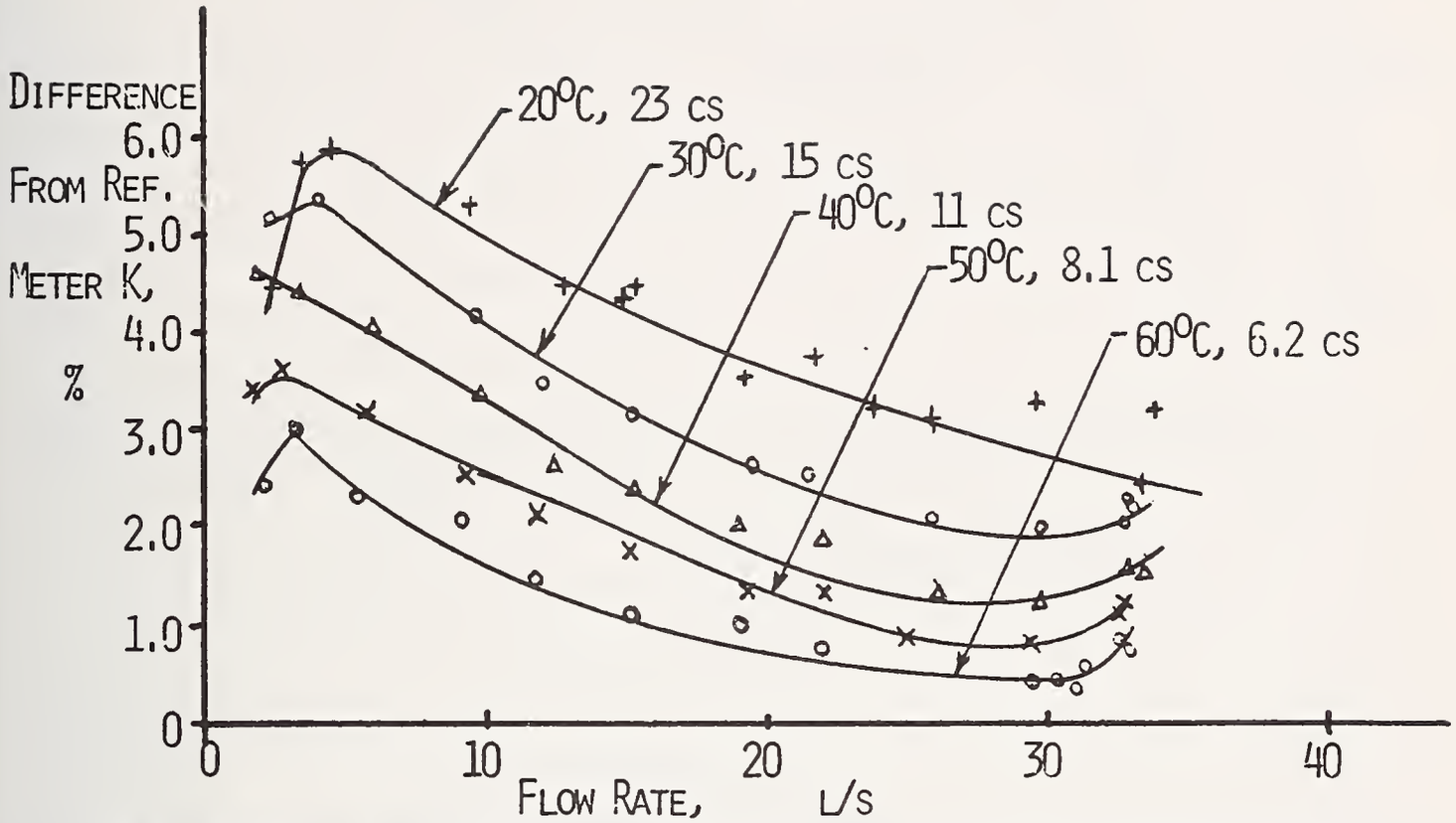

PERFORMANCE OF ONE FLOWMETER WITH DIFFERENT OILS AND TEMPERATURES

Figure 8

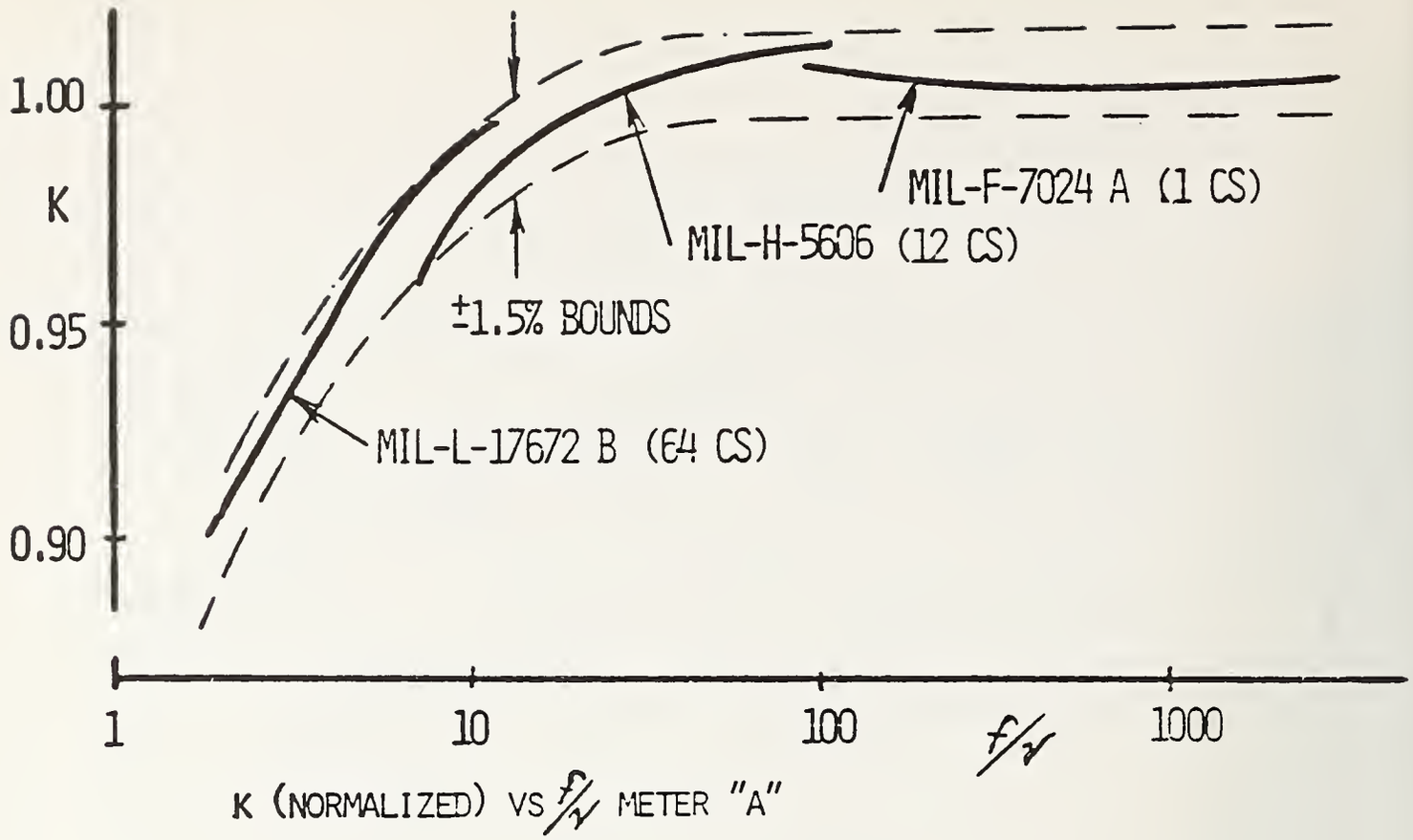

Figure 9A

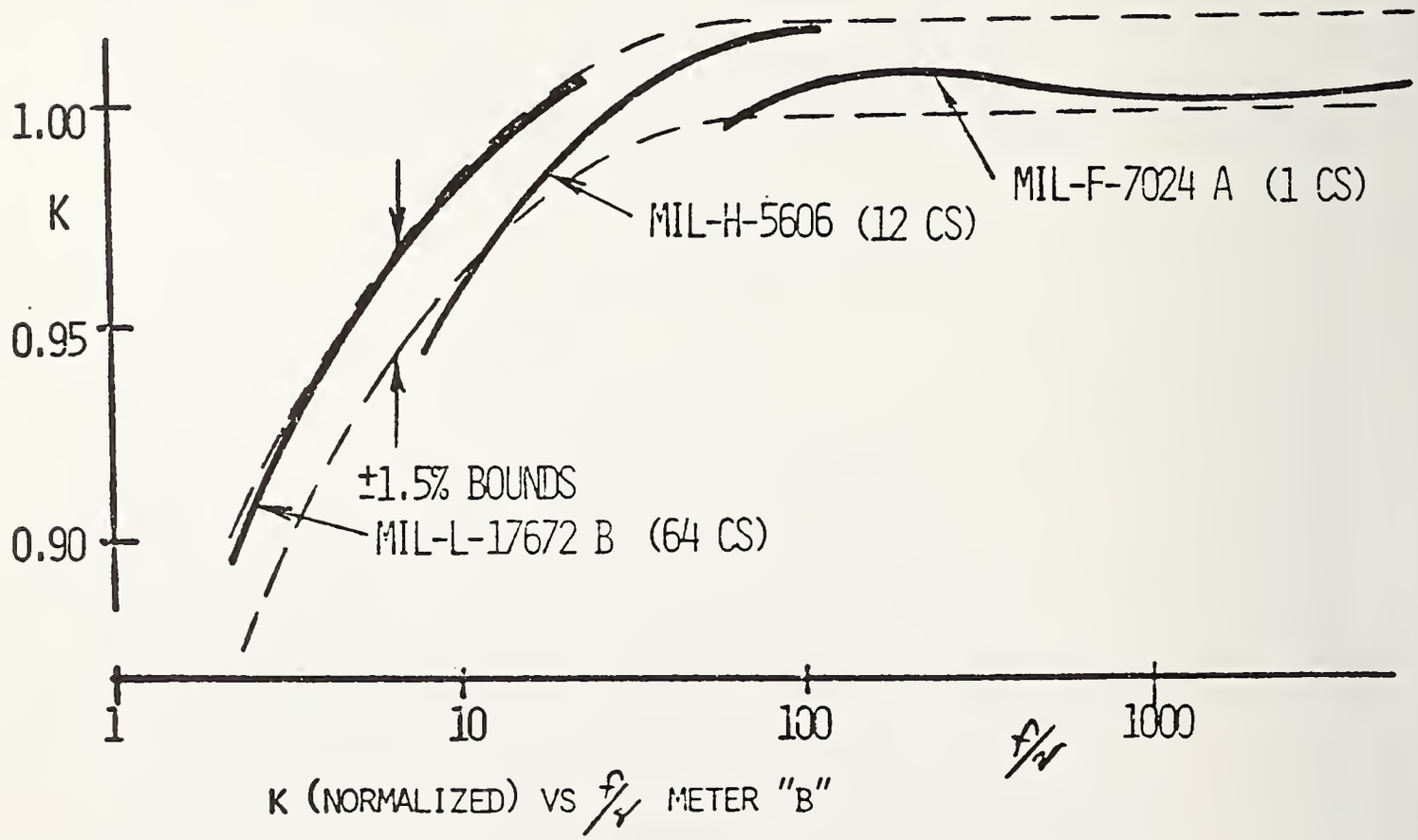

Figure 9B

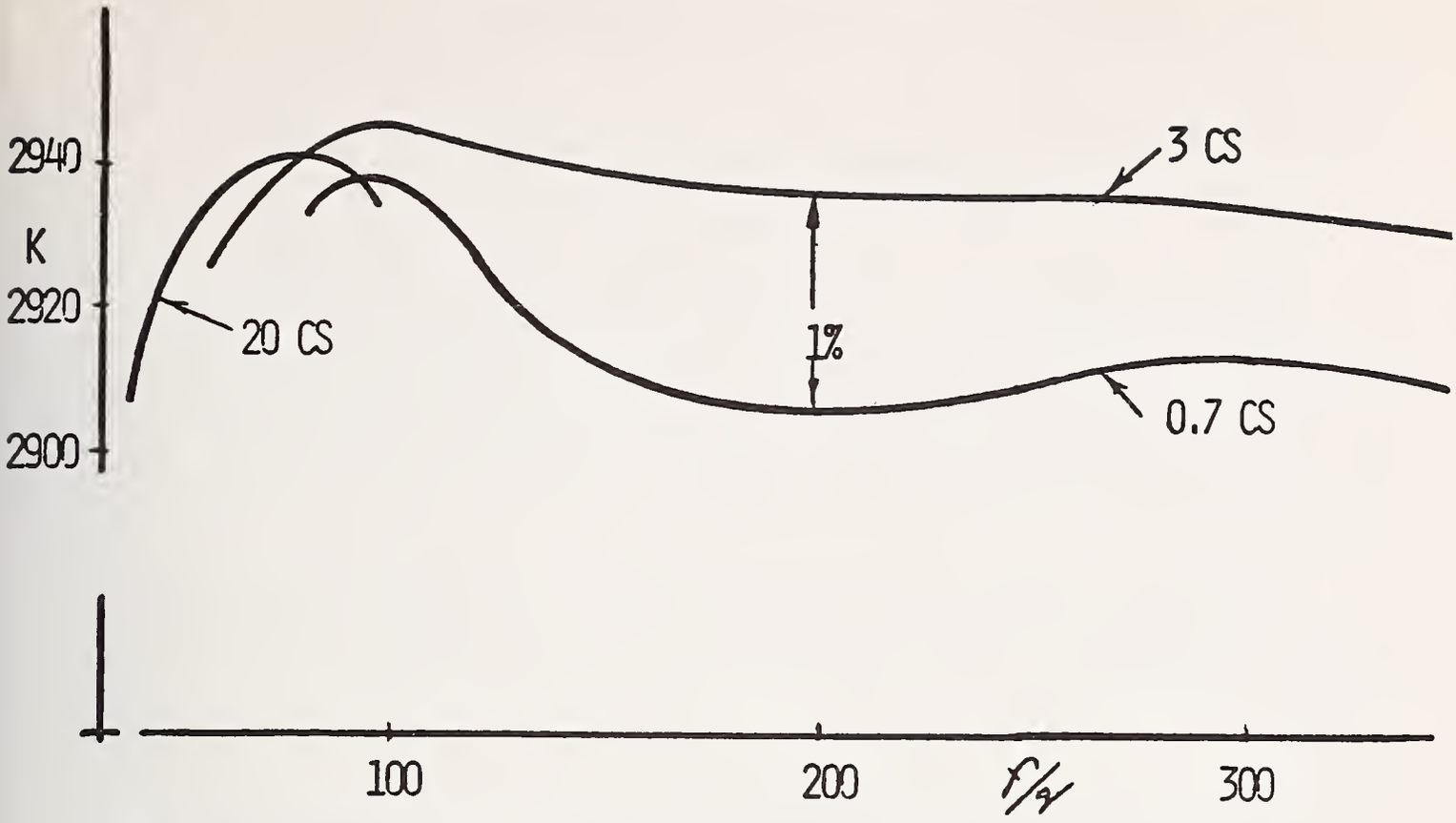

TYPICAL DISAGREEMENT RESULTING FROM DIFFERING VISCOSITY FLUIDS

Figure 9C

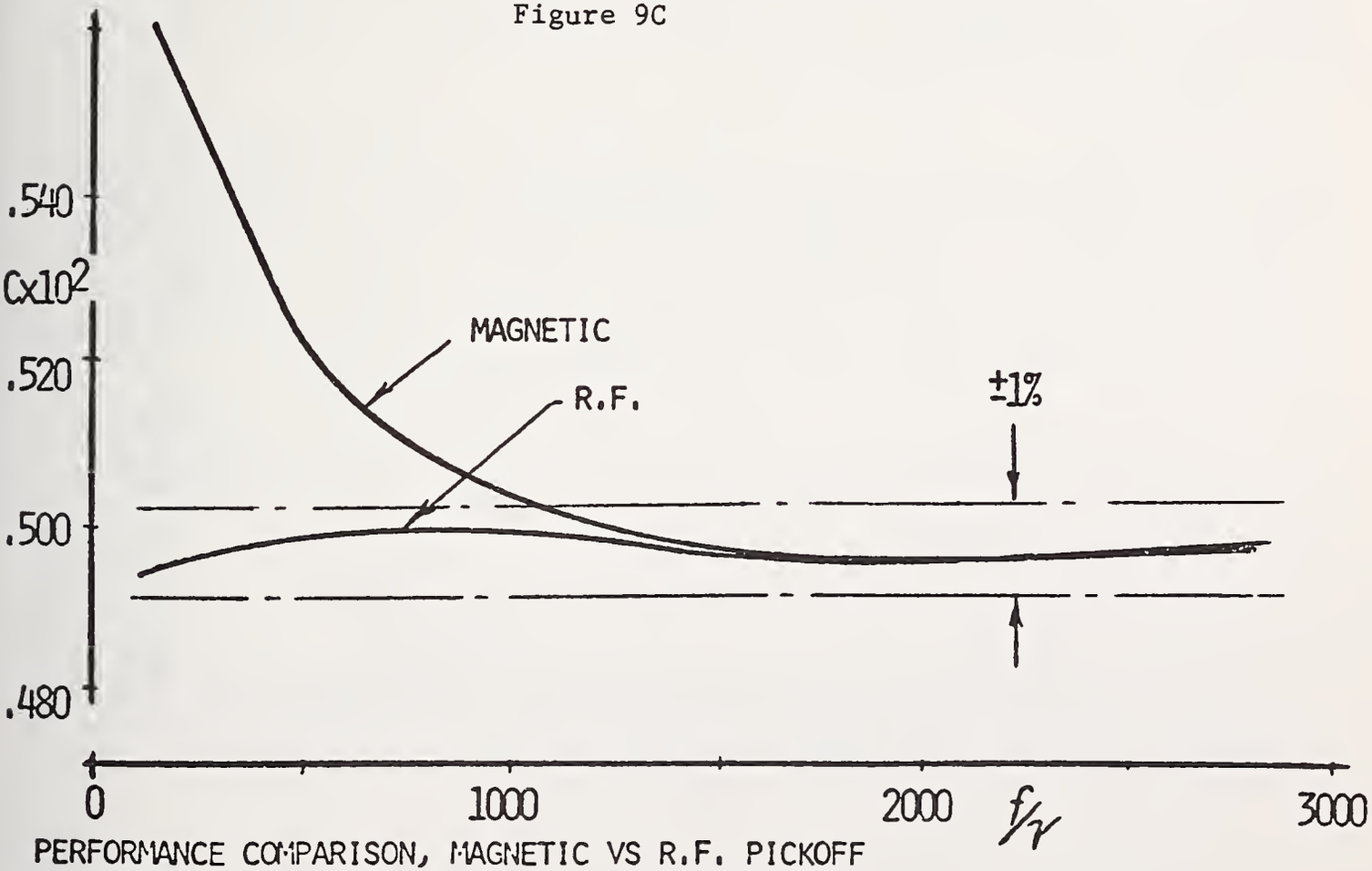

PERFORMANCE COMPARISON, MAGNETIC VS R.F. PICKOFF

Figure 10

Since this meter type is at present by far the most commonly used, most users should not expect to obtain universal curves from calibration laboratories, and those people who use a single calibration fluid curve to predict other fluid performance are quite probably introducing significant errors into their measurements unknowingly.

8. RF Flowmeter Data

Magnetic drag affects the performance curve as illustrated in Figure 10. A flowmeter was calibrated in the same fluid under the same conditions, first as a magnetic meter, and then as a modulated carrier (RF) meter. This was accomplished by changing pickoffs between calibrations. Note that the curves run together at higher frequencies, but that the effect of magnetic drag is more pronounced at the lower end of the range.

It might be expected, based upon the more nearly linear response of the RF meters at low frequencies that this type of meter would perform better in multiple fluids, and even that a single ϕ_1 might exist for such meters.

9. Test Results

Unfortunately, sample turbine meters of the RF type from several manufacturers were not available in sufficient numbers, and so the results which follow are based primarily upon the periodic calibration and recalibration of approximately 100 RF turbine flow transducers purchased by the US Army for use as transfer standards (all of which are manufactured by the same company).

Illustrated in Figure 11 and the Appendix are typical multiple fluid C factor curves, and typical single fluid curves for these meters. Note the random error percentage in the multiple fluid example of $\pm$ .037% (99.7% confidence). The random error is a measure of the fit of the computer generated curve to the real data (both the computer generated curve and the real data points are shown). For these 100 meters typical random errors ranged from about .05% to about .25% of reading.

The curve was generated based upon the assumption that a function ϕ_1 existed, and, while the exact form of ϕ_1 might not be determinable, it was assumed that ϕ_1 would be well behaved enough to be approximated by the polynominal series

$$C = (f/\nu) = A + B\ f/\nu + C\ (f/\nu)^2 + \_\ \_\ \_\ \_ + P\ (f/\nu)^{N-1}$$

Due to the performance of the meters at the "minimum" point, (See Figure 11 and Appendix), we used two polynominal approximating functions, one from the start of the curve to the frequency corresponding to the "minimum", and a second from the "minimum" onward.

TYPICAL COMPUTER GENERATED MULTIPLE FLUID CURVE FOR TRANSFER TURBINE METERS

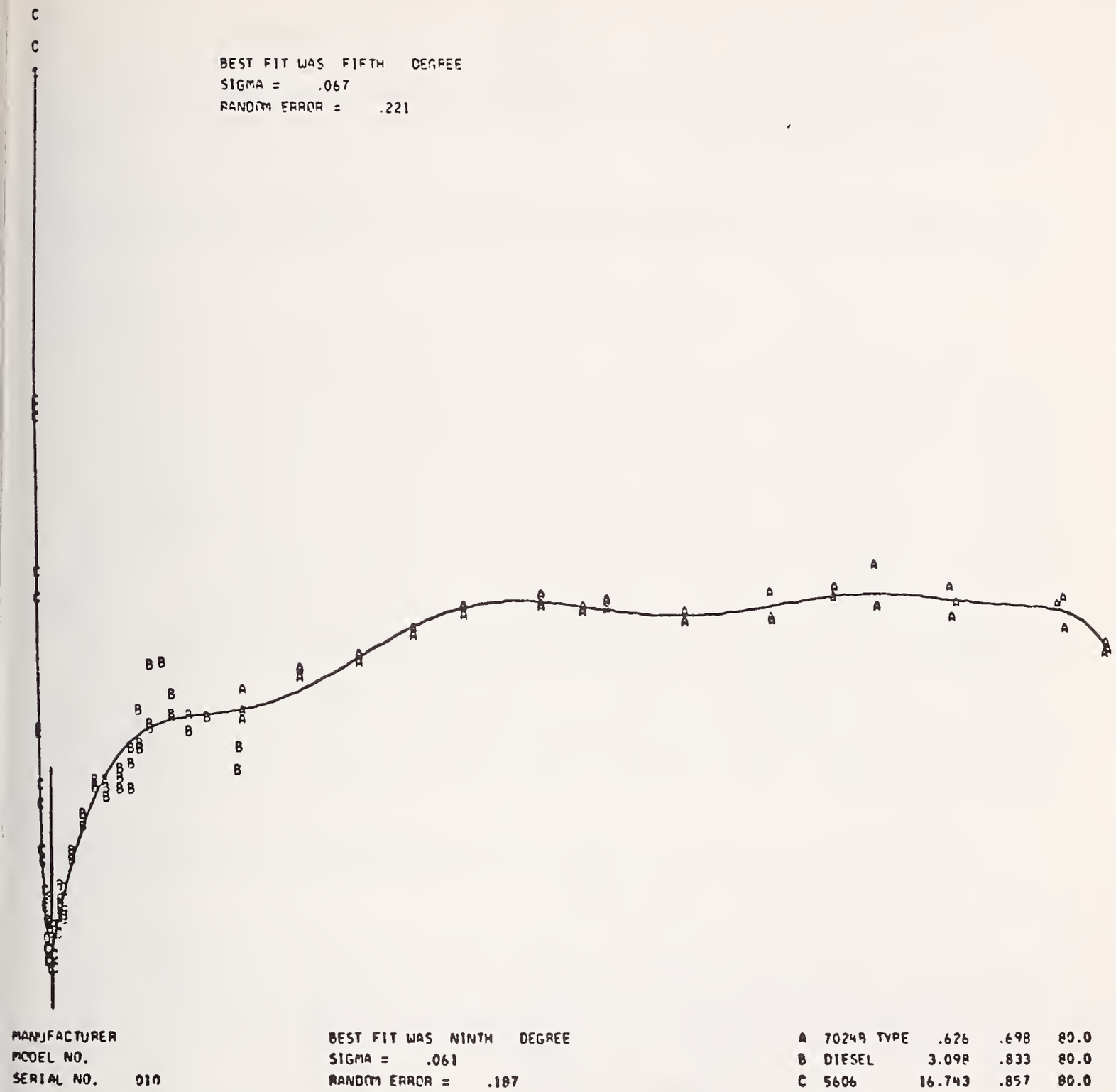

Figure 11

Typical orders of the polynominal curve for "best fit" on each side of the "minimum" for the 1" meter were 8th and 8th respectively, and for the 1/2" meter 10th and 9th respectively, with a spread through the group of about $\pm$ 30%.

The minimum point was found to occur at a Reynolds Number of about 5000 for the 1" and about 4000 for the 1/2" meter. This would add weight to those theories which have contended that the shape of the performance curve is due to changes in the flow regime from laminar to transition to turbulent (See Lee and Karlby).

These 100 meters have been found to repeat their original curves to better than $\pm$ .1% after being fielded and used for one year; then being returned to our laboratory (See Figure 12).

10. Conclusions

Our results show that universal viscosity curves accurate to better that $\pm$ .5% can be routinely produced by certain precision RF meters of the variety available to the general public, and that such performance generally cannot be expected from magnetic pickoff meters or from meters of less than 1/2" bore. A meter should always be calibrated in the fluids in which it is to be used. Interpolations from one fluid to another should not be performed unless calibration data demonstrates that such is possible, and the errors introduced by interpolating considered (which increases the uncertainty of the measurement).

The need for accurate and frequent viscosity measurements is demonstrated. Especially in the low range, the universal curve is worthless without an accurate measure of ν to divide into the frequency (note the response to ν in Figure 1). The accuracy required of the viscosity measurement is illustrated in Figure 13. Figure 13 shows the likely error introduced by viscosity error, and that the viscosity induced error in the "high" range (solvents, fuels, etc.) is small except at the lower frequencies.

Factors which affect the viscosity such as pressure and temperature must be included in calibration reports, if the universal cuvre is to be used, because both affect the viscosity.

Even though several sources of error remain which are not considered here (such as the effect of line pressure on the turbine meter), there are turbine meters which do show a single ϕ_1 and for which a universal curve or table can be used to routine accuracies of $\pm$ .5% or less.

11. References

1. Hochreiter, H. M.: "Dimensionless Correlation of Coefficients of Turbine-Type Flowmeters,"Transactions of the ASME, October, 1958.

2. Lee, W. F. Z., and Karlby, H.: "A Study of Viscosity Effect and its Compensation on Turbine-Type Flowmeters,"Transactions of the ASME, Journal of Basic Engineering, September, 1960.

3. Olsen, L. O.: "Introduction to Liquid Flow Metering and Calibration of Liquid Flowmeters,"N. B. S. Technical Note 831, June, 1974.

4. Shafer, M. R.: "Performance Characteristics of Turbine Flowmeters," Transactions of the ASME, Journal of Basic Engineering, Paper No. 61-WA-25, 1961.

5. Withes, V. R. Inkley, F. A., and Chesters, D. A.: "Flow Characteristics of Turbine Flowmeters,"Proceedings of the International Conference at Harwell, England, September, 1971.

6. Tan, P. A. K., and Hutton, S. P.: "Experimental Analytical, and Tip Clearance Loss Studies in Turbine-Type Flowmeters," OP. CIT.

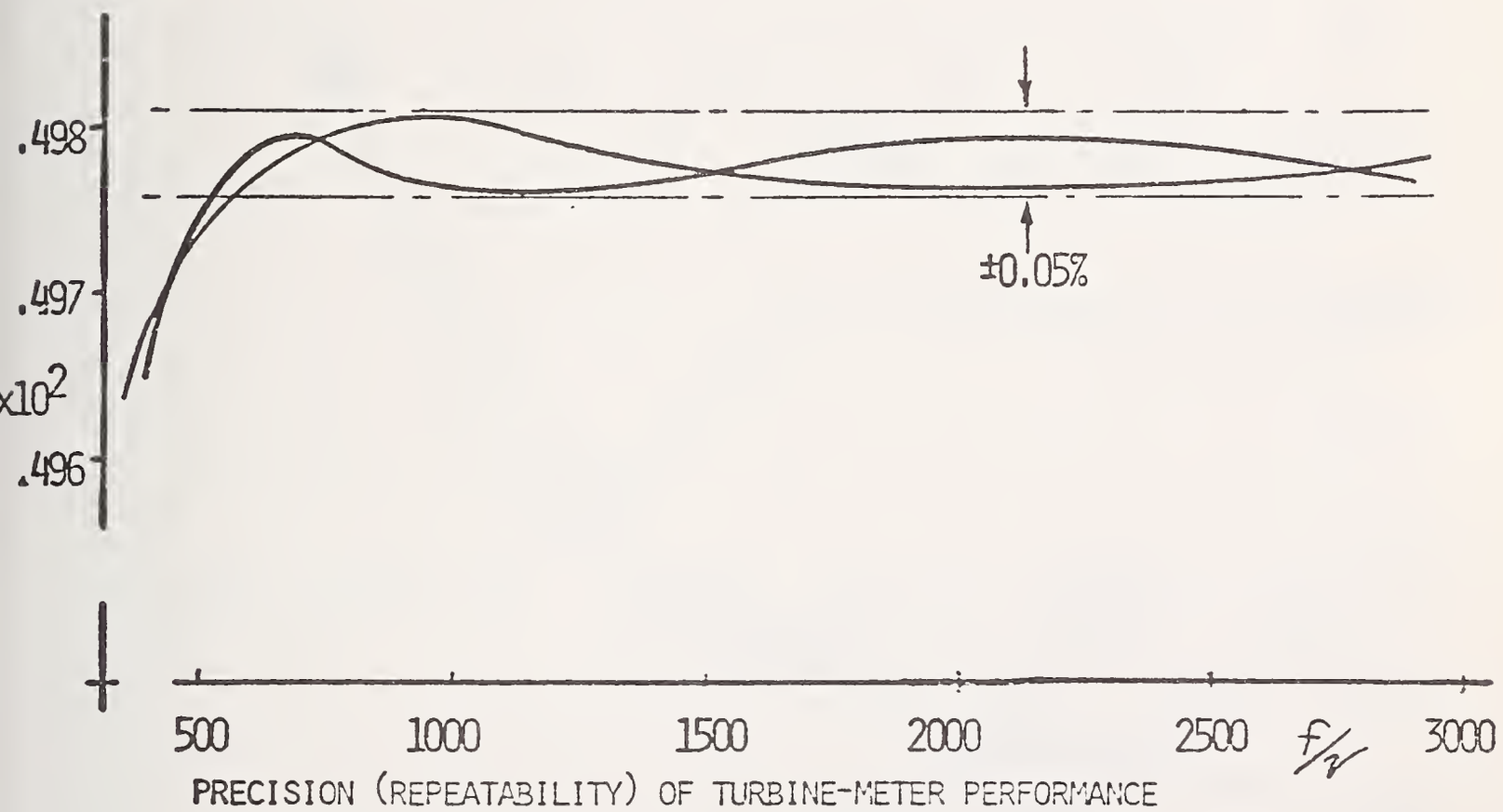

Figure 12

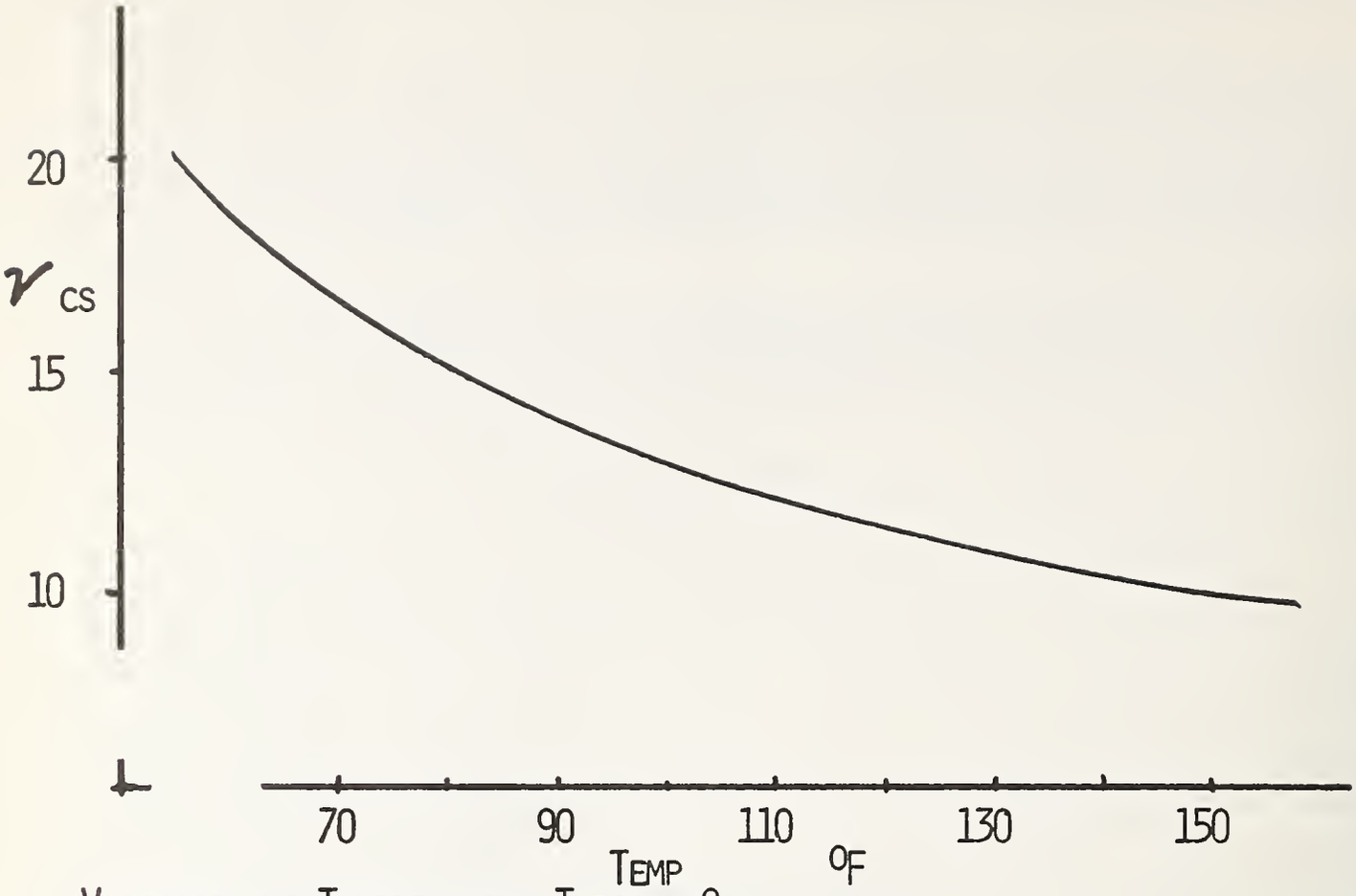

Viscosity vs Temperature, Typical Oil

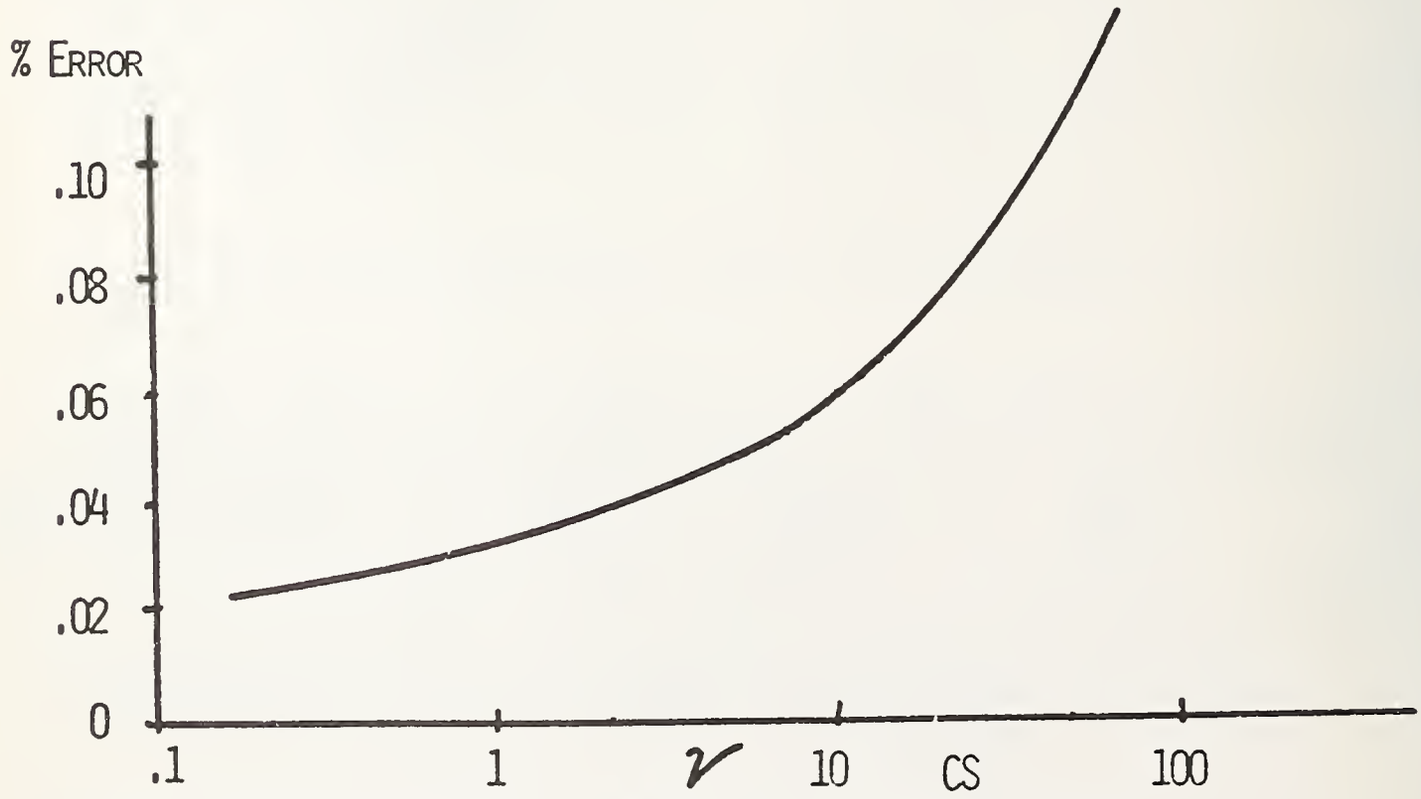

Typical Error in K Due to a 1% Error in Viscosity Value

Figure 13

Samples of US Army transfer turbine meter response curves. Figures A1 through A3 are single fluid response curves, and Figures A4 through A6 are multiple fluid (ϕ_1) curves.

All of these curves are computer generated plots of real data points (represented by letters) and computer generated curves (shown by X's and lines). The illustration below will aid in interpreting the figures which follow.

These plots are not printed to a uniform scale, but both X and Y scales vary from figure to fugure.

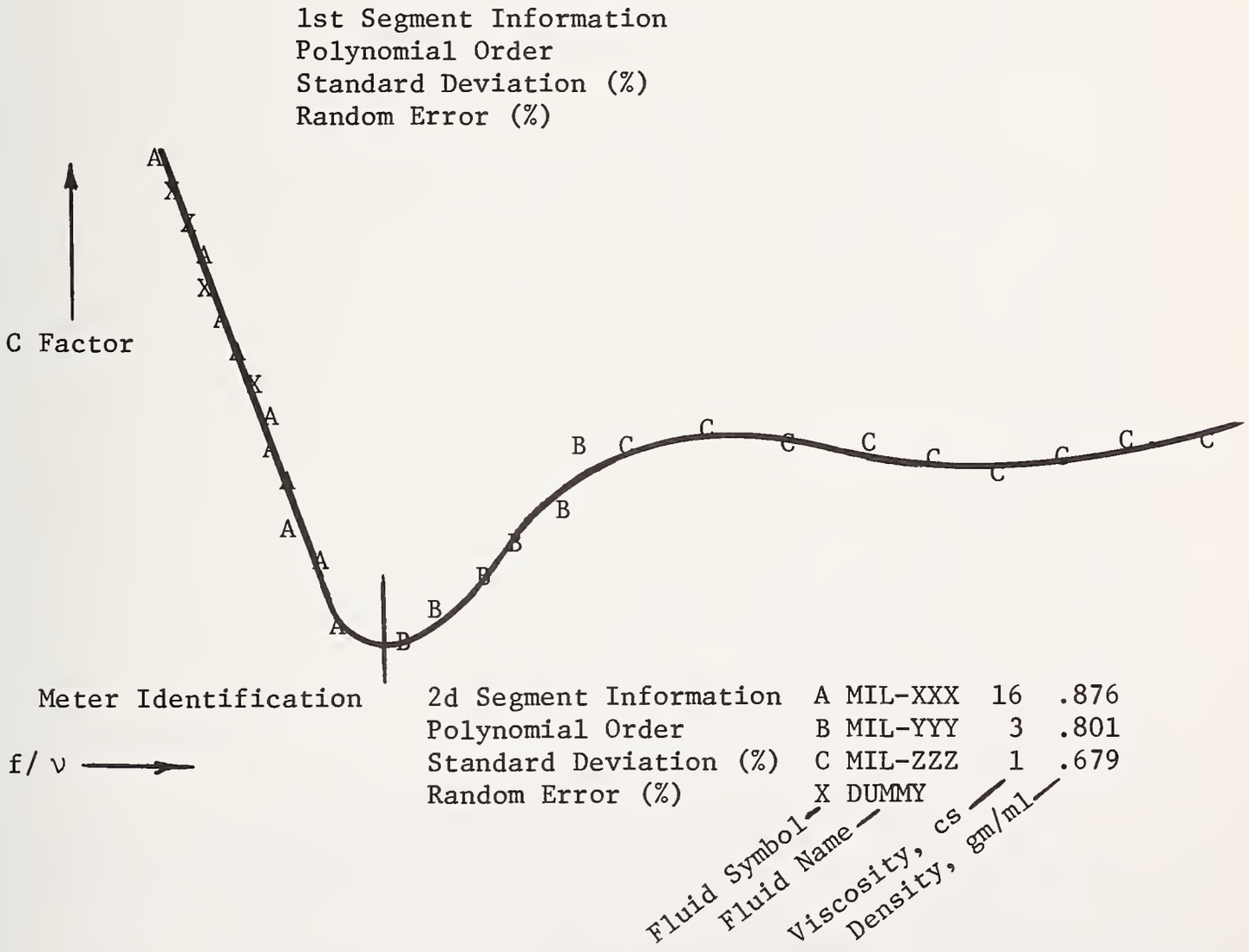

TYPLICAL SINGLE FLUID RESPONSE CURVES

MANUFACTURER
MODEL NO.
SERIAL NO. 091

BEST FIT WAS NINTH DEGREE
SIGMA = .112
RANDOM ERROR = .363

A 5606 19.290 .859 80.0
X DUMMY

A 1

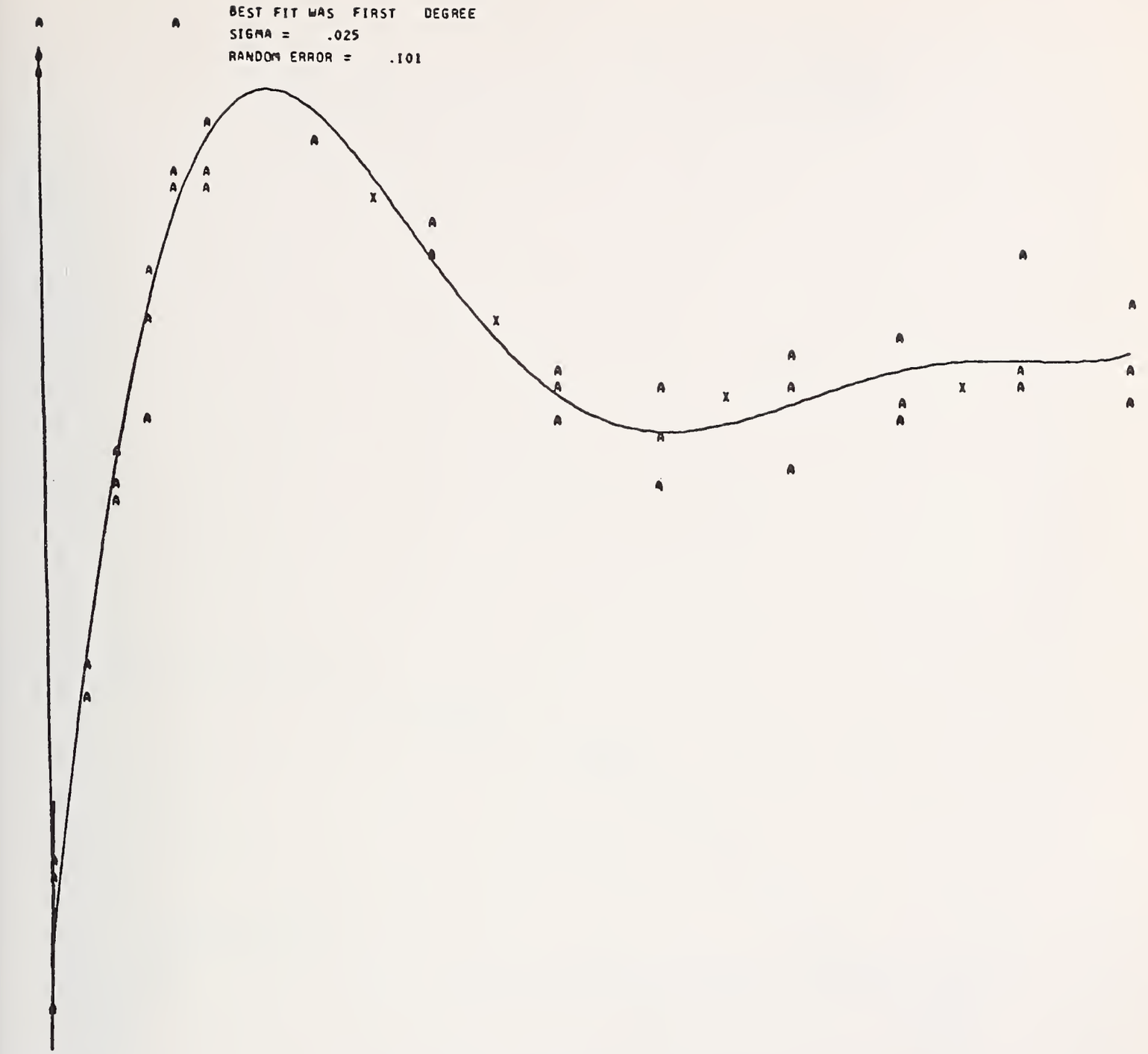

MANUFACTURER
MODEL NO.
SERIAL NO. 047

BEST FIT WAS FIFTH DEGREE
SIGMA = .033
RANDOM ERROR = .105

A TYPE 2 1.168 .74680.0
X DUMMY

A 2

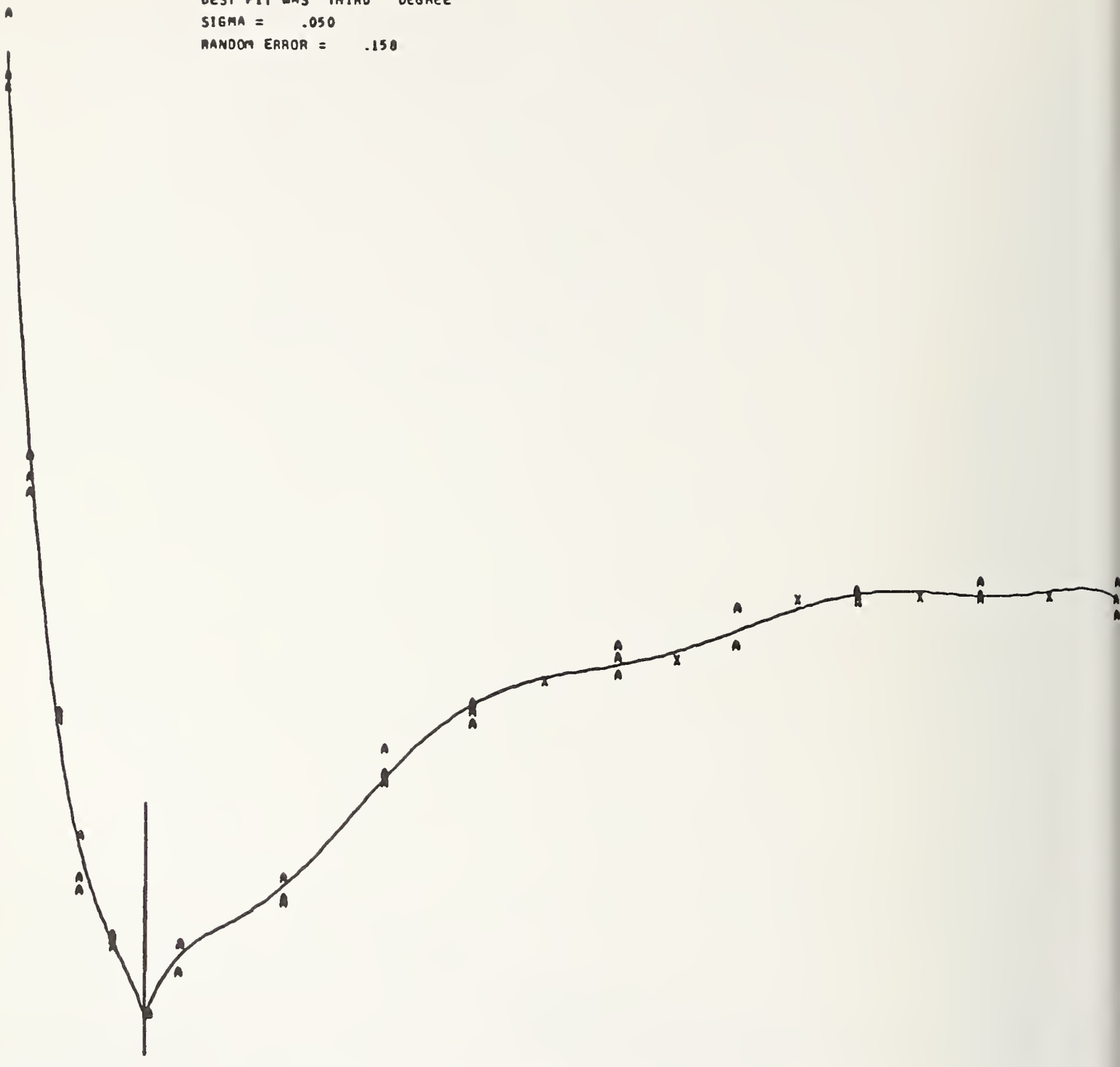
BEST FIT WAS THIRD DEGREE
SIGMA = .050
RANDOM ERROR = .158
MANUFACTURER
MODEL NO.
SERIAL NO. 349
BEST FIT WAS EIGHTH DEGREE
SIGMA = .033
RANDOM ERROR = .111
A DIESEL 3.171 .03580
X DUMMY

TYPICAL MULTIPLE FLUID RESPONSE CURVES

BEST FIT WAS FIFTH DEGREE
SIGMA = .139
RANDOM ERROR = .445

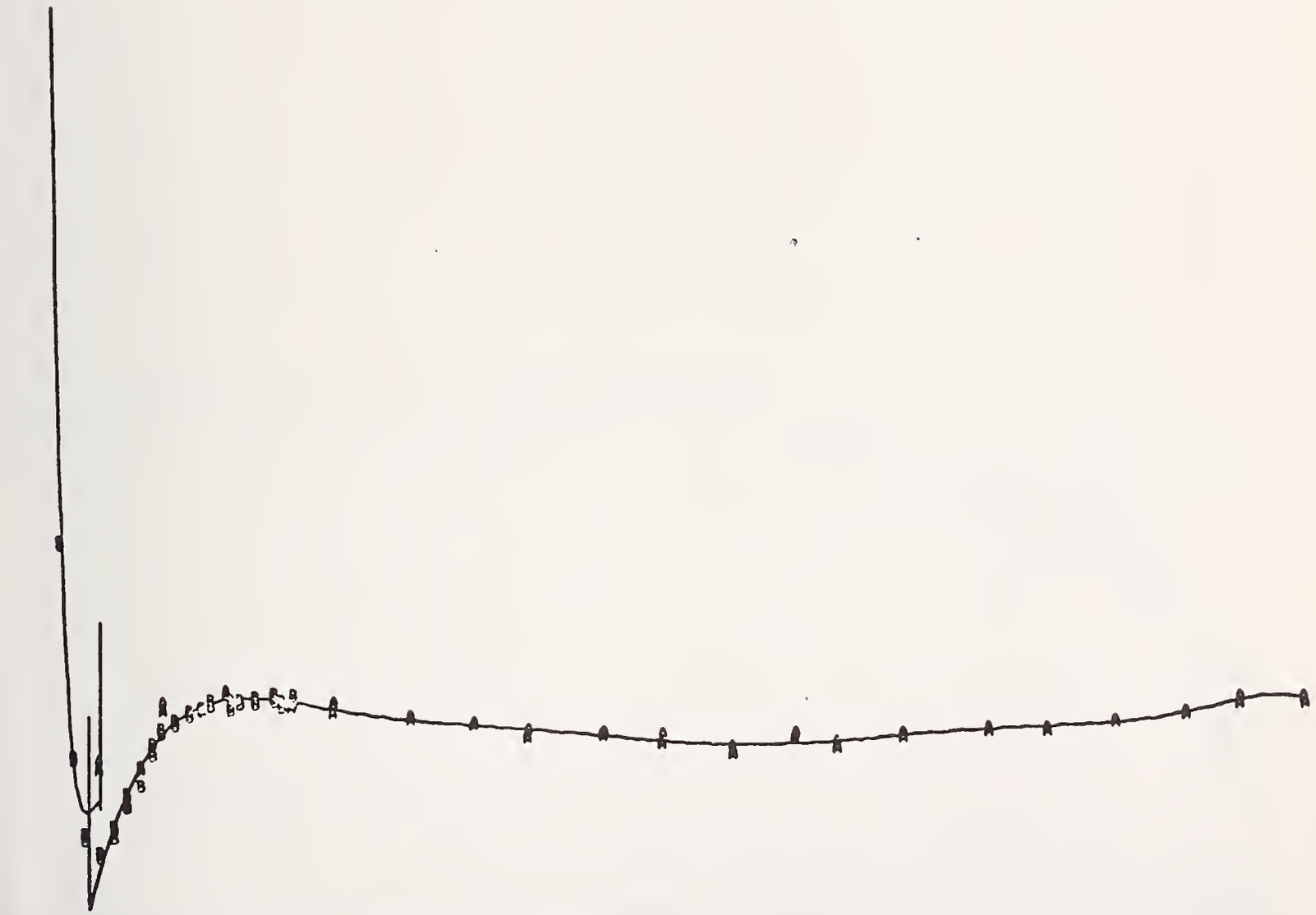

MANUFACTURER
MODEL NO.
SERIAL NO. .014

BEST FIT WAS NINTH DEGREE
SIGMA = .035
RANDOM ERROR = .108

A	7024B TYPE	.626	.698	80.0
B	DIESEL	3.098	.833	80.0

MANUFACTURER
MODEL NO.
SERIAL NO.

BEST FIT WAS NINTH DEGREE
SIGMA = .061
RANDOM ERROR = .187

A	7024B TYPE	.626	.698	80.0
B	DIESEL	3.098	.833	80.0
C	5606	16.743	.857	80.0

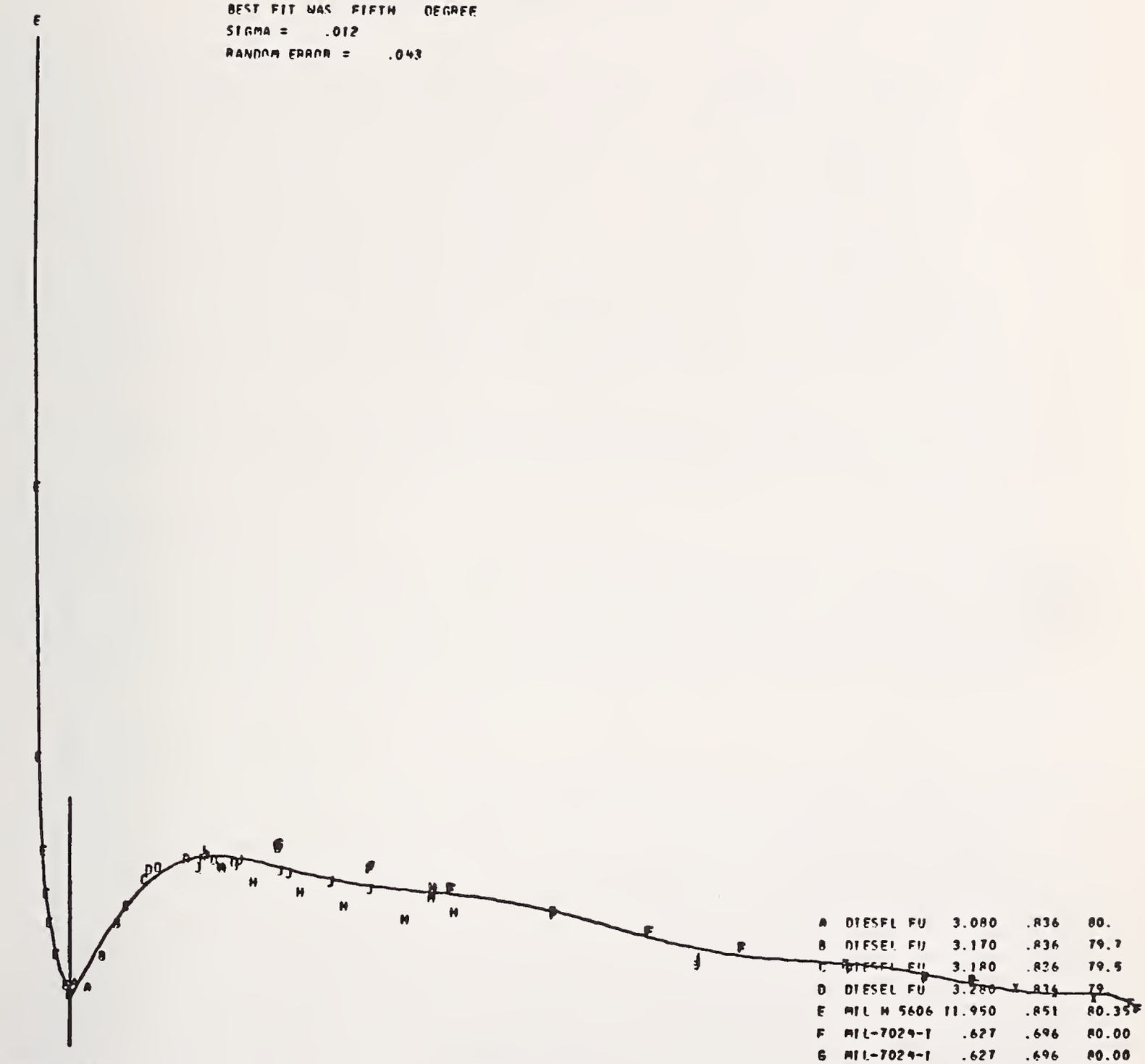
BEST FIT WAS FIFTH DEGREE
SIGMA = .012
RANDOM ERROR = .043
E
A DIESEL FU 3.080 .836 80.
B DIESEL FU 3.170 .836 79.7
C DIESEL FU 3.180 .836 79.5
D DIESEL FU 3.280 .836 79.
E MIL H 5606 11.950 .851 80.35
F MIL-7024-1 .627 .696 80.00
G MIL-7024-1 .627 .696 80.00
H JP 4 .990 .751 30.
J JP 4 1.040 .751 25.5
X DUMMY
MANUFACTURER
MODEL NO. 8
SERIAL NO.
BEST FIT WAS NINTH DEGREE
SIGMA = .022
RANDOM ERROR = .069

National Bureau of Standards Special Publication 484, Proceedings of the Symposium on Flow in Open Channels and Closed Conduits held at NBS, Gaithersburg, MD, February 23-25, 1977. (Issued October 1977)

TURBINE METERS FOR THE MEASUREMENT OF GASEOUS HYDROCARBONS

Paul J. LaNasa
Daniel Industries, Inc.
Houston, Texas 77024

Turbine meters for the measurement of gaseous fluids have been available for many years. However, their application in the United States to the measurement of hydrocarbon fuel gases has occurred over the last fifteen years. The evolution of the turbine meter for this particular application has resulted in specific design consideration to insure its continued reliability and performance. In addition to specific design considerations, this particular measurement application requires the accuracy of the turbine meter be verified on location, thus necessitating the development of accurate high pressure field testing methods.

Key Words: Turbine meter, gaseous hydrocarbons, fundamentals, fuel gas measurement, field testing, installation, performance characteristics, design considerations.

INTRODUCTION

During the last decade the gas turbine meter has become established as a very useful instrument for the measurement and control of gas flow. This paper will present a summary of the principles of operation, the basic construction and the performance characteristics of the gas turbine meter.

PRINCIPLE OF OPERATION

The gas turbine meter is a velocity measuring device. The theory of its operation is as follows: The gas enters the meter and is constricted increasing its velocity. It then passes through a free turning rotor which is mounted coaxially on the pipe centerline and exits the meter. In passing through the meter the gas imparts an angular velocity to the rotor proportional to the linear velocity of the gas in the meter. As the gas velocity is directly proportional to the volume flow rate it follows that the speed of rotation of the rotor is also directly proportional to the volume flow rate. Therefore, by accurate measurement of the rotor speed and the application of a predetermined calibration constant the volume flow rate can be obtained. The necessity of the calibration constant stems from the difference between the theoretical and the actual. In theory, as the gas passes through the meter it encounters a free

running rotor on which to impart its energy. However, in actuality the rotor has certain retarding forces which impede its movement. These retarding forces are due mainly to bearing friction and aerodynamic forces. As flow is increased from zero through the turbine meter a certain amount of gas is allowed to pass through the rotor unaccounted until a point is reached where the gas imparts enough force to overcome the frictional retarding forces of the rotor bearings. At this point the rotor begins to turn and the frictional forces in the bearing becomes negligible. From here on the aerodynamic forces become the predominate retarding force and control the rotor's speed. The existence of these retarding forces create a difference between the theoretical rotor speed and the actual rotor speed. This difference is accounted for by the calibration constant.

BASIC CONSTRUCTION

The essential elements of the gas turbine meter's construction are shown in Figure 1. As the gas enters the meter it encounters a flow deflector which constricts it into a smaller annular passage. This annular passage is approximately one-third the area of the pipe and serves to increase the velocity of the gas before it passes through the rotor. The resulting increase in velocity gives more driving force to the rotor thereby improving the accuracy at low flow rates.

Parts List

A	Housing
B	Cover Plate
C	Flow Deflector
D	Inner Housing
E	Rotor Hub
F	Bearings
G	Rotor
H	Magnet Housing
J	Coil Housing
K	Cover Plate & Outlet Tube
L	Boss
M	Preamp Housing
N	Preamp
O	Pressure Tap
P	"O" Ring
Q	Swagelok Nut
R	Drain Plug

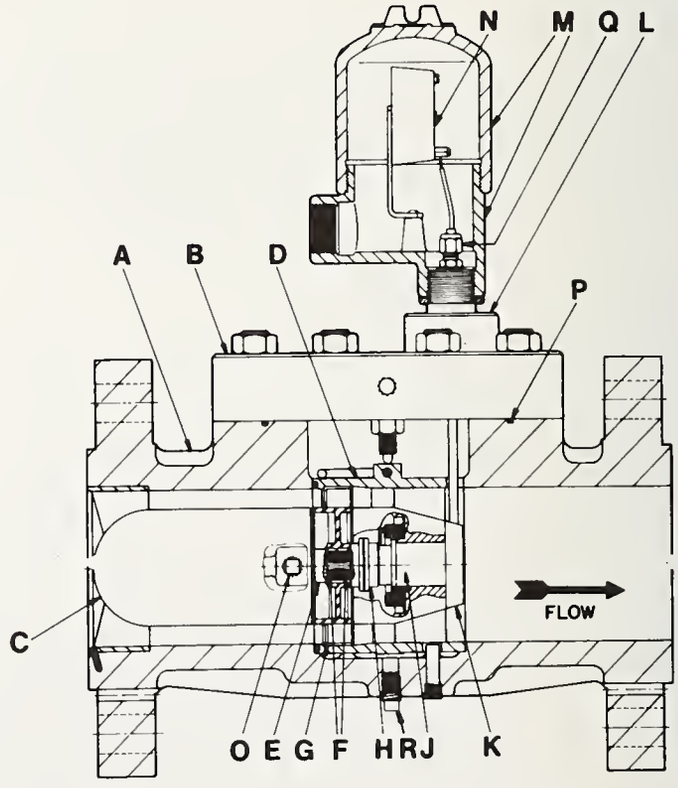

FIG. 1 Cross-sectional View of an Electro-magnetic Gas Turbine Meter.

The flow deflector also serves to lessen the thrust loads on the rotor bearings by shielding the center of the rotor from the flowing stream. As the flow continues it passes through the rotor and exits the meter. The potential accuracy of the meter is to a great extent determined by the design of the rotor. The rotor carries a number of blades set at a predetermined angle. The blades are seldom of aerofoil shape, usually being machined or molded as an integral part of the hub and may be twisted or untwisted. In most meters the rotors are made of a present day plastic with high strength and substantially impact resistant. The rotor is supported on ball bearings which are lubricated by shielding the bearing with the lubricant incorporated at the time of their manufacture, or by furnishing supplemental lubrication through wicking or external supply line. A prime advantage from the standpoint of construction is to have the bearings for the rotor centrally enclosed in an area which is not in the direct line of flow. This helps protect the bearings from contamination in the pipeline. In order to keep the frictional torque low, the bearings are of a small diameter in relation to the meter size; and, since in some meters they are the only part of the meter in running contact, the reliability and life between overhauls are solely dependent on their design.

The method for accurately measuring the rotor speed is as critical as the rotor and bearings. At this stage in the basic construction there are two distinct designs for accomplishing this measurement - mechanical and electromagnetic.

In the mechanical design the rotor is an integral part of a mechanical gear train which relates its rotation to the volume flow rate as displayed on a clock type index on the exterior of the meter housing. The extent to which the mechanical design can accurately measure the speed of the rotor is dependent on the possible gear ratios available in the gear train driving the external index. As a result of this system the mechanical readout meter incurs some retarding forces over and above the basic bearing and aerodynamic forces. Additional forces that must be overcome are gear losses, losses due to eddy currents in the magnetic coupling and any loads imposed by the meter registers or the correcting devices that might be employed. All of these forces have the effect of reducing the turbine meter range at the low flow rates.

In comparison to the mechanical design we have the electromagnetic. The electromagnetic measurement of the rotor speed is accomplished in either of two ways: 1) By placing small permanent magnets within the rotor and electrically counting the passage of these magnets with a pick-up coil. This is called the induction method. 2) By having a magnet housed inside the pick-up coil and the rotor blade tips made from, or contain suitable magnetic materials to stimulate pulses in the coil. This is called the reluctance method. With the electromagnetic design the meter encounters only a small additional retarding force due to breaking of the magnetic

line of force. In addition, with the electromagnetic design there is a high frequency digital output available for control purposes.

As a final point of construction many of the turbine meters are designed so that the inner housing containing the measurement assembly can be removed from the meter without removing the entire meter housing from the pipeline. On the larger size meter this offers a distinct advantage.

PERFORMANCE CHARACTERISTICS

The discussion of performance characteristics of gas turbine meters will be divided into the following sections: rangeability, meter capacity, effects of gas density, field test methods, and piping considerations.

RANGEABILITY

A prime characteristic of the turbine meter is its rangeability. This is defined as the ratio of the maximum meter capacity to the minimum capacity for a stated set of operating conditions and during which the meter retains its specified accuracy.

In comparison to other types of meters, the turbine meter increases its linear rangeability with increases in gas density. This increase in rangeability results from a decreasing of minimum velocity required for linear operation. The minimum velocity required is a function of the gas density, as the density increases the minimum velocity required is allowed to decrease. A relationship for approximating the variation of rangeability with density is developed by examining the minimum kinetic energy necessary to achieve linear meter performance:

$$KE_r^* = 1/2\ \rho_r\ V_r = \text{Const.}$$

As ρ increases V is allowed to decrease maintaining the energy necessary for linear meter performance.

$$V_x = V_r \sqrt{\rho_r / \rho_x}$$

KE_r = Minimum Kinetic Energy Required

ρ_r & ρ_x = Gas Density at Respective Conditions

V_r & V_x = Gas Velocity at Respective Conditions

The rangeability of most present day gas turbine meters at atmospheric pressure is 10 to 1 greater as shown in Table 1.

*Available kinetic energy per unit volume for steady flow of a frictionless, incompressible fluid along a streamline.

TYPICAL TURBINE METER PERFORMANCE

METER SIZE	MAX. FLOW RATE SCFH	RANGE	MIN. FLOW RATE SCFH	APPROX. DIFF. INCHES W.C.
2	4,500	10:1	450	2.0
4	18,000	15:1	1,200	1.2
6	36,000	15:1	2,300	1.5
8	60,000	20:1	3,000	1.8
12	150,000	20:1	7,500	1.7

METER CAPACITY

The capacity of the turbine meter is determined by many controlling factors.

The maximum capacity is determined by such factors as rotor speed, pressure drop, and gas velocity. The limitation of the meter capacity due to rotor speed is a relative matter. The bearings used in the turbine meter have a given life under a given load and at a specific speed. As the speed of the rotor is varied the speed of the bearings varies. Although the turbine meter is capable of turning at three or four times its maximum speed without immediate damage, its life can be substantially reduced if this speed is maintained for prolonged periods.

The pressure drop across the rotor also influences the maximum capacity of the turbine meter. In some applications, such as distribution systems with line pressures running from 7 to 10 inches of water above atmospheric, the pressure loss caused by measurement equipment must be at a minimum.

In most cases the pressure loss called out in the manufacturer's literature is listed for a 0.6 specific gravity.

In order to convert the pressure loss for a different gas the following relationship can be utilized:

$$\Delta P_{max\,(x)} = \Delta P_{max\,(0.6)}$$

$$Q_{max\,(x)} = Q_{max\,(0.6)} \sqrt{\frac{P_{f(x)}}{P_{f\,(.6)}} \cdot \frac{0.6}{G_{(x)}}}$$

$Q_{max\,(0.6)}$ = Maximum Volume Flow Rate of (.6) Gravity Gas

$Q_{max\,(x)}$ = Maximum Volume Flow Rate of (x) Gravity Gas

$P_{f(.6)}$ = Line Pressure of (.6) Gravity Gas

G = Specific Gravity of Gas

A further limiting factor resulting from pressure loss is a variable thrust load on the rotor shaft and bearings. This thrust component is intensified with rising pressure loss resulting from increases in line pressure or specific gravity. Therefore, holding the pressure loss to a minimum increases the life span of the meter.

The gas velocity becomes a controlling factor due to the aerodynamic characteristics of the rotor blades and also the need to avoid the possibility of obtaining sonic velocity within the meter.

The minimum capacity of the turbine meter is limited by meter accuracy. This minimum flow meter accuracy is determined by gas density, bearing friction and the aerodynamic characteristics of the rotor.

The bearings in a turbine meter are selected for their ability to carry a load while introducing a minimum amount of friction. Thus, while increasing the minimum capacity of the turbine meter by reducing friction the maximum is limited by reduced load capacity.

EFFECTS OF DENSITY

The gas density can have three principle effects on the performance of the gas turbine meter. These are:

1) Increase rangeability
2) Vary pressure differential
3) Alter calibration

As previously stated the gas density can increase the rangeability of the turbine meter by increasing the kinetic energy available for driving the rotor.

In gas flow the pressure differential across a restriction increases as the density increases. Hence, the loss through the turbine meter intensifies as the density increases. This intensification can range from 2 inches of water of atmospheric condition to 200 inches of water at 1440 psig.

Finally, as density increases it can cause a shift to occur in the turbine meter proof, normally in the positive direction. The amount of the shift, if it occurs at all, depends upon the design of the meter and seems to be a function of the rotor design and meter size.

INSTALLATION

Since the turbine meter is a velocity type meter the pattern of the velocity upstream of the meter is of basic importance. The

meter is particularly sensitive to any spiraling motion that may result from upstream piping configurations. The American Gas Association sponsored intensive testing to establish standards of construction applicable to proper design for the meter tubes used in orifice metering. The probable effect of piping configurations, pinched valves, etc., to a degree might be estimated as to the probably severity of these non-uniform conditions on turbine meters. The streamline character of the diffusor section ahead of the rotor has a tendency to minimize some of these adverse effects. The net effect, consequently, is dependent somewhat on the particular design employed by the manufacturer. It is consequently impossible to give specific rules for all makes of turbine meter; it is recommended, rather, that the recommendation of the manufacturer be employed in specifying the required piping system.

The rotor of the turbine meter is inherently of light construction and is vulnerable to damage from foreign objects in the gas stream. Depending upon the degree of cleanliness of the gas and the degree of caution warranted to safeguard the mechanism, strainers or filters might be installed upstream of the meter. The rotor and the rotor bearings can also be damaged from momentary high flow rates encountered when the shut-off valve is opened too rapidly. To protect against this condition restricting orifices can be placed downstream of the meter. The objection to a restriction orifice is, of course, that the pressure loss over the restriction can be objectionable when the meter is operating at its rated capacity.

There are two principle piping configurations recommended for turbine meter installations.

The conventional coupling utilizes ten diameters of straight full pipe upstream with straightening vanes. The downstream contains five or more full pipe diameters. Test results have shown that the conventional coupling is suitable for most installations encountered in meter station designs.

The short coupled installation consists of a full size elbow or tee upstream and downsteam. In addition to being a space saver, the short coupled configuration can be designed to provide bypass and test connections. If the short coupled configuration is utilized it is a must that the meter be calibrated in this position, particularly for high pressure service.

FIELD TESTING

There are several methods that can be utilized for field testing a turbine meter. The choice of which one will be determined by operating conditions, location of meter, number of meters involved, preference, experience of personnel, and availability of equipment. In general, the methods available for field calibrating the turbine meter are the same as those used on other high volume gas meters, such as critical flow prover or low pressure provers.

Current field test methods include the spin test and transfer proving.

SPIN TEST

The spin test consists of spinning the rotor of a gas turbine meter to a given speed in a draft-free environment and letting the rotor coast to a stop. The time it takes the rotor to coast to a stop is the spin down time (Fig. 2). The spin test of a gas turbine meter is no more a calibration than a physical inspection of an orifice plate is a calibration of a plate's flow coefficient.

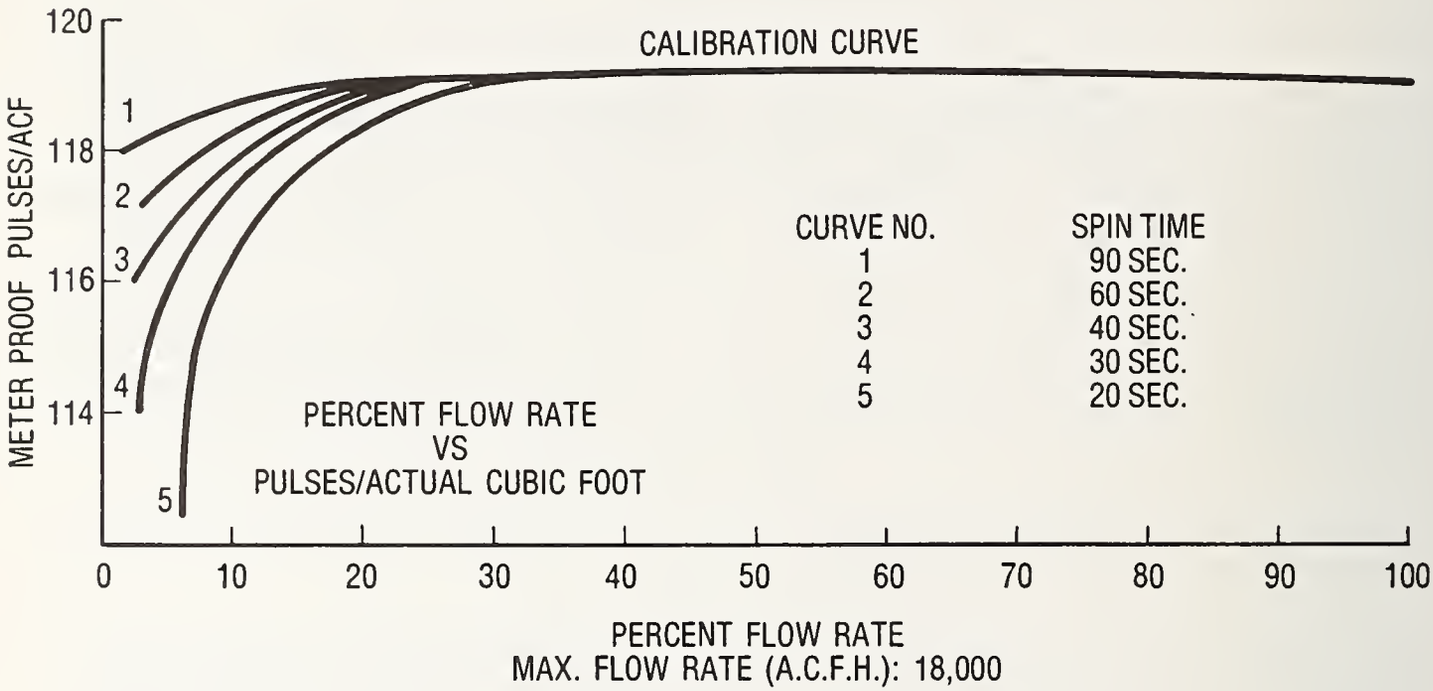

FIG. 2 Changes in proof of 4-inch gas turbine meter due to variations in spin time.

The spin test at best can be used to infer calibration; that is, if under similar conditions,there is no less of spin time then the meter can be expected to have maintained its original proof.

In comparing the spin test to the physical inspection of an orifice plate it can be pointed out that when an orifice plate is found to be dirty or poor measurement conditions exist, the plate is cleaned or replaced, the condition is corrected and the coefficient is then assumed correct because all conditions are met. Likewise, with the turbine meter, if the spin test repeats and there is no physical damage to the meter, then its flow coefficient can be expected to remain unchanged.

TRANSFER PROVING

Periodically it becomes necessary to perform a test in addition to checking the mechanics of the primary devices in order to verify accuracy. In doing this the most desirable method is to compare the device to an accepted and recognized primary standard.

In the United States the primary measurement standard for gas volume is the cubic foot bottle calibrated by the National Bureau of Standards. However, use of the calibrated bottles for production or field testing is highly impractical.

Therefore, it has become necessary to designate more practical methods for these operations and in doing so establish secondary proving standards. These proving methods obtain a statement of accuracy from a primary standard; thus, the original of the transfer prover.

It is of particular importance that the field test be conducted under steady state conditions. That is, the turbine meter is brought up to speed and allowed to run for a period of time and the pressures and temperatures are allowed to stabilize. During a test it is necessary to run a mechanical drive meter for at least two revolutions of the output shaft. This allows the slowest gears in the train to make several revolutions and balance out gearing irregularities.

Transfer proving consists of meter calibration by means of a transfer or master meter. In transfer proving the master meter and test meter are piped in series. A selected volume of gas is simultaneously passed through both meters and their registration is observed. These observations (registration) are then corrected for any temperature and pressure difference between the two meters.

A percentage error is determined for any flowing conditions by installing the master meter in the pipeline with the test meter, or at atmospheric conditions by installing the test meter in series with the master meter and using a portable blower to provide through the two meters.

Such devices as the orifice meter, critical flow provers, rotary meter and turbine meter are used as transfer provers (Fig. 3).

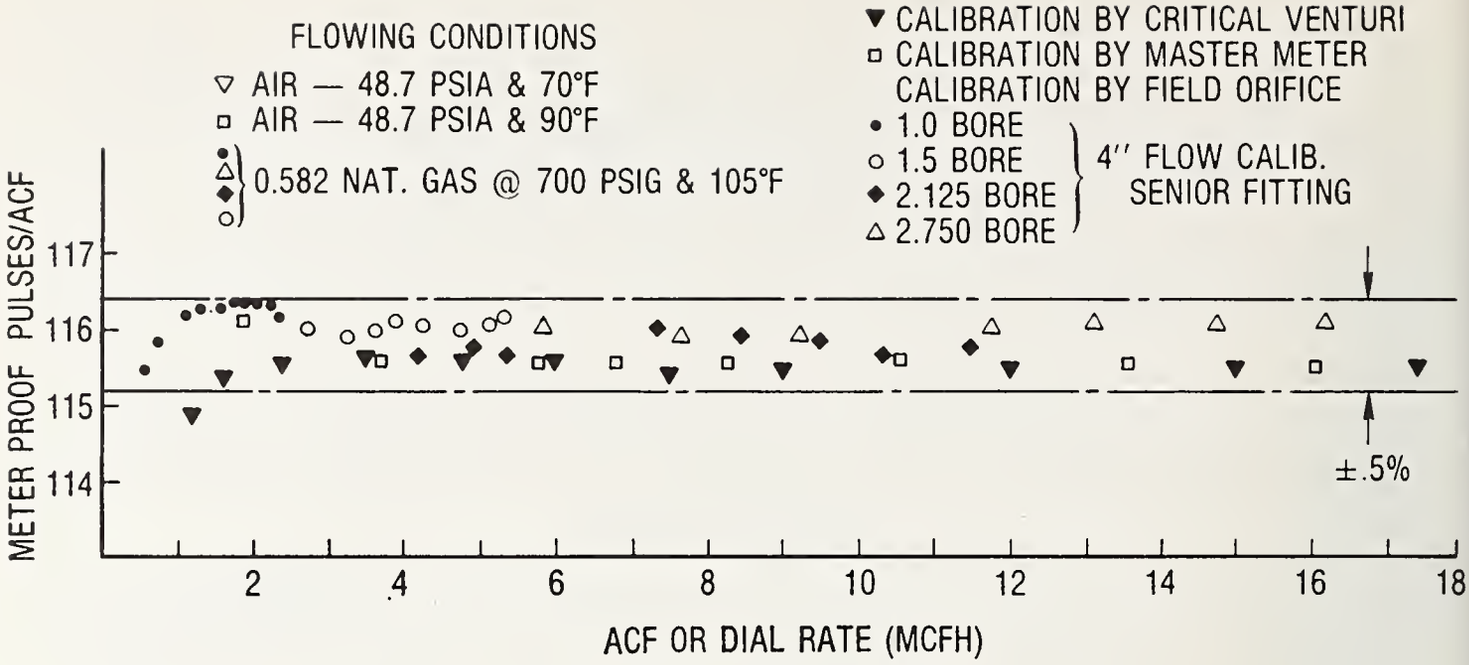

FIG. 3 High pressure orifice field calibration of a 4-inch turbine meter.

These devices obtain their statement of accuracy either by having been calibrated by a bell prover which in itself is a transfer prover calibrated by the cubic foot bottle, or by reference to tolerances as established by previous thruput tests upon which appropriate industry standards are written. Each of these methods establishes a meter's performance to within specified tolerances.

REFERENCES

1. Gebre H. and Smits J. - "A Turbine-Type Gas Flow Meter" Flow Measurement in Closed Conduits Vol. II 1962

2. Miller R.E. - "Evaluation of Turbine Meter Performance" American Gas Association Transmission Conference, 1971.

National Bureau of Standards Special Publication 484, Proceedings of the Symposium on Flow in Open Channels and Closed Conduits held at NBS, Gaithersburg, MD, February 23-25, 1977. (Issued October 1977)

ON A NEW METHOD OF GAS FLOW MEASUREMENT USING CRYOGENIC TECHNIQUES

D. B. Mann and J. A. Brennan

Cryogenics Division
Institute for Basic Standards, National Bureau of Standards
Boulder, Colorado 80302

Direct comparison of ambient temperature gas flow measurements to mass is made possible by a new continuous closed-loop measurements method. The direct comparison is made possible by modification of a proven flow reference system based on mass-time.

The complete gas flow reference system has, as yet, not been demonstrated physically; however, the liquefied gas portion has been continuously proven over a period of six years and is the flow standard for the recently developed cryogenic flowmeter code. Modifications are state-of-the-art additions of heat exchangers and process control. It is believed that the accuracy of the liquid system (less than $\pm$ 0.2%) will be maintained after modification.

If implemented, the method would be extremely valuable in improving and redefining many of the present gas flow measurements and standards. Gas and liquid meter coefficients could be related directly to mass and to each other without the tedious reliance on state equations and critical pressure and temperature measurements. The validity of liquid calibration for gas service could be confirmed on a mass basis. Current codes and recommended practices could be supported and improved with new, more accurate empirical data. The method can be extended to mixtures such as natural gas and would improve the accuracy of these measurements.

It is believed that this modification is a significant and timely improvement within measurement science which could have major impact on custody transfer and energy conservation.

Key words: Cryogenic; flow; gas; liquid; mass flow; measurement.

1. Introduction

A new and more accurate method of measuring gas flow in terms of mass is possible using existing, well developed cryogenic techniques. The method, which could be used to redefine present gas flow measurement codes and standards, is a natural and logical development from codes and standards measurements of cryogenic liquids such as oxygen, nitrogen, argon and hydrogen. The method is closed-looped allowing extended periods of observations at set gas pressures, temperatures and flow rates. Gas pressures above 1000 psi and gas temperatures above ambient temperatures are possible. The method is suitable for air, oxygen, nitrogen, argon, methane and natural gas mixtures of methane, ethane, propane, butanes, and nitrogen, and could be extended to neon, hydrogen, helium and other fluids.

Total uncertainty in mass flow is based on an existing cryogenic flow reference facility having over six years of operational experience. If successfully applied to gas flow measurements, gas flow measurements and standards could be improved by a factor of from five to ten.

Other studies made possible with this new method are:

a) Direct comparison of gas to liquid flow on a mass basis.

b) Intercomparison of gas to water or other fluid flow on a mass basis.

c) Performance of gas flowmeters operating on low temperature gases.

d) Investigation of Reynolds number variations at constant mass flow.

The new method will be described in general terms with several operating modes followed by a detailed description of the existing Cryogenic Flow Facility and modifications necessary to prove the new method.

2. Gas-Mass Flow Reference System

The system is shown in an elementary schematic in Figure 1 and thermodynamically in figure 2. The cyclic process is continuous with only power to the pump and refrigerant to the subcooler as requirements. Liquefied gas subcooled under moderate pressures (0.7 MPa) is fed to the inlet of the pressure pump 1. The pump is of the turbine type to minimize flow pulsations and capable of pressurizing the liquefied gas to above critical pressures ($\sim$ 4 MPa) at 2. This single phase compressed fluid is then fed to the first pass of the counter flow regenerative type heat exchanger where it is heated to ambient temperature or above at 3. An electric heater is installed at this point to stabilize the gas temperatures. The gas meter test section contains all necessary upstream and downstream flow conditioning such as pipe length, flow straighteners, the meter and all other standard meter run equipment. Gas leaving the gas meter test section will be at a lower pressure (depending on the meter type) and at a different temperature (depending on test and ambient temperatures) at 4. The gas

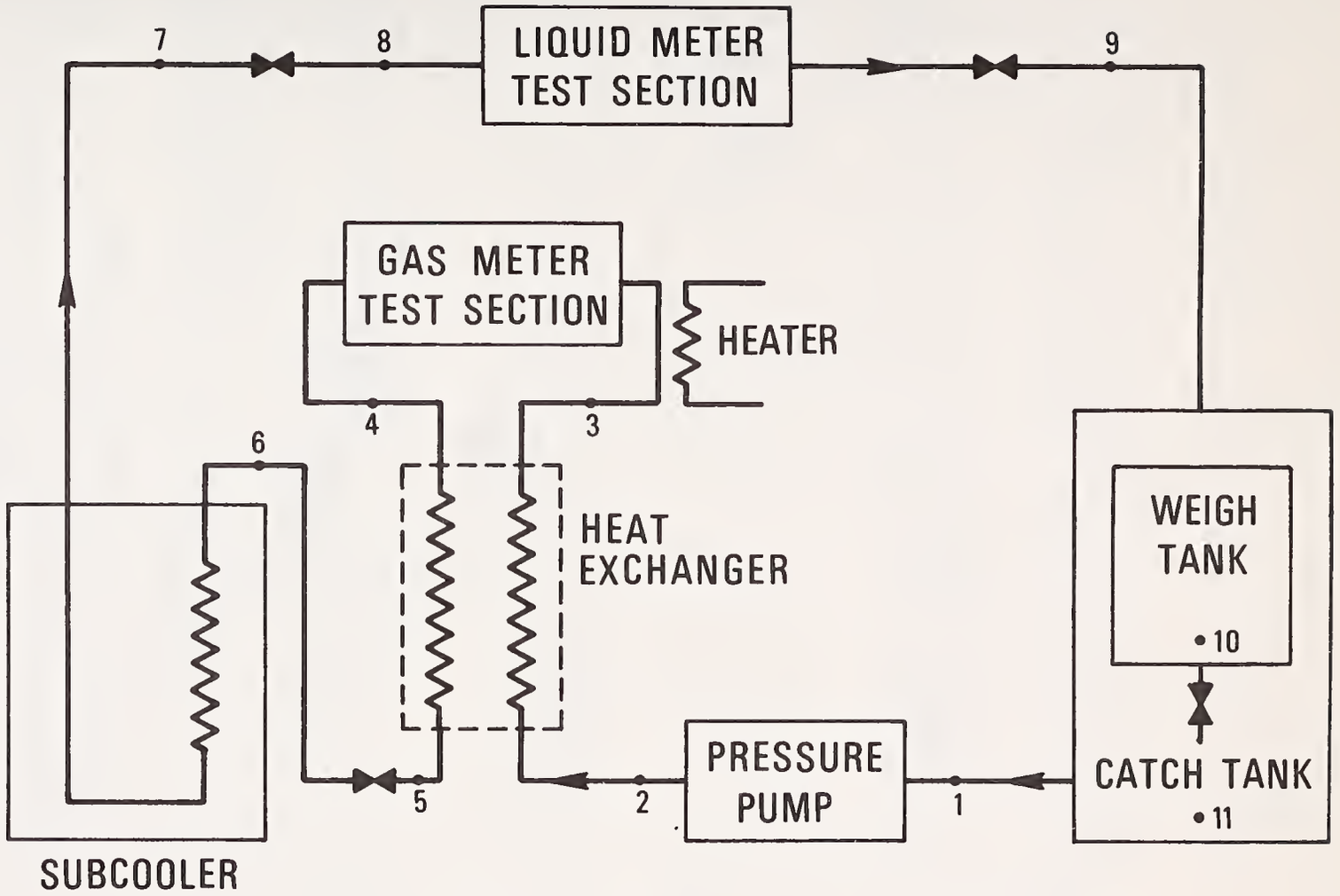

Figure 1. Gas flow measurement system schematic for operation at greater than critical pressures.

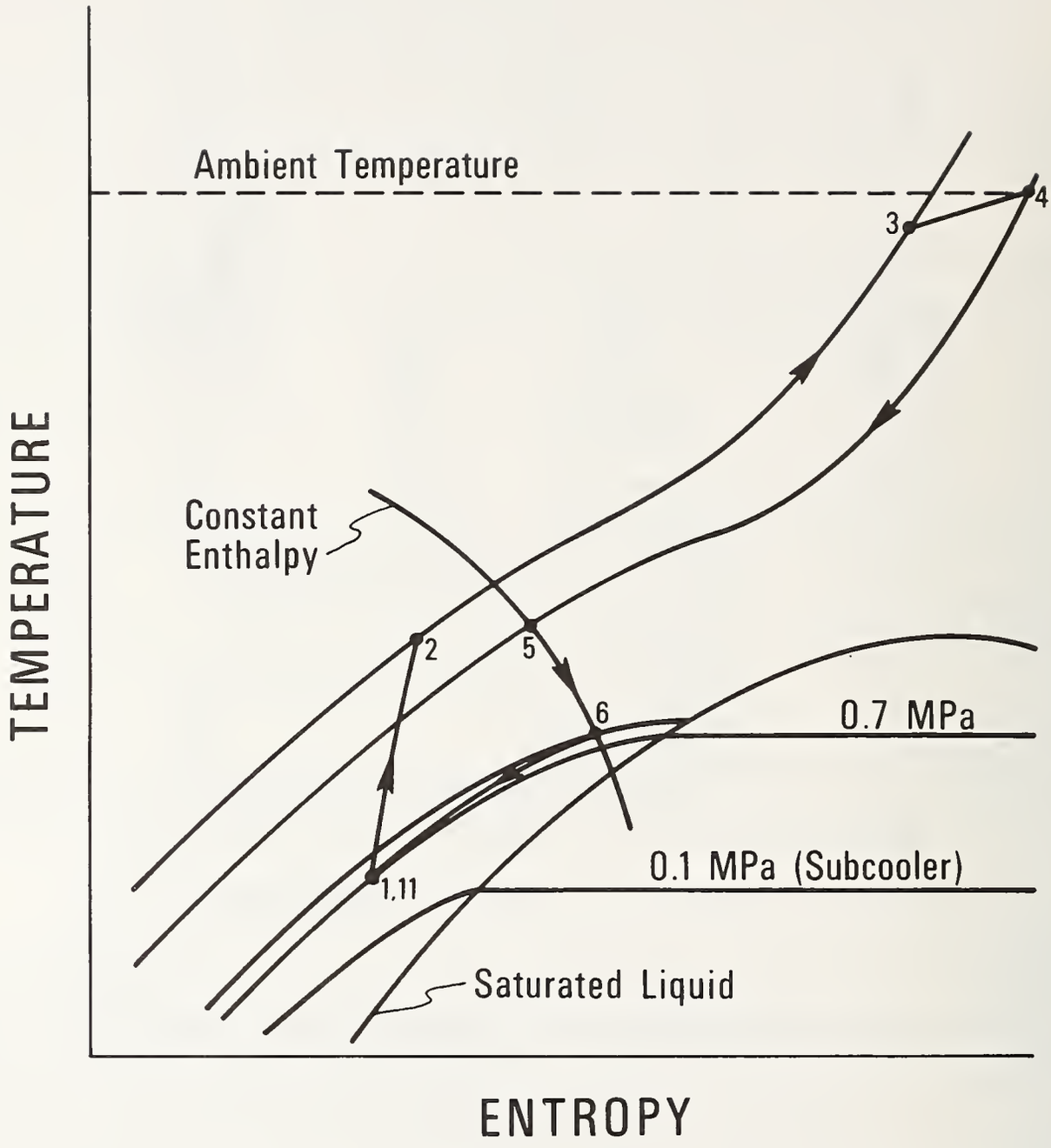

Figure 2. Operation of flow measurements system at above critical pressures.

will then be fed to the second pass of the counter flow heat exchanger where it leaves as a compressed fluid at cryogenic temperatures at 5. The pressure of the fluid is reduced by a simple expansion through an expansion valve to moderate pressures ($\sim$ 0.7 MPa) and fed to the subcooler at 6. The subcooler provides a controlled liquid temperature prior to the liquid meter test section.

The liquid meter test section contains all necessary liquid flow treatment and the cryogenic flowmeter. This meter can be of the same type and design as the gas meter or can be a proven cryogenic meter used as a secondary standard.

After metering, the liquid enters the catch and weigh system which are shown as concentric containers. The weigh tank is supported on a load string and a load cell. Load cell calibration is maintained with standard weights referenced to NBS standards of mass.

At periodic intervals the drain valve in the weigh tank is closed and a quantity of cryogenic fluid is accumulated in the weigh tank 10. The time required to accumulate a given weight of liquid is measured and the mass flow rate calculated. The weigh tank drain valve is then opened and the liquid cryogen is released to the catch tank 11.

Pressures within the catch and weigh tank are maintained above the fluid saturation pressure by inert gas pressurization to maintain subcooling and to eliminate flashing after expansion at point 6. The actual pressure selected will also depend on the pressure ratio available from the pressure pump.

The schematic of figure 1 is the simplest equipment arrangement and will allow operation of gas meters above the critical pressure and with low pressure drop through the gas meter. These conditions can be met with flowmeters with 100 in. water pressure loss such as orifice meters, venturi meters, some turbine meters and most non-intrusive type flowmeters.

For operation at pressures below critical pressure, some additional equipment must be added. Figures 3 and 4 show these modified arrangements.

In figure 3, a low-head high-volume flow circulation pump is used in place of the pressure pump. A boiler and heat source are added to vaporize the liquid prior to heating to ambient temperatures and a condenser is required to reliquefy the gas prior to subcooling. This additional equipment is made necessary because the temperature of condensation of the fluid from the gas meter test section is equal to or less than the boiling point temperature of the fluid discharged from the circulation pump. A high capacity blower could be installed at the outlet of the gas meter test section to increase the pressure and therefore the saturation temperature, but this would defeat one of the advantages of the method which is low power requirements and simplicity.

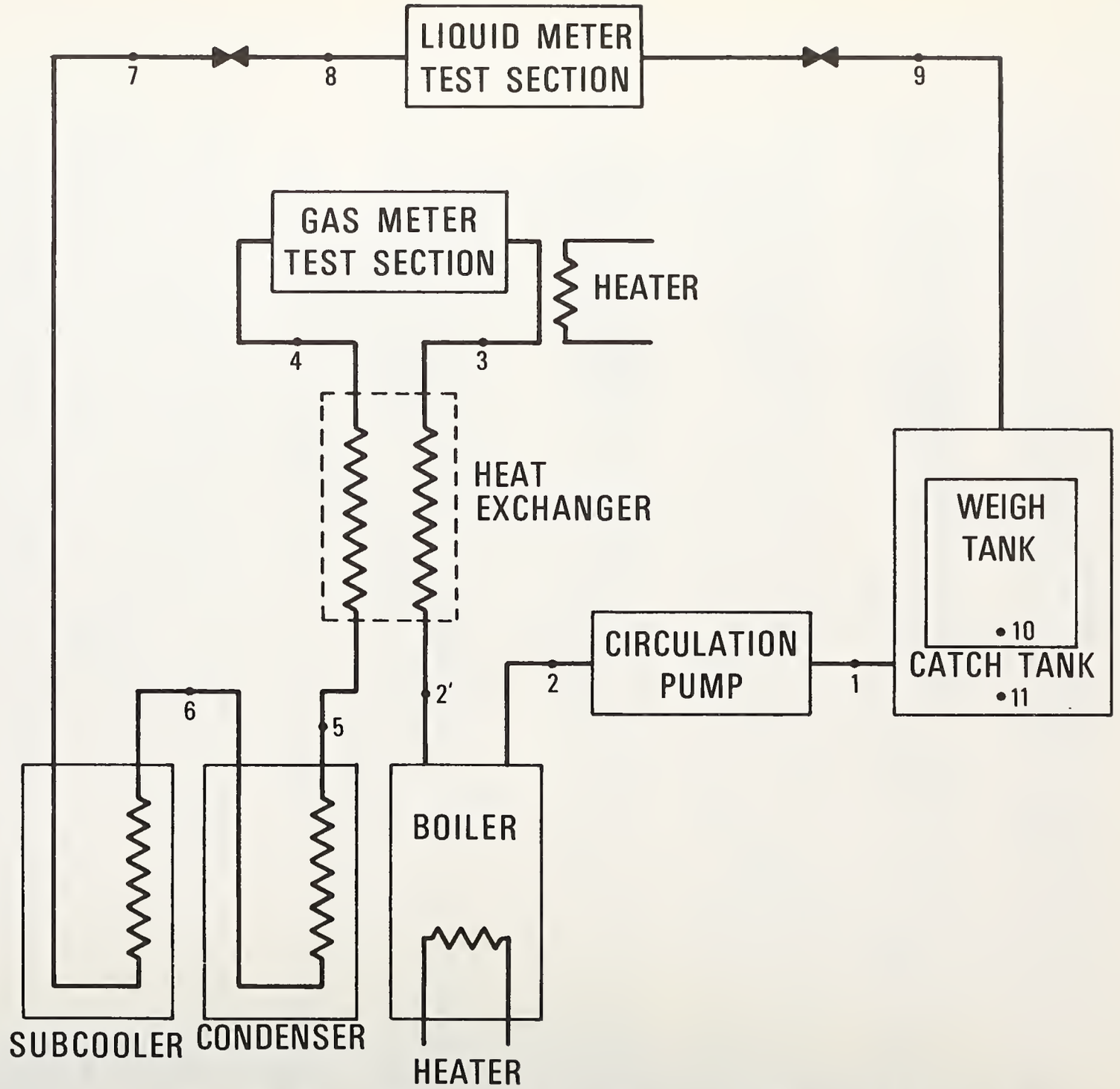

Figure 3. Gas flow measurements system schematic for operation at less than critical pressures.

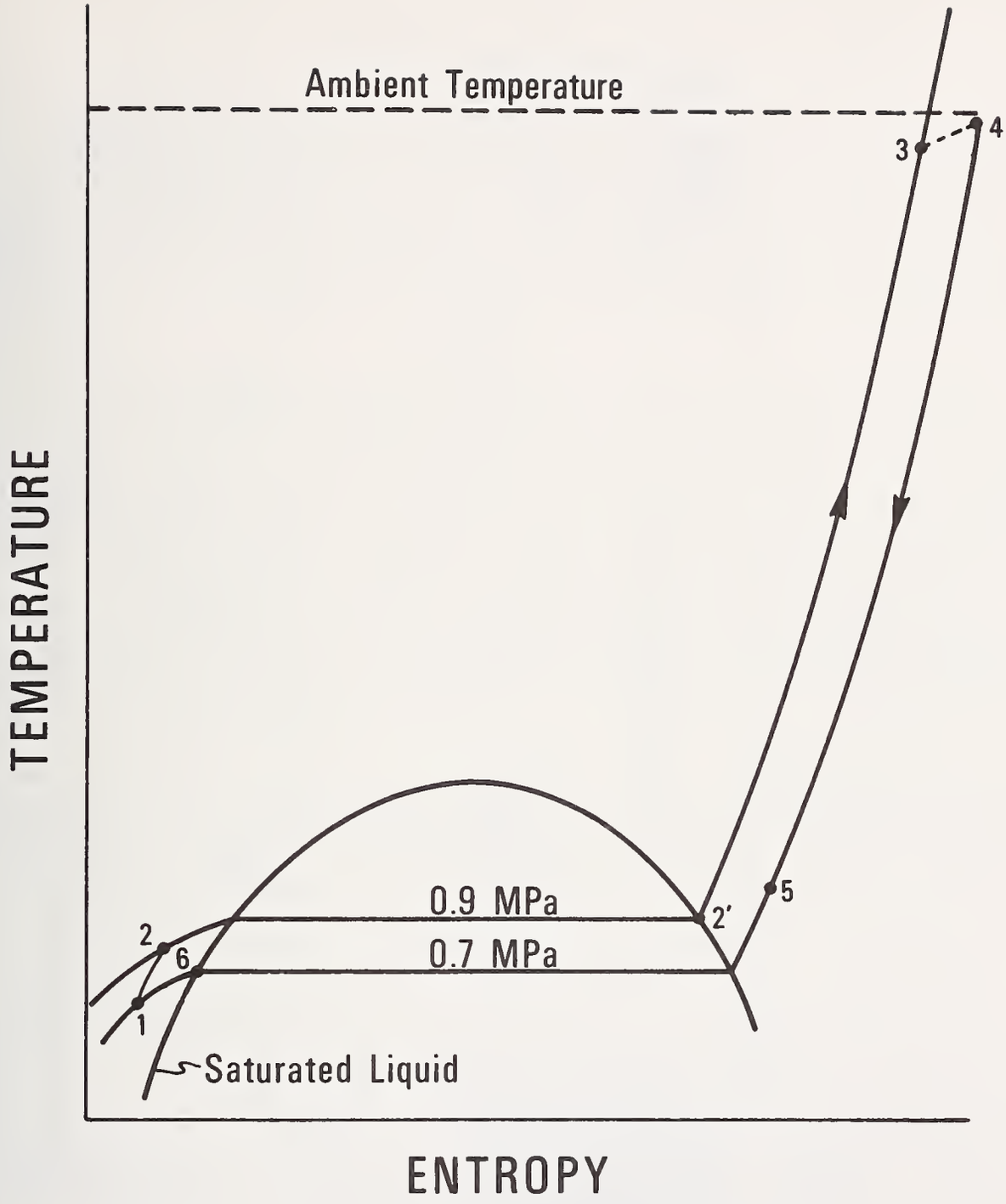

Figure 4. Operation of flow measurements system at less than critical pressures.

For the special case of large meter pressure losses, such as choked nozzle flow, a combination of the two cycles would be necessary. The pump must be a pressure pump, as in figure 1, to provide the necessary high pressure at the gas meter inlet; however, a condenser and heater will be necessary as in figure 3, to provide external heating of the high pressure stream and condensation of the low pressure stream. No pressure reducing valve would be required.

3. Liquid Mass Flow Reference System

In the gas mass flow measurement system just described, the actual mass flow measurement takes place while the gas is in its liquid phase. For commercial industrial gases such as oxygen, nitrogen, argon, methane and natural gas mixtures, the liquid phase is in the cryogenic temperature region. This is a fortunate situation because we can establish the potential limiting accuracy of the gas mass flow system by referring to an existing cryogenic liquid mass flow measurement system.

The cryogenic flow measurement reference system was established in 1968 in a joint government-industry program on cryogenic flowmetering. Under that program, NBS joined with the Compressed Gas Association and state regulatory agencies to establish a flow reference system, to evaluate existing flowmeters used in commercial service, to evaluate new measurement methods and to establish a national model cryogenic flow measurements code through the National Conference on Weights and Measures. A schematic of the facility constructed under that program is shown in figure 5. The similarity to the previously described gas mass system is obvious. The basic operating principles of the two systems will be very similar and the basis for the estimate of uncertainty in mass flow measurement should be identical.

The cryogenic flow measurement program was completed in 1976 with the acceptance of a permanent cryogenic flow measurement code by the Conference on Weights and Measures. The description of the facility and program are well documented in the literature (see references). The most pertinent reference to this discussion of the gas mass flow system is the work of Dean, et al. (1971). This report is a summary of an 18-month study to determine the accuracy of the flow reference system, "At this time the uncertainty of the measurement of totalized mass flow is estimated to be $\pm$0.18%. This figure includes an uncertainty of $\pm$0.12% for known sources of systematic errors plus an uncertainty of $\pm$0.06% for random error. The estimated uncertainty due to the random error is three times the standard deviation calculated from 23 applications of the calibrated masses over a period of three months." The report provides a complete description and data on how this accuracy statement was determined and, in addition, provides a description of the process control which allows the reference system to be kept under statistical control.

Over sixty flowmeters based on five different generic types were included in the evaluation program. Transfer standards were developed for field certification of commercial meters as well as being used in inter-laboratory

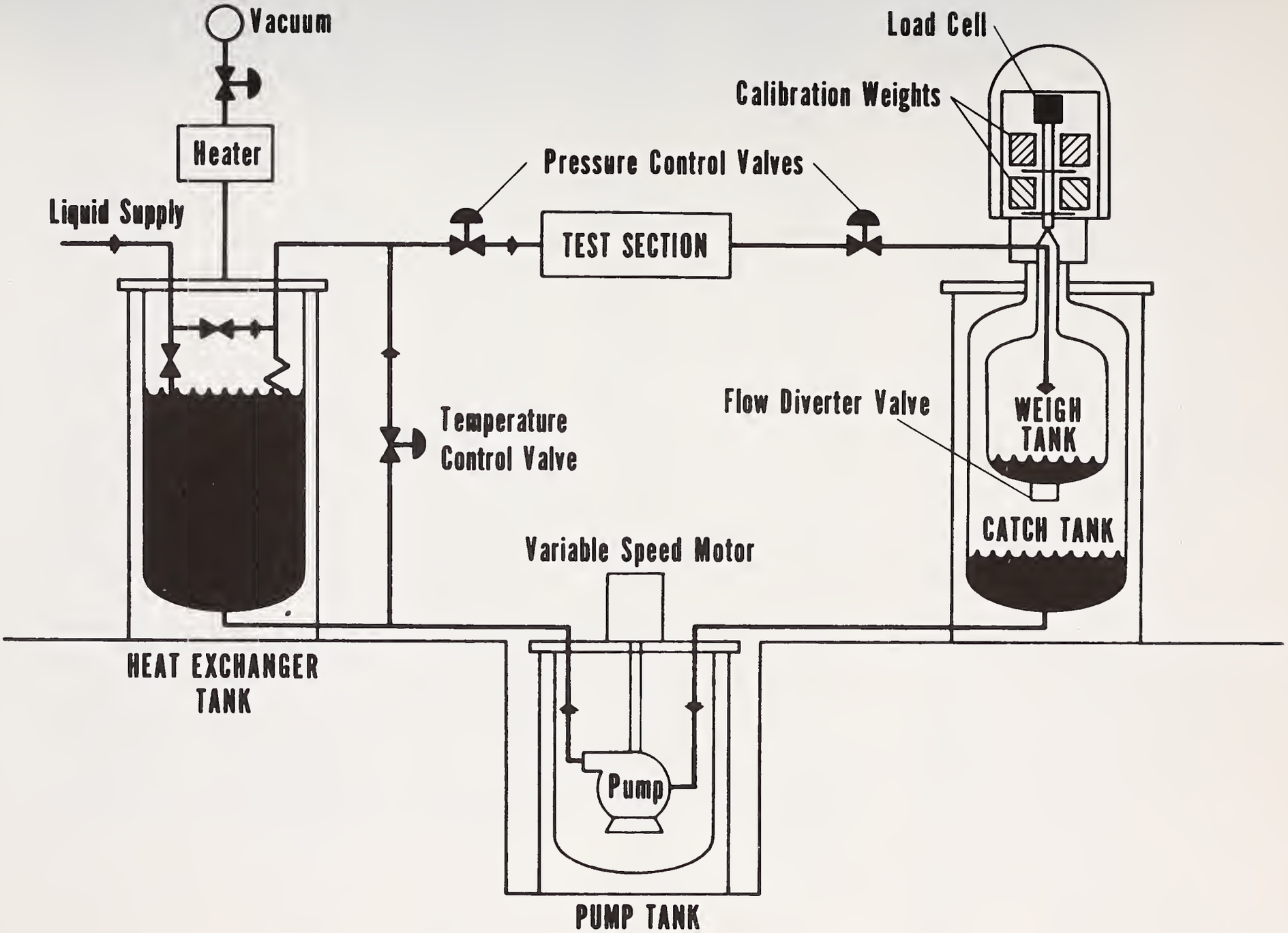

Figure 5. Cryogenic flow measurements reference facility schematic.

comparisons which provided additional validity to the accuracy statement. Confidence in the ability of this system to provide a mass flow measurement was established in almost 4000 hours of operational experience. The report itself was a provisional accuracy statement and during the six years of operation, more precise measures of systematic error have been made which should allow the uncertainty statement to be improved significantly. However, if the accuracy of this system could be maintained while adding a regenerative heat exchanger and gas flowmeter test section, the improvement in measurements of a gas mass flow reference would be significant. Present estimates of the latter are between plus or minus one and two percent, therefore, an improvement could be realized of between five and ten over present methods.

The process fluid used in the facility of figure 5 is nitrogen although argon has also been used successfully. The system itself could be adapted to other cryogenic fluids such as air, oxygen, hydrogen, methane, ethane, propane and liquefied natural gas.

4. Applications

The potential for such a system, if the total uncertainty can be maintained at $\pm$0.2% or less, is impressive and would allow the following studies:

- Redefinition of gas flowmeter factors relative to mass flow directly and continuously. No intermediate calculations or approximations are required.
- Gas flow pressures and temperatures could be controlled independently of the mass flow reference and would allow wide variations in experimental conditions. An added benefit, particularly in the case of nitrogen as the process fluid, would be that the Reynolds number can be increased by a factor of 4 or 5 by reducing the temperature and therefore the viscosity of the gas.
- Gas flowmeter performance could be compared directly with existing codes and standards which are based on volumetric or water calibration predictive calculations. Errors in predictive correlations could be identified and corrected.
- The working hypothesis that water calibration may be transferred directly to gas flow can be tested to an accuracy not previously possible. Errors in this hypothesis can be identified and corrected.
- The effects of upstream and downstream meter flow conditioning (straight runs and/or flow straighteners) can be redefined with gas flow with greater accuracy than previously available.
- Evaluations of potential gas flow transfer standards on a long term mass flow basis. This would include such devices as the choked nozzle and other new devices such as the laser Doppler velocimeter or ultrasonic meters, the success of which would make gas flow or water flow reference systems increasingly unnecessary.

- o An evaluation of velocity effects on direct reading densitometers. This work would be in support of the development of a natural gas energy meter.
- o As a precision reference system, test sections could be used to investigate the development of boundary layer and turbulence, and the effects of these phenomena on gas meter size.

Component design would be heavily influenced by the selection of the fluids to be used. If multiple fluids were to be tested, then components must be designed for the most severe conditions. This would particularly be the case in the selection of pressure pump and regenerative heat exchanger. Table 1 is the result of calculations made on two different applications. The methane/LNG system was based on a flow rate of 16.4 cubic meters per second (50 MMCFD). It is believed that a system of this size would meet many of the natural gas industry requirements for flow calibration in meter studies.

The nitrogen example is basically a modification of the existing cryogenic flow facility to demonstrate the feasibility of the gas flow measurement reference system. The gas flow rate of 1.2 cubic meters per second (2750 SCFM) would be of such a capacity as to allow testing of existing codes and practices and at the same time would not require a large investment in heat exchange or pressure pump equipment.

Other applications are also possible and a reduction in size of the facility for small flow should also be feasible. This suggests that a small portable gas measurement mass flow standard could be constructed and used routinely for field calibration and certification of meters.

5. Summary

Direct comparison of ambient temperature gas flow measurements to mass is made possible by a new continuous closed loop measurement method. The direct comparison is made possible by modification of a proven flow reference system based on mass time. The anticipated total uncertainty in mass flow of gas at operating conditions should not exceed $\pm 0.2\%$. This is an improvement of a factor of 5 to 10 over existing gas flow standards.

At a time when natural resources and raw materials are decreasing in quantity and increasing in cost, it is believed that new measurement methods, such as proposed, are essential to provide the necessary measure of accuracy and precision for establishing product quantity and value.

Table 1. Examples of application of gas mass system.

	Methane/LNG	Nitrogen
Gas Side		
Flow rate (m^3/s @ 14.73 psia to 60°F)	16.4	1.2
Pressure (MPa)	5.5	3.4
Temperature (K)	289-300	289-300
Pipe diameter (cm)	20-25	10-15
Heat Exchanger		
Heat transfer load (MJ/s)	9.27	0.52
Liquid Side		
Weigh tank capacity (m^3)	3.8	0.379
Catch tank capacity (m^3)	5.7	0.433
Pressure (MPa)	0.83	0.69
Temperature (K)	100.0	80.0
Pipe diameter (cm)	10.0	7.6
Pressure Pump		
Flow rate (m^3/s)	0.027	0.0019
Pressure ratio	6.6	5.1
Power Requirement (kJ/s)	395.0	16.04

REFERENCES

ISA, Ad Hoc Committee Report of Flow Measurements, Instrument Society of America, Pittsburgh, PA (1967).

Mann, D. B., Cryogenic flowmetering research at NBS, Cryogenics 11, 179 (1971).

J. W. Dean, J. A. Brennan and D. B. Mann, Cryogenic flow research facility of the National Bureau of Standards, Advances in Cryogenic Engineering 14, (Plenum Press, New York, 1969).

D. B. Mann, J. W. Dean, J. A. Brennan, and C. H. Kneebone, Cryogenic Flow Research Facility, (Unpublished NBS report to sponsor, Jan. 1970).

J. W. Dean, J. A. Brennan, D. B. Mann and C. H. Kneebone, Cryogenic flow research facility provisional accuracy statement, Nat. Bur. Stand. (U.S.) Tech. Note 606 (1971).

J. A. Brennan, J. W. Dean, D. B. Mann and C. H. Kneebone, An evaluation of cryogenic positive displacement volumetric flowmeters, Nat. Bur. Stand. (U.S.) Tech. Note 605 (1971).

J. A. Brennan, R. W. Stokes, D. B. Mann and C. H. Kneebone, An evaluation of several cryogenic turbine flowmeters, Nat. Bur. Stand. (U.S.) Tech. Note 624 (1972).

J. A. Brennan, R. W. Stokes, C. H. Kneebone and D. B. Mann, An evaluation of selected angular momentum, vortex shedding and orifice cryogenic flowmeters, Nat. Bur. Stand. (U.S.) Tech. Note 650 (1974).

National Bureau of Standards, Specifications, tolerances, and other technical requirements for commercial weighing and measuring devices, Nat. Bur. Stand. (U.S.) Handbook 44, 4th Ed. w/revisions (1972).

National Bureau of Standards Special Publication 484, Proceedings of the Symposium on Flow in Open Channels and Closed Conduits held at NBS, Gaithersburg, MD, February 23-25, 1977. (Issued October 1977)

AN ANATOMY OF THE INTERNATIONAL STANDARDS PRODUCING SYSTEM - FLOW MEASUREMENT

L. K. Irwin

Mechanics Division
National Bureau of Standards
Washington, D. C. 20234

The several international organizations that, collectively, form the "system" to promulgate and maintain the documents and publications that are explicit or de facto international standards are described. Included in this review are the International Organization for Standardization, International Electrotechnical Commission, International Organization of Legal Metrology, European Economic Community, European Committee for Standardization, World Metrological Organization, and International Bureau of Weights and Measures. Also, elements of organizations, that are not international by design but that generate standards used internationally, are reviewed. This second group includes the American Society of Mechanical Engineers, American Society for Testing and Materials, American Petroleum Institute, and British Standards Institution.

Summary information is given for the current activities of most of these organizations and the scope and technical output of selected technical committees as they affect standards for flow measurement or the quantitative determination of volume or mass of fluids. The efforts on coordination and apparent overlap of the work are noted. Some discussion of the existing and needed relationships between physical measurement standards and international documentary standards is given.

Key Words: Closed conduit flow; flow measurement; international standards; open channel flow; petroleum product standards.

1. Introduction

Flow measurement is usually a means to an end; to determine the quantity of material passing a point. This determination results from sets of measurements of parameters such as length, time, temperature, mass, pressure, volume, density, viscosity, and others. Thus, the complexities of the standardizing documents and of the procedures for using them are often greater than corresponding standards for other quantities. The problems of understanding and using standards are compounded when they are international standards since translations do not accommodate many of the idiomatic differences in language country-to-country and industry-to-industry.

In this country, technical managers, engineers, and purchase agents have problems when they attempt to utilize standards in their operations or to respond to contractual requirements that include standards. These arise from several causes including (a) the corruption of the meanings of "standard," (b) the multiplicity in the form and structure of standards, (c) the lack of ready access to all the required documents, particularly when there is interdependence between the documents, and (d) the absence of nationwide quality control for standards.

Except for brief comments on the meanings, form and structure, and quality control for standards, this paper will discuss a limited aspect of "ready access" to the international standards relating to fluid flow measurements.

Readers of the English-language standardization and standards periodicals have been exposed to numerous editorials and feature articles on the 'what', 'why', and 'how' for standards, on rationales to support the several viewpoints of the editors, and on definitions for standards and standardization. An extensive two-part series [1,2][1] is given in the February and March 1977 issues of ASTM[2] Standardization News. A related, intellectual discussion by Verman and Visvesvaraya [3] is given in the first issue.

The following discussions will accept Webster's Dictionary for

> standard, n- that which is established by authority, custom or general consent, as a model or example; criterion; test,

and will not attempt to establish a new, or correct, or incorrupt meaning. The study is concerned primarily with documentary standards, either explicitly entitled or de facto.

The form and structure of standards are beyond the scope of this paper except to call attention to the great variety in which users can expect to find the desired information. For example, compare the one-page ISO 5024-1976 (See Appendix 2, Table 2) with ASME PTC 3.3-1969 (See Appendix 2, Table 7). In one page, the former provides the standard reference conditions for temperature and pressure as the basis for comparing quantities measured under other conditions and the latter includes most of ASTM D 1071-55 for information on how to test gas provers and a variety of flow meters along with more than fifty pages of other material. The procedures in D 1071-55 are applicable to many non-fuel gases. But, how can all potential users of this flow measurement standard know of the multiple applications for these documents?

The proper exercise of quality control for documentary standards is an elusive goal and deserves more than the passing notice given here. Agreement on proof of "quality" is not general and, sometimes, not attempted. Some attributes of quality control would include completeness, specific scopes, demonstrable uncertainty statements for the necessary physical measurements and documented calculating algorithms. Others may be equally important.

---

[1] Figures in brackets indicate the literature references at the end of this paper.

[2] Complete titles of all organizational acronyms used are given in Appendix 1.

Those several organizations and institutions, that promulgate, maintain or influence international standards, their documentary technical outputs, and the users of these outputs are treated as a system. The elements of this system are described as they are perceived to affect flow measurement or the quantitative determination of volume or mass of fluids. The material presented and discussed may increase "ready access" to available standards by some of the many users.

2. International Organizations that Promulgate Flow Measurement Standards

Four international organizations have been identified that clearly are producing or issuing documentary standards important to the measurement of fluid flows. All details concerning the structure of these organizations are necessarily lacking due either to the continuing evolution of their programs of work or to the author's failure to locate the required documents.

2.1 International Organization for Standardization

The ISO is a voluntary organization[3] comprised of the national standards bodies of more than 80 countries, with 63 member bodies and 18 correspondent members at the end of December 1975. The technical work is carried out through more than 150 Technical Committees (TC) which operate through about 500 subcommittees (SC) and about 1000 working groups (WG). The secretariats for each technical committee, subcommittees or working groups are distributed among the member countries that choose to participate actively in the work (P-members) and other member bodies are kept informed if registered as observers (O-members).

Typically, an international standard evolves from a draft proposal (DP) of a technical committee P-member or the results of an assignment to a working group through several stages of comment and revision. When agreement is reached within the technical committee, the document is sent to the Central Secretariat for registration as a draft International Standard (DIS) and circulated to all member bodies for voting. The DIS is sent to the ISO Council for final acceptance if 75 percent of the votes cast are favorable. With Council acceptance, the document becomes an International Standard subject to review every five years or earlier when technical changes are agreed to by the members.

The ISO work is available through the approximately 3000 International Standards currently in use as published or as national standards. The annual Memento [5] and publications catalog [6] provide connecting data on available standards and the responsible participating organizations. Two technical committees, TC 30 and TC 113, have primary assignments to produce flow measurement standards, and technical committees TC 28 and TC 144 are probable sources for additional standards important to flow measurement. If the titles and scopes reflect the areas of their activity properly, twelve or more other technical committees are users of or contributors to flow standards.

Technical Committee 30, Measurement of Fluid Flow in Closed Conduits, has as its scope:

> Standardization of rules and methods for the measurement of fluid flow in closed conduits including:
> (1) Terminology and definitions,
> (2) rules for inspection, installation, operation,

[3] International organizations involved in standardization are described briefly in BSI PD4845 [4].

(3) construction of instruments and equipment required,
(4) conditions under which measurements are to be made,
(5) rules for collection, evaluation, and interpretation of measurement data, including errors.

At the beginning of 1977, seven subcommittees and four working groups were organized as shown in Figure 1 to conduct this program of work. The TC has produced seven International Standards and one Technical Report; it has ten documents advanced to DIS or DP status (See Appendix 2, Table 1); and fourteen other items of work in various stages of development and comment. The wide-spread interest in this program of work is reflected in the fifteen ISO and IEC liaisons and the five external liaisons with intergovernmental and international technical organizations.

The scope for Technical Committee 113, Measurement of Liquid Flow in Open Channels is as follows:

> Standardization of rules and methods relating to different techniques for the measurement of liquid flow with particular reference to sediment transport in open channels including:
> (1) terminology and definitions,
> (2) rules for inspection, installation, operation,
> (3) instruments and equipment required,
> (4) conditions under which measurements are to be made,
> (5) rules for collection, evaluation, analysis and interpretation of measurement data including errors.

In 1976, there were six working groups to carry out the program of work as shown in Figure 2. By the end of 1976, the TC had produced twelve International Standards, had eleven documents advanced to DIS status (See Appendix 2, Table 2) and had eighteen other working projects including revisions to three standards. There are five ISO and IEC liaisons and seven external organization liaisons.

Technical Committee 144, Air Distribution and Air Diffusion, is relatively new and had produced one standard on vocabulary by the end of 1976. The scope reads as follows:

> Standardization in the field of air distribution and air diffusion including performance testing both in the laboratory and on site, dimensional characteristics and terminology.
>
> Specifically excluded will be fans (TC 117 refers), heat exchangers (TC 116 refers), filters (TC 142 refers), cooling and air conditioning devices (TC 68 refers), but when these elements are an integral part of the air terminal device or high velocity/pressure assembly or low velocity/pressure assembly, or valve or damper, they are included.

This TC is organized with four subcommittees that have five projects in their program of work. These are (1) aerodynamic testing and rating of air terminal units, (2) aerodynamic testing and rating of constant and variable flow rate assemblies, (2c) aerodynamic testing of single duct units, dampers and valves,

(3a) technique of airflow measurements in conduit, and (4) acoustic testing and rating. There are seven liaisons with other ISO committees and two external liaisons. The membership consisted of eleven participating and sixteen observer bodies at the end of 1976.

The other significant and direct ISO involvement in fluid flow measurements is Technical Committee 28, Petroleum Products with a scope as follows:

> Standardization of methods of measurement, sampling and test, nomenclature, terminology and specifications for petroleum and petroleum products.

In 1976, there were five subcommittees and agreement to form a sixth as shown in Figure 3.

The work of this TC is an example of flow measurement being the means to an end, an aid in determining the quantity of material. A review of the titles of thirty-eight standards produced through 1976 does not show the words "flow" or "flowmeter" in any title. However, ten of these documents (See Appendix 2, Table 3) deal with fluid properties or with procedures for sampling and obtaining one or more fluid property of the product. The high level of activity in this TC is reflected in the twenty-six documents designated DIS, seventeen designated DP and thirty other projects or studies underway at the beginning of 1977. The titles of fifteen of the DIS or DP documents (See Appendix 2, Table 3) indicate the continued output of standards important to flow measurement technology. The terms[4] that occur in the titles of documents listed in Table 3 include viscosity, kinematic viscosity, temperature measurement, density, relative density, volumetric measurement, standard reference conditions, positive displacement meter, turbine meter, measurement of quantities, calculation of quantities, tank calibration, container calibration, and measurement of level.

An incomplete list of titles for other ISO technical committees that have or appear to have good reasons to use flow measurement standards or to participate in their formulation are given below. Excerpts from the scope of a few committees are given as quotations.

TC 11	Boilers and pressure vessels "Methods of inspection and testing such boilers and vessels."
TC 64	Methods of testing fuel-using equipment "Standardization of methods of testing for performance and efficiency of fuel-using equipment."
TC 67	Materials and equipment for petroleum and natural gas industries.
TC 70	Internal combustion engines.
TC 86	Refrigeration.
TC 112	Vacuum technology.
TC 115	Pumps "Standardization of methods for testing pumps on test stands, in their final installations, on models ..."
TC 116	Space heating appliances.
TC 117	Industrial fans.
TC 131	Fluid power systems and components "Standardization in the field of fluid power systems and components, comprising terminology, ... and testing and inspection methods."

[4] In some cases, the full length term has been editorially shortened.

TC 161 Control and Safety Devices for Heat Generating Systems.

It is unclear how those technical committees for equipment powered by internal combustion engines (TC's 22, 23, 110, and 127) serve their flow measurement needs since no direct liaisons are indicated with TC 30 or TC 28.

2.2 International Electrotechnical Commission

The IEC is affiliated with the International Organization for Standardization and has an organizational system and operating rules that are similar, in most respects, to ISO. The Commission consists of more than 40 National Committees, each representing one country, which are required to be as representative as possible of all electrical interests in the country concerned. The IEC produces Recommendations and Reports that are approved if not more than 20 percent of the member committees cast negative votes. It operates with more than 70 technical committees and 100 subcommittees [7] and has produced nearly 600 approved Recommendations and Reports [8,9].

Although the chief outputs of IEC deal with electrotechnical matters, some areas of the work impinge directly on flow measurement technology -- particularly the work of TC's 4, 5, and 65. TC 4 Hydraulic Turbines and TC 5 Steam Turbines have produced four recommendations (See Appendix 2, Table 4) for acceptance tests of hydraulic or steam turbines. These documents contain substantial amounts of technical information to assist with making flow measurements suitable for these applications. Subcommittee B of TC 65 Industrial Process Measurement and Control is responsible for standardization of pneumatic control devices including performance testing and has a program of work that includes the use of flow measurements. These three IEC technical committees have liaisons with ISO/TC 30.

2.3 International Organization for Legal Metrology

The OIML is an intergovernmental (treaty) organization set up to resolve the technical and administrative problems of legal metrology. It is particularly concerned with the compatibility of standards of measurement and the legislative and Government regulations which may affect such standards of measurement. See ref. 10 for a concise review of the USA involvement. As of 1976, there were 43 member states. Standards are developed through technical committees called Pilot Secretariats (PS) and subcommittees called Reporting Secretariats (RS). The responsibility for administering the Pilot or Reporting Secretariats is assigned to member states on a request basis. There are 26 active PS's and about 160 RS's that have produced more than 30 International Recommendations through 1976. The programs of work of four PS's have produced documents or have active projects relating to flow measurement. Two of these, PS 5 Measures of Liquid Volumes and PS 6 Measures of Gas Volumes, are directly involved in flow measurement standards. Organizational charts are shown in Figures 4 and 5 and their published standards or drafts in progress are given in Appendix 2, Table 5. Certain of the International Recommendations produced or being developed by PS 9 Measure of Densities, and PS 30 Physio-Chemical Measures are important for flow measurement, especially, those dealing with humidity, liquid and gas densities, viscosity and other properties of fluids.

Also, PS 7 Measure of Masses, PS 11 Measure of Pressure, PS 12 Measure of Temperatures and of Calorific Energy, and PS 24 Equipment for Legal Metrology

Bureaus have produced standards in their respective areas that are important to flow measurement laboratories and, in certain cases, to field measurements.

The liaisons of PS 5 and PS 6 are mostly with other OIML technical committees or with ISO/TC 28 and TC 30. There is one joint OIML/PS 5/RS 13 - ISO/TC 28/SC 5 task group that is trying to deal with the problem of eliminating gas during the measurement of volumes of flowing hydrocarbons.

2.4 European Economic Community

This organization, often called the 'Common Market', has a continuing interest in standardization for the primary purpose of removing technical barriers to trade among its nine member states. The EEC standards are issued as directives under Article 100 of the Treaty of Rome, 1957. The texts of proposed and adopted directives are published in the EEC Official Journal. In principle, the EEC work on standardization avoids activities which duplicate those of other organizations. From a review of a recent article [11] in Trade and Industry, it is unclear how closely they adhere to this principle. Eleven items in this article that implied flow measurement were tabulated (See Appendix 2, Table 6). These show that the EEC has a substantial involvement in promulgating flow measurement standards. Information obtained by the author to date is insufficient to comment on the extent to which these Directives are transformations of documents from other organizations or represent direct outputs of technical committees of EEC.

3. Other International Organizations

3.1 European Committee for Standardization (CEN)

The CEN is a regional, voluntary standardization organization comprising the national standards bodies of 15 EEC and European Free Trade Association countries. The technical work is conducted by working groups assigned to the member bodies with proposals coming from CEN members or international organizations. Priority is given to subjects proposed by European intergovernmental organizations. By early 1976, the approximately 60 working groups of CEN had produced 23 European Standards (EN) and had 59 draft standards in the final stages of preparation [12]. The amount of flow measurement technology that will be incorporated into the European Standards is unclear at this time. The subjects or titles of some of the working groups include metrological equipment, gas and oil pipelines, fuels, central heating boilers, gas governors, industrial valves and drainage equipment. These suggest flow measurement standards from CEN in the future.

3.2 World Meteorological Organization (WMO)

The WMO is an agency of the United Nations of which 140 states and territories are members. Its concerns include the total water resources of the world and especially the meteorological cycles through which water is transported in varying amounts over this planet. From this interest, WMO adopts "Technical Regulations" and "Guides" for use by member organizations about how to obtain useful data on precipitation, water levels, stream flow, stored water and other hydrological elements required to assess the quality and quantity of water in the world. The WMO produces and distributes numerous publications [13] for systems and instruments on data acquisition, including practices, procedures, and specifications important to water and air flow measurement.

3.3 International Bureau of Weights and Measures

The BIPM is the international metrological laboratory operated by the International Committee of Weights and Measures. This laboratory provides the means for national measurement standards to be compared with internationally agreed standards. With proper attention to measurement transfer chains from national standards to field measurements, the international documentary standards that depend upon measurements of derived quantities such as flow, viscosity, pressure, etc., will be compatible with each other and consistent within the interdependent sets of standards.

4. National Organizations Whose Documents Sometimes Serve as International Flow Measurement Standards

The transformation of national standards into international standards to effect a specific exchange of goods or services is probably as old as the existence of recognizable standards. Some special cases of national standards serving as international standards deserve comment.

4.1 The American Society of Mechanical Engineers and the American Petroleum Institute

There are at least two American organizations that have produced extensive technical information and published documents which have served as de facto standards. The American Society of Mechanical Engineers produces and maintains the Boiler and Pressure Vessel Codes and the companion Performance Test Codes (formerly, Power Test Codes), known worldwide, without "standard" occurring in either the titles or descriptive information about these documents. Several of the ASME Performance Test Codes (PTC) contain straightforward prescriptions about the measuring devices and the methods for the flow measurements performed during acceptance tests of power plant equipment. A partial list of these codes is given in Appendix 2, Table 7. When abridged flow measurement procedures are cited in these codes, there are numerous references to the book popularly known as "Fluid Meters" [14] and its supplement on applications [15]. Also, PTC documents make use of ASTM standards and, occasionally, make reference to the AGA Report No. 3 [16] (also, published as API Publication 2530) for gas flow measurement technology.

The other American source of volumetric flow measurement standards is the American Petroleum Institute whose measurement publications [17] have been used worldwide for quantifying the amounts of petroleum products. These publications will deal with volume and mass measuring systems, meter proving, measurement procedures in the field, properties of fluids, calculating procedures and other information. This manual has many of the attributes of a de facto international standard, i.e., has international acceptance and use. In fact, the activities of ISO/TC 28 reported above show that a significant amount of the measurement technology generated by API is being transferred to International Standards. Pena and Resnick [18] reported on this trend earlier.

4.2 American Society for Testing and Materials

The largest single source of standards in the United States is the American Society for Testing and Materials (ASTM) which has as the central element of

its scope "the development of standards on characteristics and performance of materials, products, systems, and services; and the promotion of related knowledge." At least four of its more than 140 technical committees have produced or have work underway on methods of flow measurement, on specifications for flow measuring devices or on measurements of properties of fluids. These committees include:

D-2 on Petroleum Products and Lubricants,
D-3 on Gaseous Fuels,
D-19 on Water, and
D-22 on Methods of Sampling and Analysis of Atmospheres.

Particular ASTM standards on flow measurement can become used internationally through reference or inclusion in other documents such as the ASME Performance Test Codes or the API Measurement Manual. To date most of the ASTM fluid flow standards (see Appendix 2, Table 8) have dealt with water in open channels or gases in closed conduits.

4.3 British Standards Institution

The recognized body [19] in the United Kingdom for the preparation and promulgation of national standards is the British Standards Institution (BSI). This organization also represents the United Kingdom in a wide variety of international standardizing activities. The international character of certain British Standards (BS) results, in part, from the use of BS documents by that economic and cultural association of nations often referred to as the British Commonwealth and to past political connections with these and other national entities. Complete sets of British Standards are maintained in 89 countries. There are five or more locations with complete BS collections in Australia, Canada, India, Malaysia, New Zealand, Nigeria, South Africa and the United States of America. Documents that deal directly with flow measurement include:

BS 1042: Methods for the measurement of fluid flow in pipes (three parts),
BS 3680: Methods of measurement of liquid flow in open channels (thirteen parts), and
BS 4161: Gas meters (six parts).

5. Discussion

The upsurge in numbers and variety of international standards has been reflected by the increasing pressures on several components of the standardization system. Until recently, the chief stimulus for international standardization has been the self (private) interest of groups of people and organizations with common technological information and goals. Now, we observe significant efforts to serve the public interest in standardization through intergovernmental organizations. As one result, there are indications of competition to produce and promulgate standards among the institutions representing the private interest and the public interest. Also, philosophical distinctions between standards and regulations [20] and bases for voluntary versus mandatory standards [1,3] are receiving attention. Additionally, the perceived present or future shortages of economically important fluids including water and liquid and gaseous hydrocarbons have caused increased activity to develop acceptable, uniform procedures

for quantifying and exchanging these commodities.

These pressures to produce more standards also lead to attempts to coordinat the work. For flow measurement, coordination is usually accomplished by liaisons between the several technical groups that produce and use the standards and through the reviews of documents that are recommended for adoption as standards. The author's observations indicate that many liaisons are not very effective except when the representative has high competence in the technical area and is a capable negotiator. Often, the liaison representative's most useful function is as a reporter. A noteworthy example of apparently effective coordination is described by Smoot [21] for hydrologic measurements. Coordination through review of documents tends to concentrate on minimizing damage rather than increasing use fulness. Documents that do not contradict accepted practices or preempt assignments of responsibility often get perfunctory study by reviewers outside of the originating committee. Other factors that contribute to limited usefulness of reviews are that significant changes or expansions of a proposed standard will almost certainly entail delay in adoption. Also, reviewing is not widely regarded as creative activity. Within the present pluralist social-economic-technical system, the mechanisms for coordinating the development of flow measurement standards probably will continue to be weak.

Reviews of the existing international standards for flow measurement and those that incorporate flow measurements do not show significant overlaps in technical content. However, examination of the programs of work [22] of several ISO and OIML committees giving the titles of draft documents and the projects being studied suggests widespread overlaps of interest and concern for standardization of flow measurement. The clearest overlaps of interest in new standards are ISO/TC 28 with TC 30 and ISO/TC 28 and TC 30 with OIML PS 5 and PS 6. In the absence of strong managerial and coordination mechanisms, these potential overlaps are logical extensions of the organizations (see Figures 1, 3, 4, and 5) and the scopes of these committees. It is unclear whether the technical content of the emerging flow measurement standards from different committees will be duplicative or contradictory or both. Administrative overlaps appear inevitable. The present flow measurement sections of IEC standards (see Table 4) are being duplicated piecemeal by new standards with inconsistencies probable unless close liaisons are maintained. The technical areas of several CEN working groups are likely to utilize flow measurement procedures that will use or overlap with activities of ISO and OIML committees.

Readers of the present measurement methods in international standards will find statements and phrases such as

". . . instruments that cannot be calibrated on site shall carry valid calibration certificates of an official institution.",
". . . scales shall be checked using certified weights . . .",
". . . shall be straight and remain vertical during use.", and
". . . water flow by collection in a tank for a measured time and weighing is an accurate absolute method."

We recognize that skilled operators with appropriate technical competences have and continue to use such qualitative information to make measurements to obtain useful and quantitative data for making decisions. However, the imprecision of these statements provides little guidance for organizations, operating at different locations or times, to establish efficient measurement

chains for assuring comparability of their results. Also, these statements are nearly useless for resolving differences in results when a standard method is used at two or more locations or times to evaluate the performance of an item of equipment or to ascertain the quantity of a shipment of material measured at locations remote to each other. Most Technical Committee working groups lack the capability to include the necessary guidelines to assure the integrity of all measurements used to implement specific standards. Also, it is seldom within the scopes of their assignments to provide the means for assuring the consistency of equivalent measurements across political or regional boundaries.

At this time, the use of physical measurement standards referenced to national metrological institutions that compare national standards with BIPM is the only recognized system that operates to establish consistent and acceptable measurements internationally. When this system can be coupled with appropriate statistical tools for testing the quality of the measurements obtained to implement each flow measurement standard, the entire system of measurements and data will have the potential for being consistent and comparable. The motivation for the separate technical committees and working groups to add criteria for ascertaining the appropriateness of the measurements probably will have to come from the parent institutions.

6. Conclusions

The international standards producing system has completed, started, or has under consideration, a wide variety of projects for flow standards. Two organizations, ISO and OIML, are clearly the leaders for producing and promulgating additional flow measurement and related standards. Some organizations that have produced flow standards with international status including IEC, API, and ASME do not appear to have significantly new work on flow measurement standards underway outside of the ISO and OIML committees.

The need for coordination to avoid duplicate work and contradictions among the several flow measurement standardizing committees is clear but the mechanisms for effective coordination are not evident.

Many existing flow measurement standards are flawed if their purpose is to assure comparability and consistency of data acquired by competent but different organizations at different times or locations. These standards are unclear about relationships with nationally maintained physical measurement standards or how users of the standards can demonstrate the appropriateness of their measurements and data to overcome this deficiency.

7. References

[1] The What and Why of Standards, Part I, *ASTM Standardization News*, Feb. 1977, pp. 24-27.

[2] The People, Process, and Principles of Standards Development, Part II, *ASTM Standardization News*, March 1977, pp. 21-25, 60.

[3] Verman, Lal C. and Visvesvaraya, H. C., A systems approach to standardization, *ASTM Standardization News*, Feb. 1977, pp. 12-23.

[4] Short Guide to International Organizations Concerned with Standards, BSI; Its Activities and Organization PD4845, *British Standards Institution*, London, March 1977.

[5] ISO Memento 1976, *International Organization for Standardization,* Geneva.

[6] ISO Catalogue 1976, *International Organization for Standardization,* Geneva.

[7] IEC Handbook, 1975, *International Electrotechnical Commission,* Geneva.

[8] Catalogue of IEC Publications 1976, *International Electrotechnical Commission,* Geneva.

[9] IEC Report on Activities for 1974, *International Electrotechnical Commission,* Geneva.

[10] United States Membership in the International Organization of Legal Metrology (OIML), *NBS LC 1059,* May 1975.

[11] Eliminating Technical Barriers to Trade Within the EEC, *Trade and Industry,* pp. 228-230, April 23, 1976.

[12] Standards and Legislation in the European Economic Community, *BSI News,* pp. 14-16, February 1976.

[13] Catalogue of Publications, Meteorology and Related Fields Such as Hydrology, Marine Sciences and Human Environment, *World Meteorological Organization,* Geneva, April 1975.

[14] Fluid Meters - Their Theory and Application, Sixth Ed., Howard S. Bean, ed., *American Society of Mechanical Engineers,* New York, 1971.

[15] Fluid Meters, Part II, Application of Fluid Meters - Especially Differential Pressure Type, *Report of ASME Research Committee on Fluid Meters, American Society of Mechanical Engineers,* New York, 1972.

[16] Orifice Metering of Natural Gas, *Gas Measurement Committee Report No. 3,* revised 1969, American Gas Association, Washington.

[17] Manual of Petroleum Measurement Standards, *American Petroleum Institute,* Washington (publication of major additions and revisions in 1977 and 1978).

[18] Pena, A. A. and Resnick, I., ANSI/ISO codes and standards for hydrocarbon measurements, *Talk at the 49th International School of Hydrocarbon Measurements,* Norman, Okla., 1974.

[19] British Standards Yearbook 1977, *British Standards Institution,* London, 1976.

[20] Ailleret, Pierre, The importance and probable evolution of standardization, *ASTM Standardization News,* Feb. 1977, pp. 8-11 (orig. pub. in *Revue Générale de l'Electricitré,* Sept. 1975).

[21] Smoot, George F., Standardization of hydrologic measurements, *Proc. International Seminar on Organization and Operation of Hydrological Services,* Ottawa, Canada, July 15-16, 1976.

[22] Private communications of technical committee secretariats and U. S. Technical Advisory Groups for ISO technical committees.

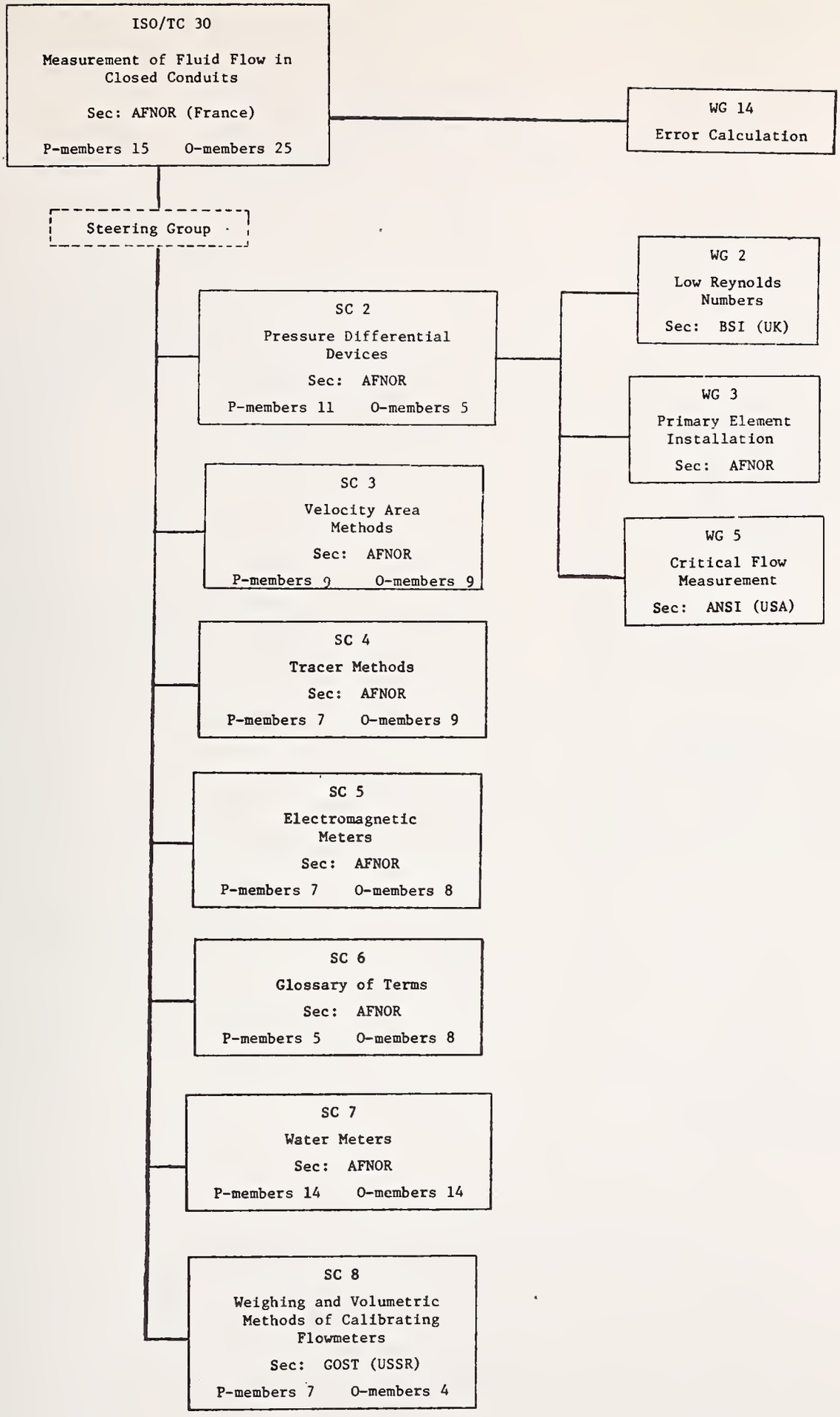

Figure 1. ISO/TC 30 Measurement of Flow in Closed Conduits

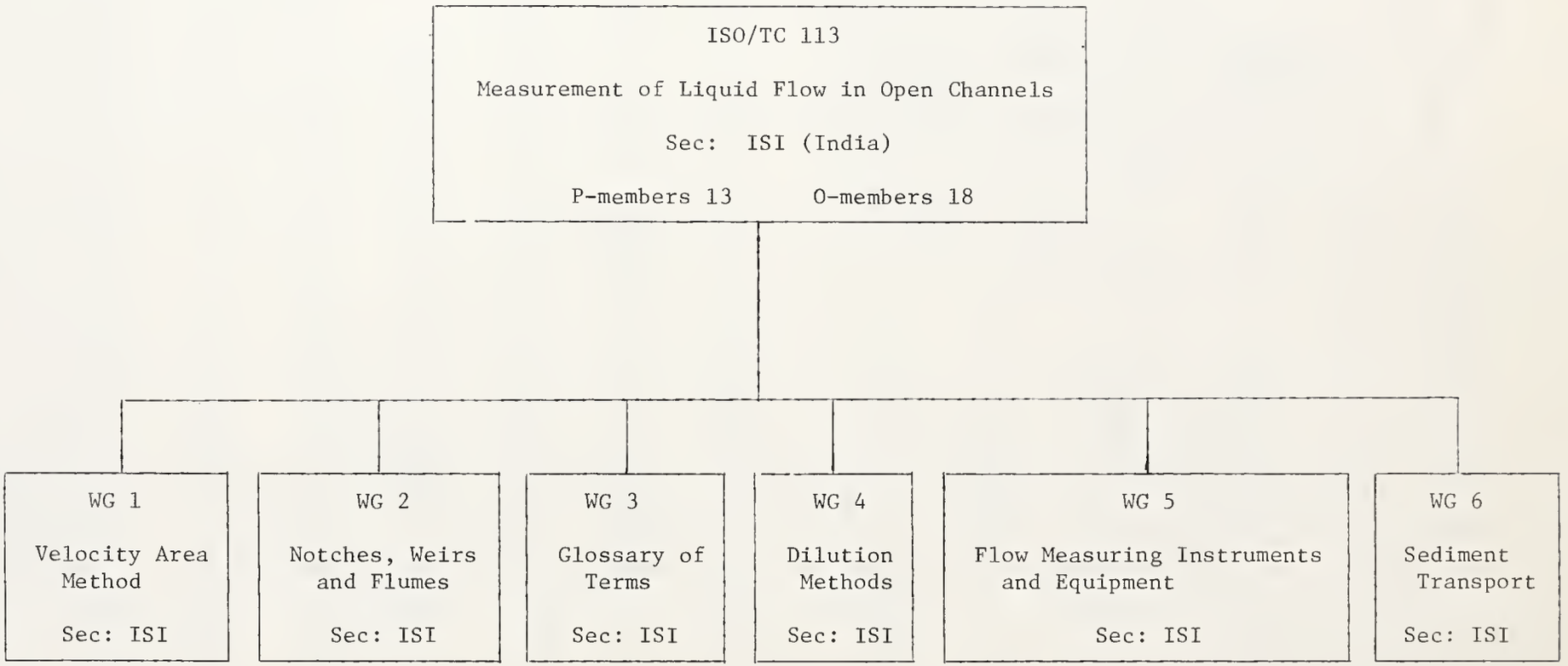

Figure 2. ISO/TC 113 Measurement of Liquid Flow in Open Channels

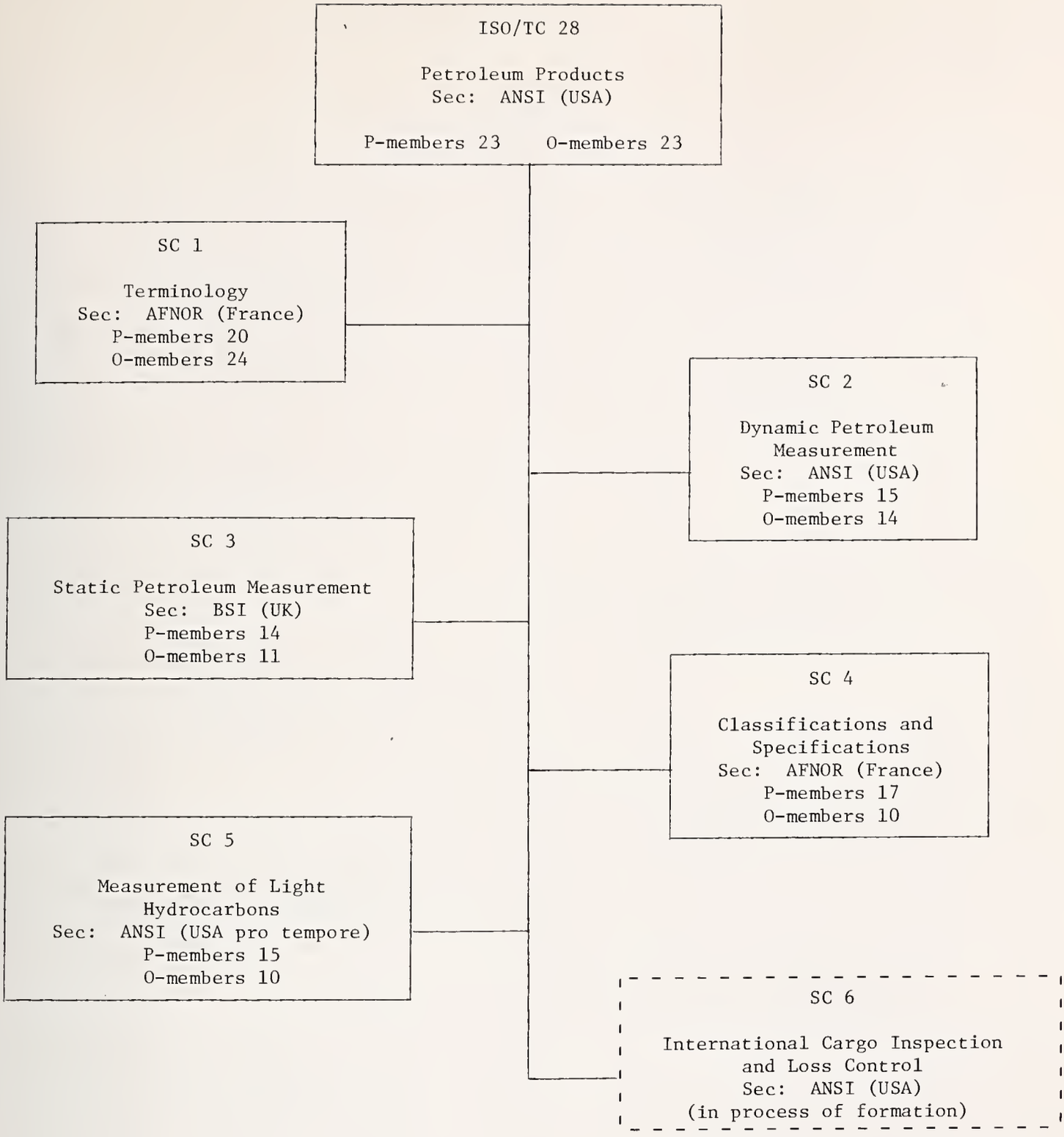

Figure 3. ISO/TC 28 Petroleum Products

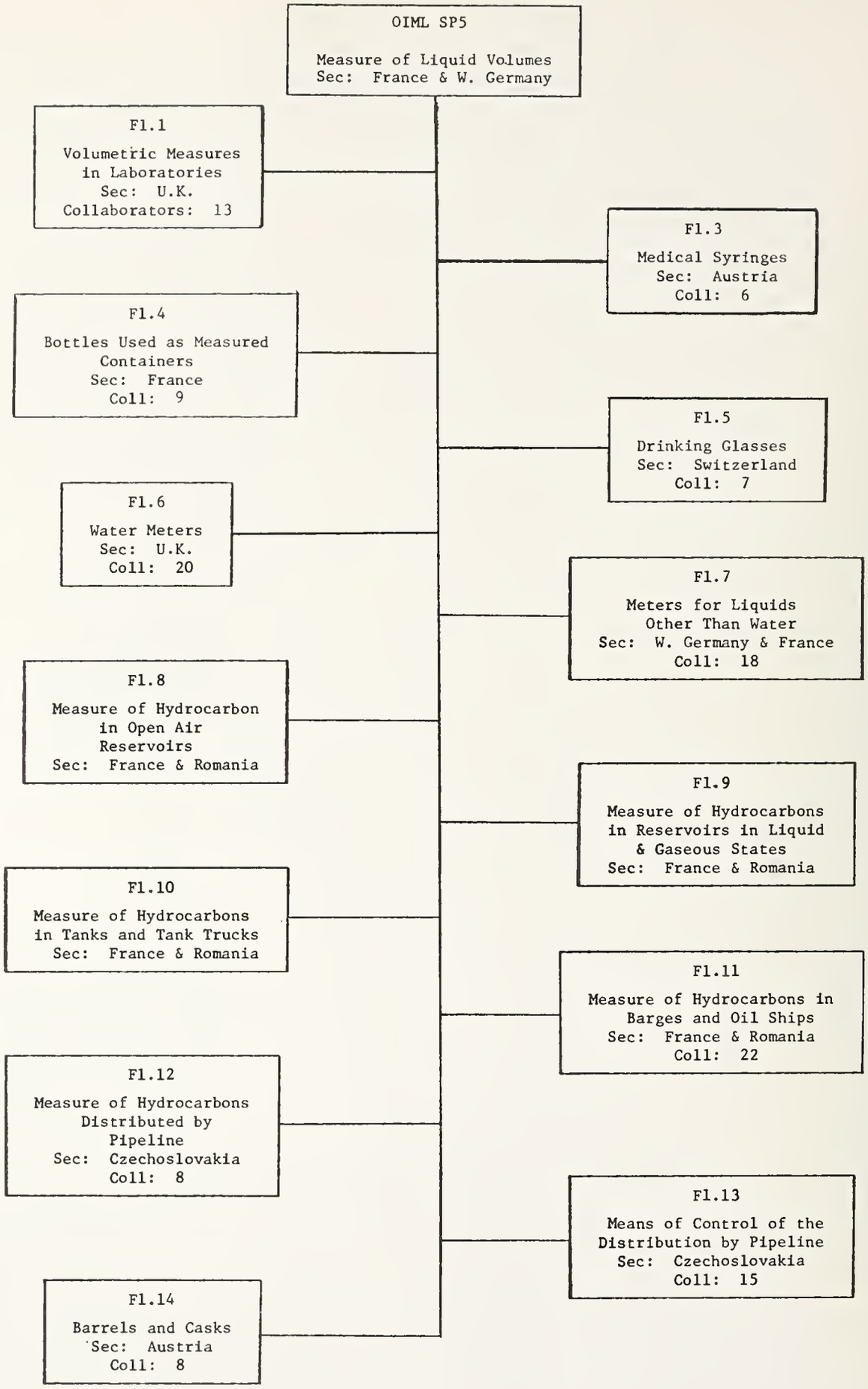

Figure 4. OIML PS5 Measure of Liquid Volumes.

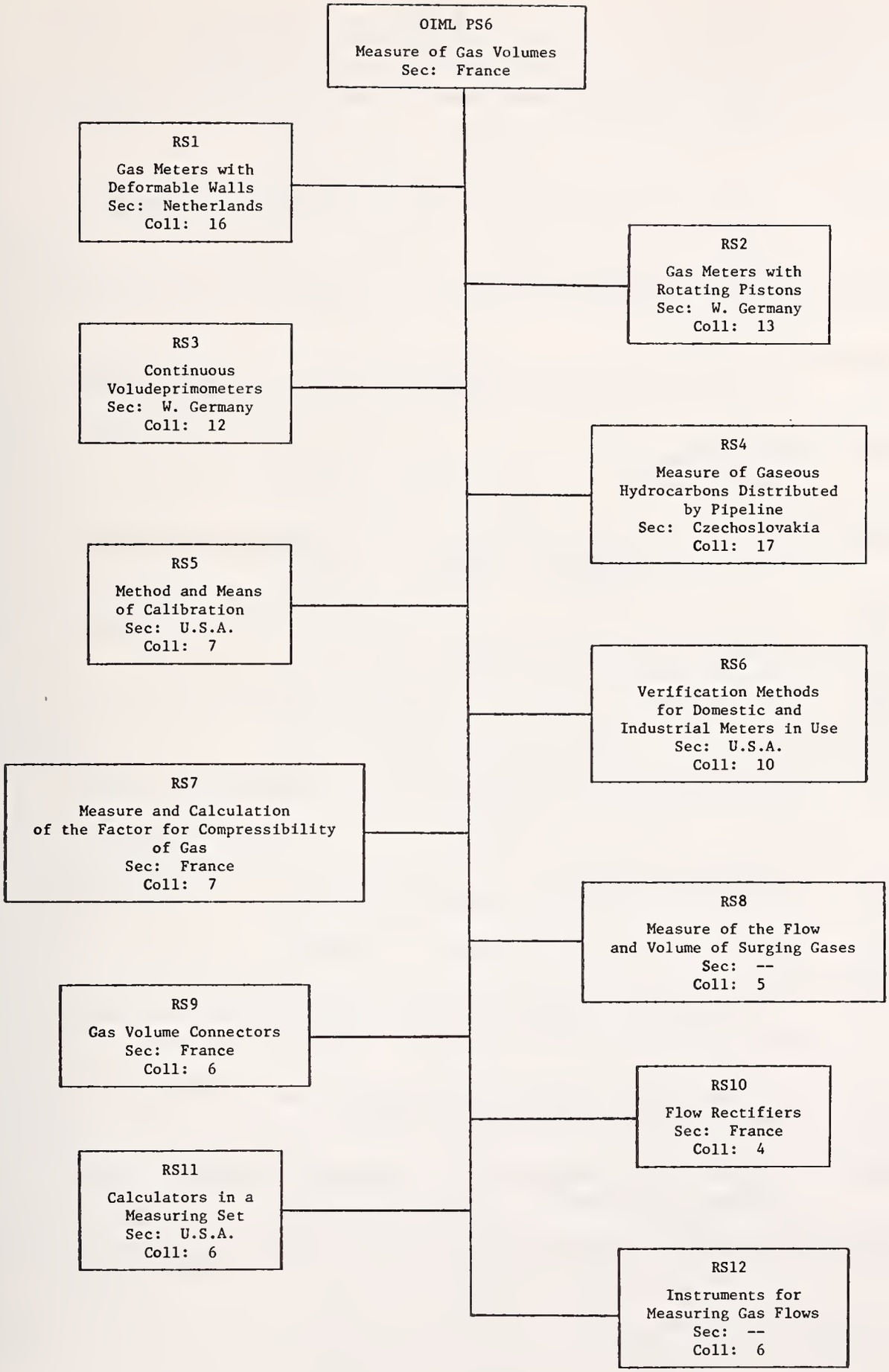

Figure 5. OIML PS6 Measure of Gas Volumes.

APPENDIX 1. Organizations Involved in Flow Measurement Standards

The organizations given below are identified as having some direct role in the system for international flow measurement standards. A brief description of most of the non-American organizations is given in a recently revised BSI publication [4].

AFNOR	Association Francaise de Normalisation, Tour Europe, CEDEX 07, 92080 Paris la Defence, France
AGA	American Gas Association, 1515 Wilson Blvd., Arlington, Virginia 22209
ANSI	American National Standards Institute, 1430 Broadway, New York, New York 10018
API	American Petroleum Institute, 2101 L Street, NW, Washington, D. C. 20037
ASME	American Society of Mechanical Engineers, 345 East 47th Street, New York, New York 10017
ASTM	American Society for Testing and Materials, 1916 Race Street, Philadelphia, Pennsylvania 19103
BIPM	International Bureau of Weights and Measures, Pavillon de Breteuil, F92-Sevres, France
BSI	British Standards Institution, 2 Park Street, London, W1A 2BS, United Kingdom
CEN	European Committee for Standardization, 5, Boulevard de 1'Empereur, B-1040 Brussels, Belgium
EEC	European Economic Community, Brussels, Belgium
IEC	International Electrotechnical Commission, 1, rue de Varembé, 1211 Geneva 20, Switzerland
ISO	International Organization for Standardization, Case postale 56, 1211 Geneva 20, Switzerland
OIML	International Organization of Legal Metrology, 11, rue Turgot, Paris IX, France
WMO	World Metrological Organization, CH-1211 Geneva 20, Switzerland

APPENDIX 2. Published Standards and Other Documents Related to Flow Measurement

Table 1. ISO/TC 30 Measurement of Fluid Flow in Closed Conduits

Designation	Title
R 541-1967	Measurement of fluid flow by means of orifice plates and nozzles
781-1968	Measurement of fluid flow by means of venturi tubes
2186-1973	Fluid flow in closed conduits - Connections for pressure signal transmissions between primary and secondary elements
2975/I-1974	Measurement of water flow in closed conduits - Tracer methods - Part I: General
2975/II-1975	Measurement of water flow in closed conduits - Tracer methods - Part II: Constant rate injection method using non-radioactive tracers
2975/III-1976	Measurement of water flow in closed conduits - Tracer methods - Part III: Constant rate injection method using radioactive tracers.
TR 3313-1974	Measurement of pulsating fluid flow in a pipe by means of orifice plates, nozzles or venturi tubes, in particular in the case of sinusoidal or square wave intermittent periodic-type fluctuations.
3354-1975	Measurement of clean water flow in closed conduits - Velocity-area method using current-meters

Note: The items below are working documents and not available for general distribution.

DIS 2975/VI	Water flow - Tracer methods - Part VI - Transit time method without tracer
DIS 2975/VII	Water flow - Tracer methods - Part VII - Transit time method with radioactive tracers
DIS 3966	Velocity-area method using pitot tubes
DIS 4006	Vocabulary and symbols
DIS 4053/I	Gas flow in closed conduits - Part I - General
DIS 4053/IV	Gas flow in closed conduits - Part IV - Transit time method with radioactive tracers
DIS 4064/I	Cold potable water meters - Part I - Specifications
DP 4064/II	Cold potable water meters - Part II
DIS 5167	Measurement of fluid flow by means of orifice plates, nozzles and venturi tubes inserted in circular closed conduits running full
DIS 5168	Computation of limit error

Table 2. ISO/TC 113 Measurement of Liquid Flow in Open Channels - Published Standards and Documents Being Developed

Designation	Title
555-1973	Liquid flow measurement in open channels - Dilution methods for measurement of steady flow - Constant rate injection method
555/II-1974	Liquid flow measurement in open channels - Dilution methods for measurement of steady flow - Part II: Integration (sudden injection) method
748-1973	Liquid flow measurement in open channels by velocity area methods
772-1973	Liquid flow measurement in open channels - Vocabulary and symbols
1070-1973	Liquid flow measurement in open channels - Slope-area method
1088-1973	Collection of data for determination of errors in measurement of liquid flow by velocity area methods
1100-1973	Liquid flow measurement in open channels - Establishment and operation of a gauging-station and determination of the stage-discharge relation
1438-1975	Liquid flow measurement in open channels using thin-plate weirs and venturi flumes
2425-1974	Measurement of flow in tidal channels
2537-1974	Liquid flow measurement in open channels - Cup-type and propeller-type current meters
3454-1975	Liquid flow measurement in open channels - Sounding and suspension equipment
3455-1976	Liquid flow measurement in open channels - Calibration of rotating-element current-meters in straight open tanks

Note: The items below are working documents and are not available for general distribution.

DRS 0748	Revision ISO 748-1973 - Liquid flow measurement in open channels - velocity-area methods
DRS 0772	Revision of ISO 772-1973 - Vocabulary and symbols

Table 2 (contd.)

Designation	Title
DIS 3716	Flow measurement - Suspended sediment load samples
DIS 3846	Free overfall weirs of finite crest width
DIS 3847	End depth method for estimation of flow in rectangular channels
DIS 4360	Liquid flow measurement in open channels by weirs and flumes - Triangular profile weirs
DIS 4363	Methods of measurement of suspended sediment in open channels
DIS 4364	Bed material sampling
DIS 4369	Measurement of liquid flow in open channels by the moving boat method
DIS 4373	Measurement of liquid flow in open channels - Water level measuring devices
DIS 4375	Cableway system

Table 3. ISO/TC 28 Petroleum Products - Published Standards and Documents being Developed that Relate to Flow Measurement

Designation	Title
R 91-1970	Petroleum measurement tables (2nd Edition)
R 91/Addendum I-1975	Petroleum measurement tables based on a reference temperature of 20°C
2909-1975	Petroleum products - Calculation of viscosity index from kinematic viscosity
3104-1976	Petroleum products - Transparent and opaque liquids - Determination of kinematic viscosity and calculation of dynamic viscosity
3105-1976	Glass capillary kinematic viscometers - Specification and operating instruction
3170-1975	Petroleum products - Liquid hydrocarbons - Manual sampling
3171-1975	Petroleum products - Liquid hydrocarbons -Automatic pipeline sampling
3448-1975	Industrial liquid lubricants - ISO Viscosity classification
3675-1976	Petroleum and liquid petroleum products - Determination of density and relative density - Hydrometer method
5024-1976	Petroleum liquids and gases - Measurement - Standard reference conditions

Note: The items below are working documents and not available for general distribution.

DIS 2714.2	Liquid hydrocarbons - Volumetric measurement by positive displacement meter systems other than dispensing pumps
DIS 2715.2	Liquid hydrocarbons - Volumetric measurement by turbine meter systems
DIS 3658	Crude or liquid petroleum products - Determination of density and relative density - Graduated bicapillary pyknometer method
DIS 3829	Petroleum products - Determination of density and relative density - Jaulmes pyknometer method

Table 3 (contd.)

Designation	Title
DIS 3838	Crude and liquid or solid petroleum products - Determination of density and relative density - Capillary stoppered pyknometer method
DIS 3967	Liquid hydrocarbons and petroleum distillates - Determination of density and relative density - Bingham pyknometer method
DIS 3993	Petroleum products - Light hydrocarbons - Determination of density and relative density - Pressure hydrometer method
DIS 4256	Liquefied petroleum gases - Determination of vapour pressure - LP Gas method
DP 4266	Petroleum and liquid petroleum products - Measurement of temperature and level in storage tanks - Automatic methods
DP 4267	Petroleum and liquid petroleum products - Calculation of oil quantities
DP 4268	Petroleum and liquid petroleum products - Temperature measurement - Excluding averaging thermometers
DP 4269	Petroleum and liquid petroleum products - Tank calibration - Liquid measurement methods
DP 4270	Petroleum products - Determination of density and relative density - Reischauer pyknometer method
DP 4271	Petroleum products - Determination of density and relative density - Capillary stoppered conical pyknometer
DP 4273	Vocabulary of petroleum measurement terms
DP 4511	Petroleum and liquid petroleum products - Measurement of oil quantities and free water - Manual methods
DP 4512	Petroleum and liquid petroleum products - Measurement equipment - Manual measurement and container calibration

Table 4. IEC/TC 4 Hydraulic Turbines and TC 5 Steam Turbines - Published Standards That Relate to Flow Measurement

Publication Number	Title
41(1964)	Recommendations for international code for the field acceptance tests of hydraulic turbines
46(1962)	Recommendations for steam turbines, Part 2: Rules for acceptance tests
193(1965)	Recommendations for international code for model acceptance tests of hydraulic turbines
198(1966)	Recommendations for the field acceptance tests of storage pumps

Table 5. OIML/PS 5 Measures for Liquid Volumes and PS 6 Measures for Gas Volumes - Published Standards and Other Documents That Relate to Flow Measurement

Recommendation*	Title
IR 5(1970)	Meters for liquids other than water with measuring chambers
IR 6(1976)	Gas meters - General
IR 27(1973)	Meters for liquids other than water - Complementary devices
IR 31(1973)	Gas meters with deformable walls
IR 32(1973)	Gas meters with rotary pistons and turbine meters
IR --(1975)	Water meters
Draft (1973)**	Orifice meters
Draft (1975)**	Measuring systems for liquids other than water - Equipped with metering devices
Draft (1975)**	Measurement of gaseous hydrocarbons distributed by pipeline

*Number in parentheses is the year of adoption of last revision or last draft.

**Not available for general distribution.

Table 6. EEC Directives Related to Flow Measurements That are Listed in ref. 11

Reference or latest draft	Status	Title
71/349/EEC of 10/12/71	Directive (OJ 10/25/71)	Calibration of ships, tanks
71/319/EEC of 7/26/71	Directive (OJ 7/26/71)	Meters for liquids other than water
COM(75)577 FINAL	Commission Proposal	Meters for liquids other than water - measuring systems
71/348/EEC of 10/12/71	Directive (OJ 10/25/71)	Meters for liquids other than water - ancillary equipment
71/318/EEC of 7/26/71 Adapted to technical progress by 74/331/EEC of 6/12/74	Directive (OJ 9/6/71) Commission Directive (OJ 7/12/74)	Gas volume meters
75/33/EEC of 12/17/74	Directive (OJ 1/20/75)	Cold water meters
Work not yet started	-	Hot water meters
Work not yet started	-	Heat meters
COM(74)877 FINAL	Commission proposal (OJ 9/13/74)	Head and gas tanks used as measuring containers
111/1919/72	Preliminary draft in abeyance. Further work in hand	Manometers
Work not yet started	-	Differential pressure gas meters

Table 7. ASME Performance Test Codes* That Include or Require Standardized Flow Measurement Methods

Designation	Title
ASME PTC 3.3-1969 ANSI PTC 3.3-1974	Performance Test Code - Gaseous Fuels
ASME PTC 4.1-1964 ANSI PTC 4.1-1974	Performance Test Code - Steam Generating Units
ASME PTC 6-1964 ANSI PTC 6-1974	Performance Test Code - Steam Turbines
ASME PTC 6 Report-1969 ANSI PTC 6 Report-1974	Performance Test Code Report - Guidance for Evaluation of Measurement Uncertainty in Performance Tests of Steam Turbines
ASME PTC 6S Report-1970 ANSI PTC 6S Report-1974	Performance Test Code Report - Simplified Procedures for Routine Performance Tests of Steam Turbines
ASME PTC 9-1970 ANSI PTC 9-1974	Performance Test Code - Displacement Compressors, Vacuum Pumps and Blowers

*Partial list given here.

Table 8. ASTM Standards for Flow Measurement

Designation	Title
D 1071-55(1975)	Measurement of Gaseous Fuel Samples
D 1941-67(1975)	Open Channel Flow Measurement of Industrial Water and Industrial Waste Water by the Parshall Flume
D 2034-68(1975)	Open Channel Flow Measurement of Industrial Water and Industrial Waste Water by Weirs
D 2458-69(1975)	Flow Measurement of Water by the Venturi Meter Tube
D 3154-72	Test for Average Velocity in a Duct (Pitot Tube Method)
D 3195-73	Recommended Practice for Rotometer Calibration
D 3464-75	Test for Average Velocity in a Duct Using a Thermal Anemometer
F 317-72	Test for Liquid Flow Rate of Membrane Filters

National Bureau of Standards Special Publication 484, Proceedings of the Symposium on Flow in Open Channels and Closed Conduits held at NBS, Gaithersburg, MD, February 23-25, 1977. (Issued October 1977)

OIML AND EEC, THEIR IMPACT ON THE INTERNATIONAL STANDARDS PRODUCING SYSTEM

D. E. Edgerly
Office of International Standards
National Bureau of Standards

ABSTRACT

Existing relationships of three major international organizations involved in producing standards are explored. These are the International Organization of Legal Metrology (OIML), the International Organization for Standardization (ISO), and the International Electrotechnical Commission (IEC). Emphasis is given to differing government versus industry needs in the production and use of standards and examples are provided in the flow measurement field which illustrate these differing needs. The technical directives program of the European Economic Community and its impact on the international standards producing system is also considered. Discussion is provided on existing and needed relationships among these organizations to ensure compatibility of technical requirements and to prevent duplication of effort.

Key Words: Flow measurement; industry; intergovernmental; international standards; legal metrology; measurement; trade facilitation.

1. Introduction

Nations seeking to participate in international standards activities quickly learn that the system that has evolved to produce such standards is diffuse and complex. Such complexity is in part due to the sheer number of international organizations involved in standards activities and to the differing needs of government and industry within the system. There also exists a degree of duplication and overlap of activities among standards organizations and a general lack of concern over instituting effective means to counter such duplication. Further, regional multi-national organizations, some of which are intergovernmental, are developing standards in the name of trade facilitation which impact the international standards producing system. In some instances these regional efforts become counterproductive to the international system when technical requirements are adopted and followed at the regional level which fail to gain acceptance in the international standards arena.

This paper explores existing relationships of three major international organizations involved in producing standards. These are the International Organization of Legal Metrology (OIML), the International Organization for Standardization (ISO), and the International Electrotechnical Commission (IEC). The paper also considers the impact on these organizations of the European Economic Community (EEC) and its technical directives program designed to facilitate trade within the Community.

2. Discussion of OIML, ISO, and IEC

The International Organization of Legal Metrology (OIML), was founded in 1955 as an intergovernmental organization to promote uniformity of national legal requirements for measuring instrumentation and to foster the development of Metrology Services within its member nations. The principal task of OIML is to achieve international uniformity in the definition of and approach to legal measurements. That is, to define and set into International Recommendations, acceptable criteria that a measuring instrument or system must meet to be declared "legal for use" by a national authority. In the United States "legal for use" predominantly applies to measuring instruments in trade and industry which directly impact the consuming public. In the flow measurement field within the United States there is very little regulation over the measurement end of custody transfer between producers and transporters of liquids such as natural gas and petroleum. In many other nations, particularly in Europe, national authorities have much greater control over flow measurements throughout the commerce chain from producer to the consumer. Similarly, the concept of "legal for use" in other nations includes measuring instrumentation and systems found not only in trade and industry but also in science and medicine. Thus, the scope of OIML is very broad and includes all types of measurement instrumentation whether found in a retail food store or in a hospital. The definition of acceptable criteria for a legal measurement primarily involves international agreement on such basic metrological factors as accuracy and precision and agreement on the degree of errors that should be permitted in measurement. However, OIML also establishes recommendations on the verification of instrument and system design and performance as a means of assuring that devices and systems are adequate for intended use and will perform within reasonable error limits established by national authority.

OIML is by reasonable definition an international standards producing organization. It functions on a technical level in the same fashion as the International Organization for Standardization (ISO) and the International Electrotechnical Commission (IEC), the world's two major nongovernmental standards bodies. The principal difference between OIML on the one hand, and ISO and IEC on the other, is the governmental character of OIML and its outputs which are drafted as model laws and regulations designed to be adopted and enforced as law by its member nations. ISO and IEC produce standards which are voluntary and whose content are slanted towards a prescribed set of conditions and requirements designed to assure acceptable quality or performance of products, materials, or processes. A principal task of ISO and IEC is to facilitate the international exchange of goods and services through standards which offer some assurance of product quality. OIML has a similar goal of trade facilitation which is to achieve international agreement on legal requirements governing acceptable measurement practices in the exchange of goods and services. The two goals are not in conflict and can be complimentary, providing there is some agreement among the standards organizations covering their intended scope of operation.

There are many technical areas in ISO and IEC involving flow measurement, for example, that are oriented towards agreement on acceptable characteristics for flow control and measurement whether concerning pipeline systems or electronics involved in flow control. The purpose of such work should be the development of a good flow measurement technology base. While their flow measurement standards do cover inherent system or device errors and methods for testing and control of such errors, they should be oriented towards a documentation of inherent errors in various flow equipment, the purpose being to inform the user of the standard what he may expect in the way of operating characteristics of a meter or a flow system. Such standards should not preempt OIML's task, for example, of recommending error limits for acceptance and use of these devices or systems as legal in trade, industry, science, etc. Similarly, the technical involvement of OIML in flow measurement should be governed by like conditions. For example, OIML efforts in developing the conditions and requirements for flow measuring instrumentation to be legal for use should only center on the development of metrological and technical requirements which influence the measuring capability of an instrument or system and on recommended means for use by national authorities in verifying that instruments or systems meet the prescribed requirements.

Metrological requirements are those which relate to measuring errors and are approached by examining errors occurring in a measurement system so as to establish error limits which may not be exceeded in legal measurements. Technical requirements relate to an examination of those properties of an instrument which influence measurement errors and those which determine the practical usefulness of an instrument for legal metrology purposes. Examples of technical requirements which might be imposed on a manufacturer of flow measurement equipment by OIML recommendations are as follows:

1. requiring that the primary indicating elements and primary recording elements of a flow measurement system be readily returnable to a definite zero indication; or,

2. requiring that a retail motor-fuel dispensing system be constructed such that after a particular delivery cycle has been completed by movement of the starting lever to any position that shuts off the device, an effective automatic interlock will prevent a subsequent delivery from being started until the indicating elements and recording elements have been returned to their correct zero positions.

These technical requirements are imposed to ensure suitability of equipment for use in commerce and to prevent, as far as practicable, the facilitation of fraudulent measurement practices. The requirements, however, are couched in performance language and for the most part do not specify design requirements to meet stated performance needs. OIML should not become involved in specifying the design of measuring instrumentation or systems as a means of assuring adherence to metrological and technical requirements.

Concern with design criteria in OIML primarily results from experience gained in those national metrology laboratories which conduct pattern approval of measuring instruments or systems as the first step in verifying that they are adequate for intended use and legal for trade and industry within that country. The government experts who conduct such testing are the same experts who attend technical meetings of OIML and who bring with them practical experience gained in the laboratory on the performance of various instruments. In many cases, these experts feel that the solution to a measuring problem is to require specific design criteria which will assure acceptable instrument performance. The difficulty with this thinking is that if design criteria are written into legal requirements there is the possibility of creating trade barriers and of stiffling technological innovation. A recent experience in OIML illustrates this concern quite clearly.

In December 1975, a technical level meeting was held in London to discuss a first draft OIML International Recommendation entitled "Measuring Systems for Liquids Other than Water, Equipped with Volumetric Meters." The draft was written by France and the Federal Republic of Germany, and intended as a general legal code for various flow measurement systems including retail motor fuel dispensers; tank truck metering systems; receiving systems for unloading of ships, rail tankers and road tankers; liquefied petroleum gas systems; pipeline systems; and, even milk measuring systems. For the most part, the draft Recommendation was found acceptable. The requirements written into the draft covering the operation of measuring systems prescribe, in performance terms, generally accepted specifications for the operation of transfer points; filling of the meter and pipework; draining; anti-vortex devices; by-passes; and so forth, as such components affect the measuring elements of the system. However, in its discussion of air or vapor elimination, the draft shifted to very specific design requirements. For example, requirements were contained which specified that the volume of an air or vapor elimination device be at least equal to 8% of the product volume delivered in one minute at maximum flow rate. This requirement could not be met by United States manufacturers without substantial and costly design and construction changes to incorporate larger air or vapor elimination devices within motor fuel or tank truck dispensing systems. Fortunately, other member nations joined the United States in objecting to such a design requirement and the matter was resolved by creating a joint OIML/ISO Task Group to study the question of air or vapor entrapment in liquid and to propose technical recommendations which would be acceptable to both bodies. It should be added that this joint working group between ISO and OIML is the first to be established. Hopefully, other common problem areas between these international organizations will be approached in a similar manner as it is through this type of government/industry relationship that technical conflicts and duplication of effort are minimized.

3. Discussion of EEC

The problems of duplication of effort and technical conflict are not confined solely to ISO, IEC, or OIML. There are other international organizations and multinational regional organizations which, though perhaps not primarily chartered as standards bodies, do produce technical recommendations which impact the standards producing

system. These organizations and their interactions with ISO, IEC, or OIML have already been discussed. However, some special emphasis should be given to the European Economic Community (EEC), and the important impact it has on the international standards producing system. EEC is important because it is a major trading partner of the United States and it is an important technology contributor to the international standards producing system. However, it also competes with the system and in some cases works counter to the system by preempting actions under consideration within ISO, IEC, or OIML.

The EEC operates a technical directives program oriented towards achieving harmonization of laws, regulations and administrative actions among its nine member nations as directly affects the operation of the Common Market. The intergovernmental character of the EEC and the obligation of its members to adopt Council Directives makes it an important organization to reckon with. Basically, the EEC Directives program generates standards for use by its nine members in facilation of trade within the Community. At the present time, for example, the EEC is pursuing the development of technical directives in many subject areas which are common with technical activities in ISO, IEC, or OIML, including: motor vehicles; tractors and agricultural machinery; metrology and measuring instrumentation; electronics; construction materials; rubber and plastics; and many other areas. In the flow measurement field, the EEC now has five final Directives in force covering such areas as petroleum and natural gas flow meters, water meters, ancillary equipment used with flow meters, and calibration of ship, rail and road tanks. There are another five Directives at the draft level covering general requirements for flow measuring systems, differential pressure gas meters, and electronic devices fitted into measuring instruments. Basically, the approach taken by the EEC in standards generation is to use international standards when available as the foundation for its technical directives. However, when international standards do not exist, or when there are unique regulatory needs which cannot be satisfied by adopting a given international standard, the EEC will produce and adopt technical requirements within its directives without going to an international forum such as is provided through ISO, IEC, or OIML. This has an important impact on the international standards producing system because once efforts are underway internationally to achieve agreement on standards, the Common Market nations by virtue of preemptory action speak as a unified bloc of nine ISO, IEC, or OIML members, thereby exerting considerable influence over the final technical content of the international standard.

Another action by the EEC which is not uncommon and which also impacts the international standards producing system is the practice of introducing draft ISO, IEC, or OIML international standards into its technical directives program and moving the drafts through the program to final adoption as EEC Directives before the standard comes into fruition at the international level. The danger in this practice is adopting Directives having legal status within the Community, whose technical content may differ from the final standard eventually accepted by ISO, IEC, or OIML. The net effect of such a practice is technical conflicts which could result in non-tariff trade barriers.

4. Summary

OIML and the EEC are standards generating organizations that have important impacts on the international standards producing system. Though they are intergovernmental bodies with standards needs differing from those of industry they nevertheless impact commercial standards through the adoption of laws and regulations which govern the flow of commerce. If commerce is to be unrestrained among nations then the technical requirements written into law by OIML and the EEC must be compatible with each other and with standards generated by ISO and IEC. As has been stated, insuring this compatibility is not as simple as having OIML or EEC or any other governmental body adopt ISO or IEC standards as the basis for mandatory regulations covering trade and industry. There are regulatory decisions involving commercial equity and public health and safety which are not and should not be within the purview of voluntary bodies such as ISO or IEC. Thus, the only apparent solution to government versus industry generation and use of standards seems to be greater interaction and participation by the two within the international standards producing system. At present, nations face somewhat of a resource burden in having to be vigilant and active within many international organizations in order to ensure that both industry and governmental needs are being met and that the various organizations are not working counterproductively to national aims. Unfortunately, this situation is not likely to change for some time to come.

BIBLIOGRAPHY

National Bureau of Standards Handbook 44; Fourth Edition, "Specifications, Tolerances, and Other Technical Requirements for Commercial Weighing and Measuring Devices," Issued December 1976.

Referowski, Z., "Remarks on the Work Topics of OIML Secretariats," Draft of an OIML Bulletin article, September 1976.

National Bureau of Standards Special Publication 484, Proceedings of the Symposium on Flow in Open Channels and Closed Conduits held at NBS, Gaithersburg, MD, February 23-25, 1977. (Issued October 1977)

THE INTERFACE BETWEEN INDUSTRIAL, NATIONAL AND INTERNATIONAL STANDARDS

Wallace N. Seward
American Petroleum Institute
2101 L Street, N. W.
Washington, DC 20037

The oil and gas industries, throughout more than 100 years of historical development, have been able to capitalize on the rationalization of sophisticated document and technology through industry-wide standardization efforts. The essential incentives of the original industrial standardization programs were threefold:

First, to decrease capital costs and long-term maintenance expenses through the interchangeability of parts and the establishment of uniform operating, procurement, and training procedures.

Second, to ascertain and develop optimum levels of performance, safety, and reliability without inhibiting technological development.

Third, to promote economic viability and incentive among supply and service organizations associated with the resource industries.

There are essentially two end uses for proprietary measurement standards developed by industry. A significant number were developed by industrial users to aid in the purchase, operation and maintenance of equipment common to various companies making up the industry. Conversely, as the product line of a manufacturing industry multiplied, the manufacturers themselves generated quality or definition standards to describe common product characteristics to the customer or user level.

One of the more perplexing aspects of the world's industrial standards development process is the huge number of organizations involved in preparing technical literature. Overall, there are at least 12,000 known sources of industrial standards (or proprietary support data). In the U. S., approximately 360 trade associations and professional suppliers are currently engaged in on-going standards development.

So, recalling that industrial standardization first got its impetus in the U.S., and generally throughout the world, as mass-production replaced craft manufacture, it followed that companies faced with expanding their operations or markets

sought uniform inventory control and were inherently drawn into the process. Competitively, however, national markets caused similar products to be produced by different suppliers in a multiplicity of ways, often because of differing regulatory expectations. One way or another, conflicting national industrial standards emerged through trade associations and professional societies. Domestically, if the end-product or methodology impacted on the general public, then an industrial standard was further reviewed for voluntary national adoption as a consensus of technical, legal and economic interests by the public, labor, government and private enterprise. Ultimately, if the commodity or service was offered multinationally, it was usually submitted to a broad review at an international level. In those cases where the consuming public or national interests were significantly affected, individual governments themselves may require and adopt or legislate the use of the standard after negotiation and modification, thus making it directly enforceable by law. This act is called regulation by reference to standards. But, in many countries, this process is significantly modified because the authority to create and adopt standards is simply vested in the government, even though it often has an overriding financial stake in export sales of equipment or value-added taxes on imported hydrocarbons. Thus, in some nations, the tax on crude oil may easily be 500 percent greater than the commercial value, so a measurement shortage is a greater penalty to the state than to a company.

Application of Standards

Direct enforcement is much more difficult internationally, so for commercial measurement of hydrocarbons, it is quite common to reference voluntarily-developed standards within a contract negotiated between a specific buyer and seller. But, even if governments and private concerns are involved, the voluntary label is misleading because each contract carries with it the right of equitable enforcement through a mutually agreed legal protocol or judicial process. With this in mind, such non-government standards should best be described as a pre-negotiated package of technical information, which, when referenced in contract, allow any affected party recourse to due process. That such standards are applied time after time without gross penalty suggests the satisfaction of all parties, even though they may contain contradictions to domestic regulations. This attribute is sometimes overlooked when governments alone seek to promote and unilaterally enforce conflicting national measurement regulations on petroleum commerce. Especially when pattern approval or prototype testing is demanded, responsibility is not shared; rather, this stance assumes that government is somehow invariably right while the supplier and user are invariably deficient. However, since hydrocarbons are measured at least 12 times between wellhead and consumer, it is evident that cooperative international standardization offers the only path to rational economic equality.

Organizations Engaged in Oil and Gas Measurement Standardization

Recalling the complexities resulting from the evolutionary process of standards development, it seems preferable to categorize rather than simply list standards organizations involved in preparing technical material. Since we are primarily concerned with the measurement of hydrocarbon fluids and fluid properties, it is not possible to be either all-inclusive or free of technical overlap in describing the organizations involved. Thus, there are:

I. Domestic Equipment and Manufacturing Interests

   a. Instrument Society of America (ISA)

   b. Scientific Apparatus Makers Association (SAMA)

   c. Electronic Industries Association (EIA)

   d. Fluids Controls Institute (FCI)

   e. Manufacturers Standardization Society of the Valve and Fittings Industry (MSS)

   f. Oilfield Production Equipment Manufacturers Association (OPE)

II. User Industry Interests

   a. American Gas Association (AGA)

   b. American Petroleum Institute (API)

   c. Compressed Gas Association (CGA)

   d. Manufacturing Chemists Association (MCA)

   e. Natural Gas Processors Association (NGPA)

III. Professional Societies

   a. American Society of Mechanical Engineers (ASME)

   b. American Society for Testing and Materials (ASTM)

IV. National Standards Management

   a. American National Standards Institute (ANSI)

   b. National Bureau of Standards (NBS)

   c. National Conference on Weights & Measures (NCWM)

V. International Standards Development

a. International Organization for Standardization (ISO)

b. Organization of International Legal Metrology (OIML)

c. International Bureau of Weights & Measures (BIPM)

To clarify one point immediately, there are four organizations included in this list which are not classifiable as industrial standardizing bodies. These are shown in the latter two categories for convenience. The NBS, NCWM, and the OIML engage in standards development to the extent that they draft model codes for ultimate adoption and enforcement by regulatory bodies while the BIPM establishes by treaty scientific definitions of units of measure, including the legal interrelationship of one unit to another. It also houses such necessary articles as the prototype kilogram and the prototype litre measure on which virtually all national calibration equipment is based.

As is self-evident, each category represents a unique interest having as its objective the satisfying of what it perceives to be in the common good of its respective constituency. Governments respond to "national interests;" industries to "markets." Personally, I think of a market as a selective interest with a limited amount of money. A "national interest" is usually politically ascertained with greater regard to continuation in power than to economic efficiency or limits.

But many of the contradictions and conflicts in the international arena, including both measurement equity and useful standardization, are created because existing social "systems" cannot resolve whether best objectives are obtainable through an educationed commercial marketplace, or traditional regulatory prescription or intervention in the "national interest."

Thus, a measurement equipment supplier is primarily interested in meeting his customer's expectations in terms of accuracy, convenience, and budget. The user industry, the hydrocarbon companies, tend to wish for reliable and provable performance expectations at a defensible cost for each specific application. Most governments wish to insure that their national interest will not be harmed, that export markets will be expanded and that tax revenues are optimized.

Thus, we are faced with which constituency is to be pleased, so there are variations in enforcement expectations, performance versus prototype test requirements, and, not least of all, a paradox in evaluating who is technically most competent to judge when a reasonable balance of competence has been achieved.

Although internationally we still lack the ultimate resolution of this problem, we have made great progress by isolating and examining its foundation through ISO and OIML. However, I also believe that in a world that is as sophisticated and complex as ours, no one interest can exist to the exclusion of others, including government. I rest my case by observing that OPEC officially is a treaty organization, not a cartel of competing companies. Even though its commercial impact cannot be avoided in the immediate future, its political consequences can only be overcome by the combined talents - economic, technical, and political - of an inter-dependent world.

Even trade and commerce by OPEC nations must be based on three principles that, when negotiated and agreed, will result in the exchange of a commodity. First, the level of quality offered must meet the expectations of the purchaser. Second, the total amount of material to change hands must be specified and delivered within reasonable and reliable limits. Third, a price for either the total exchange or per unit basis can only be concluded after the first two conditions are clearly understood and acceptable.

The new role of measurement standardization is to provide standing roles and test methods, composed by the best available technical talent, to evaluate the level of quality and degree of quantitative accuracy that is acceptable to all parties engaged in petroleum commerce. With such agreements in hand, trade can be assured subject only to price agreement, without hidden manipulation or prolonged and misdirected negotiations or even worse, including threat of war. The contribution of measurement standardization is that it is responsibly carried out by the technical community in advance of market pressures. Measurement standardization must not become subject to the hazards of political bargaining. To suggest diplomacy as the only recourse is to run the risk of irreconcilable failure.

Conclusion

Recent changes in the politics and economics of the oil industry have placed new strains on the contractual system which have, to an increasing extent, become supplanted by governmental negotiations. Domestically, the Energy Conservation Act of 1975 for the first time authorizes our government to directly purchase and own crude oil.

In the past, the API Committee on Petroleum Measurement was able to assist in resolving technical disputes by arbitration based on the industry's integrity reflected through equitable consensus standards. In that 45 percent of U.S. oil is now imported, with one party more frequently a soverign

agency, this procedure has diminished in effectiveness. Therefore, technical support from all affected interests is also mandated by the inherent conflict between OPEC governments, consumer governments, and commercial interests.

Leadership in ascertaining the limits to accuracy and precision, technically rather than legislatively, is a serious need which must be shared. Our mutual involvement in the Organization of International Legal Metrology and the International Organization for Standardization has highlighted the degree of competence that may be brought to bear now and in the future.

To maintain measurement integrity, it is essential that the National Bureau of Standards continue a program in fluid measurement standardization and related fluid dynamics at a sufficient level in support of the historic U.S. reputation in this field. But overall, API supports work with all those dedicated to developing useful programs that will be most beneficial in meeting the needs of the world.

National Bureau of Standards Special Publication 484, Proceedings of the Symposium on Flow in Open Channels and Closed Conduits held at NBS, Gaithersburg, MD, February 23-25, 1977. (Issued October 1977)

THE ADEQUACY OF THE DATA BASES AVAILABLE FOR PROMULGATING INTERNATIONAL STANDARDS

H. H. Dijstelbergen

N. V. Nederlandse Gasunie
Groningen
The Netherlands

1. Introduction

The number of international standards for measuring flow rate or quantity is gradually increasing. In the light of experience with existing ones questions rise with respect to the validity of certain figures or tolerances. To answer the questions raised implicitly in the title, for all fields of standardization is beyond the competence of the author and the rest of the paper will therefore be limited to two specific fields. From the observations in these fields some conclusions might be drawn which are more generally valid.

In general international standards are based on national ones which have been in existence for some time. In some instances, the data bases underlying these standards have not been published and are lost in forgotten file cabinets. If they would be found, hardly anybody would be able to find his way in the chaos of insufficiently specified data. The adequacy of the data basis can, therefore, be rarely tested directly on the data itself. If, however, the claims put in the standards show not to hold, it can be concluded indirectly that the data base must be inadequate. Instead of speaking of adequacy of the data base one could put the question more gently by asking whether the right standard is based on the available data. The paper restricts itself to two standards. The first is not an international standard in the usual sense but the EEC regulations on gas turbine flowmeters. The second one is the international standard on flow measurement by means of orifice plates.

2. The EEC Regulations on Turbine Gas Flow Meters

The practice and philosophy of gas metering in a number of EEC countries is substantially different from the United States. In these countries the way to measure gas is limited by law to certain approved measuring devices. This originates from protecting the (domestic) user - the weaker economic party - by requiring each and every meter to be calibrated in a flow rig under legal supervision. Furthermore, the meter had to be of an approved type to warrant a trouble-free and stable performance over its lifetime.

The rules were not limited to domestic gas meters but also larger size meters were included. One of the most important aspects of the law was to avoid the possibility of interference by user or supplier. So, much emphasis was placed on sealing of parts and of course orifice plate metering was originally not accepted as being too easy to interfere with. In fact in Germany orifice plate measurement while accepted in principle, was not applied until very recently for this reason and in the Netherlands it is still not officially accepted. Type approval of a meter depended not only on the fulfillment of the legal regulations but also on tests carried out by the official

bodies and field trials supervised by the same. It took, for example, three years for approval of the first gas turbine flowmeter in the Netherlands.

In 1971, the EEC countries prepared under the secretariat of Germany and the Netherlands a rule on gas meters. It was largely based on current practice in these two countries, amended by the other members. Highlights of metrological aspects of the rules are:

Specifications for the indicating counters to facilitate the check of individual meters in a calibration flow-rig,
Limits to error,
Limit to average error over the measuring range,
Calibration at defined points in the measuring range,
Type approval with air of atmospheric pressure,
Type approval by tests on a number of meters (three to seven),
Specified maximum derivative of error curve with respect to flow rate at approval,
Endurance tests of 1000 hours at maximum throughput at approval, and
Specified maximum change of error during endurance test.

The data on which the rules are based are very diffuse. Let us investigate what would be needed.

Evidence that the tests are sufficient to warrant good performance under actual conditions.
Evidence that the performance does not deteriorate over the lifetime of the meter or the time between two calibrations.

As to the first point it is striking that no limits have been put on either pressure range or temperature of the gas nor on the ambient conditions. Installation conditions have not been taken into consideration. It is obvious that the evidence for such a large field of conditions and applications does not exist. The data reported in the literature are limited to the influence of pressure on the meter [1][1]. Furthermore, the base consists of the theory that the slip of the blades in a turbine gas flow meter is relatively small and remains so independent of conditions. In reference 1, there is a further theory on the influence of density especially at the lower end of the range. The check of this theory has been carried out on too small a number of meters to be statistically significant.

The second point is to a certain extent covered by the endurance test. However, it does seem limited when considering the field of application which includes dust-laden gases and gases more aggressive than air at atmospheric pressure. The fact that every meter has to be tested individually under controlled conditions assures, however, that at least under those conditions the meter is capable of a guaranteed performance. The extrapolation of this performance is rather daring, especially in view of the dependence of the error curve on pressure and installation conditions [2,3]. As a conclusion it can be said that the data base underlying the EEC rules is insufficient. Furthermore, because of the inaccessibility of the data it is impossible to weigh the degree of extrapolation for a particular application.

3. The ISO Standard on Flow Measurement with Orifice Plates [4]

The philosophy behind the standardization of these devices is significantly different from the one behind the rule on turbine gas flowmeters. Instead of

[1] Figures in brackets indicate the literature references at the end of this paper.

individual calibration of each meter in a calibration flow rig the standard controls closely all geometrical dimensions. This insures a high degree of geometrical similarity with a number of tested installations which served to establish the equations or tables relating the differential pressure to the flow rate. The main reason for this inferential method of calibration is of course that, for the chief applications, either no primary calibration facilities were available or the cost of using these would be prohibitive.

The fact that no individual calibration on a flow rig is needed puts a very high value on the geometrical similarity with the original devices. These original devices form in fact the kernel of the data base. In principle these tubes and orifice plates should therefore have been carefully conserved. The ISO standard on flow measurement with orifice plates standardizes flange taps, vena contracta taps and corner taps. It is presently under revision and this will result in the incorporation of D-D/2 taps whereas the vena contracta taps will be left out. The data for the D-D/2 taps and the flange taps originate from the United States and the corner taps from Germany.

The only readily available data base are the U. S. data. The report [5] issued in 1935 by the joint AGA-ASME committee on orifice flow meters was not distributed on a large scale, but copies do exist. It gives a comprehensive account of a multitude of tests which served as a basis for the present standard. As such it should serve as an example for those involved in standardization.

The coefficient and the tolerance in these were largely derived from tests on a water calibration rig at the Hydraulic Laboratory of the Ohio State University, carried out under the supervision of Professor S. R. Beitler. The analysis of the data was made by Dr. E. Buckingham and Mr. H. S. Bean of the National Bureau of Standards. In a thorough investigation [6], Dowdell and Chen clearly show that "Since computers were not available ....., the accuracy figures given must represent, to a certain degree, the judgement of the people involved in the analysis." Although the accuracy quoted in ISO R 541 and the underlying standard, AGA Report No. 3 [7] is 0.5 percent, the study, by employing statistical methods on all the Columbus data clearly shows that even when the range of Reynolds, diameter and diameter ratio are limited a *standard deviation* of 0.5 percent is found. This means that an accuracy figure should rather be 1 percent instead of 0.5 percent. Apart from an analysis of the Columbus data alone, data from six other sources from recognized hydraulic laboratories in the U. S. were analyzed. When all these data were included and the range of Reynolds number, line size and diameter ratio was limited to the same values as above, the same order of magnitude for the standard deviation was found. Curve fitting by regression analysis and eliminating data wherever there is a justification yields a curve which reduces the standard deviation of the measuring points with respect to this curve to 0.37 percent.

Other comparisons with different sources give striking results. If for example, flange tap coefficients are compared with corner tap coefficients these should be the same for large diameters. Likewise, the coefficients for flange taps and for D-D/2 taps should be the same for 2 inch pipe. In Figure 1, which is derived from [8], differences of up to 0.5 percent show.

An important problem arises from the fact that the range of diameter ratios, flow rates and pipe diameters is more limited for the data itself than the standards derived from these data. Furthermore, the distribution of data

points over the whole field is rather uneven. High Reynolds numbers correlate with large orifice diameters and measuring points reflect the technical limitations of the flow rig used. The present standards are therefore a rather far extrapolation on the original data, especially in those areas where the original data are few. Although in at least one case such an extrapolation was carefully checked [9], this was certainly not always the case. Another extrapolation is the application of coefficients derived in water calibration rigs to gas.

Of course, measurements have been made using primary gas standards such as bell-provers, but it is improbable that the accuracy of these measurements was sufficient to detect anything else but first order deviations. After all the Reynolds similarity is a hypothesis which for these simple configurations holds to a first approximation. When, however, it is used for extrapolation over such a wide range and in the accuracy brackets of 0.5 percent it should be checked whether there are no other effects.

As stated earlier on, it is a pity that the original equipment was not preserved. The roughness and roundness of the adjacent pipes are now only qualitatively known as is the fact with the edge sharpness. It is now quite possible that due to improvement of manufacturing techniques there has been a systematic change in the true coefficient of orifice plates.

The source of the installation requirement in the ISO standard is hazier. Again one of the best documented set of tests appears in the AGA-ASME report [5]. Another basis is the DIN-standard [10]. The last one even gives for some upstream disturbances not only the increase in tolerance but also the direction and average magnitude of the shift. Data supporting this have been published by Schröder [11].

When comparing the installation requirements in AGA Report No. 3 [7] with the ones of R 541 it shows that the lengths required for the same accuracy are according to ISO twice the ones needed according to AGA. A recent study of the data on disturbance tests given in the AGA-ASME report shows that even the strict ISO requirements are not sufficient to eliminate the influence of upstream conditions. Some results are listed in Figure 2, where for specific tests the difference between two orifice meter runs in series is listed together with the undistrubed lengths required by both ISO and AGA. The disturbance upstream one orifice plate consisted of three angles in two planes, the other being preceded by a very long length of the tube.

Field experience from two large gas measuring stations in series at the French-Belgian border [12], both meticulously instrumented and maintained, indicate that on the average one of the stations indicates a flow rate 0.4 percent higher than the other. Both stations are equipped with several lines in parallel and installed according to ISO R 541. When changing orifice plates the difference between the two stations can amount to one percent depending on the particular orifice used. The difference would remain stable over weeks. Interchanging orifices between the stations indicated that the systematic difference can only be attributed to the installation conditions.

From these facts, based both on reanalysis of existing data and on field experiments, the conclusion that the standards claim too high an accuracy and extrapolate too much on the existing data is unavoidable.

4. Possible Improvements

Possible improvements of the standards can only be achieved by better use of existing data or the generation of new data.

An improvement to the new ISO standard on flow measurement by means of orifice plates was proposed by Stolz [13]. By making use of the existing equations and tables for D-D/2 taps, flange taps and corner taps, Stolz managed to mold these into one simple single equation which ironed out some inconsistencies in the old standards. It it is admitted that all of the original data are based on serious measurements, the odds are on the result being closer to the truth than the original. The proposed equation incorporates measurements in the vicinity of the plates by Herning, Witte and Schröder. The coefficient has the following general form

$$C(L_1,L_2') = C_\infty(0,0) + \Delta(L_1) - \Delta(L_2') + B\ (\frac{10^6}{Re_D})^{0.75}$$

where,

L_1 and L_2'	indicate the locations of upstream and downstream tap respectively (normalized with respect to the diameter)
$C(L_1,L_2')$	indicates the discharge coefficient of a meter equipped with L_1 and L_2' taps
$C_\infty(0,0)$	indicates the discharge coefficient for corner taps for $Re_D = \infty$
$\Delta(L_1)$	correction for the distance of the upstream tap from the orifice plate face
$\Delta(L_2')$	correction for the distance of the downstream tap from the orifice plate face

The full equation is written:

$$C(L_1,L_2') = 0.5920 + 0.0376\ \beta^{1.55} - 0.1543\ \beta^{6.7} + 0.900\ L_1\ \beta^4\ (1 - \beta^4)^{-1} - 0.0156\ L_2'\ \beta^{1.2} + 10^{-4}\ [5.27\ \beta + 38.4\ \beta^4 - 20.2\ \beta^8]\ [\frac{10^6}{Re_D}]^{0.75}$$

Interesting features of the equation are:

as β goes to zero the Re term comes to zero too,
for large diameters corner taps and flange taps give the same coefficient,
for pipe diameters of 2", flange taps and D-D/2 taps give the same coefficient,
the Re_D term is the same for all tappings,
the discharge coefficient C comes to one single value for β equal to zero regardless of tappings.

Another improvement which is suggested for the new ISO standard is the introduction of straighteners. The required length between orifice and straightener and between straightener and disturbance is specified on the basis of measurements carried out by Plunian and Sens [14] which were confirmed by experiments at British Gas by Jepson. The introduction of a straightener does not decrease the required straight length but serves to enable the user to put unspecified disturbances, such as regulators, upstream of the orifice plate. This was hitherto not allowed.

If, however, it can be shown, for example by Pitot-tube traverses, that at the location of the orifice plate the flow profile is fully developed, any length or arrangement is permitted. The changes are being proposed to bring the standard in line with presently available data.

For the EEC regulations on gas meters, being a legal document, it is much more difficult to bring about a change. However, in the Netherlands ways have been opened to calibrate meters individually with gas at operating conditions within the still valid national legal framework. There is little doubt that in the long run the data now available will influence the EEC regulations.

A second possibility would be to gather new data. In fact this is the only possibility to substantially improve the standards. Of course this has been obvious to many people, but several reasons prevented the collection of new data. Mainly this is a matter of cost. If new data bases have to be collected, which would be adequate for present day needs and possibly for tomorrow's, a massive program would have to be carried out covering the whole field of parameters. In order to avoid any bias, it would be necessary to cross-check between different laboratories and to use equipment from a large number of sources, operated with liquids as well as gas. This is very important as the required accuracy is higher today than it was in the thirties and certainly higher than the apparent accuracy of existing data bases.

One thing that certainly needs exploration is the stability of orifice plates measurement. There is evidence that in some cases the repeatability of a measurement is rather bad although over very long periods it appears to be better [9]. The same phenomenon showed up, for example, in the Refugio tests in 1954. In none of the cases an explanation of the instability could be found. In very small orifices a true instability of the discharge coefficient has been reported [15], and it would be necessary to investigate if something similar could occur with normal size orifice plates.

Anyhow in order to get reliable standards, calibration facilities capable of operating close to the actual practical conditions of the measuring equipment are needed. Several calibration laboratories do exist for water and oil and up to large flowrates. For high pressure gas the number of calibration facilities is much more limited. To investigate instruments under the conditions prevailing in gas transportation, our company built a high pressure calibration rig for 144 000 m^3_o/h (5.10^6 SCF/H) [2] and started building one for $2.5.10^6$ m^3_o/h (9.10^7 SCF/H). The first operates at pressures between 8 and 60 bar, the second at pressures between 50 and 60 bar. To check the absolute accuracy of these installations a comparison is now being made with an installation at Gaz de France and one at the National Engineering Laboratory in Glasgow. These last installations are also capable of calibrating high pressure gas flowmeters although with a more limited capacity. The three installations are based on totally different principles. The comparison takes place under the auspicies of the EEC.

Generally there is a large reluctance to accept evidence that standards are not as they were believed to be. At the Pittsburgh flow conference in 1971 one of the speakers drew attention to instrument manufacturers supplying specifications to the wishes of their customers without changing their instruments. He coined the word 'specmanship' for this activity.

It is the feeling of the author that in the case of standards a considerable degree of 'specmanship' is displayed by users. Instead, a realistic approach would be more commendable and either the standards should be adapted to the available data or data should be generated to support the required standard.

5. References

[1] Eujen; Untersuchungen über die Messeigenschaften von Hochdruck gaszählern, II Teilbericht, Messungen an Schraubenradzählern; *Gas- und Wasserface*, 105 (1964), p. 1192-1199.

[2] Bellinga; Calibration of turbine flowmeters under operating conditions; *Paper B2, Conference on Fluid Flow in the mid 1970's*, 8-10 April 1975, East Kilbride, Glasgow.

[3] Peignelin, Pellous; Etude expérimentale a 1'aide de tuyères fonctionnant en régime sonique de la précision du comptage de gaz sous pression; *Communication IGU/C 21-73*, presented at the 12th World Gas Conference, Nice 1973.

[4] Measurement of fluid flow by means of orifice plates and nozzles, *ISO Recommendation, R541*.

[5] Report by the joint AGA-ASME orifice coefficient committee to the gas measurement committee, Natural gas department AGA and the Special research committee on flow meters of the ASME - 1935.

[6] Dowdell, Chen; A statistical approach to the prediction of discharge coefficients for concentric orifice plates, *Trans. ASME, J. Basic Engineering*, (1970) p. 752-765.

[7] Orifice metering of natural gas, *Gas Measurement Committee Report No. 3*, American Gas Association, Arlington, Va., 8th printing 1972.

[8] Stolz; An Approach towards a general correlation of discharge coefficients of orifice plate meters; *Paper K-1, Conference on Fluid Flow in the Mid 1970's*, 5-10 April 1975, East Kilbride, Glasgow.

[9] Gorter, DeRooy; An investigation in widening the Reynolds number range for flow measurement in closed conduits by means of orifice plates, *Paper A-1*, presented at the *Conference on Fluid Flow in the Mid 1970's*, 8-10 April 1975, East Kilbride, Glasgow.

[10] VDI/VDE; Richtlinie, Entwurf VDI 2040 Berechnungsgrundlagen für die Durchflussmessung mit Drosselgeräte, Blatt 1, Durchflusszahlen und Expansionszahlen genormter Drosselgërate und Abweichungen von den Normvorschriften. Beuth Vertrieb, Berlin, Köln.

[11] Schröder; Notwendige störungsfreie Rohrstrecken für Dusen und Blenden; *Brennstoff, Wärme, Kraft*, 13 (1961) Nr. 1, January, p. 20-23.

[12] Roman, Lagier, Blié, Ballez; Comptage de grands débits de gaz au moyen de diaphragmes et de calculatrices numériques aux postes de Taisnières et de Blaregnies; *Communication au Congrès de l'Association Technique de Gaz* (1973).

[13] Stolz; A general coordinated equation for discharge coefficients of orifice plate meters, *DOC N 75 ISO/TC 30/SC 2* (Sept. 1976).

[14] Plunian, Sens; Etude experimentale de redresseurs d'écoulement dans la mesure de débit au moyen de diaphragmes; *Communications IGU/C - 22 - 73,* presented at the *12th World Gas Conference,* Nice 1973.

[15] ARAKI; Flow instabilities in air orifices; *Fourth International Fluid Symposium,* April 1975, organized by BHRA at the University of Sheffield, England.

[16] Bean; Fluid meters, their theory and application, 6th ed., *American Society of Mechanical Engineers,* New York, N. Y., 1971.

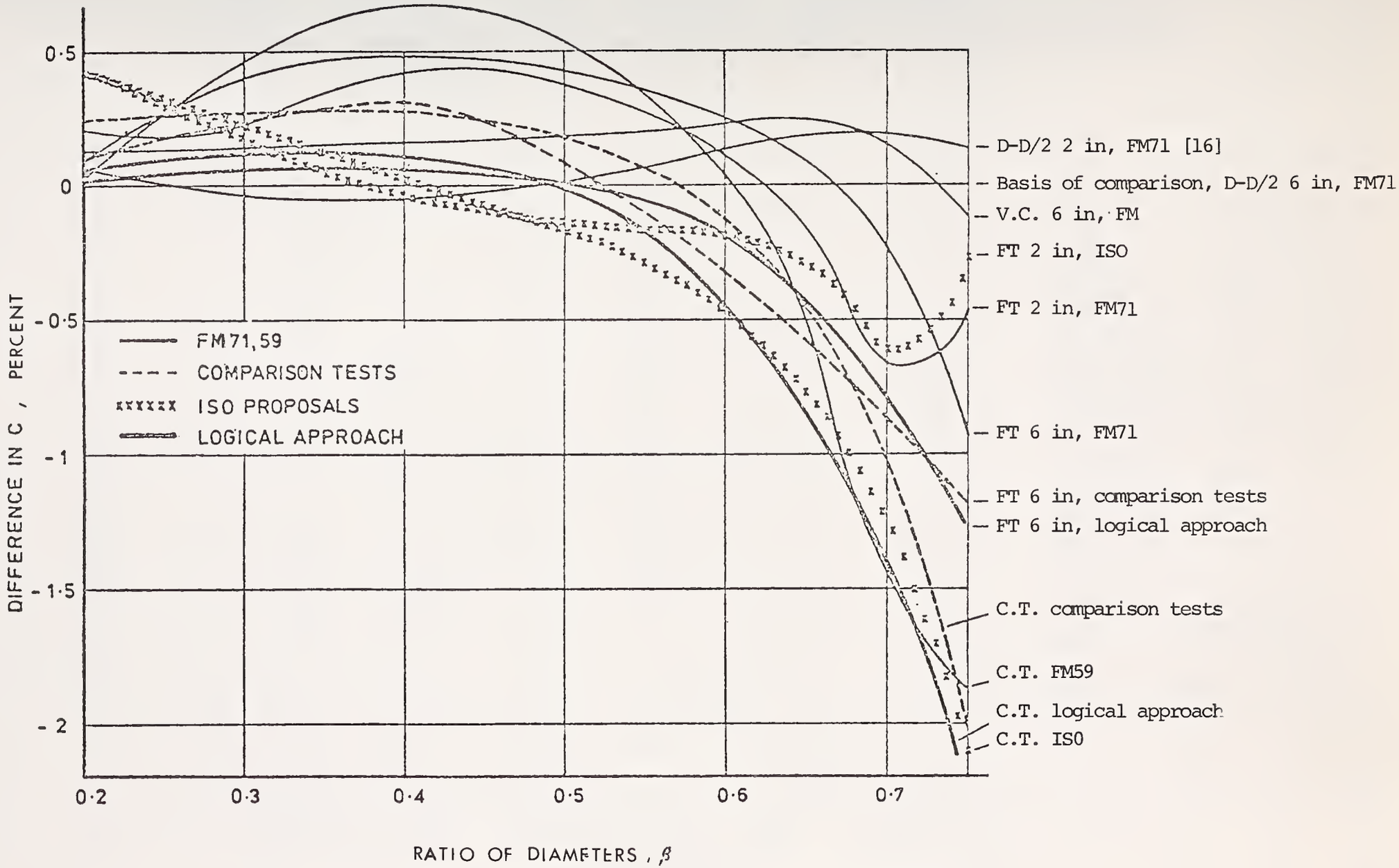

Fig. 1 A comparison of the discharge coefficients for 2" and 6" pipe diameter for several tapping arrangements and several standards, reference 8.

Group No.	No. of Measurement First	No. of Measurement Last	Test Orifice No.	β of Test Orifice	L, distance between disturbance and orifice in diameters	L_{ISO} required by ISO R581	L_{AGA} required by AGA No. 3	$(1 - \overline{Q/Q})$ %	L/L_{ISO}	L/L_{AGA}
7	58	63	23	.25	55.25	34.0	15.0	-.61	1.62	3.68
8	112	117	23	.25	35.25	34.0	15.0	-1.48	1.04	2.35
9	213	219	31	.25	14.60	34.0	15.0	-4.61	.43	.97
17	631	634	31	.25	58.25	34.0	15.0	-.38	1.71	3.88
37	31	32	25	.49	55.25	40.0	20.0	-1.95	1.38	2.76
39	64	69	25	.49	55.25	40.0	20.0	-1.40	1.38	2.76
42	95	99	25	.49	35.25	40.0	20.0	-3.00	.88	1.76
59	237	242	33	.49	14.60	40.0	20.0	-5.63	.36	.73
65	381	384	33	.49	4.25	40.0	20.0	-9.71	.11	.21
80	39	44	35	.68	55.25	62.0	30.0	-3.99	.89	1.84
87	554	557	39	.74	33.60	70.0	35.0	-4.21	.48	.96
89	603	607	39	.74	12.90	70.0	35.0	-1.93	.18	.37
91	615	618	39	.74	58.25	70.0	35.0	-3.81	.83	1.66
104	106	111	39	.74	35.25	70.0	35.0	-5.19	.50	1.01
108	350	354	39	.74	8.50	70.0	35.0	.10	.12	.24
113	371	380	39	.74	4.25	70.0	35.0	1.06	.06	.12
139	871	874	2	.25	10.00	34.0	15.0	1.47	.29	.67
142	884	888	6	.50	10.00	40.0	20.0	-1.37	.25	.50
145	897	900	6	.50	25.00	40.0	20.0	.42	.63	1.25
159	957	960	2	.25	17.00	34.0	15.0	4.98	.50	1.13
160	961	964	6	.50	15.00	40.0	20.0	-2.40	.38	.75
163	973	976	6	.50	23.75	40.0	20.0	.42	.59	1.19
172	1011	1014	6	.50	8.50	40.0	20.0	-3.14	.21	.42

Fig. 2 Results of tests without a straightener and three angles in two planes as disturbance.

National Bureau of Standards Special Publication 484, Proceedings of the Symposium on Flow in Open Channels and Closed Conduits held at NBS, Gaithersburg, MD, February 23-25, 1977. (Issued October 1977)

EQUITABLE IMPLEMENTATION OF NATIONAL AND INTERNATIONAL ALLOCATION PROGRAMS
(Summary of Remarks to the Panel)

James A. West
Assistant Administrator
International Energy Affairs
Federal Energy Administration
Washington, D.C. 20461

Following the 1973-74 Arab Oil Embargo of the United States and the Netherlands and a reduction of Arab oil supplies, the United States and 18 other nations formed the International Energy Agency (IEA). These nations consume about 85 percent of the world's oil supplies and formed IEA in order to establish cooperative measures in the event of any future large-scale interruptions in petroleum supplies. Its major programs include an international emergency allocation program, oil market monitoring, producer-consumer relations, and long-term cooperation on energy problems.

The Federal Energy Administration (FEA) was formed to administer the national regulatory programs in petroleum product allocations and pricing. FEA has the major role in the U.S. Government's participation in the IEA international allocation program. Flow measurement standards are not a major concern in national allocations but are of very considerable concern in the international emergency program (IEP).

In the IEP allocation program, the United States and the other 18 nations have agreed to allocate available oil supplies during an emergency in order to share such supplies equitably among the participating countries.

Emergency measures are activated when there is a seven percent reduction in oil supplies (based on average yearly consumption) to the group or to individual countries. The program requires mandatory demand restraint and maintenance of 70 days, eventually 90 days, of petroleum imports as stocks. Allocations are based upon computed supply rights and obligations derived from allowable consumption levels reduced by stock drawdown obligations.

Basically, the allocation is a crude oil program. All stocks and allocations are based upon crude oil and crude oil equivalents for broad categories of petroleum products (gasolines, middle distillates, fuel oils and other products).

In general, each country has its own measurement standards and product definitions or follows API or other petroleum measurement practices.

This raises several problems relative to flow measurements. The allocations are complicated by use of broad petroleum product groupings and lack of international standard definitions of these product categories. This complicates product exchanges and deliveries of desired products in allocating supplies. Allocations and stocking obligations are skewed because of duel use of certain fuels, such as residual fuel oils and naphthas.

So far, measurement problems have not been addressed in IEA but are left to national entities for applying standards, settling disputes and rationalizing transactions. There is a need for adoption of acceptable measurement standards in IEA.

National Bureau of Standards Special Publication 484, Proceedings of the Symposium on Flow in Open Channels and Closed Conduits held at NBS, Gaithersburg, MD, February 23-25, 1977. (Issued October 1977)

OF FORM AND SUBSTANCE FOR EFFECTIVE STANDARDS

Dr E. A. Spencer

Department of Industry
National Engineering Laboratory
East Kilbride
Glasgow, G75 0QU

With the expansion of demand and consequent increase in world trade, the need for international standardization has intensified. The various types of such standards include product specifications, methods of test and codes of practice: all are relevant to flow measurement. Their effectiveness can be measured by how well the operator attains in practice the objectives set out in the standards and these are reviewed.

Three ISO Draft International Standards, which can be used for hydrocarbon fluid flow measurement, are taken as examples of product specifications and codes of practice. The importance of their interrelationship with national regulations is examined.

1. Introduction

Standardization of speech and writing makes communication possible and we accept this form of standardization without question as being eminently desireable and necessary. Though standards have existed, however, from earliest times their scope in man-made products was limited until recently. Indeed their advantages have only become indisputable in the past century when the diversity of production which followed the industrial revolution became overwhelming. Major rationalizations then became crucial to provide simplifications which would result in economies in terms of effort and materials, and thus meet the world's increasing demands.

In addition to the benefits gained by simplification, standardization can also give benefits by setting up minimum requirements. These in a sense discipline society, but at the same time, for example by defining requirements for quality or safety, they are aimed at the protection of the individual or consumer interests.

Flow measurement can show examples of both these aims of standardization. The standards on pressure difference devices which emerged nationally about 50 years ago represented a coalescing of local experience in each country and an acceptance of a few prescriptions in place of each instrument maker's own pattern. Simplification of this kind is perhaps best exampled, however, by one of Britain's very first standards in 1901 which reduced the existing 75 different sizes which were in use for tramway rails to five. Though it is hard to imagine such a process being applied

to the whole of flow measurement with its hundreds of different flowmetering systems available today, there can be useful rationalizations as discussed later.

Oil and gas were being supplied to consumers well before the above dates and agreements were often individually negotiated. Legal regulations were later introduced for the protection of the consumer covering the measurement of the quantity of the fluid, its composition and so on and took on a role of quasi-standardization. Pattern approval and verification of each flowmeter used for sales to the public was supervised by government representatives. Thus, while national standards were being used extensively in the design of plant and pipelines, they were virtually excluded from the measurement side.

On the other hand, bulk measurements at custody transfer points were also required and here the interface between regulations and standards was being shifted. Now with the further expansion of demand and the development of international trade and operational groups, the need for common ground both at the national and international level has intensified. The pace is, indeed, such that the evolutionary process of earlier times is having to be replaced by strong guidance from governments and associations of users and manufacturers.

2. Types of Standards

If the aims of standardization are to promote economies wherever practicable, to protect the consumer either individually or collectively and to provide a means of communication and understanding between all parties, then it is important to establish what sort of standards can be used to achieve these aims in the flow measurement world.

While a standardized glossary is valuable in promoting understanding and clarity in the more practical standards, it is often left until they have been completed. These latter fall broadly into three categories: product specifications, methods of test and codes of practice.

Simplification must clearly depend on the selection of a few from the many available and these few must be considered as capable of standing up successfully on their own. Implementation of this selection must involve change for both suppliers and users, and calls for considerable co-operation. Thus, standard sizing to permit interchangeability can be a first stage and product standardization can in initiated in this way. Interestingly this had not taken place in the case of orifice plate fittings, where the ISO standard [1] while specifying the geometry of the plate leaves considerable latitude in its housing as well as variety in pressure tappings and coefficients. A "standard orifice plate unit" in the fullest sense could well benefit many users.

Dimensional specifications with stipulated tolerances provide one line of approach whether they cover overall or detailed requirements. Product specifications can also deal with the meeting of performance levels either on the basis that by meeting the requirements the appropriate performance will be achieved or that a level of performance is given which it is

required that the product must be shown to satisfy.

Within the specification standard or separately a different type of standard can therefore be adopted which lays down an acceptable method of test. As the name implies, this is a specification of the way in which a product can be measured and it must be sufficiently explicit that the values obtained by the method will be reproducible to within the expected level for any set of conditions which are permitted.

Less rigorous than either of the above is a code of practice. Having drawn together various procedures which have been established separately through experience in different areas, this is a standard which distills from them a composite set of instructions or guidelines. Thus, these guidelines provide the user with what is considered to be the best available advice to meet the objective of the standard, but they inevitably allow a fair amount of latitude. The code is lower down in the hierarchy of standardization, but vitally important in ensuring that a minimum set of criteria can be used.

It is logical to conclude from the above description of the sorts of standards which can be written that they all result from a pruning of existing information which must involve discarding a tremendous amount of data. Indeed it could be argued that the longer standardization is postponed, the greater will be the amount of wasted effort which will have been put into the development of information that is no longer needed.

It is certain that there is a propitious moment for the introduction of a standard. This is the moment which represents the optimum timing between missing improvements which were in the making, and delaying to include them. It is probable that nearly always standardization is left too long. Indeed it must be remembered that a standard can only be effective if it has time to be used properly and as a corollary it must therefore, once it is issued, remain frozen without changes for a reasonably long period. Committees preparing draft standards are often over-conscious of this and delay publication until they believe they are as near perfection as they can get in the hope that the standard will last a very long time. Though it is clear that, if it is known that a standard is to be amended after only a short period, there will be a disincentive for it to be adopted in its first form; nevertheless delay in publication can have serious consequences, just as will failure to revise it subsequently to take account of technological advances.

It can be asserted that standards in general should not be aimed at covering too large a field. If they are, they can take an inordinate time in preparation and then be left unaltered for too long. Instead the aim should be to conceive a limited series of objectives and deal with each separately. A steadily broadening coverage will be achieved and each part will contain the most up-to-date information. Revisions or supplements which permit additional ways of meeting the limited objective of each part are then much more easily prepared and accepted.

3. Limiting Objectives For Individual Standards

Certainly the timescale and the scope to be covered must be in the forefront of the drafting committee's first considerations when they tackle each project. No hard and fast rules can be laid down but a task which is likely to take more than five years before it is published and in use could well be said to be too comprehensive in its inception and would be better split up into a number of stages. For example, it is ambitious to prepare a standard to cover in depth the design, installation and performance, operation and maintenance of a particular type of flowmeter manufactured in variety throughout the world. A preliminary survey could well show that certain aspects can be cleared more quickly than others, and hence indicate a more amenable set of stages which can be tackled separately. The ISO standards on the use of tracer methods of flow measurement [2] have followed this pattern.

The scope of a standard must define explicitly the objectives which are aimed at. The standard will then be effective if it has no ambiguities and the user can achieve the objectives set out with a minimum of uncertainty. Objectives can be simple or complex, narrow or wide, but they should never be contradictory. The simplest would be where a single route is laid down to achieve the objective, for instance for accepting or rejecting carburettor jets. This could be solely on the basis of whether they gave flow rates under certain specified conditions which when compared to the flowrate through a fully specified critical flow nozzle package came within a defined bandwidth. No other way would be permitted.

The objective could still be the same as in the example above but a number of different routes might be permitted. This could arise in an international standard because different methods used in different countries are so strongly supported as being of equal merit that they are all adopted. Inevitably there will then be jets which if tested by one route would succeed, but would fail by another. If the quality of the production line would be virtually unaffected in total by such individual differences there is no real significance in their occurrence. Cross-checking rigorously between such alternative routes is often sparse, however, and so there must be a danger of incompatibilities occurring. For example, there could be a systematic bias between the overall mean value of a batch tested by the different routes or the resulting bandwiths could be different. This should be recognized and sufficient intercomparison made for some indication to be given in the standard of its likelihood, for example by increasing the overall uncertainty estimate for all the routes.

An example of such an incompatibility is in the International Standard ISO R541 [1] where the predicted discharge coefficients for an orifice plate installed in a pipeline of 32 inches or above are different depending on the arrangement of the pressure tappings used. Though technically specifications for the locations of the flange and corner tapping arrangements differ, their proximity is such that at this size they can be regarded as identical. The pressure differences across the tappings are found to be the same, so that it is clearly wrong that using the two relevant discharge coefficients the calculated flowrates will be different. This clear anomaly has arisen because the coefficients evolved from different sources

of data and were analysed independently of each other. A fresh and comprehensive re-assessment of the various predictions has been made so that this and similar discrepancies can be resolved in future editions. Without new data or the almost impossible task of re-analysis of all earlier data, it must be accepted that the new solution must have an increased uncertainty to take into account such incompatibilities.

Another situation arises where although the objective of the standard may be quite clear some extrapolation is in reality involved. Thus there could be applications permitted in the standard for which the information is only tentative. For example this could be especially true when the limits of the operating range of temperatures over which the standard can be used are set. It is very unlikely that strict tests will have been carried out at the extreme conditions. Again the increase in uncertainty must be acknowledged in the standard.

Summarizing therefore it can be said that a standard can only be fully effective if the objectives have been closely checked for all the conditions and methods which are covered in the standard. Neglect of this rule will lead to errors of unknown size of which the user is unaware. Its observance means that if necessary the scope will have been suitably modified to allow for these special areas.

4. The Form of The Standard

If it is the principle condition in setting out to write a standard that the objectives should be clearly understood, it is proper that when the standard is published these should be brought together to constitute its first clause and not be scattered through it. There can be justification for expressly stating what is not covered in the standard where such exclusions might be overlooked and the standard thus misused. Normally, however, the scope can be expected to prescribe the actual limits within which it it expected to apply. References can then be given to any overlapping or fringe standards or to any standards which may be required to be used in order to comply with the one being published.

Since for most users it is likely that an international standard will not be printed in their own native language the importance of selecting words and phrases which are well understood is easily appreciated. Yet all too often the final editing is hurried and points of this kind are overlooked. A lesson could be taken from the EEC Commission where Directives in their final stages of preparation are subjected to detailed examination by both legal and linguistic experts.

Understanding is also greatly aided if the presentation in the text follows a logical sequence, though in a long or complex standard the best sequence may not be automatically self-evident. The form or framework most usually adopted is for the equipment to be specified fully before its performance is considered.

The tests to be used to check its performance, the methods of computation and analysis and the method of presentation of the results can then follow. While the method of estimation of the overall uncertainty may

be left to an appendix, there should always be a clause in the main text requiring the estimated uncertainty to be given as an essential part of the statement of results. This should apply whether this statement is a single line giving the flowrate or quantity or a full test report.

Appendices or footnotes should be used wherever possible to separate non-essential material from that required for the operation of the standard. It is worth recalling that formally such appendices become a mandatory part of a standard only if they are defined as such in the main text of the standard. Similarly tables and figures need a direct reference if they are to be of similar force to the text.

5. The Substance of Standards

For the purposes of this essay a collection of standards are to be available which have as their aim the correct measurement of the quantity of a hydrocarbon fluid passing a particular point in a given time. They may be used by individuals or organizations being supplied with these fluids; they may be used at custody transfer points between one distributor and another or at the source; or they may be used for control purposes at any stage. The government will be concerned with such measurements both for their own purposes in taxation and wherever legal transactions between parties involving flow measurements are subject to the enactments by the legislature.

Many different standards will therefore be needed to provide full coverage since the range of hydrocarbon fluids is considerable and the number of possible metering systems for its measurement is large. The first breakdown can be into liquids and gases; for in general, the metering devices normally used for these will be different. With mixtures of liquids and gases, separation is necessary if the measurement is to be reliable, since the methods which are available at present for the measurement of two-phase flows are only very approximate. Indeed no standardization has even been attempted yet.

The question of contamination which generally occurs at an early stage in the process, is an important one since precautions must be prescribed and followed if false measurements are to be avoided. Provided the amount and size, for example, of solid particles being carried in suspension is low enough, their influence can be taken into account so long as they do not change or damage the measuring system. Similarly, if a small percentage of water is mixed with the oil it can be allowed for. In all cases where contaminants may exist it will be imperative that sampling techniques are laid down which can adequately assess the amount of the extra constituent being passed.

The only ISO standards so far published dealing with flowmeters for general use in pipelines and closed conduits are R541 [1] and R781 [3], covering the design and use of orifice plates, nozzles and venturi tubes. These documents, which are product specifications, have been the subject of revision and are combined in the Draft International Standard DIS 5167 at present awaiting ratification [4]. Several other proposals for other metering devices are also at this DIS stage while there are also a number

at the drafting stage.

The R541 and R781 standards have been adopted nationally in a number of countries, and there and elsewhere they are being used for hydrocarbon measurements. It has to be remembered that these standards were drawn up for general use in industry and it is left to the user to judge the overall accuracy he has achieved in his measurement since a number of factors are not controlled within the conditions laid down in the standard. For example, there are no specified methods for measuring the density of the fluid. Also the measurement of the pressure difference is not prescribed and uncertainties in this could play a significant part in the assessment of the overall uncertainty.

If then an agreed level of accuracy is to be the objective for standards concerned with the use of pressure difference devices for hydrocarbon fluid measurements, subsidiary standards are required laying down how these various additional measurements are to be made. In addition, since ISO DIS 5167 covers all industrial measurements, the requirements for these specific gas and oil applications have to be considered and the necessary extra constraints then added in a supplementary document to ensure that the objective in the hydrocarbon standard can be achieved under all the conditions which are likely to be met.

Intercomparison between the ISO standard and the AGA Report No 3 [5], so long used in the USA for natural gas measurement, has shown up differences too substantial to be disregarded. Among these, the most important relate to differences in acceptable installation conditions and their effect on the estimation of the uncertainty to be associated with the discharge coefficients which are adopted. On the other hand, it must be recognized that to be effective the standard needs also to be supplemented to give full coverage to all aspects making up the final measurement.

In oil flow measurement the dominance of the positive displacement meter has given way especially in the larger pipeline sizes to the turbine meter, but between them they provide the vast majority of measurements on which payment is made. International draft standards are available on both these devices; ISO/DIS 2714 deals with positive displacement meters [6] and ISO/DIS 2715 with turbine meters [7]. It is perhaps surprising in view of the importance attached to the use of these meters that publication of these standards has not occurred earlier. The ISO Committee concerned is however simultaneously proceeding with the drafting of a large number of standards covering various aspects of the measurements involved, including meter proving.

The coverage aimed at in these two draft standards (2714 and 2715) is very considerable, though it is fair to note that in substance these standards are essentially codes of practice. While guidance is given of the manifold problems which can arise during measurement, there are no details of how to deal with these problems. The user is left to find this out from other sources.

Both standards are inevitably limited in their treatment since it is stated at the commencement that no tolerance or accuracy limits are being

set, but in following sentence in each, however, it is claimed that the provisions of the standard should prove adequate to achieve a degree of measurement accuracy acceptable to any metering requirement. These objectives are obviously contradictory, for the user cannot determine how rigorously he must meet provisions which have been so written as to allow for a wide range of different levels of accuracy to be attained. For example, having stated that turbine meter performance is affected by swirl and non-uniform velocity profiles, it is recommended quite rightly that "sufficient" lengths of straight pipe or a combination of straight pipe and straightening vanes be used to overcome this problem. No definition of what is "sufficient" is given for any particular layouts and the recommended flow straightener assembly is described as "effectively assisting in achieving flow conditioning" without expressly stating the level which it has been found to achieve.

If then these two standards on oil flowmeters are to be regarded as the first steps towards fully comprehensive international standards how are they to be followed up. One way must be to set explicit performance criteria and associate with these more detailed information on what has been found to be sufficient in design, installation and operational requirements to achieve this performance. At present any matters covered in national regulations or private agreements have been excluded because of their legal implications. Differences between such regulations are inevitable since they will have been established, in some instances, many years ago in accordance with procedures developed separately in the different countries. If such differences can be reduced to a matter of degree and not of contradiction then a major restraint to progress will be removed.

The aims of the International Organization for Legal Metrology are to promote unification in the measurement practices followed by the governments of member states. This is achieved by publishing Recommendations agreed by the member states as representing acceptable compromises between their individual regulations; the members also agree to implement these harmonized versions. OIML Working Groups are active in the field of hydrocarbon fluid measurements so that progress towards rationalization is being made. Indeed the countries within the EEC are also seeking to obtain a common pattern in this field; this time through the publication of Directives which are to take the place of the individual country's rules.

It is clearly of considerable importance that there should be very close liaison between such govermental organizations and the ISO and IEC. For the immediate future there is bound to be an overlap of interests, and aspects that may be more appropriate to standardization could well be included in the model regulations. Ultimately, however, the greatest benefit to industry as a whole will be achieved by the extension of the coverage of the standards; for example, by dealing with specific ranges of applications at various levels of accuracy. The necessary regulations can then be framed in such a way that they require the user to conform to appropriate sections of the international standards, rather than themselves prescribe the technical provisions to be met.

There is a marked contrast between bulk metering of oil using, for example, the draft standards on turbine meters with dedicated pipe proving

systems and that of natural gas using the detailed specification for orifice plates. Both can be made more effective for operational use by extending their scopes to include areas covered by the other.

6. Conclusion

The main aims of standardization can be said to be to promote economies, protect the consumer and provide the means of understanding between parties. These have all been very amply demonstrated in flow measurement by the extensive use of "standard" pressure difference devices over the past fifty years and by the development of acceptance test methods. Such standards have not been static and they are still being modified and improved as fresh analyses and evidence become available.

As more and more flowmetering systems are introduced so the advantages of a standards framework for their intercomparison and operation increase. The form of the standard can vary to suit the requirement, whether this be for the simplification of face-to-face dimensions to allow interchangeability, or the specification of performance criteria at codified levels, or yet again the guidance given in a Code of Practice. Each such standard can be effective for a period of time if its provisions unambiguously permit the operator to achieve the objectives laid down in the standard.

The rapid expansion of industrial activity and the increase in international trade has meant that it is no longer worthwhile pursuing solely national standards as a goal. Instead international agreement must be sought and this is especially true of the measurement of hydrocarbon fluids. The existence of differing national regulations, however, has been a restraint which will be overcome only when present efforts to harmonize these are successful. Indeed the importance of collaboration between organizations such as OIML, ISO and IEC is recognized and closer liaison is being developed. This will enable more positive international standards to be promulgated for the general benefit of industry while allowing governments to incorporate suitable references to mandatory aspects of these standards in their own regulations.

Acknowledgement

This paper is presented with the permission of the Director, National Engineering Laboratory, Department of Industry. It is British Crown copyright.

[1] Measurement of fluid flow by means of orifice plates and nozzles, ISO/R541-1967, 1st Ed., (International Organization for Standardization, Geneva, 1967).

[2] Measurement of water flow in closed conduits. Tracer methods, ISO Standard 2975, Parts I-VII, (International Organization for Standardization, Geneva).

[3] Measurement of fluid flow by means of venturi tubes, ISO/R781-1968, 1st Ed., (International Organization for Standardization, Geneva, 1968).

[4] Measurement of fluid flow by means of orifice plates, nozzles and venturi tubes, ISO/DIS 5167, (International Organization for Standardization, Geneva, 1976).

[5] Orifice metering of natural gas, AGA Report No 3, (American Gas Association, Arlington Va, 1969).

[6] Liquid hydrocarbons - volumetric measurement by positive displacement meter systems other than dispensing pumps, ISO/DIS 2714, (International Organization for Standardization, Geneva, 1976).

[7] Liquid hydrocarbon - volumetric measurement by venturi meters, ISO/DIS 2715, (International Organization for Standardization, Geneva, 1976).

National Bureau of Standards Special Publication 484, Proceedings of the Symposium on Flow in Open Channels and Closed Conduits held at NBS, Gaithersburg, MD, February 23-25, 1977. (Issued October 1977)

COMMENTS ON: ROLE OF INTERNATIONAL STANDARDS IN MEASURING AND ALLOCATING HYDROCARBONS - A PROGRAM FOR SOLUTION OF OUR PRESENT PROBLEMS

Frederick H. Abernathy
Harvard University
Cambridge, Mass. 02138

The four members of the panel concentrated their discussion on different aspects of the hydrocarbon measurement problem, which are associated with the international trade in hydrocarbons. There are a number of features of the present problem that makes the situation qualitatively different from that which existed in the past. Increasingly the buyers and sellers of hydrocarbon are units of government rather than individual corporations. The total mass or volume of hydrocarbons in international trade is rising and likely to continue to rise over the next decade. The amount of hydrocarbons primarily trans-shipped through nations is also rising. Lastly the value of a unit of hydrocarbons has risen by at least a factor of four in so short a period of time that it can be thought of as a discontinuous change.

In the past when the buyers and sellers of hydrocarbons were individual corporations, the method of settlement of measurement dispute was through negotiation of a satisfactory price. National prestige and techniques of measurements were not necessarily involved, or at the forefront of the discussion. Now as the unit price of hydrocarbons has risen, monetary value associated with discrepancy in measurements has also risen. The attention devoted to discrepancy in measurements of these large volumes and flow rates naturally increases. In addition, one has the possibility of different measurement techniques and standards used by each nation in a hydrocarbon transaction. Each party to the transaction is generally satisfied with its technique and standards, and when measurements of pipe line flow across national borders disagree, or when measurements of mass of oil in a tanker disagree from on-loading to off-loading, then one has a technical problem complicated by international political considerations. The question then is really how does one resolve all of these conflicting points of view and interest. An obvious answer is that each of us do our task a little bit better and a little more carefully. We should decrease the uncertainty in our measurements by more carefully defining procedures and increasing the accuracy of our measurements. This is easily said and not very easily done, and might in the long run not even resolve the problem. The differences between many standards cannot be resolved by increasing the data base alone unless one changes the range of validity of various standards and/or incorporates additional

variables. What should be done? The need for more precise measurements exists - many of the problems have been identified, but can we agree on how best to resolve these difficulties?

Let me advance a particular point of view, namely that increased testing, calibration, and measurement will not alone solve the problem without simultaneously expanding our understanding of the various fluid metering processes. Let me give just two examples:

(1) Because the bulk coefficient of expansion of petroleum depends on its chemical composition in addition to the state variables, no amount of data taking or curve fitting without awareness of this property will remove this dependence of the coefficient of expansion on composition.

(2) Axial swirl apparently affects turbine meter measurements in pipe flow even when they are installed under conditions which meet some current standards.

A much longer list of examples could be compiled. From my point of view, it is only necessary to agree that such a list could now be made of parameters whose importance is not recognized in present standards. If one accepts the premise that such a list could currently be devised, and with additional research could probably be expanded, then one is naturally led to the conclusion that we need to expand our basic understanding of flow metering processes. While one might always wish to expand our basic understanding, the question can be raised, is now a relatively more important time than the immediate past, and if so are our chances of success greater than they have been in the recent past? I believe the answer to both questions is yes.

We have a greater need for more fundamental understanding now, because the uncertainties in measurements currently involve very substantial sums, and because increased understanding appears, to me, in the long run to be the only way to avoid complex political or judicial solutions of what are in fact technical problems. The likelihood of achieving increased understanding of the fluid dynamics of flow metering problems is, in my opinion, excellent, if we find the strength and courage to move vigorously on the problem. I believe this to be true primarily for two reasons. We have reached a state where we are able to numerically calculate solutions to pipe metering flows and open channel flow from first principles provided we independently know the wall shear stress variation and the turbulent eddy diffusivity. Because such codes exist, or can be developed, it is now possible to explore fairly inexpensively the importance of variations in initial conditions, the effects of variation of viscosity on temperature, etc. on a theoretical basis and check these results against special experiments designed to test the calculations. The second factor that makes advances in understanding likely is the improvements in instrumentation. It is not only that spatial resolution and time response of velocity and pressure probes have been improved, but also that non-intrusive velocity probes are now available for the first time.

In addition, the introduction of the mini-computer to the laboratory is in the process of changing our entire view of what it is possible to measure and analyze. As a result, for example, it seems likely that we will be able to routinely acquire spectral information about velocity fluctuations that we always considered important but rarely measured because of the enormous effort involved in acquiring and reducing the data.

It no longer appears visionary to expect on line instrumentation systems to automatically account for spatial changes in state variables in real time. Existing integrated circuit technology makes relatively large volume data storage for use with complex algorithms economically possible. We can now acquire data at a high rate and manipulate large data bases with inexpensive reliable solid state devices. The technology is available to handle problems with a large number of parameters quite easily. Our difficulty is that instrumentation and computing technology is well ahead of our understanding of the parameters which control the flow processes in metering devices. In the relatively recent past, this was not true, which diminished our drive to increase our knowledge. We should recognize that times have changed; the need exists, the technology to exploit additional knowledge exists, and now our lack of understanding is holding us back.

I believe that we should and can move vigourously with programs which enlarge our understanding, confident in the knowledge that the results of such efforts will be used quickly in the international field.

AUTHOR INDEX

Abernathy, F. H. 957
Allion, H. 33
Annett, John 145
Appell, Gerald 109

Bajura, R. A. 523
Baker, Milton 803
Ball, John M. 847
Baumoel, J. 267
Berte', Frank J. 447
Bradshaw, J. E. 293
Brennan, J. A. 881
Brower, W. B. Jr. 719
Bruner, Ronald F. 277

Clark, M. E. 479
Cullen, J. T. 549

Dang, Clement 187
Davis, L. M. 55
Davis, R. W. 219, 491
DeCarlo, J. P. 549
Delisi, Donald P. 423, 783
Dijstelbergen, H. H. 935
Durgin, William W. 471
Dussauge, J. P. 649

Edgerly, D. E. 921

Fabris, Gracio 659
Flandro, G. 335
Flemons, R. S. 319

Gad-el-Hak, Mohamed 571
Gaviglio, J. 649
Gold, D. S. 621
Grant, D. M. 91
Greenleaf, J. F. 335
Guthrie, D. L. 173

Halmi, Dezsoe 61
Haney, Robert A. 755
Hayward, A. T. J. 1
Holley, E. R. 395

Irwin, L. K. 895

Jennings, Roger 821
Johnson, S. A. 335

Kempf, D. 361
Kirchhoff, Robert H. 783
Koenig, H. L. 145
Kondic, N. N. 765
Kulin, G. 123
Kullman, C. G. 25

LaNasa, Paul J. 871
Lin, Jung-Tai 423
Liu, Hsien-Ta 423
Lowell, Francis C. Jr. 243
Lynnworth, L. C. 293

Mann, D. B. 881
Martig, Kenneth W. Jr. 83
Mattingly, G. E. 33, 491
McQuivey, S. 109
Meagher, Thomas F. V. 687
Mero, Thomas 109
Miller, R. W. 549
Moore, E. 33
Morel, P. R. 293
Morgan, W. H. 361

Neale, Lawrence C. 471

O'Brien, Joseph F. 145

Peckham, Vernon D. 687
Pedersen, N. E. 293
Pellegrin, M. T. 523
Phillips, R. E. 361
Pierce, F. J. 621
Pontius, P. 33

Replogle, John A. 201
Robben, Frank A. 423
Robertson, J. M. 479
Rudland, R. S. 705
Ruff, James F. 187

Sachs, Donald C. 687
Saxton, Keith 187
Scottron, V. E. 737
Servoz, Alan 719
Seward, Wallace N. 929
Singley, G. Wayne 145
Skridulis, James 145
Spencer, E. A. 947
Suhoke, Robert B. 597

Tabler, J. H. 25
Tanaka, M. 335

Vincenty, C. 173

Washington, D. R. 173
West, James A. 945

U.S. DEPT. OF COMM. BIBLIOGRAPHIC DATA SHEET	1. PUBLICATION OR REPORT NO. SP 484 -- Volume 2	2. Gov't Accession No.	3. Recipient's Accession No.

4. TITLE AND SUBTITLE

Flow Measurement in Open Channels and Closed Conduits
Volume 2

5. Publication Date: October 1977

6. Performing Organization Code

7. AUTHOR(S)
Lafayette K. Irwin, Editor

8. Performing Organ. Report No.

9. PERFORMING ORGANIZATION NAME AND ADDRESS

NATIONAL BUREAU OF STANDARDS
DEPARTMENT OF COMMERCE
WASHINGTON, D.C. 20234

10. Project/Task/Work Unit No.

11. Contract/Grant No.

12. Sponsoring Organization Name and Complete Address *(Street, City, State, ZIP)*

National Bureau of Standards

13. Type of Report & Period Covered: Final

14. Sponsoring Agency Code

15. SUPPLEMENTARY NOTES

Library of Congress Catalog Card Number: 77-14243

16. ABSTRACT *(A 200-word or less factual summary of most significant information. If document includes a significant bibliography or literature survey, mention it here.)*

The wide range and complexity of problems and potential solutions that must be considered for useful flow measurements are emphasized by the papers contained in these proceedings. Fifty-three presentations cover: characteristics of new and improved instruments; applications of traditional and new measuring devices in field environments; procedures for identifying and analyzing errors or uncertainties in data under specific conditions; uses of physical and numerical models; politico-economic changes that affect international standards for flow measurement; and philosophical bases for making measurements. The fluids of most interest are water and waste water, petroleum and related refined products, air, natural gas and stack gas.

Experimental and analytical investigations on instrument performance and interpretation of results include innovative applications of traditional and new flow measurement techniques to fluid flows in open channels and closed conduits. The traditional devices or techniques include weirs, flumes, current meters, orifice plates, turbines, hot-wires, pitot-static tubes, velocity traverses, dye-dilution, and others. More recent instrumentation developments and procedures such as laser doppler anemometry, acoustic and thermal imaging, acoustic pulse velocity and doppler anemometry, numerical modeling, vortex shedding and digital computation are covered for particular measurement purposes.

The most significant trend reflected in these presentations is the general awareness that uncertainties in measured quantities at the lowest point in the measurement chain, i.e., in the field or plant, are more important than accuracy statements derived from controlled laboratory studies. Other trends in evidence are the rising importance of turbine meters for use as transfer standards and in-line measurements of liquids and gases in filled pipes and the increasing number of applications for acoustics and laser technology for flow measurements in both open channels and closed conduits.

17. KEY WORDS *(six to twelve entries; alphabetical order; capitalize only the first letter of the first key word unless a proper name; separated by semicolons)*

Acoustic flow meters; closed conduit flows; current meters; dye-dilution methods; errors in flow measurement; flow measurement; fluid flow modeling; fluid velocity; flumes; gas flow standard; hot-wire anemometry; international flow standards; laser anemometry; open channel flows; orifice meters; pitot-static meters; turbine meters; weirs.

18. AVAILABILITY

☐ Unlimited

☐ For Official Distribution. Do Not Release to NTIS

☒ Order From Sup. of Doc., U.S. Government Printing Office Washington, D.C. 20402, SD Cat. No. C13.10:484/Vol.2

☐ Order From National Technical Information Service (NTIS) Springfield, Virginia 22151

19. SECURITY CLASS (THIS REPORT): UNCLASSIFIED

21. NO. OF PAGES: 490

20. SECURITY CLASS (THIS PAGE): UNCLASSIFIED

22. Price: $12.25 Per 2 Part Set

USCOMM-DC 29042-P74

☆ U. S. GOVERNMENT PRINTING OFFICE : 1977 246-328/6596

NBS TECHNICAL PUBLICATIONS

PERIODICALS

JOURNAL OF RESEARCH reports National Bureau of Standards research and development in physics, mathematics, and chemistry. It is published in two sections, available separately:

• **Physics and Chemistry (Section A)**
Papers of interest primarily to scientists working in these fields. This section covers a broad range of physical and chemical research, with particular emphasis on standards of physical measurement, fundamental constants, and properties of matter. Issued six times a year. Annual subscription: Domestic, $17.00; Foreign, $21.25.

• **Mathematical Sciences (Section B)**
Studies and compilations designed mainly for the mathematician and theoretical physicist. Topics in mathematical statistics, theory of experiment design, numerical analysis, theoretical physics and chemistry, logical design and programming of computers and computer systems. Short numerical tables. Issued quarterly. Annual subscription: Domestic, $9.00; Foreign, $11.25.

To begin publication as a single journal, July-August, 1977

DIMENSIONS/NBS (formerly Technical News Bulletin)—This monthly magazine is published to inform scientists, engineers, businessmen, industry, teachers, students, and consumers of the latest advances in science and technology, with primary emphasis on the work at NBS. The magazine highlights and reviews such issues as energy research, fire protection, building technology, metric conversion, pollution abatement, health and safety, and consumer product performance. In addition, it reports the results of Bureau programs in measurement standards and techniques, properties of matter and materials, engineering standards and services, instrumentation, and automatic data processing.

Annual subscription: Domestic, $12.50; Foreign, $15.65.

NONPERIODICALS

Monographs—Major contributions to the technical literature on various subjects related to the Bureau's scientific and technical activities.

Handbooks—Recommended codes of engineering and industrial practice (including safety codes) developed in cooperation with interested industries, professional organizations, and regulatory bodies.

Special Publications—Include proceedings of conferences sponsored by NBS, NBS annual reports, and other special publications appropriate to this grouping such as wall charts, pocket cards, and bibliographies.

Applied Mathematics Series—Mathematical tables, manuals, and studies of special interest to physicists, engineers, chemists, biologists, mathematicians, computer programmers, and others engaged in scientific and technical work.

National Standard Reference Data Series—Provides quantitative data on the physical and chemical properties of materials, compiled from the world's literature and critically evaluated. Developed under a world-wide program coordinated by NBS. Program under authority of National Standard Data Act (Public Law 90-396).

NOTE: At present the principal publication outlet for these data is the Journal of Physical and Chemical Reference Data (JPCRD) published quarterly for NBS by the American Chemical Society (ACS) and the American Institute of Physics (AIP). Subscriptions, reprints, and supplements available from ACS, 1155 Sixteenth St. N.W., Wash. D. C. 20056.

Building Science Series—Disseminates technical information developed at the Bureau on building materials, components, systems, and whole structures. The series presents research results, test methods, and performance criteria related to the structural and environmental functions and the durability and safety characteristics of building elements and systems.

Technical Notes—Studies or reports which are complete in themselves but restrictive in their treatment of a subject. Analogous to monographs but not so comprehensive in scope or definitive in treatment of the subject area. Often serve as a vehicle for final reports of work performed at NBS under the sponsorship of other government agencies.

Voluntary Product Standards—Developed under procedures published by the Department of Commerce in Part 10, Title 15, of the Code of Federal Regulations. The purpose of the standards is to establish nationally recognized requirements for products, and to provide all concerned interests with a basis for common understanding of the characteristics of the products. NBS administers this program as a supplement to the activities of the private sector standardizing organizations.

Consumer Information Series—Practical information, based on NBS research and experience, covering areas of interest to the consumer. Easily understandable language and illustrations provide useful background knowledge for shopping in today's technological marketplace.

Order **above** *NBS publications from: Superintendent of Documents, Government Printing Office, Washington, D.C. 20402.*

Order **following** *NBS publications—NBSIR's and FIPS from the National Technical Information Services, Springfield, Va. 22161.*

Federal Information Processing Standards Publications (FIPS PUBS)—Publications in this series collectively constitute the Federal Information Processing Standards Register. Register serves as the official source of information in the Federal Government regarding standards issued by NBS pursuant to the Federal Property and Administrative Services Act of 1949 as amended, Public Law 89-306 (79 Stat. 1127), and as implemented by Executive Order 11717 (38 FR 12315, dated May 11, 1973) and Part 6 of Title 15 CFR (Code of Federal Regulations).

NBS Interagency Reports (NBSIR)—A special series of interim or final reports on work performed by NBS for outside sponsors (both government and non-government). In general, initial distribution is handled by the sponsor; public distribution is by the National Technical Information Services (Springfield, Va. 22161) in paper copy or microfiche form.

BIBLIOGRAPHIC SUBSCRIPTION SERVICES

The following current-awareness and literature-survey bibliographies are issued periodically by the Bureau:

Cryogenic Data Center Current Awareness Service. A literature survey issued biweekly. Annual subscription: Domestic, $25.00; Foreign, $30.00.

Liquified Natural Gas. A literature survey issued quarterly. Annual subscription: $20.00.

Superconducting Devices and Materials. A literature survey issued quarterly. Annual subscription: $30.00.

Send subscription orders and remittances for the preceding bibliographic services to National Bureau of Standards, Cryogenic Data Center (275.02) Boulder, Colorado 80302.

U.S. DEPARTMENT OF COMMERCE
National Bureau of Standards
Washington, D.C. 20234

OFFICIAL BUSINESS

Penalty for Private Use, $300

POSTAGE AND FEES PAID
U.S. DEPARTMENT OF COMMERCE
COM-215

U.S.MAIL

SPECIAL FOURTH-CLASS RATE
BOOK